# Partial Discharge Diagnostics in Medium Voltage Cables

*A dissertation submitted to the department of electronic and electrical engineering and the committee for postgraduate studies of the University of Strathclyde in partial fulfilment of the requirements for the degree of doctor of philosophy.*


*By*

**Faisal Peer Mohamed**


*Glasgow, 2013*

*To my beloved parents and wife*

# Declaration

This thesis is the result of the author's original research. It has been composed by the author and has not been previously submitted for examination which has led to the award of a degree. The copyright of this thesis belongs to the author under the terms of the United Kingdom. Copyright Acts as qualified by University of Strathclyde Regulation 3.50. Due acknowledgement must always be made of the use of any material contained in, or derived from, this thesis**.**

_____

**Faisal Peer Mohamed**

# Acknowledgement

It would never have been possible to write this doctoral thesis without the grace of the Almighty and the support and kindness of people around me. I would like to express my deepest gratitude to my principal supervisor, Dr. Wah Hoon Siew for his excellent guidance; caring; patience; freedom and providing me with an excellent atmosphere for doing research. I am also thankful to him for arranging industrial funding to continue my research from the master project. I wish to express my deep thanks to second supervisor Prof. John Soraghan for his help and suggestions in the area of signal processing. I wish to express my special thanks to Dr. Scott Munro Strachan for his endless help throughout the project in arranging site trials and valuable discussions. Also my sincere thanks to Mr. Douglas Grant, Dr. Martin Judd and Dr. Tee Chong Lim for useful discussions.

This research project was very dependent on the provision of utility assets from Scottish Power Plc. I would like to thank Mr. Jamie Mcwilliam for his kindness and his efforts through these years. Indeed without Jamie, many of the substation field tests would be impossible. I also wish to express my sincere thanks to Mr. Brian Boys, Mr. Paul Cunningham and Mr. Neil McDonald for their patience and time during field trials.

Being an electrical engineer, It was more challenging to enter the field of embedded systems. I wish to express my sincere thanks to Mr. Bob Elkind and Mr. Austin Lesea of Xilinx for their on-line suggestions and advice. Also I wish to express my thanks to Mr. Frank Cox for his technical support in building printed circuit boards. I wish to thank Dr. Karl Liu for his support during debugging of hardware and many thanks to Mr. Yuxian Tao for very useful discussions especially in the hardware design. My appreciation goes to all of my colleagues, especially Mr. Ahmad Syahrir Ayub and Mr. Farhan bin Hanafi for their effort to make such a pleasant working environment.

I would like to thank my wife for her patience and understanding of my long hours in the lab and consistent support throughout the period. Also I would like to thank my uncle Mr. Mohamed Ghani for his endless moral and financial support especially in tough situations. Last and certainly not least, I would like to express my gratitude to my parents and sisters, especially to my mum Mrs. Subaitha Beevi for her prayers which hopefully leads to success.

# *Abstract*

Most of the high voltage cables installed in the United Kingdom for power transmission and distribution are approaching the end of their designed life. This is likely to lead to an increased prevalence of circuit faults resulting directly from insulation degradation and breakdown due to ageing. This will lead to customer interruption and regulatory penalties. A program for the wholesale replacement of vast cable networks is impracticable, not economically viable and most likely unnecessary. A more pragmatic and affordable approach to extending the life time of these ageing assets, incorporating targeted cable replacement, may be achieved through the use of condition based maintenance strategies utilizing online partial discharge monitoring technologies. Partial discharges (PD) are the early symptoms of insulation degradation that can ultimately lead to complete breakdown of the insulation system.

Presented in this thesis are novel contributions to the area of online PD diagnostics for underground medium voltage cables. The work encompasses various issues with installation of PD sensors in cable networks, data acquisition procedures and signal processing techniques for post processing of PD data. A novel approach of using power frequency current transformer for detecting PD is proposed. This approach is validated using laboratory tests and on-site trials using the PD monitoring hardware developed.

PD source location using double ended method is widely accepted due to the accuracy in discharge site location compare to single ended approach. However, this method is not widely used due to its complex system design, time synchronization and communication requirement between measurement units at both ends of the cable network. In this thesis, double ended PD source location system using a novel time based triggering logic is implemented in field programmable gate arrays with GPS. System design, laboratory results and on-site trials are presented.

Denoising of PD signals using second generation wavelet transform are comparatively faster than classical wavelet based techniques. This second generation wavelet transform using kurtosis based thresholding is developed and tested using synthetic and on-site data. A PD signal interpretation algorithm is applied to analyse the data acquired from the 11kV PILC cable network from 33/11kV substation using the system developed.

# Table of Contents

# List of Figures

# List of Tables

# List of Acronyms and Abbrevations

| | |
|---|---|
| (AC) | Alternating Current |
| (ADC) | Analogue to Digital Converter |
| (ADL) | Address Decode Logic |
| (AE) | Acoustic Emission |
| (AM) | Amplitude Modulated |
| (AUI) | Advanced User Interface |
| (BCR) | Bus Configuration Register |
| (BNC) | Bayonet Neill–Concelman |
| (CDMA) | Code Division Multiple Access |
| (CDF) | Cohen-Daubechies-Feauveau |
| (CI) | Customer interruption |
| (CML) | Customer Minutes Lost |
| (CMOS) | Complementary-Symmetry Metal–Oxide–Semiconductor |
| (CPLD) | Complex Programmable Logic Devices |
| (CT) | Current Transformers |
| (CTS) | Clear to Send |
| (CWT) | Continuous Wavelet Transform |
| (DAC) | Damped Ac Voltage |
| (DAC) | Digital to Analogue converter |
| (DAQ) | Data Acquisition |
| (DC) | Direct Current |
| (DCM) | Digital Clock Manager |
| (DFT) | Discrete Fourier Transform |
| (DGA) | Dissolved Gas Analysis |
| (DIDR) | Device Identification Register |
| (DLL) | Delay Locked Loop |
| (DSO) | Digital Storage Oscilloscopes |
| (DWT) | Discrete Wavelet Transform |
| (EHV) | Extra High Voltage |
| (EMD) | Empirical Mode Decomposition |
| (EPR) | Ethylene Propylene Rubber |

| | |
|---|---|
| (ESD) | Electrostatic Discharge |
| (ETSI) | European Telecommunications Standards Institute |
| (FAA) | Federal Aviation Administration |
| (FDMA) | Frequency Division Multiple Access |
| (FF) | Flip Flop |
| (FFT) | Fast Fourier Transform |
| (FIFO) | First in First Out |
| (FIR) | Finite Impulse Response |
| (FM) | Frequency Modulated |
| (FPGA) | Field Programmable Gate Arrays |
| (FRA) | Frequency Response Analysis |
| (GIS) | Gas Insulated Substations |
| (GLONASS) | Globalnaya Navigatsionnaya Sputnikovaya Sistema |
| (GNSS) | Global Navigation Satellite Systems |
| (GPS) | Global Positioning System |
| (GUI) | Graphical User Interface |
| (HDL) | Hardware Descriptive Language |
| (HFCT) | High Frequency Current Transformer |
| (HOS) | Higher Order Statistics |
| (HPLC) | High Performance Liquid Chromatography |
| (HV) | High Voltage |
| (ILS) | Instrument Landing System |
| (IMF) | Intrinsic Mode Function |
| (I/O) | Input Output |
| (ISM) | Industrial, Scientific and Medicine |
| (ITU) | International Telecommunication Union |
| (KBT) | Kurtosis Based Thresholding |
| (LED) | Light Emitting Diodes |
| (LMS) | Least Mean square |
| (LPT) | Line Print Terminal |
| (LR-WPAN) | Low Rate Wireless Personal Area Network |
| (LSB) | Least significant bit |
| (LV) | Low Voltage |

| | |
|---|---|
| (MAF) | Moving Average Filter |
| (MLE) | Maximum Likelihood |
| (MOM) | Method of Moments |
| (MDPE) | Medium Density Polyethylene |
| (MRA) | Multi Resolution Analysis |
| (MRTIE) | Maximum Relative Time Interval Error |
| (MSE) | Mean Square Error |
| (MTIE) | Maximum Time Interval Error |
| (MV) | Medium Voltage |
| (NDT) | Non-Destructive Testing |
| (NPL) | National Physics Laboratory |
| (OWTS) | Oscillatory Wave Test System |
| (PAR) | Post Place and Route |
| (PCI) | Peripheral Component Interconnect |
| (PD) | Partial Discharge |
| (PDDN) | PD Detection Node |
| (PFCT) | Power Frequency Current Transformer |
| (PLD) | Programmable Logic Devices |
| (PMU) | Phasor Measurement Unit |
| (PPM) | Parts Per Million |
| (1PPS) | One Pulse per Second |
| (PPS) | Precise Position Service |
| (PQM) | Power Quality Monitor |
| (PRC) | Primary Reference Clock |
| (PSRAM) | Pseudo Static RAM |
| (PVC) | Poly Vinyl Chloride |
| (RDBMS) | Relational Database Management System |
| (QMF) | Quadrature Mirror Filters |
| (RAM) | Random Access Memory |
| (RCR) | Refresh Configuration Register |
| (RDBMS) | Relational Database Management System |
| (RF) | Radio Frequency |
| (RMU) | Ring Main Unit |

| | |
|---|---|
| (RSI) | Remote Server Interface |
| (RTL) | Register Transfer Level |
| (RTS) | Request to Send |
| (SDA) | Steepest Descent Algorithm |
| (SGWT) | Second Generation Wavelet Transform |
| (SNR) | Signal-to-Noise Ratio |
| (SPS) | Standard Positioning Service |
| (STFT) | Short time Fourier Transform |
| (SURE) | Stein's Unbiased Risk Estimator |
| (TBTL) | Time based triggering logic |
| (TCVCXO) | Temperature Compensated Voltage Controlled Crystal Oscillator |
| (TDR) | Time Domain Reflectometry |
| (TDM) | Time Division Multiplexing |
| (TR-XLPE) | Tree Retardant Cross Linked Poly ethylene |
| (TTL) | Transistor Transistor Logic |
| (UART) | Universal Asynchronous Receiver Transmitter |
| (UHV) | Ultra High Voltage |
| (USAF) | U.S. Air Force |
| (UTC) | Coordinated Universal Time |
| (VCTCXO) | Voltage Controlled Temperature Compensated Crystal Oscillator |
| (VLF) | Very Low Frequency |
| (VPN) | Virtual Private Network |
| (VT) | Voltage Transformers |
| (WSN) | Wireless Sensor Network |
| (WiMax) | Worldwide interoperability for Microwave Access |
| (XLPE) | Cross Linked Poly ethylene |

# Chapter 1 :
# Introduction

## 1.1 Partial discharge diagnostics

In the United Kingdom the majority of cable installation was completed between the 1950s and 1960s. The typical design life of MV cables prescribed by manufacturers is around 70 years and so in the near future any of these cables may approach the end of life. This is likely to lead to an increased prevalence of circuit faults resulting directly from insulation degradation and breakdown due to ageing. A program for the wholesale replacement of vast cable networks is impracticable and not economically viable and most likely unnecessary. Hence a condition based maintenance strategy can help prevent forced outages and improve supply reliability and availability for customers. On-line detection and location of PD is considered an integral part of a condition based maintenance strategy for underground cable networks.

PD is a localized electrical discharge, which partially bridges the insulation between conductors. PD offers early symptoms of insulation degradation, which can ultimately lead to complete breakdown of the insulation system. Conventional PD monitoring requires off-line measurement where the cable needs to be isolated from the power system network. Consequently, the power industry considers it is necessary to develop robust on-line methods for close monitoring of cable condition, and in particular the on-line detection, measurement and location of PD activity in power cables.

On-line PD monitoring can be done in two ways, namely spot testing and continuous monitoring. Spot testing is normally carried for a short duration, unlike continuous PD monitoring. Spot testing has major disadvantage in that this method cannot pick up the intermittent nature of PD activity. This is due to the fact that PD occurs in regular cycles with varying magnitude which depends upon circuit conditions, weather condition and asset condition. There are commercially available PD monitoring systems which include HVPD, Power PD, Doble Lemke etc. Lifetime prediction of cable upon initiation of PD is not well defined. HVPD has formulated “ knowledge rules ” based on their global PD database which allows the plant owner to assess the

condition of their MV Cables and Cable accessories through the on-line PD Test results (Appendix H)[HVPD 2009].

## 1.2 Research Motivation

The motivation for this research in the area of online PD detection and location for underground cables stems from several perspectives.

- PD originates from the defective site of the cable or from the cable joints. This discharge induces fast rising low power signals into the surrounding conductors which propagates to both ends of the cable. PD measurements are normally done at the cable ends either at the substation or at the RMU. PD pulses undergo attenuation and dispersion due to the propagation characteristics of the cable. HFCTs clamped in the earth strap of a cable are most widely used to detect such fast varying pulses caused by PD. This type of measurement requires the earth trap of the cable to be insulated from the switchgear earth. Furthermore older substations have completely enclosed switchgear which prohibits access to the earth strap. In these circumstances HFCT sensors needs to be installed in the phase conductors of the cable, but this retrofit requires a circuit outage, and is invasive.
- PD monitoring can be done in two ways, namely spot testing and continuous monitoring. Spot testing is normally carried for short durations of around 5 to 30 minutes, which depends upon site permission, but can be carried out for longer periods based on the network owner's interest. Spot testing has the major disadvantage that this method cannot pick up the intermittent nature of PD activity. This is due to the fact that PD occurs in regular cycles with varying magnitude which depends upon circuit conditions, weather condition and age. Hence continuous monitoring is essential to understand the PD trend. However continuous monitoring needs highly-sophisticated data loggers, data storage, and fast communication.
- PD induces rapidly varying pulses in the neighbouring conductors which can be used as an apparent variable to quantify the discharge magnitude. Also these pulses can be used to locate the origin of PD source using a single ended and double ended approach based on TDR. Accuracy in PD source location reduces

cable repair time which ultimately reduces all the costs involved in repair. Accuracy of single ended method is fully determined by the signal power of reflected signals, which is determined by the characteristic impedance mismatch between RMU/cable termination and the cable itself. Moreover, cable propagation characteristics and PD measurement systems will also affect the signal power of a reflected PD pulse which makes it difficult to locate PD, sometimes not possible. By monitoring PD at both sides of the cable uncertainty introduced by a reflected pulse can be eliminated. Such double ended monitoring of PD needs two monitoring systems, one at each end of the cable with accurate time base alignment and a communication link between measurement units. This makes the double ended approach more complex and expensive.

- PD signals acquired from on-site are more prone to noise and it becomes more challenging to extract PD information from the raw data. Wavelet based denoising has been widely used to extract PD signals from the raw data. This approach involves three stages namely decomposition, thresholding and reconstruction. The number of decomposition levels in wavelet based denoising is chosen based on the noise level in wavelet coefficients. This requires experience based personnel. Also widely applied universal thresholding for PD denoising is level dependent which may sometime over-smooth the signal, which leads to undetect PD pulse from the raw data. Furthermore wavelet based techniques uses convolution for the filter operation which needs higher hardware resources in on-board signal processing.

## 1.3 Research objectives

This research project has four objectives.

- Investigate an alternative method of PD detection using conventional PFCT principally used for protection and measurement purposes. This investigation assesses the feasibility of this approach by conducting a magnetic study of the transformer core material, FRA and finally capturing and analyzing onsite PD data using conventional PFCTs with PD data acquisition/interpretation system**.**
- Design a remote controlled PD data acquisition/interpretation system**.** This system will enable remote on-line capture and remote analysis of data for PD

diagnostics and location. This system should eliminate the requirement for frequent site visits to collate PD cable data. The system will be adaptable for connection to cable earth straps and PFCT (protection and measurement).

- Investigate various issues associated with PD source location methods based on TDR using single ended and double-ended approaches. This would lead to the design of double-ended PD monitoring system incorporating accurate time synchronization for reducing the error in PD source location.
- Develop signal-processing algorithms for denoising of PD raw data acquired from insulated power cables. Signature preservation, PD source location error and processing time are the prime concerns.

## 1.4 Summary of Contributions

The research documented in this thesis includes original contributions to the field of PD diagnostics for medium voltage underground cables. These contributions are as follows:

I. Technical feasibility of using existing, pre-installed protection/measurement PFCT as surrogate PD sensors for the detection of PD signals from cables is investigated. This investigation includes modelling of transformer core materials and frequency response analysis experiment using PFCTs. This approach is also validated using on-site measurements from 11 kV PILC cable network. A hardware system for gathering data from PFCTs is not commercially available. Remote controlled PD data acquisition system from previous research is inherited followed by introducing additional features. Features included are protection algorithms, remote database storage, hardware upgrade, PC controlled switch design and software development. This system is fully remote controlled and can be used for continuous monitoring of PD in substation with less frequent site access. The system has been installed successfully in 11 kV PILC cable at a 33/11 kV substation using both cable core via PFCT terminal and earth strap via HFCT.

II. PD source location methods using single ended and double ended approach is simulated using lossy transmission line model of the cable network under various scenarios of PD source location. In the case of interconnected cable networks, it is more challenging to identify the origin of PD source. Also a non invasive method is proposed to discard the PD pulses from the neighbouring cable. Double ended approach for detecting PD is not commercially available. In this research project, double ended PD detection using GPS based time synchronization with mobile broadband is developed. This system has a novel time based triggering approach unlike level triggering in conventional systems. Such time based triggering approach needs less hardware resources which reduces the overall cost of the system. Furthermore accuracy of the system is evaluated in the laboratory and can be used to locate PD with a maximum error margin of ± 10 meters. This system has been installed and tested successfully in 33 kV PILC cable, Edinburgh.

III. SGWT using kurtosis based thresholding with stopping criterion is developed to denoise PD signals. This algorithm is implemented in matlab. Denoising performance of this algorithm is evaluated by comparing with existing wavelet thresholding methods used for denoising namely “universal”, “minimax” and “sure” using both synthetic and on-site data. It is found that error introduced by this method in PD source location and PD quantification is smaller compare to the existing thresholding methods. Furthermore, this approach is faster than classical DWT based denoising which will reduce the cost of DSP processor when on-line denoising is required. This is due to the fact that the so called lifting operation in SGWT requires lower memory allocation compare to convolution operation used in classical wavelet based denoising techniques.

## 1.5 Organisation of the Thesis

This thesis includes nine chapters. Organisation of the thesis is as follows.

### Chapter # 1

In this chapter introduction to PD diagnostics is presented. Motivations and contributions made in this research project are included in this chapter. Finally organisation of this thesis into various chapters is described.

### Chapter # 2

In this chapter, fundamental mechanism of PD in high voltage system is presented. Presented are the different forms of PD described based on the electrode geometry and the associated PRPD patterns. Properties of PD signals and structure of high voltage cables are also included. Various PD detection methods used in high voltage systems including electrical and non electrical methods are presented. Furthermore PD detection in cables using inductive couplers is described in detail which also includes the various issues in installing inductive couplers for detecting PD from cables.

### Chapter # 3

In chapter # 3 high frequency signal propagation characteristics of insulated power cables are presented. PD source location methods using both single ended and double ended methods based on time domain reflectometry are described. Also simulation study is included for single ended and double ended method using lossy transmission model of cable in PSPICE for various scenarios. Various time synchronization methods used in double ended methods are also included. GPS based time synchronization is analysed and laboratory measurement results are included. Furthermore methods to distinguish forward and reverse travelling wave in cables is reviewed, and a non invasive method is proposed to discard the PD pulses from the neighbouring cable network.

## Chapter # 4

Chapter # 4 covers various signal processing techniques to denoise partial discharge signals acquired from on-site. Various signal processing techniques discussed in this chapter includes matched filter, moving average filter, adaptive filtering and wavelet based techniques. Second generation wavelet transform using lifting scheme is presented with full analytical base. The Data driven technique empirical mode decomposition is also included in this chapter. Furthermore various signal processing methods used in the area of PD diagnostics in cables is also presented.

## Chapter # 5

Chapter # 5 describes an alternative approach for PD detection in insulated power cables using PFCTs meant for protection and measurement purposes. This includes theory of current transformers, simulation study on magnetic performance of transformer core and frequency response analysis measurement. Also Remote PD monitoring systems design which includes hardware design, software design, laboratory tests and on-site trial are presented.

## Chapter # 6

Chapter # 6 describes a double ended PD monitoring system design. This includes hardware, firmware and software design. A novel approach of time based triggering is also presented. Laboratory measurements, namely GPS receiver drift measurements, PD source location accuracy tests and synchronized data acquisition are included. On-site installation and measurements using the developed system in is also presented.

## Chapter # 7

In chapter # 7 a novel kurtosis based thresholding method using second generation wavelet transform is described. Denoising performance of this method on the basis of PD detection and location error with existing thresholding method is presented. Then denoisng results using on-site data is also discussed. Furthermore kurtosis based thresholding approach using empirical mode decomposition is included. Also

comparison results of second generation wavelet transform with empirical mode decomposition using synthetic data and on-site data are presented.

## Chapter # 8

In this chapter, the signal processing and PD signal interpretation techniques are applied to the field data acquired from the 33/11 kV substation using the PD monitoring system described in chapter # 5. Timely variation of load and signal power in the substation is also included. Feature extraction using statistical parameters and phase resolved PD pattern is also included.

## Chapter # 9

Finally, Chapter # 9 concludes with the summary of the contributions presented in this thesis and the conclusions drawn. Discussion of the potential future research directions that may be employed in the area of detection and location of partial discharges in underground cables is also included.

# Chapter 2 :
# Partial discharge phenomena in dielectrics

## 2.1 Introduction

A common cause of insulation degradation in cables or any high voltage equipment is due to PD's. The danger of PD activity is that it promotes further degradation of insulation condition and eventually leads to permanent electrical breakdown. As a result PD monitoring is considered as one of mostly widely used tools to assess the insulation degradation of these ageing assets, thereby condition based maintenance strategies can be formulated. In this chapter various the topics discussed are basics physics of PD, structure of insulated power cables, physical properties and characteristics of cables, various forms of PD and PD detection methods in power cables.

## 2.2 Partial Discharge Phenomena

Electric discharges that do not completely bridges the electrodes are known as partial discharges. The term PD is defined by IEC 60270 (Partial Discharge Measurements) "localized electrical discharges that only partially bridges the insulation between conductors and which can or cannot occur adjacent to a conductor. PD's are in general a consequence of local electrical stress concentrations in the insulation or on the surface of the insulation. Generally, such discharges appear as pulses having duration of much less than 1 μs". PD can originate from voids in solid insulation (paper/polymer insulation), along the interfaces of multi layer solid insulation systems, on boundaries between the solid and the electrodes, gas bubbles in liquid insulations,and around sharp points of an electrode (corona discharges).

PD's can be triggered from normal working conditions in high voltage equipment which is due to the ageing of the insulator, stresses (electrical/thermal) in the insulation, improper insulation due to poor workmanship, and contaminants in the insulator such as metal particles and voids. In reality insulation systems often contain cavities or voids within the dielectric material. These cavities are usually filled with gas or liquid having a lower breakdown strength than the solid insulation [E. Kuffel 2006].

Moreover, the permittivity of the filling medium is frequently lower than that of the solid insulation. This makes the field enhancement in the cavity t higher than in the dielectric which leads to breakdown in the cavity. Once PD is initiated, it can propagate and develop electrical tree, thereby forming an interfacing track which leads to complete breakdown between ground and phase or between different phases in a three phase system at somepoint. Figure 2-1 shows photograph of damaged insulation due to PD. From the initiation of PD, complete breakdown can take anything from several hours to several years. It depends upon the size and location of PD source. In cables, common PD sources are defects in the polymeric insulation, cable joints such as voids, shield protrusions, contaminants; advance stage of water trees etc. shows the photograph of damaged insulation due to PD.

Electrical breakdown in gas is sequence of irreversible events which leads to transition of gas from insulation state to conducting state. This transition state occurs in ranging from ns to ms which depend upon several factors. For breakdown to happen two conditions need to be satisfied namely sufficient background electrical field and primary electron. Primary electron is created by photoionization, or other physical processes including cosmic rays, x-rays or nuclear radiations. Ionization by cosmic rays is a continuous process which produces ions and electrons [Crichton, Karlsson et al. 1989; Mazen Abdel-Salam 2012].

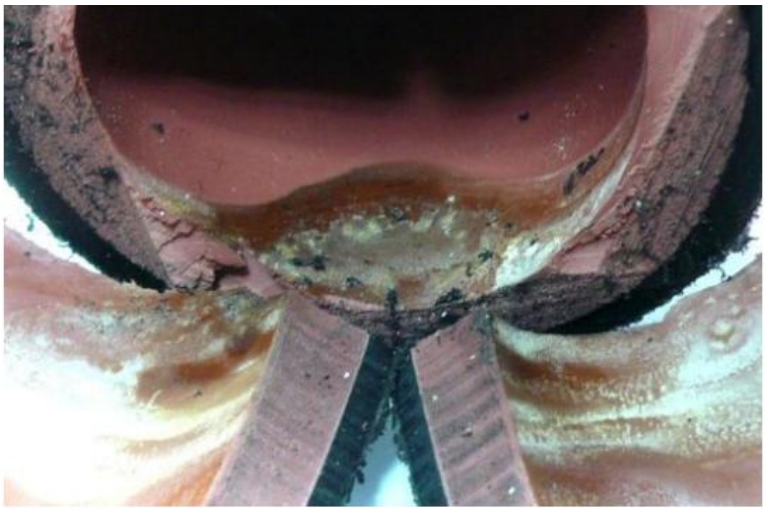

Figure 2-1 Evidence of PD found[**Carl Eastham 2011**]

When the applied voltage to the insulator exceeds the breakdown voltage, breakdown will be triggered by a primary electron. This electron being accelerated by the background field to energy levels higher than the ionisation potential of the insulator molecules. These electrons collide with gas atoms or molecules thereby dislodging further electrons from the gas atoms. This process leads to electron multiplication causing further ionization which leads to the formation of electron avalanche, which eventually ends up with a conduction channel between the electrodes. This process of electron multiplication is given by

$$N = N_0 e^{\alpha d} \qquad 2\text{-}1$$

$N$, nunber of electrons produced at a distance $x = d$ form the cathode
$N_0$, Initiatory elecrtron at distance $x = 0$ from the cathode
$\alpha$, Townsends frist ionisation coefficient which is related to probability of ionization caused by the initiatory electron

In an ideal insulator electrical field distribution is uniform between the electrodes. In practice, this cannot be achieved due to the imperfections caused by the tolerances during the manufacturing process. These imperfections become gas filled cavities or voids in the bulk insulation. Dielectric permittivity of this gas filled void is lower compare to the rest of the dielectric, which leads to enhancement in electrical filed distribution, which eventually leads to breakdown of the gas in the void.

Figure 2-2 shows the pictorial representation of electrical field distribution in a dielectric with void. As a result charges will be transported across the cavity. Positive charge will be accumulated in the direction of the background field while negative charge is in the opposite direction as shown in Figure 2-3 . As a result an electric field will be developed across the cavity which opposes the background field. At any instant total field is the sum of background field and the field due to space charge inside the cavity. Due to the high resistance in the insulation, charge inside the cavity will not leak. As the applied voltage increases, voltage across the cavity also increases until it reaches the break down voltage. Once it reaches the cavity breakdown voltage, the cavity breaks so that voltage across the cavity decreases to a very low value, nearly

zero. Since the applied voltage is increasing continuously, cavity voltage again starts to increase. The process repeats and second discharge occurs.

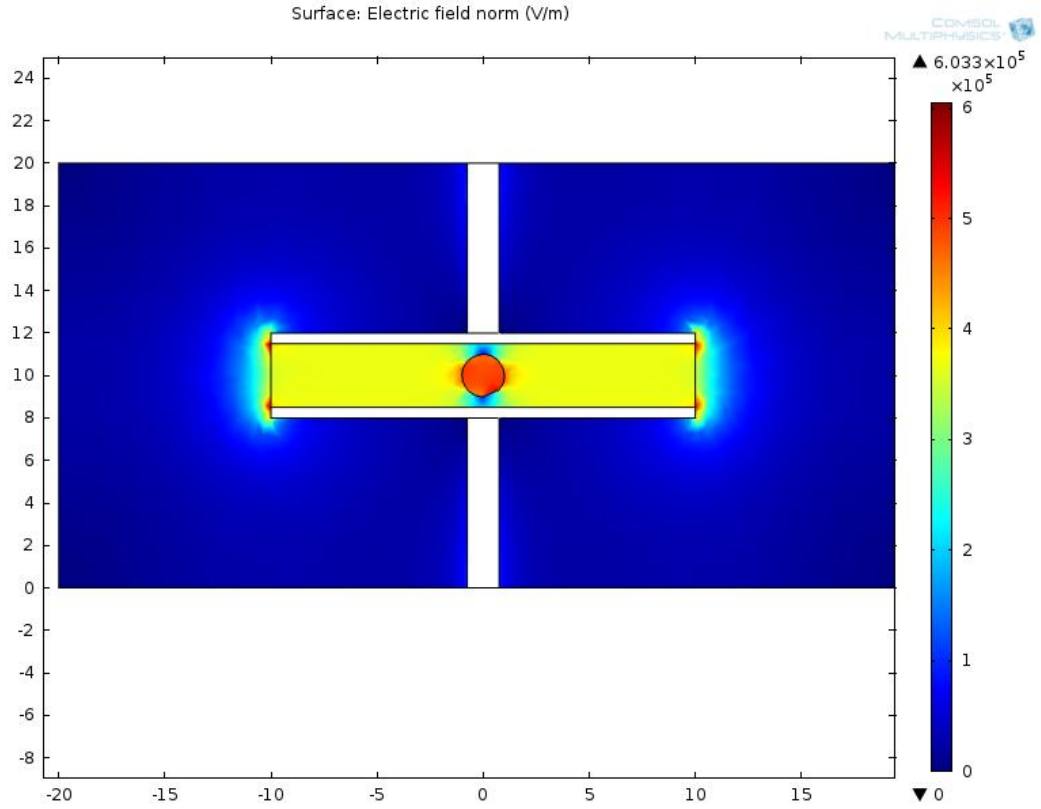


Figure 2-2 E field enhancement in dielectric

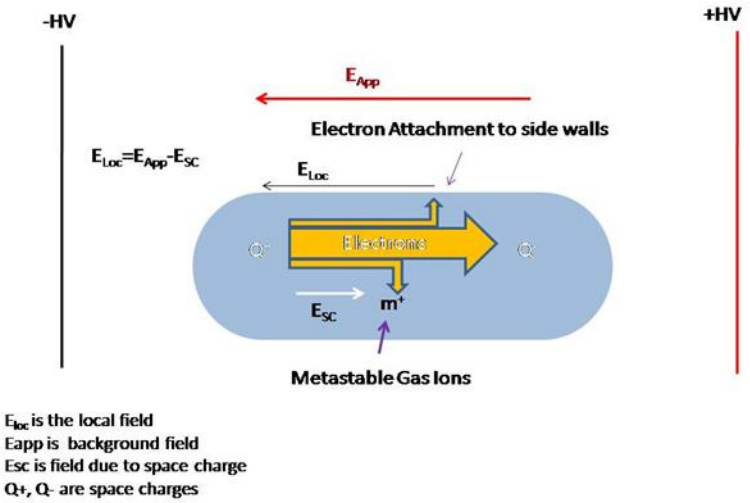


Figure 2-3 Background field and fields due to space charge

Sequence of such partial discharges under the sinusoidal background field is discussed with referrence to Figure 2-4. In Figure 2-4, waveform in red colour indicates the applied voltage while blue colour indicates the voltage across the cavity if the cavity does not break. Voltage waveform of the cavity has the same shape as the blue line but displaced down wards by an amount equal to the break down voltage of the cavity. After second discharge, voltage across the cavity increases but this time it will not reach the breakdown voltage of the cavity since the applied voltage starts to fall. As a result cavity voltage increases in reverse direction continuously and reaches the breakdown voltage. Third discharge occurs in this way.

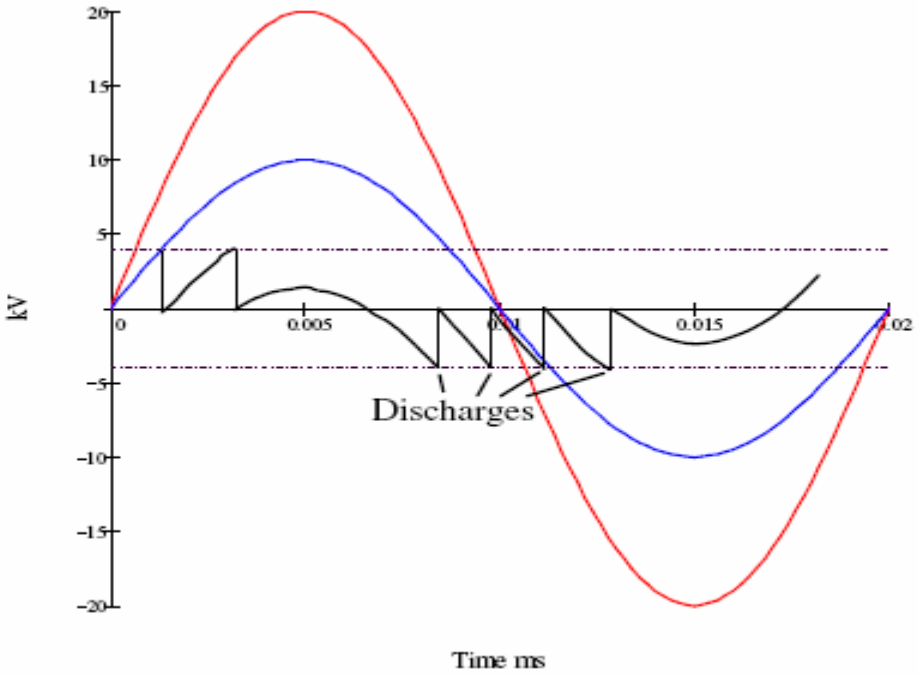


Figure 2-4 PD sequence under ac waveform [Boggs 1990]

## 2.3 Forms of Partial Discharges

The various categories of PD are simplified into four types of physical discharges, namely surface discharges, internal discharges, electrical trees, and corona discharges. Various types of discharges are discussed in the following section.

### 2.3.1 Surface Discharges

Surface discharge is a form of partial electrical breakdown which occurs across the interface between a gas and a solid dielectric in the presence of high voltage stress. Such discharges can occur in transmission lines and gas insulated systems where the insulator provides isolation among the conductors as well as mechanical support. Surface discharges have been shown to propagate distances in excess of 4 meters when guided by earthed conductors beneath the dielectric surface. Figure 2-5 shows typical electrode setup for surface discharge and Figure 2-6 shows the associated PRPD pattern [Song 2009].

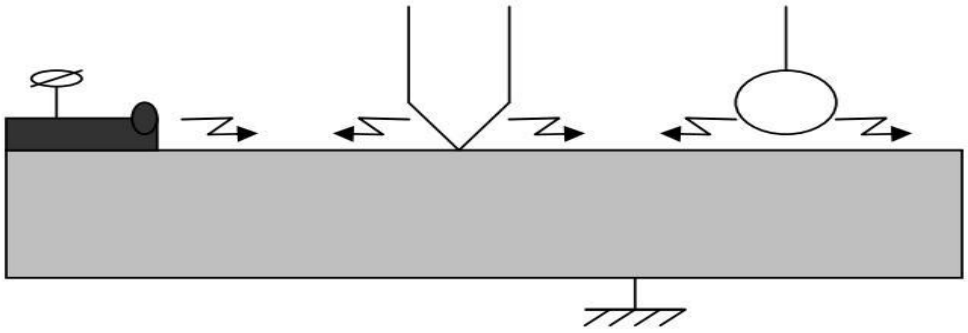

Figure 2-5 Surface discharges [Foo 2003]

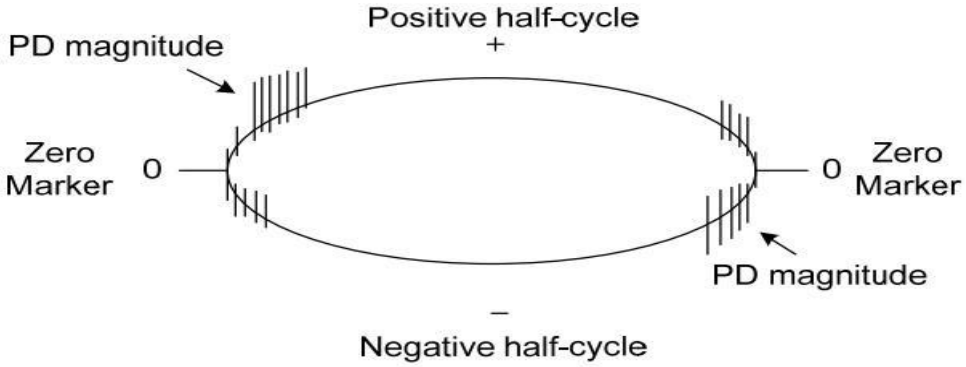


Figure 2-6 PRPD pattern of surface discharge [Song 2009]

### 2.3.2 Corona Discharges

Corona discharges occur at sharp edges from electrodes in gaseous dielectric shown in Figure 2-7. But conditions are insufficient to cause complete electrical

breakdown. In power systems non uniform fields are unavoidable. “In uniform field and quasi uniform field gaps the onset of measurable ionization usually leads to complete breakdown of the gap”. In the case of non uniform field, various symptoms like luminous and audible discharges will be evident before the complete breakdown. These discharges are known as coronas. These types of discharges occur when the potential gradient around the point exceeds a certain value, corona inception point. Figure 2-8 shows PRPD pattern for corona discharge.

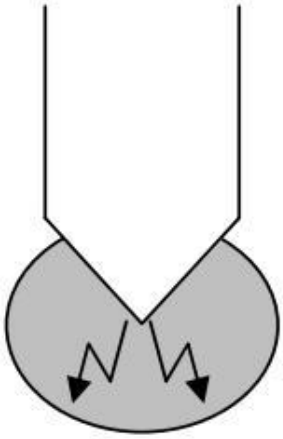

Figure 2-7 Corona discharges [Foo 2003]

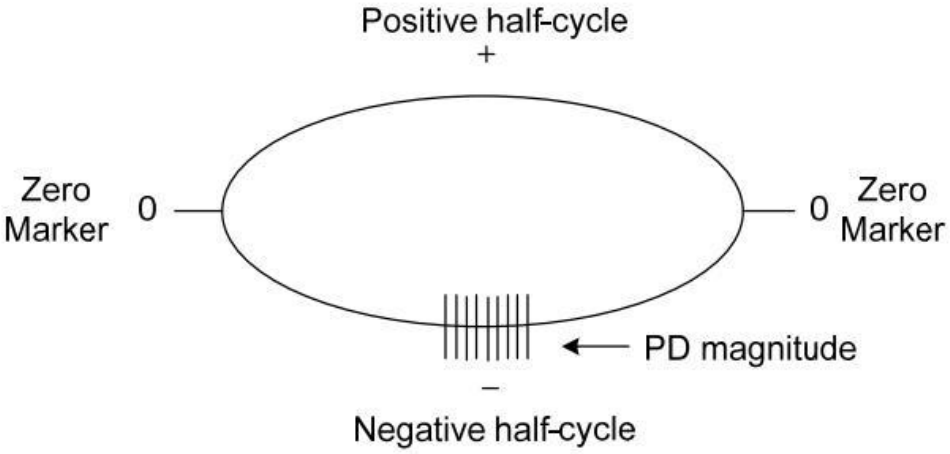


Figure 2-8 PRPD pattern of corona discharges [Song 2009]

### 2.3.3 Electrical Treeing

Electrical treeing is one of the major factors influencing the long term breakdown of polymers. Electrical trees can originate from sharp conducting particles or from a cavity in solid insulation. It is a process by which small tree like structures

appear on the surface of the solid dielectric due to cumulative PD activity. A typical tree consists of small cracks which form a branch-like structure or bush like structure with some portions of the branches having a melted appearance. A typical tree structure is shown in Figure 2-9 and the corresponding PRPD pattern for electrical treeing is shown in Figure 2-10.

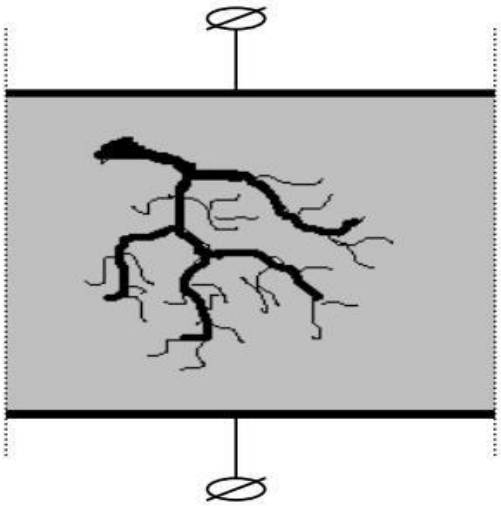

Figure 2-9 Electrical treeing [Foo 2003]

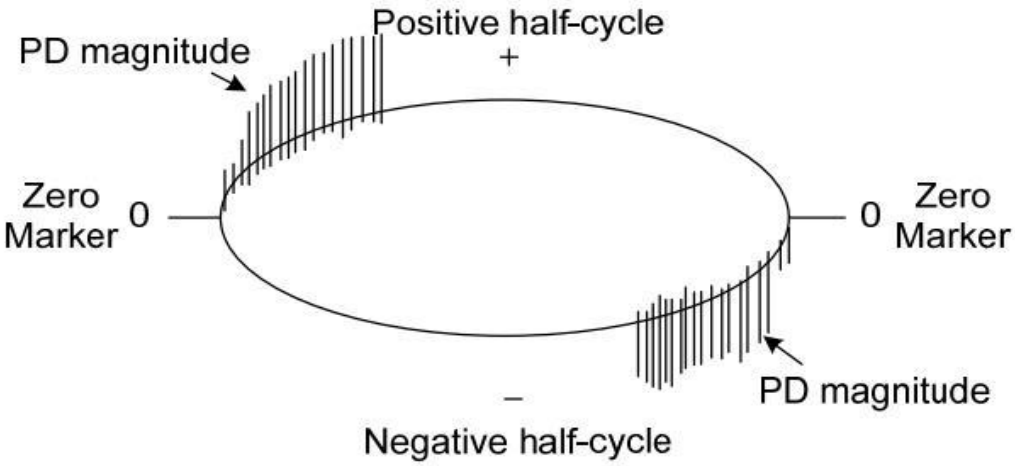


Figure 2-10 PRPD pattern of electrical treeing [Song 2009]

### 2.3.4 Internal Discharges

Voids or cavities and inclusions are the major sources of internal discharges. Inclusions can arise from dirt, paper or textile fibres and other foreign particles impregnated into the insulating material during the manufacturing process. The low

dielectric strength of such inclusions will cause internal discharges to occur. In gas filled voids or cavities, the discharge properties and characteristics are governed by their orientation and size [McAllister 1997]. Internal discharge patterns in the insulator are as shown in Figure 2-11 and the corresponding PRPD pattern is shown in Figure 2-12.

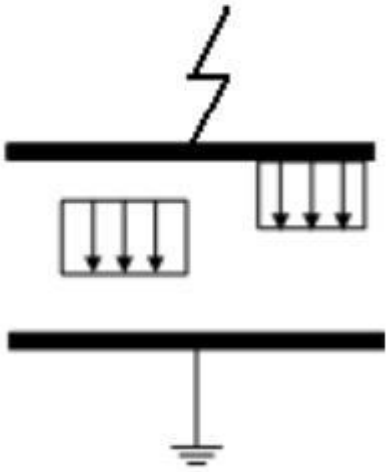

Figure 2-11 Internal discharges [Foo 2003]

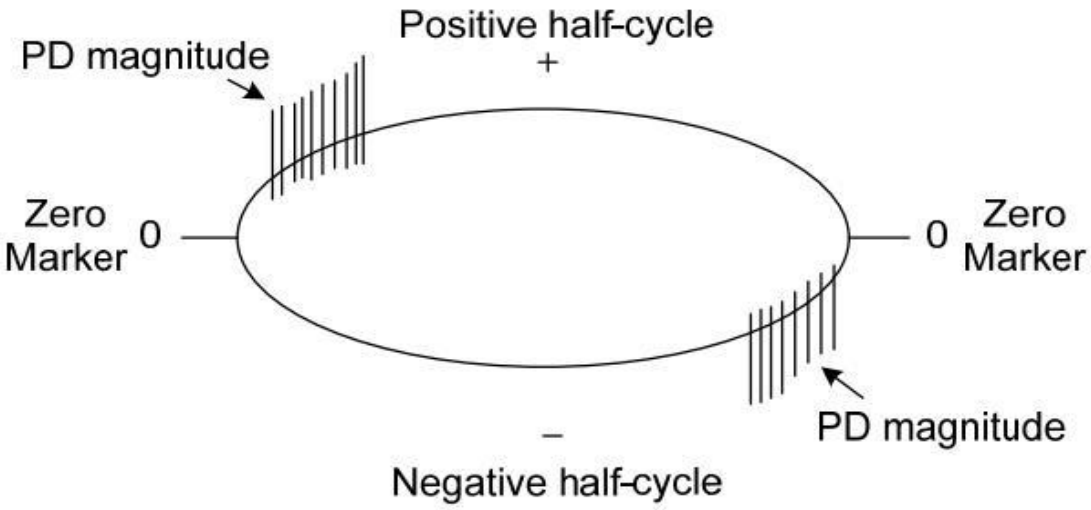


Figure 2-12 PRPD pattern of internal discharges [Song 2009]

## 2.4 Characteristics of PD signal

PD tests are applied to a wide range of high voltage power apparatus from miniature power supplies to multi-tone power transformers. Various techniques employed to detect PD sources contained in the dielectric are discussed in the later

sections. In this thesis electrical detection of PD is applied. Hence generation of electrical impulses due to PD is explained in this section.

A PD sequence consists of a flow of electrons and ions across a very small distance. Since the velocity of electrons is much greater than ions in gaseous medium, measurement of the PD current will have short duration pulse (caused by electrons) followed by a longer duration, lower magnitude pulse of the same polarity (caused by ions). PD's in void or tree tubule as shown in Figure 2-13, results in a pulse which lasts less than 1 ns, whereas the ionic portion has a duration of about 100 ns. As a result, sensors used to detect PD must be of wider bandwidth [Boggs 1982; Bogg 1990; Company 1997]. Integrated value of PD current source will give the apparent charge magnitude. Figure 2-14 shows the PD waveform recorded from void test cell.

Figure 2-13 Typical tree tubule structure [Seralathan and Nandini 2006]

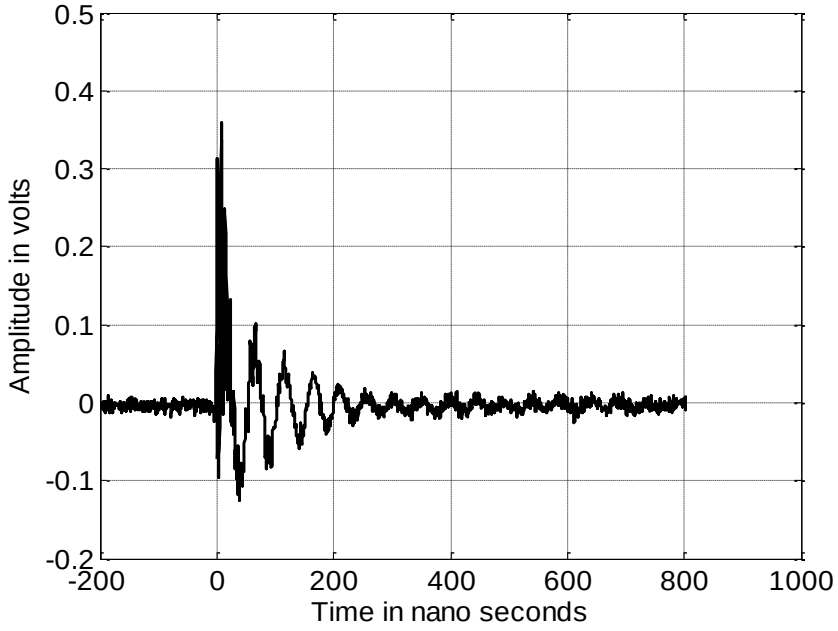


Figure 2-14 PD test using void test cell

## 2.5 Power Cables – Theory

Power cable technology has been increasingly developing to meet the demands of growing urbanization. The need to replace conventional overhead transmission lines with underground cables for power transmission and distribution has grown. In major cities, rapid growth of illumination under some circumstances is impossible to accommodate with the number and size of feeders required using the transmission line approach. As long ago as 1884 in New York City, an ordinance law was passed requiring the removal of the overhead line structures and their replacement by underground cables due to the dangers posed and to safety hazards. The first cable specification was formulated by British Standard (B S).7. in 1910. This includes paper insulated electric cable, solid type paper insulated lead sheathed armoured (PILC) cables which became established in the United Kingdom as the standard for underground distribution at voltages of up to 33kV [Gracias 1994].

Selection of power cable is determined by the application, voltage rating, thermal rating and environmental factors. Various applications include underground, submarine and HVDC cables. Depending on the operating voltage level based on IEC 60038, cables are classified as low voltage (LV≤ 1 kV), medium voltage (MV ≤ 35 kV), high voltage(HV≤ 230 kV), extra high voltage (EHV> 230 kV) and Ultra High Voltage (UHV, around 1 million volts). The operating voltage level of the cable determines the insulation requirements. The thermal rating of the cable is determined by the ampacity of the cable. The environmental factors that need to be considered are recycling of cable insulation, health concerns relating the restriction of hazardous substances (RoHs) and magnetic induction towards the neighbouring metal pipe. Insulated power cable is designed based on the above applications and various facets of the cable design are electrical, mechanical, thermal, environment and site-specific [Battacharya 2011; Gary stevens 2011; Geraldo De Almedia 2011; Kwang Hoi Ku 2011; Liu Ying 2011]. Figure 2-15 shows typical 11 kV XLPE cable. Various building blocks of the cables are conductors, insulation, semi conducting screen, sheath and armour which are discussed in the next section.

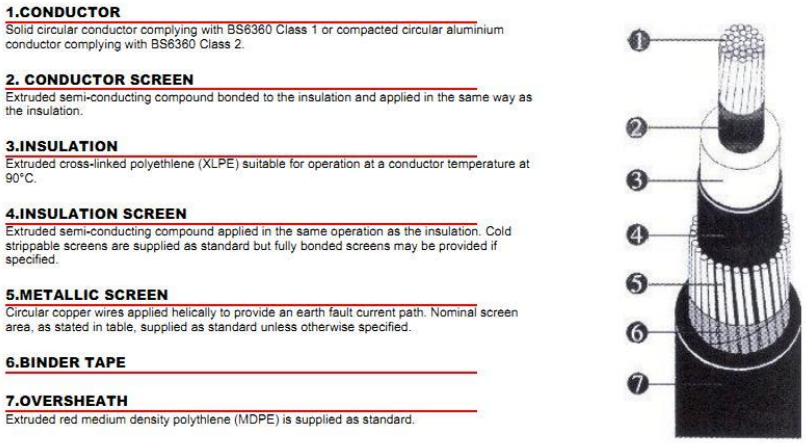


Figure 2-15 11 kV XLPE cable

## 2.5.1 Conductor

Copper and aluminium are widely used as the materials for the conductors of power cables. The conductivity and mechanical strength of copper are far better than aluminium. The only unsatisfactory feature of copper is its price fluctuation. Due to the economic benefits, aluminium is preferred over copper. Some of the drawbacks of using aluminium are low conductivity, less immune to corrosion and lower mechanical strength [Ericsson 2009].

The selection of conductor for power transmission has various criteria, namely electrical considerations, thermal design, environmental impact, installation technique, mechanical stresses etc. Most designers choose the smallest diameter conductors allowing the required maximum operating temperature to limit the investment cost. Conductors of large diameters have disadvantages namely increased investment cost, higher weight, larger accessories, larger ducts. However there are substantial technical advantages like low losses, safety margin to cope with peak loads, circuit upgrading, and overload margin etc. Cross sectional area of the conductors varies and extends up to 2500 $mm^2$ [Federic Leuser 2011; Francois Gahungu 2011]. Conductors are designed in strands or solids as shown in Figure 2-16 and Figure 2-17 . Stranded conductors are flexible and larger in diameter than solid conductors of same area. Diameters of stranded conductors vary depending upon the exact type of construction. These constructions include concentric round, compressed, compact and compact sector. Solid conductors are beneficial for soldering and compression jointing, but have a low

flexibility. In the UK, solid conductors have been extensively used for the 600/1000V cables and 19/33kV cables with paper and polymeric insulation [Foo 2003].

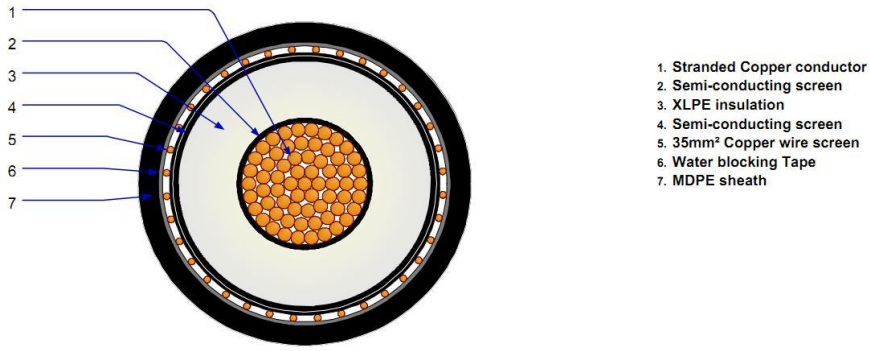


Figure 2-16 11 KV MDPE cable with stranded conductors

[Courtesy: www.prysmian.com]

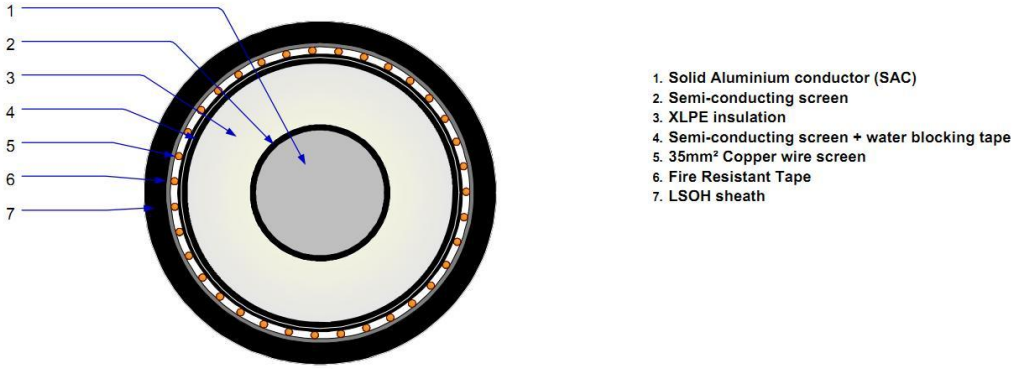


Figure 2-17 11 kV XLPE cable with solid conductors

[Courtesy: www.prysmian.com]

## 2.5.2 Insulation

Dielectric material forms an integral part of high voltage cables. The purpose of the dielectric in cables is to provide mechanical support and isolation between the conducting parts [E. Kuffel 2006]. The majority of conventional power cables are insulated with either solid extruded dielectrics or liquid impregnated papers. Impregnated paper is the most common dielectric used for high voltage cables. This type of insulation consists of multiple layers of paper tapes, wrapped helically around the conductor to be insulated. The total wall of paper tapes is then heated, vacuum dried, and impregnated with an insulating fluid. Impregnated paper insulation has excellent electrical properties, such as high dielectric strength, low dissipation factor, and low dielectric loss (ERICSSON 2009).

The origin of extruded dielectric insulation stems from the design of polyethylene in 1941. Two major types of extruded insulation used are cross linked polyethylene (XLPE) and ethylene propylene rubber (EPR). Conventional polyethylene is comprised of long chain polymers which are comprised of ethylene groups. XLPE can be considered to be a branched polyethylene where the branch is connected to a different polyethylene chain. Cross linking adds certain desirable properties to the polyethylene. From a cable perspective, stability is maintained at elevated temperatures. Water treeing can reduce the life time of XLPE cables. In the 1980s, tree retardant cross linked poly ethylene (TR-XLPE) was popular which has improved resistance to water treeing. This type of insulation uses the additive union carbide to XLPE (ERICSSON 2009). XLPE insulated cables have a rated maximum conductor temperature of 90$^{\circ}$C and an emergency rating of up to 140$^{o}$C.

EPR cable became more popular in 1980s. Polymerization of ethylene with propylene results in EPR. In order to have desired dielectric properties, EPR is cross linked. A thermal and mechanical property such as thermal conductivity and thermal expansion of EPR cable is far better than TR-XLPE cables. The upper temperature limit for operation of XLPE is often limited to 90°C or 105°C, and EPR cable dielectrics can be operated safely to 140°C [Xiaoguang and Boggs 2006].

Though XLPE has been widely used due to higher thermal stability, it cannot be recycled due to the chemical cross linking in XLPE, this makes it a threat to the environment. [Kwang Hoi Ku 2011]et al proposed new XLPE cable dielectric using physical cross linking rather than chemical cross linking and can be recycled

### 2.5.3 Semi Conducting Layer

A semi conducting layer is placed between the conductor and dielectric to obtain uniform electrical field distribution due to the imperfections in the cable conductors [Yonghua, Changshun et al. 2006]. The semiconducting screen needs to be inserted in two places, namely one between conductor and dielectric and the other between dielectric and sheath. The semi-conducting screen in the power cable is named conductor screen and insulation screen. The semicoducting screen has greater influence in attenuating high frequency signals like PD's.

### 2.5.4 Sheath and Armour

Sheath is used over the cable to increase abrasion resistance and to protect the cable from the local environment. Ideally, a jacket will provide immunity to water ingress and foreign ions out of the insulation. Sheathing materials have varying properties that is controlled by their molecular structure and compound ingredients. Plasticized PVC was used as jacket in the olden days and is now rarely used as a cable jacket though it is quite inexpensive relative to other materials. For low voltage cables, it is common to use other materials such as neoprene (poly chloroprene) or hypalon (chlomulphanated polyethylene) [Moore 2006]. Cable armour is the outermost layer of a cable. It functions to protect the cable in many aspects such as from chemical corrosion, animal gnawing and sharp objects and it has to withstand strong pressure forces especially for buried cables. Two universal types of armour are steel tapes and galvanized steel wires [Moore 2006]. It also represents the ground return path for any external earth fault currents.

## 2.6 PD detection Methods

The detection and measurement of partial discharges in insulators is based on the exchange of energy taking place during the discharge. These exchanges are manifested as electrical current pulses, dielectric losses, electromagnetic radiation (light), sound(noise), increased gas pressure and chemical reactions. Therefore, discharge detection and measuring techniques may be based on the observation of any of the above phenomena. The above mentioned phenomena can be detected and analysed to ascertain the PD activity. Methods applied to detect PD are broadly classified into two, namely non electrical and electrical methods.

### 2.6.1 Non Electrical Detection Methods

As the name suggests non electrical detection of PD activity measures non electrical parameters resulted from PD. Various non electrical detection methods of PD activity are discussed below.

### 2.6.1.1 Optical Method

Optical method of PD detection is based on the detection of light produced due to various processes like ionization, excitation and recombination during PD. Though all forms of discharge emits electromagnetic radiation, the optical spectrum depends upon the nature of discharge [Schwarz and Muhr 2007]. For example the wavelength of faint corona is less than 400 nm, appearing as  as purple, the ultraviolet region occupies the main part. In the case of strong flash discharge, the optical spectrum spans from 400 nm to 700 nm [Xn, Yn et al. 2000]. The optical spectrum resulted from partial discharges depends upon the chemical composition of the dielectric material. The choice of optical sensors is determined by the optical spectrum. This method of PD detection shows higher immunity to electromagnetic interferences and acoustic disturbances. Figure 2-18 shows a typical optical spectra of discharges in oil. This spectra included $H_\alpha$ and $H_\beta$ are hydrogen balmer lines and vibration, rotation band structres from $C_2$ radical. Figure 2-19 shows optical spectra for corona discharge [M. Muhr 2009].

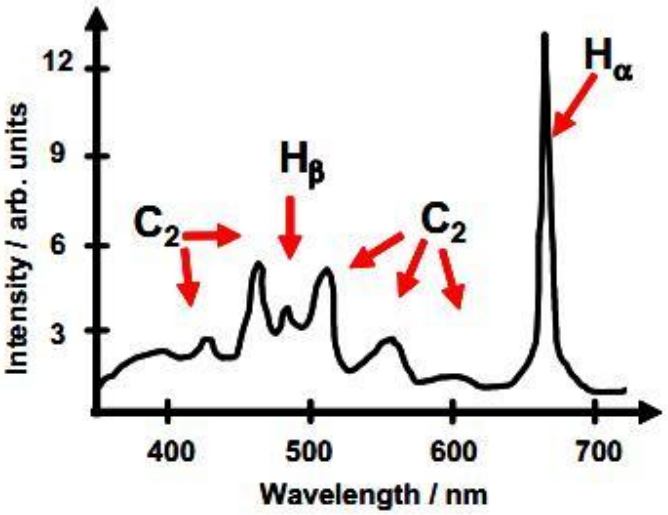


Figure 2-18 Typical optical spectra of discharge in oil [Schwarz, Muhr et al. 2005]

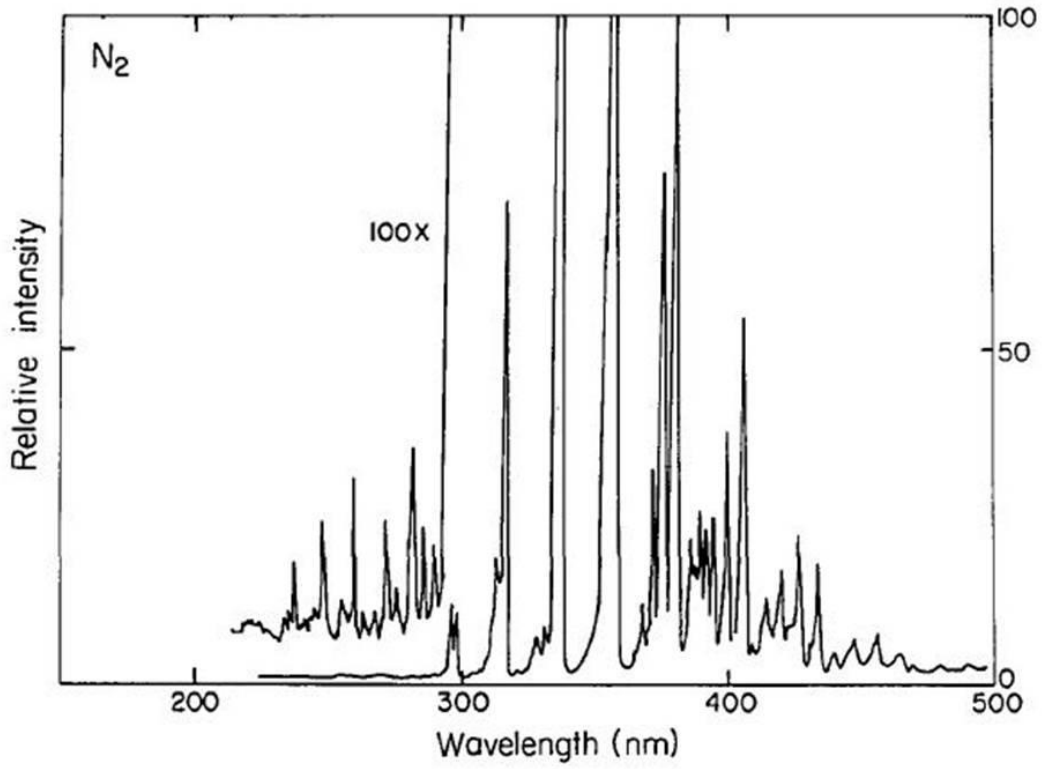


Figure 2-19 Typical optical spectra of corona discharge [M. Muhr 2009]

### 2.6.1.2 Chemical detection

Streamer due to PD across the void can cause break down of the surrounding materials into different chemical components. These changes can be used in the detection of PD activity in a power plant. Two of the commonly used chemical detection techniques are high performance liquid chromatography (HPLC) and dissolved gas analysis (DGA) [Song 2009]. HPLC measures the byproducts, produced from the degradation of the insulation such as glucose and degraded forms of glucose [Guven 2012]. DGA provides the information of partial discharge in terms of the volume of gas produced. DGA is used to determine the concentrations of gases dissolved in the insulating oil of transformers. Insulation faults causes transformer oil, pressboard, and other insulating materials to decompose and generate gases, some of which dissolve in the oil [Lelekakis, Martin et al. 2011]. These concentrations can be used as a benchmark to diagnose insulation faults. Nature, Intensity and location of PD source can't be identified in chemical detection of PD's [Karmakar, Roy et al. 2009].

#### 2.6.1.3 Acoustic detection

Acoustic emission (AE) is a non-destructive testing (NDT) technique which is used to detect the propagation of acoustic waves produced by the discharge site through the insulation. Acoustic detection of PD activity involves detecting an acoustic wave which propagates from the discharge site through the insulation. These acoustic waves which are in ultrasonic range (20 KHz- 1 MHz) can be detected through piezoelectric transducers. This type of PD detection is widely used in transformers and gas insulated substations (GIS) [Zhu, McGrail et al. 1994; Kemp 1995]. By installing sensors along the length of the cable , discharge location can be identified based on the energy contained in the AE signal. Acoustic methods are not suitable for PD detection in cables because of the reduced sensitivity with variations of distance from the discharge source. Furthermore, for underground cables the application of acoustic methods is limited since the cable surface may not be accessible.

### 2.6.2 Electrical Detection Methods

As name suggests electrical detection of PD activity measures the electric quantity resulted from PD's. Various electrical detection of PD activity are discussed below.

#### 2.6.2.1 Dielectric Loss (Tanδ) Measurements

If the dielectric of the cable is free from defects, water trees, electrical trees, moisture and air pockets etc, the cable exhibits the properties of a perfect capacitor. In a pure capacitor voltage and current follows a $90^{o}$ phase shift. If there exists impurities in the dielectric, this will reduces the dielectric resistance which makes a resistive current flow through the dielectric. Hence the current and voltage no longer exhibit 90 degree phase shift as shown in Figure 2-20. Drift in phase shift from 90 degree can be used as a indicator of level of contamination in dielectric material [GJ Catlin 2010].

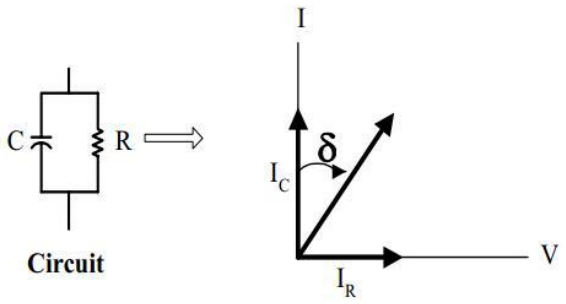


Figure 2-20 Dielectric loss measurements

Based on IEC Standard Publication 502, 1978, the maximum value of tan delta (dissipation factor) at ambient temperature is 0.004 at the rated power-frequency voltage between conductor and earth or metallic screen for which the cable is designed. Figure 2-21 shows typical tanδ vs applied voltage for three core 11 kV cable of age 3 to 5 years. When the tanδ value of a cable insulator is high, the potential for this cable to breakdown during service is also high. Charge transfer during PD in the void leads to a sudden change in tanδ and can be used to ascertain the PD activity [Foo 2003; Ponniran 2008]. Higher harmonic content present in the voltage and current waveforms which is used to calculate tanδ has influence on the phase of fundamental component which introduces error in tan measurements [Song, Gao et al. 2007].

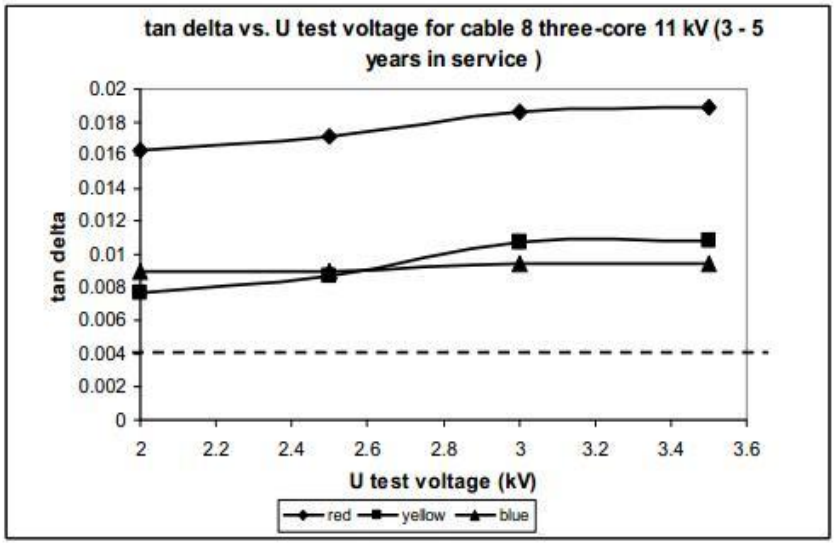


Figure 2-21 tan delta for three-core cable after 5 years (Ponniran 2008)

### 2.6.2.2 Very Low Frequency Technique

VLF testing is used for testing of higher capacitive loads, cables, motors, surge arrestors etc. VLF testing normally uses frequencies in the range from 0.01Hz to 1Hz [guide 2005]. Since these tests are conducted at lower frequencies lower current is needed to energize the capacitive elements contained in the dielectric. VLF test systems are essentially composed of an HVAC power source with very low frequency output to supply capacitive loads and detection impedance in series with a coupling capacitor as shown in Figure 2-22 [Bodega 2004].

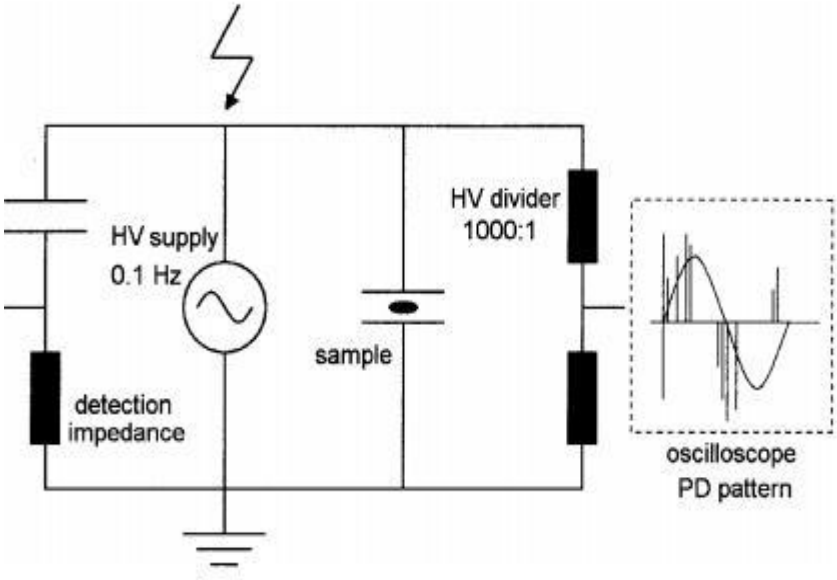


Figure 2-22 VLF test setup [Bodega 2004]

In VLF testing, the supply voltage is gradually increased until discharges are detected [60270]. Since the cables have been taken offline before the energising, the supply voltage can vary from $1U_o$ up to $3U_o$. Higher stress is required to initiate the first PD that will cause the chain of PD's to occur. This is one of the reasons why offline techniques can be dangerous.

VLF testing methods can be categorized as voltage withstand or diagnostic testing. In voltage withstand testing the test object should withstand a specified voltage level applied across the insulation for a specified period of time without breakdown. Diagnostic testing allows the determination of a relative amount of degradation of insulation. Diagnostic test results obtained from VLF test may not correlate with those values obtained during power frequency tests. For example, the dissipation factor is

much larger at 0.1 Hz than at power frequency and also PD may differ in terms of magnitude and inception voltage [guide 2005]. Energization of cable or any high voltage equipment has the disadvantage of continuous stress that is exerted on the cable throughout the testing [Foo 2003].

### 2.6.2.3 Oscillatory Wave Test System Technique

To obtain a sensitive picture of PD's in dielectrics, it is preferable to use a power frequency voltage source to ignite, detect and locate PD's. This type of PD ignition resembles true on-site conditions of cables. Unfortunately, this method is not suitable for on-site testing due to the requirement of a large 50 Hz power supply needed to energize the cable samples with lengths of a few kilometres [Gulski, Smit et al. 1998]. The OWTS method is used to overcome this difficulty which uses damped ac voltage for detecting PD sources in cables. This method is also known as damped ac voltage (DAC) test. The Test setup for OWTS is shown in Figure 2-23. The method of using DAC to test the PD has a frequency range from 50 to 500 Hz. The test system consists of a variable D.C. voltage source which gradually raises the voltage to test voltage level for a period of time. A solid sate switch having lower closure time connects air core conductor to the cable which leads to the formation of a damped oscillatory voltage with oscillating frequency [Gulski, Smit et al. 2005]

$$f = \left( \frac{1}{2\pi\sqrt{LC}} \right)$$

2-2

where $L$ : Inductance of the air core inductor

$C$ : Capacitance of the cable

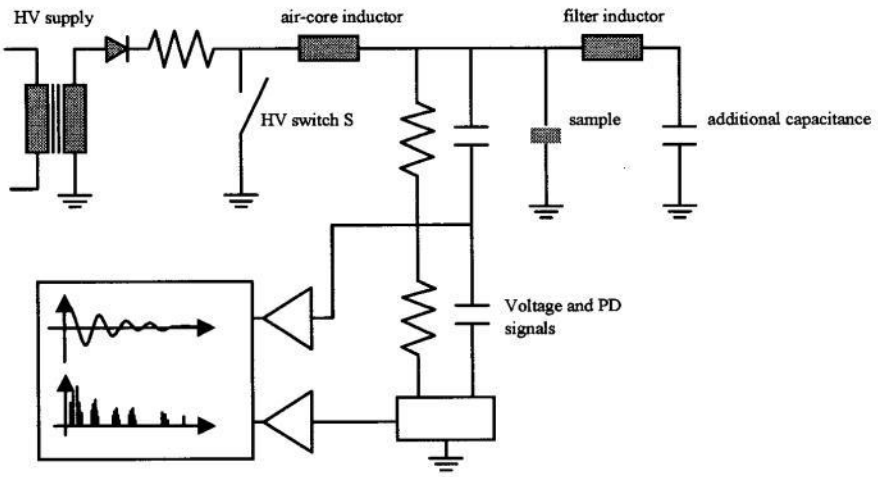


Figure 2-23 OWTS method [M.E. Ardeleanu 2008]

This oscillating voltage will initiate the PD's in the cable specimen. Typical PRPD pattern for the polyester resin using 264 Hz OWTS is shown in Figure 2-24. [Bodega 2004] studies the effect of frequency and shape of the applied voltage on PD inception using OWTS method.

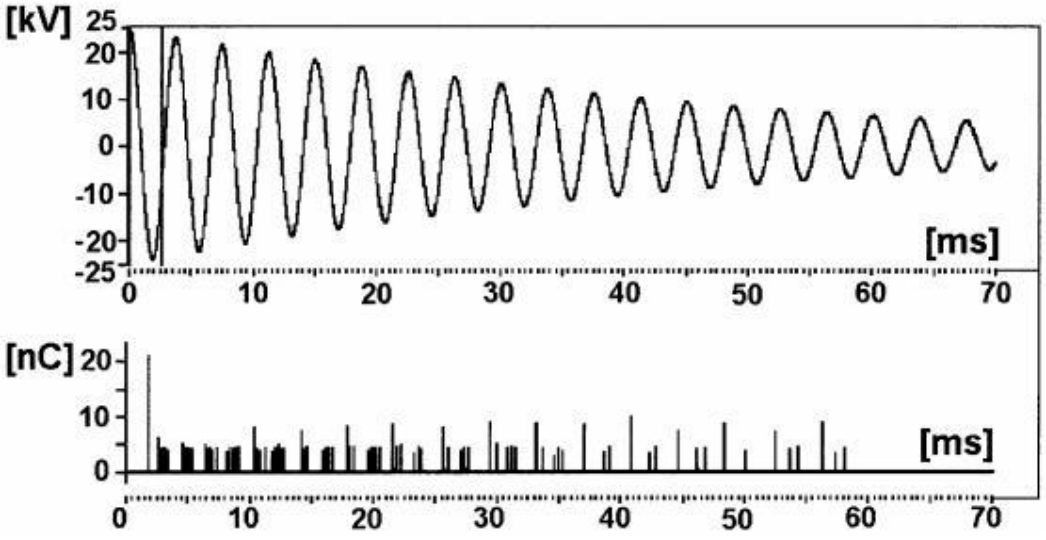


Figure 2-24 PRPD for the polyester resin using 264Hz [Bodega 2004]

## 2.7 PD detection in Power Cables

Pulses induced in a neighbouring electrode due to PD's are of high frequency electromagnetic waves that travel through the conductor and shielding of the cable in both directions from the discharge source. The stray magnetic field resulting from these

discharges could be detected by an inductive coupler. A Rogowsky coil or high frequency current transformer (HFCT) is commonly used as inductive sensors for detecting PD's from cables. In 1912, Rogowski and Steinhaus proposed a method for measuring magnetic potentials using an air cored coil known as Rogowski coil [T.Exon 1993]. It has been used for the detection and measurement of transient electric currents for decades. A Rogowski coil is widely used for PD detection in rotating machines since motors normally carry large load currents which will not saturate such air-cored CTs. The bandwidth of a Rogowski coil is purely determined by its design. [Hemmati and Shahrtash 2012] desgined an unshielded Rogowski coil having bandwidth of 1 kHz – 12 MHz.

Cables having helical metal screens of individual wires exhibit higher magnetic field strength, which can be detected using rowgowski coils. In solid shielded cables, magnetic field generated outside the cable due to fast varying PD pulses is of low power. In such cases high frequency current transformers are preferred [Carl Eastham 2011] over a rogowski coil since it has higher sensitivity . High frequency ferrite materials are used as core material in HFCTs. These materials exhibits higher initial permeabilities over a wide frequency range which makes them more suitable to detect fast varying weak magnetic fields developed by PD in solid shielded cables.

When HFCT is used for detecting PD, there are certain criteria related with network configuration needed to be met to detect PD signals. HFCTs can be installed either in the earth strap or the core (phase conductor) of the cable. Figure 2-25 shows typical HFCT installation in cable earth screen.

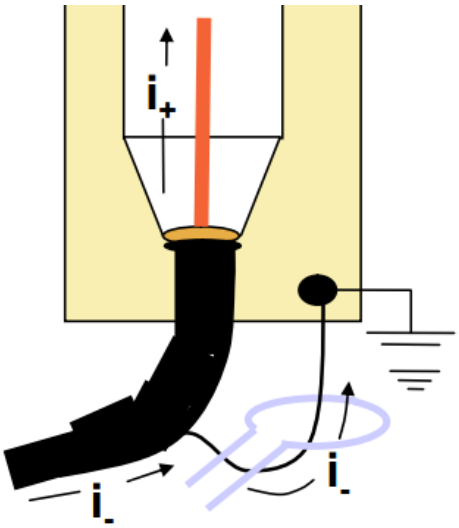


Figure 2-25 Typical HFCT installation in cable screen [Ltd 2009]

This type of installation is non invasive and does not require any outage. However this needs the cable earth strap to be isolated from switchgear earth as shown in Figure 2-26, otherwise PD signals from cable core and earth cancel each other leaving behind a very low signal which is difficult for the HFCT to detect.

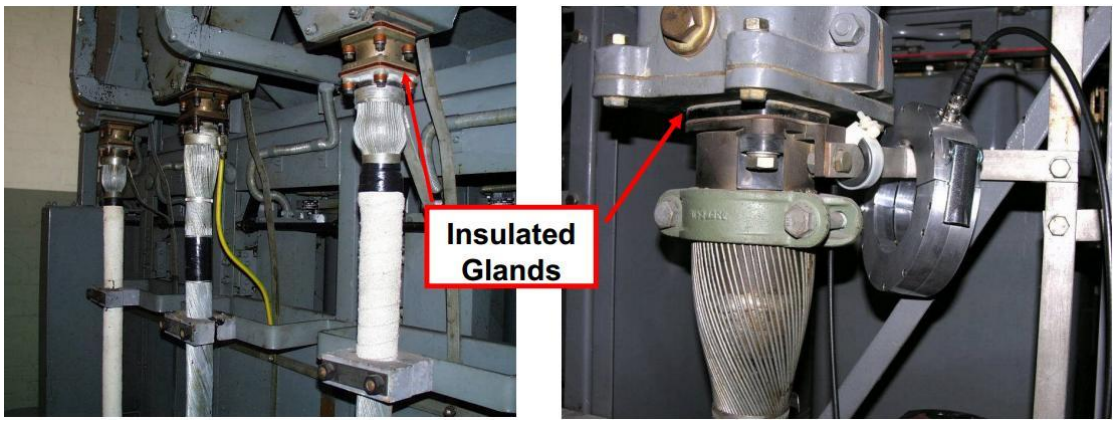


Figure 2-26 Earth strap with insulated gland [Ltd 2009]

Typical HFCT installation in cable core is as shown in Figure 2-27. This type of installation needs outage and also HFCT is located in the electrical field of the cable termination which is not recommended by plant owners or switch gear manufacturers.

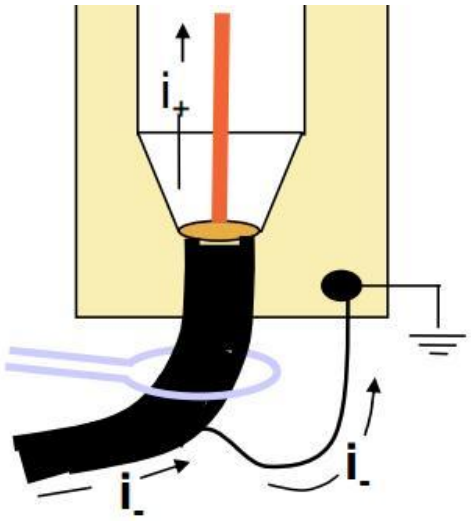


Figure 2-27 Typical HFCT installation in cable core [Ltd 2009]

Typical installation of HFCT which is the most preferred as shown in Figure 2-28. This type of installation involves a cable core earth strap loop. This type of

topology will cancel out PD signals and noise from coupling to the cable core from the earth strap thereby leaving PD signals from the cable core.

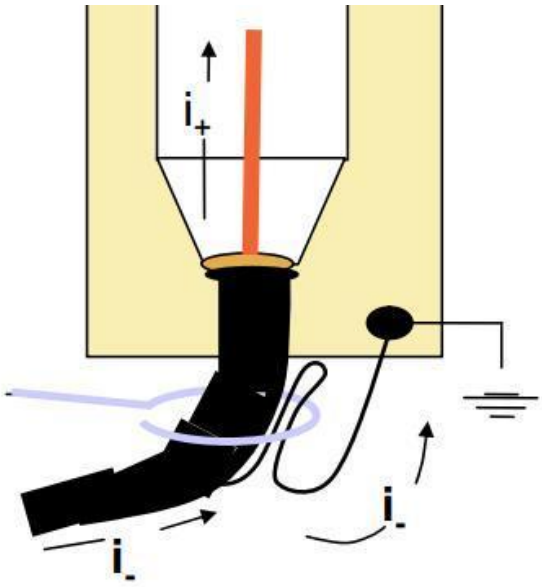


Figure 2-28 Typical HFCT installation in cable core with earth loop [Ltd 2009]

In older secondary substation design, distribution transformers are enclosed which makes the earth screen inaccessible to install HFCT as shown in Figure 2-29. Such type of solidly bonded cable terminations makes PD measurements difficult to achieve [Ivy Shim 2000].

Figure 2-29 Solidly bonded termination

## 2.8 Conclusion

Insulation degradation in cables or any high voltage equipment is caused by PD's. Such discharges do not completely bridges the electrodes in between the insulation. PD's can be triggered from normal working conditions in high voltage equipment which is due to the ageing of the insulator, electrical,thermal or mechanical stresses in the insulation, improper insulation due to poor workmanship, and contaminants in the insulator such as metal particles and voids. PD's can occur in different forms namely surface discharges, internal discharges, electrical trees, and corona discharge. These discharges shows unique signature in PRPD pattern, which can be used as fingerprint to classify those discharges. PD's in cables can be detected using non-electrical and electrical methods. Electrical methods of PD detection using inductive couplers as a non-invasive technique are widely used since non-electrical detection of PD activity cannot be able to locate the origin of the PD source. Though PD detection using inductive couplers is easy to impelement, older switchgear with completely bonded design, crosslinking of switchgear earth and substation earth often limits this technique to detect PD's from cables.

# Chapter 3 :
# Partial Discharge Location Methods in Cables

## 3.1 Introduction

PD's originate from a defective site of cable or from cable joints. It induces fast rising low power signals into the surrounding conductors which propagates towards both ends of the cable. Since PD measurements are normally done at the cable ends either at the substation or at RMU, attenuation and dispersion characteristics of a cable network can diminish signal power and alter the PD signature. This will cause inaccurcaies in PD source location. Accuracy in PD source location reduces repair and outage times and subsequently CML cost and CI cost. In addition, accurate PD source location can mean that only the damaged or degraded section of cable is replaced rather than an entire circuit or suspected circuit area, reducing cable replacement costs. Travelling wave method based on TDR is widely used to locate PD source using single ended and double ended monitoring. The success rate of the single ended method is not fully guaranteed due to the underlying factors of cable network design such as length of the cable and impedance mismatch between cable termination and the cable itself. The double-ended method of PD source location gives better PD source location accuracy compared to the single ended approach. However, this method is not widely used due to its complex system design, time synchronization and communication requirement between measurement units at both ends of cable.

In this chapter high frequency signal propagation characteristics of single core and three core cable are discussed. PD source location methods based on TDR using both single ended and double ended PD monitoring are reviewed. Simulation studies of single ended and double ended PD source location using a lossy transmission line model of single core cable for various scenarios of PD source location are included. Furthermore various invasive methods to discard PD pulses from the neighbouring cable network are discussed. A non invasive method is proposed to distinguish PD from the neighbouring cable. Various time synchronization methods used for double ended PD source location are also discussed and a feasible time synchronization technique is identified.

## 3.2 Signal Propagation in Cables

Understanding of high frequency signal propagation characteristics of insulated power cable including velocity of propagation, characteristic impedance, and frequency dependent attenuation, frequency dependent dispersion are important for many cable diagnostic techniques such as TDR, PD source location, cable fault location etc. Induced PD pulses get attenuated and distorted by the propagation characteristics of the cable. High frequency attenuation depends on the conductivity of the main dielectric and the conductivity of the semi conductor screen together with the cable conductor [Ulaby 2006]. In case of off-line PD detection, diagnosis is performed one phase at a time, therefore a two conductor transmission line model is sufficient to characterize the high frequency behaviour of the cable. Based on the and well known telegrapher equations with referrence to transmission line model shown in Figure 3-1, the following equations can be written.

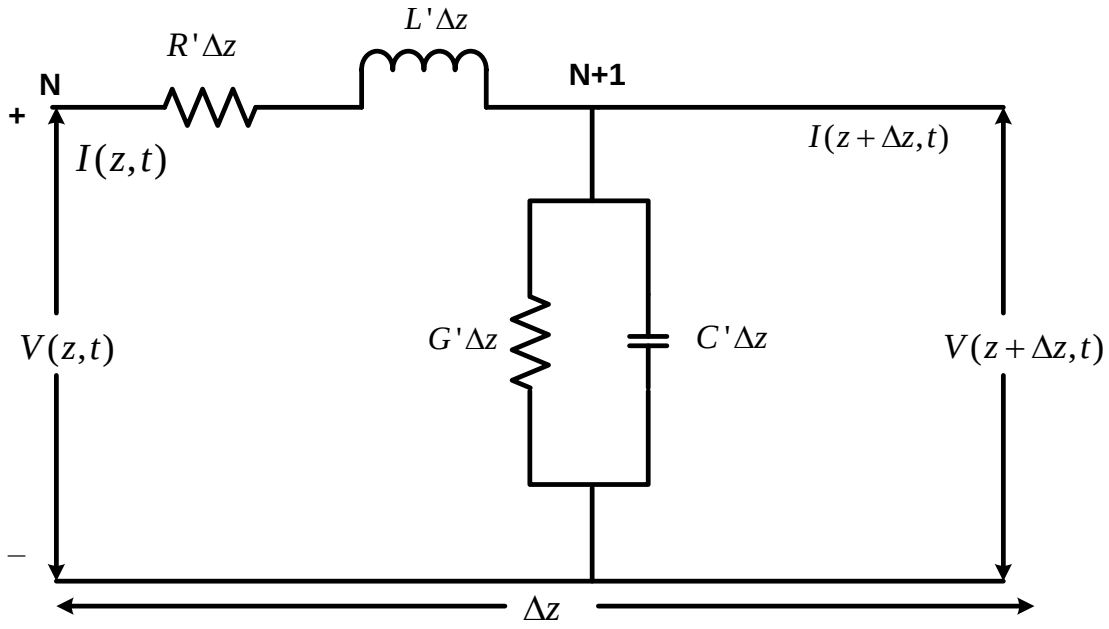


Figure 3-1 Transmission line model

$$\frac{d^2V(z)}{d(z)^2} - (R' + J\omega L')(G' + J\omega C')V(z) = 0 \qquad 3\text{-}1$$

$$\frac{d^2V(z)}{d(z)^2} - \gamma^2 V(z) = 0$$

3-2

Where, $\gamma^2 = (R' + J\omega L')(G' + J\omega C')$

3-3

$$\gamma = \sqrt{(R' + J\omega L')(G' + J\omega C')}$$

3-4

$$\gamma = \alpha + j\beta$$

3-5

Where

$\alpha = \mathrm{Re}\left(\sqrt{(R' + J\omega L')(G' + J\omega C')}\right)$ Neper/meter

3-6

$\beta = \mathrm{Re}\left(\sqrt{(R' + J\omega L')(G' + J\omega C')}\right)$ Rad/second

3-7

Attenuation constant α leads to reduction in power, while dispersion β leads to change in signature of the signal. Attenuation is the result of two phenomena, viz., (i) dielectric loss (tanδ) of the dielectric and (ii) propagation of the radial displacement current through the resistance of the semi conducting layers. Different frequency components of a pulse travel along the cable at different speeds which gives frequency-dependent phase shift. This phenomenon is known as dispersion. It is a function of the distance traveled by the pulse and of the frequency which causes temporal wave spreading [Cavallini, Montanari et al. 2007]. Absorption of moisture or water ingress changes the dielectric and semiconductor properties of the cable which in turn alters the attenuation and dispersion properties of the cable [Shu and Boggs 2008].

When wavelength λ of the signal is comparable to length of an unmatched line $l$, such that $\frac{l}{\lambda} > 0.01$, it may be necessary to consider the transmission line effects. This not only effects the phase shift associated with time delay between generator and load, but also for the reflected signals that may have been bounced back by the load towards the generator. Due to reflection, forward and reverse travelling waves were generated as follows.

$$I(z) = I_0^{+} e^{-\gamma z} + I_0^{-} e^{\gamma z}$$

3-8

$$V(z) = V_0^{+} e^{-\gamma z} + V_0^{-} e^{\gamma z}$$

3-9

Where

$e^{-\gamma z}$ - Propagation in positive z direction
$e^{+\gamma z}$ - Propagation in negative z direction

$$\frac{V_0^{+}}{I_0^{+}} = Z_0 \ = -\frac{V_0^{-}}{I_0^{-}}$$

3-10

Where $Z_0$ is characteristic impedance.

Characteristic impedance or zurge impedance denoted as ($Z_0$) is an expression relating to electric and magnetic field intensities in electro magnetic wave propagation through the respective medium. Theoretically $Z_0$ is independent of wavelength and is considered to be a physical constant. Characteristic impedance of insulated power cable normally lies in the range 10 and 60 ohms. However $Z_0$ depends upon propagation modes, common mode or differential mode.

A travelling wave may undergo reflections when it arrives at a termination of the transmission line. The reflections are governed by the value of load impedance connected at the end of the line. The reflection coefficient is given by

$$\Gamma = \frac{Z_L - Z_0}{Z_L + Z_0}$$

3-11

$Z_L$ : Impedance of termination
$Z_0$ : Characteristic impedance of the cable

For an open circuited termination incident, the reflected pulse will be in phase while for a short circuited termination incident, the reflected pulse will be out of phase with each other. The Amplitude of the reflected pulse is determined by the reflection coefficient.

Signal propagation velocity is normally expressed as a fraction of the electromagnetic propagation velocity in vacuum, and is given by [Shu and Boggs 2008].

$$V(s) = \frac{1}{\sqrt{\mu\varepsilon}} = \frac{1}{\sqrt{L(s)C(s)}}$$

3-12

where $\mu$ is permeability, ε is dielectric constant, $L$ is inductance per unit length, and $C$ is capacitance per unit length of the cable.

In the case of three core cable different propagation modes, exists namely common and differential modes. Multi conductor transmission line model of three core cable based on telegrapher equations were found in [Veen, van der Wielen et al. 2002]

## 3.3 PD source location using TDR

The conventional method for PD source location in cables based on signal point of view is TDR which is also known as travelling wave method. [Lowe 1968; Shim, Soraghan et al. 1999].A fast rising pulse from PD source propagates simultaneously in both directions of the cable and get reflected due to the mismatch between characteristic impedance of the cable under test and impedance at the termination/ RMU [Zhifang, Willett et al. 1997]. Signal power of the reflected pulse depends upon the magnitude of the reflection coefficient. As a result, PD pulse travels in opposite directions till the signal is completely attenuated. Figure 3-2 shows an off line TDR experiment results using 24 meter XLPE cable for termination having variable impedance. Based on Figure 3-2 , as the termination impedance increases, the amplitude of the reflected pulses gets increased. The optimum PD detection bandwidth and maximum cable length over which PD is detectable are determined by frequency dependent propagation characteristics of the cable. PD source location based on TDR method can be done using single ended and double ended measurements which are discussed in the following sections.

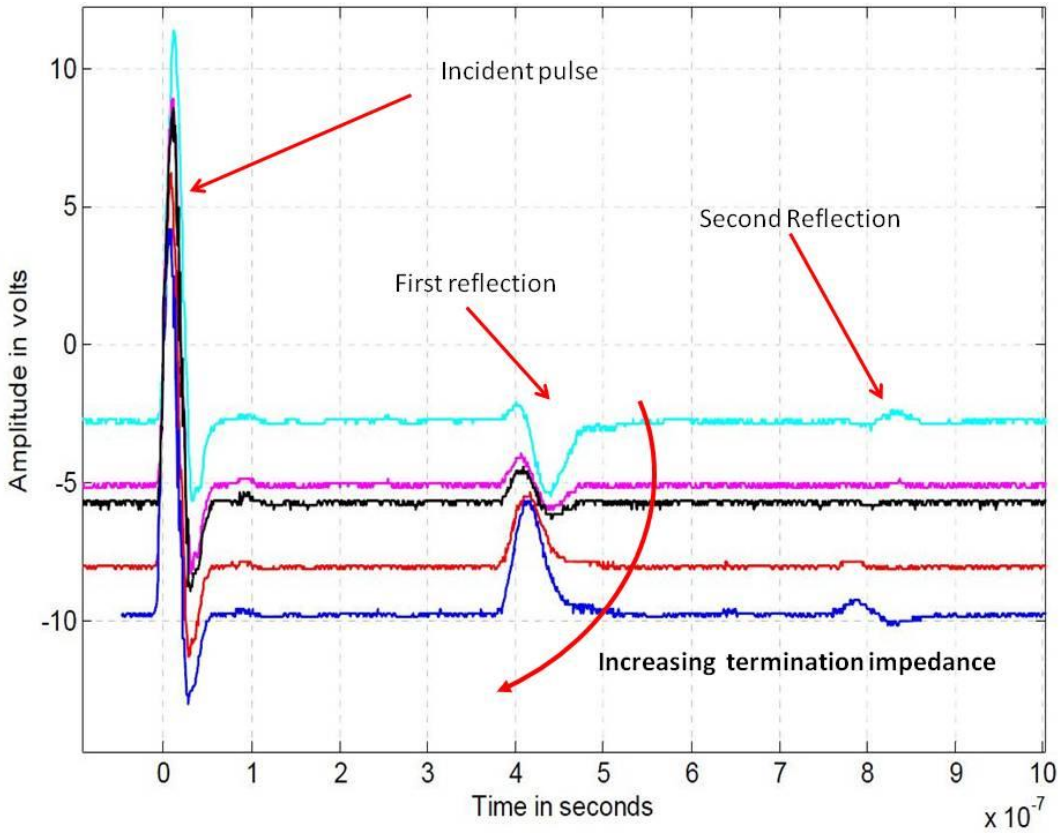


Figure 3-2 TDR pulses in XLPE cable of length 24 meters

## 3.4 Single ended PD source location

In the single-ended method, the PD source location is obtained using the data acquired from one end of the cable. It involves monitoring of both incident and reflected PD pulses using oscilloscopes installed at any one of the cable end. A block diagram of the measurement system for the single-ended PD source location is shown in Figure 3-3. Measurement setup consists of a high pass filter to remove the power frequency component, a digitizer and a PC for data storage and analysis. Location of PD source can be obtained from the time offset between incident and reflected pulse. This can be illustrated using bewley lattice diagram as shown in Figure 3-4 [Bewley 1931; Company 1997]

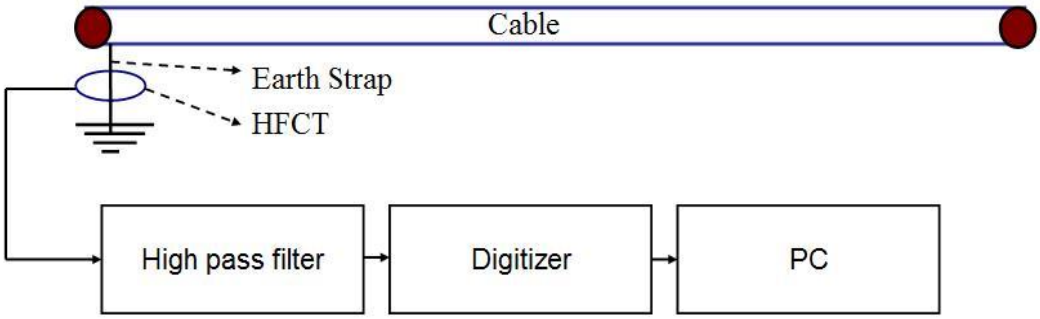


Figure 3-3. Single ended PD source location block diagram

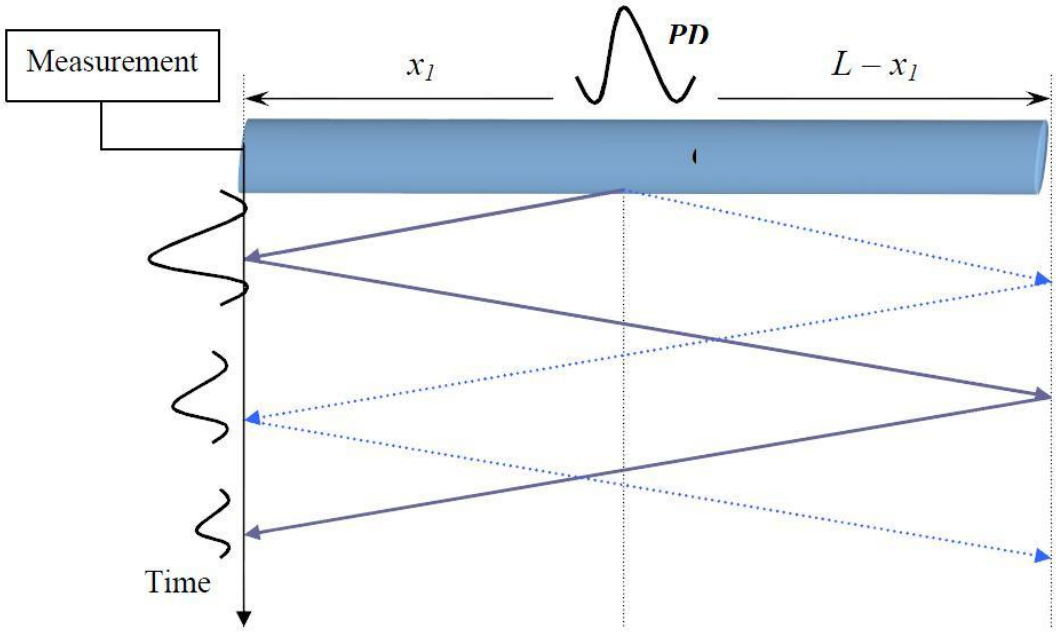


Figure 3-4 Bewel Lattice diagram [Bewley 1931; Company 1997]

Based on Figure 3-4, incident PD pulse which is the first pulse needs to travel a distance $x_1$ from the PD source to reach the measurement unit. Reflected PD pulse which is the second pulse needs to travel $2l - x_1$ to reach the measurement unit. Time offset between first pulse and second pulse is given by

$$\Delta t_1 = \frac{2(l - x_1)}{v} \qquad 3\text{-}13$$

Location of the PD source is given by

$$PD_l = l - \frac{v * \Delta t_1}{2}$$

3-14

Where, v is the velocity of signal propagation in the respective medium,

$\Delta t_1$ is the time offset between incident and reflected pulse.

When TDR is used to locate PD source , there are a few parameters which need to be considerd in the data acquisition system such as sampling rate, bandwidth, dynamic range and data length [Zhifang, Willett et al. 1997]. For clear understanding of PD source location using TDR, simulation study using PSPICE is included in this chapter. Transmission line model *TLOSSY* is used to model a single core cable. The aim of the simulation is to give a better view of PD source location using TDR for various location of PD source. Hence parameters selected for PD source location have no physical existence with single core cables.

This cable network has total length of 1500 meters made up of 15 sections. Each section has a length of 100 meters. Transit time is given by 350μs/meter. Distributed model parameters used to model the cable are R= 15 Ω /meter, L= 175 μH/meter, G=9 μ/meter, C= 70 nF/meter, v =2.8571e+005 meter/second, and transit time per 1 meter cable section of 3.5 e-006 seconds. PSPICE schematic of the cable network is as shown in Figure 3-5. PD source location under various scenarios of discharge source using single ended method are discussed in the next section.

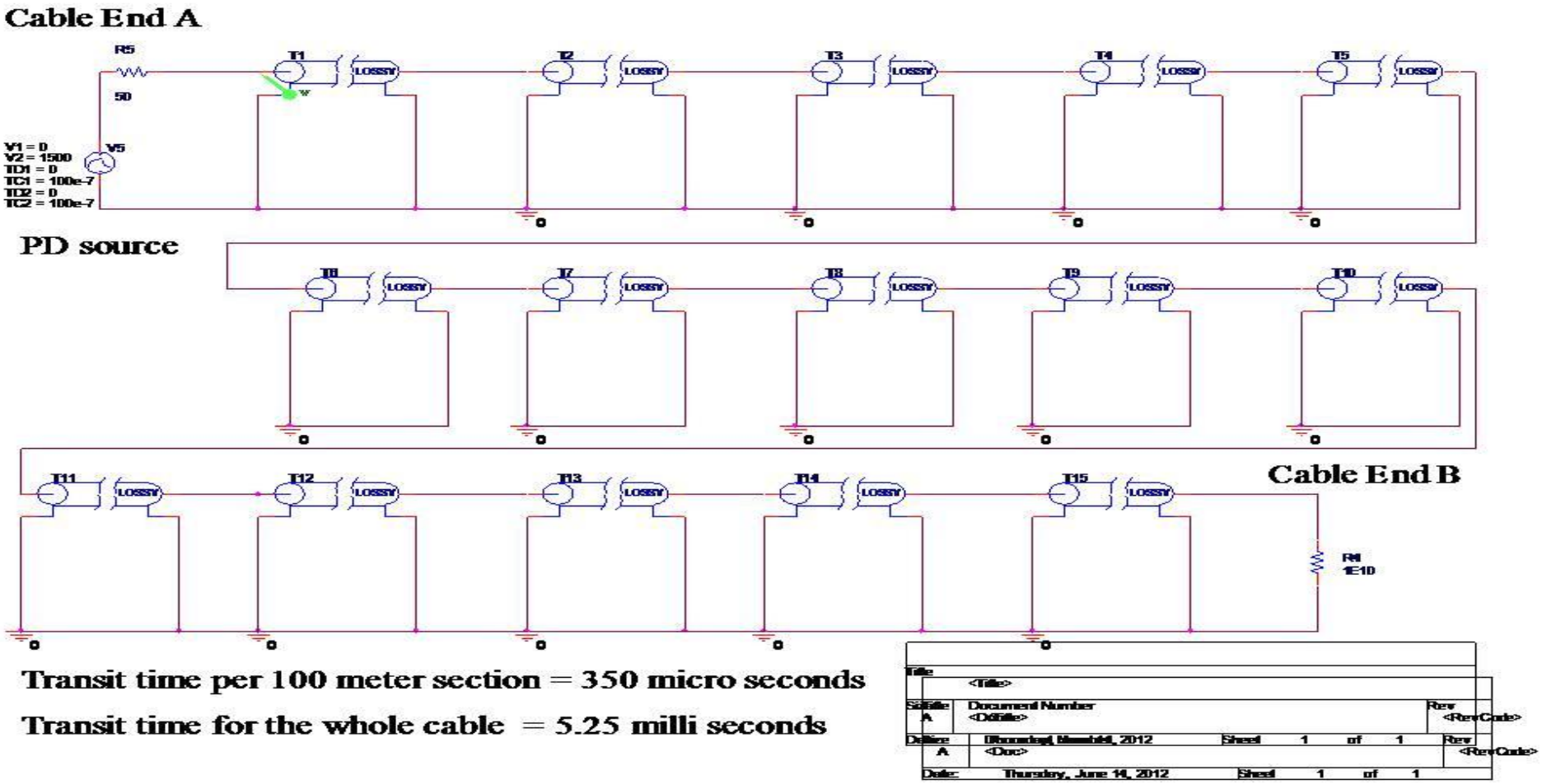


Figure 3-5 PSPICE model of cable network

### 3.4.1 Scenario # 1 , Internal PD source

In Figure 3-6 PD monitoring equipment at cable end A, PD source at cable end A and cable end B is open circuit. TDR plot is shown in Figure 3-7.

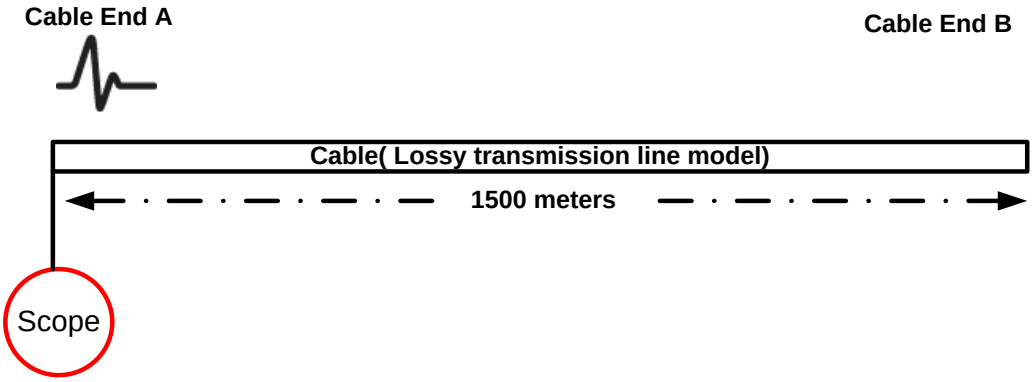


Figure 3-6 Scenario # 1, Cable network single ended method

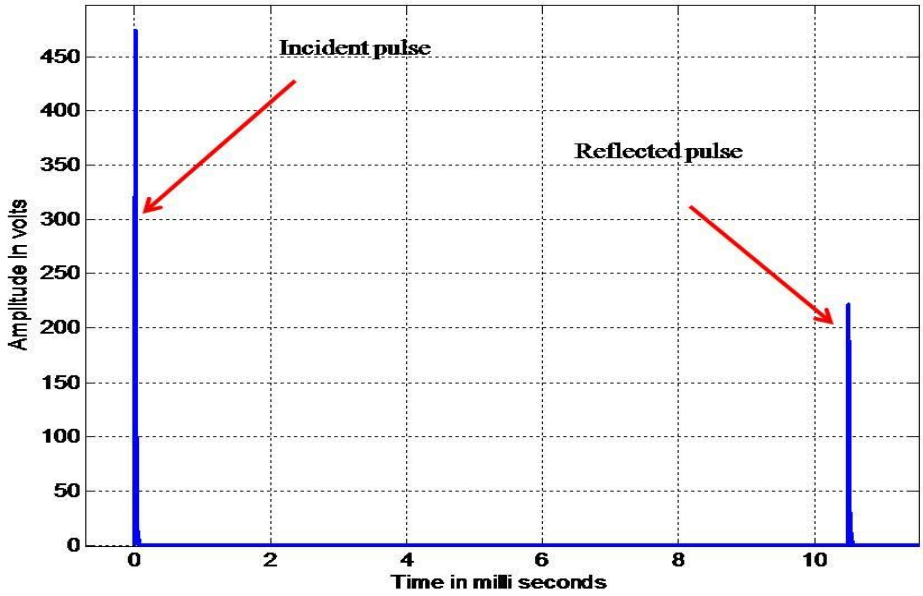


Figure 3-7 Scenario # 1, TDR plot, single ended method

Applying the formula in 3-14 ,

$\Delta t = 10.5\times10^{-3}$ seconds

$$\text{Location is given by } :1500 - \frac{10.5\times10^{-3} \ * \ 2.8571\times10^{5}}{2}$$

$$: \ 0.0225 \text{ meters}$$

$$\approx 0 \text{ meters}$$

$$\approx \text{ PD source is from the cable end A}$$

### 3.4.2 Scenario # 2, Internal PD source

In Figure 3-8 monitoring equipment at cable end A, PD source at 500 meters from cable end A, and cable end B is open circuit. TDR plot is as shown in Figure 3-9.

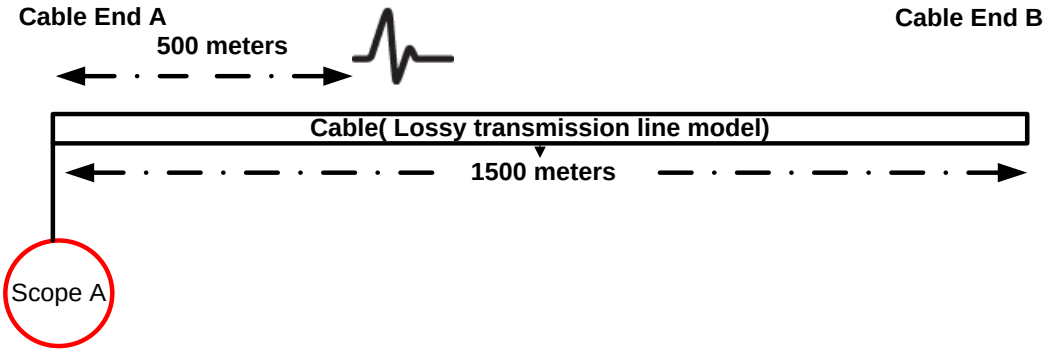


Figure 3-8 Scenario # 2, cable network single ended method

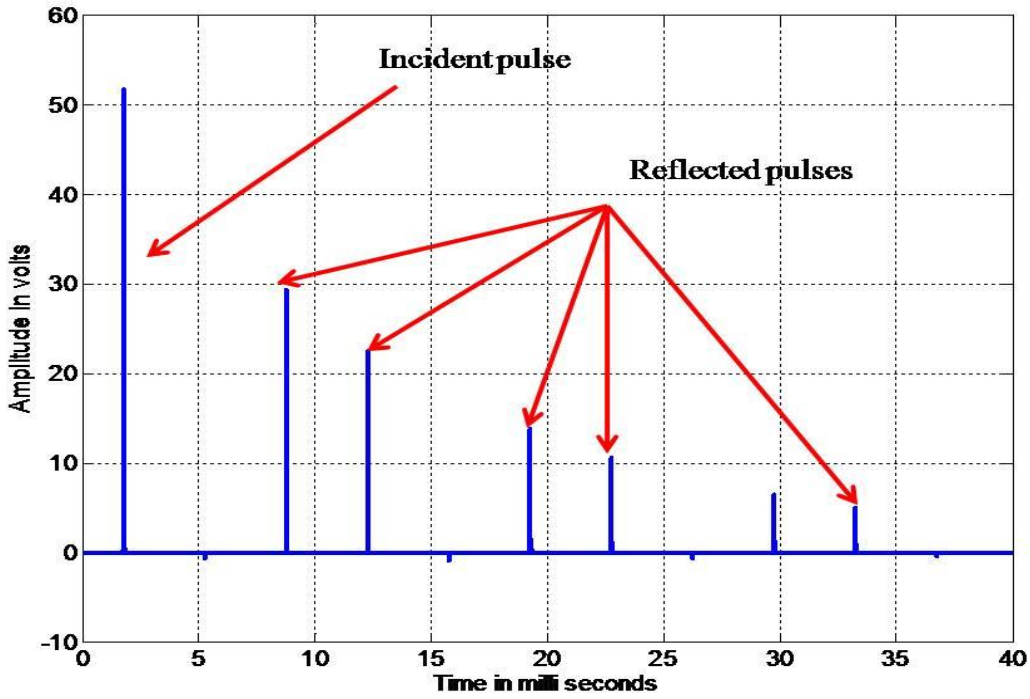


Figure 3-9 Scenario # 2, TDR plot, single ended method

Applying the formula in 3-14 ,

$$\Delta t = 1.75\times10^{-3} \sim 8.75\times10^{-3} \text{ seconds}$$
$$= 7\times10^{-3} \text{ seconds}$$
$$\text{Location is given by } : 1500 - \frac{7\times10^{-3} * 2.8571\times10^{5}}{2}$$
$$: 500.015 \text{ meters}$$
$$\approx 500 \text{ meters from cable end A}$$

### 3.4.3 Scenario # 3, External PD source

In Figure 3-10 monitoring equipment at 500 meters from cable end A, PD source at cable end A, and cable end B is open circuit.TDR plot is shown Figure 3-11.

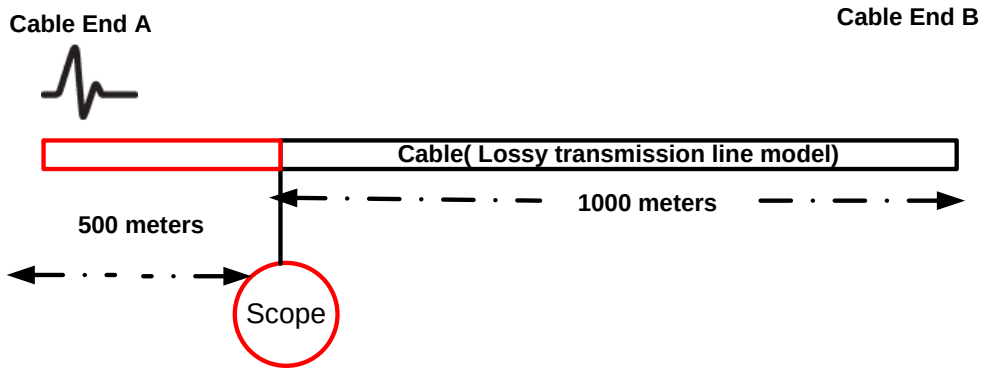


Figure 3-10 Scenario # 3, cable network single ended method

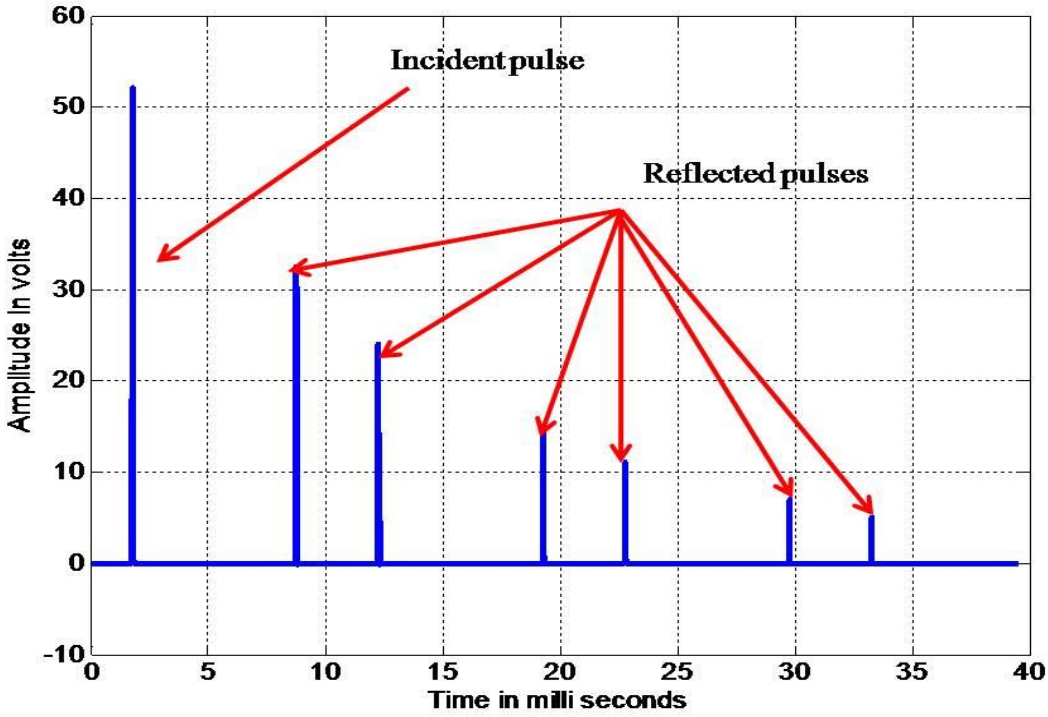


Figure 3-11 Scenario # 3, TDR plot, single ended method

Applying the formula in 3-14 ,

$$\text{Location of PD source} = \frac{\Delta t * V}{2}$$

$$\Delta t = (8.75\times10^{-3} - 1.75\times10^{-3})$$

$= 7\times10^{-3}$ seconds ,Since $\Delta t$ is twice the transit time of the cable of length 1000 meters, PD is most likely from outside the cable. Hence it can be ignored.

### 3.4.4 Scenario # 4, Multiple PD sources from the cable

In Figure 3-12 PD monitoring equipment cable end A, two PD sources one at 500 meters from cable end A and other at 700 meters from cable end A, and cable end B is open circuit. TDR plot is shown Figure 3-13.

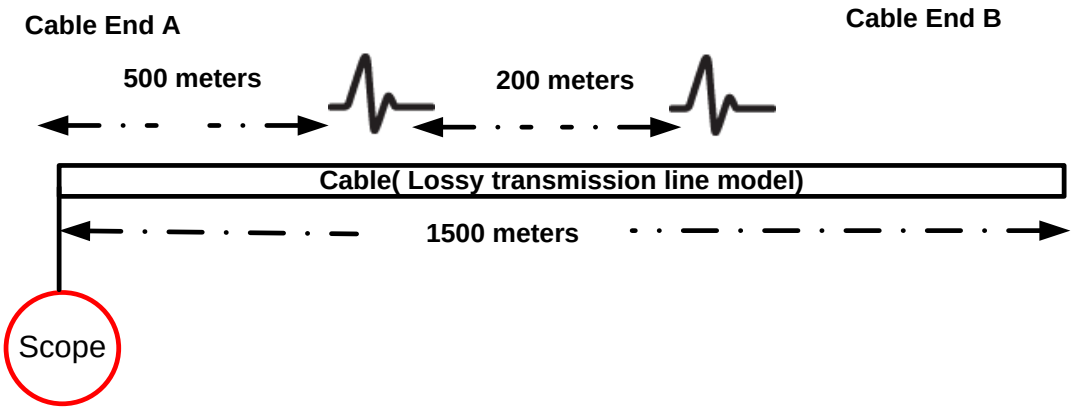


Figure 3-12 Scenario # 4, cable network, single ended method

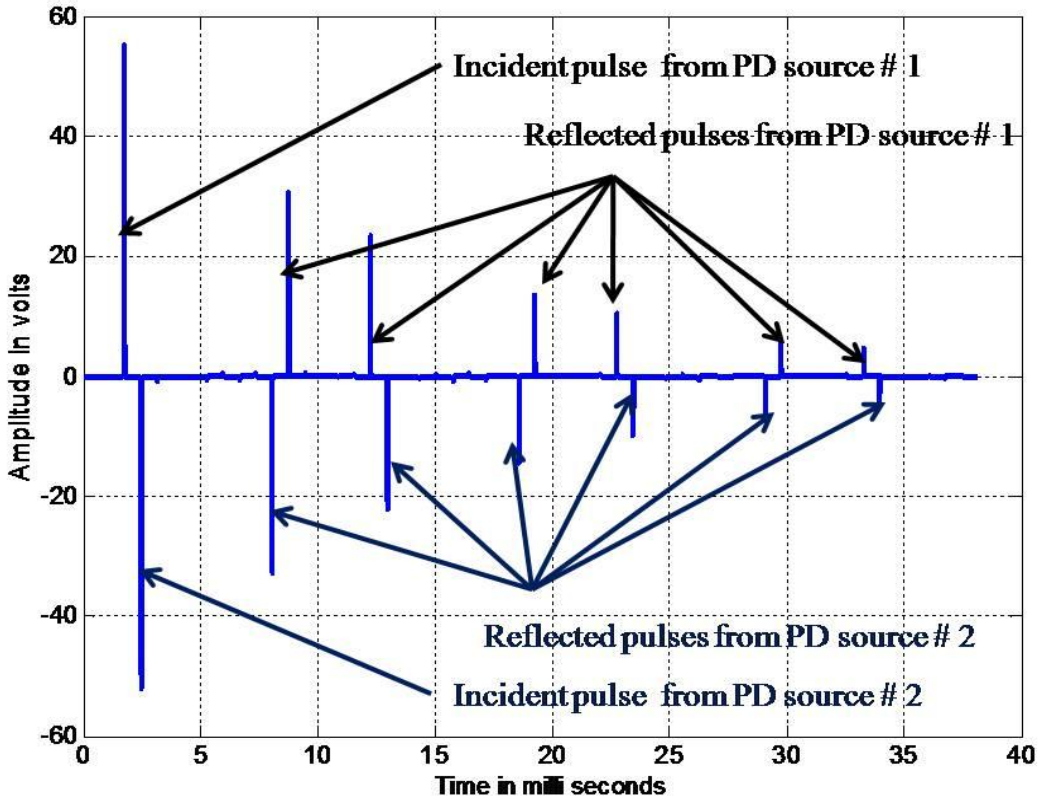


Figure 3-13 Scenario # 4, TDR plot, single ended method

### 3.4.4.1 Pulse Selection Method

Since there are multiple PD pulses from different sources, care must be taken to choose incident and reflected pulses. I Assumed there are n PD sources from the cable which will appear as n incident pulses and n+ reflected pulses in the measurement units. Incident pulse and reflected pulse required to calculate the PD source location are selected based on the pulse selection diagram as shown in Figure 3-14. This method is applied successfully to locate the PD source in scenario 4 discussed in the above section 3.4.4.

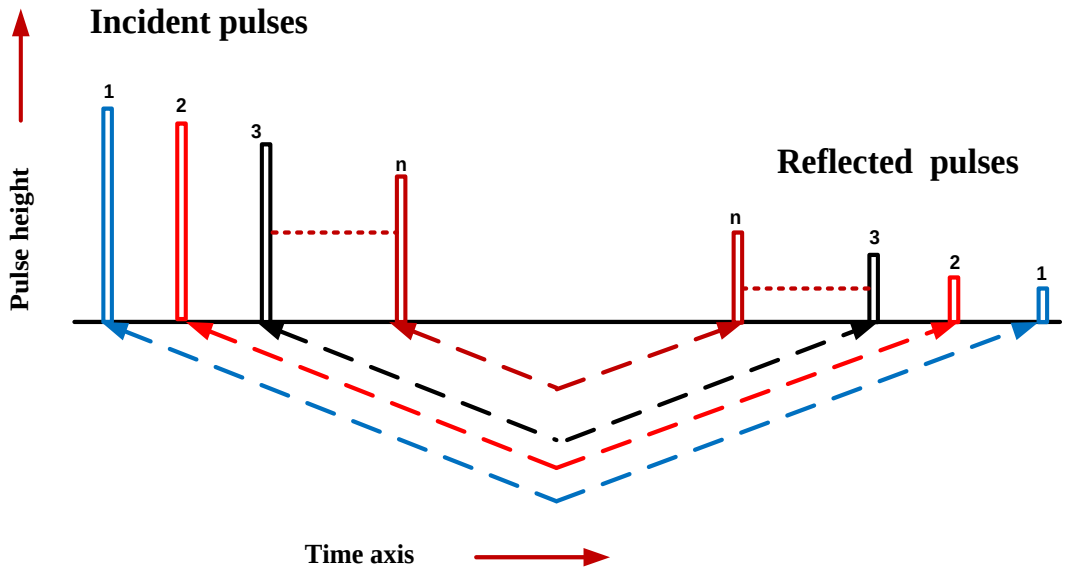


Figure 3-14 Pulse selection method for single-sided PD source location

Applying the formula in 3-14

PD source #1

$\Delta t_1 = 7\times10^{-3}$ seconds

$$\text{Location is given by } :1500 - \frac{7\times10^{-3} \ * \ 2.8571\times10^{5}}{2}$$

$$: \ 500.015 \text{ meters}$$

$$\approx \text{PD source \# 1 is 500 meters from cable end A}$$

PD source # 2

$\Delta t_2 = 5.6\times10^{-3}$ seconds

$$\text{Location is given by } :1500 - \frac{5.6\times10^{-3} \ * \ 2.8571\times10^{5}}{2}$$

$$: 700.012 \text{ meters}$$

$$\approx \text{ PD source \# 2 is 700 meters from cable end A}$$

### 3.4.5 Scenario # 5, Multiple PD sources close and far end

In Figure 3-15, PD monitoring equipment cable end A, Two PD source one at 500 meter from cable end A and 1400 meter from cable end A and cable end B is open circuit. TDR plot is shown in Figure 3-16.

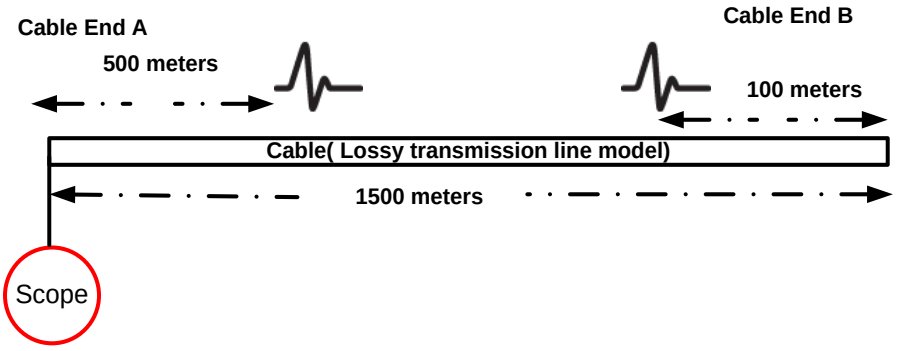


Figure 3-15 Scenario # 5, cable network single ended method

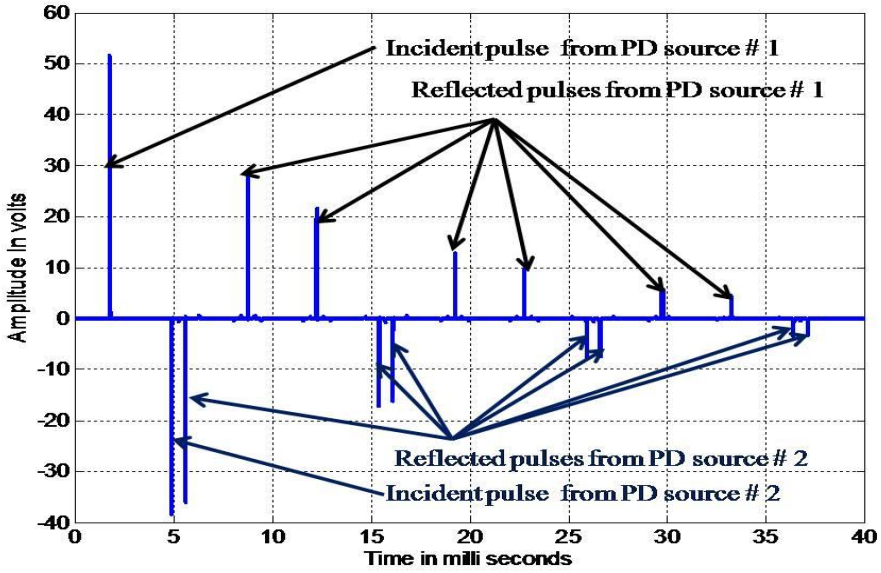


Figure 3-16 Scenario # 5, TDR plot, single ended method

Applying the formula in 3-14 and pulse selection method in section 3.4.4.1

$$\Delta t_1 = 1.75 \times 10^{-3} \sim 8.75 \times 10^{-3} \text{ seconds}$$

$$\text{Location is given by } : 1500 - \frac{7 \times 10^{-3} * 2.8571 \times 10^{5}}{2}$$

$$: 500.015$$

$$\approx \text{ PD source \# 1 is 500 meters from cable end A}$$

$$\Delta t_2 = 4.9 \times 10^{-3} \sim 5.6 \times 10^{-3} \text{ seconds}$$

$$\text{Location is given by } : 1500 - \frac{0.7 \times 10^{-3} * 2.8571 \times 10^{5}}{2}$$

$$: 1400.015 \text{ meter}$$

$$\approx \text{ PD source \# 2 is 1400 meters from cable end A}$$

### 3.4.6 Scenario # 6, internal and external PD

In Figure 3-17, PD monitoring equipment at 500 meter from cable end A, Two PD sources at 200 meters and 500 meters from cable end A and cable end B is open circuit. TDR plot is shown in Figure 3-18.

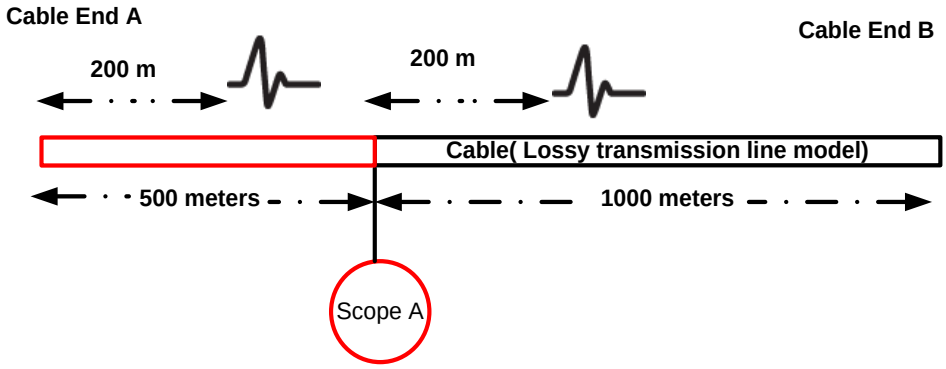


Figure 3-17 Scenario # 6, cable network single ended method

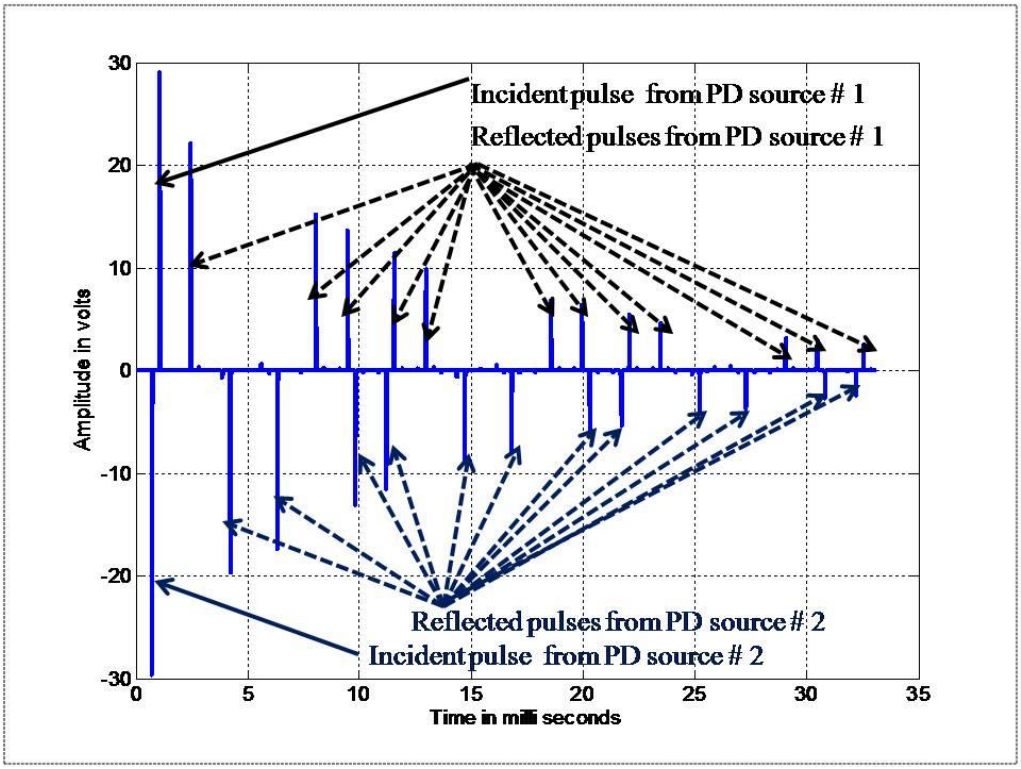


Figure 3-18 Scenario # 6, TDR plot, single ended method

In this scenario there is ambiguity in choosing the right pulses based on the pulse selection method discussed above. In this case the single ended method fails to distinguish pulses from internal and external PD.

## 3.5 Double Ended PD source Location

Success rate of locating PD using the single ended method depends upon the reflected pulse which is determined by mismatch in characteristic impedance between RMU or Cable termination and the cable itself. RMU impedance does not often have a significant impedance change from the characteristic impedance of the cable. So PD signals can propagate through RMU without generating reflected PD pulse [Lee Renforth 2009]. Moreover cable propagation characteristics and measurement systems will also reduce the amplitude of a reflected pulse which makes the PD source location difficult, sometimes not possible. This makes the single ended method more suitable for off-line PD source location since open circuit reflection can be generated by opening the remote end of the cable. Various issues affecting the accuracy of PD source location using the single ended method may be overcome by detecting PD at both ends of the cable with high accurate time base alignment between the measurement systems. Block diagram of typical double ended method is shown in Figure 3-19.

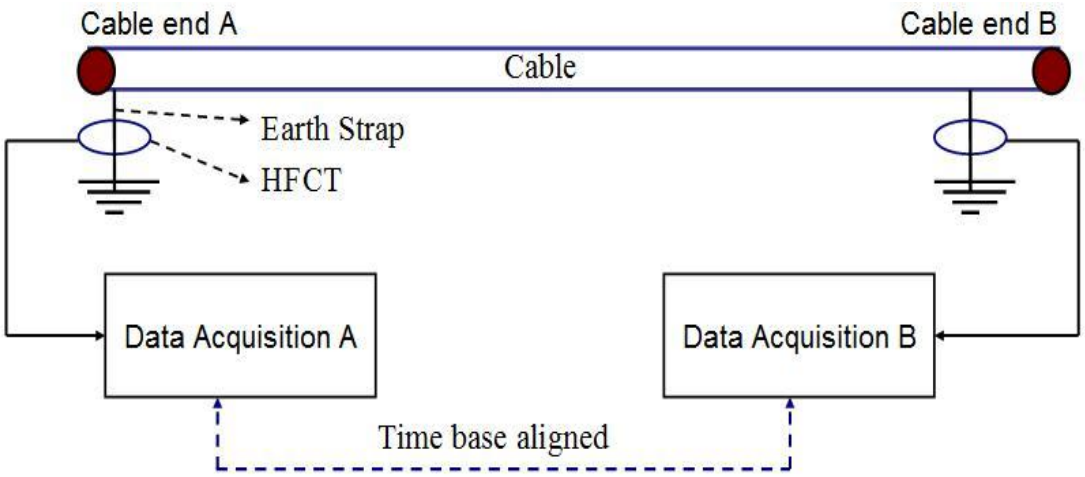


Figure 3-19 Double ended PD source location test setup [Mohamed, Siew et al. 2011]

In this method time offset in arrival time between first pulse in both measurement systems together with propagation velocity and cable length are used to calculate the PD source location and is given by:

$$PD_l : \frac{l - (\Delta t_2 \times v)}{2} \qquad 3\text{-}15$$

Where, $l$ : length of the cable section

$\Delta t_2$ : time offset between incident pulses

$v$ : velocity of propagation

Attenuation and dispersion effects are reduced to greater extent and the effect of substation or RMU impedance is eliminated [Mohamed, Siew et al. 2011]. Accurcay of this method is fully determined by the time synchronization method. PD source location under various scenarios of discharge source in double ended PD location method are discussed in the next section.

### 3.5.1 Scenario # 1, Internal PD source

In Figure 3-20, PD monitoring equipment at both ends of the cable ends A and B, PD source at cable end A. TDR plot is shown in Figure 3-21.

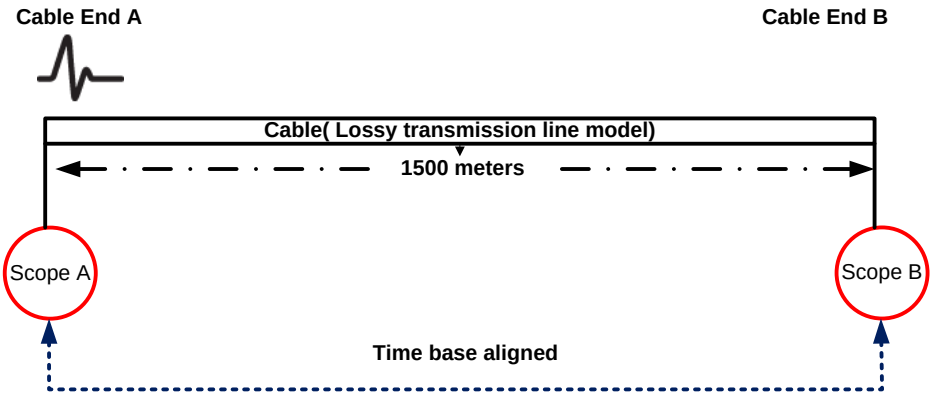


Figure 3-20 Scenario # 1, cable network, double ended method

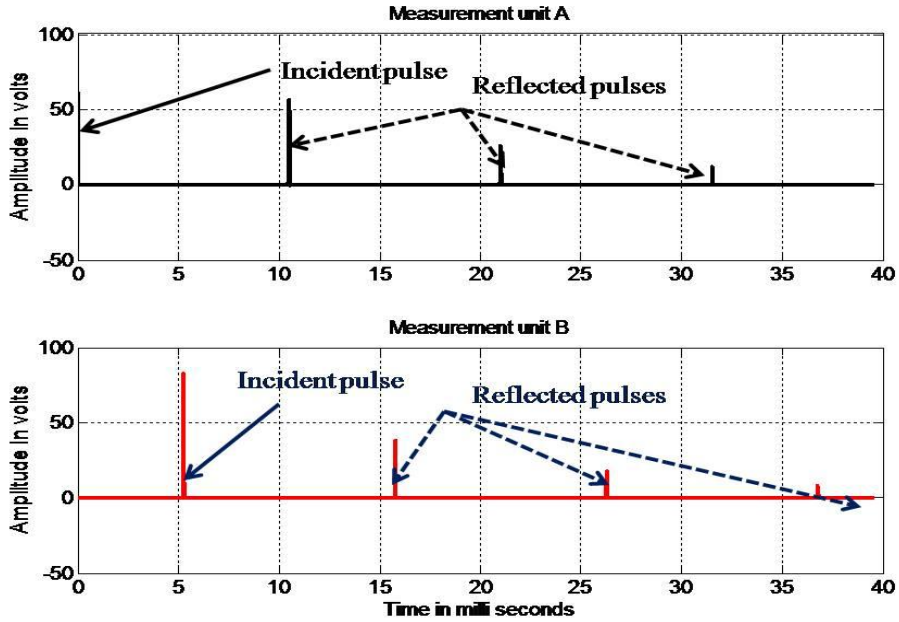


Figure 3-21 Scenario # 1, TDR plot, double ended method

Based on equation 3-15,

$$\Delta t = (0) \sim \left(5.25 \times 10^{-3}\right) \text{seconds}$$

$$= 5.25 \times 10^{-3} \text{ seconds (Which is the trasit time of the whole cable network)}$$

$$PD_l : \frac{1500 - \left(5.25 \times 10^{-3} \times 2.8571 \times 10^{5}\right)}{2}$$

$$: 0.01125 \text{ meters}$$

$$\approx \text{ PD source is from Cable end A}$$

### 3.5.2 Scenario # 2, Internal PD source

In Figure 3-22, PD monitoring equipment at cable end A and B, PD source at 500 meters from cable end A. TDR plot is shown in Figure 3-23.

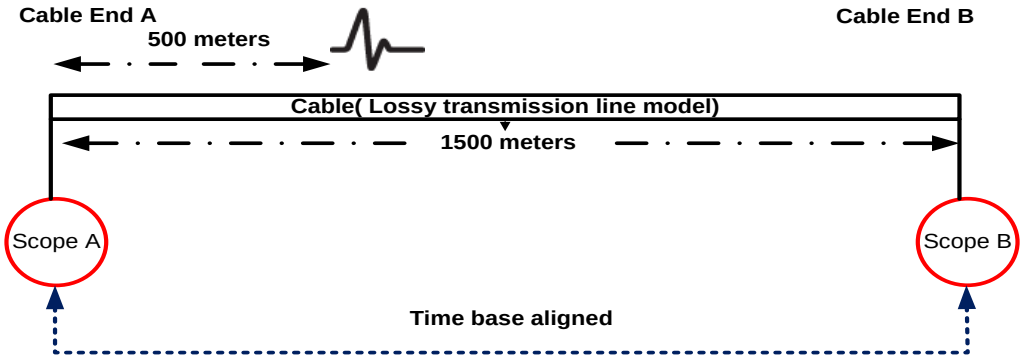


Figure 3-22 Scenario # 2, cable network, double ended method

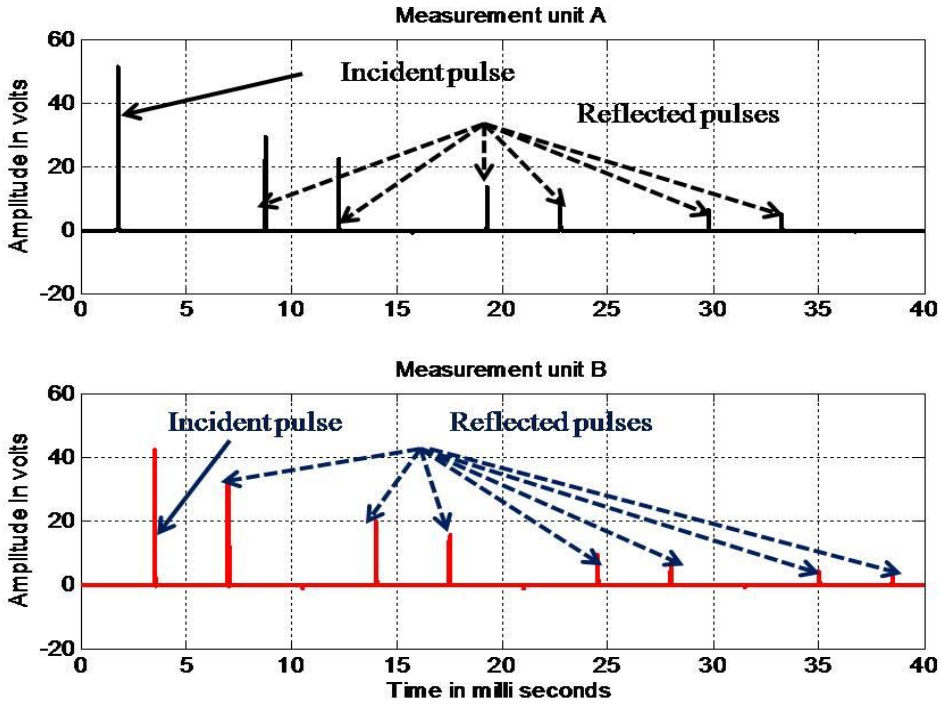


Figure 3-23 Scenario # 2, TDR plot, double ended method

Based on equation 3-15,

$$\Delta t = \left(1.75\times10^{-3}\right) \sim \left(3.5\times10^{-3}\right) \text{seconds}$$
$$= 1.75\times10^{-3} \text{ seconds}$$
$$PD_l \;:\; \frac{1500\text{-}\left(1.75\times10^{-3} \times\ 2.8571\times10^{5}\right)}{2}$$
$$: 500.00375 \text{ meters}$$
$$\approx 500 \text{ meters from Cable end A}$$
$$\approx (1500\text{-}500) \text{ meters from Cable end B}$$

### 3.5.3 Scenario # 3, External PD source

In Figure 3-24, PD monitoring equipment 700 meter from cable end A and at cable end B, PD source at cable end A.TDR plot is shown in Figure 3-25.

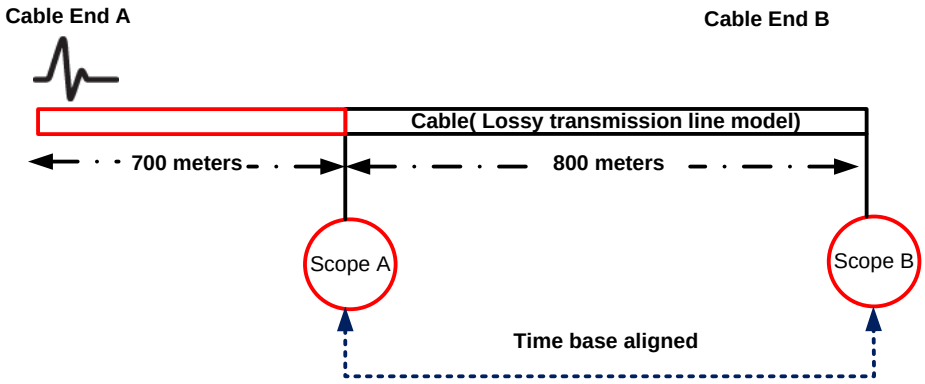


Figure 3-24 Scenario # 3 Cable network, double ended method

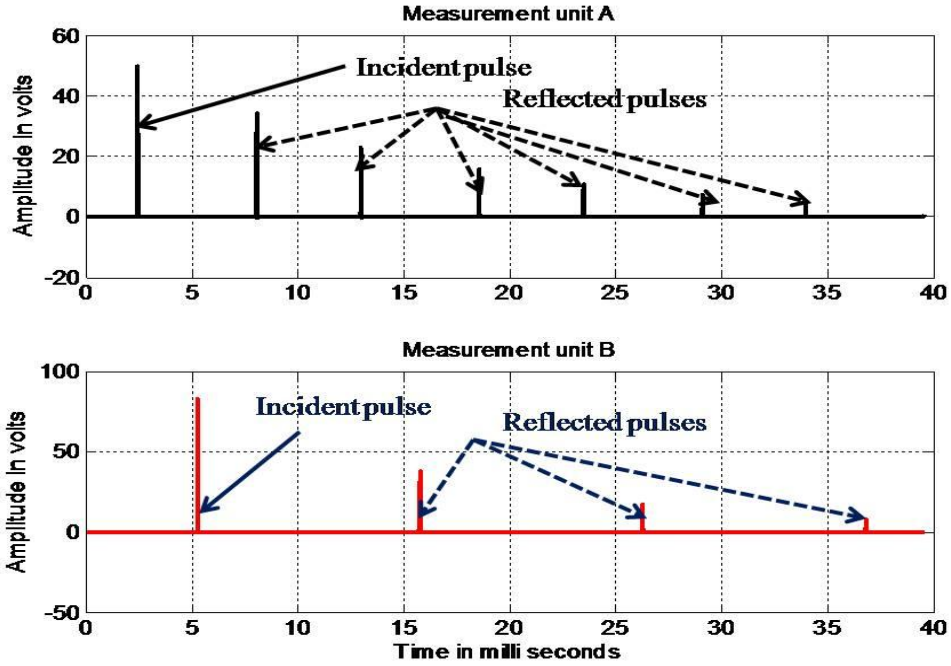


Figure 3-25 Scenario # 3 TDR plot, double ended method

Based on equation 3-15,

$$\Delta t = (2.45\times10^{-3}) \sim \left(5.25\times10^{-3}\right) \text{seconds}$$

$$= 2.8\times10^{-3} \text{ seconds}$$

Since $\Delta t$ equals transit time of the cable section between two measurement units , PD source is either coming from or away the cable end A

### 3.5.4 Scenario # 4, Multiple PD sources from the cable

In Figure 3-26, PD monitoring equipment at cable end A and at cable end B, PD sources at 500 meters from cable end A and 700 meters from cable end B. TDR plot is shown in Figure 3-27.

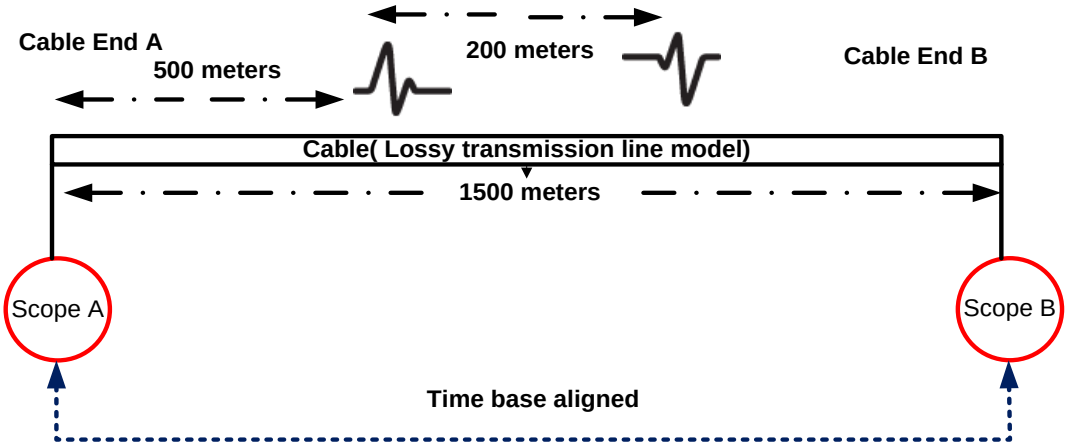


Figure 3-26 Scenario # 4, cable network, double ended method

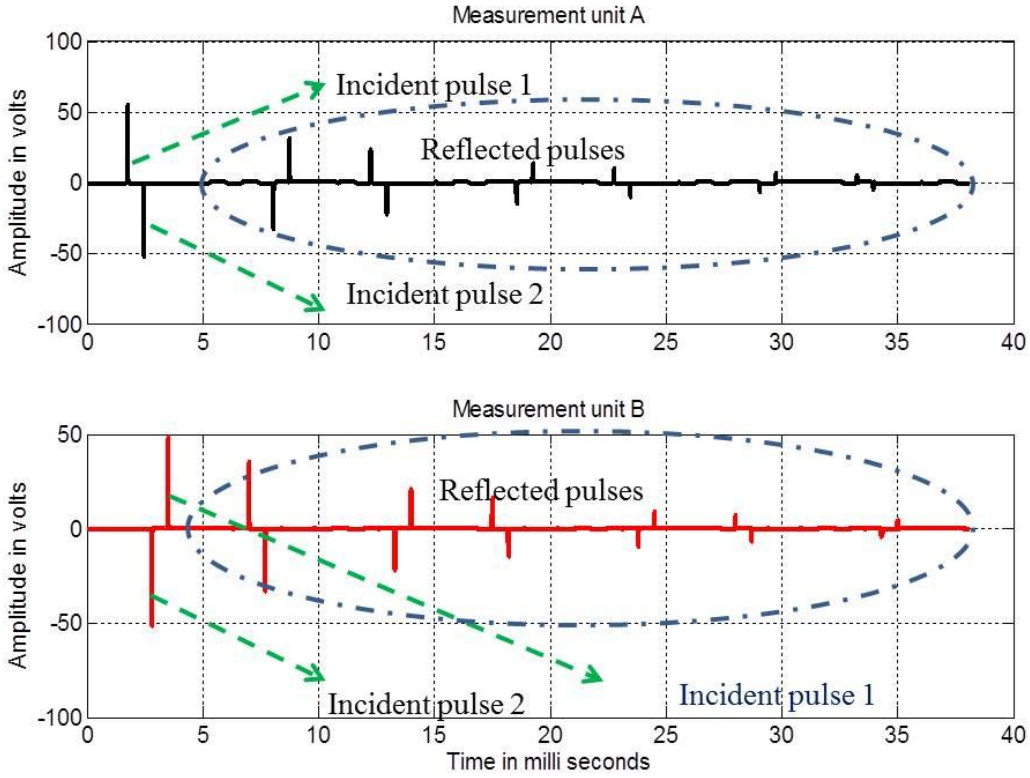


Figure 3-27 Scenario # 4, TDR plot, double ended method

### 3.5.4.1 Pulse Selection Method

Since there are multiple pulses from different PD sources, care must be taken to choose the incident and reflected pulses. Assume there are n PD sources from the cable which will appear as n incident pulses in both measurement units. Incident pulses required to calculate the PD source location are selected based on the diagram as shown in Figure 3-28. This method is applied successfully to locate the PD source in scenario-4 discussed in section 3.5.4. Further example is included in the Appendix A-1.

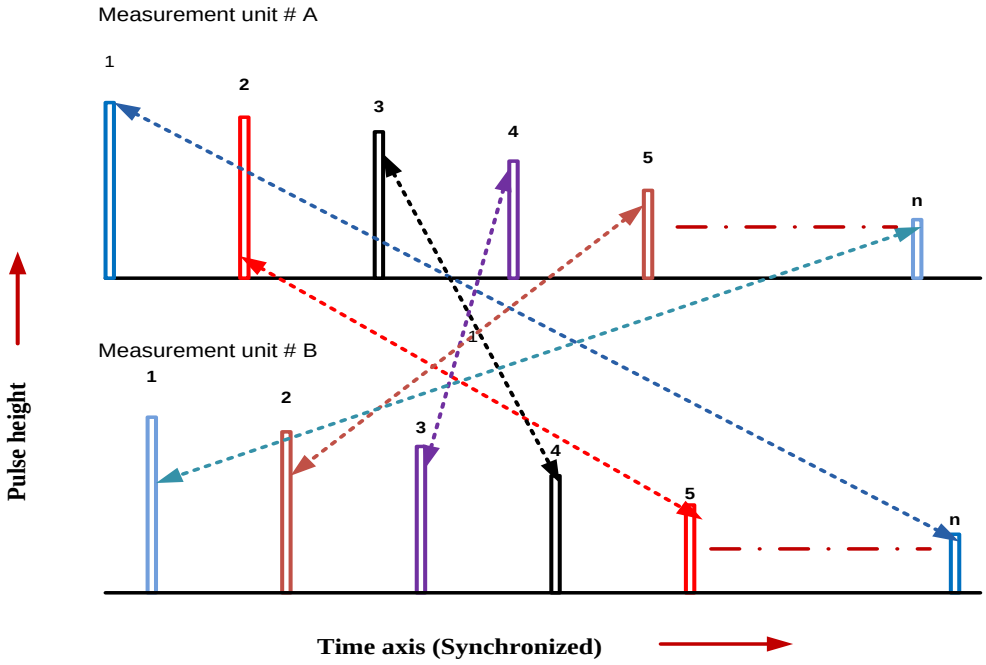


Figure 3-28 Pulse selection method for double-ended PD source location

Based on equation 3-15 and pulse selection method

PD #1

$$\Delta t = \left(1.75\times10^{-3}\right) - (3.5) \text{ seconds}$$

$$PD_l = \frac{1500 - \left(1.75\times10^{-3} \times 2.8571\times10^{5}\right)}{2}$$

$$= 500.00375 \text{ meters}$$

$$\approx \text{from Cable end A}$$

$$\approx (1500\text{-}500) \text{ meters from Cable end B}$$

PD # 2

$$\Delta t = \left(2.45\times10^{-3}\right) - \left(2.8\times10^{-3}\right) \text{seconds}$$

$$= 0.35\times10^{-3} \text{ seconds}$$

$$PD_l = \frac{1500 - \left(0.35\times10^{-3} \times 2.8571\times10^{5}\right)}{2}$$

$$= 700.00075 \text{ meters}$$

$$\approx 700 \text{ meters from Cable end A}$$

$$\approx (1500\text{-}700) \text{ meters from Cable end B}$$

### 3.5.5 Scenario # 5, Multiple PD sources

In Figure 3-29, PD monitoring equipment at 500 meter from cable end A and at cable end B, one PD source at 200 meters from cable end A and other PD source at 700 meters from cable end A. TDR plot is shown in Figure 3-30.

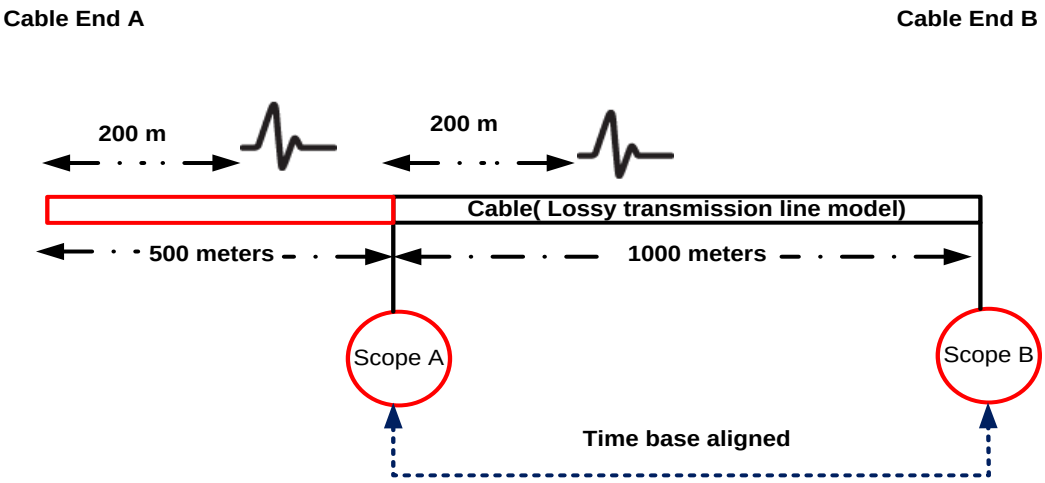


Figure 3-29 Scenario # 5 , cable network, double ended method

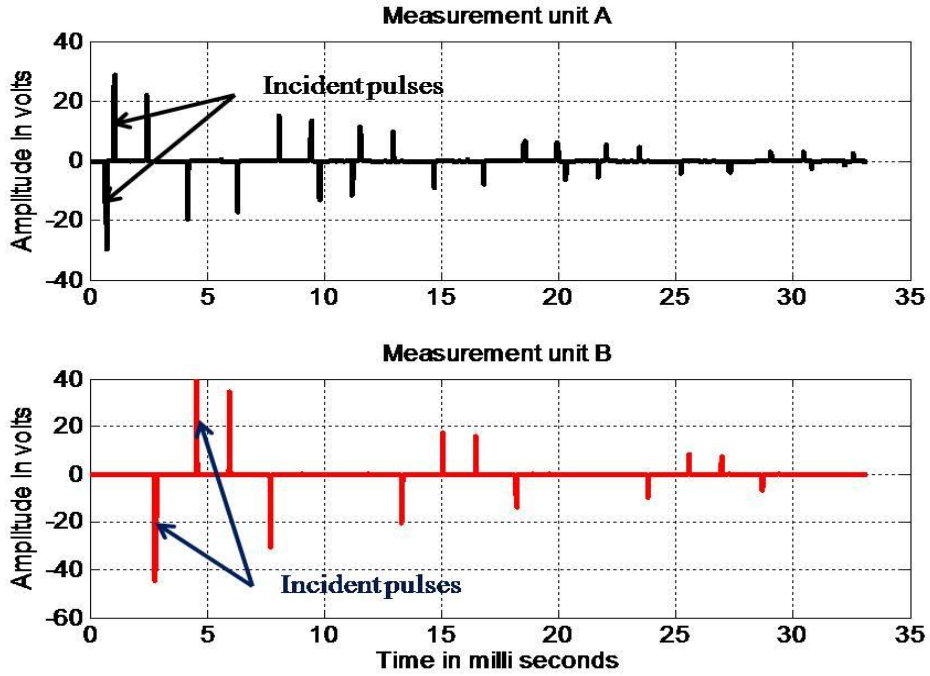


Figure 3-30 Scenario # 5 , TDR plot, double ended method

There is ambiguity in choosing the relevant incident PD pulses based on the pulse selection method discussed above. PD source away from the cable can be misinterpreted as the PD from the cable itself.

## 3.6 How to discard through pulses

The single ended method uses both incident and reflected pulses from the cable to compute the PD source location. Accuracy of this method depends upon cable parameters and termination impedance. On the other hand the double ended method uses incident pulses from both ends of the cable. The effect of cable parameters on PD source location is much less compared to the single ended method thereby this method can be used to locate PD's in longer cables. Also the effect of termination impedance on PD source location is eliminated. Hence the probability of getting PD source location is higher compared to the single ended method. However this method is not cost effective since two data acquisition units with time base alignment are required. In both methods there is a difficulty to distinguish internal PD source from external PD source (scenario # 6 , section 3.4.6 and scenario 5 section 3.5.5).

[Lundback, Nordebo et al. 2008] proposed a digital directional coupler which separates forward and backward travelling waves on a transmission line. This method is based on two independent wideband measurements of voltage (capacitive coupler) and current (inductive coupler) and frequency-domain digital wave splitting using a FFT. [Lemke, Strehl et al. 1999] proposed the method of using directional couplers for identifying the PD from and outside the cable. Both of these methods are invasive and may not be possible to implement on-line.

### 3.6.1 Dual measurement system method

In this thesis the dual measurement unit method is proposed to differentiate forward and reverse travelling waves in the cable under test. Block diagram of the method is shown in Figure 3-31.

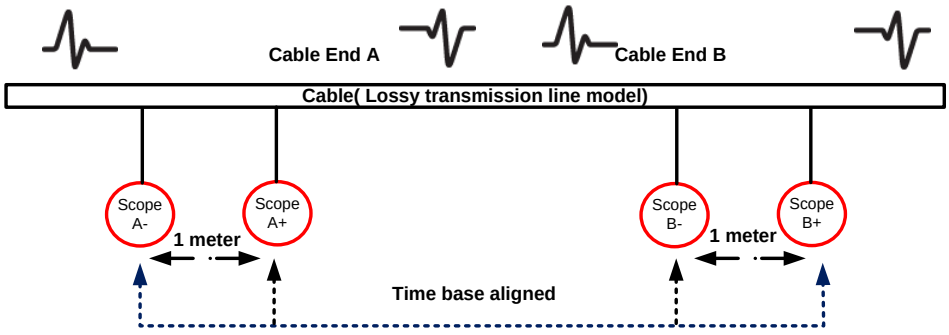


Figure 3-31 Dual measurement unit method

In this method, two data acquisition pair namely scope $A^-$ and scope $A^+$, scope $B^-$ and scope $B^+$ which are placed at 1 meter distance apart in the cable under test. Cable under test spans from scope $A^+$ and scope $B^-$. Forward and backward travelling waves were differentiated using the waveform signature and from the spatial map as shown in Figure 3-32 and Figure 3-33, based on the distance of separation between the pulses which is 1 meter in this case. In this way PD pulses from and outside the cable can be differentiated.

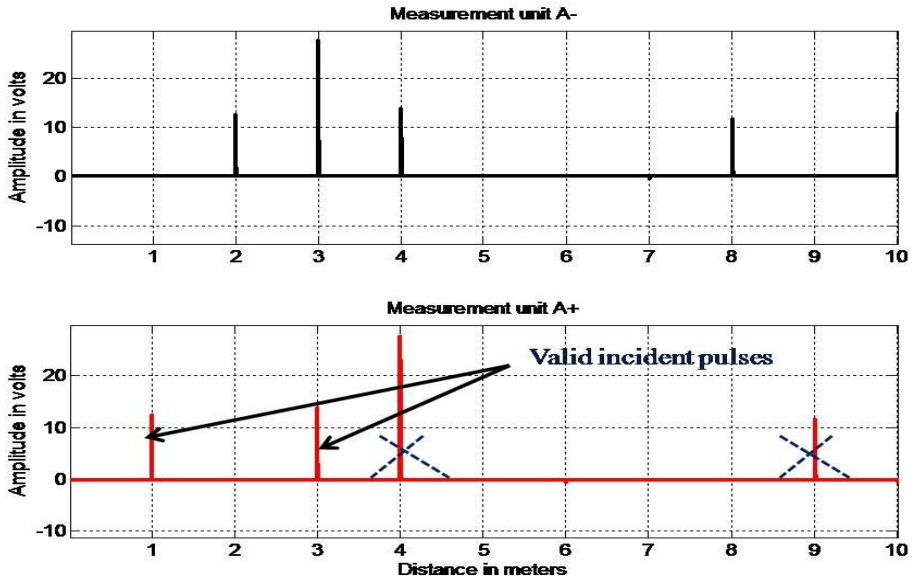


Figure 3-32 Spatial TDR map End A, dual measurement method

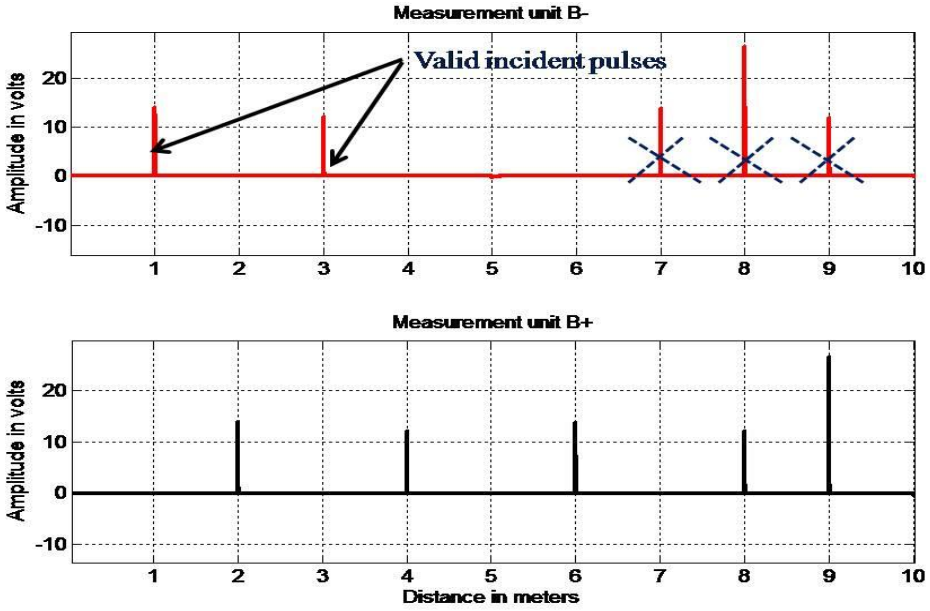


Figure 3-33 Spatial TDR map End B, dual measurement method

Though this method looks simple and easy to implement, based on author's experience in on-line PD measurements in few subsations, it may be difficult to get 1 meter seperation in the earth strap of the cable. In this simulation, in order to discard PD signals from neighbouring cables, sampling rate of 1 Gsamples/second is used to differentiate forward and reverse travelling waves. Hence, hardware requirement for this method such as sampling rate and resolution of the data acquisition system needs to be high so that forward and reverse PD pulses can be separated. High speed oscilloscopes including Agilent U1065A, Tektronix DPO5204, etc [Technologies 2013; Tektronix 2013] are commercially available,therefore this method can be implemented. Futhermore, accurcay of this method also depends upon the rise time, pulse width and time domain signature of the waveforms.

PD location methods discussed in section 3.4 - 3.6 assumes that multiple PD sources were resulted from same PD incipient voltages. PD pulses from various defective sites with different inception voltages exhibit unique signal profiles. This produces unique energy distribution in time and frequency domain. Using the energy distribution approach, PD pulses from various sources can be discriminated. [Hao, Lewin et al. 2011] proposed method of PD signal discrimination from various sources using principle component analysis based classical wavelet based decomposition. However, discrimination of mutiple PD sources is beyond the scope of this research work and hence, it will not be considered in this thesis. Accuracy of PD source location is also affected by sampling frequency of the data acquisition system and error in velocity of propagation factor. As discussed in the Section 3.5, double ended PD location method required high resolution time synchronization between the measurement units. Various time synchronization methods are discussed in the next section.

## 3.7 Time Synchronization Methods

In order to locate PD with reasonable accuracy of 10 meters in insulated power cables, it is necessary to have time base alignment accuracy of 100 nano seconds approximately based on the velocity of propagation of electromagnetic wave in PILC cables. In this section various time synchronization methods are discussed.

### 3.7.1 Stable Independent Clocks

All clocks have two basic elements namely regular constant repetitive process and displaying repetition process in the form of digits. Accuracy of the clocks rely on accuracy of the repetition frequency. An atom, when excited by an external energy source, enters into a higher energy state and then back to a lower energy state. In this transition, the atom releases photons of energy at a very precise frequency which is the characteristic of the type of atom. This is like a signature for the type of material used. Thus atoms constitute a potential pendulum which performs oscillatory motion and can be used as basis for highly accurate atomic clocks. Atomic clocks can be constructed by detecting the characteristic frequency of the atom and feeding it as an input to a counter, [F.Ramsey 1983].

There are various types of atomic clocks based on the element used e.g hydrogen, ammonia, rubidium, caesium. Within a limited time span these clocks provide a high degree of accuracy. Navigation systems and internet synchronizations are using atomic clocks. The first caesium atomic clock was built by NPL in 1955 which led to the internationally agreed definition of a second. One second corresponds to 9,192,631,770 periods of caesium -133. The accuracy of this clock is 1 second in 15 million years [Dong-Jun, Il-Yop et al. 2002]. Accuracy of a rubidium atomic clock is 3 seconds in one million years. Hydrogen maser atomic clocks are used on Gallileo navigation systems. It has better shortime accuracy of 6 *10^(-15) s in 24 hours which is better than a caesium clock [Wang 1989]. Earlier in 2011 Symmetricom, of San Jose, Calif., introduced the first commercial chip-scale atomic clock, the SA.45s. It measures 4 × 3.5 × 1.1 centimetres and weighs 35 grams. The tiny clock is accurate to within about “less than half a microsecond per day”[Jones 2011]. Accuracy of these clocks is far beyond the accuracy of the time base alignment required for PD source location. These clocks are highly expensive and are not affordable for applications like PD source location methods.

### 3.7.2 Navigation Systems

Navigation is the science of getting a craft or person from one place to another. Everyone in day to day life conducts some form of navigation for example walking to the store or driving to work using fundamental human navigation skills using eyes,

common sense and landmarks. In some cases a more accurate and precise knowledge of position is required which can be achieved through radio navigation aids. Navigation aids are classified as ground based and space based. ILS is the ground based navigation system used by FAA for automatic landing of aircraft. Space based navigation aids are satellite based which are normally known as GNSS. Space based navigation systems are discussed in the following section.

#### 3.7.2.1 Global Positioning System (GPS)

GPS is a space-based radio navigation system which is managed for the government of the United States by USAF, the system operator. GPS was originally developed as a military force enhancement system and also demonstrated a significant potential to benefit the civil community in an increasingly large variety of applications. GPS provides accurate, precise, continuous, world-wide, three-dimensional position and velocity information to users with GPS receiver. It disseminates a form of UTC. The satellite constellation consists of 24 satellites arranged in 6 orbital planes with 4 satellites per plane as shown in Figure 3-34 [Kaplan and Hegarty 2006].

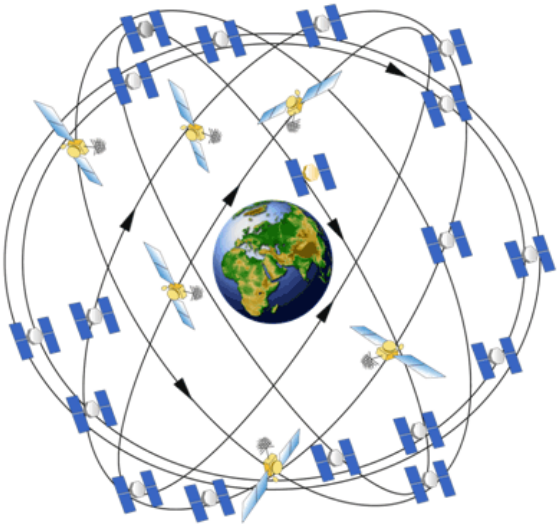

Figure 3-34 GPS constellation satellites [http://www.gps.gov/multimedia/images/]

Each orbit makes a $55^0$ angle with the equator, which is referred to as the inclination angle. The orbits are separated by $60^0$ to cover the complete $360^0$. The radius of the satellite orbit is 26,560 km and it rotates around the earth twice in a sidereal day. GPS can provide service to an unlimited number of users since the user receivers operate passively (i.e., receive only). GPS receivers calculate its position based on the

data received from satellite. Each satellite transmits data at a rate of 50 bits per seconds. Data stream consists of the status of the individual broadcasting satellite and whole satellite configuration data. Satellite clock error and satellite position referred to as satellite ephemeris are of primary importance for the GPS receiver to provided location and timing information. At least four satellites data are required to set a 3D position fix so that the location of the receiver in the earth can be computed.

The GPS receiver calculates its own position based on the orbital information received from satellites and also a local oscillator used inside the GPS receiver will be synchronized with GPS clock [Doberstein 2011]. Once the receiver sets 3D position fix, It will start to send 1PPS followed by NMEA stream through serial data line using RS232 standard. 1PPS signal measured using two GPS receivers (GPS 610 F) at the same location with clear view of sky is shown in Figure 3-35 .

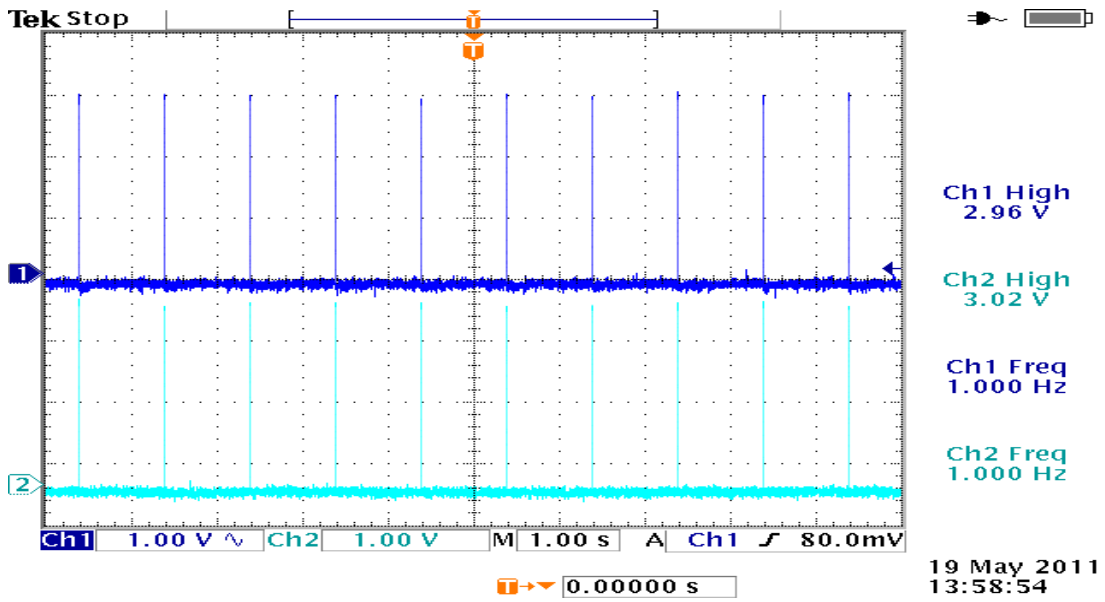


Figure 3-35 1PPS pulse measured from GPS receiver (GPS 610 F)

NMEA stream contains time, position and number of satellites in the range e.tc. Typical decoded NMEA sentence acquired from GPS 610F receiver is shown in Figure 3-36. Detailed list of NMEA commands can be found [Rabbany 2002].

After 3D position fix, if the receiver loses satellite reception 1PPS will be provided from the local oscillator and NMEA stream updates the time using the local oscillator. In this case accuracy of the 1PPS is solely determined by the frequency stability of the local oscillator in the GPS receiver. The local oscillator will be synchronised again once the satellite reception is available. For time base alignment

between PD monitoring systems used in the double ended method using GPS, both 1PPS and NMEA stream are required.

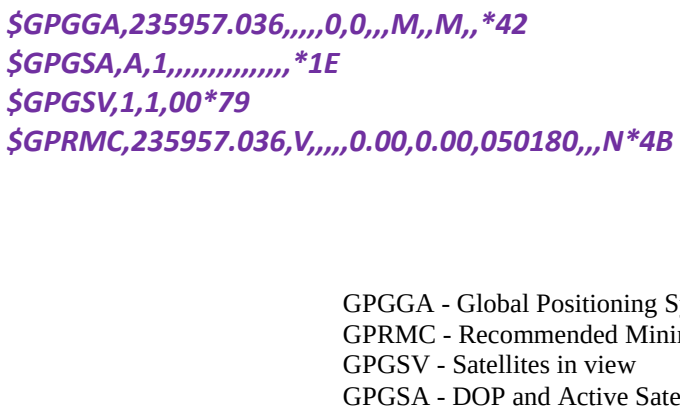


Figure 3-36 Typical NMEA sentence from GPS 610F

The satellites broadcast ranging codes and navigation data on two frequencies L1 (1,575.42 MHz) and L2 (1,227.6 MHz) using CDMA technique. GPS provides two separate services for civil and military users namely SPS on L1 and PPS on L2 respectively. Accuracy of SPS and PPS are the same in space, however PPS users can perform ionospheric correction since PPS uses two different broadcast frequencies. Ionospheric correction is a technique that reduces radio degradation caused by the Earth's atmosphere. With less degradation, PPS provides better accuracy than the basic SPS [Kaplan and Hegarty 2006].

### 3.7.2.2 Other Navigation Systems

Besides GPS, there are other space based navigation systems namely GLONASS operated by Russian Aerospace Defence Forces and the Gallileo satellite navigation system operated by European Space Agency which is in the test phase and expected to fully operate in 2020. Combinations of these GLONASS with GPS enables more comprehensive tool with huge set of services to the end user. GLONASS constellation satellites as on 07.12.2012 consist of 29 satellites in total. GLONASS is based on FDMA unlike CDMA in GPS. Galileo is expected to have more signal strength and be more accurate than GPS [Alkan, Karaman et al. 2005] .

### 3.7.3 Pulse Injection Technique

[Shim, Soraghan et al. 1999] proposed a pulse injection technique for synchronizing the measurement units at both ends of the cable. This method was later used by [Wielen, Veen et al. 2005] . This technique needs two data acquisition cards one at each end of the cable and a pulse injection unit at one end. Technical details of this method can be found (Shim, Soraghan et al. 1999 [wielen 2005]. Fast rising timing pulses are injected at one end of the cable using an inductive coupler such as HFCT or Rogowski coil. Data acquisition systems used at both ends of the cable are triggered by PD pulses from the cable using level triggering. Acquired data contains both PD pulses and timing pulses. By aligning the data sets and making use of the time delay between PD pulse and timing pulse, PD source location can be obtained. This method of time synchronization uses the power cable as transmission medium for timing pulses which is better compared to navigation systems which suffer the drawback of satellite invisibility and atmospheric condition problems. Such intrusive method need to inject pulses into the cable which is depending on the substation layout. In a closed RMU, switch gear is fully bonded with metal screen of the cable which makes it difficult to get access to the earth strap. Also as the accuracy of this method is inversely proportional with the length of the cable due to attenuation and propagation effects and also cost of this method is fairly higher compare to GPS. Most of the substations have built in GPS antennae for DFR, PMU, PQM [Mohamed, Siew et al. 2012]. With the use of these antennas, satellite visibility problem while using GPS can be minimized. Due to these inherent advantages, time synchronization using GPS method is more feasible .

### 3.7.4 Low range wireless synchronization

Many applications of WSN require the measurement nodes to maintain a common notion of time. Data from different measurement nodes often need to be temporarilly correlated in order to extract the information of interest. WSN using WiFi(IEEE/802.11g), Bluetooth(IEEE/802.15.1) and ZigBee(IEEE/802.15.4) using 2.4 GHz ISM license free band are more common in these days. ZigBee is an emerging standard for WSN which implements a LR-WPAN. Low cost battery operated measurement nodes target using ZigBee due to its low cost and low power consumption. [Ferrari, Flammini et al. 2008]. [Liu, Siew et al. 2010] proposed diverse measurement of

radiated transient pulses from substation environment due to switching using distributed measurement nodes which employ wireless time synchronization using ZigBee. [Liu 2009] _ENREF_66 proposed time synchronization WSN using Zigbee and WiFi . This type of wireless synchronization can work in the range of few meters to 100 meters. These methods can't be applied for time synchronization requirement in PD diagnostics. WiMax (IEEE/802.16) is an emerging wireless communication system with large scale coverage of the order of 50 kilometres. This method of wireless communication uses the license free 5.8 GHz band and is installed in underserved areas as well as under developed countries. WiMax peer to peer mode has potential for time synchronization applications [Bojan Angelov 2010]. However propagation delay between the two WiMax modules needs to be quantified.

## 3.8 Which is feasible time synchronization?

In order to locate PD having an accuracy of 1 % of the cable length, time offset error in time base alignment between two PD detectors should be in the order of 100 ns in case of a 2 km long cable (assuming a pulse velocity of 200 m/µs) [Wielen, Veen et al. 2005]. Various methods of time synchronization were discussed in the previous section. In this research project, GPS based time synchronization is applied due to non invasiveness, low cost and required accuracy of 100 ns [Berns and Wilkes 2000].

MRTIE and MTIE are the two important international standards used for specifying clock stability requirements in telecommunication standards. "MTIE is the maximum peak to peak delay variation of a given timing signal with respect to an ideal timing signal within an observation time ($\tau$) for all observation times of that length within a measurement period ($T$)" [Dobrogowski and Kasznia 2002; Riley 2008]. MRTIE is characteristic of the time difference between two timing signals usually having similar quality. In this research project MRTIE between two similar GPS receivers from the same manufacturer is measured for a time period of 1 second having observation interval of two hours with clear vision of sky in the city of Glasgow using the measurement setup shown in Figure 3-37. The measurement setup includes two GPS receivers and a digital storage oscilloscope (DSO) in infinite persistence mode [Hewlett-Packard 1996]. The eye diagram is shown in Figure 3-38.

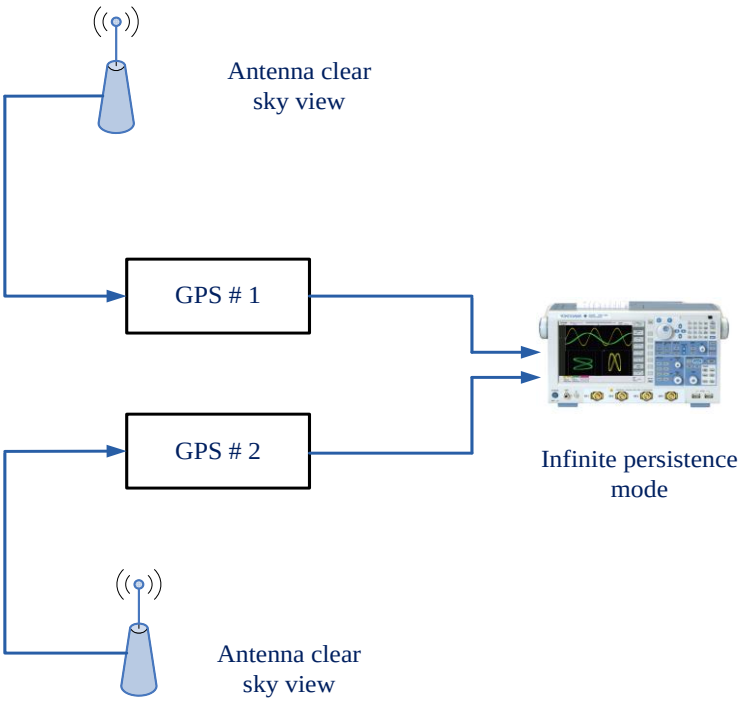


Figure 3-37 Measurement setup for 1 PPS rising edge alignment error

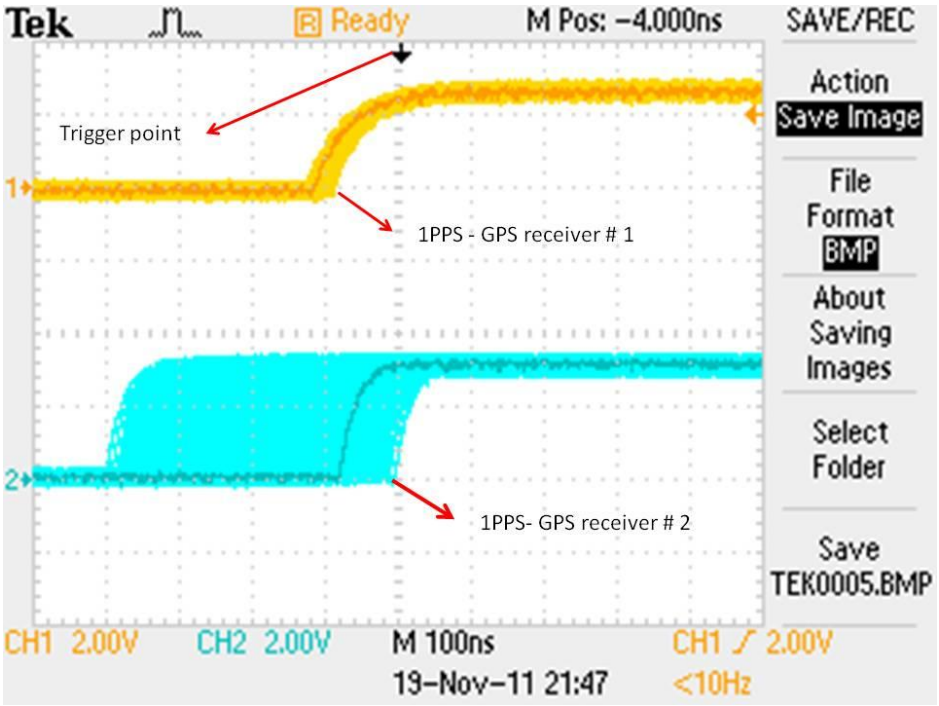


Figure 3-38 MRTIE, GPS receiver with same specification (GPS 610 F)

In Figure 3-38 each division is 100 nsecs. It is observed that MRTIE follows patterns with a maximum drift of approximately 300ns for a duration of 2 hrs. As a

result this error window can alter the PD source location accuracy from 1m to 30m which is based on the velocity of propagation of PD's in PILC cables. The performance of GPS time synchronisation is generally sufficient for most navigation applications in rural and suburban environments. In contrast, urban environments with a high density of tall buildings present a challenging environment for most GPS receivers. In urban areas satellite signals undergo multi path reflections which will degrade the MTIE performance [Soloviev and van Graas 2008]. The cause for the measurement drift includes multi path effect, RF interferrence, satellite data errors, temporary loss of GPS signal, spoofing, changes in the atmospheric conditions e.tc [Kaplan and Hegarty 2006]. Moreover atomic clocks (ceasium, rubidium and hydrogen masor) used in the GPS constellation satellites has a drift of 10^(-11) based on ETSI-ITU standard. Based on ETSI (PRC) mask, GPS constallation clock has a frequency stability of 10^(-11) seconds. This clock will have a total drift of 465.2 ns over a duration of 46520 seconds which is shown in Figure 3-39 [Helwig, Offermans et al. 2006].

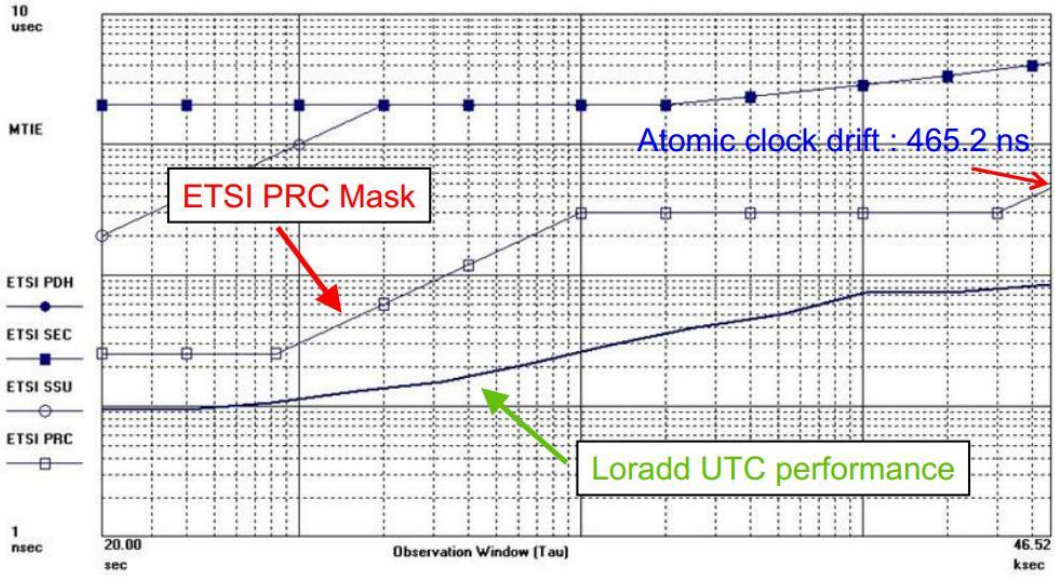


Figure 3-39 ETSI PRC Mask[Helwig, Offermans et al. 2006]

## 3.9 Conclusion

PD measurements in cables are normally done at the cable terminations. PD pulses from discharge source propagate towards the cable terminations. Due to frequency dependent attenuation and dispersion charcateristics of the cable, amplitude and shape of PD pulses get affected. Travelling wave method based on TDR is widely used to locate PD source using single ended and double ended approaches. In this chapter PD location methods based on TDR were studied using PSPICE circuit siumlation. Also various time synchronization methods for double ended PD location were reveiwed with experimental results using GPS receiver.

In single ended method of PD detection time offset between incident and reflected pulse are used to calculate the PD location while in double ended method time offset between incident pulses at both ends of the cable are used to calculate PD location. Based on simulation and experiment results, it has been established that the single ended method is not suitable for on-line PD location since impedance of RMU and cable characteristis limit the accurcay of this method. Therefore, the double ended method of PD location is preferred due to its higher accurcay. However, time synchronization and communication between the measurement units in the double ended PD location method often limits on-line implementation of this technique . In order to locate PD with reasonable accuracy of 10 meters in insulated power cables, it is required to have time base alignment accuracy of 100 nano-seconds approximately based on the velocity of propagation of electromagnetic waves in PILC cables. Hence time synchronization using GPS is applied over the exisiting techniques. However, accurcay of GPS is affected by multi-path effect, RF interferrence, satellite data errors, temporary loss of GPS signal, spoofing, changes in theatmospheric conditions, e.tc.

The pulse selection method discussed in this chapter to separate pulses from multiple PD sources were based on the assumption of same PD incipient voltages. However, multiple PD sources with different inception voltages can be sperated based on their unique energy distribution in time and frequency domain. It is often more challenging to differentiate internal PD's from external PD's. In this chapter, the dual meausrement system method was proposed to differentiate forward and reverse travelling waves uisng high speed DSO's and this method is easy to implement based on the accessibility of earth strap.

# Chapter 4 :
# Signal Processing Techniques for Denoising PD signals in Cables

## 4.1 Introduction

On-line PD measurements were often hampered by various noise sources namely radio transmissions, mobile towers, corona from high voltage equipment, PD from adjacent cables etc. These noise sources make the process of extracting PD from the raw data a more difficult task. In this chapter various signal processing tools used to denoise the raw data are discussed. Denoising techniques using digital filters which includes matched filter, moving average filter and adaptive filter is discussed. The most widely accepted denoising tool for denoising a partial discharge signal using wavelet transform is presented which includes DWT using the dyadic filtering scheme and DWT based on the lifting scheme. Most of the mathematical relations in DWT approach are derived in z domain for better understanding of this approach.

Recently Hibert Huang etal proposed a new data analysis method known as EMD. Though this method is not popular, there could be potential in using this method to denoise PD signals. In this chapter theory of EMD is discussed. Various thresholding methods in signal denoising and various denoising algorithms for denoising PD signals are also discussed.

## 4.2 Matched Filter

Matched filter was introduced in 1940 in the area of radar application. It has become a standard technique for signal detection in the presence of noise [Veen and van der Wiellen 2003]. Matched filters are a basic signal-processing tool for extracting known wavelets from a signal, which is contaminated with noise. These filters are widely used in TDR based application since the prior information-relating incident and reflected pulses are known in advance. Matched filtering is accomplished by cross correlating the signal with the wavelet to be extracted. Consider a signal *s(t)* of length *T* has a wavelet *w(t)* and white noise *n(t)*, then matched filter theory states the maximum

SNR at the output will be achieved when the filter has an impulse response which is simply the time-reverse of the input wavelet *s(t)*. Convolution of time-reversed wavelet with signal is identical to cross correlation. Once the impulse response matches the wavelet to be extracted itself, which is the case for the matched filter, then the filter output signal equals the autocorrelation function of the waveform [Bellanger 2001]. Impulse response of the matched filter is given by

$$h(t) = Aw(T - t)$$

4-1

Where *A* is the gain of the filter.

[Veen and van der Wiellen 2003] proposed semi automated PD detection using matched filter banks. These filter banks includes a range of matched filters with impulse response defined based on the PD propagation model in the cable. Filter kernel based on the PD propagation model includes pulse width of PD wavelet, frequency dependent dispersion, substation impedance and phase response of detection circuit. Further to [Veen and van der Wiellen 2003], [Wagenaars, Wouters et al. 2011] proposed an adaptation algorithm for updating the existing matched filter kernel based on the detected PD pulses. Though this methods updates or creates a new template for a matched filter bank, the adaptation process still depends on the initial filter kernel used. In general, perfect match between the desired pulse shape and the matched filter is required to produce maximum effect. Factors like variation in the PD pulse shapes due to dispersion, similarity in wavelet signature between transient noises and PD reduces the effectiveness of a matched filter when applying on-line PD diagnostics [Foo 2003].

## 4.3 Moving Average Filter

A Moving Average Filter (MAF) operates by averaging a number of points from the input signal to produce each point in the output signal. Mathematical formula of MAF is given by

$$y[i] = \frac{1}{M} \sum_{J=0}^{M-1} x(i + j)$$

4-2

Where *x [i+j]* is the input sequence, *y [i]* is the output sequence and *M* is the number of points in the average. For example, in a 5 point moving average filter, 10 $^{th}$ sample of the output sequence is given by

$$y[10] = \frac{x[10] + x[11] + x[12] + x[13] + x[14]}{5}$$

MAF operation is a convolution of the input signal with a rectangular pulse having an area of one. Frequency Response of MAF is simply the fourier transform of the filter kernel which is rectangular pulse, given by

$$H[f] = \frac{\sin\left(\prod fM\right)}{M \sin\left(\prod f\right)} \qquad 4\text{-}3$$

Where M represents number of taps in the filter. Frequency response of the MAF is shown in Figure 4-1. It exhibits low pass characteristics and the roll off rate is slower and higher stop band ripple for lower value of M. MAF cannot separate one band of frequencies from other. Time domain performance of MAF is as shown in Figure 4-2 and Figure 4-3 using a recursive algorithm for various values of SNR and M.

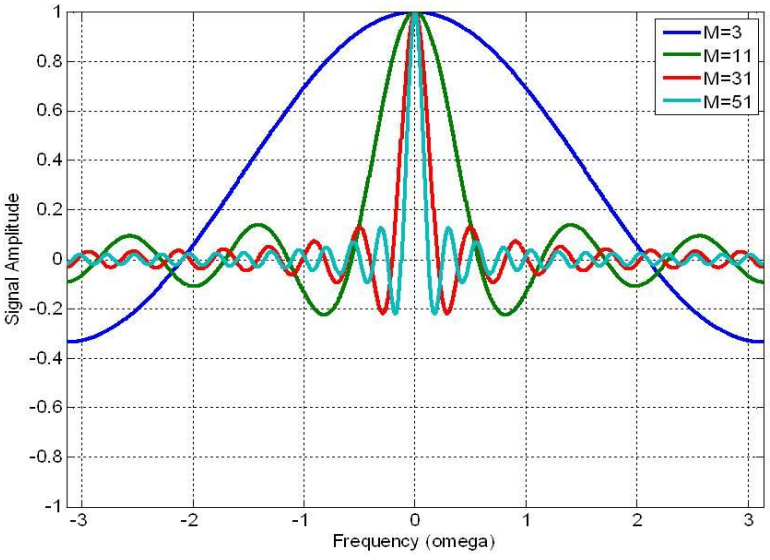


Figure 4-1 Frequency response of MAF

In Figure 4-2 and Figure 4-3, square pulse with blue colour is the original signal while the waveform in red is the extracted signal after applying MAF. Based on Figure 4-2 and Figure 4-3, increased value of M gives higher noise cancellation which leads to loss of edges. Also, the value of M cannot be fixed. Even recursive implementation of this filter consumes more resources in hardware. MAF can be considered as a smoothing filter in time domain. Conversely poor low pass filter frequency domain. This type of filter may introduce error in interpreting and location PD pulses.

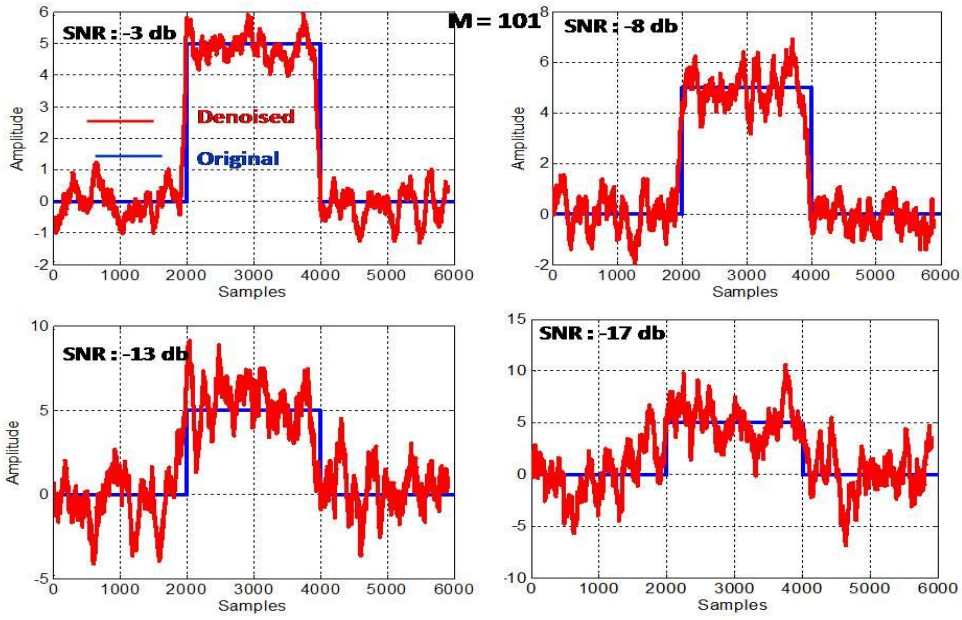


Figure 4-2 Time domain performance of MVF for M=101

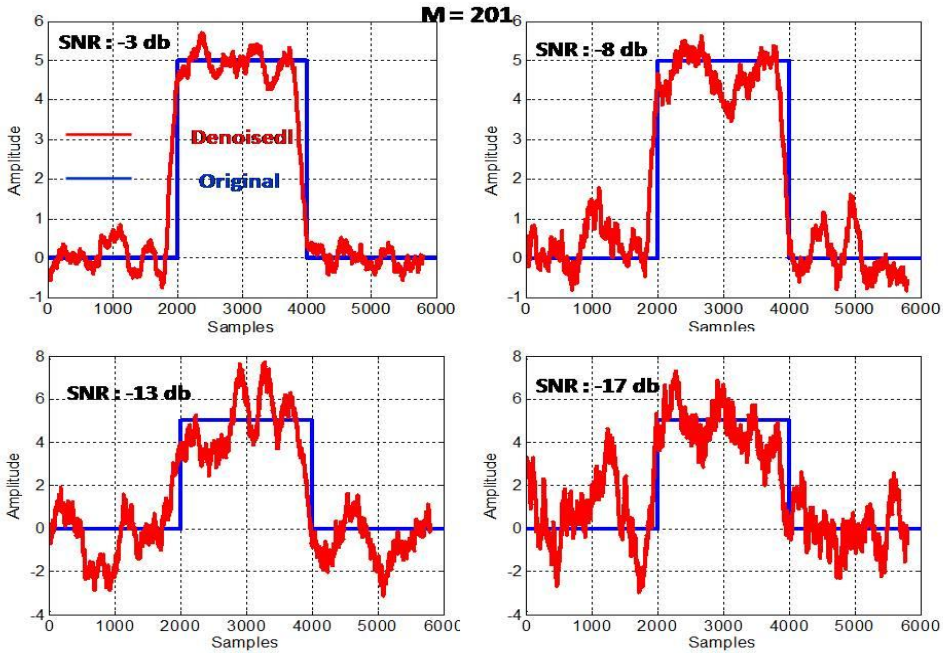


Figure 4-3 Time domain performance of MVF for M=201

## 4.4 Adaptive Filtering

Adaptive filters have been widely used in applications like process control, medical instrumentation, speech processing, echo and noise cancellation, channel equalisation etc. Adaptive filtering for noise removal was first designed at Stanford University [Widrow, Glover et al. 1975]. Adaptive filters are not fixed filters in the sense that filtering coefficients are updated with priory information. This means that an adaptive filter automatically adjusts its own impulse response based on the criteria used in the adaptive algorithm. Basic building blocks of adaptive filtering include digital filter structure, performance evaluator and adaptive algorithm to modify the weights of the filter coefficients in the digital filter. Performance evaluator calculates the error estimate followed by tuning the filter coefficients using the adaptive algorithm. Widely used adaptive algorithms are SDA and LMS [Foley and Boland 1987]. Basic theory behind adaptive noise cancellation is explained as follows [Vaseghi 2000; Bellanger 2001].

Let *H(n)* be the filter coefficients, *y(n)* be the raw data and x(n) be the noise uncorrelated with signal but correlated with noise present in *y(n)* some unknown way

$$H(n)=\begin{bmatrix} h_0(n) \\ h_1(n) \\ . \\ . \\ . \\ h_{N-1}(n) \end{bmatrix}, X(n)=\begin{bmatrix} x(n) \\ x(n-1) \\ . \\ . \\ . \\ x(n+1-N) \end{bmatrix} \quad \text{4-4}$$

$$Y^{\wedge}(n)=H^{T}(n)X(n) \quad \text{4-5}$$

The adaptation algorithm is based on the minimization of the mean square error criterion which is given as

$$E(\varepsilon^{2}(\mathrm{n}))=E\left[\left(Y(n)-Y^{\wedge}(n)\right)^{2}\right] \quad \text{4-6}$$

$$\varepsilon(\mathrm{n})=Y(n)-Y^{\wedge}(n) \quad \text{4-7}$$

Where $\varepsilon(n)$ is the error sequence

Structure of adaptive filter is shown in Figure 4-4

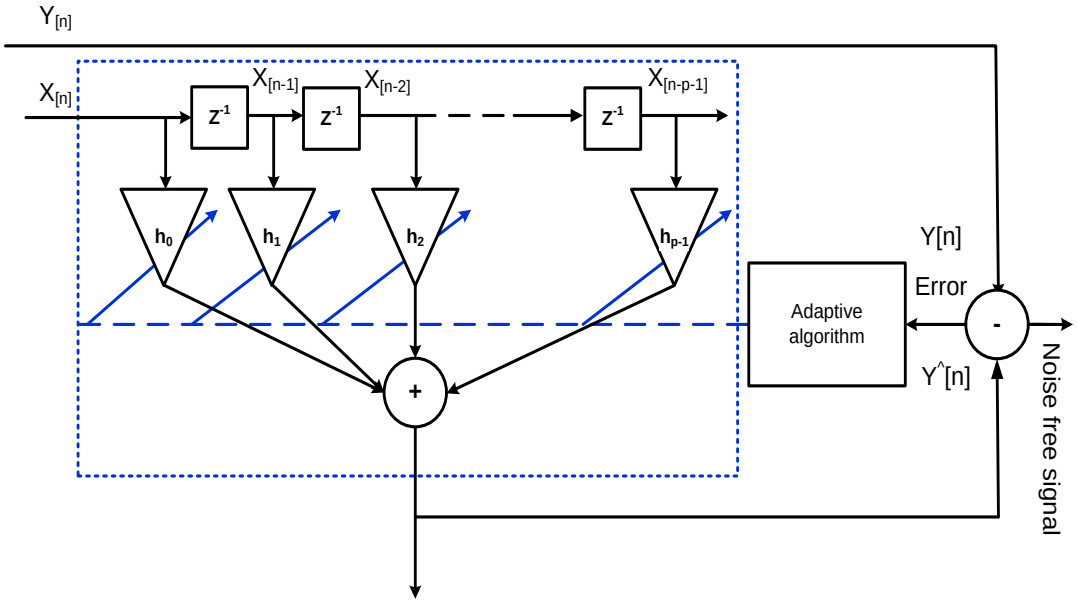


Figure 4-4 Adaptive filter structure

Basically, the adaptive filter needs two inputs to perform noise cancellation. One serves as the primary input *y[n]*, which consists of PD signal and noise. The other input *x[n]* contains mainly noise. This type of filter is mostly suited for estimating stationary signals. An adaptive filter is effective in rejecting stationary noise and becomes less effective in rejecting white noise and switching noise which makes it less suitable for denoising partial discharge signals. [Ferrara and Widrow 1981] proposed a time sequenced adaptive algorithm to extract signals from non stationary noise. Due to the computational complexity and hardware resources requirement, an adaptive filter is not widely used to denoise partial discharge signals.

## 4.5 Wavelet Transforms

Most of the signals we measure day to day are in time domain. In most cases more relevant information is hidden in frequency domain rather than in time domain. For e.g. charcaterization and classification of ECG are obvious in frequency domain [Afonso and Tompkins 1995]. Conversion from time domain to frequency domain is done through Fourier series analysis, devised by by French mathematician Jean Baptist Joseph Fourier. Based on Fourier series analysis, any periodic waveform can be

decomposed into an infinite sum of sine and cosine functions of various frequencies. In the real world most of the signals are aperiodic in nature. This aperiodic or non periodic nature can be used to resolve the complex spectrum of frequencies known as Fourier Transform. This is similar to a sunlight which can be split-up into colours (VIBGYOR) of various frequencies [Ramachandran 2000]. In case of discrete time signals, Fourier transform is termed as DFT and is given by

$$X(k) = \sum_{n=0}^{N-1} x[n] e^{\left(\frac{-j2\pi kn}{N}\right)}, k = 0,1,...N-1$$

4-8

Where *x[n]* is a discrete sequence and *N* is the length of sequence. Due to increased computational time required for DFT, FFT is used,which is an algorithm for fast computation of DFT. So FT can convert time domain information contained in a signal to frequency domain. However FT cannot provide time frequency localization of the signal of interest. The problem of time-frequency localization leads to the development of the windowed Fourier transform known as STFT. STFT extracts time vs frequency information contained in a signal over short time duration window in which the signal is assumed to be stationary.

STFT involves multiplying the signal *f(t)* with a compactly supported window function ω, centred around 0, followed by computing the Fourier coefficients of the product *g(t)* . These coefficients give an indication of the frequency content of the signal f in the neighbourhood of $t = 0$. This procedure is then repeated with translated versions of the window function (i.e., *g(t)* is replaced by $\omega(t + to)$, $\omega(t + 2t)$ [Daubechies 1990]. STFT of a time domain signal x(t) is given by

$$STFT(t, f) = \int_t x(t) * \omega(t - nt_0) e^{-jm\omega_0 t} dt, \quad (m, n \in Z)$$

4-9

Figure 4-5 shows STFT of signal having frequency components 80 Hz and 160 Hz at different times along the time axis. Both frequencies can be seen in FT plot, while frequency vs time information can be seen in STFT plot.

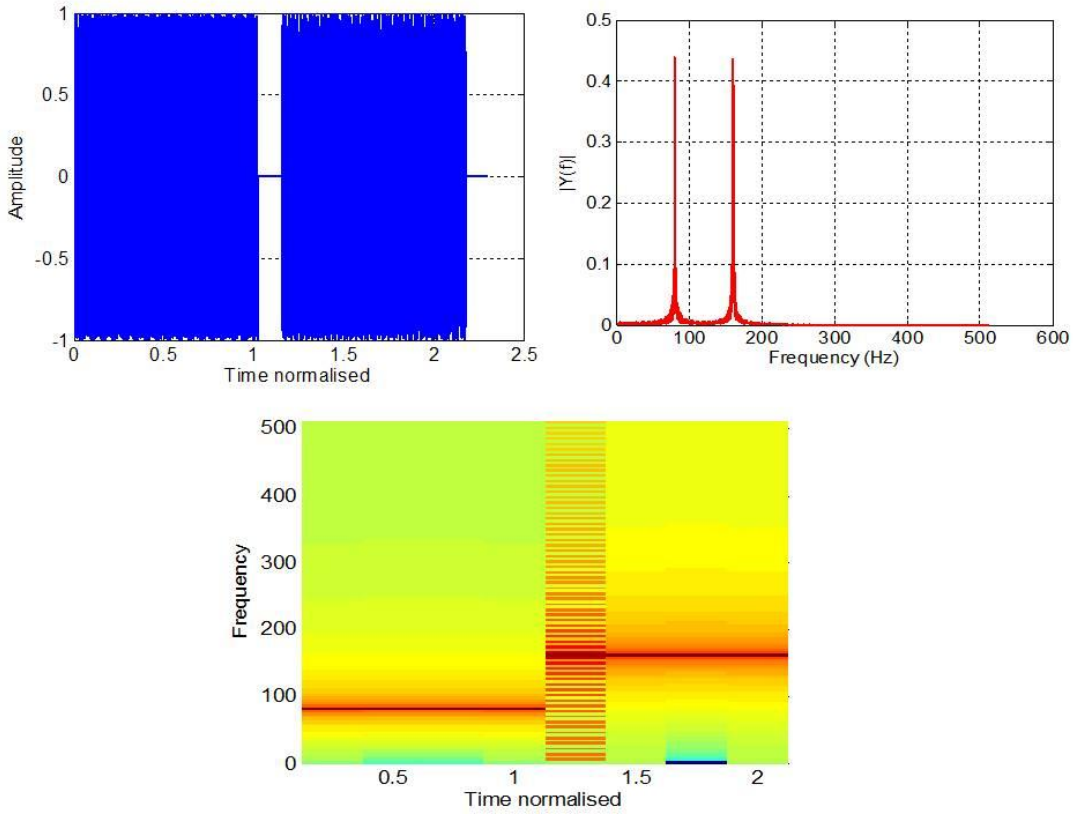


Figure 4-5 STFT of non stationary signal

STFT suffers a problem of time and frequency resolution which goes back to the Heisenberg uncertainty principle which states that exact time vs. frequency information of a signal can not be obtained in practice. However time duration vs frequency band can be obtained at one place by compromising the resolution in time and frequency domain. Since window function used in STFT is of fixed duration, time and frequency resolution cannot be met at one place. Although the time and frequency resolution issues are results of a physical phenomenon regardless of the transform used, it is possible to analyze any signal by using an alternative approach termed as MRA. As the name suggests, in MRA, a signal is viewed at various levels of approximations or resolutions. The idea was developed by Meyer and Mallat. By applying the MRA , a signal can divided into several simpler ones and studied separately. Signals which exhibit in nature are high frequency pulses which exists for short duration and low frequency signals which exists for longer durations. So MRA is designed to give good time resolution and poor frequency resolution at higher frequencies while good frequency resolution and poor time resolution at low frequencies. There are several instances of functions which can be used for MRA. All of these functions are termed as

wavelets. Wavelets have been widely used by researchers for isolation and manipulation of specific patterns hidden from the mass of data. Though the signal processing community started to apply wavelets in the late 1990s, the use of wavelets was as far back to 1909 by a Hungarian Mathematician Alfred Haar which is now known as Haar wavelets [Jaideva C. Goswami 2010].

### 4.5.1 Continuous Wavelet Transform

CWT on a signal produces wavelet coefficients by scaling and shifting versions of the mother wavelet with convolution. The wavelet coefficients are decomposed into frequency scales, which are weighted by the similarities or correlation of the wavelet function and the input signal. CWT of a function x(t) is given by

$$CWT(s,\tau) = \frac{1}{\sqrt{s}} \int x(t) * \psi(\frac{t-\tau}{s}) dt$$

4-10

$\psi(\frac{t-\tau}{s})$,wavelet basis function or mother wavelet
$\tau$,Scaling operator
$s$,Shifting operator

CWT transforms a continuous signal into a wavelet domain defined by variables $\tau$ and $s$. Once the wavelet basis function is chosen, the computation starts with s= 1 by placing the mother wavelet at t=0 in the signal. The Mother wavelet function is multiplied with the signal and integrated over time followed by energy normalization. This procedure is repeated until the wavelet reaches the end of the signal. One row of points on the time-scale plane for the scale $s$=1 is now completed. Then $s$ is increased by a small value and the procedure is repeated. Every computation for a given value of $s$ fills the corresponding single row of the time- scale plane. When the process is completed for all desired values of $s$, the CWT of the signal is over. So shifting the wavelet in time based on τ gives time localization while changing the value of s (compressed or dilated) gives frequency localization. Lower value of $s$ corresponds to better time resolution and poor frequency resolution and vice versa. In order to compute CWT using a computer, it is necessary to discretize the time and scale axis. In this case, CWT is the discrete version or sampled version of CWT [Jaideva C. Goswami 2010]. As usual any transform needs to be bilateral. The original signal can be perfectly

reconstructed from the wavelet coefficients. For successful reconstruction, admissibility condition needs to be satisfied which is given by

$$C\phi = \int \frac{|\phi(\omega)|2}{\omega} \partial\omega \langle \infty$$

4-11

Where,

$$\phi(\omega) = F(\phi(t))$$

Mathematical Expression for reconstruction process is as follows

$$x(t) = \frac{1}{C\phi 2} \iint_{s\tau} \Psi_x^{\phi}(\tau, s) \frac{1}{s^2} \psi\left(\frac{t-\tau}{s}\right) \partial\tau \partial s$$

4-12

In sampled or discretized CWT, the parameters $\tau$ and $s$ are varied in steps which lead to data redundancy. Such data redundancy causes increased computation time and high usage of hardware resources. Such data redundancy problem makes CWT approach difficult to implement for signals having higher data length.

### 4.5.2 Discrete Wavelet Transform

The data redundancy problem in discretised CWT is solved by Mallat by implementing dyadic filtering schemes. Mallat's algorithm is also known as the classical two channel sub-band coding scheme [Mallat 1989]. A Sub-band coding scheme will split the frequency band of the signal into various sub-bands and the filters used are QMFs. A two channel filter bank with perfect reconstruction is shown in Figure 4-6. It consists of a pair of analysis (high pass, $H_0$ and low pass, $H_1$) and synthesis (high pass, $G_0$ and low pass, $G_1$) filters. Decimation or down sampling, Interpolation or up sampling are the part of multi rate signal processing [Rad 2003]. In the sub-band coding scheme, the input signal is split into two bands, low-frequency and high-frequency using analysis filters. Frequency responses of the analysis filters $H_0$ and $H_1$ are shown in Figure 4-7.

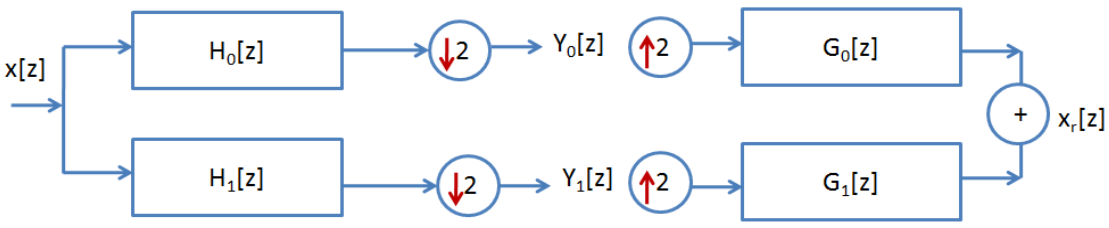


Figure 4-6 Two channel filter bank with perfect reconstruction

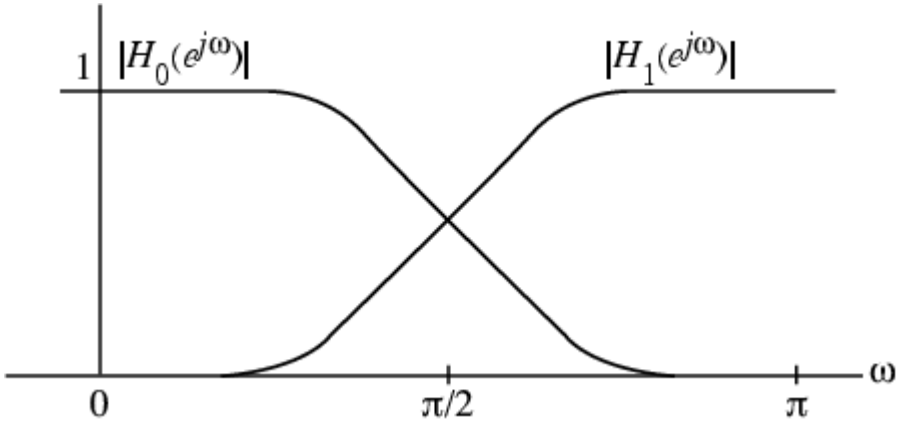


Figure 4-7 Frequency response of analysis filters

Wavelet filters are not ideal brick wall filters so frequency responses overlap each other at the stop band due to transition bandwidth. So the down sampled signals $Y_0$ and $Y_1$ are not perfectly band limited which will have an impact on the perfect reconstruction. However by properly choosing the synthesis filters, perfect reconstruction can be achieved. Analysis of these filter structures is discussed below. Mathematical formulae of upsampling and downsampling are included in the Appendix B.

Down sampling operation of sequence *x[n]* in frequency domain is given by

$$X_e(z) = \frac{1}{2}\left\{X(z^{1/2}) + X(-z^{1/2})\right\}$$

Referring to Figure 4-6

$$Y_0(z) = \frac{1}{2}\left\{H_0(z^{1/2})X(z^{1/2}) + H_0(-z^{1/2})X(-z^{1/2})\right\} \quad 4\text{-}13$$

$$Y_1(z) = \frac{1}{2}\left\{H_1(z^{1/2})X(z^{1/2}) + H_1(-z^{1/2})X(-z^{1/2})\right\} \quad 4\text{-}14$$

$$\begin{pmatrix} Y_0(z) \\ Y_1(z) \end{pmatrix} = \left(\frac{1}{2}\right)\begin{pmatrix} H_0(z^{1/2}) & H_0(-z^{1/2}) \\ H_1(z^{1/2}) & H_1(-z^{1/2}) \end{pmatrix}\begin{pmatrix} X(z^{1/2}) \\ X(-z^{1/2}) \end{pmatrix}$$

4-15

Up sampling operation in frequency domain is given by

$$X_u(z) = X\left(z^2\right) \text{ [ Ref Appendix B]}$$

$$X_r(z) = \left\{Y_0\left(z^2\right)G_0(z) + Y_1\left(z^2\right)G_1(z)\right\}$$

4-16

$$Y_0(z^2) = \frac{1}{2}\left\{X(z)H_0(z) + X(-z)H_0(-z)\right\}$$

4-17

$$Y_1(z^2) = \frac{1}{2}\left\{X(z)H_1(z) + X(-z)H_1(-z)\right\}$$

4-18

Upon substituting 4-17 and 4-18 in 4-16

$$X_r(z) = \left[\frac{1}{2}\left\{X(z)H_0(z) + X(-z)H_0(-z)\right\}G_0(z)\right] + \left[\frac{1}{2}\left\{X(z)H_1(z) + X(-z)H_1(-z)\right\}G_1(z)\right]$$

$$= X(z)\left\{\frac{H_0(z)G_0(z) + H_1(z)G_1(z)}{2}\right\} + X(-z)\left\{\frac{H_0(-z)G_0(z) + H_1(-z)G_1(z)}{2}\right\}$$

4-19

For perfect reconstruction, $X_r(z) = X(z)$.

This gives the condition for perfect reconstruction as

$$H_0(z)G_0(z) + H_1(z)G_1(z) = 2$$

4-20

and aliasing term or mirror image *X(-z)* should be zero, which leads to

$$H_0(-z)G_0(z) + H_1(-z)G_1(z) = 0$$

4-21

Condition for perfect reconstruction is given by

$$\underbrace{\begin{pmatrix} H_0(z) & H_1(z) \\ H_0(-z) & H_1(-z) \end{pmatrix}}_{D(z)} \begin{pmatrix} G_0(z) \\ G_1(z) \end{pmatrix} = \begin{pmatrix} 2 \\ 0 \end{pmatrix}$$

4-22

Where $H_m$ (z) is modulation matrix of analysis filter. Synthesis filters $G_0$ and $G_1$ can be computed as follows. In order to solve this

$D(z) = \begin{pmatrix} H_0(z) & H_1(z) \\ H_0(-z) & H_1(-z) \end{pmatrix}$ should be invertible.

Filters $H_0(z)$and $H_1(z)$ are FIR filters and $D(z)$ will hold Laurent polynomial. For $D(z)$ to be invertible, $|D(z)| = [H_0(z)H_1(-z) - H_0(-z)H_1(z)]$ should be monomial.

Let

$$\begin{aligned} |D(-z)| &= [H_0(-z)H_1(z) - H_1(-z)H_0(z)] \\ &= -[H_0(z)H_1(-z) - H_0(-z)H_1(z)] \\ &= -|D(z)| \end{aligned}$$

$H_0(z)$ is even , such that $H_0(z) = H_0(-z)$

$H_1(z)$ is odd , such that $-H_1(z) = H_1(-z)$

Hence $D(z)$ is odd. Monomial $|D(z)|$ can be expressed as

$$\begin{aligned} |D(z)| &= \frac{2}{cz^{(2k+1)}} \\ &= 2c^{-1}z^{-(2k+1)} \end{aligned}$$

Upon applying crammers rule

$$\begin{aligned} G_0(z) &= \frac{\begin{pmatrix} 2 & H_1(z) \\ 0 & H_1(-z) \end{pmatrix}}{|D(z)|} \\ &= \frac{\begin{pmatrix} 2 & H_1(z) \\ 0 & H_1(-z) \end{pmatrix}}{2c^{-1}z^{-(2k+1)}} \\ &= \frac{2H_1(-z)}{2c^{-1}z^{-(2k+1)}} \end{aligned}$$

$$= cz^{(2k+1)}H_1(-z)$$

Similarly $G_1(z)$ can be obtained as

$$G_1(z) = \frac{\begin{pmatrix} H_0(z) & 2 \\ H_0(-z) & 0 \end{pmatrix}}{|D(z)|}$$

$$= \frac{\begin{pmatrix} H_0(z) & 2 \\ H_0(-z) & 0 \end{pmatrix}}{2c^{-1}z^{-(2k+1)}}$$

$$= \frac{-2H_0(-z)}{2c^{-1}z^{-(2k+1)}}$$

$$= -cz^{(2k+1)}H_0(-z)$$

$$G_0(z) = cz^{(2k+1)}H_1(-z) \qquad \text{4-23}$$

$$G_1(z) = -cz^{(2k+1)}H_0(-z) \qquad \text{4-24}$$

This is how the dyadic filtering operation is performed. A dyadic filtering scheme can be applied in multi level. The number of levels depend on the features to be extracted. Multi level DWT analysis and synthesis tree are shown in Figure 4-8 and Figure 4-9 respectively.

DWT suffers from the drawback of shift variant or translational variance. Shift variance causes two similar transient signals which are considerably different even if the two signals just differ by time shift. Shift variance is caused by the critical sampling used in classical DWT algorithm discussed above which makes the signature and energy conserved in the wavelet coefficients highly depend upon the position in the critical sampling space. This property will distort the reconstructed waveform to a higher extent [Foo 2003]. The shift variant property of DWT will have implications on transient analysis and pattern recognition. In the context of PD, shift variance properties of DWT has implications in identifying the edge of PD pulses which will introduce PD source location errors [Wasim Ahma 2010]. Various research methods has been proposed in recent years to solve the shift variant problem in DWT and most of the methods bypass the dyadic decimation steps [Pesquet, Krim et al. 1996]. These schemes enable the restoration of shift invariance in wavelet domain, but they increase the computational complexity and data redundancy. In addition to that, convolving signal with filter kernel in multiple level of decomposition as in DWT needs higher hardware resources when implementing in real time systems.

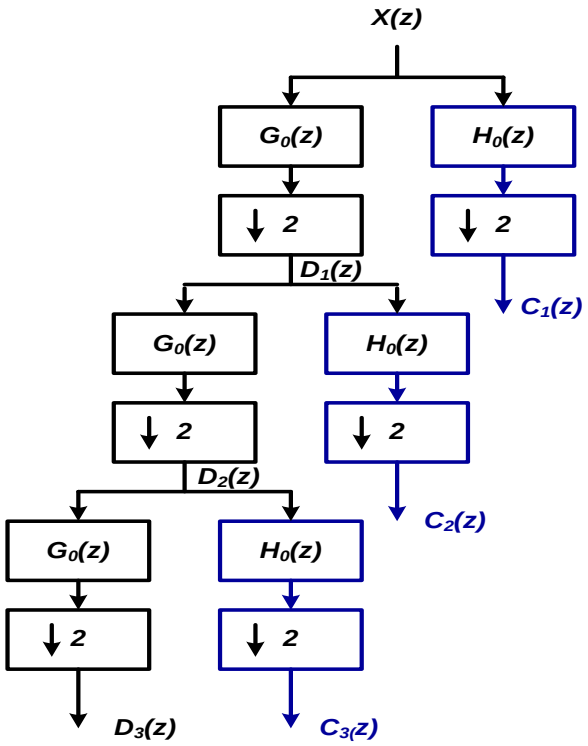


Figure 4-8 Three level DWT analysis tree

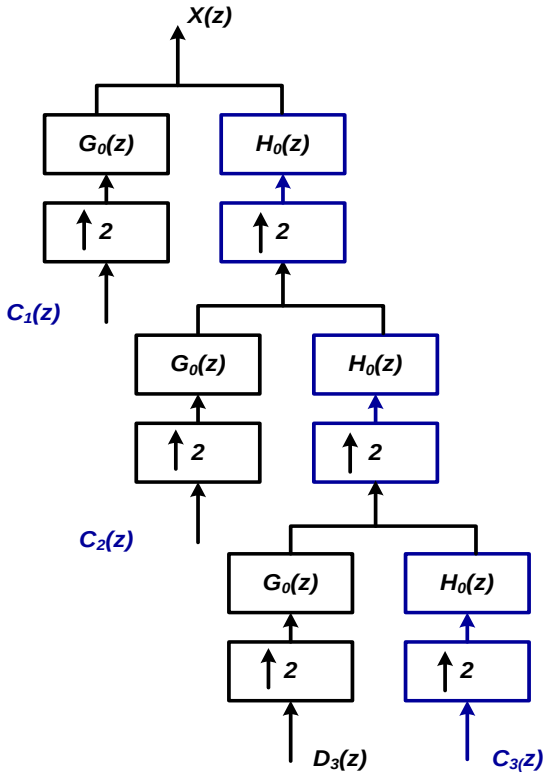


Figure 4-9 Three level DWT synthesis tree

*H(z)* - High pass filter, *C(z)* detail coefficient
*G(z)* - Low pass filter, *D(z)* approximation coefficient

## 4.6 Discrete Wavelet Transform by Lifting

Wavelets have been proved to be a highly versatile tool in various applications namely, signal and image processing, data compression, data transmission, and noise reduction. Traditional wavelets or classical wavelets translates or dilates one particular function. Mallat and Meyer provided the connection between sub-band filters and wavelets which enabled a fast way of computing wavelet transform. Later many wavelet families were introduced. All of these wavelet basis or mother wavelet are generated using fourier transform. This is known as first generation wavelets.

In this thesis DWT decomposition based on the lifting scheme is used which is also knows as SGWT. So lifting is explained on the basis of feature extraction rather than wavelet generation. Lifting scheme is completely spatial unlike classical wavelet scheme which needs frequency analysis. Though lifting is a technique for wavelet generation it can also be applied to DWT decomposition since it preserves reversibility [Sweldens 1996] [Song 2009]. Lifting scheme involves three steps namely split, predict and update. Using lifting scheme, wavelet filters can be created adaptively using the prediction and update process.

### 4.6.1 Splitting

The Splitting process divides an input sequence x[n] into two disjoint subsets. This means splittng the signal x[n] into even and odd indexed sequences [Claypoole, Baraniuk et al. 1998].

Let a finite sequence

$$x[n], n = 0,1,2,3.....$$

$$x_e[n] = x[2n] \qquad \text{4-25}$$

$$x_o[n] = x[2n+1] \qquad \text{4-26}$$

Where $x_e[n]$ and $x_o[n]$ are even and odd indexed sequences.

$$Z(x_e[n]) = X_e(z) = \sum_n x[2n]z^{-n}$$

*substitute* $2n = k$

$$= \sum_k \frac{1}{2}\left\{x[k]\left[z^{1/2}\right]^{-k} + x[k]\left[-z^{-1/2}\right]^{-k}\right\}$$

$$X_e(z) = \frac{1}{2}\left\{X(z^{1/2}) + X(-z^{1/2})\right\}$$

4-27

Odd sequence is given by

$$Z(x_o[n]) = X_o(z) = \sum_n x[2n+1]z^{-n}$$

*substitute* $2n+1 = k$

$$X_o(Z) = \sum_n x[k]z^{-\left(\frac{K-1}{2}\right)}$$

$$= \sum_n x[k]z^{-\left(\frac{K}{2}\right)}z^{\left(\frac{1}{2}\right)}$$

$$= Z^{\left(\frac{1}{2}\right)}\left\{\sum_n x[k]z^{-\left(\frac{K}{2}\right)}\right\}$$

$$= \left(\frac{z^{\left(\frac{1}{2}\right)}}{2}\right)\left[\sum_k \left\{x[k]\left[z^{1/2}\right]^{-k} + x[k]\left[-z^{-1/2}\right]^{-k}\right\}\right]$$

$$\left(\frac{z^{\left(\frac{1}{2}\right)}}{2}\right)\left\{X(z^{1/2}) + X(-z^{1/2})\right\}$$

$$= z^{\left(\frac{1}{2}\right)}X_e(z)$$

$$X_o(z) = \frac{z^{\left(\frac{1}{2}\right)}}{2}\left\{X(z^{1/2}) + X(-z^{1/2})\right\}$$

4-28

Even and odd polyphase components are highly correlated and it should be possible to accurately predict each odd polyphase coefficient from the nearby even polyphase coefficients.

### 4.6.2 Prediction

Prediction gives the detail coefficient similar to convolution based DWT which can be written as ,

Detail coefficient = Odd sample + Prediction filter (Even samples)

$$d[n] = x_o[n] + P(x_e[n])$$

4-29

Where $d[n]$ : detailed coefficient

$x_o[n]$ : odd sequence

$x_e[n]$ : even sequence

$P$ : prediction filter or prediction operator

Prediction operator $P$ which depends on the lifting scheme used. Based on the lifting scheme CDF (2, 2) (named after: Cohen, Daubechies and Feauveau), detail coefficient is given by

$$x[2n+1] - \frac{\{x[2n] + x[2n+2]\}}{2}$$

4-30

Converting back to z domain

$$= z\left(x[2n+1]\right) - \frac{\{z\left(x[2n]\right) + z\left(x[2n+2]\right)\}}{2}$$

$$z\left(x[2n+1]\right) - \frac{\{z\left(x[2n]\right) + z^2\left(x[2n]\right)\}}{2}$$

$$= X_0(z) - \left(\frac{X_e(z) + zX_e(z)}{2}\right)$$

4-31

Where

where $z\left(x[2n+1]\right) = X_0(z)$, odd samples

$z\left(x[2n]\right) = X_e(z)$, even samples

$z\left(x[2n+2]\right) = zX_e(z)$, means shifting the even samples to one index left

Now

$$= X_0(z) - \left(\frac{1+z}{2}\right) X_e(z)$$

$$= X_0(z) - T(z) X_e(z)$$

4-32

Where

$$T(z) = \left(\frac{1+z}{2}\right)$$

4-33

Eq 4-33 can be wrteen as using the relation , $Z(x_e[n]) = X_e(z) = \sum_n x[2n] z^{-n}$

$$\left(\frac{1+z}{2}\right) X_e(z) = \frac{1}{2}\left\{\sum_n \left[x[2n] z^{-n} + x[2n+2] z^{-n}\right]\right\}$$

Eq 4-32 can be wrteen as using the relation , $Z(x_o[n]) = X_o(z) = \sum_n x[2n+1] z^{-n}$

$$\left(X_o(z) - T(z) X_e(z)\right) = \sum_n x[2n+1] z^{-n} - \left\{\frac{1}{2}\left[\sum_n \left[x[2n] z^{-n} + x[2n+2] z^{-n}\right]\right]\right\}$$

$$= \sum_n \left\{x[2n+1] - \frac{x[2n]}{2} - \frac{x[2n+2]}{2}\right\} z^{-n}$$

Transition of $\begin{pmatrix} X_e(z) \\ X_o(z) \end{pmatrix}$ resulted from splitting process

to $\begin{pmatrix} X_e(z) \\ X_0(z) - T(z) X_e(z) \end{pmatrix}$ resulted from prediction based on CDF (2, 2)

$$\begin{pmatrix} Xe(z) \\ X_0(z) - T(z) X_e(z) \end{pmatrix} = \begin{pmatrix} 1 & 0 \\ -T(z) & 1 \end{pmatrix} \begin{pmatrix} X_e(z) \\ X_o(z) \end{pmatrix}$$

4-34

This implies that , prediction is simply multiplication of $\begin{pmatrix} X_e(z) \\ X_o(z) \end{pmatrix}$ with $\begin{pmatrix} 1 & 0 \\ -T(z) & 1 \end{pmatrix}$

where $T(z) = \left(\frac{1+z}{2}\right)$ based on CDF(2,2)

$$P(z)=\begin{pmatrix} 1 & 0 \\ -T(z) & 1 \end{pmatrix}$$

4-35

where $P(z)$ is prediction filter
Predication operation can be written as

$$\begin{pmatrix} X_e(z) \\ X_o(z) \end{pmatrix} = \begin{pmatrix} 1 & 0 \\ -T(z) & 1 \end{pmatrix} \begin{pmatrix} X_e(z) \\ X_o(z) \end{pmatrix}$$

4-36

### 4.6.3 Update operation

Update operation gives approximation coefficients similar to convolution based DWT. This can be written as

Approximation coefficient = Even sample + Update filter (Detail coefficient)

$$c[n]=x_e[n]+U(d[n])$$

4-37

Where c[n] : approximation coefficient
$x_e$[n] : even sequence
d[n] : detail coefficient
U : Update filter or update operator

In Z domain eq (4-39) can be written as

$$C[z]=X_e[z]+U(D[z])$$

4-38

Based on CDF (2, 2), (named after: Cohen, Daubechies and Feauveau) update operator is given by

$$U(D_i)=\frac{1}{4}(D_{i-1}+D_i)$$

4-39

In Z domain, 4-39 can be written as

$$U(z)=\left[\frac{1+z^{-1}}{4}\right]$$

This gives

$U(d[n])$ using 4-39 and eq 4.6-5

$$U[D(z)] = \left[\frac{1+z^{-1}}{4}\right] \underbrace{\{X_0(z) - T(Z)X_e(z)\}}_{\text{Prediction block , Detail coefficients}} \qquad 4\text{-}40$$

Let $S(z) = \left[\frac{1+z^{-1}}{4}\right]$

$$U[D(z)] = S(z)[X_0(z) - T(z)X_e(z)]$$

$$= S(z)X_0(z) - S(z)T(z)X_e(z) \qquad 4\text{-}41$$

Upon substituting Eq (4-41) in Eq 4-38 gives

$$C(z) = X_e(z) + S(z)X_0(z) - S(z)T(z)X_e(z)$$
$$= X_e(z)\{1 - S(z)T(z)\} + S(z)X_0(z)$$

Update operation can be expressed in matrix form as as

$$\begin{pmatrix} X_o(z) \\ X_e(z)\{1 - S(z)T(z)\} + S(z)X_o(z) \end{pmatrix} = \begin{pmatrix} 1 & 0 \\ S(z) & 1 - S(z)T(z) \end{pmatrix} \begin{pmatrix} X_o(z) \\ X_e(z) \end{pmatrix} \qquad 4\text{-}42$$

$$U(z) = \begin{pmatrix} 1 & 0 \\ S(z) & 1 - S(z)T(z) \end{pmatrix} \qquad 4\text{-}43$$

This implies that update opeation is

multiplying the $\begin{pmatrix} X_o(z) \\ X_e(z) \end{pmatrix}$ with $\begin{pmatrix} 1 & 0 \\ S(z) & 1 - S(z)T(z) \end{pmatrix}$

From prediction

$$\begin{pmatrix} X_e(z) \\ X_o(z) \end{pmatrix} = \begin{pmatrix} 1 & 0 \\ -T(z) & 1 \end{pmatrix} \begin{pmatrix} X_e(z) \\ X_o(z) \end{pmatrix} \qquad 4\text{-}44$$

From updation

$$\begin{pmatrix} X_e(z) \\ X_o(z) \end{pmatrix} = \begin{pmatrix} S(z) & 1-S(z)T(z) \\ 1 & 0 \end{pmatrix} \begin{pmatrix} X_o(z) \\ X_e(z) \end{pmatrix}$$

4-45

Splitting and update operation in combined form can be written as

$$\begin{pmatrix} X_e(z) \\ X_o(z) \end{pmatrix} = \begin{pmatrix} S(z) & 1-S(z)T(z) \\ 1 & -T(z) \end{pmatrix} \begin{pmatrix} X_o(z) \\ X_e(z) \end{pmatrix}$$

$$\begin{pmatrix} X_e(z) \\ X_o(z) \end{pmatrix} = \begin{pmatrix} 1-S(z)T(z) & S(z) \\ -T(z) & 1 \end{pmatrix} \begin{pmatrix} X_e(z) \\ X_o(z) \end{pmatrix}$$

$$\begin{pmatrix} X_e(z) \\ X_o(z) \end{pmatrix} = \begin{pmatrix} 1 & S(z) \\ 0 & 1 \end{pmatrix} \begin{pmatrix} 1 & 0 \\ -T(z) & 1 \end{pmatrix} \begin{pmatrix} X_e(z) \\ X_o(z) \end{pmatrix}$$

4-46

Prediction followed by update operation means multiplying

$$\begin{pmatrix} X_e(z) \\ X_o(z) \end{pmatrix} \text{ with } \begin{pmatrix} 1 & S(z) \\ 0 & 1 \end{pmatrix} \begin{pmatrix} 1 & 0 \\ -T(z) & 1 \end{pmatrix}$$

Prediction filter is given by $P(z) = \begin{pmatrix} 1 & 0 \\ -T(z) & 1 \end{pmatrix}$

Updation Filter is given by $U(z) = \begin{pmatrix} 1 & S(z) \\ 0 & 1 \end{pmatrix}$

$S(z)$ and $T(z)$ are Laurent polynomials

Z transform representation of lifting filters (prediction, update repeated N times) and normalization can be written as

$$H(z) = \begin{pmatrix} K & 0) \\ 0 & K^{-1} \end{pmatrix} \begin{pmatrix} 1 & S_N(z) \\ 0 & 1 \end{pmatrix} \begin{pmatrix} 1 & 0 \\ -T_N(z) & 1 \end{pmatrix} \cdots \begin{pmatrix} 1 & S_1(z) \\ 0 & 1 \end{pmatrix} \begin{pmatrix} 1 & 0 \\ -T_1(z) & 1 \end{pmatrix}$$

4-47

S(z) and T(z) were defined from CDF (2,2)

Matrix H(Z) is populated with laurent polynomial and can be written as polyphase form as

$$H(z)=\begin{pmatrix} H_{00}(z) & H_{01}(z) \\ H_{10}(z) & H_{11}(z) \end{pmatrix}$$

4-48

Block diagram representation of forward lifting scheme is shown in Figure 4-10.

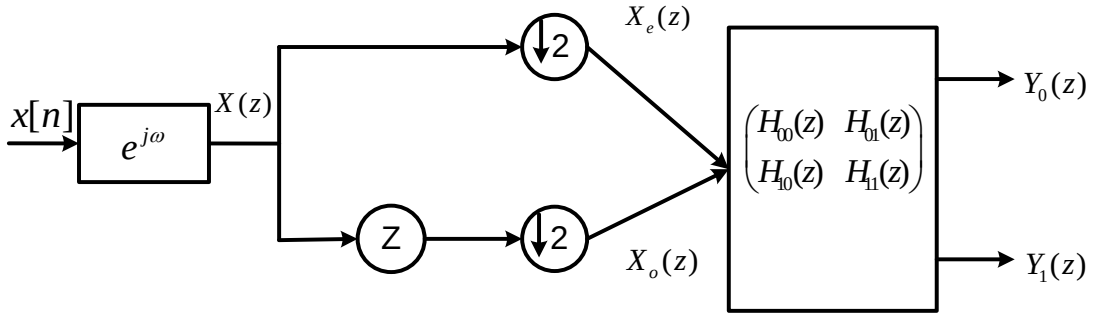


Figure 4-10 Forward lifting scheme

where

$$\begin{pmatrix} H_{00}(z) & H_{01}(z) \\ H_{10}(z) & H_{11}(z) \end{pmatrix}=\begin{pmatrix} K & 0) \\ 0 & K^{-1} \end{pmatrix}\begin{pmatrix} 1 & S_N(z) \\ 0 & 1 \end{pmatrix}\begin{pmatrix} 1 & 0 \\ -T_N(z) & 1 \end{pmatrix}\cdots\begin{pmatrix} 1 & S_1(z) \\ 0 & 1 \end{pmatrix}\begin{pmatrix} 1 & 0 \\ -T_1(z) & 1 \end{pmatrix}$$

### 4.6.4 Invertibility of lifting filters

It is necessary requirement that every transform should be invertible. From eq(4-35) and eq(4-43)

$$P(z)=\begin{pmatrix} 1 & 0 \\ -T(z) & 1 \end{pmatrix}$$

$$U(z)=\begin{pmatrix} 1 & S(z) \\ 0 & 1 \end{pmatrix}$$

$$[P(z)]^{-1}=\begin{pmatrix} 1 & 0 \\ T(z) & 1 \end{pmatrix}$$

$$[U(z)]^{-1}=\begin{pmatrix} 1 & -S(z) \\ 0 & 1 \end{pmatrix}$$

$$\left[U(z)P(z)\right]^{-1}=\left[P(z)\right]^{-1}\left[U(z)\right]^{-1}$$

4-49

Invertible filter for *N* level for *H(z)* in can be written as

$$G(z)=\begin{pmatrix}1 & 0\\ T_1(z) & 1\end{pmatrix}\begin{pmatrix}1 & -S_1(z)\\ 0 & 1\end{pmatrix}\cdots\begin{pmatrix}1 & 0\\ T_N(z) & 1\end{pmatrix}\begin{pmatrix}1 & -S_N(z)\\ 0 & 1\end{pmatrix}\begin{pmatrix}K^{-1} & 0)\\ 0 & K\end{pmatrix}$$

4-50

Matrix *G(z)* populated with Laurent polynomial and can be written in polyphase form

$$G(z)=\begin{pmatrix}G_{00}(z) & G_{01}(z)\\ G_{10}(z) & G_{11}(z)\end{pmatrix}$$

Reverse lifting block diagram is as shown in Figure 4-11

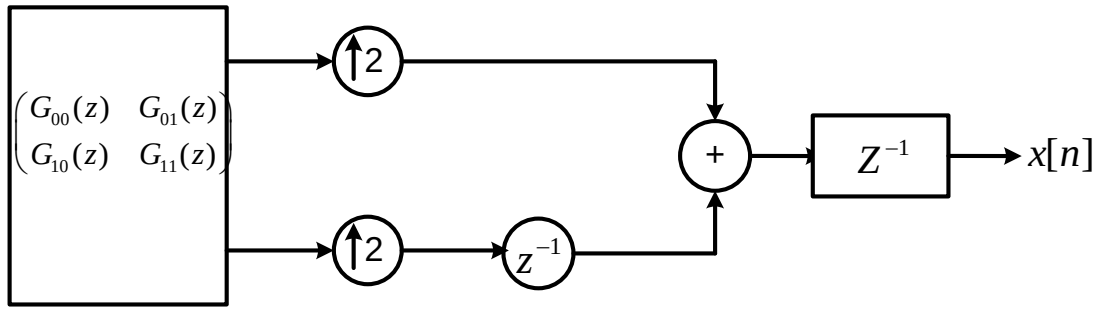


Figure 4-11 Reverse lifting scheme

where

$$\begin{pmatrix}G_{00}(z) & G_{01}(z)\\ G_{10}(z) & G_{11}(z)\end{pmatrix}=\begin{pmatrix}1 & 0\\ T_1(z) & 1\end{pmatrix}\begin{pmatrix}1 & -S_1(z)\\ 0 & 1\end{pmatrix}\cdots\begin{pmatrix}1 & 0\\ T_N(z) & 1\end{pmatrix}\begin{pmatrix}1 & -S_N(z)\\ 0 & 1\end{pmatrix}\begin{pmatrix}K^{-1} & 0)\\ 0 & K\end{pmatrix}$$

## 4.7 Filter coefficients used for lifting

Various steps involved in the lifting process were discussed in the previous section. The lifting procedure needs a pair of analysis filters and synthesis filters from a wavelet base. A prediction filter and update filter can be extracted from the particular wavelet base used. Underlying theory is discussed here analytically.

Follow from Figure 4-10

$$\begin{pmatrix}Y_0(z)\\ Y_1(z)\end{pmatrix}=\begin{pmatrix}H_{00}(z) & H_{01}(z)\\ H_{10}(z) & H_{11}(z)\end{pmatrix}\begin{pmatrix}X_e(z)\\ X_o(z)\end{pmatrix}$$

$$\begin{pmatrix} Y_0(z^2) \\ Y_1(z^2) \end{pmatrix} = \begin{pmatrix} H_{00}(z^2) & H_{01}(z^2) \\ H_{10}(z^2) & H_{11}(z^2) \end{pmatrix} \begin{pmatrix} X_e(z^2) \\ X_o(z^2) \end{pmatrix}$$

$$\begin{pmatrix} Y_0(z^2) \\ Y_1(z^2) \end{pmatrix} = H\left(z^2\right) \begin{pmatrix} X_e(z^2) \\ X_o(z^2) \end{pmatrix}$$

4-51

$\begin{pmatrix} X_e(z^2) \\ X_o(z^2) \end{pmatrix}$ means upsampling of $X_e(z\ )$ and $X_o(z\ )$

$$X_e(z) = \frac{1}{2}\left\{X(z^{1/2}) + X(-z^{1/2})\right\}$$

$$X_e(z^2) = \frac{1}{2}\left\{X(z) + X(-z)\right\}$$

4-52

$$X_o(z) = \frac{z^{\left(\frac{1}{2}\right)}}{2}\left\{X(z^{1/2}) + X(-z^{1/2})\right\}$$

$$X_o(z^2) = \frac{z}{2}\left\{X(z) + X(-z)\right\}$$

4-53

Substituting eq 4-52 and eq(4-53) in eq(4-51) yields

$$\begin{pmatrix} Y_0(z^2) \\ Y_1(z^2) \end{pmatrix} = H\left(z^2\right) \begin{pmatrix} \frac{1}{2}\left\{X(z) + X(-z)\right\} \\ \frac{Z}{2}\left\{X(z) + X(-z)\right\} \end{pmatrix}$$

4-54

$$\begin{pmatrix} Y_0(z^2) \\ Y_1(z^2) \end{pmatrix} = \begin{pmatrix} H_{00}(z^2) & H_{01}(z^2) \\ H_{10}(z^2) & H_{11}(z^2) \end{pmatrix} \begin{pmatrix} \frac{1}{2}\left\{X(z) + X(-z)\right\} \\ \frac{Z}{2}\left\{X(z) + X(-z)\right\} \end{pmatrix}$$

$$= \begin{pmatrix} H_{00}(z^2)\left[\frac{1}{2}\left\{X(z) + X(-z)\right\}\right] + H_{01}(z^2)\left[\frac{Z}{2}\left\{X(z) + X(-z)\right\}\right] \\ H_{10}(z^2)\left[\frac{1}{2}\left\{X(z) + X(-z)\right\}\right] + H_{11}(z^2)\left[\frac{Z}{2}\left\{X(z) + X(-z)\right\}\right] \end{pmatrix}$$

Classical DWT based dyadic scheme using convolution is shown in Figure 4-12.

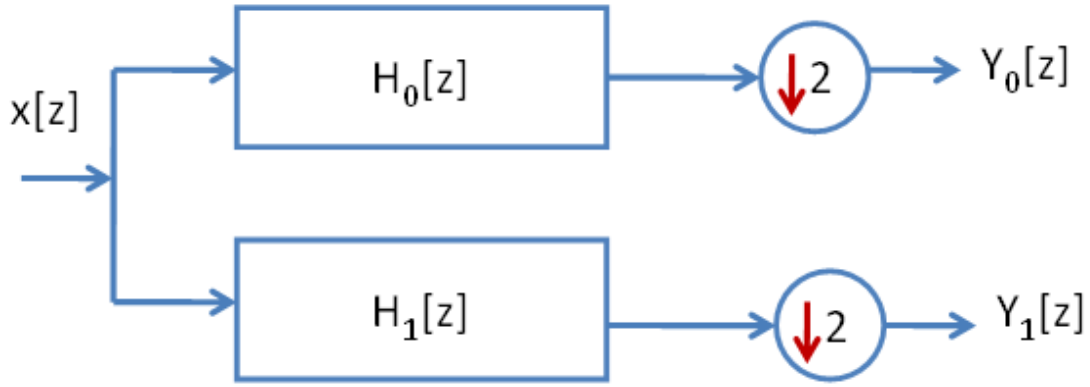


Figure 4-12 Classical DWT based on convolution

Based on two channel filter bank discussed in section 4.5.2 with reference to eq (4-15)

$$\begin{pmatrix} Y_0(z) \\ Y_1(z) \end{pmatrix} = \left(\frac{1}{2}\right)\begin{pmatrix} H_0(z^{1/2}) & H_0(-z^{1/2}) \\ H_1(z^{1/2}) & H_1(-z^{1/2}) \end{pmatrix}\begin{pmatrix} X(z^{1/2}) \\ X(-z^{1/2}) \end{pmatrix}$$

$$\begin{pmatrix} Y_0(z^2) \\ Y_1(z^2) \end{pmatrix} = \left(\frac{1}{2}\right)\begin{pmatrix} H_0(z) & H_0(-z) \\ H_1(z) & H_1(-z) \end{pmatrix}\begin{pmatrix} X(z) \\ X(-z) \end{pmatrix}$$

$$\begin{pmatrix} Y_0(z^2) \\ Y_1(z^2) \end{pmatrix} = \left(\frac{1}{2}\right)\begin{pmatrix} H_0(z)X(z) + H_0(-z)X(-z) \\ H_1(z)X(z) + H_1(-z)X(-z) \end{pmatrix} \quad 4\text{-}55$$

Substituting eq (4-55) with eq(4-54)

$$\begin{pmatrix} H_{00}(z^2)\left[\frac{1}{2}\{X(z)+X(-z)\}\right] + H_{01}(z^2)\left[\frac{z}{2}\{X(z)+X(-z)\}\right] \\ H_{10}(z^2)\left[\frac{1}{2}\{X(z)+X(-z)\}\right] + H_{11}(z^2)\left[\frac{z}{2}\{X(z)+X(-z)\}\right] \end{pmatrix} = \left(\frac{1}{2}\right)\begin{pmatrix} H_0(z)X(z) + H_0(-z)X(-z) \\ H_1(z)X(z) + H_1(-z)X(-z) \end{pmatrix}$$

$$\begin{pmatrix} H_{00}(z^2)\left[\{X(z)+X(-z)\}\right] + H_{01}(z^2)\left[z\{X(z)+X(-z)\}\right] \\ H_{10}(z^2)\left[\{X(z)+X(-z)\}\right] + H_{11}(z^2)\left[z\{X(z)+X(-z)\}\right] \end{pmatrix} = \begin{pmatrix} H_0(z)X(z) + H_0(-z)X(-z) \\ H_1(z)X(z) + H_1(-z)X(-z) \end{pmatrix}$$

$$H_{00}(z^2)\left[\{X(z)+X(-z)\}\right]+H_{01}(z^2)\left[z\{X(z)+X(-z)\}\right]=H_0(z)X(z)+H_0(-z)X(-z)$$
$$H_{10}(z^2)\left[\{X(z)+X(-z)\}\right]+H_{11}(z^2)\left[z\{X(z)+X(-z)\}\right]=H_1(z)X(z)+H_1(-z)X(-z)$$

4-56

$$\left[H_{00}(z^2)+zH_{01}(z^2)\right]X(z)+\left[H_{00}(z^2)+zH_{01}(z^2)\right]X(-z)=H_0(z)X(z)+H_0(-z)X(-z)$$

4-57

$$\left[H_{10}(z^2)+zH_{11}(z^2)\right]X(z)+\left[H_{10}(z^2)+zH_{11}(z^2)\right]X(-z)=H_1(z)X(z)+H_1(-z)X(-z)$$

4-58

Equating the coefficients gives $H_0$ (z) and $H_1$ (z) from eq 4-57 and eq 4-58

$$\underbrace{\begin{aligned}H_0(z)&=H_{00}(z^2)+zH_{01}(z^2)\\H_1(z)&=H_{10}(z^2)+zH_{11}(z^2)\end{aligned}}_{\text{AnalysisFilters}}$$

4-59

Analogously $G_0$ (z) and $G_1$ (z) is given by

$$\underbrace{\begin{aligned}G_0(z)&=G_{00}(z^2)+z^{-1}G_{01}(z^2)\\G_1(z)&=G_{10}(z^2)+z^{-1}G_{11}(z^2)\end{aligned}}_{\text{SynthesisFilters}}$$

4-60

To implement forward lifting, choose analysis filters $H_0(z)$, $H_1(z)$, Factorise into poly phase components followed by normalization. Similarly for reverse lifting choose synthesis filters $G_0(z)$, $G_1(z)$ and factorise into polyphase components. Schematic representation of perfect reconstruction using lifting scheme is shown Figure 4-13.

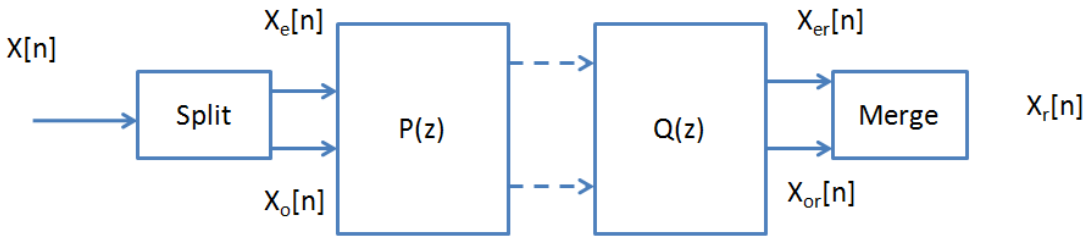


Figure 4-13 Prefect reconstruction based lifting scheme

For perfect reconstruction, P(z).Q(z) = 1 , this implies that

$$Q(z) = [P(z)]^{-1}$$

$$P(z) = \begin{pmatrix} H_{0e}(z) & H_{1e}(z) \\ H_{0O}(z) & H_{1O}(z) \end{pmatrix}$$

$$Q(z) = \begin{pmatrix} G_{0e}(z) & G_{1e}(z) \\ G_{0O}(z) & G_{1O}(z) \end{pmatrix}$$

4-61

$$[P(z)]^{-1} = \frac{1}{\left(H_{0e}(z)H_{1O}(z) - H_{1e}(z)H_{0O}(z)\right)} \begin{pmatrix} H_{1O}(z) & -H_{1e}(z) \\ -H_{0O}(z) & H_{0e}(z) \end{pmatrix}$$

for, $\left(H_{0e}(z)H_{1O}(z) - H_{1e}(z)H_{0O}(z)\right) = 1$

$$G_{0e}(z) = H_{1O}(z)$$
$$G_{0O}(z) = -H_{0O}(z)$$
$$G_{1e}(z) = -H_{1e}(z)$$
$$G_{1O}(z) = H_{0e}(z)$$

4-62

Examples of obtaining prediction and update filter using Euclidian algorithm can be found in [C. Valens 1999]. Flowchart of DWT decomposition based on lifting scheme shown in Figure 4-14.

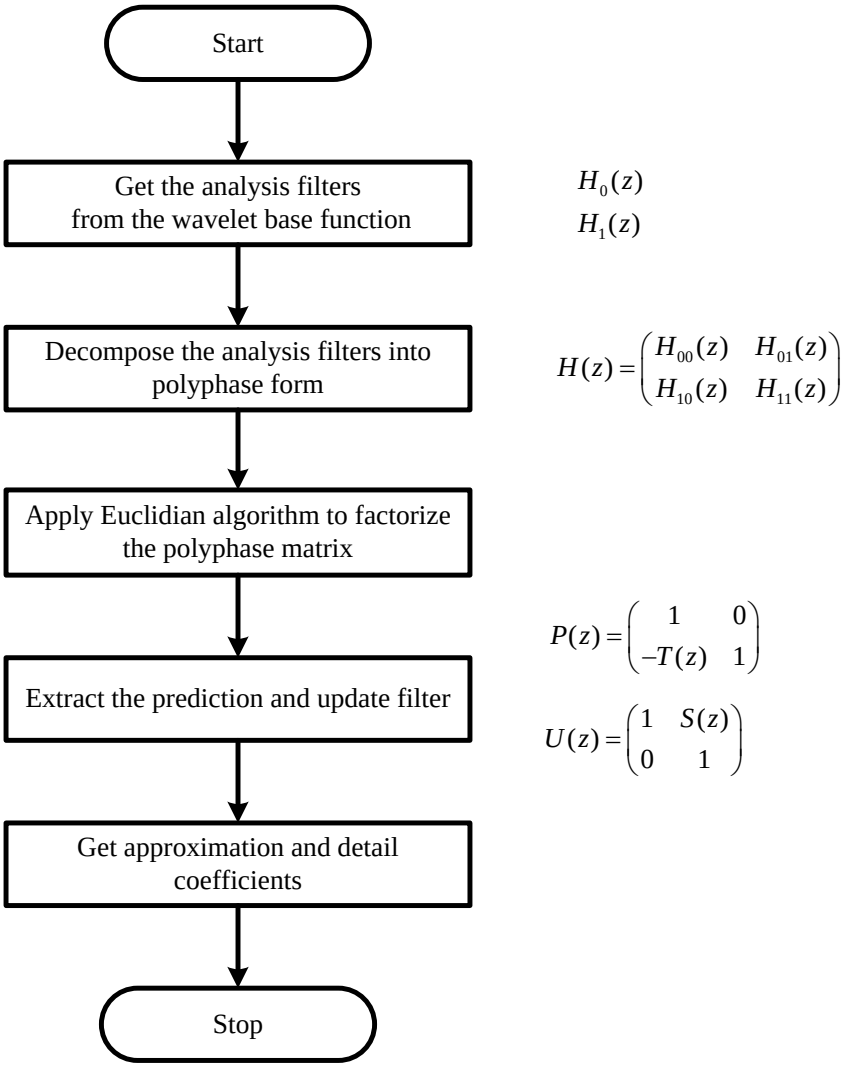


``

Figure 4-14 Lifting scheme

## 4.8 Empirical Mode Decomposition

In 1998, Hibert Huang proposed a new data analysis method intuitively based empirical mode decomposition (EMD) which will extract the energy associated with various intrinsic time scales, the most important parameters of the system. [Norden E. Huang1 1998]. So this technique is data driven since it does not not use any basis functions like wavelets. EMD decomposes a signal in time domain into set of AM and FM type components known as IMFs. The underlying theory of decomposition is picking up the fast oscillations locally in the signal. Local oscillations contained in the signal are obtained by interpolating local maximum and minimum points present in the signal. This will give an upper and lower envelop of the signal under test using the local minima and maxima. The mean envelope is computed and subtracted from the initial signal. The same interpolation scheme is applied to the difference resulted from the subtraction. The so called sifting process terminates when the envelope vanishes, in this way a well defined stopping criterion is achieved [Delechelle, Lemoine et al. 2005]. Pictorial representation of sifting process is shown in Figure 4-15.

$$x(t) = \sum_{i=1}^{N} h_i(t) + r(t)$$

4-63

x(t) : Signal in time domain
$h_i(t)$ : IMF
$r(t)$ : Residue

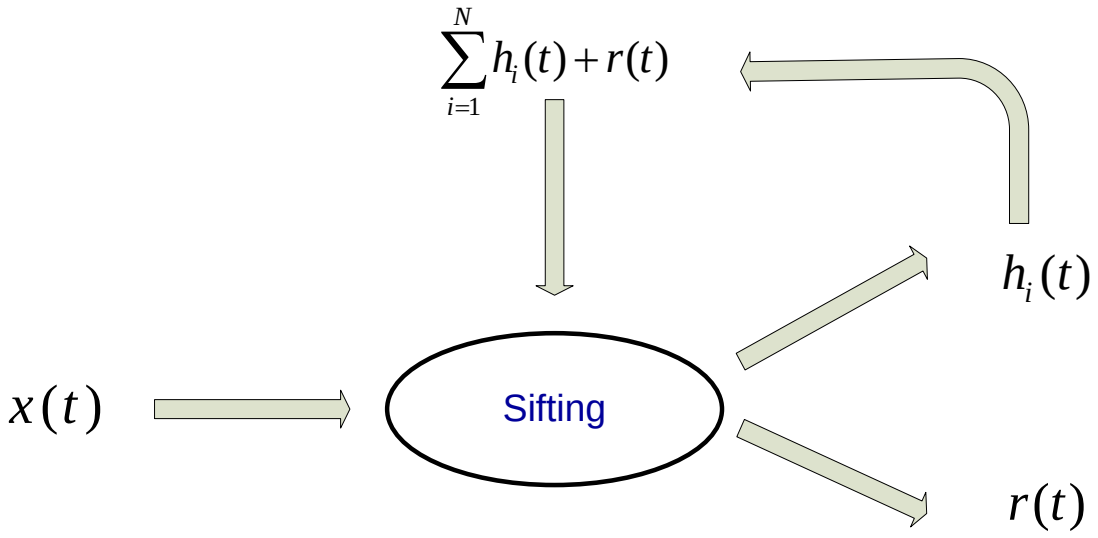


Figure 4-15 Sifting process, pictorial representation

Two conditions need to be satisfied for a decomposition component from EMD to be an IMF. The first condition is the number of local minima and local maxima should be the same or at least differ by one. Secondly, the mean of the upper and lower envelop should be zero which physically means that there will not be any additional fluctuation in the instantaneous frequency. IMF can be both amplitude and frequency modulated. In fact, it can be non-stationary. So frequency or amplitude modulated functions can be IMFs. Figure 4-16 shows a typical IMF from the same number of zero crossings and extrema, and symmetry of the upper and lower envelopes with respect to zero [R.T. Rato 2008]

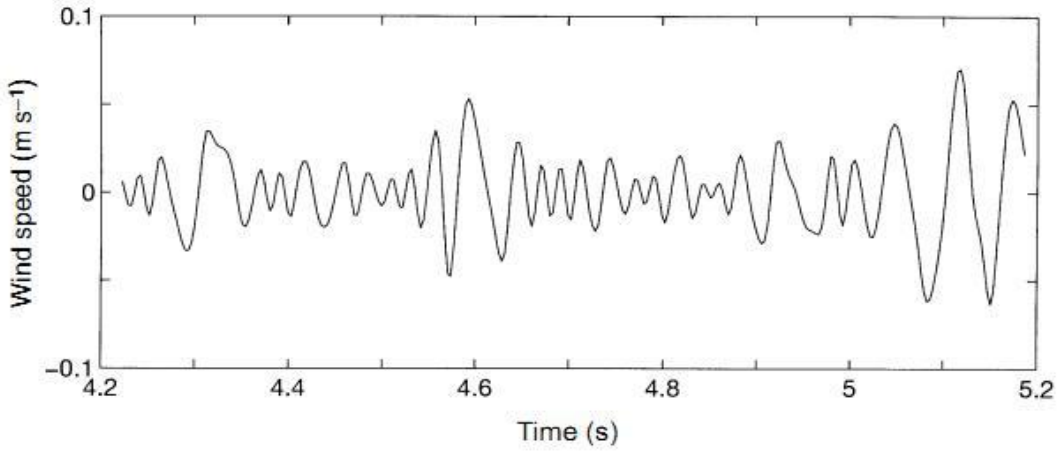


Figure 4-16 Typical IMF from EMD

A detailed flow chart of the EMD sifting process is as shown Figure 4-17. Though this technique is purely data driven with well defined stopping criterion, there is a lack of

analytical framework which makes it difficult to analyse and characterize [Niang, Dele et al. 2010]. Criterion using null local mean sometimes leads to over decomposition. Also cubic spline function based on upper and lower envelope generation introduces overshoot and undershoot in the decomposition process [Delechelle, Lemoine et al. 2005]. Applications of EMD includes speech enhancing, vibration monitoring, and anti jamming GPS signals etc. In case of PD denoising using EMD, limited research publications were found [Giscard F. C. Veloso 2009; Veloso, da Silva et al. 2009; He, Liu et al. 2011]. Apart from the drawbacks cited above, time consumption of iterative processes in EMD is fairly high compare to DWT which makes this method less feasible for signals which are sampled at high frequencies.

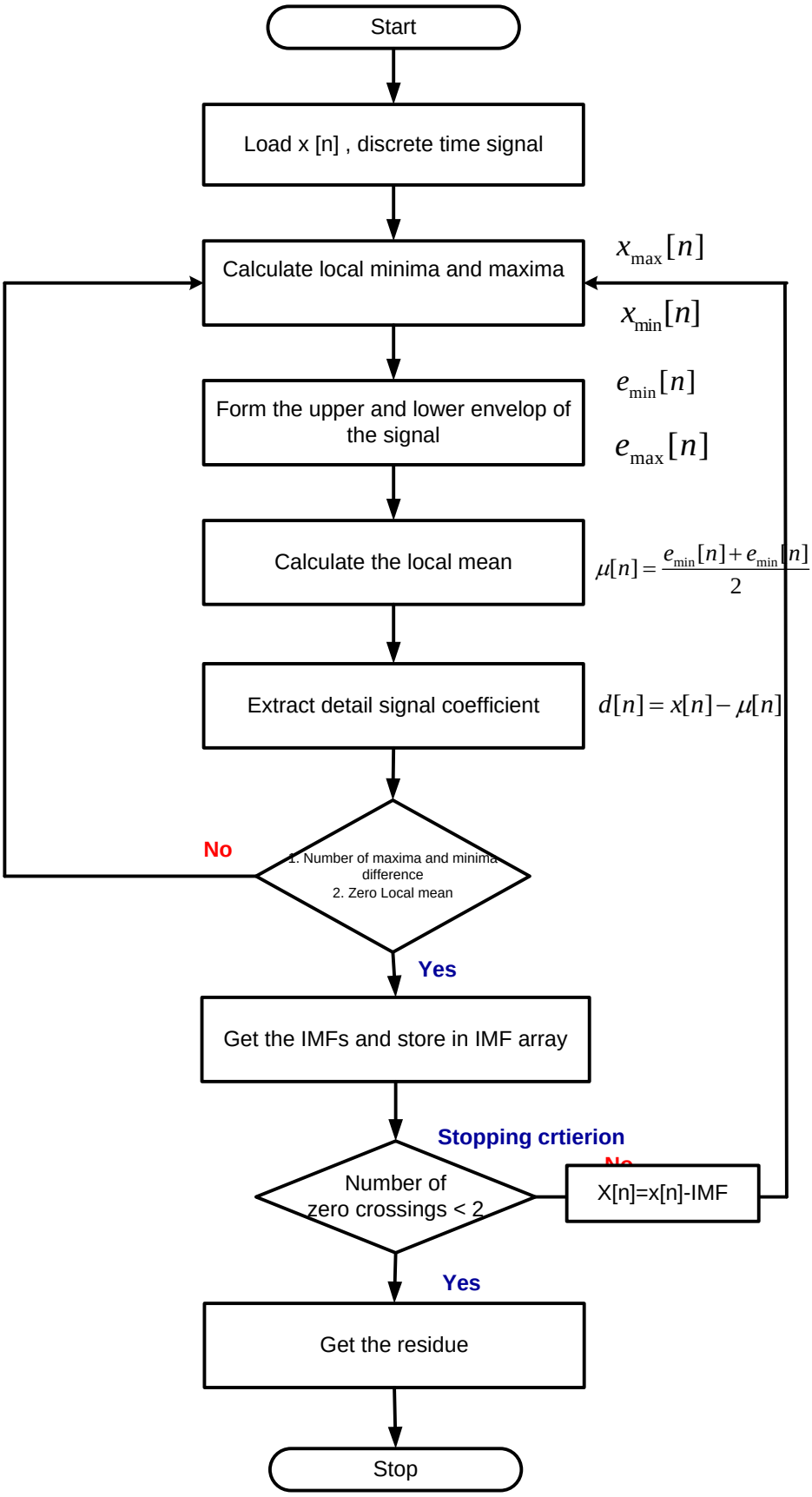


Figure 4-17 EMD decomposition tree

## 4.9 Denoising of PD signals

Denoising of PD signals is apre-processing step for interpreting and classification of PD contained in the raw data. In general, denoising is a three stage process which includes analysis or decomposition, thresholding and synthesis or reconstruction. Analysis of signals using wavelets and EMD were discussed in the previous section. In this section various threshloding methods are discussed.

The basic theory behind thresholding in wavelet domain is that energy of a signal will be often be concentrated in fewer coefficients while the noise energy spectrum spans over the entire wavelet coefficients [Qu, Wang et al. 2002]. Thresholding is a two step process, the first step defines an operator to determine the threshold. The second defines another operator which gives modified wavelet coefficients which will be used for reconstruction. Thresholding in general fall into two categories namely hard and soft thresholding. Hard thresholding retain the coefficients above the threshold and diminish the coefficients below the threshold. Soft thresholding discards coefficients whose absolute value is below the threshold, while shrinking down the remaining coefficients towards absolute by subtracting them from the threshold setting.

Hard thresholding is given by and

$$x[n] = \begin{cases} x[n], & |x[n]| \geq \lambda \\ 0, & |x[n]| < \lambda \end{cases}$$

4-64

Soft thresholding is given by

$$x[n] = \begin{cases} sign(x[n])(x[n] - \lambda), & |x[n]| > \lambda \\ 0, & |x[n]| < \lambda \end{cases}$$

4-65

Where x[n] : Wavelet decomposition coefficients
λ : Threshold value

Pictorial representation of hard and soft thresholding is shown in Figure 4-18 and Figure 4-19 respectively. The hard thresholding method creates discontinuities at the borders of the zeroed values whilst soft thresholding does not, however hard

thresholding preserves features e.g. peak heights. Soft thresholding provides a visually smoother appearence than hard thresholding. However there will be loss of high frequency information which will lead to edge blur or loss of edges. In some instances it may be beneficial to use hard thresholding to retain the original peak within a signal [Donoho 1995; Gu 2009]. There are various threshold setting $\lambda$ rules namely universal threshold, minimax threshold, rigsure and heursure. These thresholding methods have their own advantages and disadvantages. Selection of a thresholding method depends upon the denoising requirement which means type of data. Various threshold selection methods are discussed in the next section.

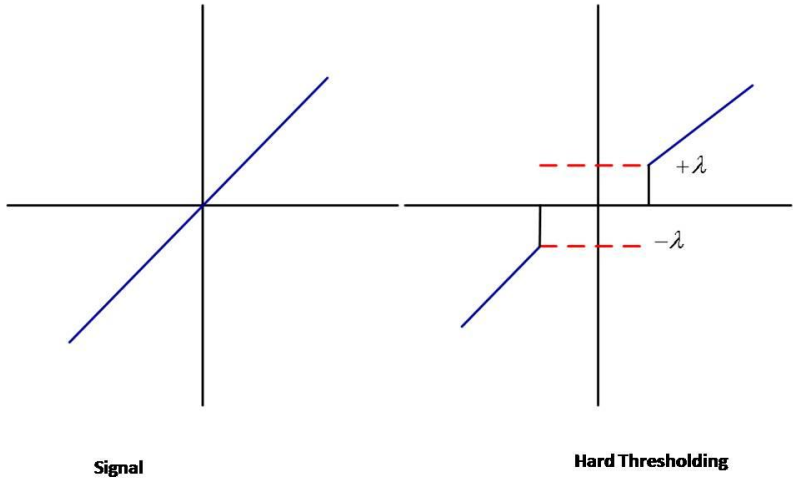


Figure 4-18 Hard thresholding

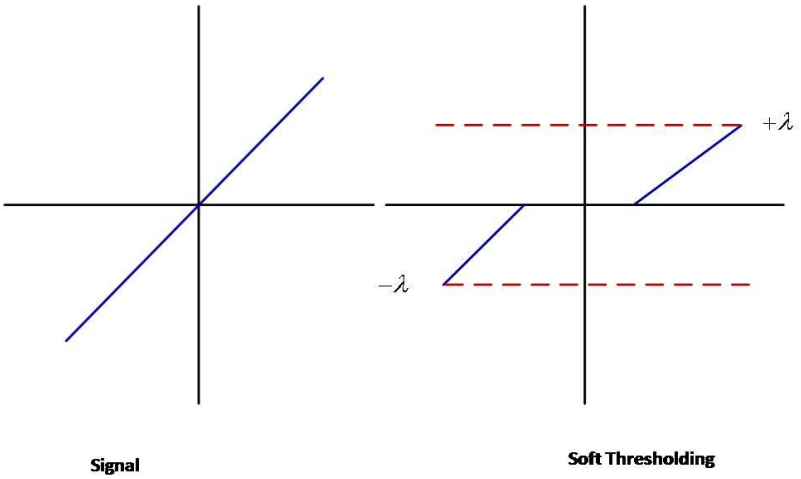


Figure 4-19 Soft thresholding

### 4.9.1 Universal Threshold

Universal threshold was proposed by Donoho (Donoho 1995) also known as visushrink. This algorithm uses a fixed threshold λ and is given by

$$\lambda = \sigma\sqrt{2\log_e(n)}$$

where

$\sigma$ : Noise variance

$n$ : Length of the signal

In real problems $\sigma$ has a scaling factor which is the estimate of some common standard noise present in the signal. The threshold is given by

$$\lambda = \frac{\sigma}{0.6745}\sqrt{2\log_e(n)}$$

4-66

### 4.9.2 Minimax threshold

Minimax thresholding involves optimal threshold which is derived from minimising a constant term in an upper bound of the risk involved in the estimation of a function [M.C.E . Rosas orea M Hernandezdias Universidad de las Américas 2005]. Commonly used estimators are MOM, MLE and bayesian estimators. Minimax threshold minimizes the risk in the loss function [Mellon 2010]. For example if the loss functions is squared error.

$$R(\theta - \theta\hat{}) = E(\theta - \theta\hat{})^2$$

4-67

Where, θ is the estimate from the best estimator $\hat{\theta}$

Estimator $\theta\hat{}$ is minimax if

$$\sup_\theta R(\theta, \theta\hat{}) = \inf_{\theta\hat{}} \sup_\theta R(\theta, \theta\hat{})$$

4-68

Where ,

*Inf* is the infimum and *Sup* is spremum

### 4.9.3 Stein's Unbiased Risk Estimator

Thresholding methods discussed in the previous section are termed as global thresholds, which means thresholds computed should be applied to all wavelet coefficients. SURE is level based thresholding. Loss function of any estimator depends upon the unknown parameter therefore it can't be calculated exactly. SURE estimates the accuracy of an estimator by estimating the mean squared error in an unbiased way. SURE can be used to choose a parametric form for an estimator. Thus one can minimize this estimate and find the optimized values [Seifzadeh, Rostami et al. 2011]. Donho and Johnston applied SURE to determine the optimal shrinkage in wavelet denosing [David L. Donoho 1995]. Thresholding using SURE shrink is nearly a minimax thresholding. Mathematical base for SURE can be found in [Anestis Antoniadis 2001]

## 4.10 Denoising Methods For PD signals From Cable

Application of wavelets for processing data in electrical engineering problems goes back to 1990s. [Robertson, Camps et al. 1996] applied wavelets to characterize the source of transient disturbances from a power frequency voltage waveform. Most popular applications of wavelet based denoising in the area of electrical engineering includes power system protection, power quality, transients, partial discharges, load forecasting, power system measurements etc. Figure 4-20 shows statistics of wavelet research publication in power engineering areas [Rosa M de castro M fernandez 2002].

[Shim, Soraghan et al. 2001] applied the universal threshold method to denoise PD signals using a db5 wavelet. Selection of an appropriate wavelet basis function is the key for extracting the relevant patterns contained in the raw data. Optimum wavelet selection maximizes the wavelet coefficient values in the time-scale plane which means generating the highest local maxima of the signal of interest. [Ma, Zhou et al. 2002] proposed automated wavelet selection using cross correlation between signal of interest and wavelet base. [Satish and Nazneen 2003] applied wavelet transforms, FIR filtering and IIR filtering for PD de-noising and compared their performance with various noise sources. [Hao, Blackburn et al. 2007] proposed a wavelet threshold method in which noise threshold level is obtained from background noise. This method needs two data sets namely background noise which has no PD and raw PD data which contains both PD and noise. This data is acquired based on PDIV as trigger. However, setting PDIV

as the trigger in on-line PD diagnostics using a data acquisition card may not be feasible since the short bursts that appear in the data may be of any means for example PD, switching noise or PD from neighbouring cable. Though the noise threshold by this method produces better denoising, on line gathering of data is difficult. [Zhang, Yu et al. 2002; Xiaodi, Chengke et al. 2007] applied DWT based on lifting scheme to denoise PD signals using universal threshold. This method is much faster compared to classical wavelet based denoising techniques.

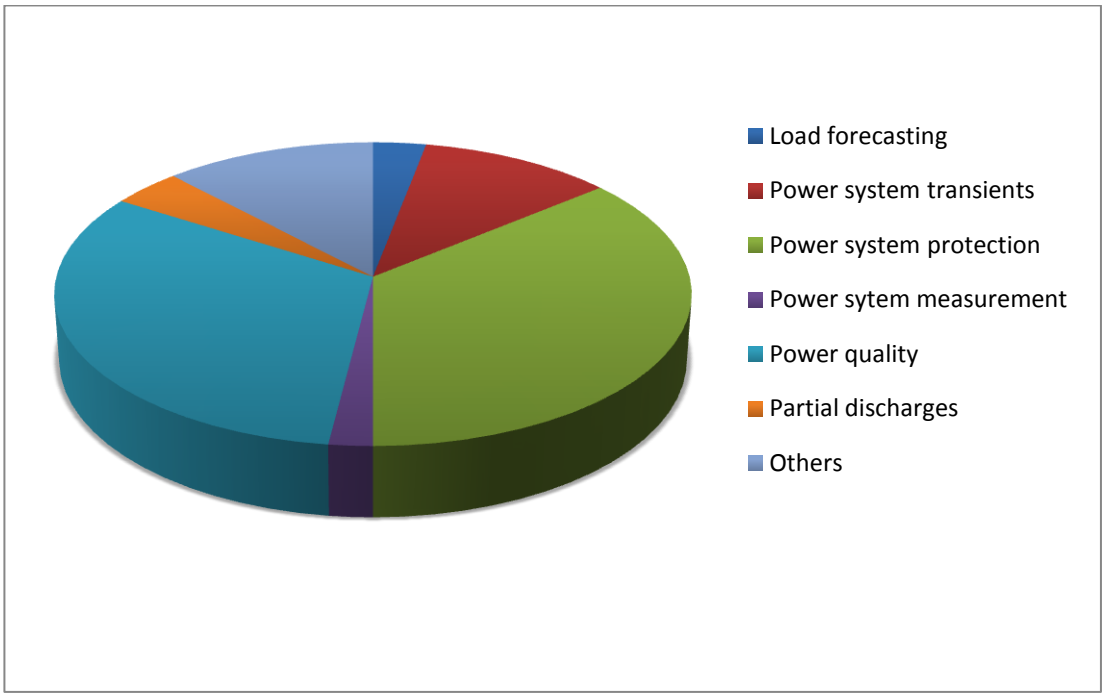


Figure 4-20 Wavelet research publications in power engineering[Rosa M de castro M fernandez 2002].

## 4.11 Conclusion

Analysis and detection of PD's in cables is often hampered by various noise which makes extracting PD from the raw data a more difficult task. Various signal processing tools are used to denoise raw data acquired from cables. Due to stochastic nature of PD actvity and hardware requirements , design of digital signal processor for denoising PD signals from cables require experience in on -site PD signals. In this chapter various signal processing techniques for denoising PD's were reviewed.

Matched filters apply cross correlating method between information to be extracted and filter kernel. Various sources of interference namely propagation characteristics of cable, PD's from neighbouring cable, transient noise sources which exhibits similar PD signatures makes difficult to select filter kernel. MAF can be considered as smoothing filter for random noise and has poor performance in frequency domain. Over smoothing by MAF leads to loss of edges in the signal which will introduce error in PD source location. In case adaptive filters, filter coefficients are updated with priory information. Though this method of denoising is applied to PD diagnostics, computational complexity and hardware resources requirement makes this method less suitable for on-line PD diagnostics.

EMD proposed by Hibert Huang et. al. has found applications in speech enhancing, vibration monitoring, anti-jamming GPS signals etc. This method has advantages such as no prerequisites required and well defined stopping criterion. These advantages make this method as fully automatic. However, mathematical base for this method is not well defined and is still in research and also this technique is slower and may require higher hardware resources for on-site PD signal processing. This emerging technique finds limited applications in denoising of PD signals.

DWT using dyadic filtering scheme based on universal threshold is a mature technique in denoising PD signals. However this technique still needs to select wavelet basis function with higher degree of correlation to PD signature to get better denoising performance. Also the number of decomposition levels in the wavelet method is chosen empirically and makes this approach semi automatic. Denoising of PD signals using SGWT is relatively faster then classically DWT and also customization of filter cofficients in SGWT enhances the PD signals which provides better PD signature extraction. In this research work denoising using SGWT is implemented.

# Chapter 5 :
# Partial Discharge Detection in Cables Using Power Frequency CT

## 5.1 Introduction

Various issues of PD detection from insulated power cables using earth strap were discussed in section 2.7. Though HFCT installed on the earth strap at the cable termination are widely used to detect the fast varying pulses resulting from PD, due to constructional reasons, earth strap accessibility in underground cables is often limited. Furthermore, in three core cables, phase angle dependency of pulses resulting from PD sometimes fails to induce pulses in the earth screen. In this chapter, an alternative method of PD detection using conventional PFCT principally used for protection and measurement purposes is investigated. This investigation assesses the feasibility of this approach by conducting a magnetic study of transformer core, frequency response analysis, and finally capturing and analyzing onsite PD data in 11 kV PILC 3 core cable using conventional PFCTs and the developed PD data acquisition/interpretation system. Hardware design, software design laboratory measurements and on-site measurements are included in this chapter.

## 5.2 Need of an alternative PD detection sensor

Inductive couplers are the most widely used non intrusive technique for PD detection in cables. Rogowski coils and HFCTs are widely used inductive couplers which need to be installed in the earth strap of the cable to detect PD. This type of PD measurement presents two issues namely the cable earth strap needs to be isolated from the switchgear earth to detect cable PD signals, and in the UK, many substations have completely enclosed switchgear units at one end of the cable circuit, which prohibit access to the earth strap [Foo 2003]. In three core cables with a common earth screen, induced currents or charges in the conductors due to PD depends on the location of discharge source and the eccentricity of the 3 phase rotating field [van der Wielen, Wouters et al. 2002]. This means that charge displacement may not occur in all

conductors to the same extent. Consequently, if PD detection is performed at only the earth screen, a PD may remain undetected [van der Wielen, Steennis et al. 2003]. These issues result in the installation of sensors at the cable core, which requires a planned outage to remove the cable from service causing customer supply interruption and regulatory penalties. This research investigates the possibility of using preinstalled PFCTs in cable networks, to detect PD signals which may eventually lead to the development of a low cost, non intrusive method of cable condition monitoring.

## 5.3 Instrument Transformers - Theory

Instrument transformers are primarily used to provide isolation between circuits which are at different voltage levels. This isolation is achieved by establishing a magnetically coupled path between circuits. In addition to isolation, levels in magnitude (voltage and current) are reduced to safer levels. Instrument transformers are divided into two categories namely VT and CT. Only CT is discussed in this thesis. The primary winding of CT is connected in series with busbar. Secondary current is replica of primary current which is scaled down depending on the transformation ratio of CT [Moore 2004]. Measuring devices such as ammeters are connected in series with the secondary winding of the measurement CT while relay coils are connected in series with secondary winding of protection CT. Impedance of the ammeter or relay coil together with lead impedance is referred as CT burden. Typical wiring diagram of CT and VT is as shown in Figure 5-1. CTs are available in several different styles such as bushing type, wound type and bar type.

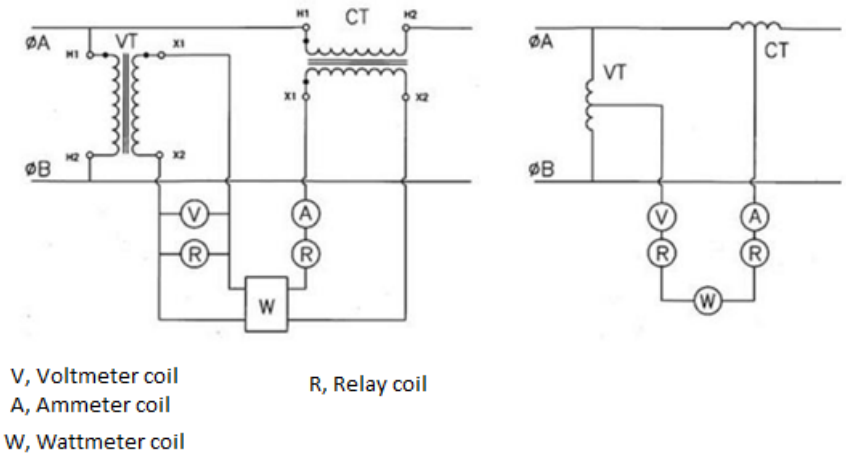


Figure 5-1 Wiring diagram of CT and VT

Bushing type CT consists of annular shaped core with an insulated secondary winding which is permanently assembled on the magnetic core. This type of current transformer has a fully insulated conductor which is used as the primary winding. Bushing type CT is typically used around bushings on circuit breakers and transformers.

Bar type CT has a fixed and straight single primary winding turn passing through the magnetic circuit. Primary winding and secondary winding(s) are insulated from each other and from the core(s) and are assembled as an integral structure. Primary conductor bar is usually bolted to the current carrying line.

Wound type CT consists of primary winding with one or more turns wound on the core or cores. A wound type transformer has no primary winding as an integral part of the structure. One turn of the line conductor is passed through the window to provide the primary winding [Siemens 2009]. In this thesis only wound type CTs are considered which are widely used as in switch gear panels. Photograph of CTs in a switchgear panel is as shown in the Appendix C-1.

Figure 5-2 shows the connection diagram for a measurement CT. Current flows through the secondary winding, which is the replica of the primary current but reduced in magnitude by a factor N which is denoted as CT ratio.

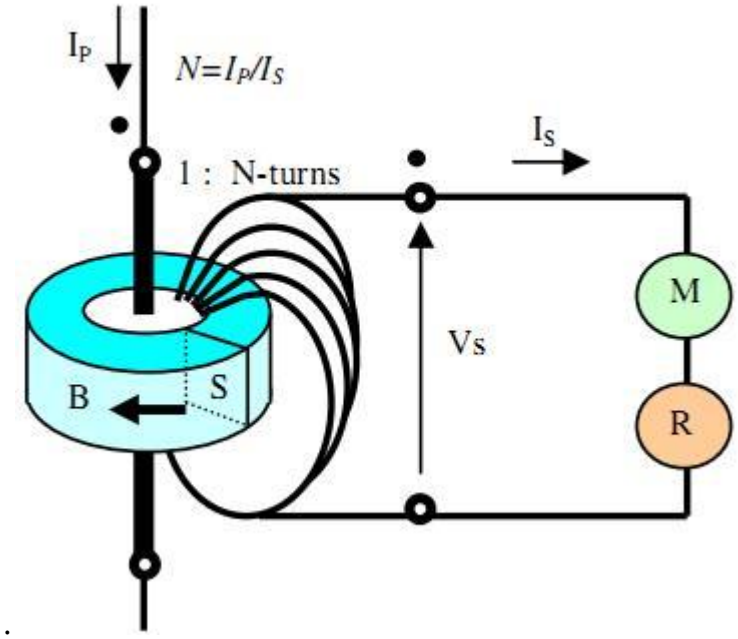


Figure 5-2 connection diagram of measurement CT [F P Mohamed 2011]

With reference to the Figure 5-2

$$I_s = \frac{I_p}{N} \quad (5\text{-}1)$$

$$V_s = 4.44 * f * S * B_m * N_r \quad (5\text{-}2)$$

Where

$I_p$ : Primary current
$I_S$ : Secondary current
$V_S$ : Secondary voltage
$f$ : Supply frequency
$N$ : Rated turns ratio
$B_m$ : Maximum flux density in the core
$S$ : Area of cross section of the core

Magnetic characteristics of a CT can be obtained from excitation characteristics. These characteristics can be plotted using the data obtained from open circuit tests with an open circuit primary. Figure 5-3 and Figure 5-4 shows the simulation and experimental excitation test conducted on a 400/5 A, 15 VA torroidal CT.

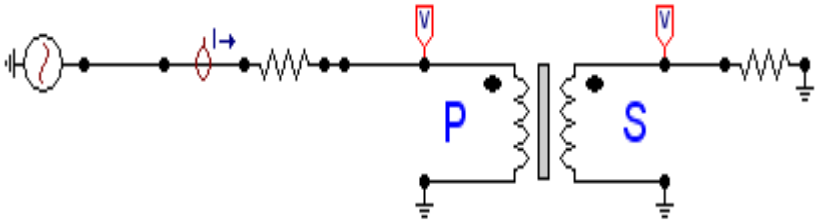


Figure 5-3 Open circuit test for excitation characteristics

Based on Figure 54, the excitation current is negligible in the linear operating region. Secondary current measured in this region will be the exact replica of scale down version of the primary current. Linearity is maintained till the knee point region is reached. Knee point region is the point on the excitation curve where the tangent is at 45° to the abscissa. The excitation curve shall be plotted on log-log paper with square decades. This definition is for nongapped cts. When the CT has a gapped core, the knee-point voltage is the point where the tangent to the curve makes an angle of 30° with the abscissa [1996]. In this region maximum permeability of the magnetic core is used. Further increase in current from the knee point saturates the CT. Measurement CTs are

normally operated in linear region so that metering errors can be avoided. In protection CTs design, knee point voltage is set above the fault current current level with suitable allowance for possible dc component so that CTs will not be pushed into saturation during abnormal conditions.

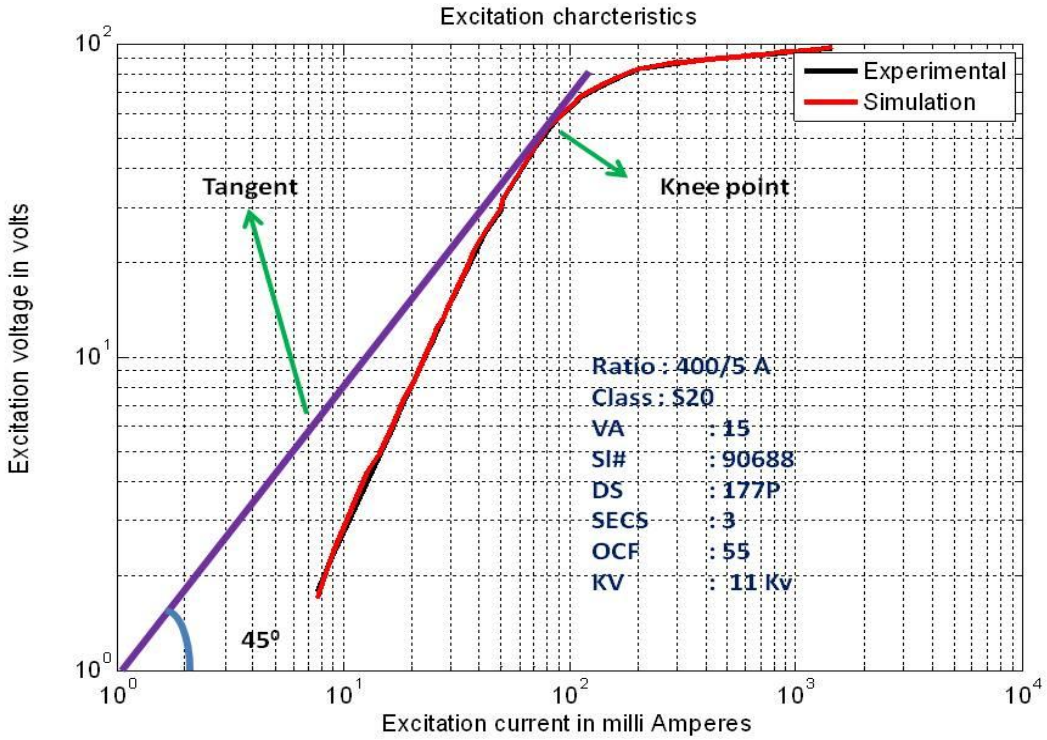


Figure 5-4 Excitation characteristics

### 5.3.1 PFCT Magnetic Circuit

The magnetic core of a transformer provides a flux path to facilitate flux linkage. Soft core materials are generally used as transformer cores since these materials have higher permeability and lower coercivity. This means these materials can easily be magnetized and demagnetized. Permeability is often used to evaluate the magnetic performance of core material used in transformers. It is a measure of how much magnetic induction is generated by the magnetic material in a given magnetic field. Permeability depends on temperature, material composition, frequency of the excitation current etc. The material used exclusively for high power transformers cores is grain oriented silicon-iron. This material contains about 3-4% silicon to reduce conductivity and eddy current losses and also they have high magnetic induction. These materials

work well at lower frequencies, but become less effective at high frequencies [Abbruzzese 1989].

Metallic oxide materials, known as ferrites, are essentially ceramics which are used as core material in HFCTs due to their relatively high resistivity and high usable frequency range. The most common ferrite contains about 50% iron oxide; the remaining 50 % classifies the type of grade of ferrite. The most common type is made up of oxides of manganese (Mn) and zinc (Zn). Mn-Zn ferrites are used for lower frequency work exhibiting high permeability, but low resistivity increases the eddy current losses. The other main type of ferrite has a nickel and zinc oxide (Ni ZnO) composition and has a lower permeability, on average, but will work well at higher frequencies. For high frequency applications, core material with a higher initial permeability is preferred. In addition to the material composition, the magnetic efficiency of a ferrite based CT depends on the design, for example shape of core, uniformity of core cross sectional area and air gap [Makky, Abo-Zied et al. 2008].

A magnetic design Engineer can get first order evaluation of the magnetic material by looking at the hysteresis loop. When the magnetic material is subject through a complete cycle of magnetization and demagnetization, a trend of permeability with respect to B and H can be traced as BH loops. Figure 5-5 shows typical BH loop.
In Figure 5-5 as $H$ is increased, the flux density $B$ increases along the initial magnetization path to the saturation point $Bs$. When $H$ is decreased, B-H loop transverses a path to $B_r$, where H is zero and the core is still magnetized. The flux at this point is called remanent flux, and has a flux density, Br. The magnetizing force, H, is now reversed in polarity to give a negative value. In practice, the magnetization of a core in an excited transformer never follows this curve, because the core is never in the totally demagnetized state, when the magnetizing force is first applied. The hysteresis loop represents energy lost in the core. The best way to display the hysteresis loop is to use a DC current, because the intensity of the magnetizing force must be so slowly changed that no eddy currents are generated in the material. Only under this condition is the area inside the closed B-H loop indicative of the hysteresis. The enclosed area is a measure of energy lost in the core material during the cycle of magnetization. In AC applications, this process is repeated continuously and the total hysteresis loss is dependent upon the frequency.

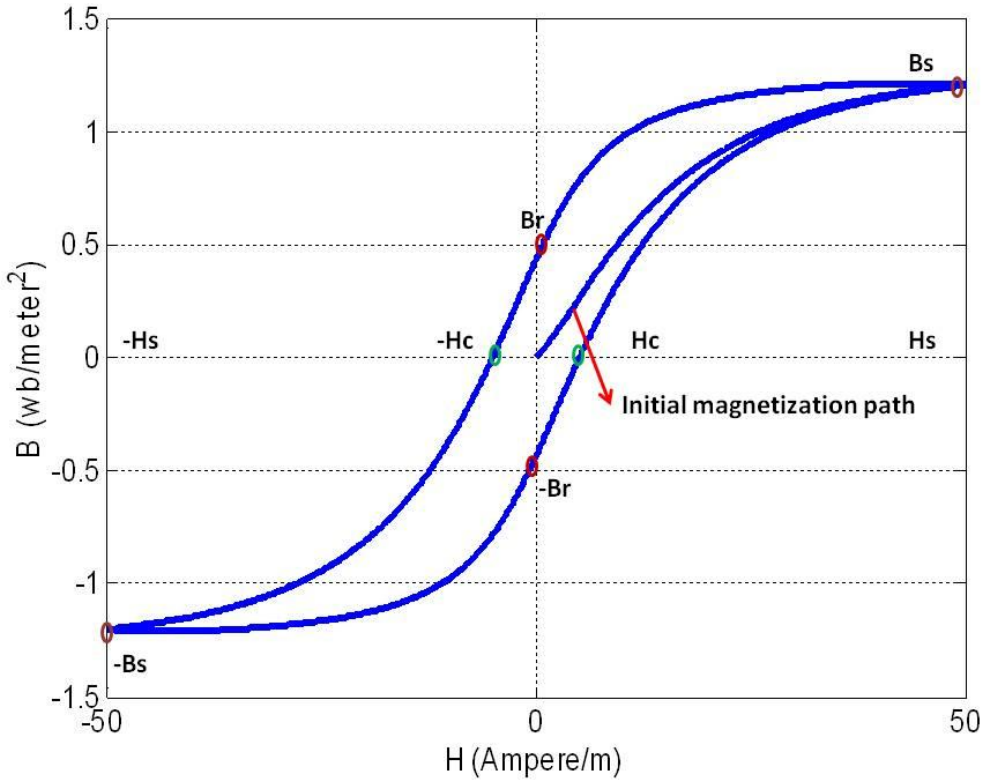


Figure 5-5 Typical B-H Loop

The magnetization curves or hysteresis loops of ferromagnetic materials varies as a function of the frequency and waveform of the applied magnetic field. The Jiles-Atherton (J-A) theory is widely used to characterize the hysteresis property of ferromagnetic material using underlying physcis in magnetic materials [Jiles, Thoelke et al. 1992; Jiles 1994; Jiles 1998; Naus 2002]. The advantage of this model over other hysteresis models is that it is based on a consideration of the underlying physics of hysteresis, and has a small number of physically interpretable parameters. J-A describes bulk magnetization into reversible magnetization due to domain wall bending and irreversible magnetization due to domain wall movement. Theory of J-A model can be found from [Jiles 1998]. In this thesis J-A model is applied to study the behavior of core material with varying permeability when subjecting excitation of fast varying fields from PD.

From the theory of J-A model of ferromagnetic hysterisis

In the absence of time-dependent effects, the energy balance equation is given byEnergy supplied to the conducting material = (change in magneto static energy + hysteresis loss + eddy current loss)

$$\mu_0 \int M_{an}(dH_e) = \mu_0 \int M(dH_e) + \mu_0 \int \frac{n\varepsilon_\pi}{2M_s}\left[\frac{dM}{dH}\right](dH) + \frac{\mu_0 d^2}{2\rho\beta}\left(\frac{dM}{dt}\right)^2 dt$$

5-3

Where,

$M$ - magnetization vector, $M_s$ - saturation Magnetization (Amperes/meter), $\mu_0$ - permeability of free space, $n$ - Number of pinning sites, $\varepsilon_{pi}$ - domain wall pinning in $180^o$

$\rho$ - resistivity of core material (Ω-meter), $d$ - the cross-sectional dimension (meters) (thickness for laminations, diameter for cylinders and spheres), $\beta$ geometrical factor which varies from $\beta = 6$ (in laminations) to $\beta = 16$ (in cylinders) and $\beta = 20$ (in spheres), and $M_{an}$ - the anhysteretic magnetization defined by Langevin function given by [Jiles, Thoelke et al. 1992]

$$M_{an} = M_s * \left(\coth\left(\frac{H_e}{b}\right) + \frac{b}{H_e}\right)$$

5-4

Where He - Effective H field which composes of external H field and internal magnetization M given by the following relation:

$$H_e = H + \alpha M$$

5-5

Where, $\alpha$ : mean field parameter this provides inter domain coupling

$a$ : shape parameter,

Magnetization vector $M$ is expressed as the sum of a reversible component $M_{rev}$ due to domain wall bending and an irreversible component $M_{irr}$ due to wall displacement, and is given by

$$M = M_{irr} + M_{rev}$$

5-6

Where,

$$M_{irr} = M_{an} - k\delta\left(\frac{dM_{irr}}{dH_e}\right) - \frac{\mu_0 d^2}{2\rho\beta}\left(\frac{dM}{dt}\right)\left(\frac{dM}{dH_e}\right)$$

5-7

$$M_{rev} = c\left(M_{an} - M\right)$$

5-8

Where

$k$ : pinning parameter which determines the amount of energy dissipated

$c$ : measure of the amount of reversible change in magnetization

Hysteresis parameters *Ms, α, a, c* and *k* needed to describe hysteresis on the basis of the Jiles- Atherton theory can be calculated from experimental measurements of the coercivity, remanence, saturation magnetization, initial anhysteretic susceptibility, initial normal susceptibility, and the maximum differential susceptibility for a particular frequency [Jiles, Thoelke et al. 1992]. In case of PD detection using PFCT, power frequency signals will magnetize the core and establish a flux path. Later at t>0, fast varying, low magnitude pulses resulting from PD activity begin to flow into the primary conductor of the CT. The H field required to characterize the behavior of the core material when subject to PD activity can be approximated as:

$$H = H_{fundamental} + H_{PD}$$

5-9

$$H_{fundamental} = H_0 \sin\left(2\pi f_0 t\right)$$

5-10

$$H_{PD} = H_1\left(e^{(-\alpha t)}\right)\sin\left(2\pi f_1 t\right)$$

5-11

$$H = H_0 \sin\left(2\pi f_0 t\right) + H_1\left(e^{(-\alpha t)}\right)\sin\left(2\pi f_1 t\right)$$

5-12

Where $f_0$ is power frequency component while $f_1$ is the frequency component of damped sinusoid. $H_{fundamental}$ is the magnetic field intensity due to the fundamental frequency component and $H_{PD}$ is the magnetic field intensity resulting from fast rising PD pulse which is approximated as a damped oscillatory signal [Foo 2003] as shown in Figure 5-7. The $H$ field due to both $F_{undamental}$ and $H_{PD}$ using eq (5-12) is shown in Figure 5-6.

The solution of J-A model in eq (5-3) for the magnetic field intensity using eq(5-12) for the material permalloy which is normally used as core material for CT with hysteresis parameters used in [Jiles 1994], give the sigmoid shape characteristics shown

in Figure 5-8. The solution of eq (5-3) using the Euler method is included in the Appendix C-2. The solution of the J-A equations gives magnetization M.

Flux density B can be obtained using the following relation:

$$\mathrm{B} = \mu\left(H + \alpha M\right) \qquad 5\text{-}13$$

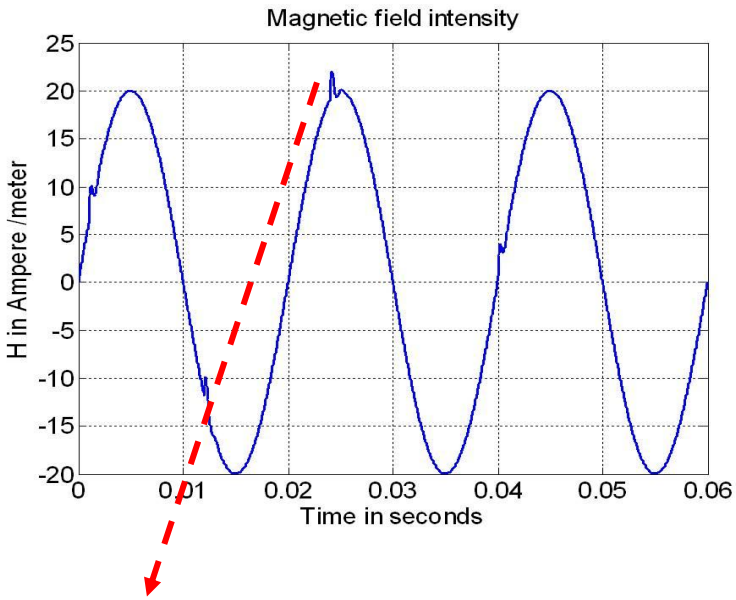


Figure 5-6 H field used to solve J-A model

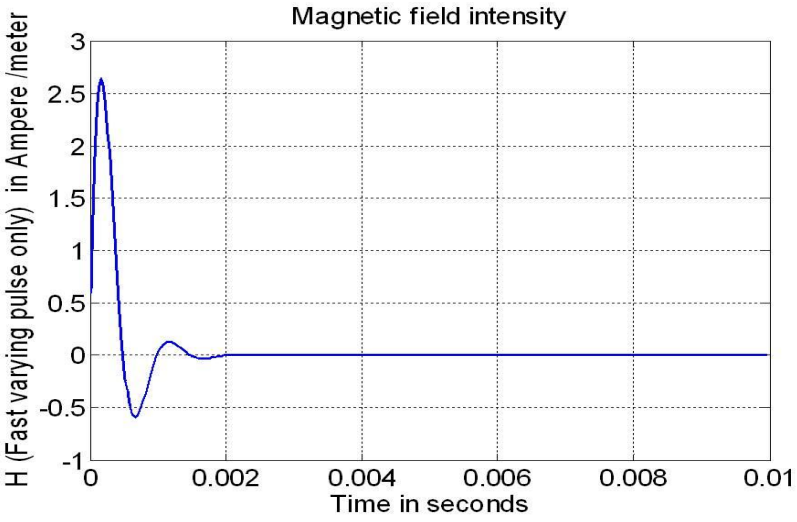


Figure 5-7 Damped sinusoid PD pulse

Figure 5-8 shows B-H loops for various permeabilities. The area under the BH loops gives the total magnetic loss which includes hysteresis and eddy current loss. The

eddy current loss depends upon the resistivity of core material and frequency (this may be negligibly small in case of ferrite material used in high frequency applications). Magnetic Parameters namely remanant magnetization, saturation magnetization varies as the permeability is varied. Harmonic components present in an excitation field will introduce minor loops in the BH loop which increases the hysteresis loss [Copeland 1966; Robertson and Zaky 1969]. The term "minor loop" is used to mean any closed B-H curve other than the fully saturated one. Minor loop can be symmetrical or asymmetrical [Carpenter 1991].

Based on the figure as shown below, effect of fast varying field due to a PD signal present in power frequency signals starts to appear as minor loops once the permeability is increased. These minor loops are resulted from the oscillatory field $H_{PD}$. This indicates that magnetic domains are aligned in the direction of the applied field. When the PFCT is used to detect PD the core is magnetized by the power frequency signal which forms a major hysteresis loop. When fast varying low power PD's occur magnetic domains aligned previously with the power frequency signal will not respond with respect to the H field caused by the PD signal. Hence this will reduce the transformer action which makes the fast varying pulses couple through the inter winding parasitic capacitance [Mohamed, Siew et al. 2009].

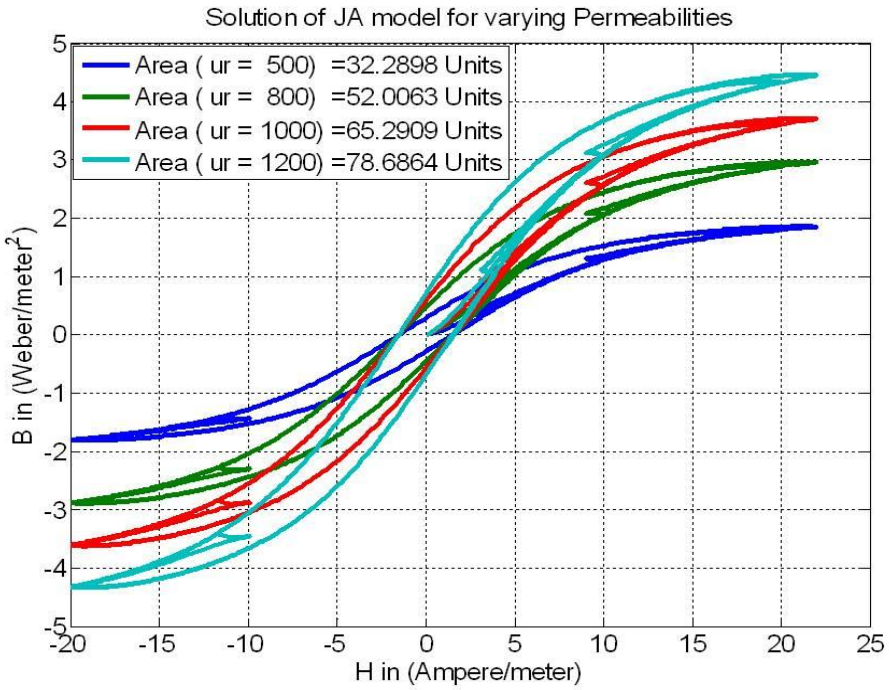


Figure 5-8 Solution of J-A equations for variable permeability

## 5.4 Frequency Response Analysis of PFCT

CTs are typically designed to operate at power frequencies. As such, the high frequency performance characteristics of these CTs are not normally provided by the manufacturer. [Redfern, Terry et al. 2004] has investigated the frequency response of transient performance of protection CTs between the frequency ranges of 1 KHz to 100 KHz. However, this frequency range is low in comparison to the typical PD frequency band. In this thesis, FRA of power frequency CT dismantled from 33/11 kV substation is conducted in a frequency band of power frequency to 50 MHz.

Figure 5-9 shows the test setup used to obtain the frequency response measurement of a PFCT. A signal generator feeds RF power amplifier, which is terminated with RF load of 50 Ω via series connected primary conductor. The secondary winding is terminated with a rated burden using wire wound resistor and the secondary current is measured using a HFCT clamped in the secondary winding terminal of the CT.

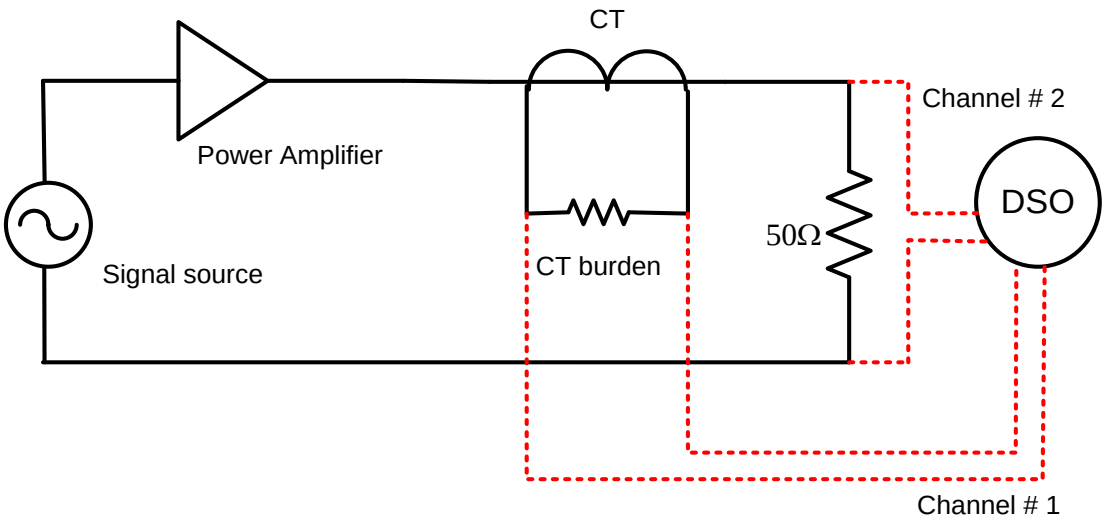


Figure 5-9 FRA test setup

The size of the primary conductor used in FRA of PFCT experimental setup plays an important role especially at high frequencies. At high frequencies, stray capacitance dominates which becomes a low resistance path for the high frequency signal. The primary conductor diameter is calculated based on the knowledge of corona and breakdown strength in air. The primary conductor together with the toroidal CT is

approximated by coaxial cylinder geometry [E. Kuffel 2006] as represented in Figure 5-10 .

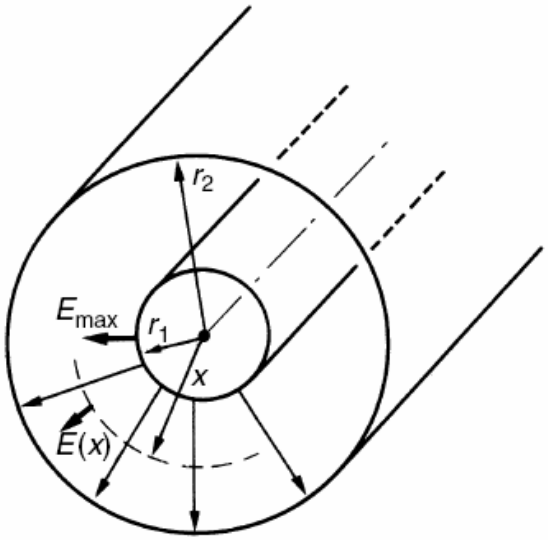


Figure 5-10. Coaxial cylindrical geometry approximation

The central conductor goes into corona whenever the electric field at the surface of the conductor exceeds a certain critical field, termed as corona inception field, which depends on the atmospheric conditions and the radius of the conductor [Cooray 2000]. Corona inception field is independent of size of the outer conductor and is given by

$$E = 3.15^{*}\ 10^{6}\ k\delta\left[1+\left(\frac{0.308}{\sqrt{\delta r_1}}\right)\right] \qquad 5\text{-}14$$

Where δ , Relative density of air which is given by $\delta = \frac{3.92b}{273+t}$

*b*, barometric pressure in centimetres

*t*, temperature in centigrade

*k*, Surface condition of the conductor which is 1 for smooth surfaces

$r_1$, Radius of the conductor in centimeters

When electrical field at the surface of the inner conductor exceeds the breakdown strength of air, the air at that point becomes conducting, or corona forms, thus in effect, increasing the size of the conductor. This increases for the given voltage until the flux density or gradient is below the rupturing gradient,when it cannot spread

any more. If this increase lowers the gradient, the breakdown will be local, and the corona is on the wire. If the conductors are veryclose together,a spark strikes between them immediately and corona cannot form.

If the ratio R/r in cylindrical geometry is such that the increase in size of the conductor by the conducting air increases the gradient, then break down area will continue to enlarge, or spark-over will occur.

The radial distribution of the electric field for the coaxial cylinder geometry as a function of radial distance from the inner conductor surface is given by the following relation

$$g = \frac{e}{x * \log\left(\frac{r_2}{r_1}\right)}$$

5-15

Where,

*e*, applied voltage between the coaxial cylinders,

$r_2$, radius of outer cylinder in centimetres,

$r_1$, radius of Inner cylinder in centimetres,

*x*, radial distance from the inner cylinder surface in centimetres,

*g*, electrical field between coaxial cylinders,

For a constant value of *e* and $r_2$, the value of $r_1$ which makes g minimum can be obtained by differentiating eq (5-15) with respect to $r_1$

$$\frac{de}{dr_1} = \mathrm{g}\left[\mathrm{r}_1\left(\frac{r_1}{r_2}\right)\left(\frac{-r_2}{r_1^2}\right) + \log_e\left(\frac{r_2}{r_1}\right)\right]$$

5-16

Equating 5-16 to zero yields

$$\log_e\left(\frac{r_2}{r_1}\right) = 1$$

$$\left(\frac{r_1}{r_2}\right) = e^{-1} = 0.368$$

5-17

The threshold value of, $r_{1/}\ r_2$ provides a condition such that partial breakdown can be avoided in a cylindrical geometry. Figure 5-11 shows the variation of g using coaxial cylinder geometry for various inner conductor diameters with a fixed outer conductor diameter and constant voltage of 11 kV between inner and outer cylinders.

When $r_1/r_2 = 0.368$, corona does not form. [F.W.Peek 1920].

Two primary conductor diameters namely $d_l$ and $d_h$ are chosen to study the effect of the primary conductor diameter on the frequency response of the PFCT obtained from Figure 5-11. Primary conductor diameter $d_l$ lies below the threshold and $d_h$ lies above the threshold in such a way that the breakdown strength of air is not reached at the specified voltage level.

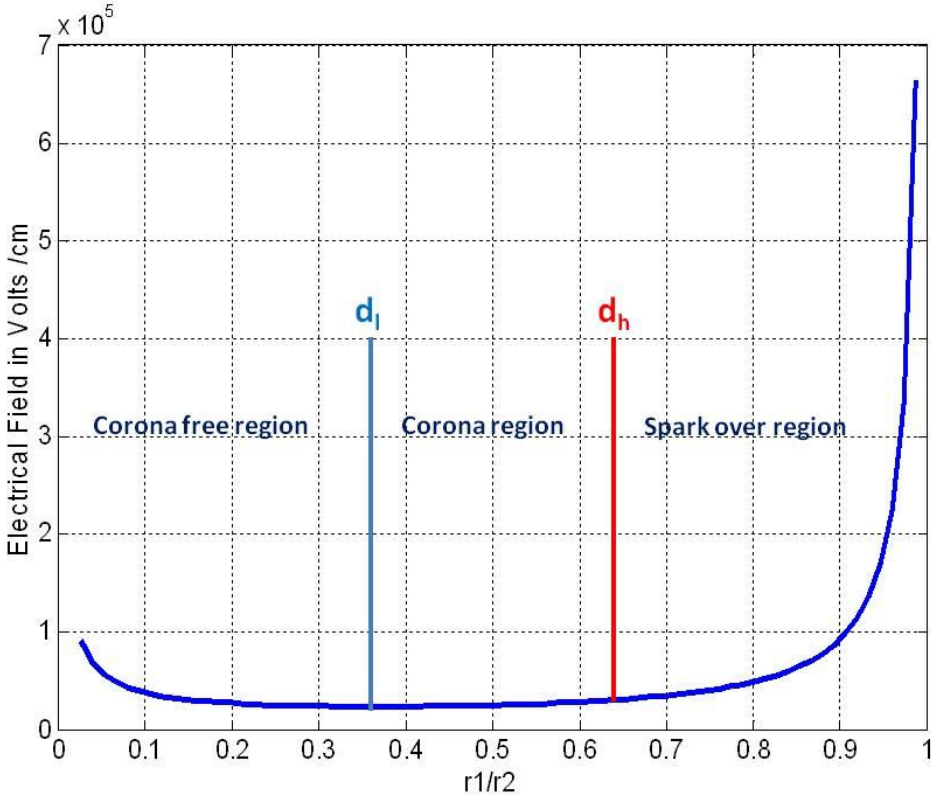


Figure 5-11 E field as a function of inner diameter of primary conductor

FRA of two different CTs, 400/5A, 11 kV 15VA, and 600/5A, 11 kV, 15VA, using primary conductors of diameter $d_l$ and $d_h$ is conducted and the results are shown in Figure 5-12 to Figure 5-15. Based on the Figure 5-12 to Figure 5-15, the FRA results show three different frequency zones exhibiting different frequency ranges and trends.

Zone A: (50 Hz $\leq$ f<100 kHz)

Zone B: (100 kHz $\leq$ f<1MHz)

Zone C: (1MHz $\leq$ f<50MHz)

The frequency response of both CTs indicates the transformer action operating satisfactorily in the frequency range represented by zone A. This is where the secondary current is an exact replica of the primary current, irrespective of conductor diameter. As the frequency is increased further from 100 kHz towards 1 MHz in zone B, the secondary current gradually decreases due to frequency dependent magnetic losses. In zone C the magnetic domains do not respond resulting in the loss of transformer action, causing the current to couple with the secondary winding through inter winding capacitance. It is in the frequency range represented by zone C where fast varying partial discharge signals can be detected. The gain for a primary conductor of diameter $d_h$ is higher than that of $d_l$, which is due to the low impedance path provided by parasitic inter winding capacitance.

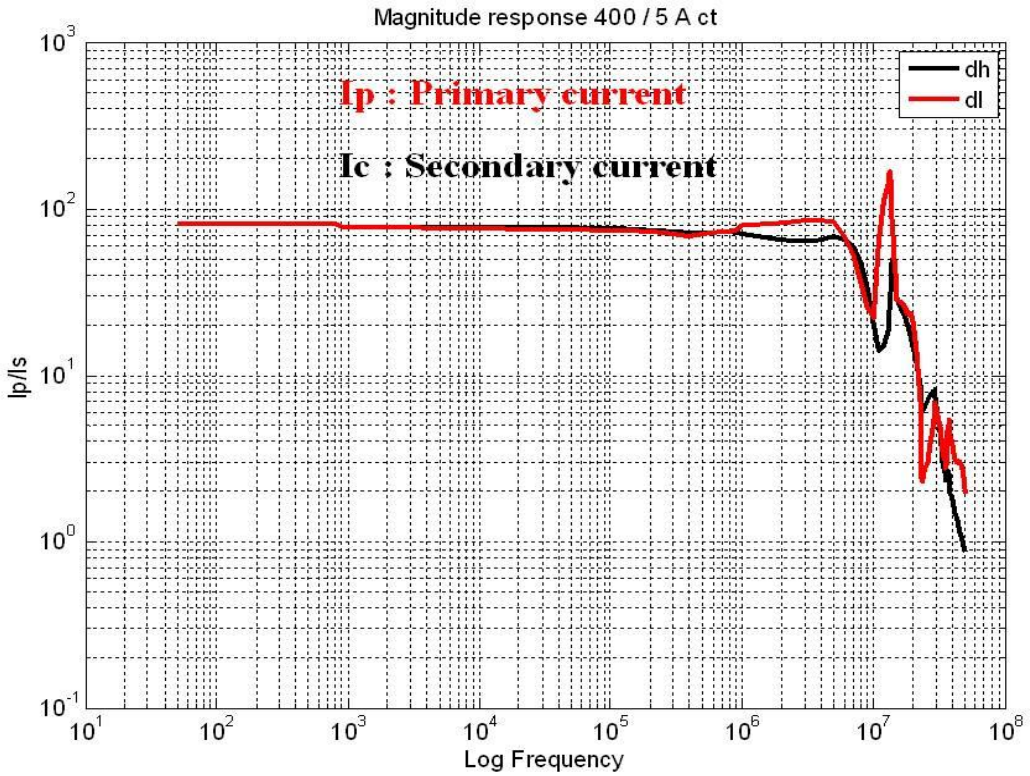


Figure 5-12 Magnitude response of PFCT #1

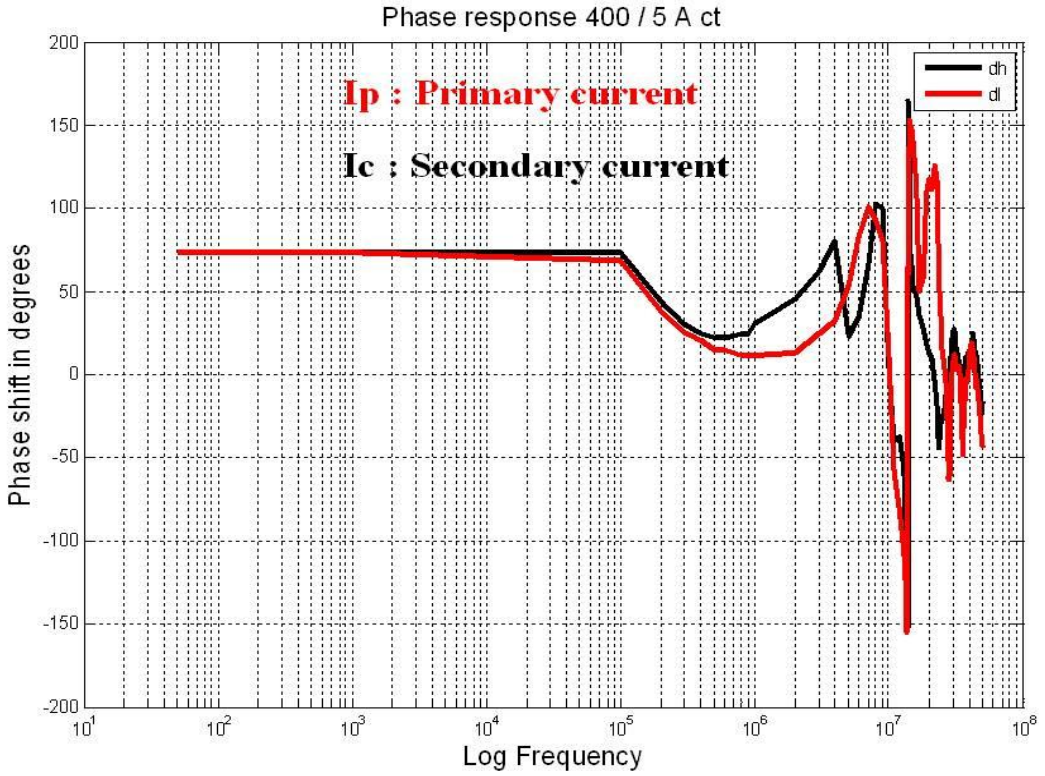


Figure 5-13 Phase response of PFCT #1

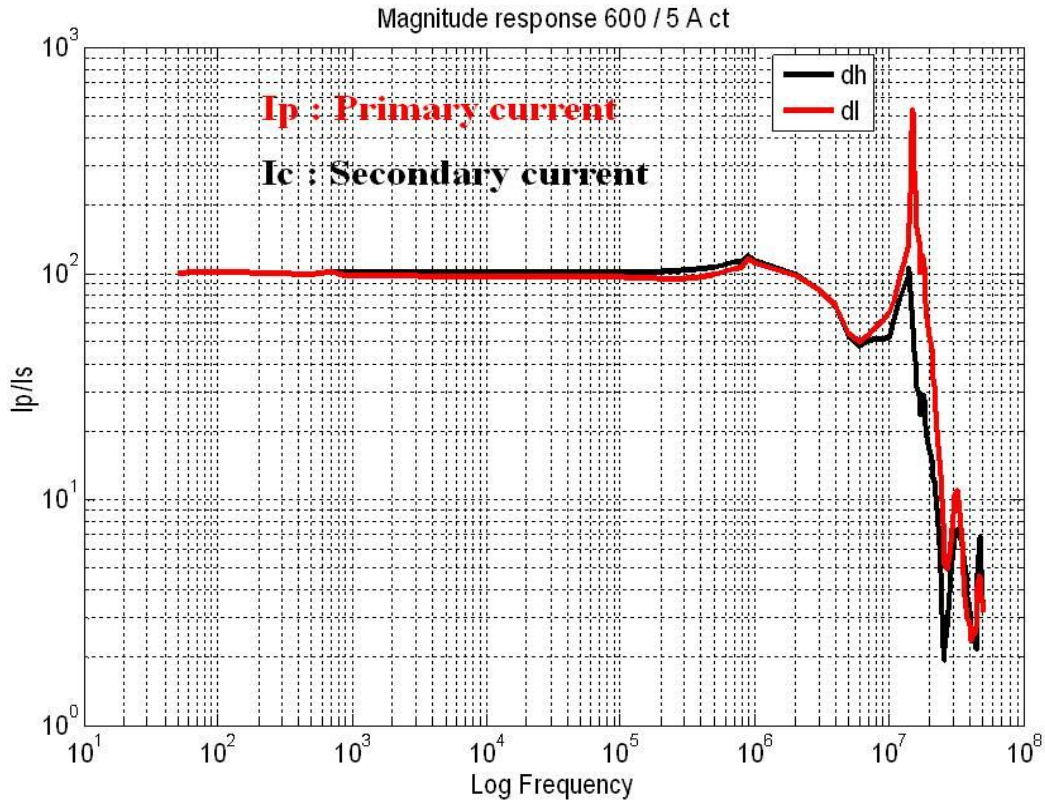


Figure 5-14. Magnitude response of PFCT #2

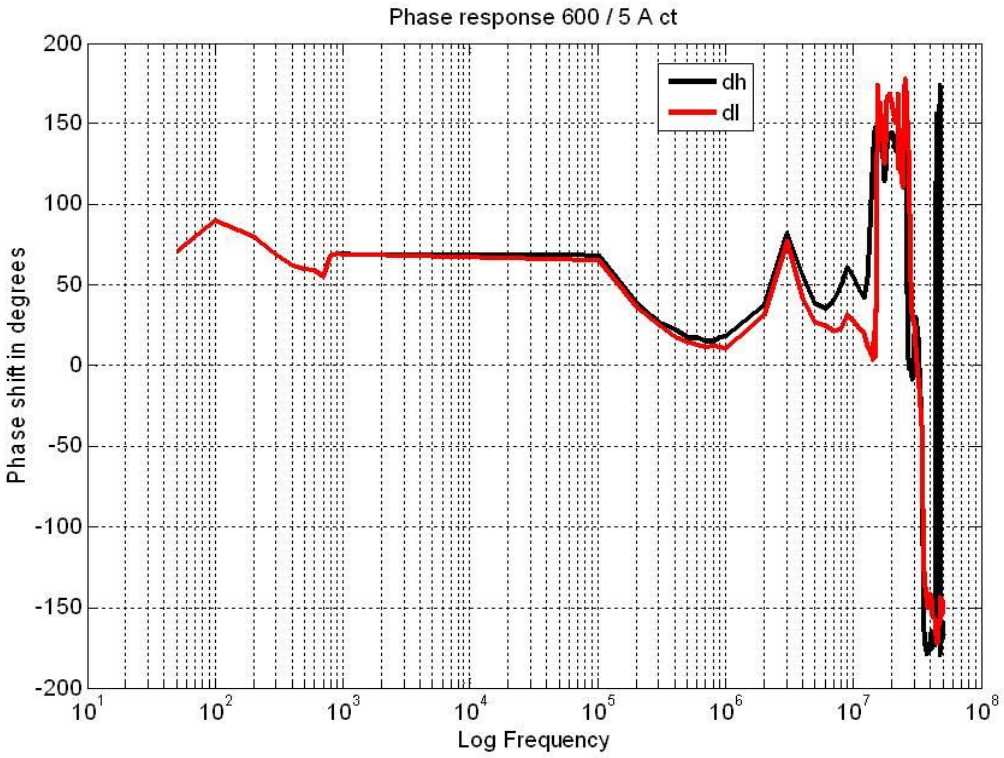


Figure 5-15 Phase response of PFCT # 2

## 5.5 Time domain measurements using PFCT

Further to frequency domain measurements, time domain measurements were also conducted by feeding an exponential pulse having rise time of 10 µs, which is generated using an arbitrary waveform generator. The same test setup discussed in Figure 5-10 is used in this case. Time domain measurements are shown in Figure 5-16. In Figure 5-16 yellow trace represents the primary current while blue trace represents the secondary current. Faithful reproduction of secondary current is achieved at this frequency based on the calculations included below.

$$I_p = \frac{9.227}{50} = 184.54\text{mA}$$

$$\mathrm{I}_S = \frac{2.413*10^{-3}}{0.5} = 4.826\text{mA}$$

$$\text{Ratio error} = \left( \frac{\left(I_p / N\right) - I_s}{I_s} \right) \times 100 \qquad 5\text{-}18$$

$$= 4.4\%$$

*Where,* $I_p$ Primary current, $I_S$ Secondry current, $N$ CTratio

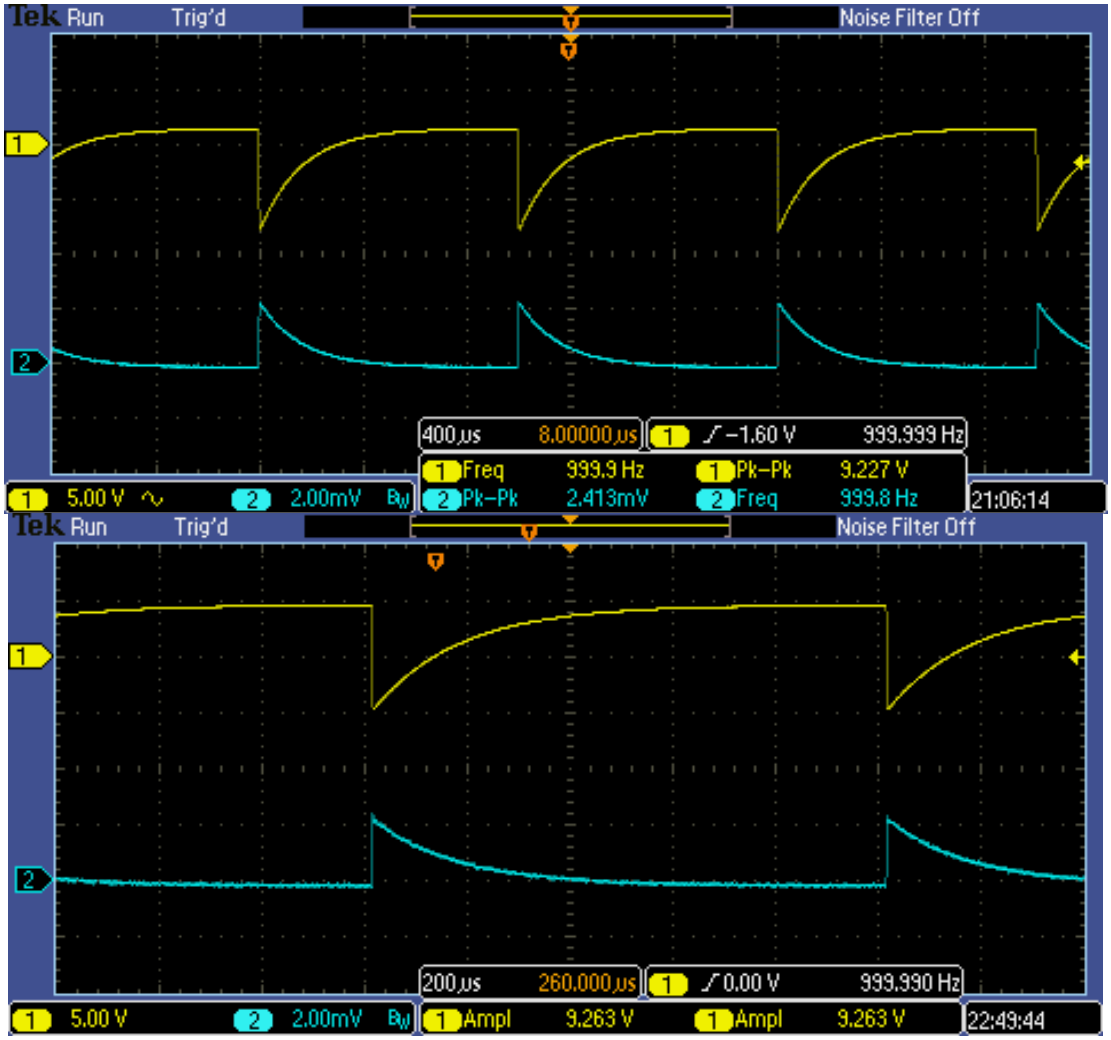


Figure 5-16 Time domain measurements in 200/5A CT

Both frequency domain and time domain measurements discussed in the above Sections 5.4 and 5.5 are based on resistive burden using wire wound resistor. However the nature of burden (resistive or inductive) connected to PFCT in on-site is determined by either relay coil as in protection CT or metering coil in measurement CT. If the burden has dominant inductive component, it can affect the frequency response of PFCT. Though the wire wound resistor used as burden in this experiment has inductive component, ratio of L/R was not known. Hence in case of using PFCT in on-site, authors suggested quantifying the burden and characterizing the CT.

## 5.6 Remote PD Monitoring System

To validate the method of using preinstalled PFCT instead of retrofitting HFCTs, on-site measurements were conducted using a PD data acquisition system developed for this research project. There are various commercial remote PD monitoring systems available to detect PD from cables using HFCTs[www.doble-lemke.eu, www.hvpd.co.uk; www.hvpd.co.uk]. [Foo 2003] proposed remote PD data acquisition systems which utilize local storage. Local storage need site visits on a regular basis to collect the data back for analysis. [Moore, Portugues et al. 2006] proposed a wireless wide-band radio frequency receiver for PD monitoring in transformers using four wideband antennae with high-speed DSO. The unit must be located near to the substation to permit free band wireless transmission [Moore, Portugues et al. 2006]. [Judd, Li et al. 2005] proposed a PC based system having high speed digitizers and ultra high frequency (UHF) sensors with automated data analysis. [Catterson 2008] proposed a remote PC based PD monitoring system for UHF monitoring of PD activity in transformers. This system uses a high speed digital storage oscilloscope controlled by an on-site PC which incorporates agent based algorithms to pick up important events from the raw data. Baker [Baker, Judd et al. 2010] proposed a low power wireless UHF detector with data acquisition and agent based on-line diagnostics. These PD monitoring systems proposed are focused on PD diagnostics in transformers.

On-line PD measurement using protection CTs can prove impracticable due to design procedures and substation access protocols. Installing PD monitoring hardware across PFCT is not straight forward since it is associated with protection issues. A hardware system for the detection and storage of PD data gathered using PFCTs is not commercially available. It is very important that any hardware used for PD measurement using PFCTs should not alter burden across the protection CT otherwise this would create invalid tripping comments from the relays. In addition, inadvertently altering the CT burden could result in metering errors.

The cost of any monitoring system needs to be weighed against benefits obtained in terms of reduction of failure rates. Proven systems using expensive off-line methods need to isolate the cable from service and these systems cannot pick up the load current dependence of PD activity since the cable under test is at no load. However

off line data interpretation is easier since the testing is done under controlled conditions. Cables exhibiting a high level of PD have a greater risk of failure than cables with little or no PD activity [Michel 2007]. As a result utilities always prefer on-line monitoring which does not require any system outage. As discussed in section 1.1, spot testing has the major disadvantage in that this method cannot pick up the intermittent nature of PD activity since PD occurs in regular cycles with varying magnitude which depends upon circuit conditions, weather condition, asset condition and age [Cliff Walton 2009]. To address this disadvantage, an asset needs to be monitored over a longer period, thus allowing a clear PD trend to be obtained.

Figure 5-17 shows typical intermittent nature of PD activity over longer period. This plot shows the importance of continuous PD monitoring over spot testing. Continuous PD monitoring needs constant site access which is difficult and may be impossible. The issues relating to CT burden,namely loading of the cable network ,intermittent nature of PD actvity and substation accessibility protocol, lead to the design of RPDMS.

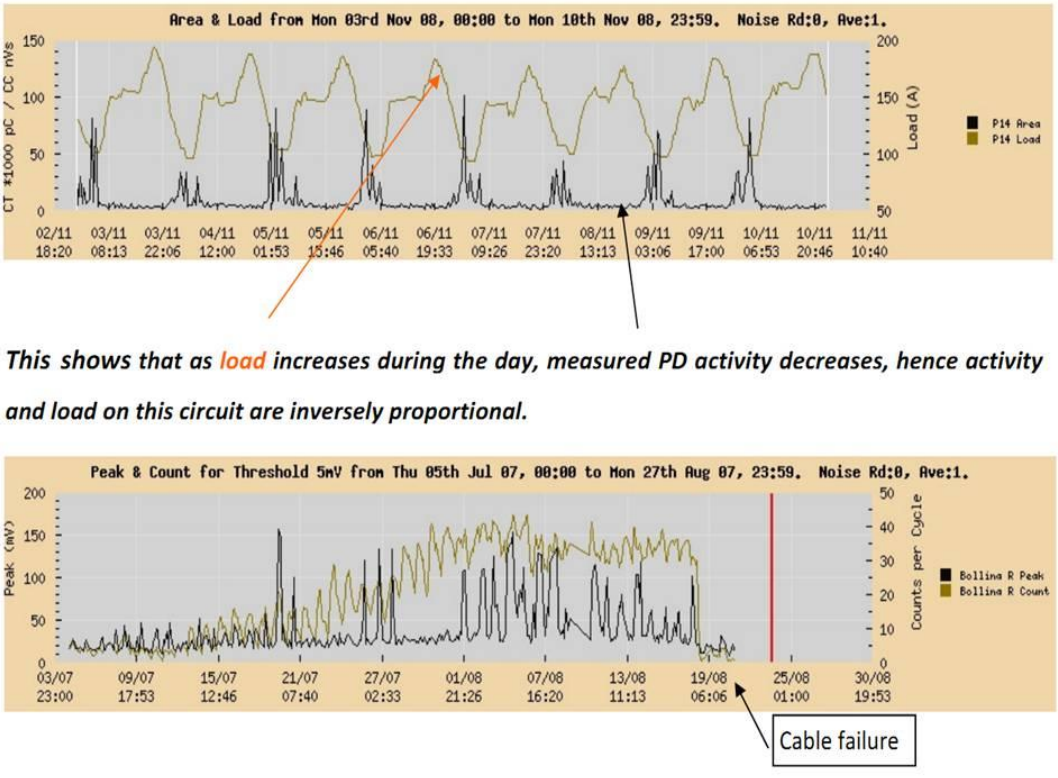


Figure 5-17 Intermittent nature of PD activity[Cliff Walton 2009]

### 5.6.1 Hardware - Design

System proposed in this thesis for PD detecion is RPDMS, a PC based single ended system which is based on client server technology. Hence two PCs are required. One PC for RPDMS/server which will be located in the on-site and other for the RPDMS/client which can be located in any of the control room. This system can be viewed as an extension of system proposed in [Foo 2003]. Functional block diagram of RPDMS for PD detection through power frequency CT is shown in Figure 5-18.

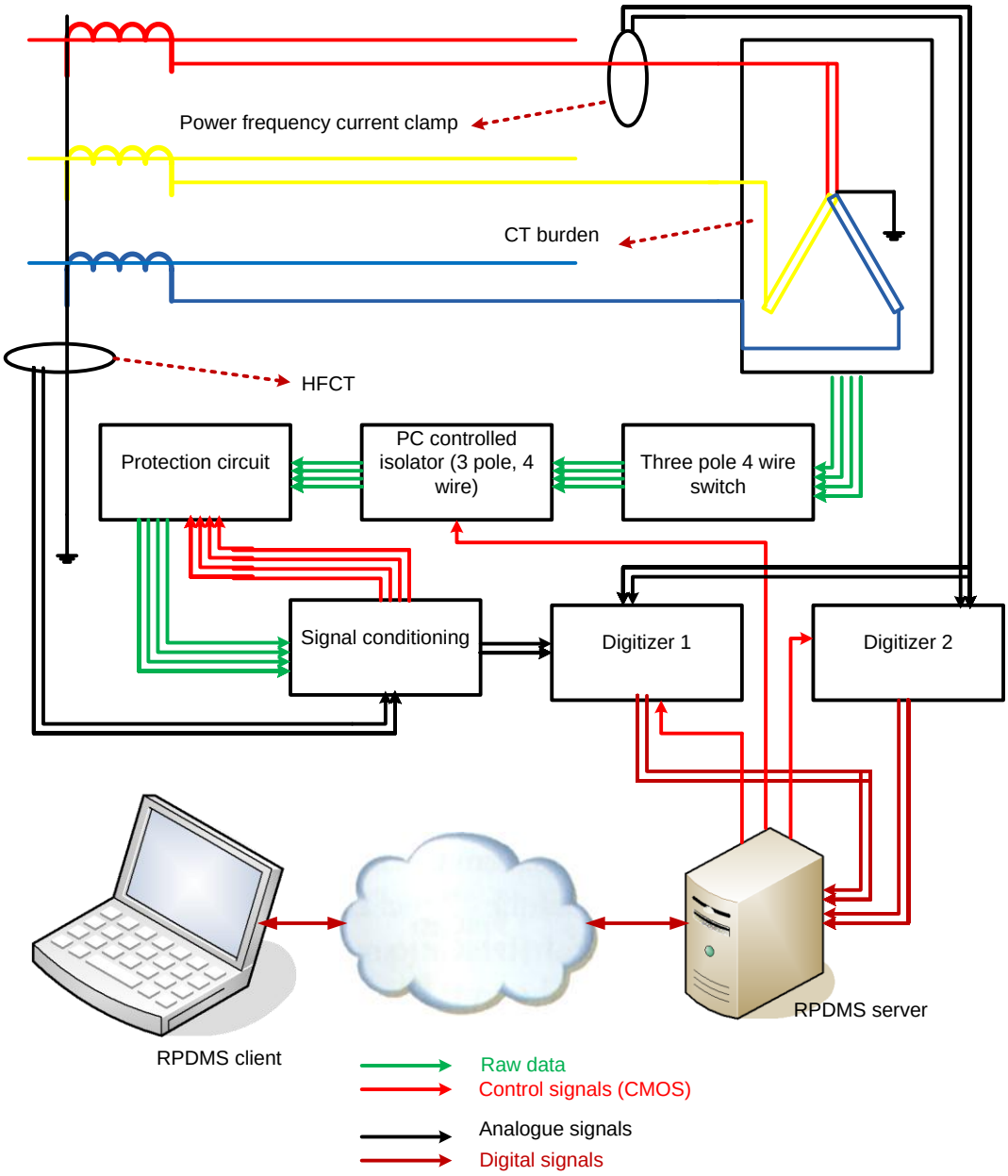


Figure 5-18 RPDMS (single ended) block diagram

RPDMS is connected across burden of PFCT to measure the voltage across the burden which contains power frequency component and PD signal. Communication between RPDMS/client and RPDMS/server is established via VPN using mobile broadband internet connection. Basic building blocks of the system included sensor units, signal conditioning, data acquisition and storage and are discussed in the following section.

#### 5.6.1.1 Protection Circuit

The functional block diagram of the protection circuit is shown in Figure 5-19 which includes a three pole switch, a source follower/buffer and a PC controlled isolator. Protection circuits serve two purposes, one is providing high input impedance to the hardware thereby maintaining the existing CT burden, and second is the isolation of the system in the event of any fault in the hardware. This means healthy systems will only be connected across PFCT using the self check algorithm discussed below.

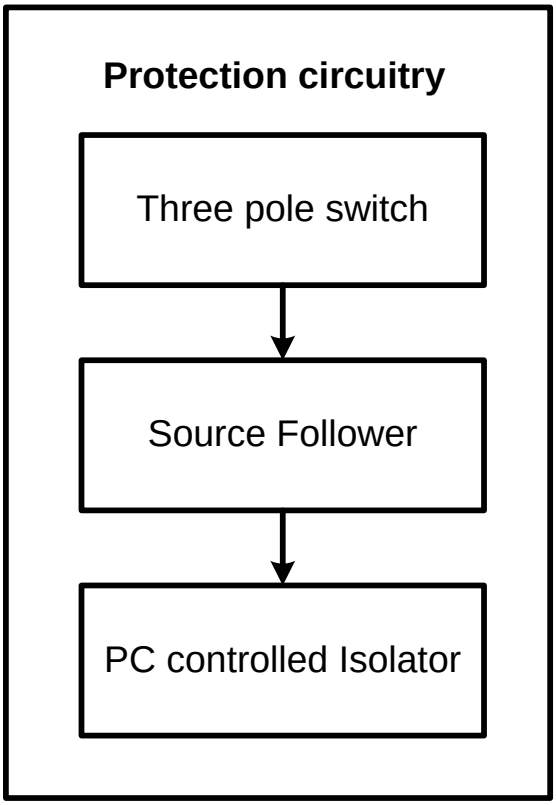


Figure 5-19 Protection circuit block diagram

The first block in the protection circuitry is three pole 4 wire switch shown in the Appendix C-3. Three poles of the input ports are connected across three single phase CTs which are connected in Y(star). The fourth wire is connected to the neutral point of the Y connection. The output port of the switch has coaxial cable with BNC connectors.

The source follower/Buffer is basically an inverting operational amplifier which provides high input impedance of a few mega ohms to the RPDMS and has a bandwidth up to 60 MHz. The schematic diagram of the source follower is shown in Figure 5-20. This circuit was inherited from previous work [Foo 2003]. Photograph of protection device is included in the Appendix C-3.

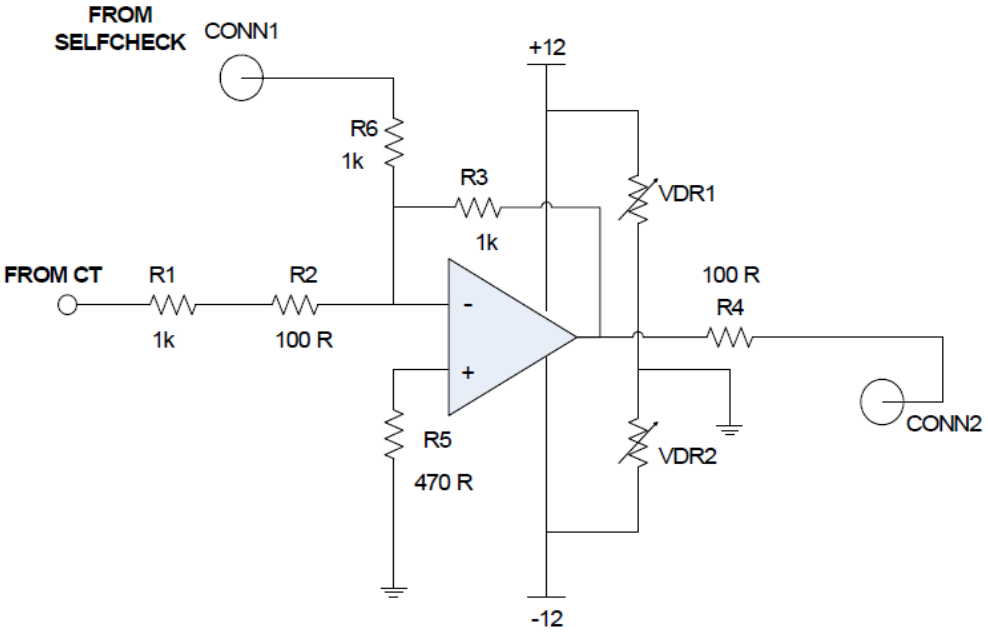


Figure 5-20 Source follower schematic [Foo 2003]

A PC controlled switch forms a vital part of the protection circuitry. It includes optical isolators(ASSR-1228-002E), freewheeling diode (IN4148), solid state relay(G7J-4A-B12 VDC from Omron) having dielectric strength of 4kV and parallel LPT interface for PC control. The schematic of the PC controlled isolator is shown in the Appendix H and a photograph is included in the the Appendix C-3.

The self-check operation is performed before each data acquisition is initiated to ensure the integrity of RPDMS. A burst of pulses having duration of 2 milli seconds is transmitted from the pre-processing filter unit (discussed in the section 5.6.1.2). inputs (SELF CHECK) of the inverting amplifier. Inverted output signals will be captured by the data acqusition card (described in the section 5.6.1.3) followed by storing the data in

the RPDMS server. The self checking algorithm in RPDMS server compares the magnitude and phase shift between of the captured waveform with an initial template from the pre-processing filter. In the event of no fault condition, phase shift of $180^0$ will be obtained with the same amplitude as the input signal. Upon successful execution of a self check operation, the PC controlled oscillator will connect the RPDMS across the PFCT installed in the cable network. Self check sequences are as shown in Figure 5-21. In this way the PC controlled isolator will connect the RPDMS to the SP network when the RPDMS is healthy. Once the PD data acquisition is finished, PC controlled switch will isolate the RPDMS from the cable network.

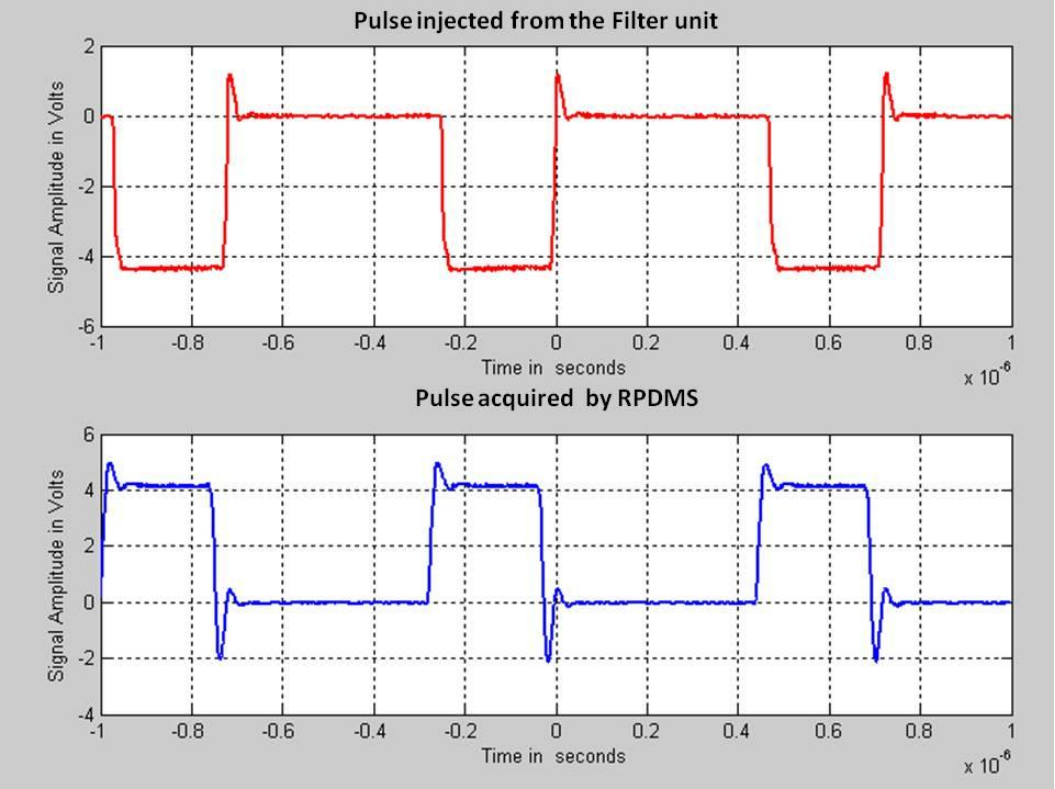


Figure 5-21 Self check signals

Since the protection circuitry includes switches and relay contacts which are not designed for high frequency application, it needs to characterize the high frequency behaviour. Frequency response of the protection circuitry using network analyser (AGILENT 4395A) is as shown in Figure 5-22. Frequency response shows attenuation of maximum 2 db at 50 MHz which can be safely ignored.

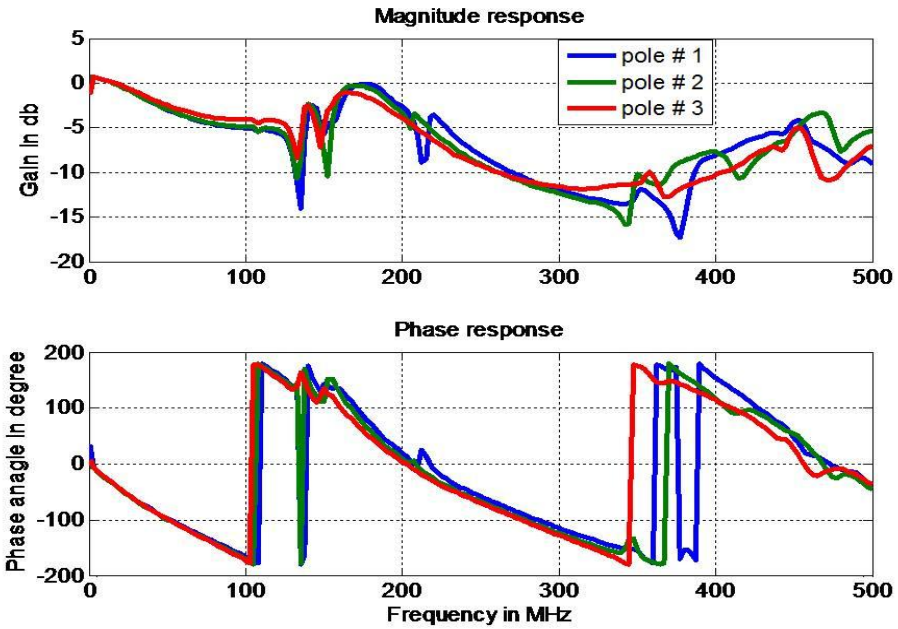


Figure 5-22 Frequency response of protection circuit

### 5.6.1.2 Signal Conditioning Unit

The signal conditioning unit provides noise reduction in addition to enhancing the PD signals. This unit consists of multi channel amplifiers, attenuators, high pass filters, band pass filters, multiplexers and pulse injection circuitry. The individual components on both channels can be activated independently, also filters can be bypassed. A block diagram of the signal conditioning unit is shown in Figure 5-23.

Gain of amplifiers and attenuators can be varied based on the SNR of the signal to be measured. High pass filters are designed specifically for the removal of the 50Hz component present in the signal. This will give wide band detection of PD with better amplitude resolutions. Narrow band PD detection is achieved using band pass filter having variable centre frequency with bandwidth up to 60MHz. Certain bandwidths of the signal with strong PD activity can be extracted through in narrow band PD detection. A Pulse injection circuit provides a burst of square pulse which exist for short duration of 2 milli seconds. This pulse is used as an input in the self checking circuitry (discussed in section 5.6.1.1). A Multiplexer unit provides the input selection for the data acquisition system. A Photgraph of signal conditioning unit is shown in the Appendix C-3.

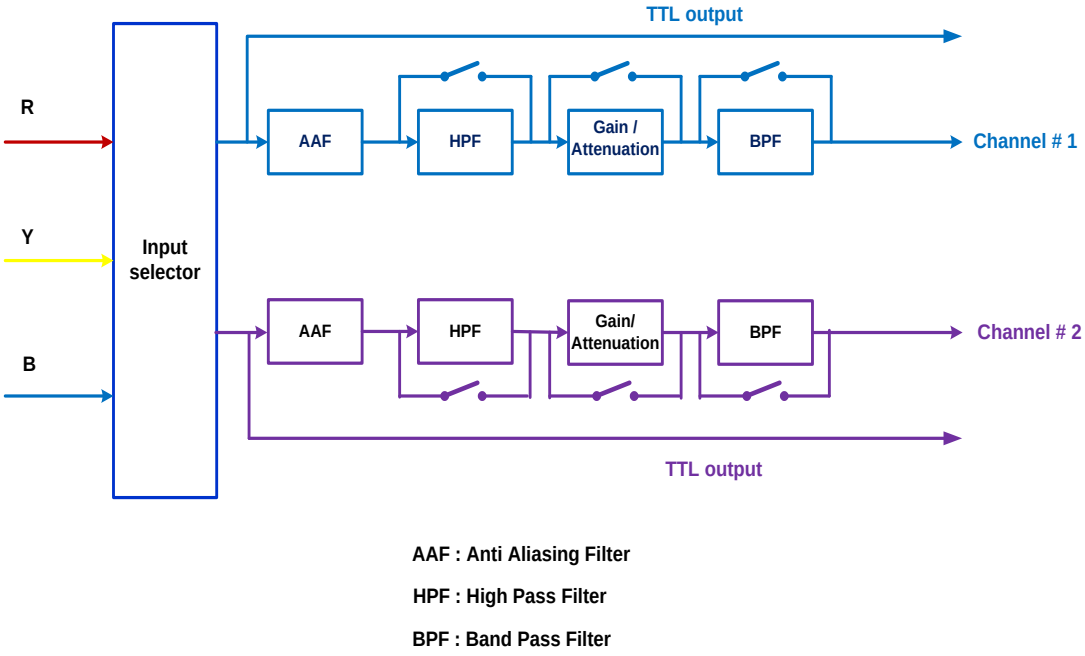


Figure 5-23 Pre-processing filter [Foo 2003]

### 5.6.1.3 Data Acquisition Card

PD signals from PFCT are acquired using a commercial data acquisition card [CS 14100, http://www.gage-applied.com]. (This card has two analogue channel inputs with sampling rates up to 100 Msps for single channel and 50 Msps for dual channel). The amplitude resolution of the card is 14 bits and has 8 Mbyte of onboard memory. This card is installed in the full length PCI slot of the industrial PC . The industrial PC is equipped with additional fans for cooling the data acquisition card. Data acquisition and control are obtained through software developed using Microsoft visual studio.net 2005 (described in section 5.6.2). A photograph of a data acquisition card CS1400 is shown in Appendix C-3.

### 5.6.1.4 High Frequency Current Transformer

To correlate the PD signals acquired using PFCT with other inductive couplers, HFCT (www.ipec.co.uk) is used. A photograph of HFCT is included in Appendix C-3. Existing PFCT in Y and B phase conductors and HFCT connected to the earth strap of the cable are connected to the RPDMS. FRA of HFCT is conducted in the laboratory and the results are as shown in Figure 5-24.

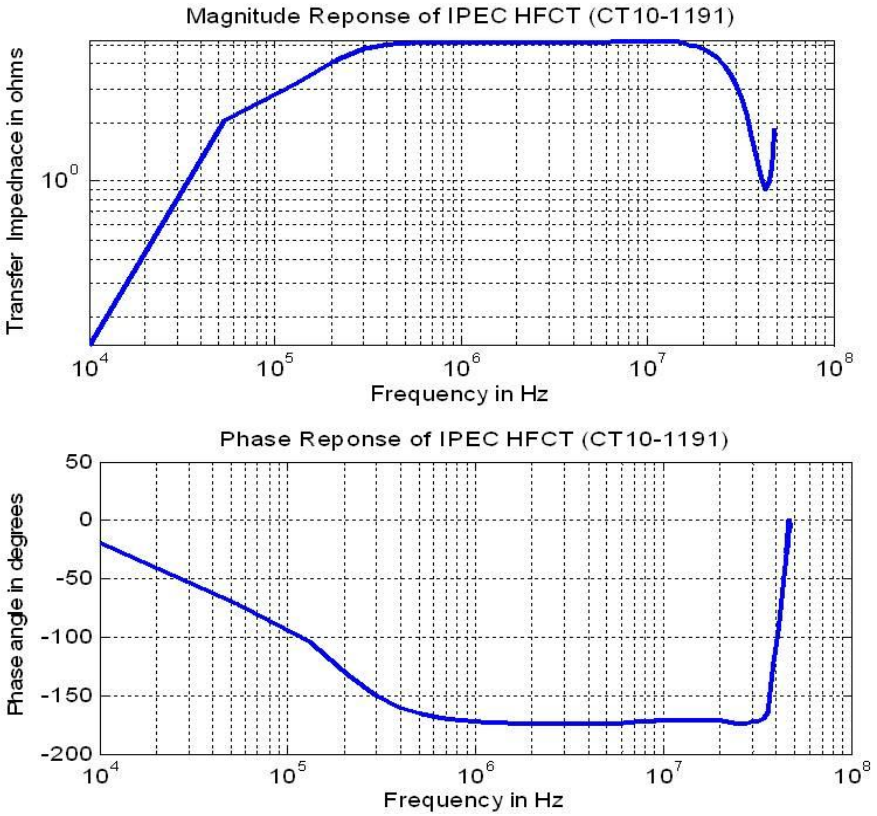


Figure 5-24 FRA of HFCT

#### 5.6.1.5 Load Current Monitoring

To study the interdependence of PD activity with cable loading, load current monitoring is employed in RPDMS. A clamp on current probe with low insertion impedance of 10 mΩ is clamped around the secondary winding of PFCT. A photograph of the current clamp used in the design is shown in the Appendix C-3. Output of the current clamp is connected to the analoge input of digitizer # 2 (NI-USB6008, http://www.ni.com). A photograph of digitizer # 2 is as shown in the Appendix C-3. The Current clamp serves two purposes namely measuring the load current and acting as external trigger source for the digitizer # 1.

### 5.6.2 Remote PD Monitoring System-Software Design

RPDMS Client and Server are controlled by the software developed using Microsoft Visual studio.net 2005. Complete software structure is incorporated into several components which runs in individual threads through distributed messaging systems. Each message is sent through TCP/IP to activate the corresponding

component. A functional block diagram of RPDMS software is shown in Figure 5-25. AUI is installed in the RPDMS client while RSI is installed in the RPDMS server.

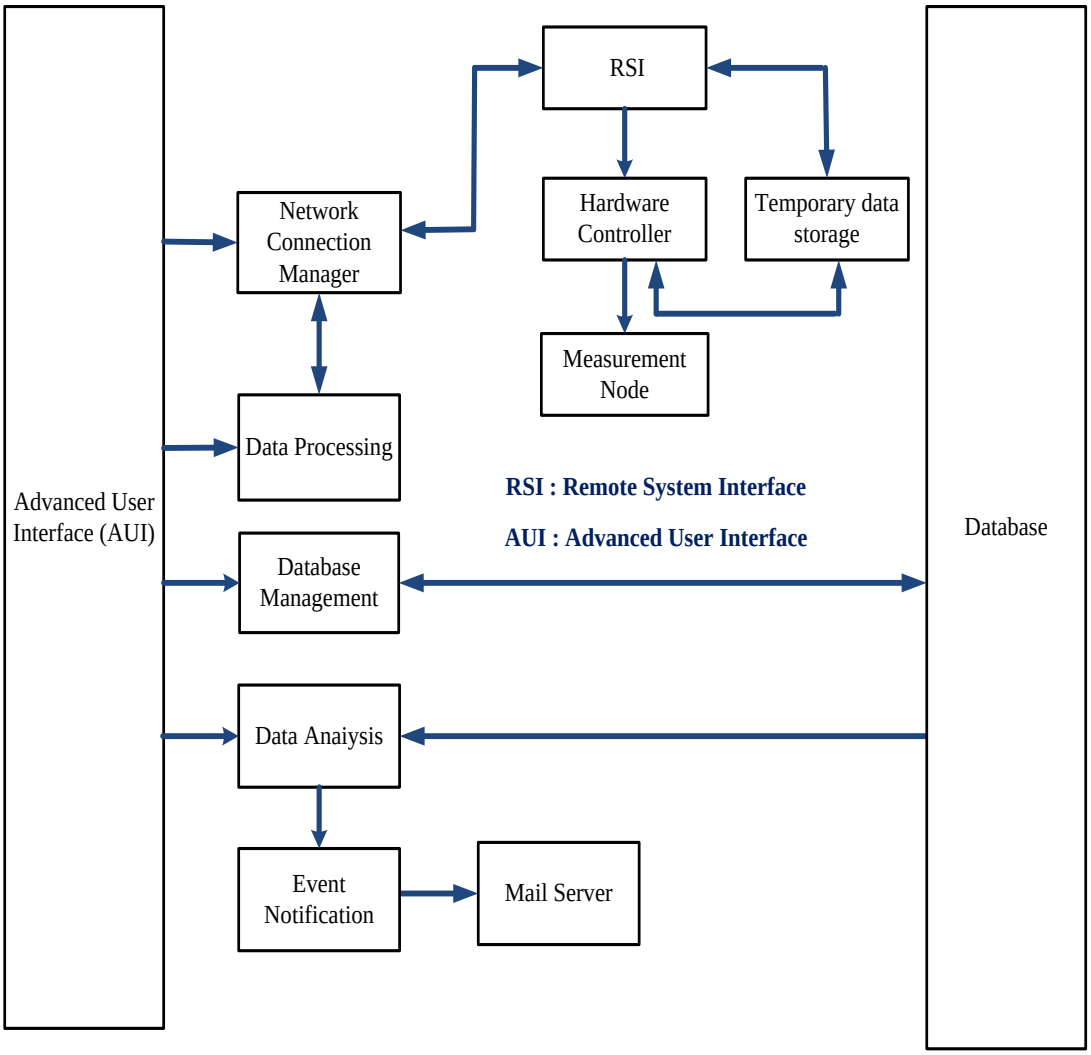


Figure 5-25 Component collaboration diagram

AUI sends a connection request to RSI using the network connection manager once VPN between RPDMS/client and RPDMS/server is established. Then the RPDMS/server will enter into command mode and wait for commands from RPDMS/client. There are two main tasks namely data acquisition and data transfer in the RPDMS/server which are done using "*ACQUIRE*" and "*TRANSFER*" commands from AUI (described in section 5.6.2.1 and 5.6.2.2). The data acquisition process involves transferring the stored data from the DAQ card memory to the RPDMS/server

hard drive. During the data acquisition process most of the PC resources are utilized by the RPDMS server and will lead to an unresponsive program.

Multithreading is implemented in RPDMS/server which shares the PC resources among the multiple threads. It is one of the most widely used techniques to tolerate the memory latency by creating parallel threads. This technique is used when a process has parallel execution paths. Any computer program can be treated as a process which contains many threads which forms subsets of the process. Each thread is a block of code which performs a specific function. In PCs having single core processor, TDM is used for multi threaded operation. Speed Difference between the processor and devices connected to the PCs makes the thread wait a long time to receive information to or from a device. Multithreading will make use of this idle time to utilise for other parallel threads which makes the whole process faster [Kwak, Lee et al. 1999].

Data transfer involves uploading the data from RPDMS server to a remote database developed in SQL server through database management component in RSI. All the events occurring in both RSI and ASI are logged through the event logger component. GUI of RSI and AUI with typical log files are shown in the Appendix C-4. Once the connection between RPDMS/server and RPDMS/client is established, RUI will send the data acquisition file generated by the DAQusing the file generation wizard. The DAQ file contains DAQ card parameters, pre-processing filter unit parameters, substation details and data acquisition interval. The DAQ file generation wizard and sample DAQ files are included in Appendix C-4.

#### 5.6.2.1 Data Acquisition

RPDMS can process two commands namely *"ACQUIRE"* and "*TRANSFER"*. Once RPDMS/server receives "*ACQUIRE* "command from the client, the DAQ file will be loaded, followed by checking necessary hard disc space. Once the conditions are satisfied an .ini file will be extracted from the DAQ file followed by the data acquisition card initialization. Then various operations which include self check operation, pre-processor filter control, and data acquisition and isolate the RPDMS from the cable network are done. Flow chart of the "*ACQUIRE*" command is included in Figure 5-26.

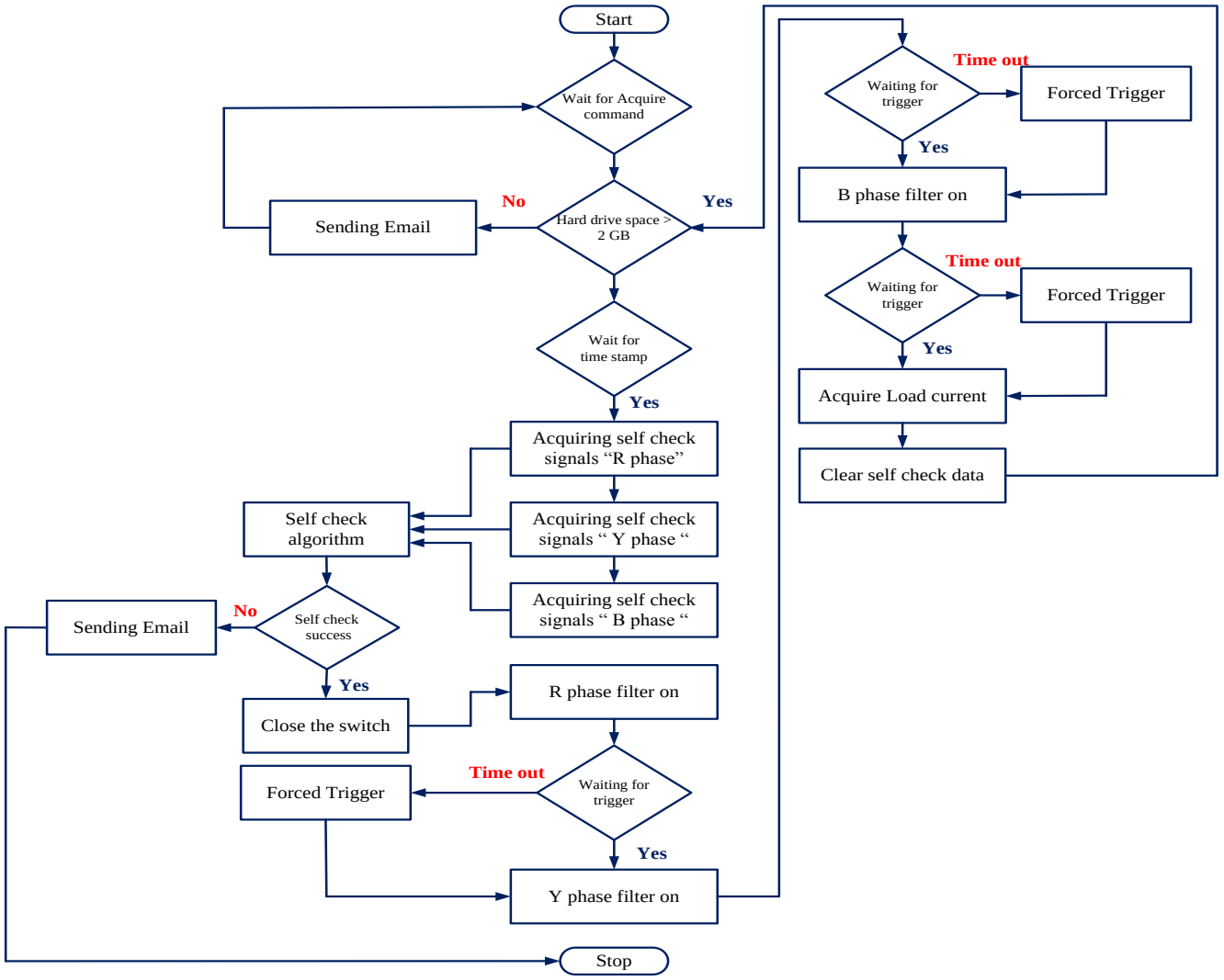


Figure 5-26 Acquire command flow chart

### 5.6.2.2 Data Transfer

RPDMS/server receives "*TRANSFER*" command from RPDMS/client for transferring the data using the data transfer algorithm (described in the section 5.6.2.3) back to the control room . Conventional PD monitoring systems use file based data storage where file management can prove to be problematic when handling large volumes of data. RDBMS using SQL server 2005 is used in this work to store the raw PD Data.

RDBMS is a well-organized collection of data that is related in a meaningful way and that can be accessed in different logical orders. In an RDBMS, data exists as data objects called data tables. Centralized data management, Data migration and system integration are the main advantages of database storage over file based storage. Centralised data management capability of the system helps to access the data from anywhere [S. Sumathi 2007]. GUI of PD Database viewer is as shown in Appendix C-4.

Once the RPDMS server receives a"*TRANSFER*" command from the RPDMS client, connection with SQL server database in the RPDMS client is established. After establishing the connection with database, two tables will be created, one for storing substation information and other for storing the acquired PD data. A flow chart of the "*TRANSFER*" command is shown in Figure 5-27.

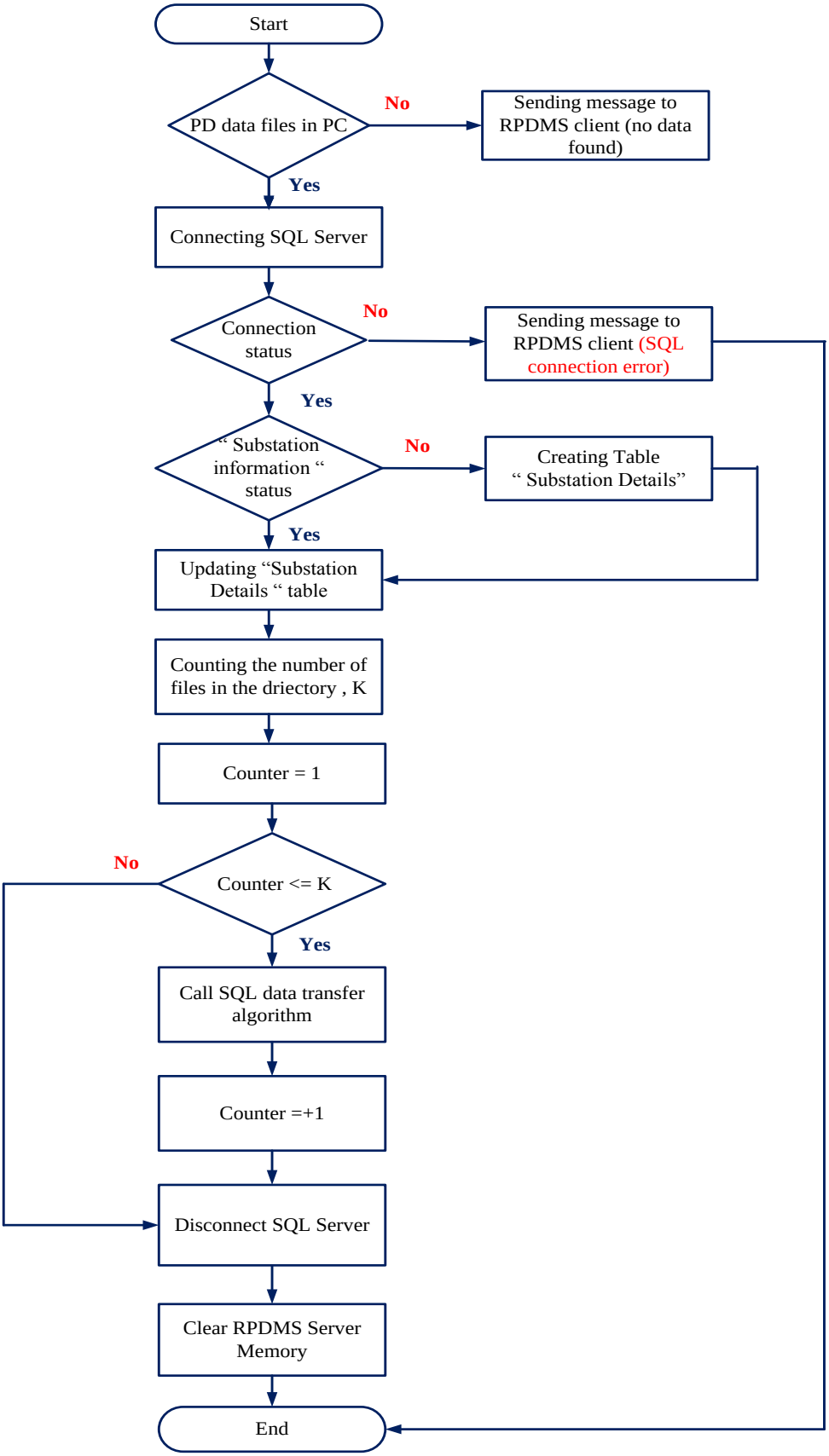


Figure 5-27 TRANSFER command flowchart

### 5.6.2.3 Flexible Data Transfer Algorithm

In order to confirm PD activity from the raw data, it is required to acquire at least one power cycle of data to interpret PD signal features such as rise time, pulse width, and PRPD and PD polarity in the respective half cycle. The RPDMS/server is configured to acquire 4 power cycles of data using 50 Msps. Such data consumes 60 MB in RPDMS/Server. To transfer such large size files back to the database, It is necessary to have a high speed stable broadband connection. Since RPDMS has mobile broadband, transferring such a large volume of data could not be possible. In such a scenario, remote database in RPDMS/client will not respond. This will lead to timeout followed by interruption in data pumping and the program becomes non responsive. One of the aims of this work is to transfer the acquired data from power cables to control room for analysis thereby reducing the frequent site visit. To solve this issue, a data transfer algorithm is developed.

This algorithm splits the data to be transferred into several pockets depending on the internet connection speed. Number of rows, L in the PD data file is obtained using a windows stream reader class [Grundgeiger 2002]. One dimensional buffers of size N lines are chosen based on the internet connection speed. In order to establish a one to one relation between network speeds and buffer length, it is necessary to have an accurate measurement of network characteristics namely delay, loss and bandwidth. Unfortunately it is difficult to measure those due to the heterogeneity of the internet, a trial and error method is used to set the buffer length with respect to network speed. Using the variables L and N, PD raw data is split into several packets which is calculated as follows.

$$\text{No of packets} = \text{Quotient}\,(L/N) + \text{remainder}\,(L/N) \qquad 5\text{-}19$$

Each packet is transferred to SQL server using the “BULKCOPY” method which is faster than entry controlled loops [Vierra 2005]. Hence internet speed, buffer size and time required for data transfer are optimised. The flow chart of data transfer algorithm is shown in Figure 5-28.

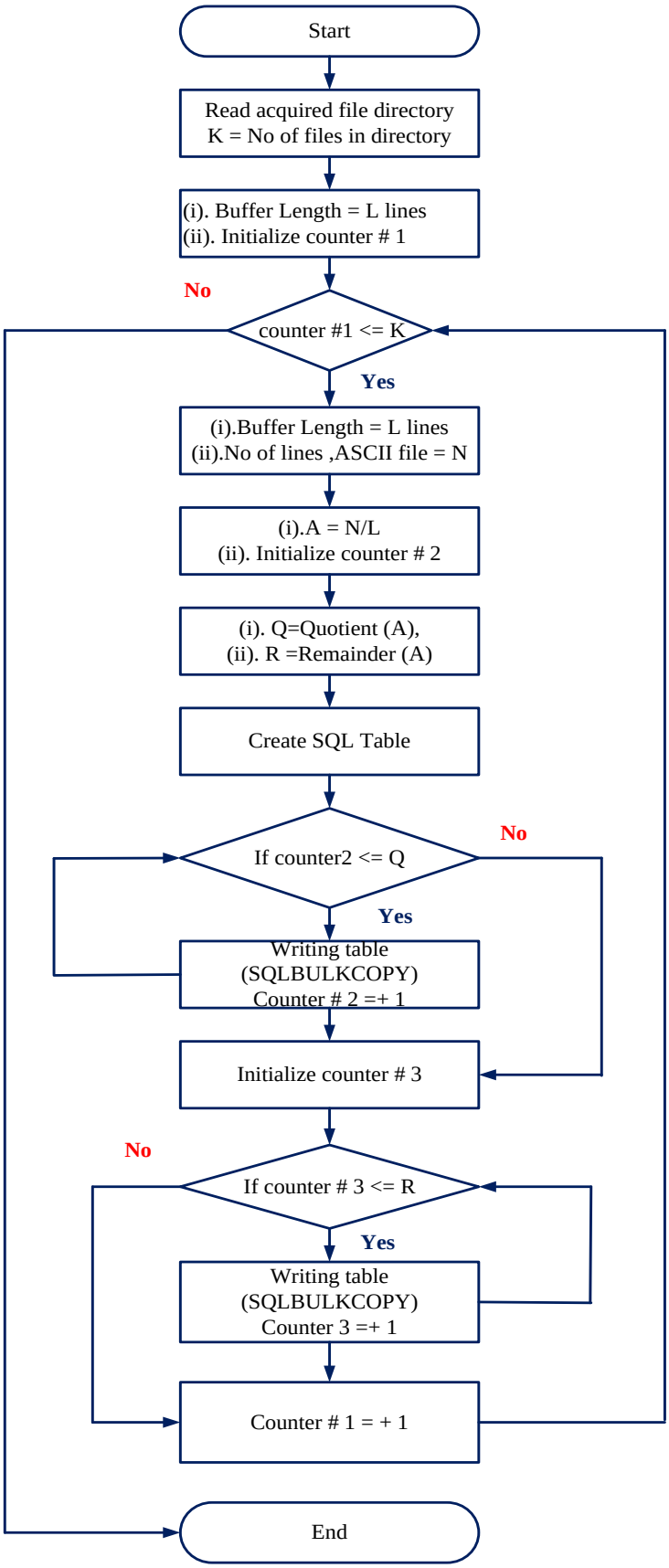


Figure 5-28 Flexible data transfer algorithm flow chart

### 5.6.3 Laboratory Tests

RPDMS is tested in the laboratory for data acquisition and remote data transfer capabilities discussed in the sections 5.6.2.1, 5.6.2.2 and 5.6.2.2. Test setup is shown in Figure 5-29 which includes signal generator and RPDMS. In this test signal generator feeds stationary signals to the RPDMS followed by capturing the signals in RPDMS/server and transfer back to RPDMS/client. Recorded waveforms are shown in Figure 5-30. Laboratory test results satisfy the requirement for PD monitoring.

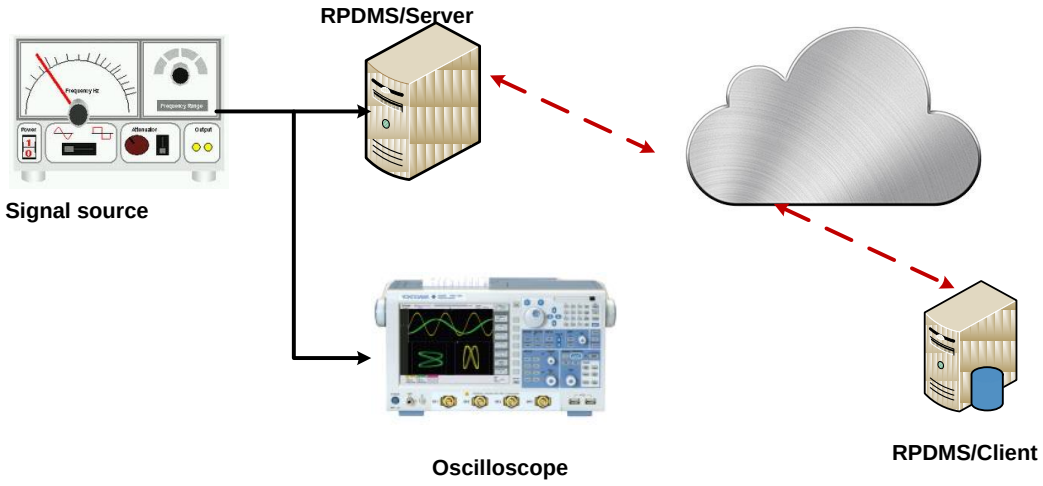


Figure 5-29 RPDMS test setup

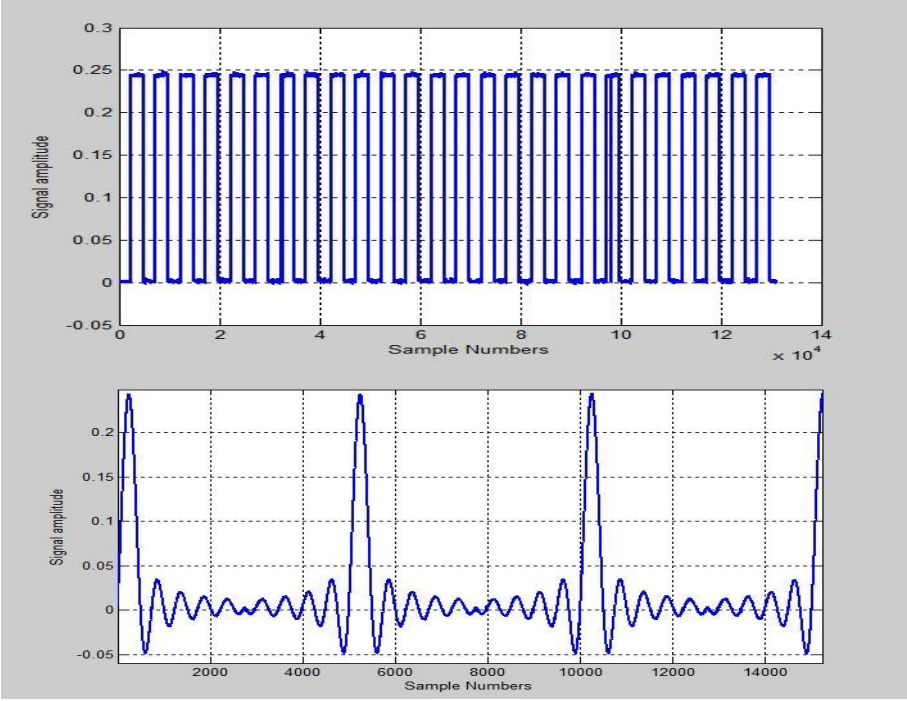


Figure 5-30 RPDMS laboratory test results

### 5.6.3.1 On-Site Measurements

In this project one of the main objectives was to investigate the possibility of using PFCT as a sensor in detecting partial discharges from cables. Though FRA of PFCT shows high gain at higher frequencies, it is important to verify this approach using on-site measurements. Though the protection systems in the PD monitoring hardware above is designed by the various issues addressed in section 5.6, It was not easy for install across the PFCTs since a robust test of the protections systems in the hardware was not available at that time rather than the laboratory tests. Few of older substation designs are equipped with Solkar PFCTs as a backup. Hence the choice was to identify a substation which has Solkar CTs rather than PD history of the cables. Hence PD monitoring equipment is installed across SOLKAR CTs at a 33/11 kV substation in Glasgow. Cable network configuration of the substation is shown in the Appendix C-5. A photograph of RPDMS installation at the 33/11 kV substation is included in the Appendix C-5. In this chapter only time domain waveforms and frequency spectrum of the data acquired using RPDMS are included in figures (Figure 5-31 -Figure 5-34). In each of the figures, the sinusoidal waveform indicates the scaled down version (400/5 A) of power frequency load current in the respective phase while noisy data with glitches is the high frequency data acquired from the respective phases.

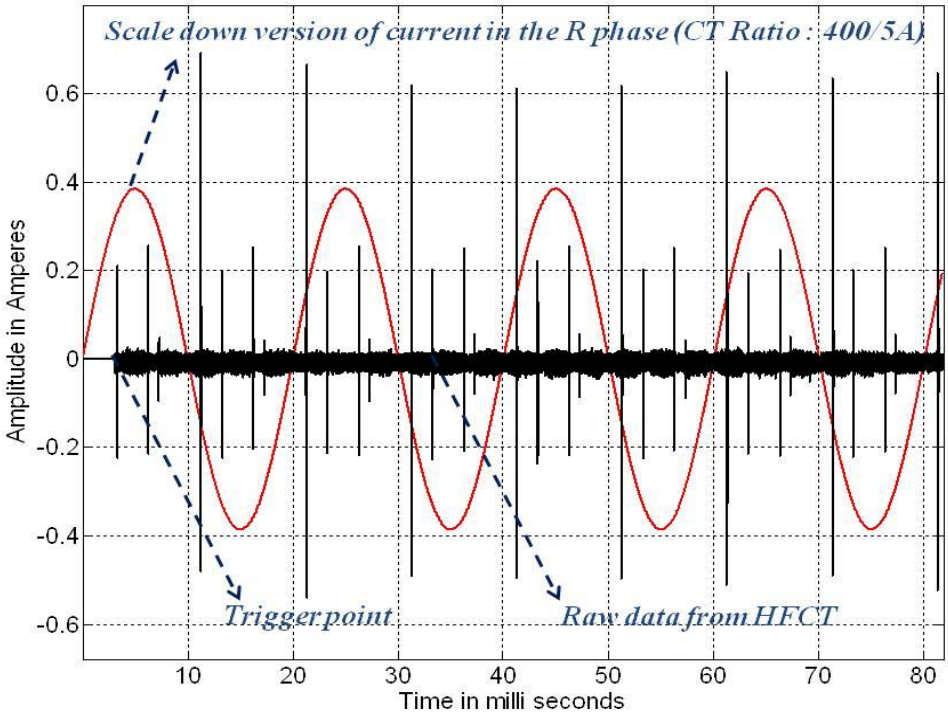


Figure 5-31 Data from earth strap (HFCT)

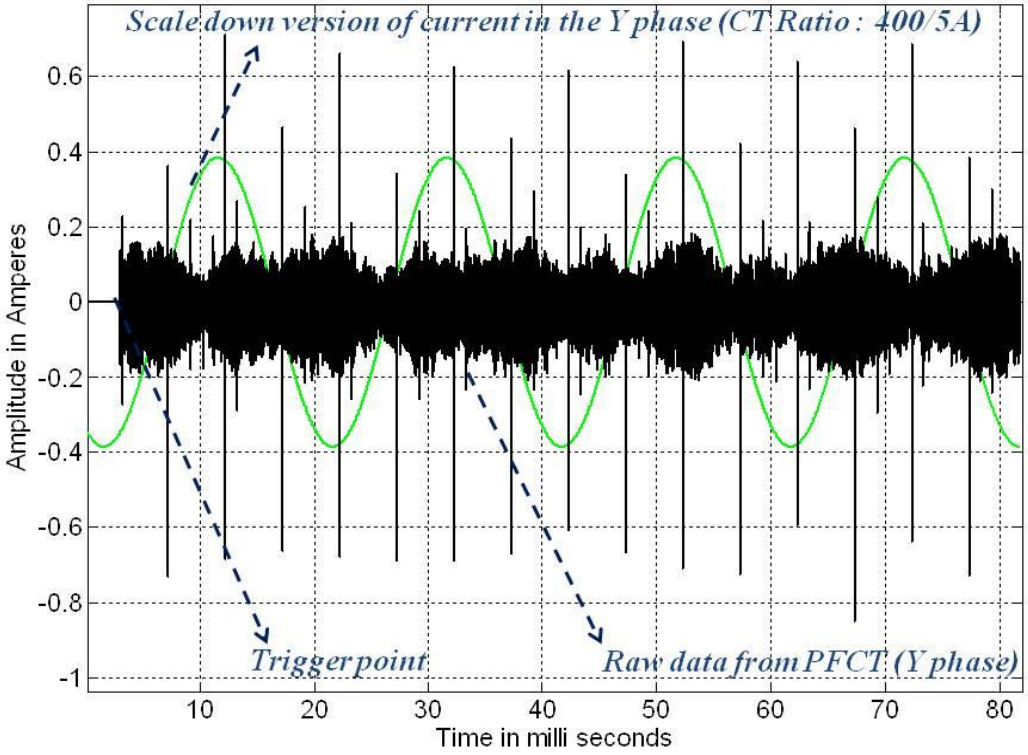


Figure 5-32 Data from Y phase (PFCT)

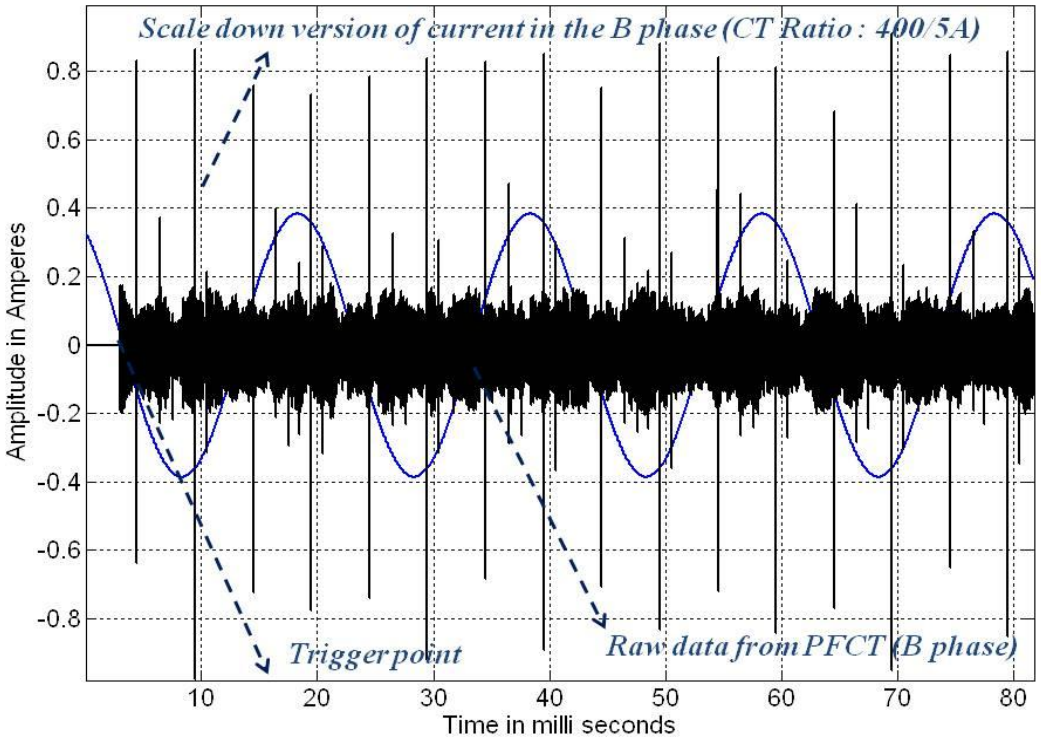


Figure 5-33 Data from B phase (PFCT)

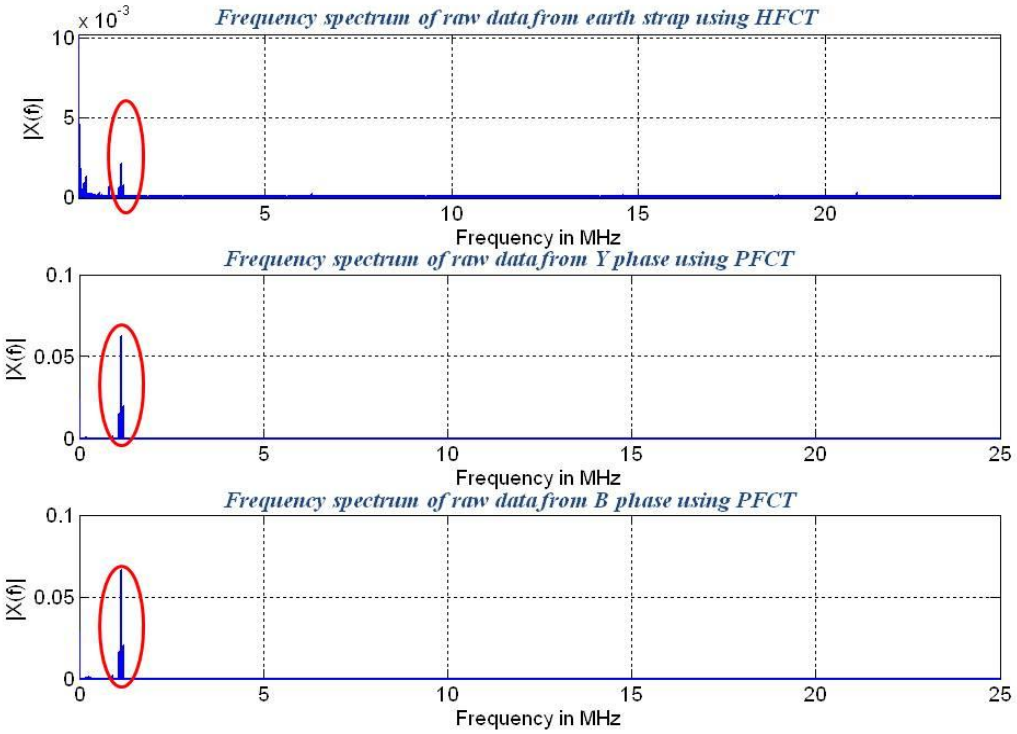


Figure 5-34 Frequency spectrum of raw data from cable core and earth strap

This high frequency data contains potential PD, which is to be ascertained using signals analysis and data interpretation, discussed in Chapter 8. Acquired data, processed data and the results of data analysis are stored in the database devloped using SQL server 2005 thereby a PD database is created which can be used for asset renewal program in the long run.

## 5.7 Conclusion

HFCT installed on the earth strap at the cable termination are widely used to detect PD. Isolation between cable earth and switchgear earth, completely enclosed older switchgear design and uneven distribution of induced charges in case of three core cables prohibits PD detection in power cables using earth strap. In this chapter, PD detection using pre-installed PFCT in cable networks for measurement/protection purposes was investigated. This investigation assesses the feasibility of this approach by conducting a magnetic study of transformer core, frequency response analysis, capturing and analysing onsite PD data in 11 kV PILC 3 core cable using conventional PFCTs and the developed PD data acquisition/interpretation system.

FRA of PFCT's were condcuted for two different primary conductor dimensions based on the parameters which determines corona and complete breakdown in cylndrical geometry using resistive burden with wire wound resisitor. FRA shows increased gain due to paraistic capacitance from 1MHz onwards. Based on both frequency domain and time domain measurements, PFCTs can be considered for detecting PD's from cables.

This approach using PFCT as PD sensor is further validated using on-site measurements using the on-line measurement system, RPDMS developed for this approach. One of the other requirement in designing RPDMS is for continuous monitoring of PD without frequent site access. This is achieved using remote control and remote database storage. Protection circuitry in RPDMS maintains constant burden across PFCT so that protection parameters of cable network remains unaltered. A health check algorithm in RPDMS isolates the systems in the event of faults in the measurement system. A flexible data transfer algorithm implemented in RPDMS can be used to transfer large volume of data even with slow speed internet connection and database storage of raw data makes easier handling and organisation of the data. On-line detection of PD from cable is corrupted by noise interferrence.To compare the performance of PFCT and HFCT in detecting high frequency signals, denoisng and data interpretation is required. Hence, validity of this approach using PFCT is moved to Chapter 8.

# Chapter 6 :
# Double-Ended Partial Discharge Detection System

## 6.1 Introduction

PD source location techniques based on TDR using single ended and double ended methods were discussed in Chapter 3. In the single ended method, both incident and reflected pulse are necessary to locate the origin of PD source. Generation of a reflected pulse is determined by the cable termination. This makes PD source location not always possible. In the double ended method, time synchronized incident pulses from both measurement units are required. Since this method does not require a reflected PD pulse, probability of getting PD source location is higher. In this chapter a novel double ended PD detection system using time based triggering method with GPS is proposed. Hardware, firmware and software design are discussed. Also various laboratory tests and on-site measurements results are included.

## 6.2 Why New System?

On-line PD measurements in cables are normally done at the cable terminations either at the switchgear end or transformer end. The PD signal travels from the discharge source towards the PD detection sensors which are installed at both ends of the cable. The PD signals undergo attenuation and dispersion which alters the PD signal shape and signal power. Though the probability of getting PD source location using double-ended method is higher, this method is not widely used because of complex hardware requirements and time synchronization.

[Steennis, Ross et al. 2001] proposed GPS based double ended PD source location using master/slave PD detection technology. In his design,once the master detects a pulse having PD signature, it will inform the slave to store the data in the memory using one of the non-energised phases of the cable network. This system identifies the PD pulse from the raw data. There should be a filtering/denoising module at some point followed by data interpretation. All these processes need to have a

sufficient time margin for completion. This delay together with communication delay could have an effect on time synchronization error, which obviously has an effect on PD source location. However, this time delay between master and slave that exists in the system is not reported in this paper.

GPS based time synchronization are widely used in phasor and power quality measurements [Mohamed, Siew et al. 2012]. In on-line double ended PD source location technique, event based edge triggering cannot be applied since the level of PD is not known in advance. Conventional double-ended systems using GPS synchronization utilizes free running 1PPS for synchronizing system clock. This type of synchronization generates large amount of datasets, and few of the data sets may not be valid due to GPS locking time variation between two ends of the cable network. This increases the usage of hardware resources which in turn leads to increase in the cost of the system.

In this thesis, the double ended PD source location system using a novel time based triggering logic implemented in FPGA with GPS is discussed. TBTL acquires the PD data for a particular 1PPS pulse which will eliminate the invalid data, unlike conventional double ended PD source location. Also in this design, the GPS receiver is turned on just before the data acquisition. This will reduce the long time drift of the GPS receiver clock. This system can also track invalid data caused by flywheel 1PPS from the GPS receiver due to temporary loss of satellite signal, which eventually reduces PD source location inaccuracies. Network structure of the system is shown in Figure 6-1. In order to implement TBTL (described in section 6.5.3.2) low-level access to hardware is required. As this was not readily available in commercial systems, a PDDN is designed.

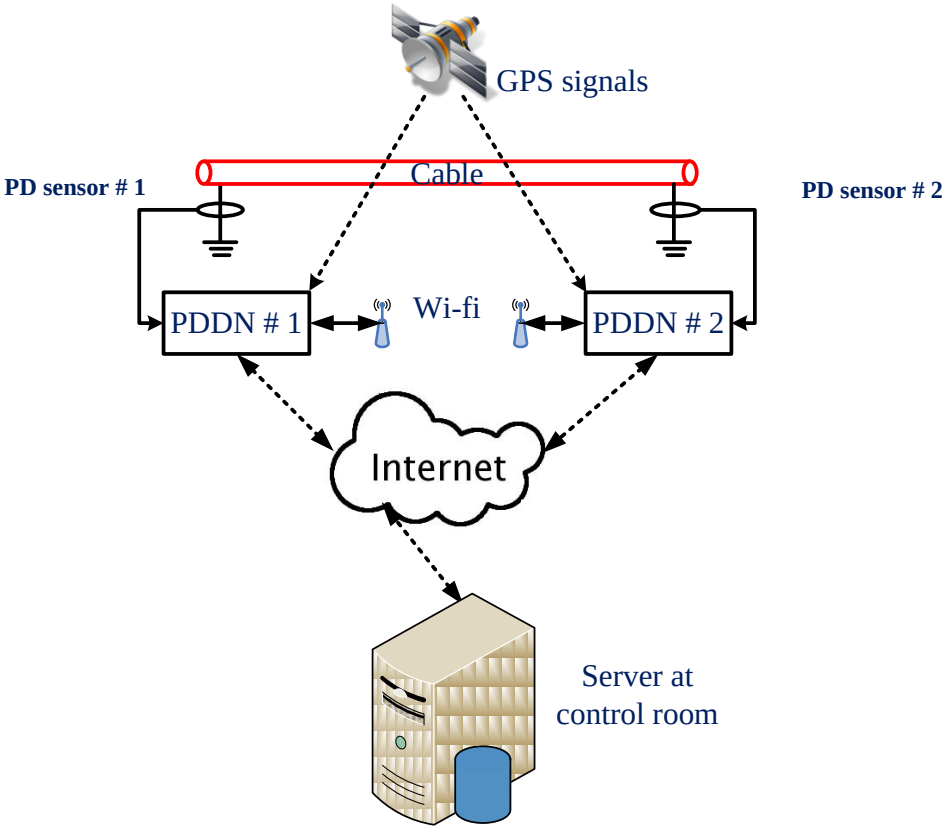


Figure 6-1 Double ended PD source location - Network diagram

## 6.3 Programmable Logic Devices

Programmable logic devices are basically silicon chips which consists of reprogrammable digital electronic circuitry or logic blocks. There are three basic kinds of ,namely memory, microprocessors and logic devices. Memory devices store information such as the contents of a spreadsheet, database or output of an ADC. Microprocessors execute software instructions like C language to perform a wide variety of tasks such as displaying texts, video games etc. Logic devices provide specific functions, including device-to-device interfacing, data communication, signal processing, data display and timing and control operations. Programmable logic is implemented in PLDs using HDL that reduces time consumption to minimize boolean expressions every time a new logical relationship is required. The advantages of programmable logic include rapid customization with relatively limited expense invested in tools and support [Balch 2003].

FPGA and CPLD are two major types of PLDs. CPLD consists of a few PLDs or micro cells on a single device with general purpose interconnections between them. A simple logic path can be implemented using a single block. Sophisticated designs require more blocks. Typical CPLD architecture is shown in Figure 6-2. CPLDs are well suited to applications involving small groups of read/write registers, which require smaller number of flops. In designs, which require many hundreds or thousands of flops, CPLDs become impractical. Advantages of CPLDs include ease of design and lower development cost [Balch 2003; Mehta 2003].

Complex applications which manipulate and parse streams of data often require large quantities of flops to serve as pipeline registers, temporary data storage registers, wide counters, and large state machine vectors. FPGA offers the highest amount of logic density, more features, and the highest performance. “The largest FPGA now shipping, part of the Xilinx Virtex™ line of devices, provides eight million "system gates" (the relative density of logic)”. Typical architecture of FPGA is shown in Figure 6-3. FPGA comes with two basic types, namely SRAM reprogrammable FPGA and one-time programmable FPGA. SRAM based FPGA is dominantly used which is reprogrammed everytime it is powered up [Balch 2003; Mehta 2003].

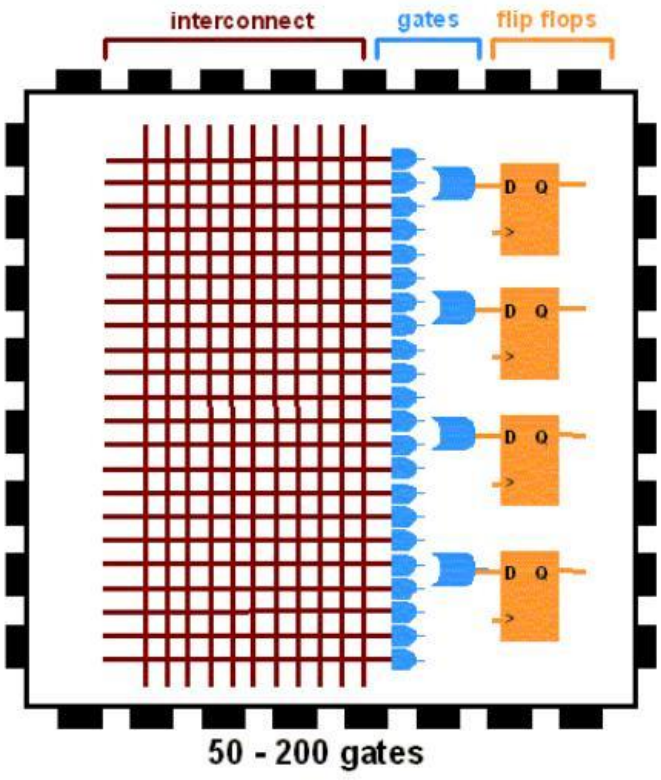


Figure 6-2 Typical CPLD architecture [Mehta 2003]

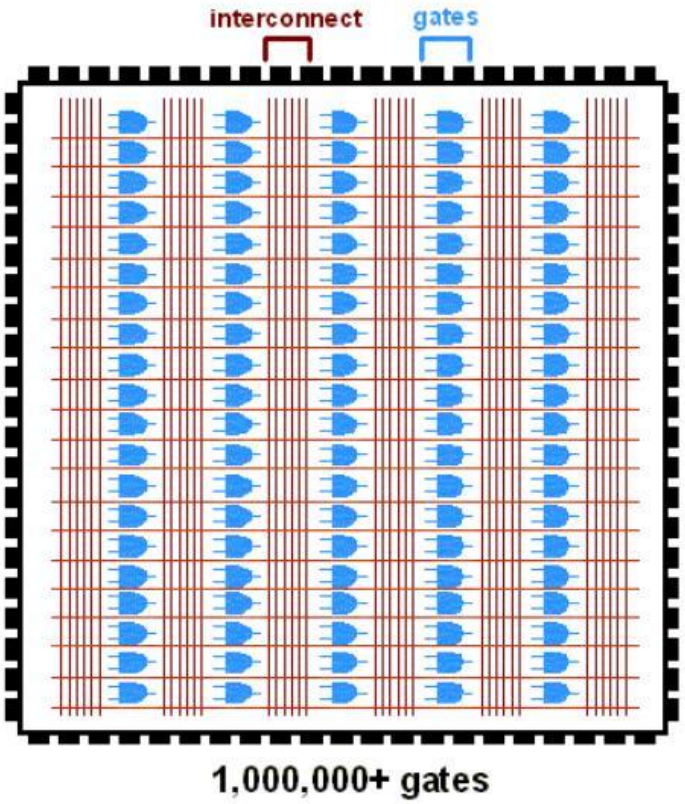


Figure 6-3 Typical FPGA architecture [Mehta 2003]

Cost and performance are probably the most debated trade-offs involved in using PLDs. The full range of applications in which PLDs or ASIC are considered can be broadly split into three categories as shown in Figure 6-4. Designs using lower clock frequencies and lower logic complexity, PLDs either FPGA or CPLD are considered. Designs using high end of technologies of ASIC is the only possible option because of leading edge timing and logic density requirements [Balch 2003].

In this particular application, the double ended PD monitoring system using time based triggering logic requires complex data processing, which needs large number of registers and memory blocks. This makes FPGA as the most suitable device for this design.

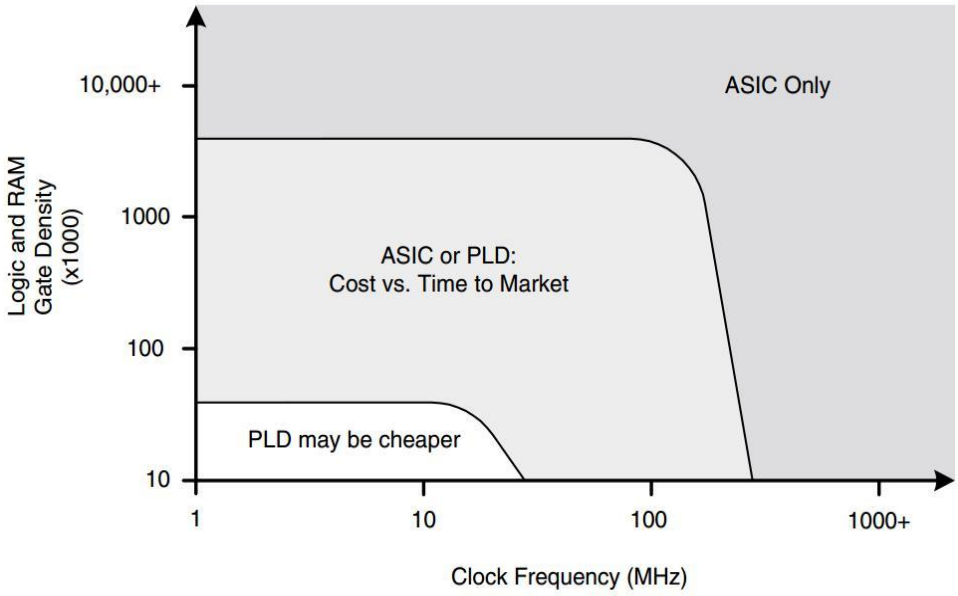


Figure 6-4 PLD vs. ASIC [Balch 2003]

## 6.4 PD Detection Node – Hardware Design

Double-ended PD detection needs two PDDN's, one at each end of the cable. A block diagram of the proposed PDDN is shown in Figure 6-5. In this design, FPGA (XC3S400) from Xilinx is used as the core processor. In PDDN design, various peripherals included in the analogue path are VCTCXO, voltage comparators, optical isolators, ADC and programmable attenuators and amplifiers. VCTCXO provides the necessary clock signal to FPGA. In this design two ADCs are used namely, ADC # 1 using a 80 MHz clock for acquiring the PD signals and ADC # 2 using a 100 kHz clock for acquiring the load current/system voltage for PRPD pattern analysis and PD intensity as a function of the load current in the cable.

Necessary protective measures are considered in the system design so that the system will be protected against over voltages and switching surges. A voltage comparator in the analogue path sets the voltage threshold. This will keep the analogue input within the limits of the ADC specification. An anti-aliasing filter in the analogue path will reduce the aliasing effect caused by high frequency signals. There are a few FPGA driven optical isolators which are used for protection purposes. They can isolate or connect the analogue part in the digital path after meeting the protection criteria. A variable gain attenuator/amplifier provides the necessary attenuation or amplification of the input signals based on the analogue signal level to exploit the dynamic range of the

ADC used. The buffer circuit is basically a source follower with optional input impedance (50 Ω and 1MΩ).

Accessories included in the digital path are a DAC, PSRAM, GPS receiver, USB-UART bridge, on-board PC and mobile broadband module. The DAC forms part of the self test logic (described in section 6.5.7) which is used to test ADC #1 before every data acquisition. It also outputs square waveforms which can be used for general purposes similar to commercially available DSO. PSRAM is used for storing high sampled data from PD's. The GPS receiver provides the time stamp information for synchronizing the measurements from both ends of the cable. The USB-UART bridge acts as an interface between the hardware and the PC, which provides the communication path for control commands from the PC and data from FPGA to PC. The mobile broadband module connects the system to the control room via the internet. Timing uncertainties such as frequency stability, phase noise and clock skew were taken into account during the PDDN design.

### 6.4.1 PD Detection Node Block Diagram.

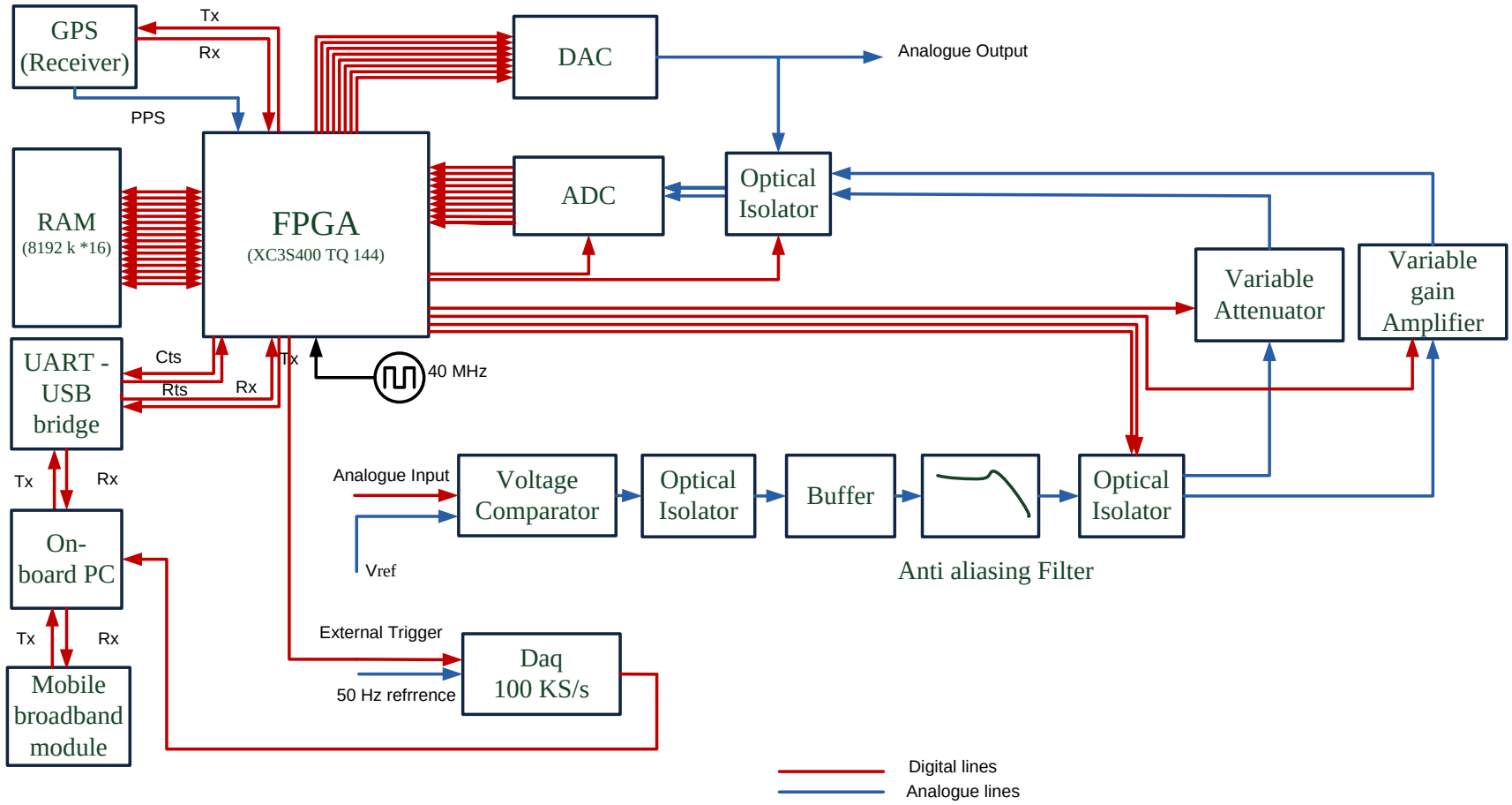


Figure 6-5 PD detection node Block diagram

### 6.4.2 PDDN - PCB design

The PDDN design discussed in the section 6.4 needs a multilayer PCB to implement the design. In order to save time designing a schematic, a PCB layout and hardware from a previous project was inherited [Liu 2009]. This hardware was designed to measure transient emissions from substations which use zigbee for wireless triggering and a Wi-Fi module for wireless communication to the PC. Details of this system can be found in [Liu 2009]. One of the difficulties faced to suit this hardware for the current design using TBTL was there were limited I/O ports available. The Zigbee module and few light emitting diodes (LED's) from the system were dismantled to get access to I/O ports . These I/Os were not enough to for the complete design, Therefore some features, namely auto gain controlling and self test logic are bypassed in the firmware design. The oscillator, GPS receiver and USB-UART bridge needs a power supply which can't be powered from the inbuilt power supply of the hardware, Therefore a power supply was designed (described in section 6.4.6).

A modified schematic of the logic circuit using FPGA is included in the Appendix H-2. Schematics of the power supply, analogue front-end, zigbee and GPS are included in the Appendix H3-H6 [Liu 2009]. Since this system needs to be tested in substations, it was necessary to consider a metal case so that any radiated field or electrostatic discharge (ESD) should not damage the hardware. A photograph of the PDDN designed is shown in the Appendix D-1.

### 6.4.3 Oscillator Selection

It is often required to have a clock source whose frequency or pulse rate needs to be highly stable and exactly known. This is important in any application when time or exact measurement is crucial. In this design, selection of the oscillator plays a dominant role in determining the accuracy of time base alignment in the TBTL. In general, an oscillator for a particular application can be selected using the following criteria

- Jitter or Phase noise
- Frequency stability (temperature, ageing and voltage)
- Jitter, clock skew introduced by the rest of the system
- Input power supply voltage to the crystal
- Cost

Jitter or phase noise is the variation in the zero crossing times of a signal, or a variation in the period of the signal. In an ideal oscillator, spacing between clock transitions is constant. In practice, the transition spacing cannot always be maintained . This uncertainty is known as clock jitter. It increases with the measurement interval as depicted in Figure 6-6. Net frequency change due to jitter in long-term is zero.

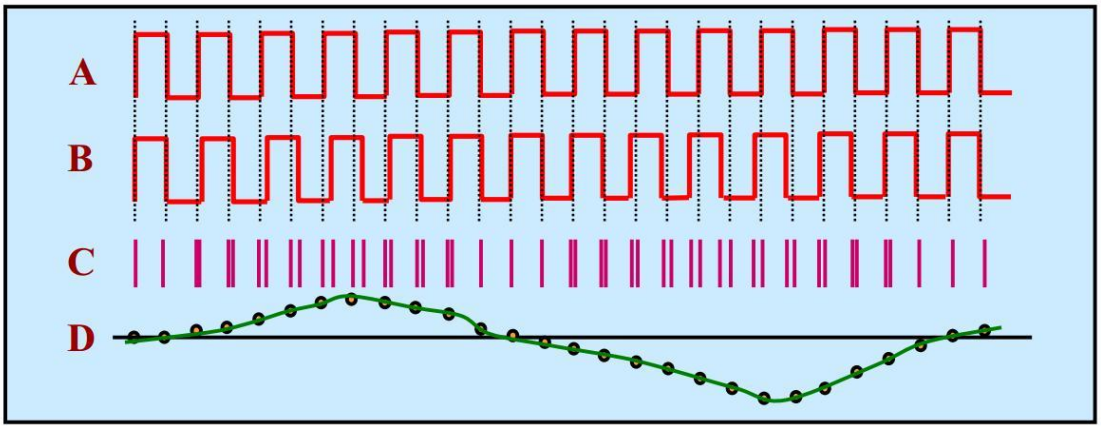


Figure 6-6 Jitter and phase deviation [Farrow 2008]

*A: Ideal Clock without noise*
*B: Jittered clock*
*C:Timing Differences*
*D: Phase (φ) deviation or Phase noise*

Frequency stability is the deviation from the nominal output frequency and can be expressed as

$$\text{Frequency stability} = \left( \frac{F_{current} - F_{nominal}}{F_{nominal}} \right) \quad 6\text{-}1$$

Where , $F_{current}$, Current frequency measurement
$F_{nominal}$, Nominal frequency

Factors such as temperature, power supply variation, load variation and ageing play dominant roles in determining the frequency stability. Stability breaks down into three categories, namely long term stability, which is usually measured over periods of a day or more; short term stability, which is usually measured over periods of perhaps 0.1 second to one day, and frequency stability, which is often expressed in PPM. For

example an oscillator with frequency 40 MHz with ± 10 PPM frequency stability has a frequency of

$$\left(40*10^6\right)\pm\left(40*10^6\right)\left(\frac{10}{10^6}\right)$$
$$=\left(40\text{MHz}\pm 400\text{Hz}\right)$$

At any instant frequency of the oscillator should be 40 MHz ± 400Hz. Progressive change in frequency over time is called drift. Drift plays a crucial role in the current design using TBTL. Hence it is a requirement to select an oscillator with lower drift. In this design a temperature compensated voltage controlled crystal oscillator (TCVCXO) of frequency 40 MHz with 1 PPM is used. The laboratory test setup for the oscillator frequency test is shown in Figure 6-7.

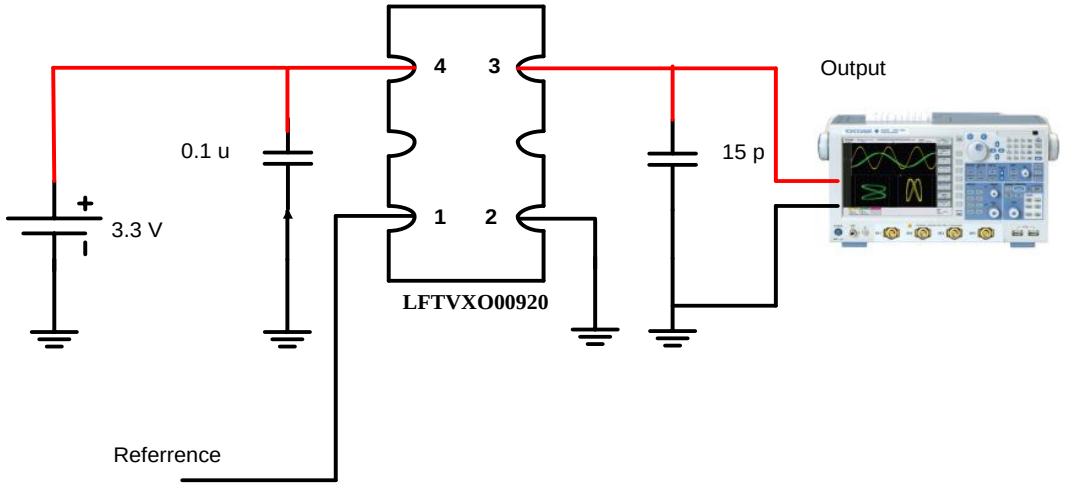


Figure 6-7 TCVCXO test

Time domain measurement results are included in Figure 6-8 and frequency spectrum is shown in Figure 6-9.

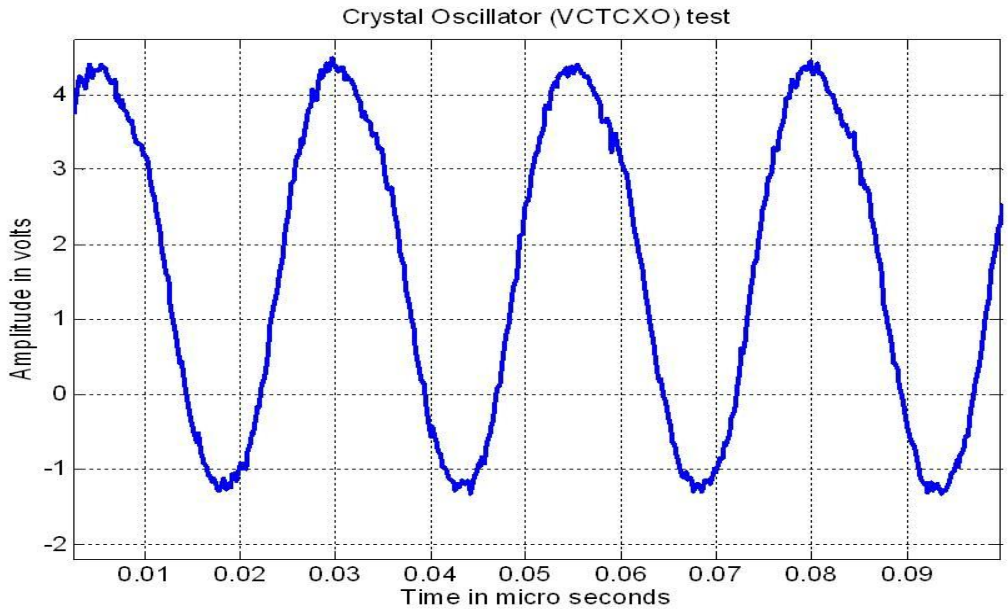


Figure 6-8 LFTVXO009920 clock output

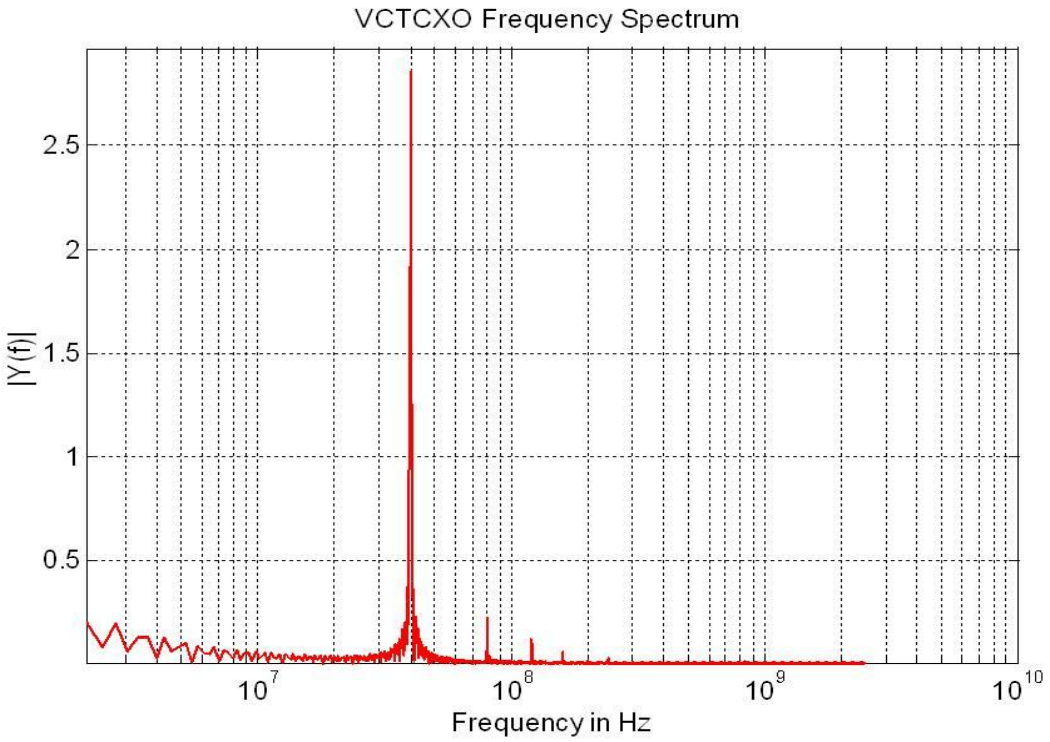


Figure 6-9 Frequency spectrum of LFTVXO009920

### 6.4.4 GPS Receiver Selection

GPS receivers are available from various suppliers. Cost, I/O standard, power consumption and NMEA data format are the criteria used for selecting a GPS receiver for a particular application. In this design, GPS module IT520 from fastrax is used. A photograph of GPS IT520 is included in the Appendix D-2. This module has a CMOS interface which consumes low power compared to the TTL based I/O standard. Some of the important electrical specifications of this chip are included in the Appendix D-2 [Fastrax 2011].

### 6.4.5 UART – USB Bridge Selection

The PDDN is interfaced with the PC using a USB-UART bridge, UM232R from FTDI. This hardware supports a baud rate up to 1 Mega Bauds. It is basically a USB to serial UART interface with optional clock generator output and hardware flow control. A photograph of UM232R is  and its electrcal specifications are included in the Appendix D-3.[Ftdi 2010].

### 6.4.6 Power Supply Design

Both GPS receiver and USB-UART bridge need to be powered which cannot be obtained from the main board (FPGA), Therefore a power supply circuit was designed. Both  peripherals need a 3.3 V power supply. The Oscillator requires a 3.3V power supply and a 1.65V for reference. 1.65V is achieved using a potential divider circuit. Schematic of the power supply circuit is shown in Figure 6-10.

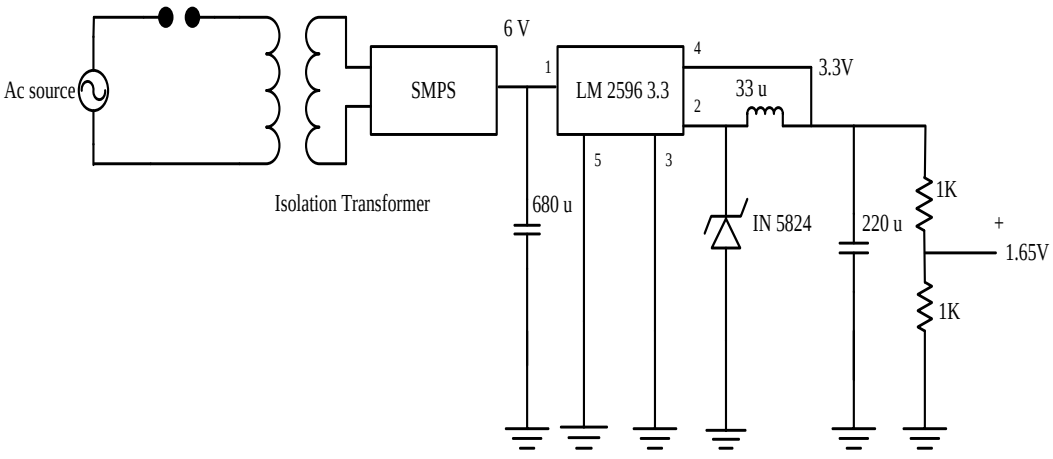


Figure 6-10 Power supply schematic

### 6.4.7 Signal Conditioning Circuit

Signals available from the cable (earth strap and cable core) are an amalgamation of PD signals with power frequency interference, also conducted and radiated noise interference from various sources. Conducted and radiated interference signals can be removed in post-processing using signal processing tools discussed in Chapter 4. Power frequency signals can be filtered in the pre-processing stage using a high pass filter. Also it is necessary to consider attenuators or amplifiers based on the signal power so that the dynamic range of the data acquisition system can be effectively used. Proposed PDDN has an auto gain controller which can provide the required attenuation and amplification. Due to the time and hardware constraints , external passive attenuators are used in the signal conditioning circuit.

A measurement system must be capable of measuring the electrical quantities without drawing any power from the measurement circuitry. Hence it is important that the PDDN should not alter the cable network parameters, it should be strictly CT burden. In this research, PFCT is used as a sensor which is a non invasive method of detecting PD signals from cable phase condutors. The PDDN needs to be connected across the CT burden to acquire PD signals. It is important that the measurement setup should not alter the CT burden. For this purpose, a signal conditioning circuit was designed. Block diagram of the signal conditiong circuit is shown in Figure 6-11 .

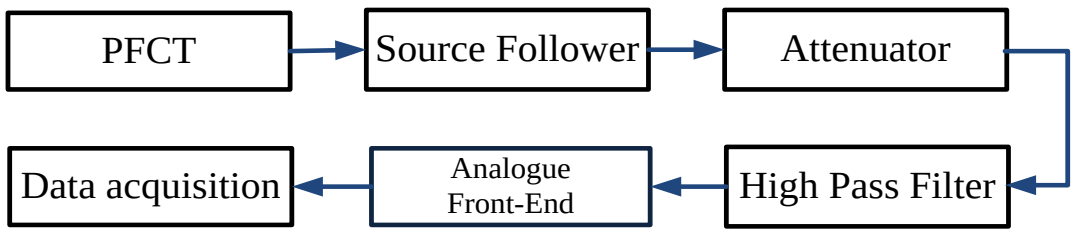


Figure 6-11 Signal conditioning

The Source follower/buffer is a 1 GHz bandwidth operational amplifier (OPA2695) having input impedance of 5 MΩ . By providing such high input impedance, the CT burden remains unaltered. The high pass filter is in series with the op-amp. It will filter out the power frequency signals contained in the raw data. In order to compensate for impedance matching with the data acquisition card, the source follower is designed for output impedance of 50 Ω.

Attenuators are basically divided into two types, namely active and passive attenuators. Passive attenuators are used in this design. Passive attenuators have three different topologies such as T type, Pi type and bridged T. Different types of attenuators and their design formulae are included in the Appendix D-4. Schematic of the signal conditioning circuit using a T type attenuator withattenuation of 10 db in series with the high pass RC filter with a – 3 db cut-off frequency of 2.34 KHz is included in the Appendix- H.Simulation and design results shown in Figure 6-12 and Figure 6-13 are in agreement. This confirms that inclusion of an attenuator between the HFCT and the high Pass filter will not alter the – 3b cut-off frequency of the high pass filter.

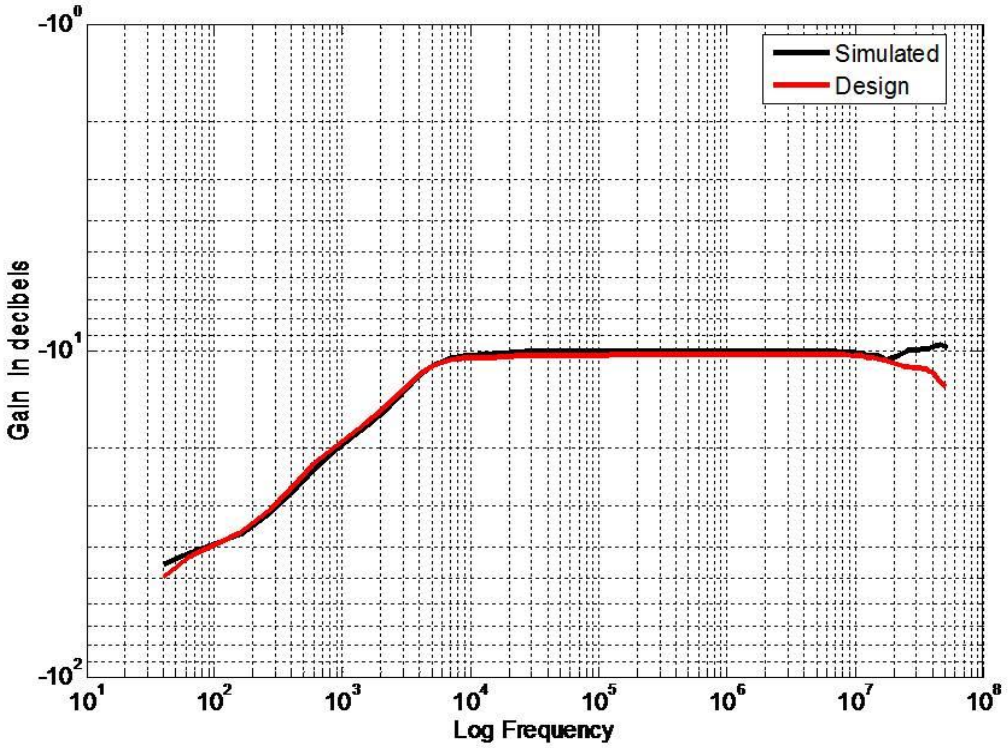


Figure 6-12 Magnitude response of signal conditioning circuit

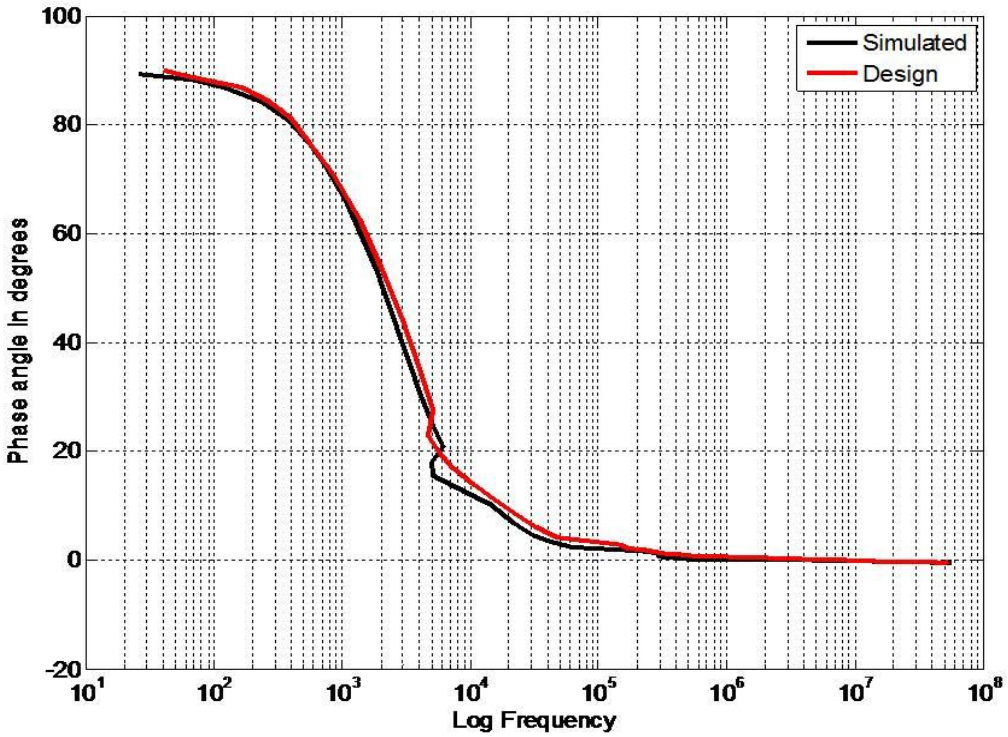


Figure 6-13 Phase response of signal conditioning circuit

## 6.5 PD Detection Node – Firmware Design

Embedded systems are controlled by programs known as firmware. These codes are stored in non volatile memory. Functional blocks of PDDN firmware are shown in Figure 6-14. Various blocks in the functional design are discussed in the following section.

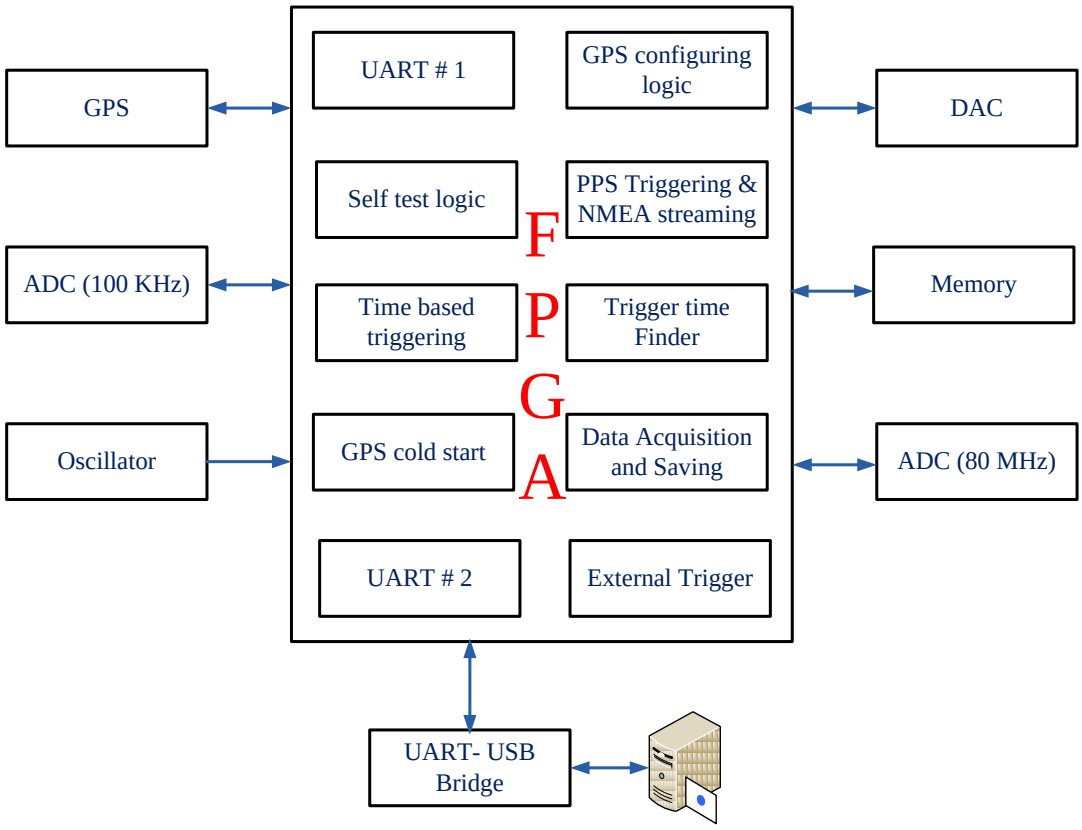


Figure 6-14 Functional block diagram PDDN

### 6.5.1 Clock Domain In FPGA

Clock domain is a part of any synchronous design driven by either a single clock or multiple clocks that have constant phase relationships. A clock and its inverted clock or its derived divide-by-two clocks are considered as a clock domain (synchronous). Conversely, domains that have clocks with variable phase and time relationships are considered different clock domains [Cadence 2011]. Spartan-3 devices provide flexible and complete control over clock frequency, phase shift and skew through the use of the DCM feature. DCM employs a DLL, a fully digital control system that uses feedback to maintain clock signal characteristics with a high degree of

precision despite normal variations in operating temperature and voltage. Basic functions of the DCM include clock skew elimination, frequency synthesis, phase shifting and status logic [Xilinx 2008]. A block diagram of the DCM is shown in Figure 6-15. A detailed description of the DCM can be found in Xilinx SPARTAN III data sheet [Xilinx 2008].

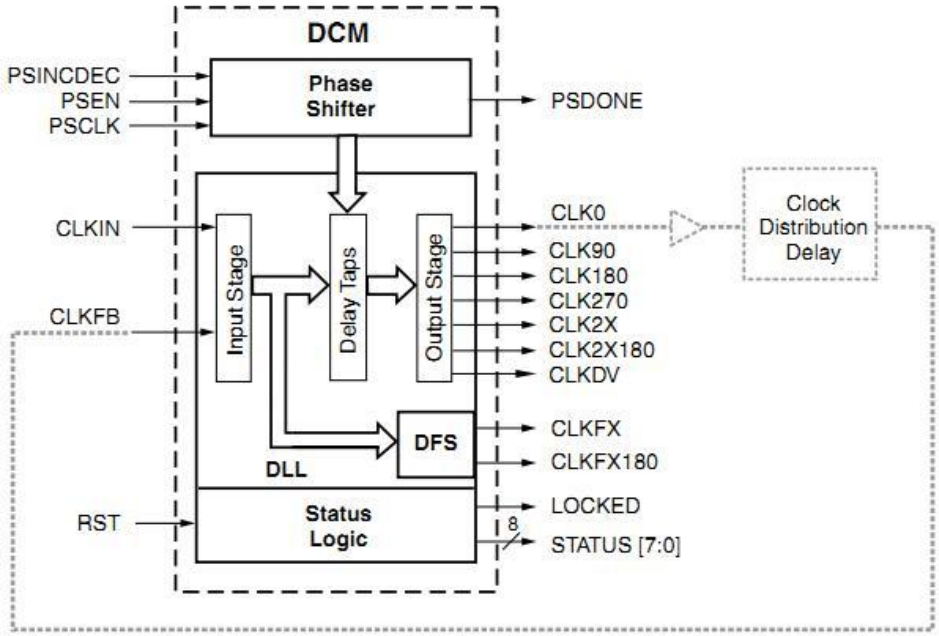


Figure 6-15 Digital Clock Manager(DCM) [Xilinx 2008].

In this design, an analogue to digital converter (AD9215) from Analogue devices (http://www.analog.com) with specifications 10-Bit, 80 Msps and PSRAM (MT45W8MW16BGX) (http://www.micron.com/)from Micron technologies with specification 16 Mbytes, 80 MHz is used.

The 80 MHz clock is generated by the DCM using the 40 MHz input clock from the VCTCXO. PAR simulation of clock generation using the DCM is shown in Figure 6-16. Based on Figure 6-16, at the beginning of the clock generation process, there is some uncertainty followed by a stable output clock signal. Once the output clock of the DCM is stable, status logic is asserted. Logical operations will be valid only if the status logic ("LOCKED") is high. After status logic is asserted, the FPGA will wait for 5 clock cycles followed by asserting the "*DEBOUNCING*" port. The FPGA will perform logic operations from this point. This is the reference point for all the state machines of RTL logic. There are four clock domains that exist in this design namely a 80 MHz

system clock, a 1PPS (1Hz) from GPS, and two serial communication protocols with different clock frequencies using UART standard in GPS and PC.

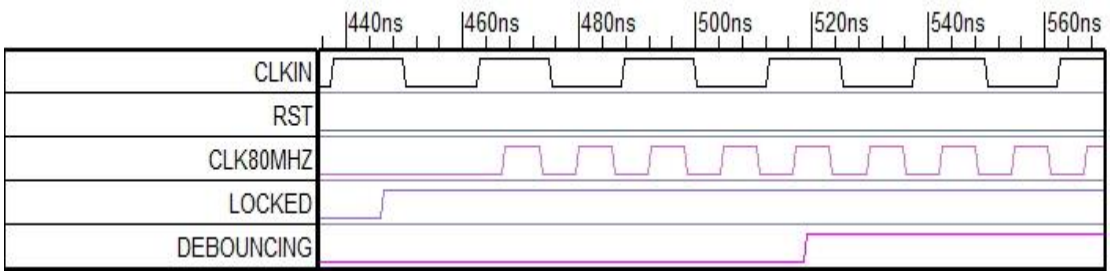


Figure 6-16 PAR simulation of DCM

## 6.5.2 Clock Domain Synchronization In FPGA

Larger designs normally involve several logic which is sampled using different clock frequencies. Some designs need to handle data asynchronously to the system clock domain. Both scenarios leads to clock domain crossing which forces the flip-flops in the FPGA to enter meta-stable state. For proper operation of a clocked flip-flop, the input must be stable for a certain period of time before and after the clock edge. This is known as setup/hold time. If the setup/hold-time requirements are met, the correct output will appear at a valid output level (either low $V_{ol}$ or high $V_{oh}$) at the flip-flop output after a maximum delay of $t_{co}$ (the clock-to-output delay). However, if these setup and hold time requirements are not met, the output of the flip-flop may take much longer than $t_{co}$ to reach a valid logic level. This is known as unstable behaviour, or meta stability. This is illustrated in Figure 6-17 with the timing diagram shown in Figure 6-18.

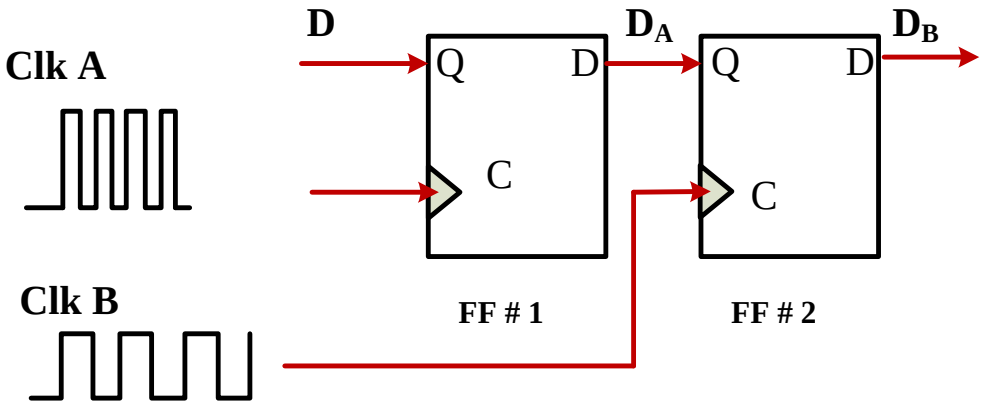


Figure 6-17 Metastability

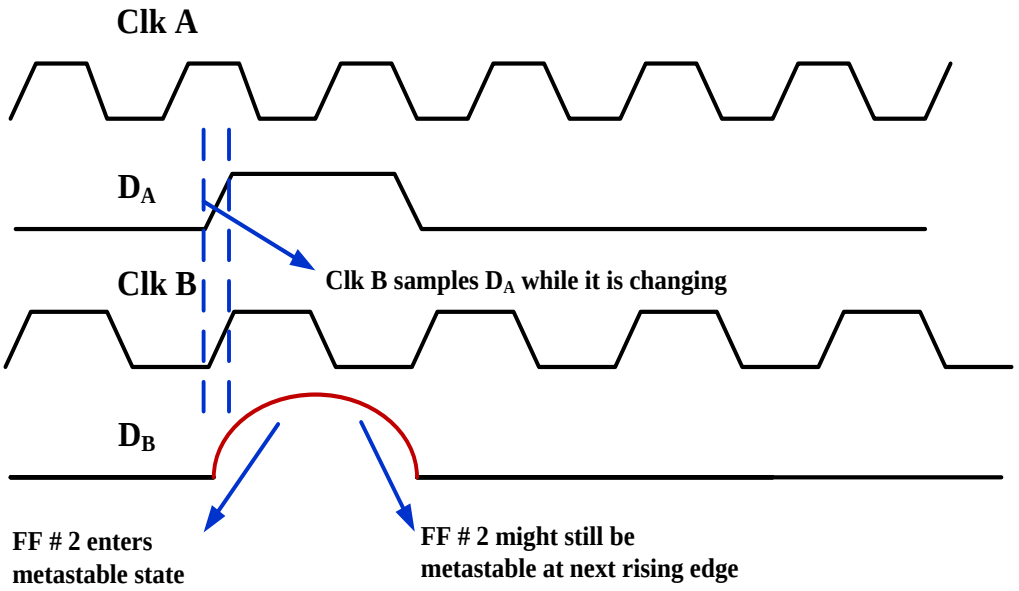


Figure 6-18 Timing diagram during metastable state

Metastability can be minimized but can't be avoided. The probability of a FF to stay in meta stable state decreases exponentially with time. Therefore a design which delays the asynchronous signal to the clock domain can be applied to reduce the metastability. In practice, delaying a signal by one clock cycle would be sufficient. The simplest and easiest way to reduce the metastability is by implementing a meta-stability filter or synchronizer in the digital path as shown in Figure 6-19. It involves two or more flip-flops which are placed in series to synchronize the incoming asynchronous signal to the clock domain.

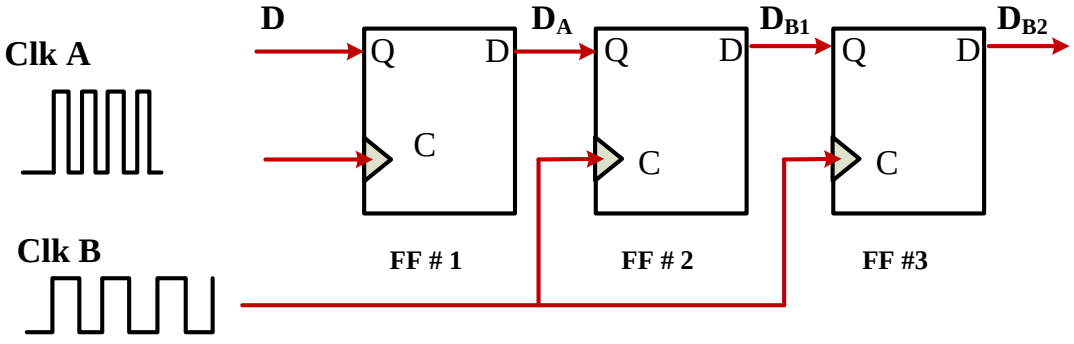


Figure 6-19 Synchronizer

The timing diagram of the synchronizer is shown in Figure 6-20. FF2 enters a meta-stable state since the input signal undergoes a transition within the setup/hold time window. Although FF2 may enter a meta-stable state, FF3 will not sample FF2 for

another clock period. The additional clock period usually provides time for FF2 to resolve to a stable state [Ginosar 2011].

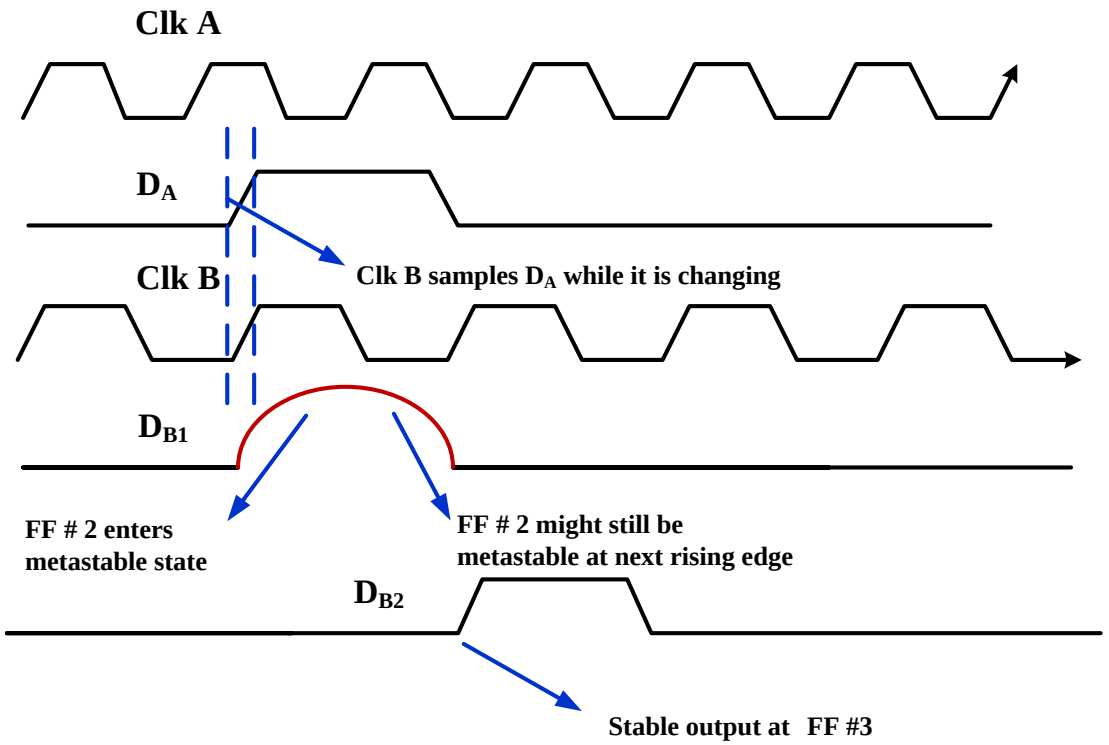


Figure 6-20 Synchronizer timing diagram

## 6.5.3 Triggering Algorithm

The triggering algorithm in the design uses time as criteria unlike level triggering in conventional double ended detection . This algorithm involves three stages, namely 1PPS detection in PDDN, start time computation of PDDN and getting trigger enable time from the remote station. These steps are explained in the following sections.

### 6.5.3.1 1PPS Triggering logic

1PPS detection is done by 1PPS triggering logic. In this design an edge triggering method is used similar to the DSO. Two parameters required for implementing edge triggering are the slope of the signal to be detected and the threshold level of the signal. The basic idea of a triggering circuit is shown in Figure 6-21. Since 1PPS is unidirectional, positive edge triggering is used. GPS receiver used in the design has CMOS standard in the range of 2.8 to 3.3 V which is used as the trigger level.

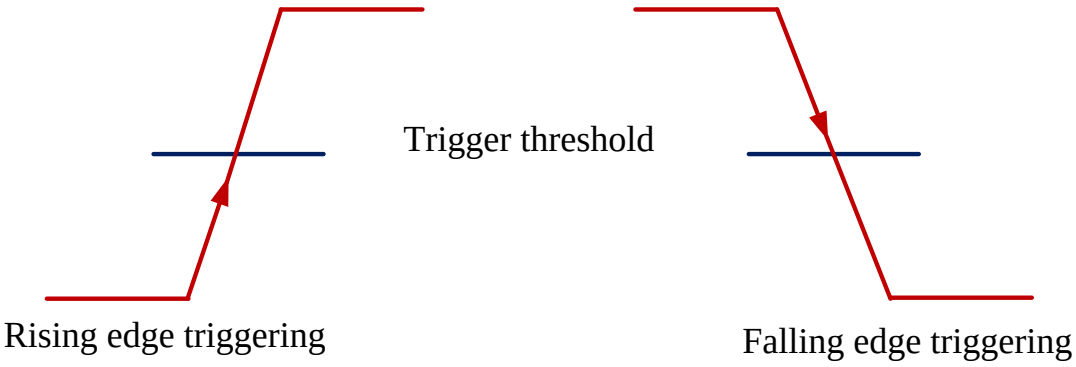


Figure 6-21 Edge trigger

The 1PPS from the GPS receiver is asynchronous to the FPGA clock domain. This will introduce meta-stability in the logic circuit, therefore a metastability filter is included. A block diagram of 1PPS triggering logic is shown in Figure 6-22. Port "*risingedgedetection*" gets asserted when the logic detects 1 PPS. PAR simulation is included in Figure 6-23. In Figure 6-23, 1PPS is shown as a high frequency pulse for demonstration. Since it is not possible to display 1PPS in 80MHz clock domain.

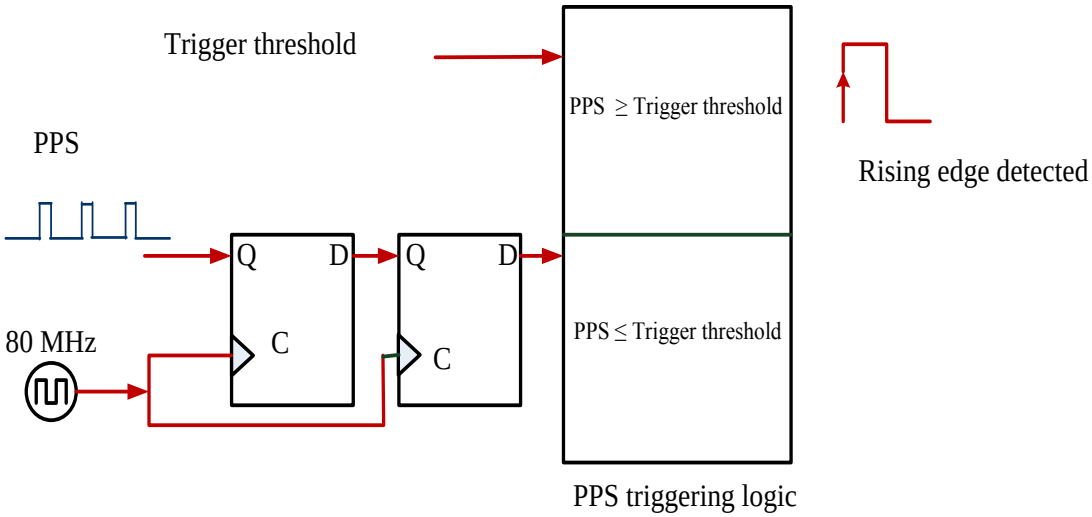


Figure 6-22 1 PPS triggering logic

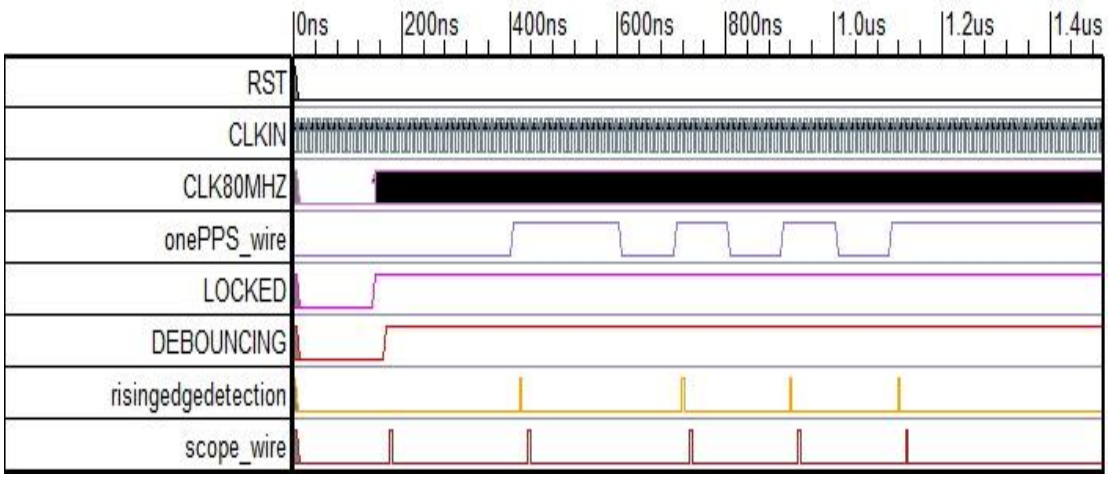


Figure 6-23 PAR simulation of 1 PPS triggering logic

Switching operations of circuit breakers and isolators in substations generates radiated emissions which may interfere with the PD detection node [Musa, Wah Hoon et al. 2010]. This interference will cause spurious triggering in the 1PPS triggering logic of the PDDN, which will eventually lead to large errors in time synchronization. To ignore the spurious triggering events, It was necessary to have robust intelligent triggering logic which is discussed as follows.

In this design there are two counters namely a top of second counter and a time based trigger counter. In a GPS receiver,the 1 PPS is followed by the NMEA stream through a serial line to the host (FPGA). The NMEA stream contains the UTC time reference and other satellite information. The rising edge of the 1PPS pulse corresponds to top of the second in the NMEA stream. Top of second resolution of the NMEA stream is in milli seconds which can't be used as time referrence for TBTL( described in section 6.5.3.2) due to the low resolution and communication delay in the serial line. Hence the top of second is calculated using a top of second counter in the FPGA, which counts between the rising edges of successive 1PPS.

This logic will calculate elapsed time between two successive 1 PPS pulses. If the two pulses detected by FPGA are from the GPS receiver , then the time elapsed should be in between 999998900 ns and 1.000001100 ns which is due to the jitter in 1PPS accuracy (± 100 ns). This criterion is used to discard the spurious pulses. In this way false triggering from spurious pulses is ignored. This logic will capture 5 numbers of 1PPS associated with NMEA stream and top of second counter followed by sending

this information to the host PC. A flow chart of the triggering logic is shown in Figure 6-24.

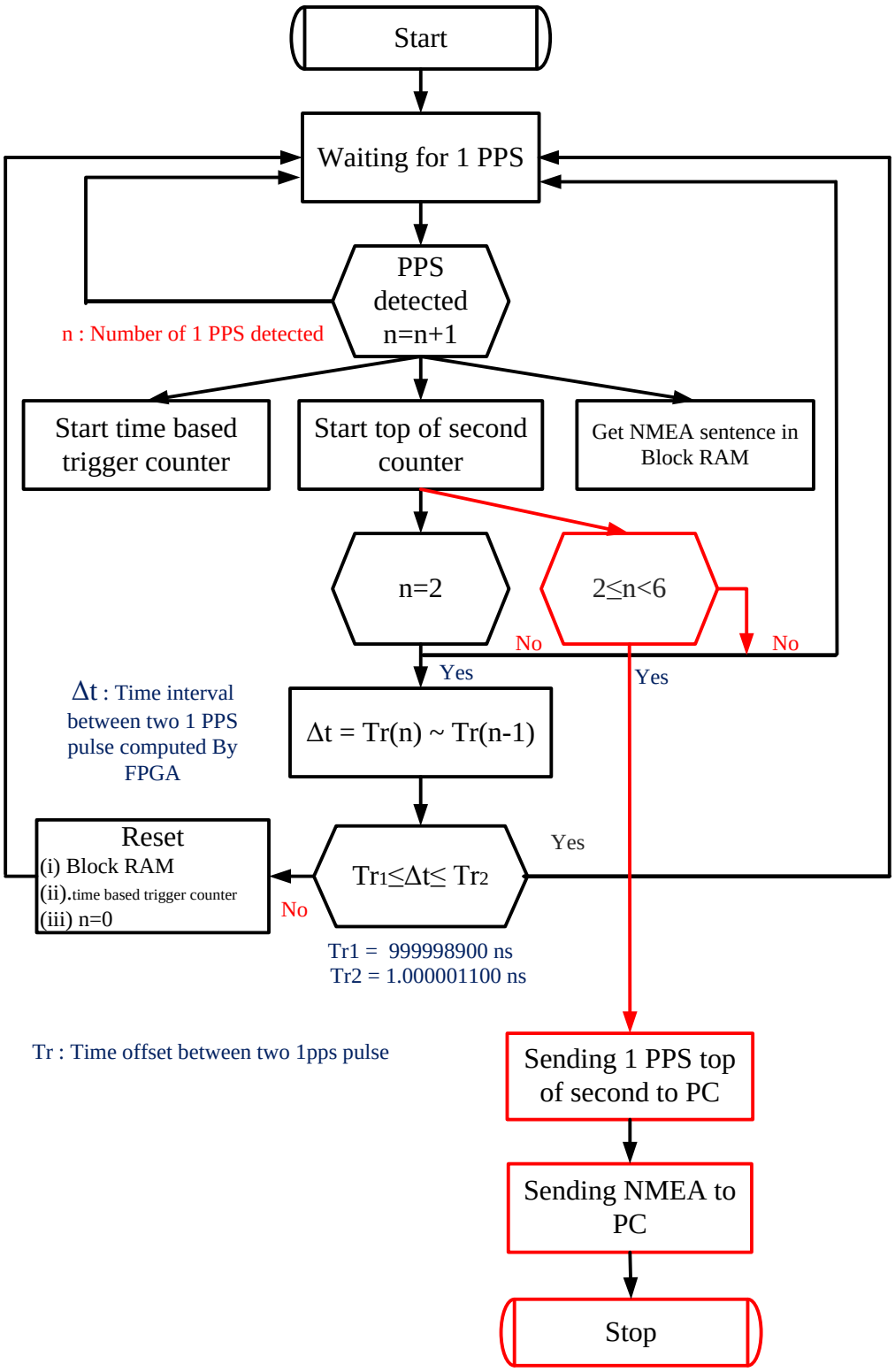


Figure 6-24 1PPS triggering logic

### 6.5.3.2 Time Based Triggering Logic

The method proposed here aims to trigger both PDDN's for a particular 1PPS using TBTL implemented on a FPGA. Once PDDN's are installed at both ends of the cable, the control room PC sends a start command to both PDDN's. Upon receiving the start command, the internal clock of both PDDN is locked with the 1PPS from the GPS receiver. This is referred to as the starting time of PDDN. Starting times of both PDDN's are sent back to control room PC. The control room PC then calculates the time delay between two PDDN's with respect to the GPS, therefore the trigger enable time is calculated and send back to both PDDN's. Pictorial representation of the time delay calculation is shown in Figure 6-25.

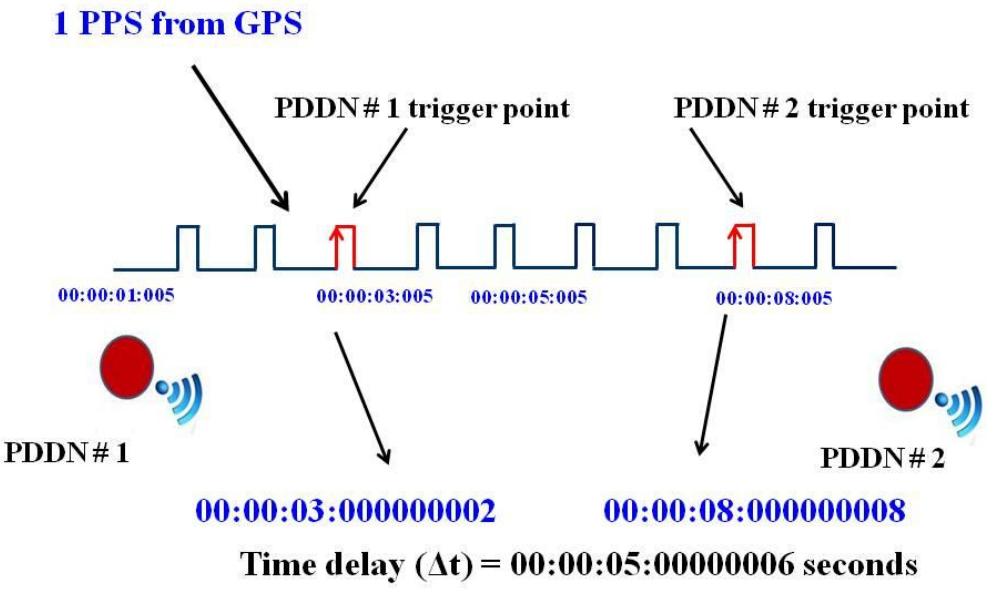


Figure 6-25 Time delay calculation, a pictorial representation

Hence, both PDDN's are triggered based on trigger enable time. In this way, PD data is acquired by both PDDN's for a particular 1PPS pulse. Trigger enable time is given by

$$T_e = \Delta T + T_a \qquad 6\text{-}2$$

$$\Delta T = Ts_1 - Ts_2$$

6-3

Where

$\Delta T$ : Time delay between two PDDN's,

$Ts_1$ : GPS locking time of PDDN # 1

$Ts_2$ : GPS locking time of PDDN # 2

$T_a$ : Data acquisition interval in seconds

$T_e$ : Trigger enables time in seconds

$T_a$ is a selectable option. It depends on the requirement based on the insulation condition of the cables to be monitored. It can be varied. The default setting is 10 minutes. A flow chart of time based trigger logic is as shown in Figure 6-26.

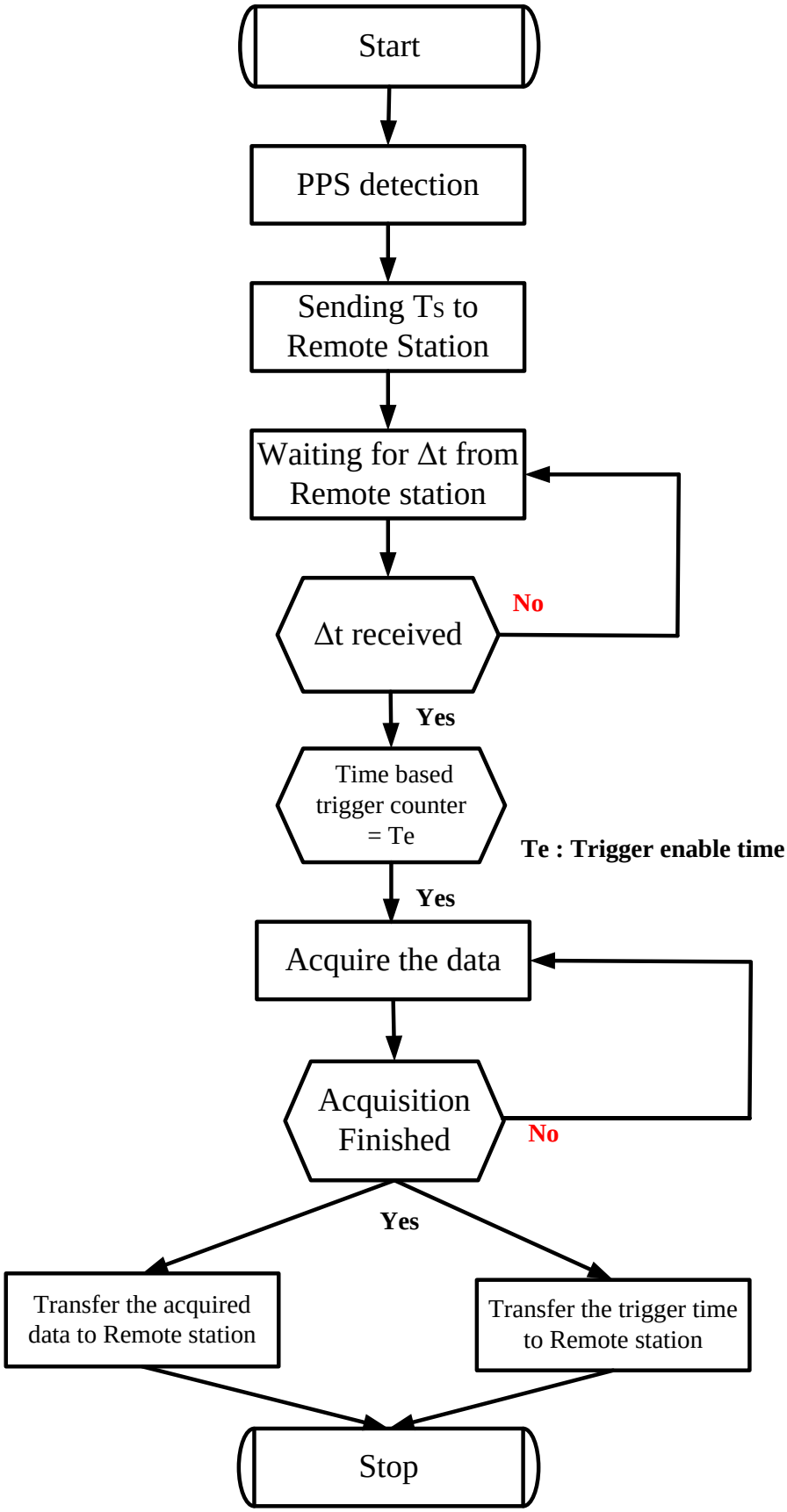


Figure 6-26 Time based triggering logic

### 6.5.4 High Speed Counter Design

TBTL discussed in the section 6.5.3.2 needs a free running counter which needs to run at a maximum of 3600 seconds from the first 1 PPS triggering point. Accuracy of this counter is crucial otherwise PDDN's will not get triggered at the same instant. Hence accuracy of the counter needs to be tested. Test setup for drift between two PDDN's for a duration of 60 minutes is shown in Figure 6-27. To measure drift between two PDDN's it is necessary to have a common reference point in time domain. This is achieved by feeding the 1PPS pulse from a single GPS receiver to the triggering logic of both PDDN discussed in section 6.5.3.1. Once the PDDN's get triggered from the 1PPS, a free running counter having a width of 38 bits is started. The same counter bits of the free running counter in both PDDN's are monitored for 60 minutes using the DSO in infinite persistence mode [Hewlett-Packard 1996]. A block diagram for the measurement setup is shown in Figure 6-27 and the corresponding flow chart for the logic is included in Figure 6-28.

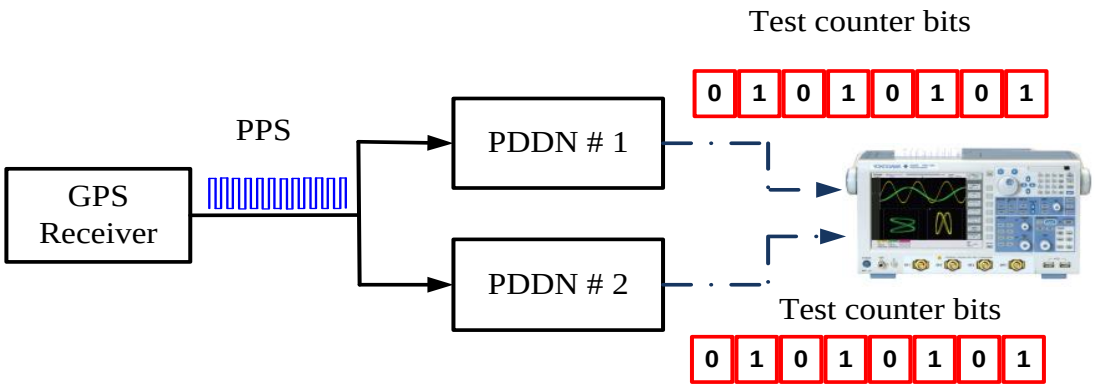


Figure 6-27 Drift measurement setup

Starting point of test counter in both PDDN's is shown in Figure 6-29 which is basically the triggering point of the 1PPS. Once a PDDN get triggered, the test counter starts counting and rolls of for every 2748 seconds for a 100 MHz clock. LSB changes for every 10 ns while higher order bits changes slower depending on the bit position.

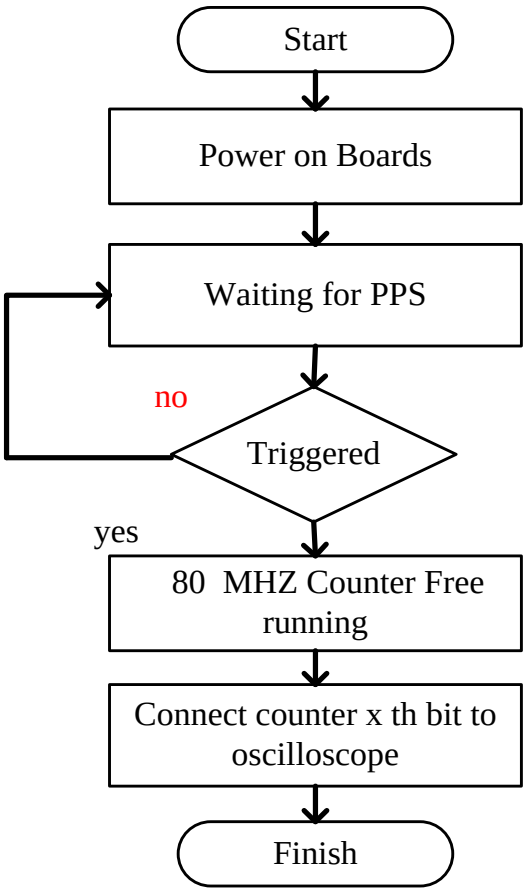


Figure 6-28 Drift measurement flow chart

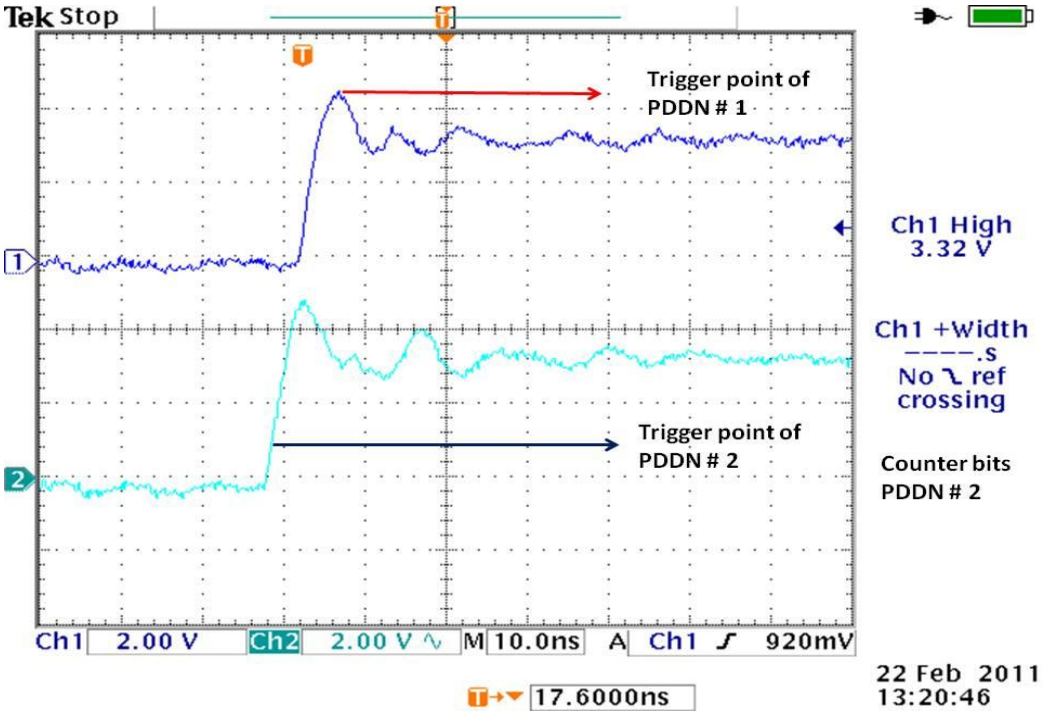


Figure 6-29 Starting point of PDDN's

In this test setup 8, 24, 32 and 37 bits were monitored. Frequency of occurrence of counter bits is given by

$$f = \frac{1}{\left[\left(2^{n} - 1\right) - 2^{(n-1)}\right]\ (2 * Ts)}$$

6-4

Where, $n$ : bit position , $n$ = 1, 2 ..., 37

$Ts$ : Sampling period

Frequency of 8 $^{th}$ bit is 393.700 KHz for 100 MHz clock. Corresponding pulses are as shown in Figure 6-30. In the case of the 32 $^{nd}$ bit, the frequency of the bit transition is 23.2 milli Hz, but this frequency is too low and is outside the capability of the DSO to display the waveform. In this case, when the counter reaches the 32 $^{nd}$ bit pulse having a pulse width of 100 µs is sent to the DSO from the FPGA. Results shown in Figure 6-31.

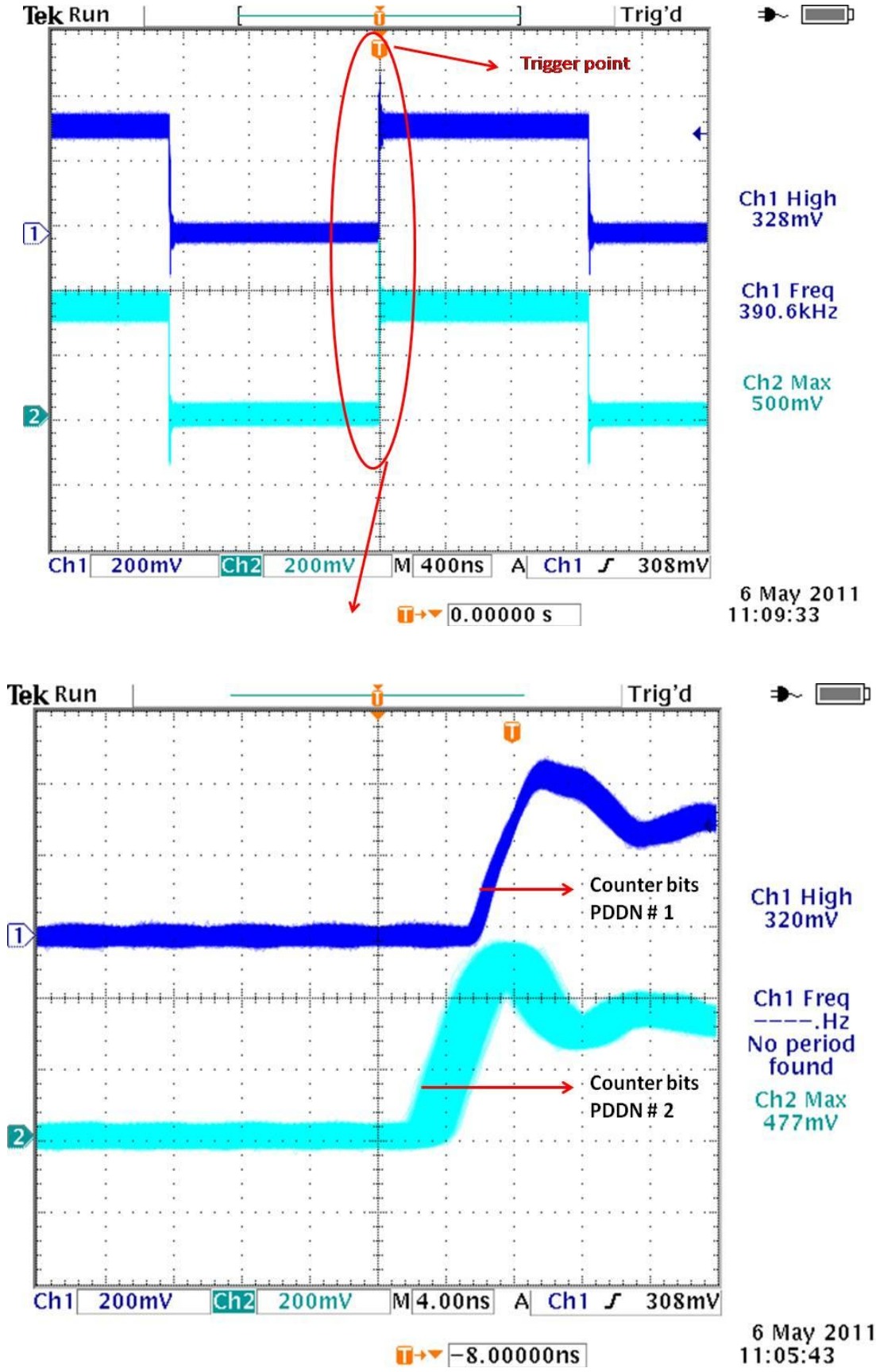


Figure 6-30 8 th bit of test counter in PDDN's

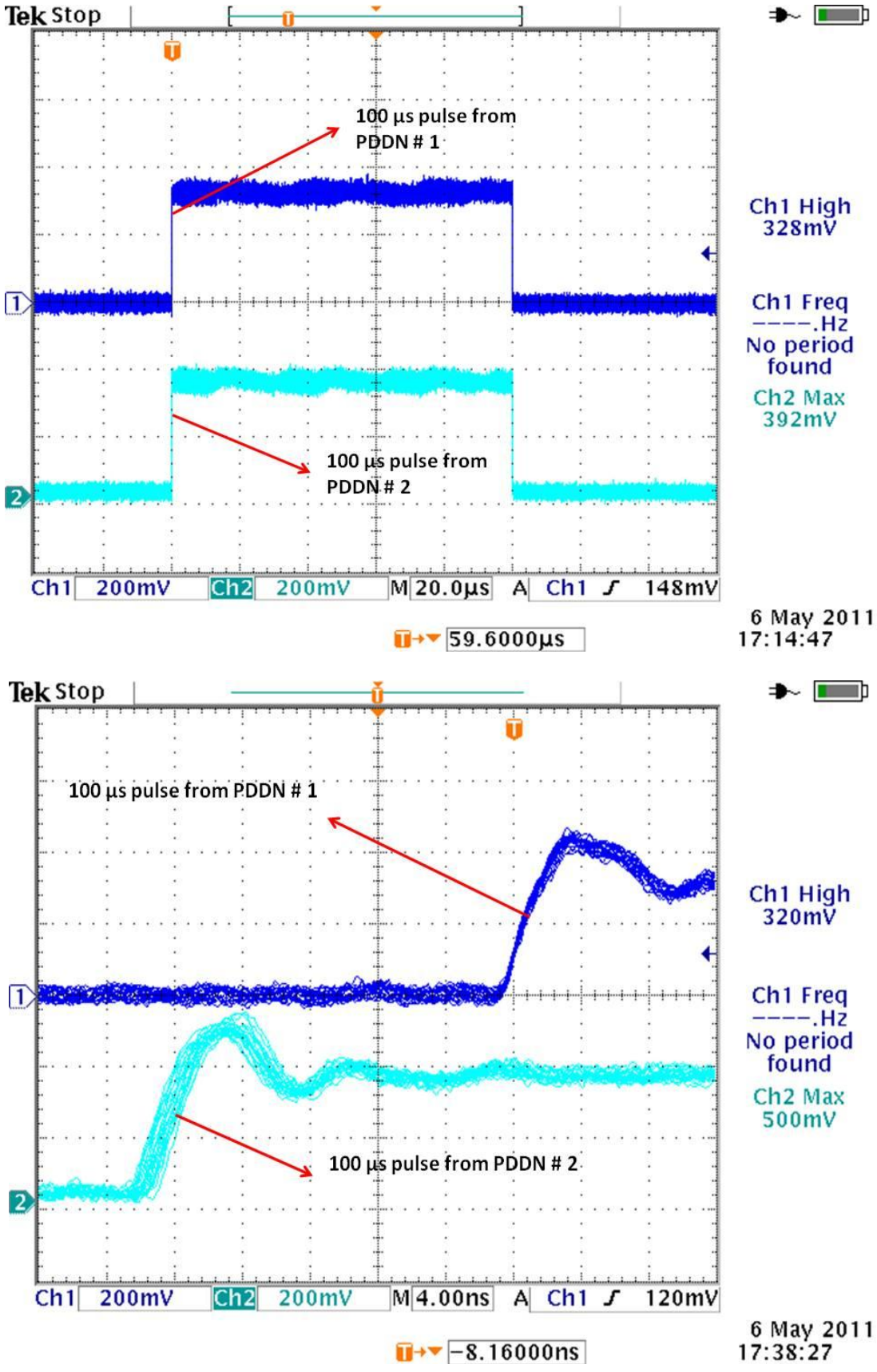


Figure 6-31 32 nd bit of test counter in PDDN

The rest of the bits (16 th and 38 th bit) monitored are included in the Appendix D-5. Drift vs counter length follows an exponential pattern as shown in Figure 6-32. The 37th bit counter exhibits a drift of 100000 nanoseconds while the8 th bit exhibits 1.6 nanoseconds. This shows that the counter is not counting correctly. Oscillator frequency stability is cumulative and may be nearly monotonic if the voltage and temperature are constant. Such varying drift is caused by two factors, namely the clocking source and the counter logic. For a 1 PPM, the VCTCXO used in the current design, cumulative drift would be approximately 3.6 milli seconds per hour. Since boards were triggered from the same trigger pulse and both oscillators are the same and of the same age, drift inroduced by oscillator could be small. Drift is possibly caused by timing margin issues in the FPGA when using such wide counters at high frequency.

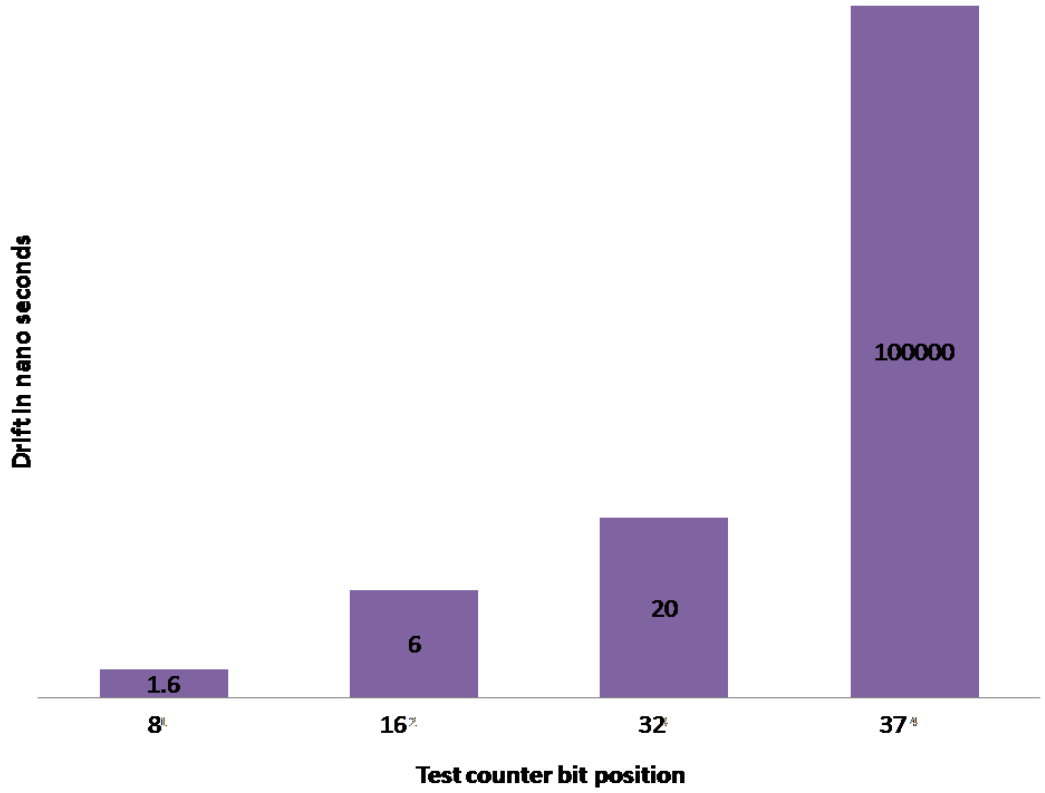


Figure 6-32, 60 minutes drift measurement using test counter bits

For 3600 seconds with a 80 MHz clock, the free running counter should be 40 bits wide. Design of such a wide, high speed counter with high accuracy in low specification boards like SPARTAN 3 in this design is more challenging unless the timing margin is enough. Synchronous counters require logic between D flip flops. If there is sufficient timing margin available, clock jitter of the time base will be covered.

In classical design of counters, all counter bits are updated on each rising edge of the clock. Roll over of such long counters will not be quick and the counter is potentially broken. Hence the classical counter design will not work in this case. Counter prescaling technique is applied in the counter design. Smaller prescaler counter (2 bit) rolls over very quickly compared the rest of counter bits [Ercegovac 1997]. Counter design logic is as shown in Figure 6-33 and the corresponding PAR simulation is shown in Figure 6-34.

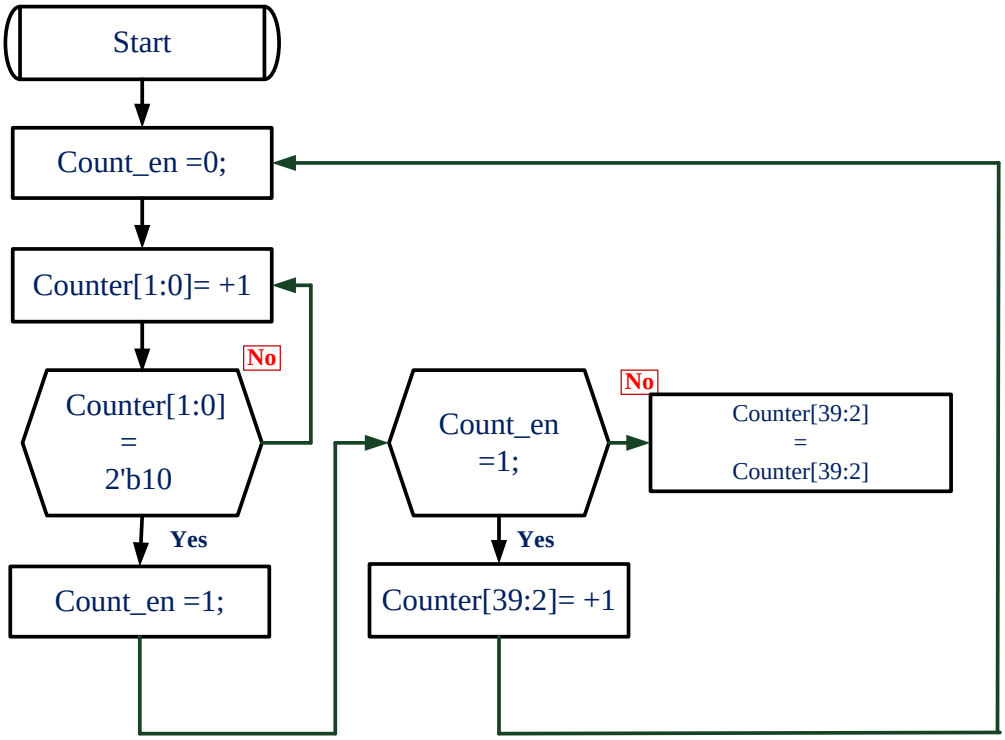


Figure 6-33 Counter partitioning logic

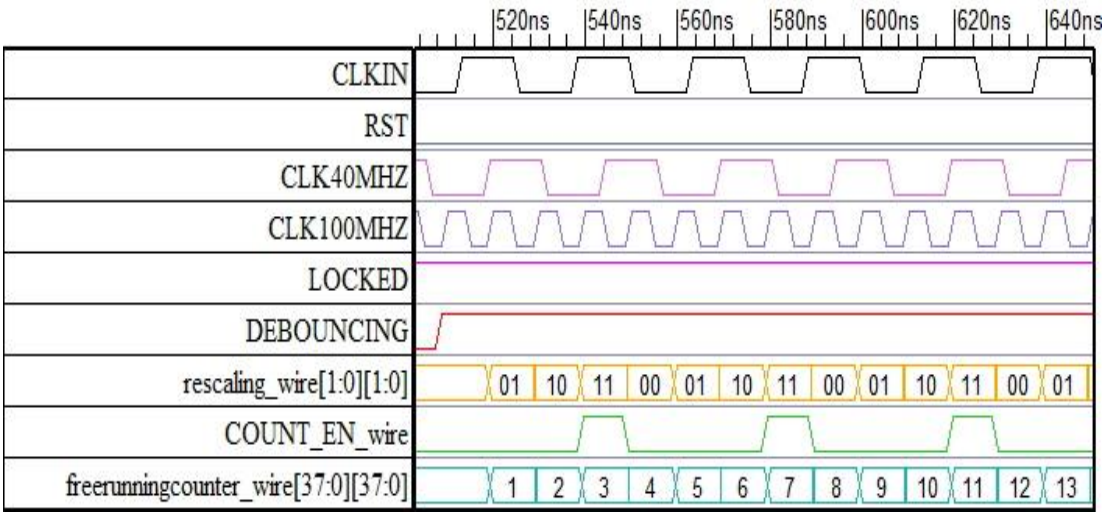


Figure 6-34 PAR simulation of counter partitioning logic

### 6.5.5 Universal Asynchronous Receiver/Transmitter

UART is widely used in embedded systems to communicate with other hardware such as PC's, GPS receivers, wifi modules etc in asynchronous mode. UART is a serial communication protocol used for short distance, low speed and low cost data transfer applications. In this design the UART serves as an interface for FPGA with PC and GPS receiver for data transfer, control and handshaking signals. The UART includes a transmitter and receiver pair. Both receiver and transmitter work in asynchronous mode. Since no clock information is conveyed between transmitter and receiver, both of them should agree on a set of parameters which includes baud rate in bits/second, start bit, data bit, optional parity bit and stop bit. The UART/Transmitter loads the data in parallel and shifts it out by bit by bit basis at specific speed which is defined by the baud rate. The UART/Receiver works serial to parallel mode which shifts the data in a bit by bit basis and then reassembles the data. In addition to a transmitter and receiver, the UART also has a buffer for temporarily storing the data during data transfer. Figure 6-35 shows a data frame of the UART. In the idle state, Tx and Rx lines of UART stay high. From the idle state, an active low alerts the UART that data is on its way. Following from the start bit, the UART treats 8 bits as data bit, 1 bit for parity and the last 1 bit for completion of the data frame. This type of implementation requires a total of 11 bits in a data frame.

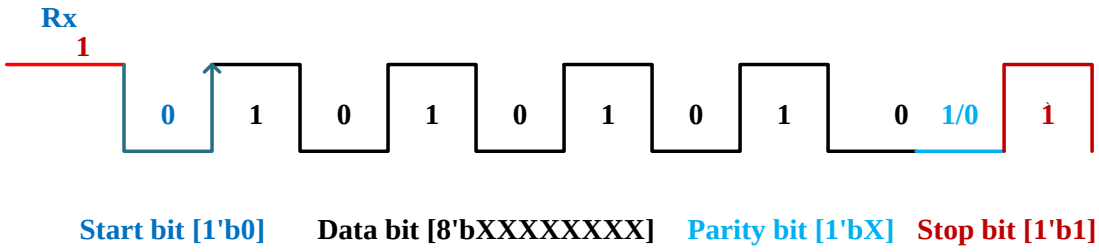


Figure 6-35 Data format UART

### 6.5.5.1 UART/ Receiver Subsystem Design

Since no clock information is conveyed from the transmitted signal, the receiver can retrieve the data bits only by using the predetermined parameters. For this purpose an oversampling scheme is implemented in the receiver to identify the midpoint of the data bits from the data frame , thereby the corresponding data bits can be retrieved to the shift register. The most commonly used over sampling rate is 16 times the baud rate, which means each serial bit is sampled 16 times. The baud rate generator generates a sampling signal whose frequency is 16 times the UART's designated baud rate. To avoid creating a new clock domain and violating the synchronous design principle, the sampling signal should function as enable ticks rather than the clock signal to the UART receiver. A typical sampling signal for the UART is calculated as follows

Baud rate : 460800 bits / second
Sampling signal : 460800 * 16
: 7372800 ticks / second

To generate sampling ticks from baud rate based on system clock domain, it is required to have a module counter which should assert the sampling ticks. The counter can be designed as

$$\text{Modulo counter , M} = \frac{80 * 10^6}{460800 * 16}$$
$$= 10.85$$
$$\approx 10$$
$$\text{Counter length} = \frac{\log_{10}(M)}{\log_{10}(2)}$$
$$= 3.32$$
$$\approx 4$$

The counter should wrap for every 16 clock cycles of the system clock thereby necessary ticks are produced. Since the UART works asynchronously with clock domain, a synchronizer is also included to reduce meta stability problems. The UART/receiver logic is shown in Figure 6-36. PAR simulation of the UART/receiver subsystem is shown in Figure 6-37.

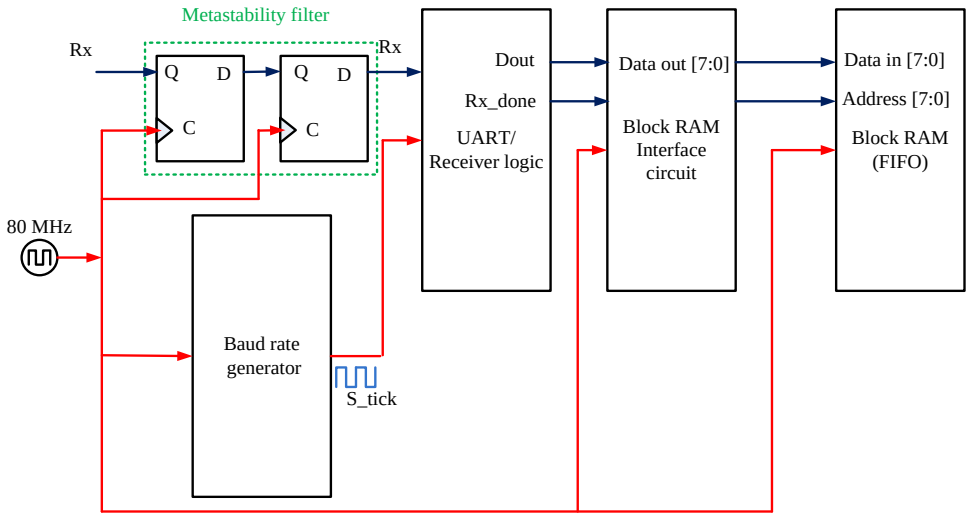


Figure 6-36 UART receiver subsystem logic

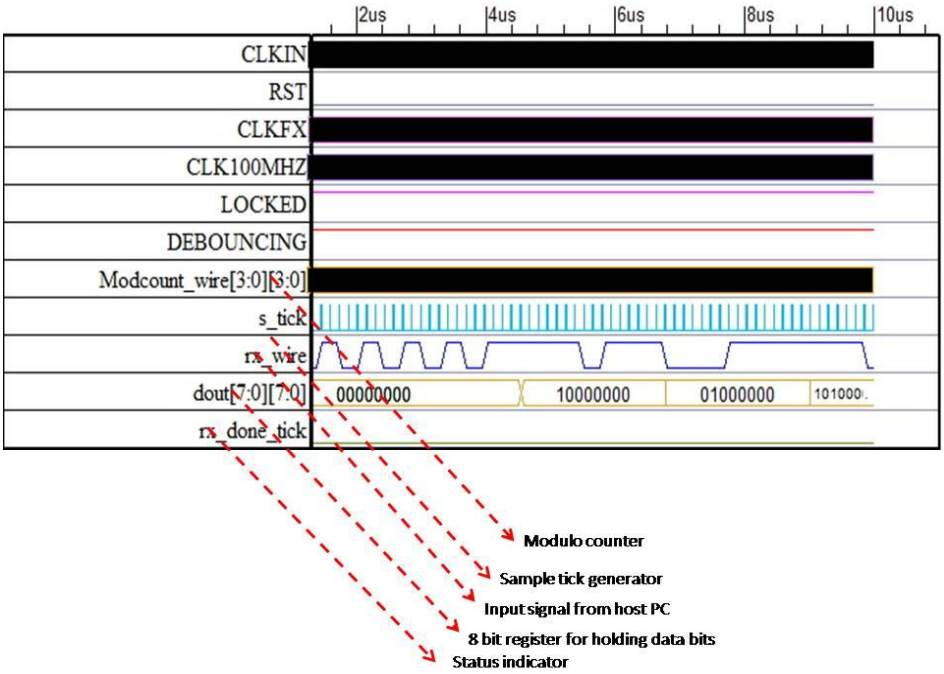


Figure 6-37 PAR simulation of UART receiver subsystem

### 6.5.5.2 UART/ Transmitter Subsystem Design

The UART transmitting subsystem is similar to that of the UART receiving sub system which includes the UART transmitter, baud rate generator, and interface circuit. The UART transmitter is basically a shift register which shifts out data bits at a specific rate. This rate is controlled by the baud rate generator. There is no over sampling process involved in the UART/transmitter unlike the UART/receiver. Frequency of the tick is 16 times slower than that of the UART/receiver. In this design three different data formats exist, namely 32 bit for top of second counter, 8 bit for NMEA and 16 bits for PSRAM and handshaking signals. A multiplexer is used to switch between different data formats. In serial communication, flow control plays an important role in determining the data integrity. Once the UART/ receiver buffer is full, and the UART/ transmitter keeps sending data, data will be lost. In this case the UART/transmitter and the UART/ receiver need mutual communication to coordinate the data. This can be achieved using flow control [Bai 2005]. Flow control can be done in two ways, namely hardware and software. In this design hardware flow control is implemented using RTS and CTS. The UART/transmitter subsystem logic is as shown Figure 6-38 and the corresponding PAR simulation is shown in Figure 6-39.

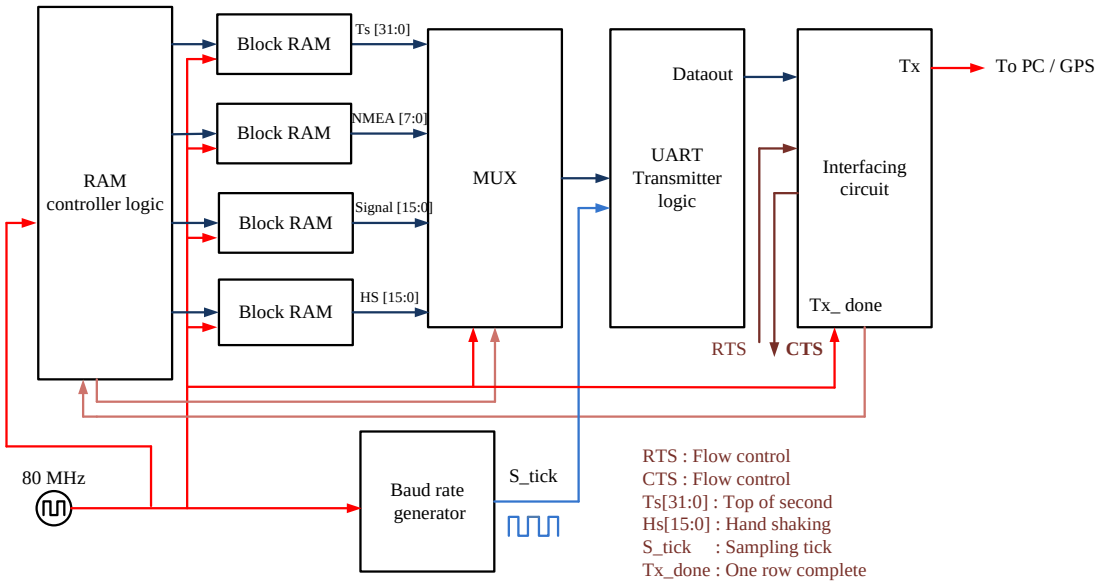


Figure 6-38 UART/transmitter subsystem logic

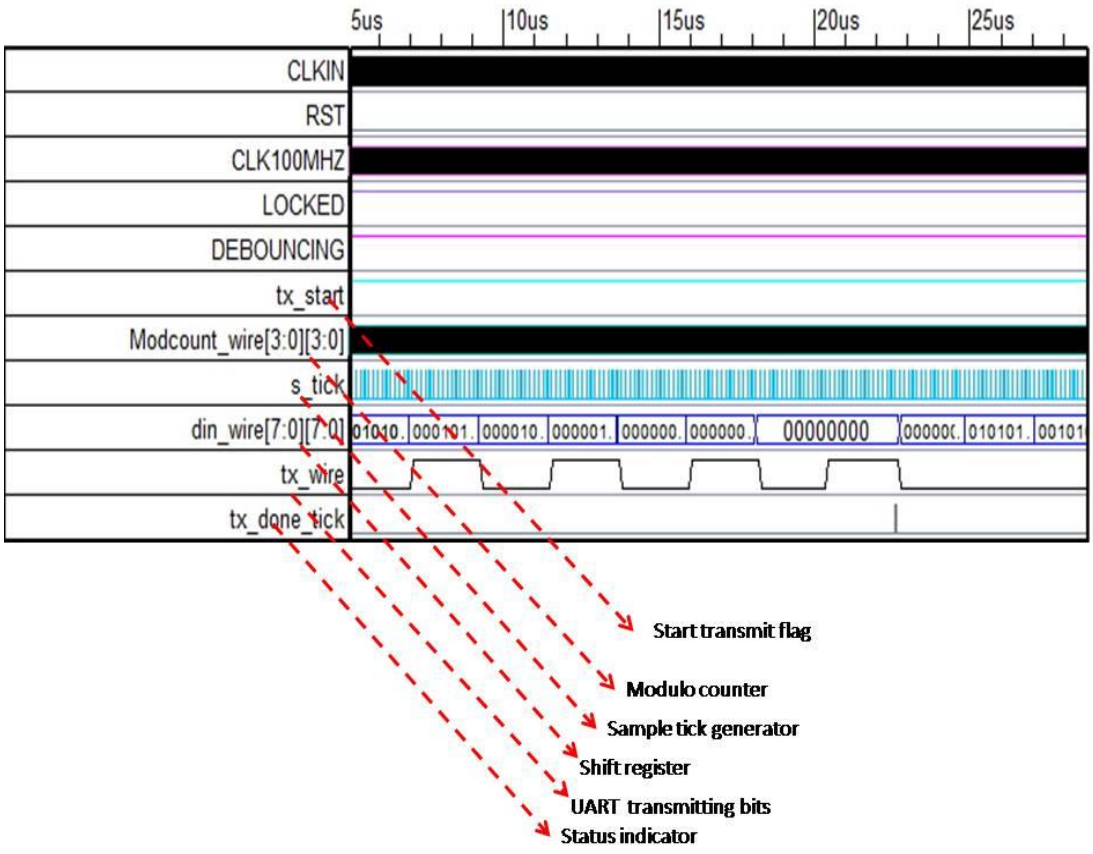


Figure 6-39 PAR simulation UART/Ttransmitter

### 6.5.6 Data Acquisition and Storage

The PSRAM used in the PDDN design is MT45W8MW16BGX-708WT from Micron, which is 128Mbits (16 Mbytes), high-speed, CMOS pseudo-static RAM for a low power, portable instrument. This chip will support a maximum clock frequency of 80MHz. At 80 Ms/s, PSRAM can hold data having a span of 104 ms which equals five power cycles and is enough for PD data interpretation. A functional block diagram of the memory chip is shown in Figure 6-40. Control logic handles nine control signals including the clock signal. These control signals inform the memory about the nature of the operation (write or read) to be performed. A bidirectional 16 bit data bus handles the data to and from the memory array via an I/O MUX and buffer. There are three control registers namely RCR, DIDR and BCR. The memory chip has 23 bit address lines which are used for initializing the control registers and row indexing during memory

write and read operations. During write and read operations only 16 bits out of 23 bits are used for row index which are latched during the operations using ADL.

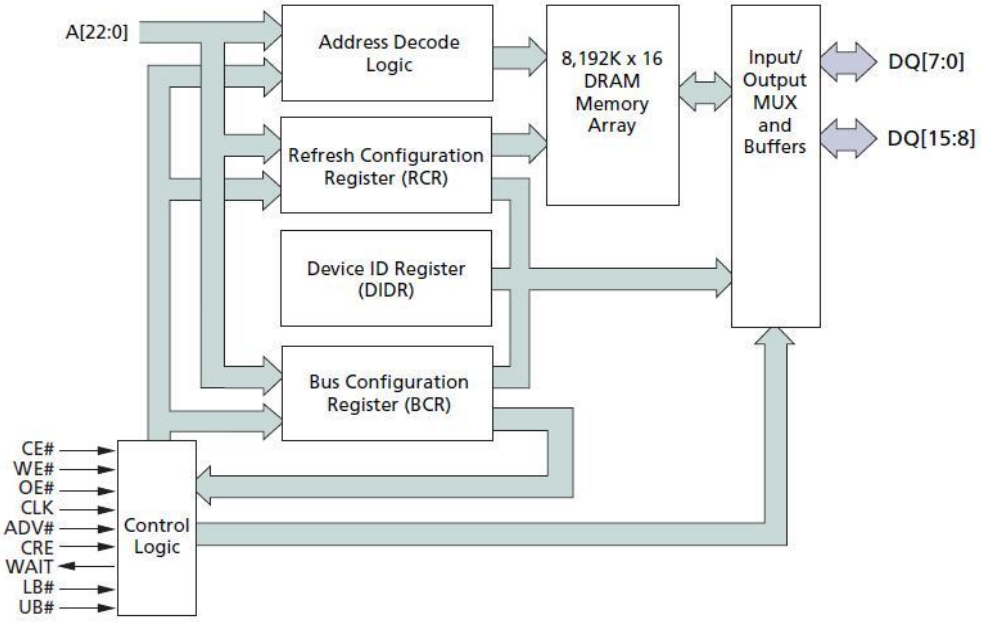


Figure 6-40 Functional block diagram of Memory Controller

Memory supports asynchronous mode, page mode, burst mode and mixed mode for writing and reading operations. The mode of operation setting will be inputted to BCR using the address lines mentioned. The DIDR provides information on the device manufacturer and the device configuration which can be used for self testing logic (described in section 6.5.7). The RCR setting is used for self refreshing operations. The Default setting is used in the current design. However the refresh parameter setting can be changed for standby applications which will reduce the current consumption dramatically and is more suitable for battery powered applications [Micron 2011].

#### 6.5.6.1 Memory Write Cycle

The memory chip used in the current design is based on half duplex mode, therefore bidirectional I/O logic needs to be implemented in the FPGA. A block diagram of bidirectional logic is shown in Figure 6-41 and the corresponding PAR simulation is shown in Figure 6-42.

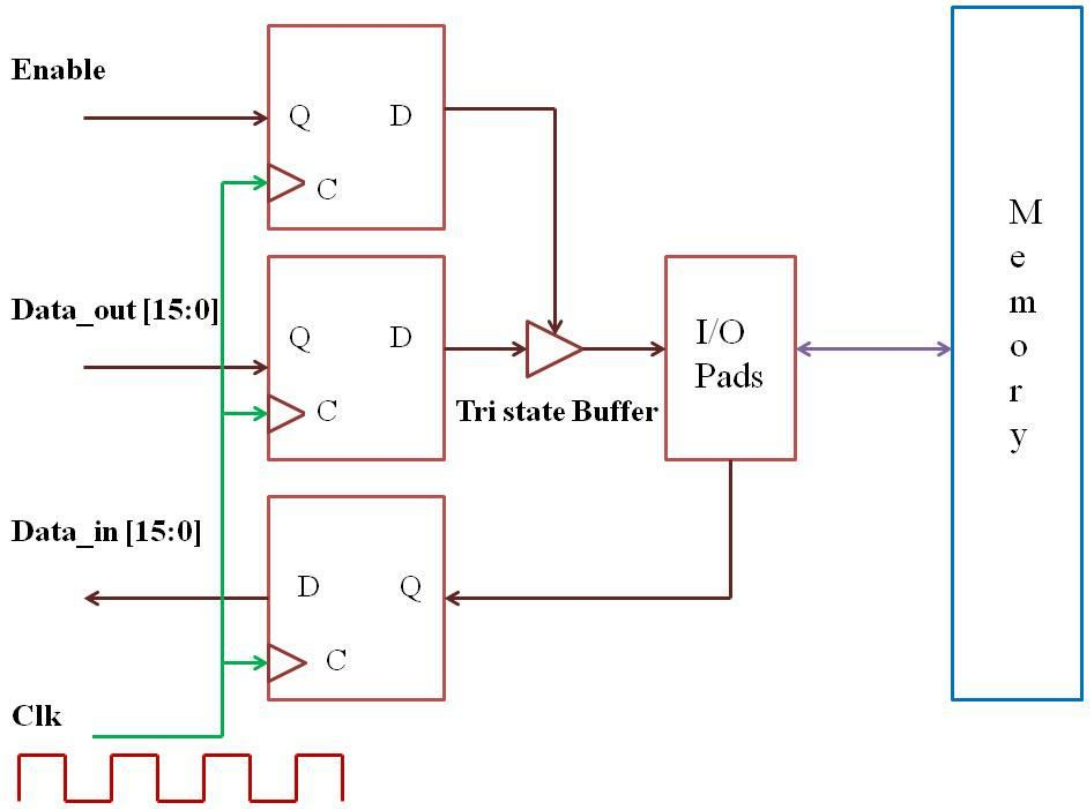


Figure 6-41 Bidirectional I/O logic

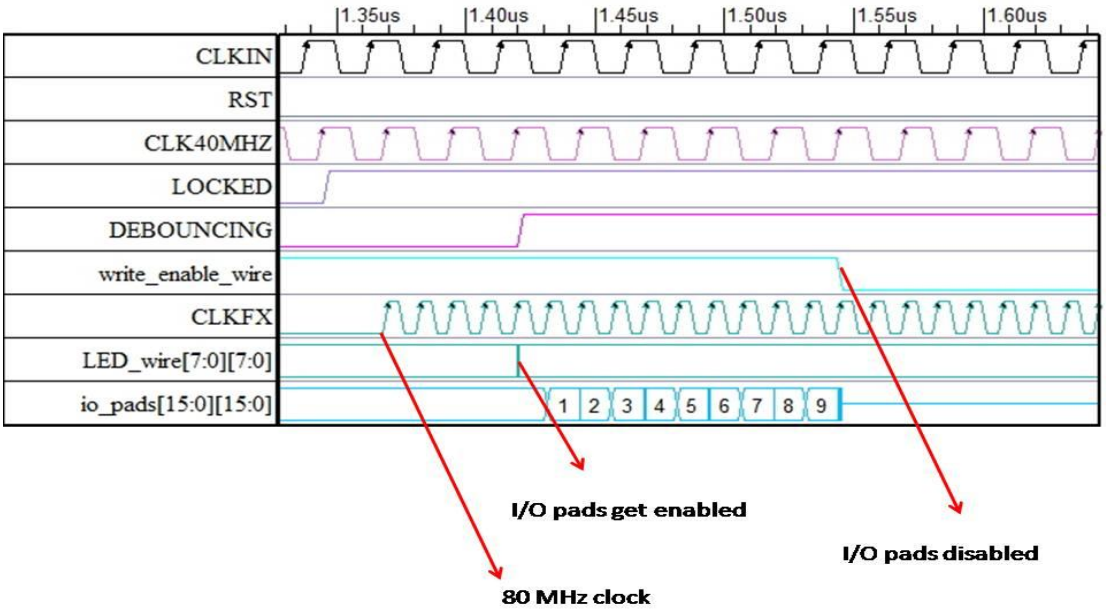


Figure 6-42 PAR simulation of Bidirectional logic

Burst mode memory operation is used in the current design which uses high speed synchronous read and write operations and also the latency period is shorter

compare to other modes. In this mode multi clock sequences are used in an ordered fashion. PAR simulation of memory timing cycle for write operation is shown in Figure 6-43.

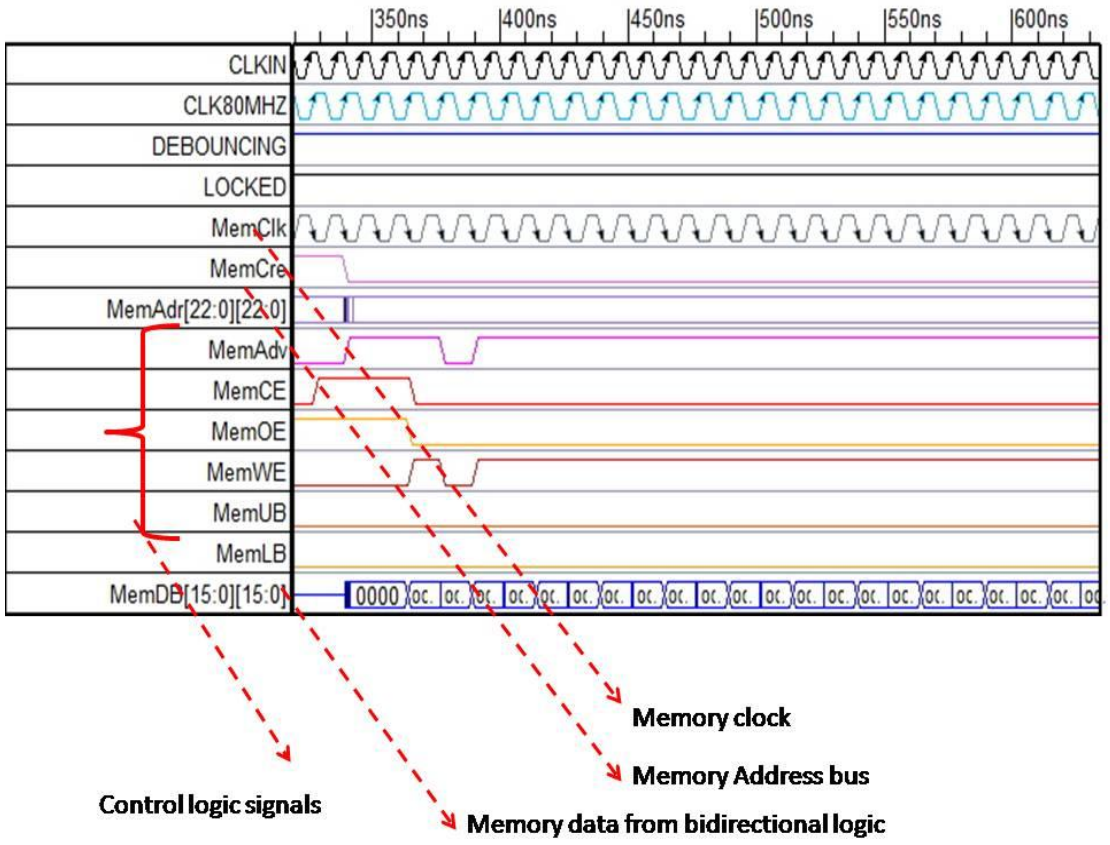


Figure 6-43 PAR simulation of memory write cycle

### 6.5.6.2 Memory Read Cycle

A Memory read operation is initiated from the PC by sending a request command to the FPGA through the UART. Then the FPGA prepares necessary control signals for memory read operation followed by transfer of the data to the PC through the UART. This type of logic requires a buffer in between the memory and the UART, since the memory read operation is faster than the UART. A block diagram of memory reading logic is as shown in Figure 6-44.

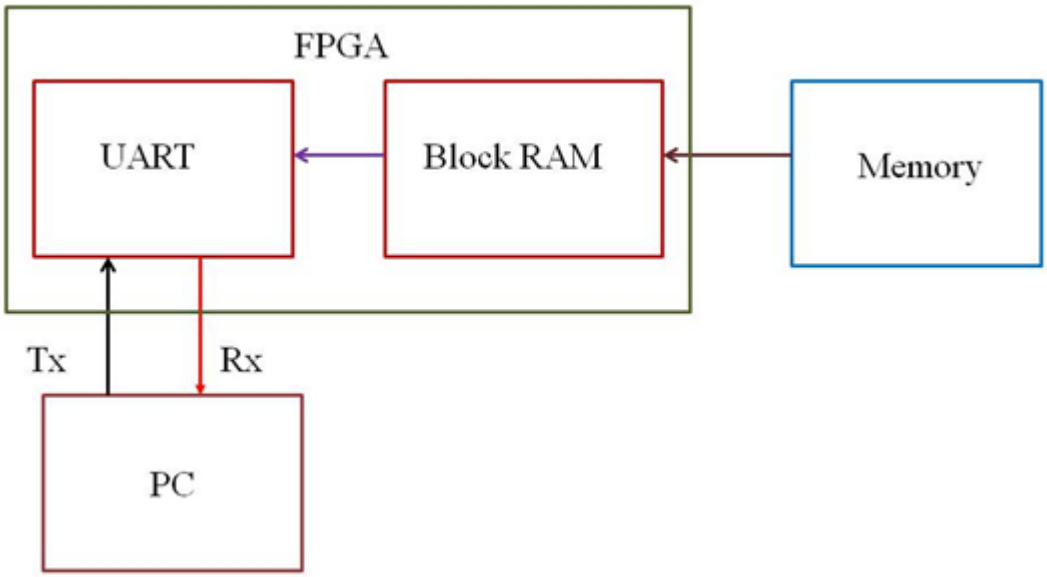


Figure 6-44 Memory reading logic

Block RAM in the FPGA acts as buffer in between the PSRAM and the PC. All Spartan-3 devices support block RAM, which is organized as configurable, synchronous 18 kilo bit blocks. Aspect ratio for example, width vs. depth, of each block RAM is configurable. Furthermore, multiple blocks can be cascaded to create wider and/or deeper memories [Xilinx 2008]. Typical block RAM used in the design is shown in Figure 6-45.

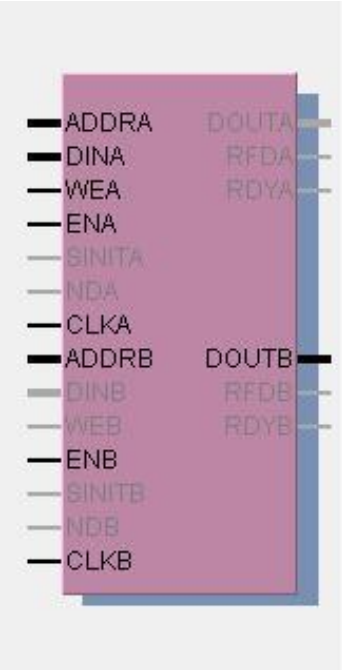


Figure 6-45 Typical block RAM used in the design[Xilinx 2008]

The timing cycle of a memory read operation involves reading each row of data from the memory and storing it in the block RAM followed by transmitting data to the PC via the UART/Transmitter. PAR simulation of the whole process is shown in Figure 6-46. Various signals included in Figure 6-46 are

PSRAM, Control logic signals (MemAdv, MemCE, MemOE, MemWE, MemUB, MemLB and MemCRV)

Data bus (MemDB)

Address bus (MemAdr)

Clock (MemClk)

Block RAM, Control logic signals(ena_wire, enb_wire, wea_wire)

Data bus(doutb_wire )

UART, Receiver bit (rx_wire)

Transmitter bit(tx_PC)

Flag(onerowdone_wire)

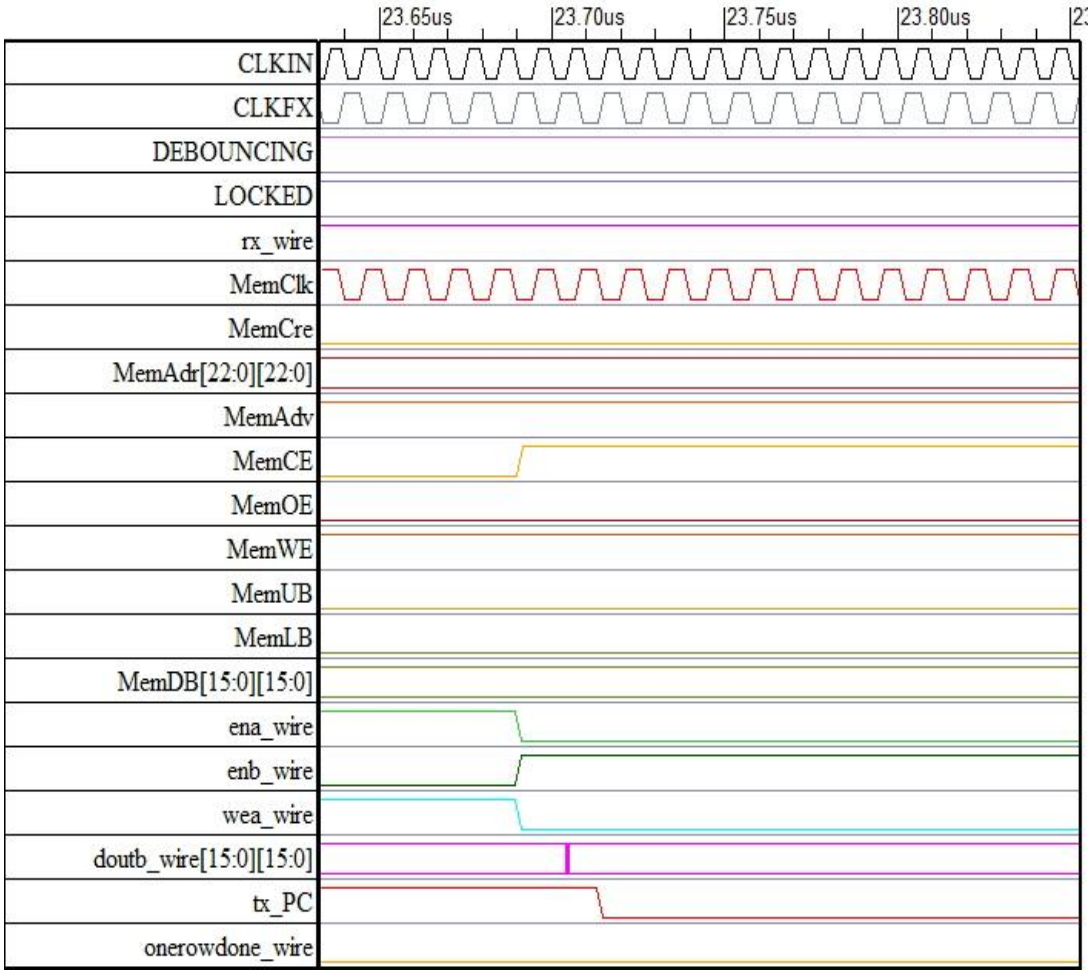


Figure 6-46 PAR simulation of memory read cycle

### 6.5.6.3 Memory Test

Memory data control logic is tested by generating a free running 16 bit counter in the FPGA followed by writing the data into memory. Then data from the memory is read and transferred back to the PC for verification. Test results are included in Figure 6-47. In Figure 6-47 certain samples (first 8 samples per row) of data were missing due to latency cycle in the PSRAM. Since the position of these samples is known, they can be interpolated while post processing the data.

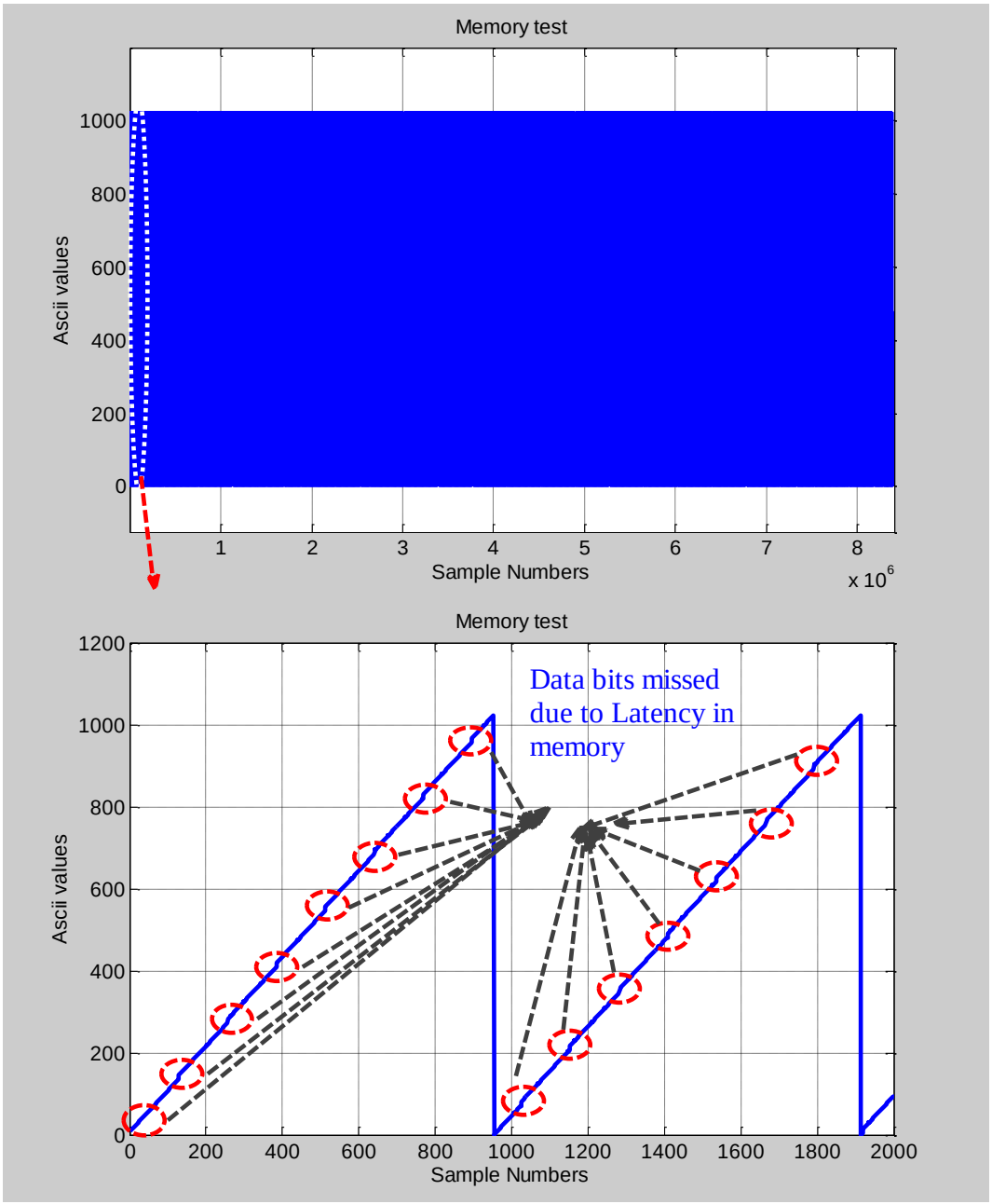


Figure 6-47 Memory test

Figure 6-48 shows the memory test setup with ADC using a signal generator and an oscilloscope. Measurement results are shown in Figure 6-49. More test results are included in the Appendix D-6.

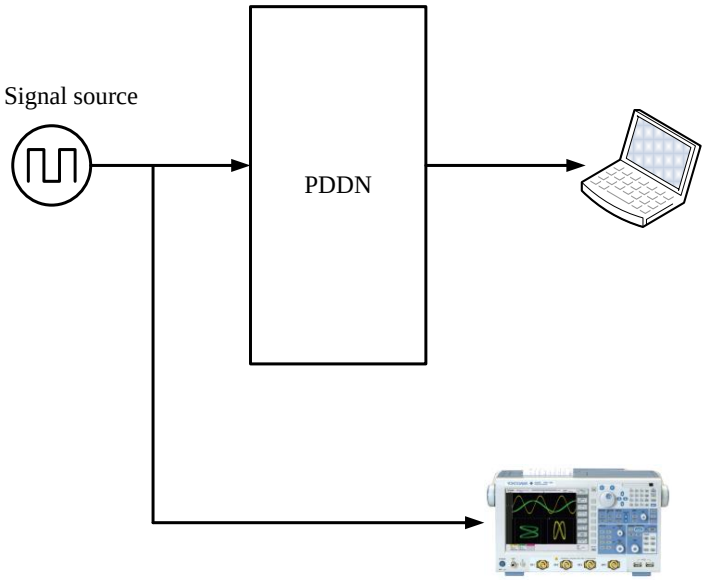


Figure 6-48 Memory test setup using ADC

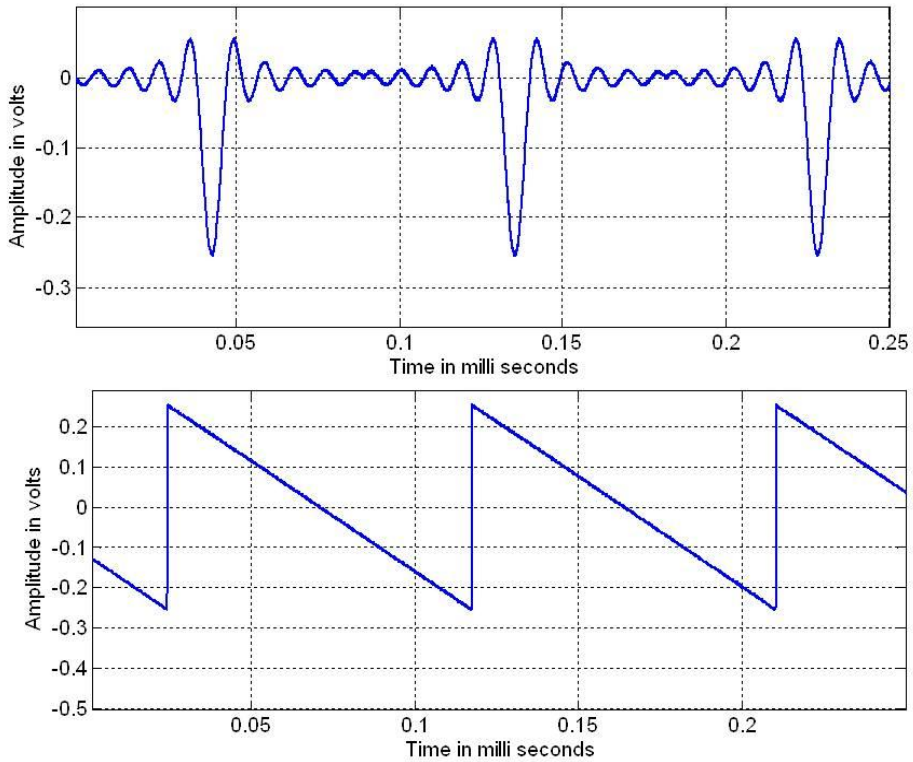


Figure 6-49 Data acquisition test # 1

### 6.5.7 Self-Test Logic

Due to the hardware constraints (discussed in section 6.4.2), self test logic is bypassed in the current design. The Method of self test logic is discussed here and can be implemented in the FPGA.

Self test logic performs initial test on the peripherals connected to the FPGA upon power up. Peripherals included in the self test are the VCTCXO, ADC, GPS and memory. Various self test logic included in the design are as follows.

The oscillator self test algorithm uses 1 PPS pulse from the GPS. A 40 MHz free running counter in the FPGA got triggered from the first 1PPS pulse and finishes at the next 1 PPS pulse. The counter value is checked with the threshold level. The timing cycle for this algorithm is as shown in Figure 6-50. This test logic runs 5 times so that any error caused by spurious triggering will be eliminated.

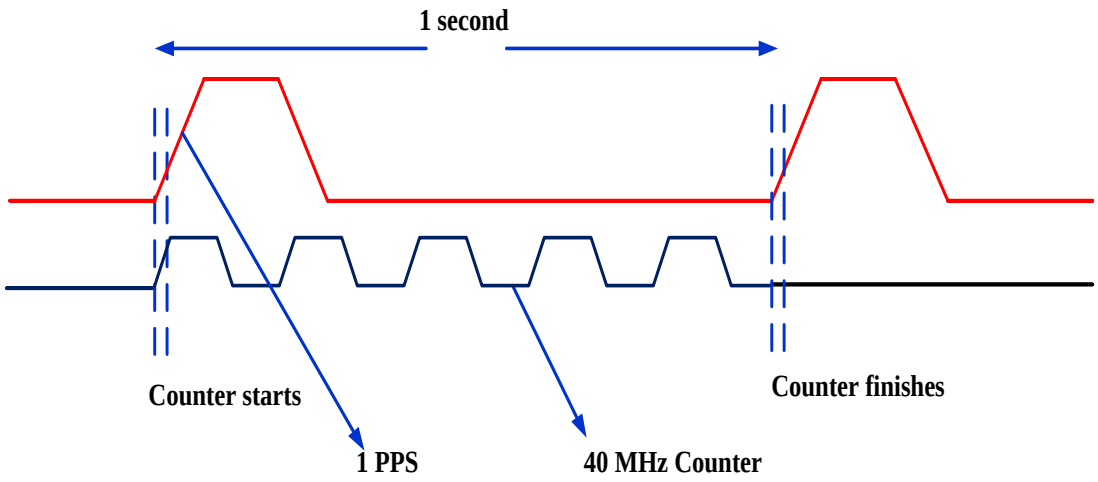


Figure 6-50 Self test logic Oscillator test

The GPS receiver is tested by sending a query from the FPGA via the UART followed by verifying handshake signals from the GPS receiver. PSRAM is tested by writing know data into the memory from the FPGA followed by reading back and comparing the data in the FPGA. The ADC is tested using the DAC and the FPGA. Digital samples are sent to the DAC from the FPGA. An analogue output from the DAC is fed back to the ADC and comparison is done in the FPGA.

## 6.5.8 Firmware Design

An ISE 10.1 Xilinx tool is used to develop the firmware. A complete state machine is shown in Figure 6-51. Hand shake signals are used which ever necessary. System can also be force restarted at any stage by sending command from control room. List of hand shaking signals used can be found in the Appendix D-7.

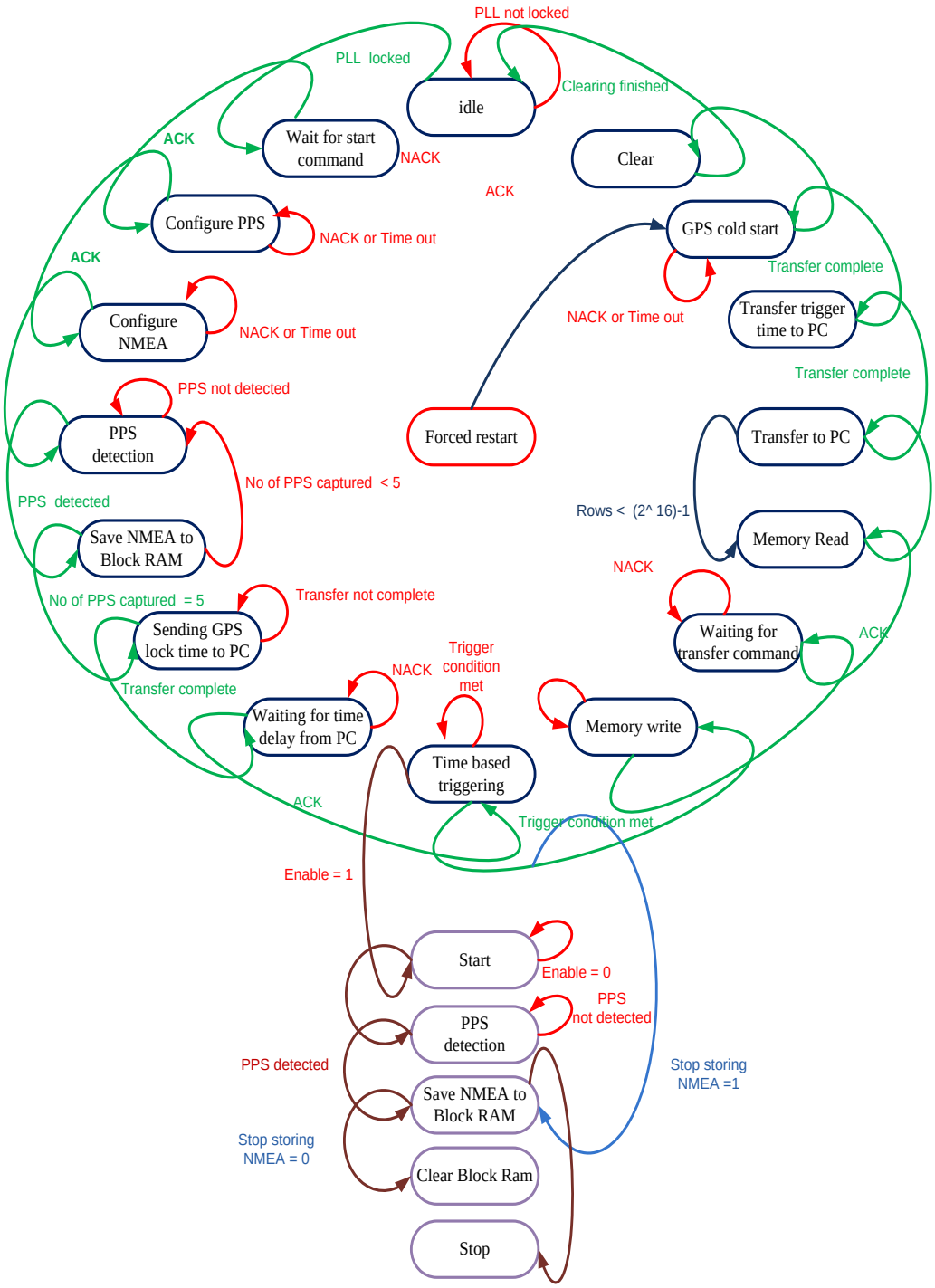


Figure 6-51 State machine

## 6.6 PD Detection Node (PDDN) – Software Design

Control, communication between remote client and servers (PDDN's), and data storage in PDDN uses software developed using Microsoft Visualstudio.net. This software includes several components which run in individual threads through distributed messaging systems and each message is sent through the TCP/IP to activate the corresponding component. A component collaboration diagram of the software is shown in Figure 6-52 in addition, the functionality of the software components is discussed below.

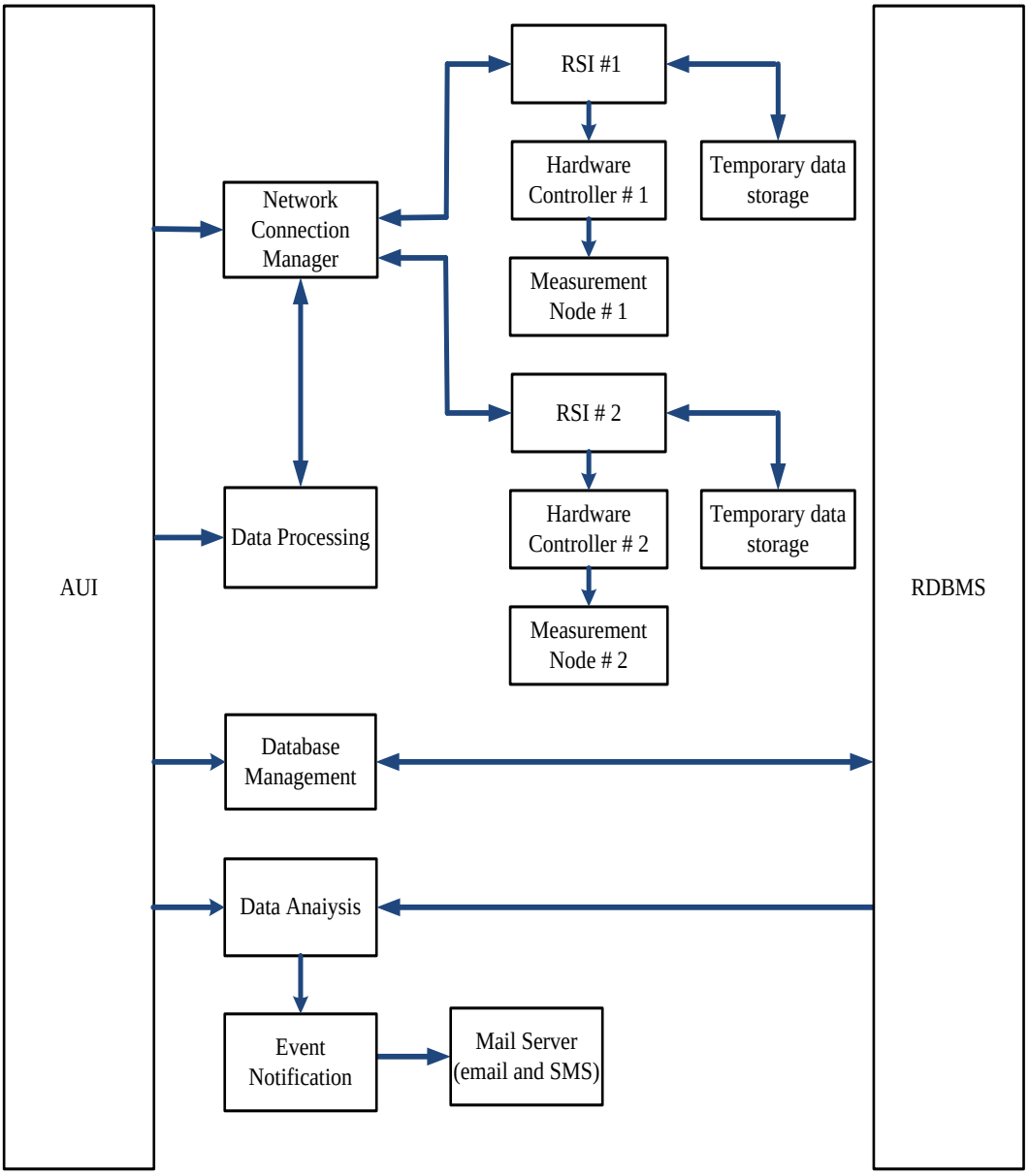


Figure 6-52 Component collaboration diagram

The AUI is installed in the client PC which can be located in the control room and a RSI is installed in both PDDN's. Both PDDN's are started first and wait for the start command from the remote client PC. The client (AUI) sends a connection request to the PDDN using a network connection manager once VPN is established. The AUI sends a start command to the RSI via the TCP/IP. Then the RSI initializes the measurement node by sending an initialize command via the hardware controller component. The PDDN's sends a GPS locking command to the AUI once a 3D position fix is set from the GPS receiver.

The data processing component in the RUI decodes the GPS locking time from both PDDN's thereby the time delay between the two PDDN's (described in section 6.5.3.2) is computed, and followed by sending the trigger enable time back to both PDDN's. Once the PDDN's get triggered based on TBTL( described in 6.5.3.2), an acquired signal data and trigger time data from the PDDN's will be sent to the RDBMS developed in the SQL server through a database management component in the RUI. All the events occurring in both the RUI and the AUI are logged through an event logger component.

The data analysis component in the RUI reads signal data and the corresponding trigger time data from the database. Data is processed using a denoising algorithms (described in section7.2) and a data interpretation algorithm (described in section 8.3 ), followed by the time base alignment of both data using the trigger time. Important events from the data analysis which includes PD level, Load current φ -q-n pattern and the PD MAP will be updated to the database followed by events sent to engineers through email or SMS. In this way history of the cable network data can be maintained, which can be used for a knowledge based expert systems so that a necessary cable renewal program can be initiated.

Software is developed using Microsoft visual studio.net which acts as the front-end, while a SQL server 2005 serves as the back end for database management. The PDDN handles binary data with different formats. For efficient operation of the software, multi threading logic is used. Decoding functions are employed in the software and the screenshots of the software tools developed are included in the Appendix D-8.

## 6.7 Laboratory Testing

Double ended PD monitoring system using time based data acquisition is tested in the laboratory using the laboratory test setup shown in Figure 6-53. The test setup involves PDDN #1, PDDN # 2, DSO, signal generator and PC. Two types of tests are necessary to validate the approach TBTL. This includes the time based trigger test and a data acqusition test. These tests are discussed in the following section.

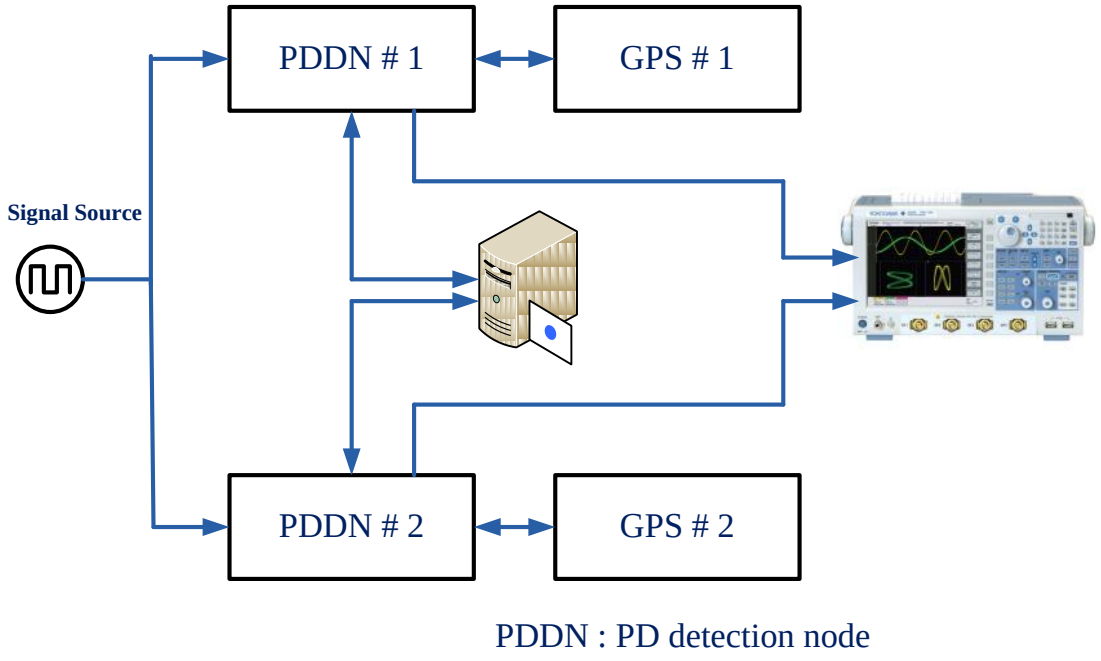


Figure 6-53 Time based trigger test

### 6.7.1 Time Based Trigger Test

In the time based trigger test, the time offset error between the triggering instants of both PDDN's is measured based on $T_e$ (described in section 6.5.3.2). This is achieved by sending a pulse having a pulse width of 1µs from both PDDN's to the DSO when $T_e$ is reached. These tests were repeated for every 10 minute interval with a measurement duration of 3 hours by making use of the infinite persistence mode in the DSO. The eye diagram of the measurement results is shown in Figure 6-54 [Hewlett-Packard 1996].

In Figure 6-54, the top trace shows the 10ns rise time corresponding to the pulse from PDDN #1, which is the trigger source for the DSO. The lower trace is from the PDDN #2. In an ideal case, rising edges of both traces should be aligned. The bottom trace in Figure 6-54 is seen to vary from the trigger point of the DSO due to the relative

drift between the PDDN's. The maximum time offset error of 160ns was recorded in the measurements. Compared to Figure 3-38 (triggering using free running 1PPS) the drift introduced by TBTL is seen to be significantly reduced. After triggering based on TBTL, digital data from the ADC output is captured and saved to the memory of the PDDN's. During this period, termed the acquisition period (104 ms), the crystal oscillator used for clocking the FPGA will introduce a drift in measurements unless the frequency stability of the oscillator for the acquisition period is sufficient. The Data acquistion test is discussed in the next section.

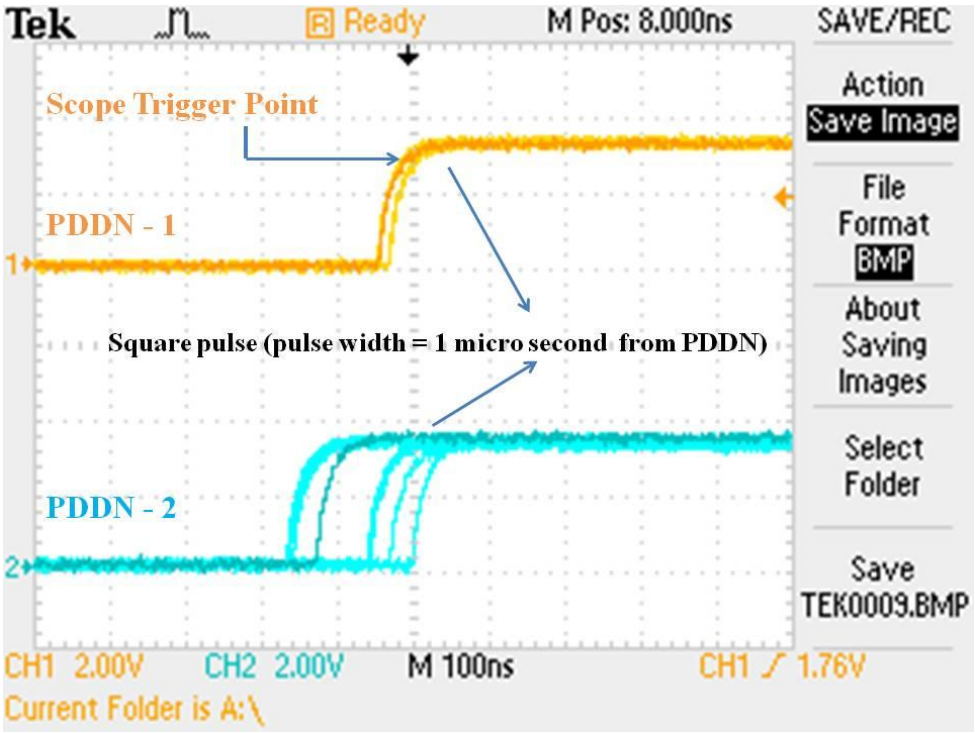


Figure 6-54 Triggering instant mismatch measurement using DSO

## 6.7.2 Data acquisition test

Figure 6-55 and Figure 6-56 shows typical data acquired from the signal generator used in the measurement setup discussed in section 6.7. Drift during the acquisition period of 104 ms is calculated using the relative time difference between the zero crossings of the data from both measurements. The measured drift of 12.5ns ncludes GPS drift and clocking uncertanity of the oscillator used in the FPGA. This drift can be safley ignored.

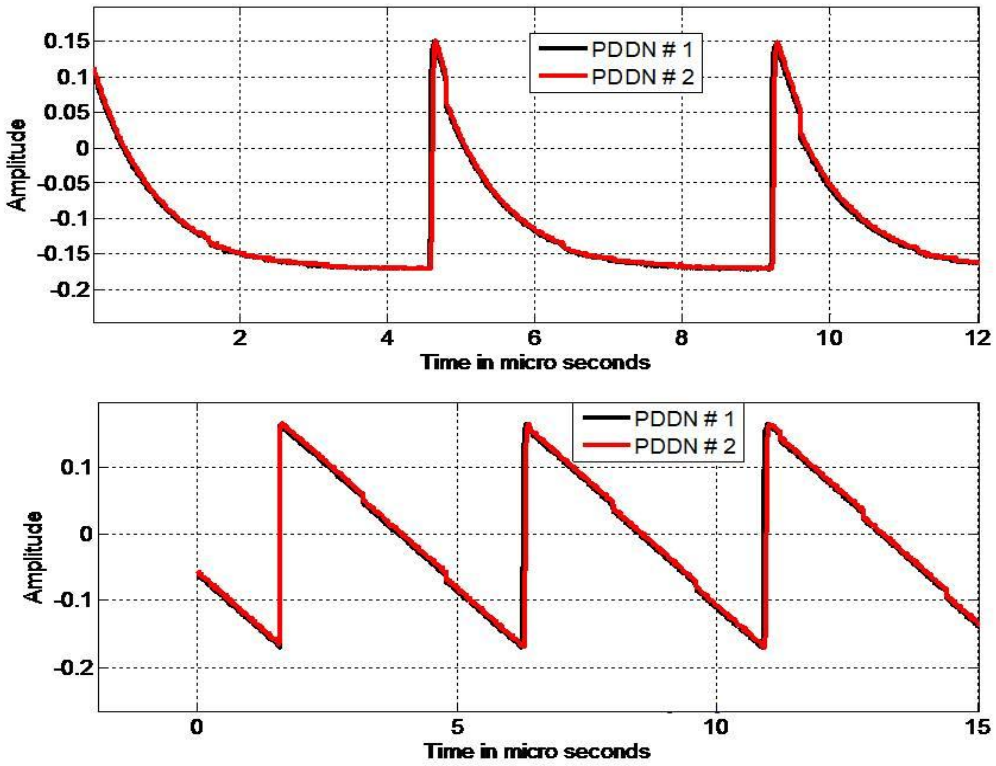


Figure 6-55 Synchronized measurements # 1 (f= 217 KHz)

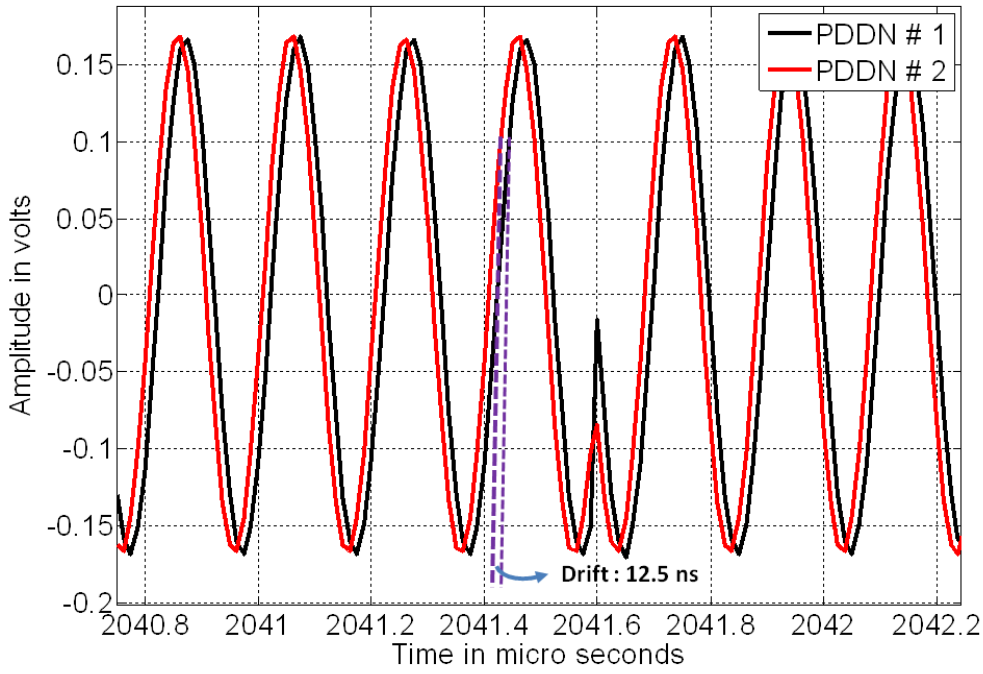


Figure 6-56. Synchronized measurements # 1 (f= 5 MHz)

## 6.8 On-site trials

Preliminary site trials were conducted in a 33/11 kV substation to calulate the PD location error of PDDN's. Figure 6-57 shows the block diagram of the on-site measurement in Sighthill substation, Edinburgh. Photograph of the measurement setup is included in the Appendix - D. In this test, both PDDN's were connected to the common earth bar from one end of the 11 KV PILC cable using HFCT's, as shown in Figure 6-58. This test setup can only give the measure of drift introduced by both PDDNs in a harsh environment like a substation. In this way PD source location accuracy of PDDN's using TBTL can be obtained.

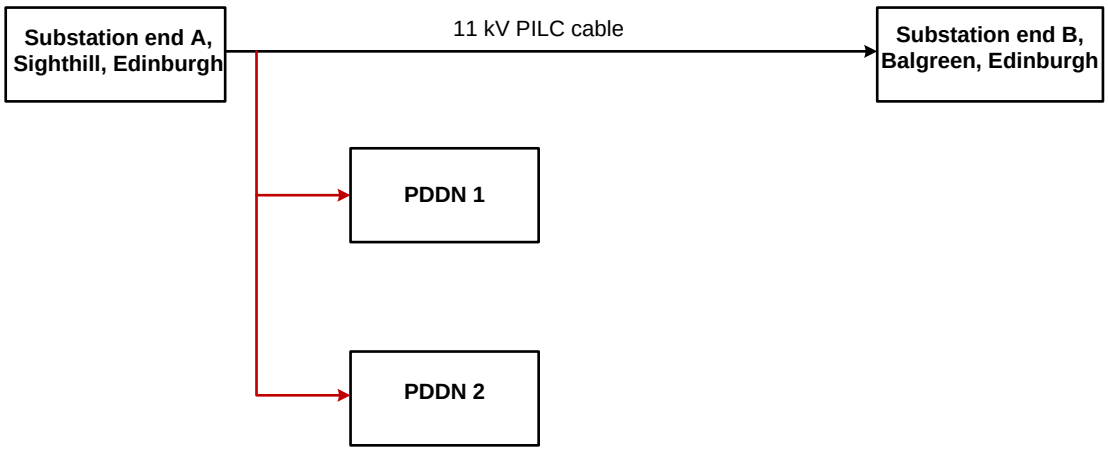


Figure 6-57 PDDN on-site trial @ 33/11 KV Substation, Edinburgh


Figure 6-58 HFCT connection @ 33/11 KV Substation, Edinburgh

Raw data acquired by the PDDN's are shown in Figure 6-59 and Figure 6-60. The MRTIE between the two PDDN's was measured by aligning fast rising pulses extracted from the on-site measurement data as shown in Figure 6-61. From a set of five measurements, the largest MRTIE values are calculated for each pulse location and the results are shown in Figure 6-62. From Figure 6-62 MRTIE for the PDDN's is approximately 60 ns. This drift is equivalent to ± 6m PD source location accuracy based on the propagation velocity in PILC cables. This drift is caused by GPS error and VCTCXO error.

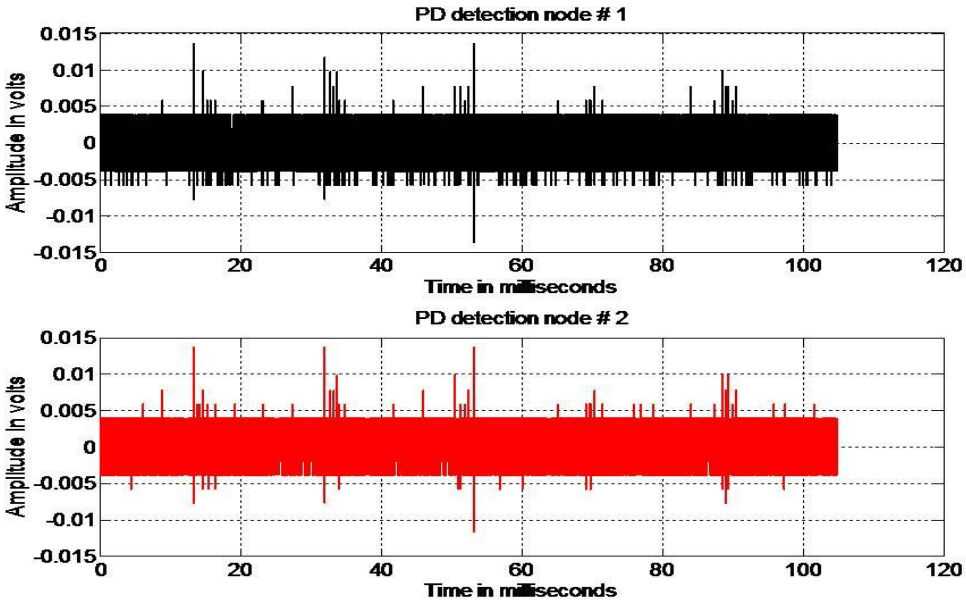


Figure 6-59 On-site trial test # 1

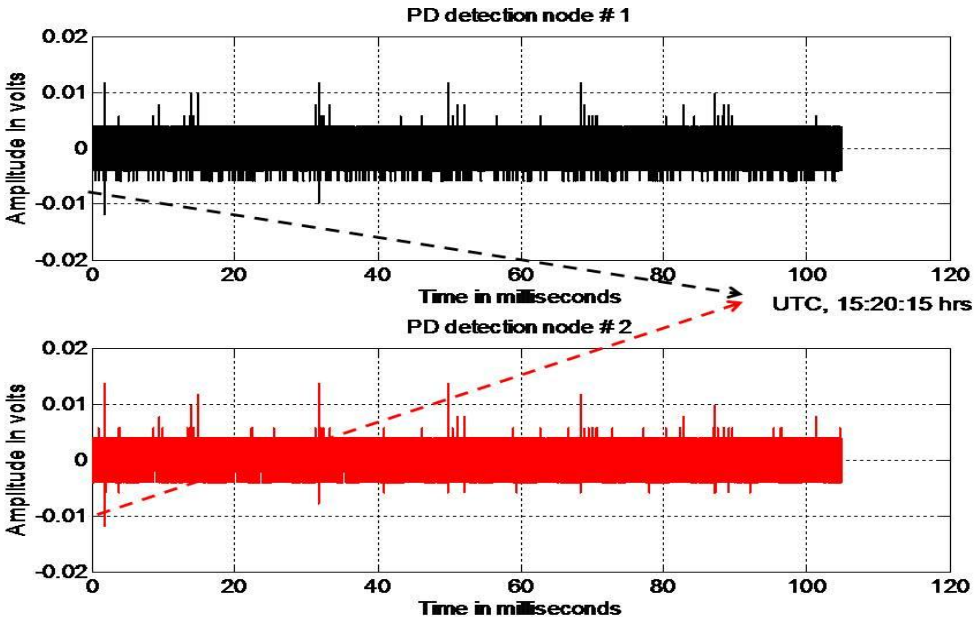


Figure 6-60 On-site trial test # 2

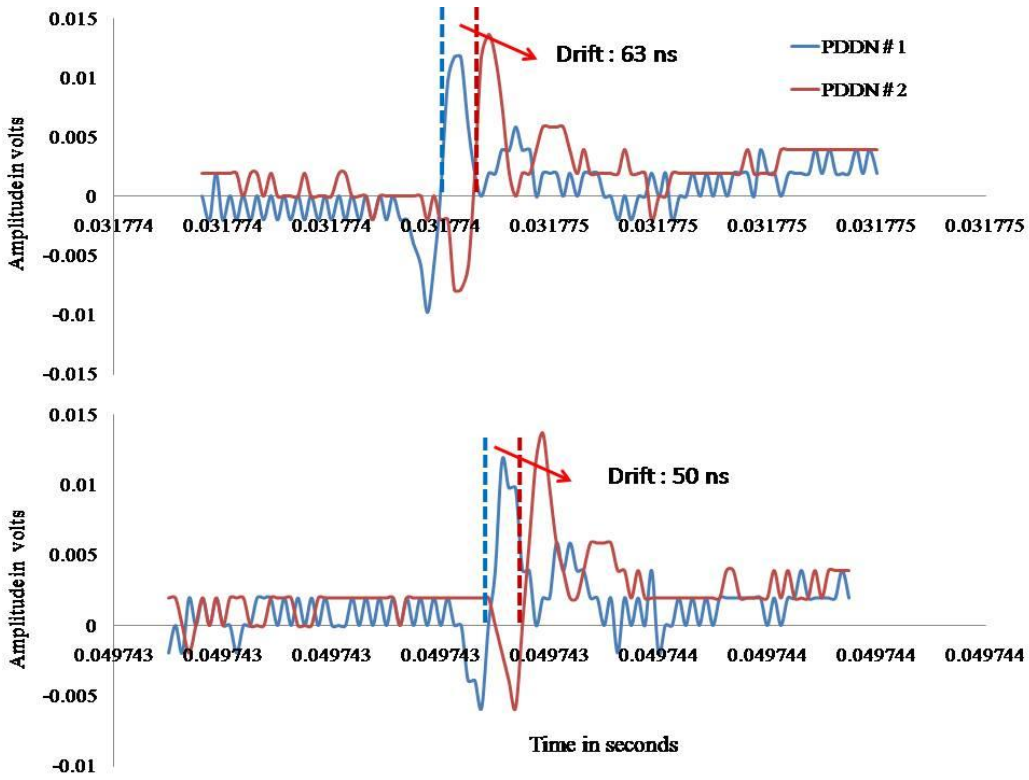


Figure 6-61 Fast rising pulses from on-site data

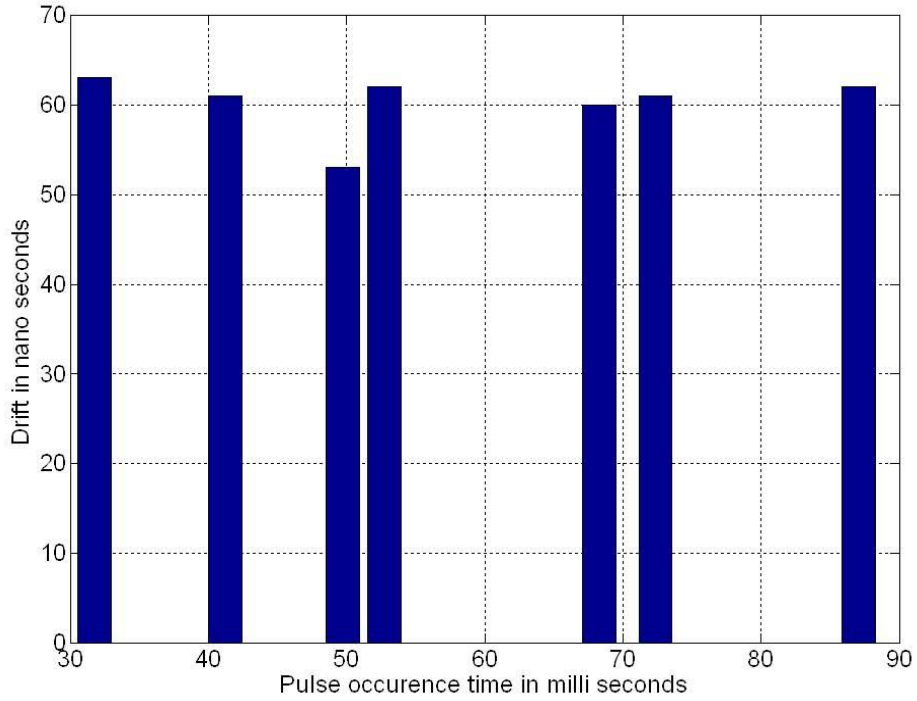


Figure 6-62 MRTIE performance of PDDN using on-site data

## 6.9 Comparison with conventional systems

The conventional method of PD source location using free running 1PPS is compared with PDDN's based on TBTL for PD source location accuracy in the laboratory. Laboratory test results are shown in Figure 6-63. Based on Figure 6-63, it is seen that the PD source location error in the proposed system using TBTL is generally lower than that of the conventional system. Furthermore PD source location accuracy can be improved by conducting a series of measurements with the proposed system. The PD source location with the lowest location in magntiude is selected.

The conventional method of PD source location using free running 1PPS node does not have communication between measurement nodes. This leads to a lack of syncronization between the measurements. This is due to the fact that the probability of the GPS receivers at both ends of the cable getting a 3D position fix at same time is much smaller. This will generate invalid data sets, thereby consuming hardware resources. The low broadcast power of the GPS satellites, approximately -160 dBw, makes these signals particularly susceptible to jamming [Reynolds, Brown et al. 1999]. Once the signals get jammed after getting a 3D position fix, the flywheel 1PPS from the GPS recever is not valid and cannot be used for locating a PD source. This uncertanity can not be tracked in conventional systems unlike the proposed system using TBTL. Generally good PD source location accuracy can be achieved using the proposed system.

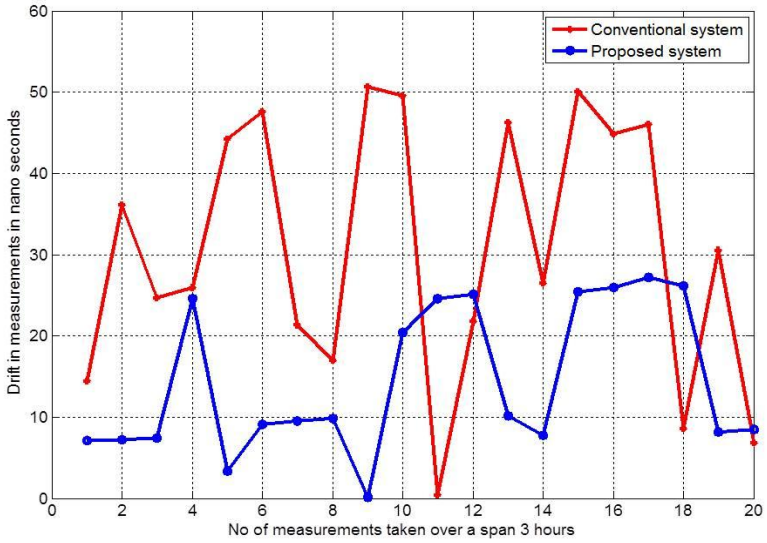


Figure 6-63 PD source location error for conventional over proposed system

## 6.10 Conclusion

The success rate of PD diagnostics relies on accuracy in identifying the origin of the PD source. This will reduce CI, CML cost and regulatory penalties. The single ended method of PD source location requires both an incident and a reflected pulse to locate PD source. Since the accuracy of this method relies on the propagation channel effects, cable network structure, length of cable network and the dynamic range of measurement systems, it is mostly applicable to offline PD source location. In the double-ended method, incident PD pulses from measurement units at both ends of the cable are measured. Hence, uncertainties introduced by propagation channel effects, cable network structure and cable length is reduced. However, double ended PD detection methods are less common due to their complexity in system design, time synchronization and the communication link required between measurement systems. In this chapter, a novel double-ended PD source location system using TBTL with a GPS receiver was proposed.

In order to implement TBTL low level access to hardware is required. As this is not readily available in commercial systems, a PDDN was designed. This system acquires the data from both ends of the cable for a specific 1PPS from a GPS receiver using TBTL. To implement TBTL, timing uncertainties such as frequency stability, phase noise and clock skew were taken into account during the PDDN design. Furthermore, GPS receiver in PDDN is turned on just before the data acquisition using FPGA. This will reduce the long-time drift of the GPS receiver clock.

Tracking of invalid data caused by flywheel 1PPS due to temporary loss of satellite signal can reduce PD source location inaccuracies which cannot be achieved using conventional methods of PD source location using flywheel 1PPS. With the use of communication between two PDDN's, invalid data acquiring is eliminated. Based on the measurements from laboratory and on-site, the proposed system with TBTL shows good PD source location accuracy compared to the conventional double ended PD source location methods. This system can be used to locate PD's with an error margin of less than ± 10 meters from the discharge source. Further advantages of this system include low cost and portability compared with existing approaches to PD source location.

.

# Chapter 7 :
# Signal Processing Algorithm for Denosing Partial Discharge Signals in Cables

## 7.1 Introduction

On-line PD signals are more prone to noise and it becomes more challenging to extract PD information from the raw data. Extracting PD information from the raw data is a two fold process, namely denoising and data interpretation. In this chapter a signal processing algorithm for denoising PD signals in cables is presented. The main objective of denoising is extracting the relevant information from the raw data by discarding the noise contained in the data [Quan, Lei et al. 1999]. Wavelet based techniques discussed in Chapter 4 are widely used to denoise the PD signals since it can provide time and frequency information simultaneously. Wavelets can decompose a signal into several scales, and at each scale the position of instantaneous structure of the signal can be obtained. This property can be used for extracting the required information from the raw data. Wavelet denoising of PD signals involves signal decomposition, thresoholding and reconstruction. The number of decomposition levels in wavelet based denoising is selected by visual examination of the SNR of the decomposition coefficients, but it may not be the optimum method [Zhou, Zhou et al. 2005]. Hence it is a requirement to determine the optimum wavelet decomposition level which will reduce the hardware resource usage and time consumption dramatically. In this chapter a KBT algorithm with stopping criterion using SGWT is proposed. This algorithm is implemented in a Matlab wavelet toolbox and is tested using synthetic data, on-site data which is followed by comparing this method with existing thresholding methods. The same approach has been tested using EMD, also with the results are compared.

## 7.2 Kurtosis Based Thresholding using SGWT

PD signals appear as a short duration bursts in the power frequency window of the applied voltage to the insulation. Signature of the PD pulses resembles transient noise [Foo 2003]. For signals composed of short duration pulses with additive white Gaussian noise, HOS allows us to detect those short duration spikes by giving higher values which are over-Gaussian and become zero for the rest of the signal corresponding with the Gaussian noise [Gottin, Ioana et al. 2009]. The signal processing algorithm proposed in this chapter decomposes the raw data into analysis and detail coefficients using SGWT followed by analysing signal trend at each level. As the level of decomposition increases, noise power get decreases, followed by a flat trend. So a number of zero crossings in the wavelet coefficients are used as criteria for terminating the decomposition. In this way stopping criterion is obtained. Then a hard threshold based on the single threshold value using kurtosis is applied to the analysis coefficients followed by reconstruction. A flow chart of this algorithm is shown in Figure 7-1.

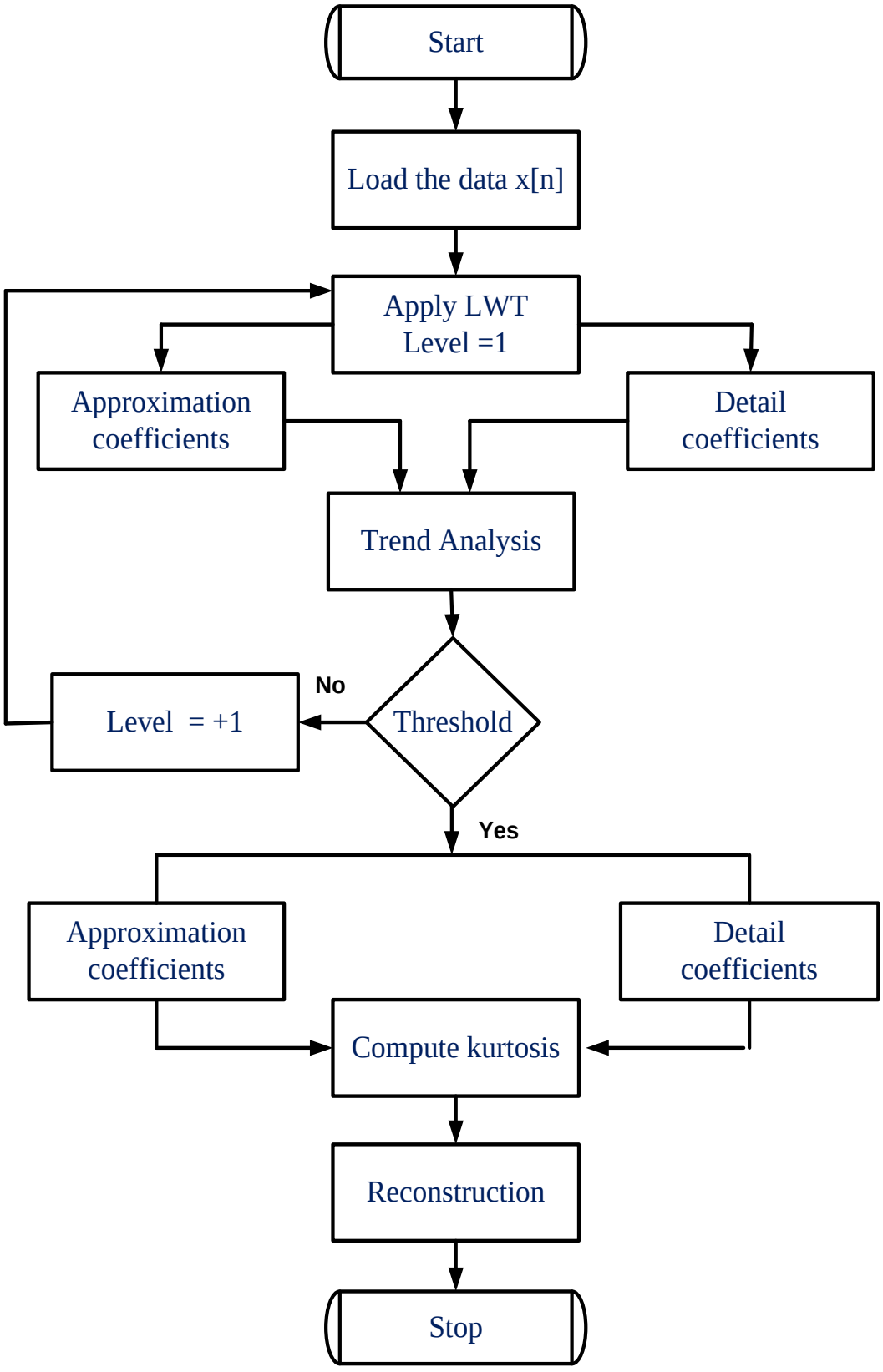


Figure 7-1 Kurtosis based denoising using SGWT

### 7.2.1 Testing the algorithm using synthetic data

Signature of the PD pulse from the discharge source is determined by factors like gas species, gas pressure, void conditions [Okubo, Hayakawa et al. 2002] and finally the propagation characteristics of the cable and transfer function of the measurement system. [Song 2009] classified PD pulses based on time domain signature in underground PILC cables detected with HFCT sensors are shown in Figure 7-2 .

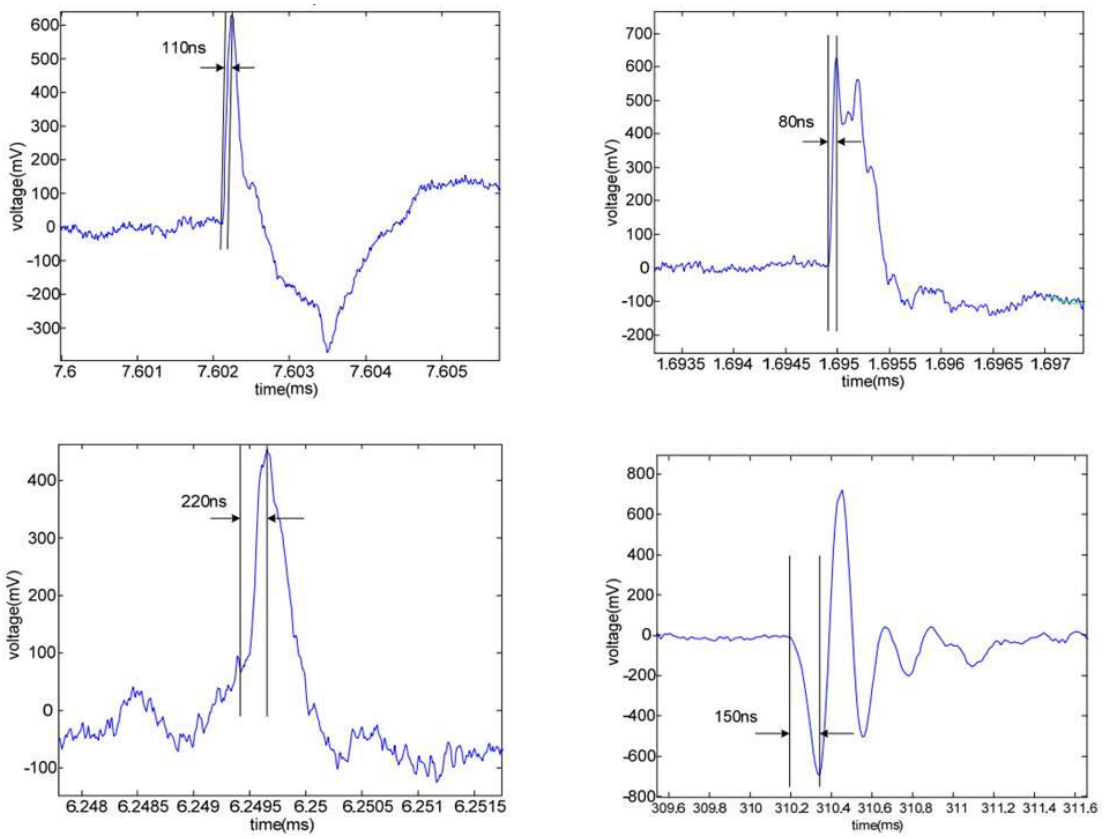


Figure 7-2 Different signatures of PD pulses from 11 kV PILC cable [Song 2009]

From Figure 7-2, the distinguishing feature is the oscillation contained in the pulses, that is the pulse with and without oscillation. Based on this information, two different sets of synthetic data are generated to represent the PD pulse as a damped oscillatory pulse and a double exponential pulse. An attenuated version of incident pulse is also included in the synthetic data for studing the densoising effect in reflected pulses. In cables, PD signals appear as positive and negative pulses depending on the phase of the PD inception voltage. Hence both positive and negative polarities of the pulses are

used. Then these pulses are then added with a wide band noise and then sent to the KBT model developed in Matlab shown in Figure 7-3.

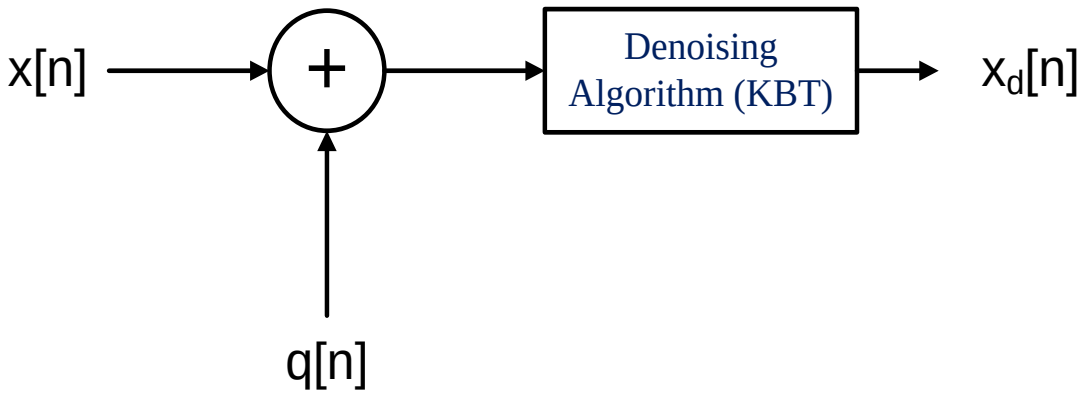


x[n] : Input signal (discretized in time)

q[n] : Wide band noise

$x_d[n]$ : Denoised signal

Figure 7-3 Denoising block diagram

The efficiency of the denoising algorithm is evaluated using the criteria of PD source location and PD magnitude shown in Figure 7-4 and Figure 7-5 respectively, which also includes the MSE between the original signal and the denoised signal. In general PD source location criterion calculates the time offset in the starting point between the original pulse and the denoised pulse. In an ideal case, time offset in starting time between both synthetic and denoised should be zero. But this can't be achieved in practice which is due to wavelet basis function and thresholding, though perfect reconstruction filters are used. Also the offset in amplitude and pulse width between the original and denoised pulse determines the accuracy in quantifiying PD magnitude. This drift in amplitude is also resulted from the thresholding which is a part of denoising. The KBT algorithm based on SGWT is tested using synthetic data as discussed in the next section.

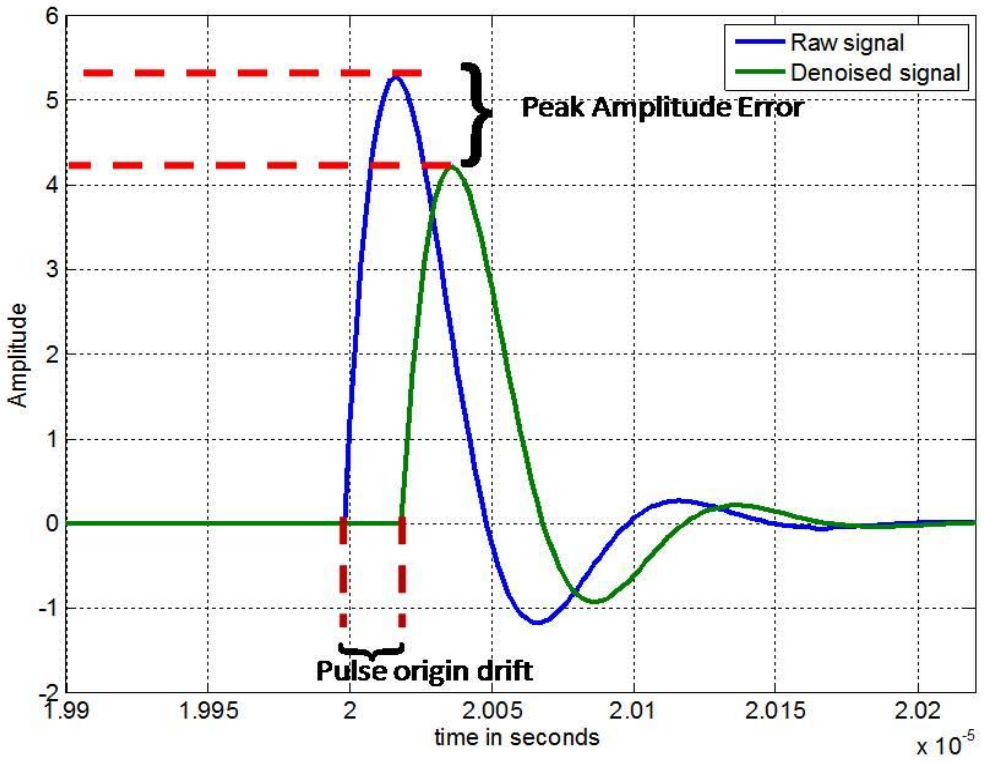


Figure 7-4 Denoising efficiency criteria

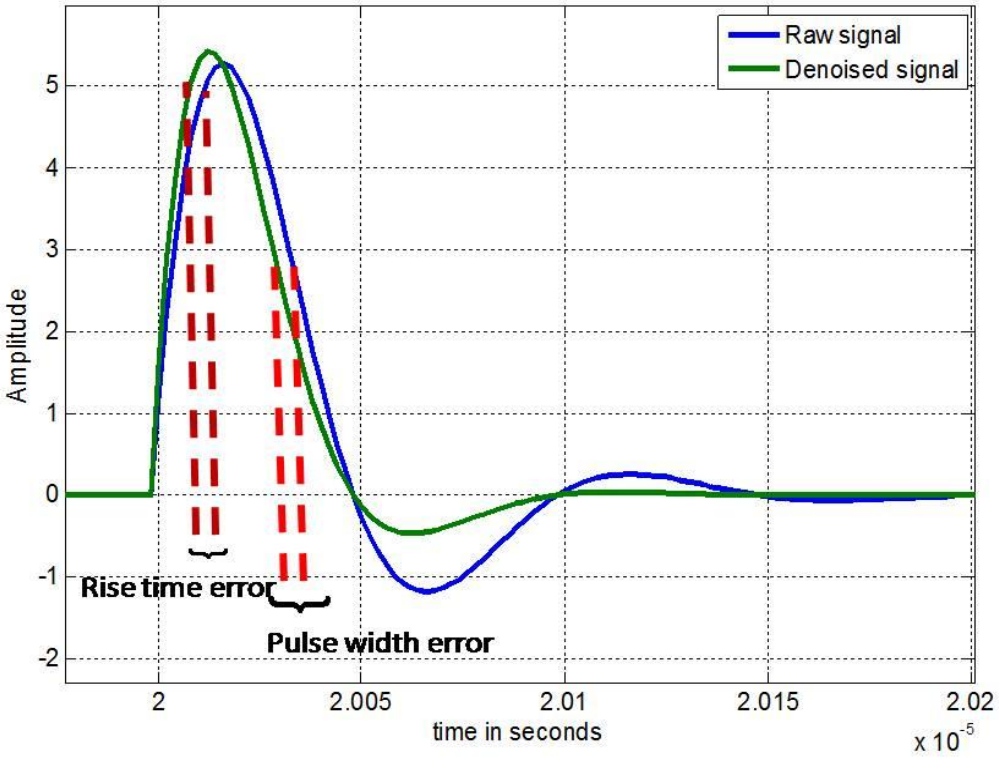


Figure 7-5 Denoising efficiency criteria

### 7.2.1.1 Experiment #1 Synthetic data using double exponential pulse

A double exponential pulse having a rise time of 100ns and a pulse width of 300ns with added wide band noise is shown in Figure 7-6. In Figure 7-6 there are three pulses, namely pulse 1 which has higher amplitude than pulse 2 and pulse 3, which are of lower amplitude. SNR with respect to pulse 1 is -13 db. Pulse 2 and pulse 3 are not visible after the adding of wide band noise, due to a lower SNR compared to pulse 1. Approximation and detail coefficients from the first level to the third level of decomposition are shown in Figure 7-7 and Figure 7-8 respectively. The rest of the decomposition coefficients are included in the Appendix E-1. Double exponential signatures can be seen in approximation coefficients, while detail coefficients are rich in noise. Higher order coefficients show a flat trend which is used as the stopping criterion.

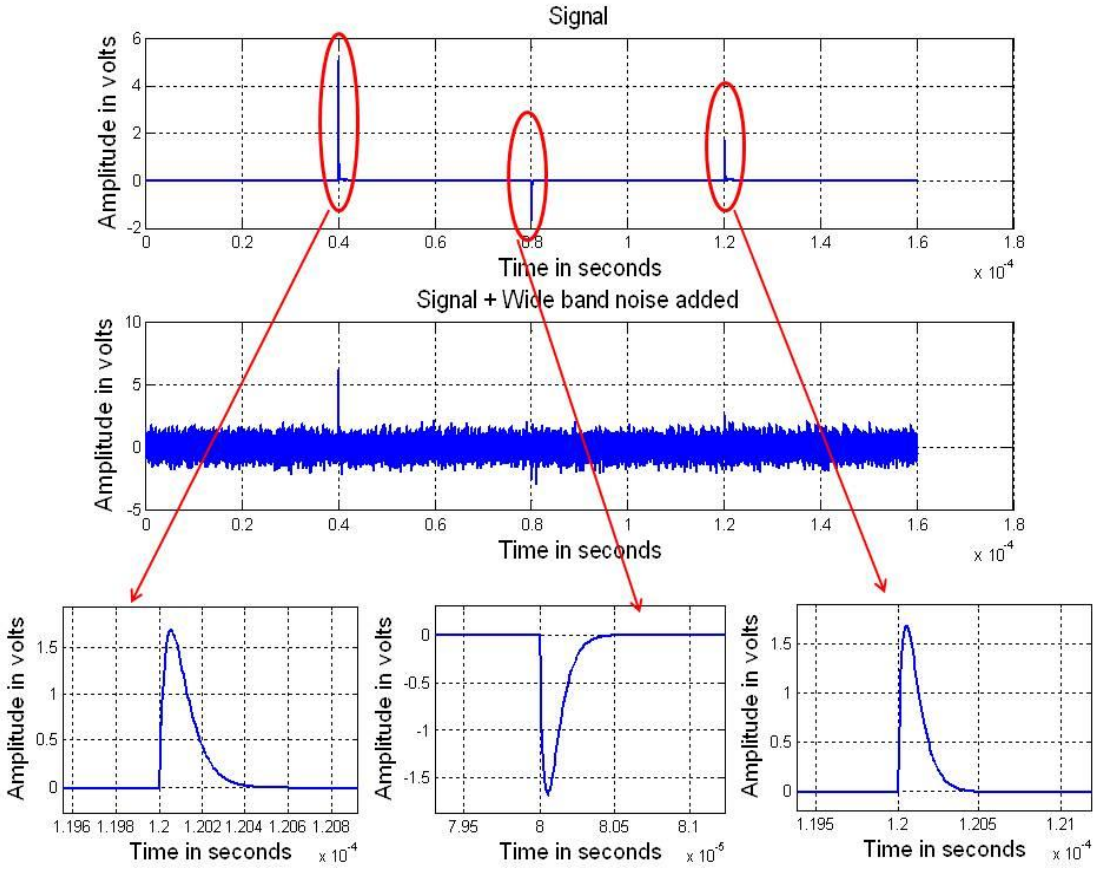


Figure 7-6 Double exponential pulse with added wide band noise (SNR : -13 db)

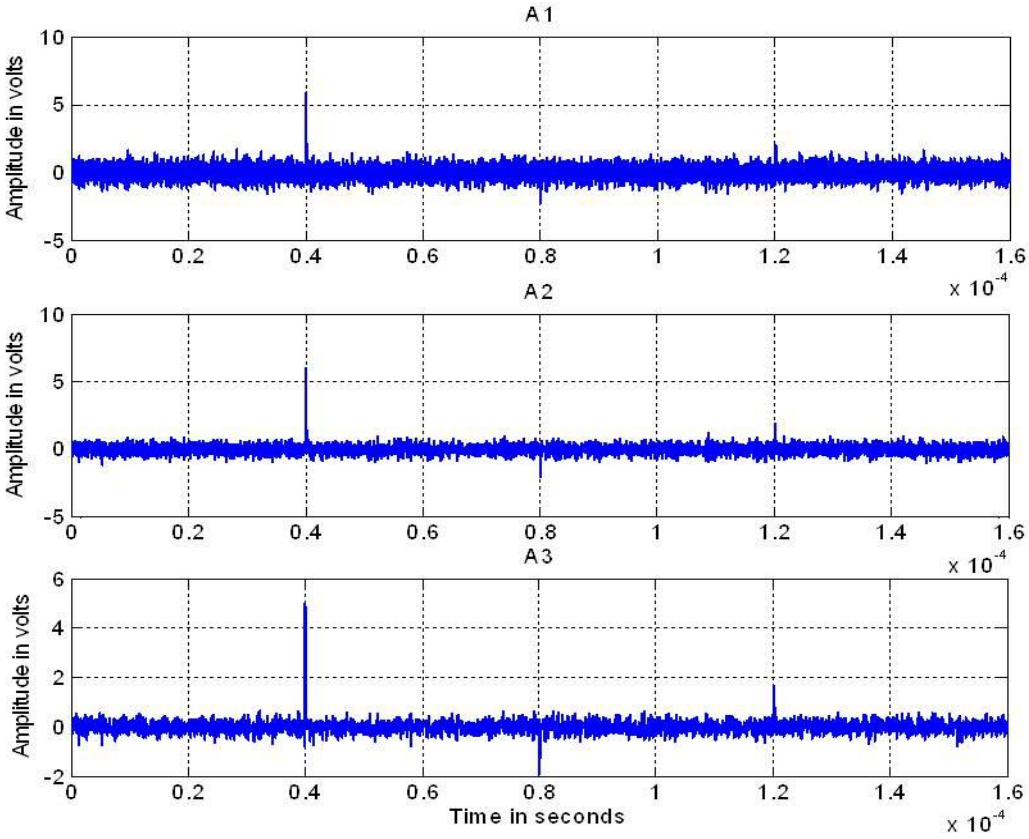


Figure 7-7 Approximation coefficients (leve1 # 1 – level # 3)

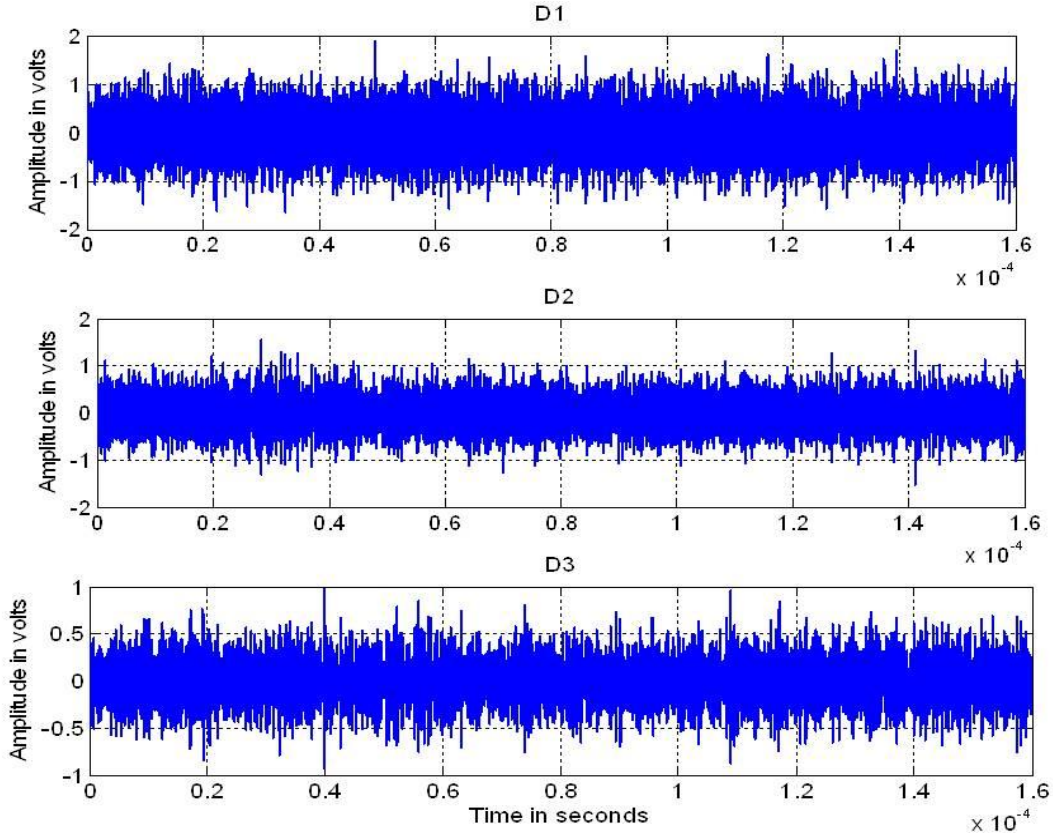


Figure 7-8 Detail coefficients (leve1 # 1 – level # 3)

Kurtosis values of the approximation coefficients from level # 1 to level # 20 are shown in Figure 7-9. Fourth level approximation coefficient ($A_4$) shows a higher kurtosis value which will be used as the threshold.

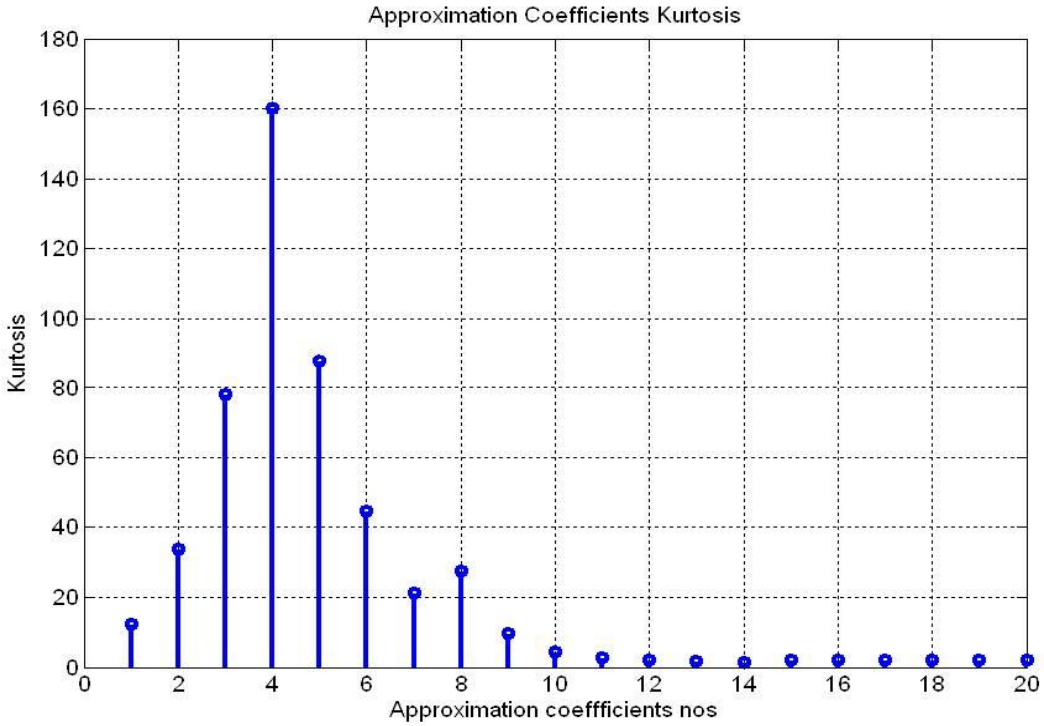


Figure 7-9 Kurtosis values of approximation coefficients ($A_1$-$A_{20}$)

Denoising based on any thresholding method causes loss of orginal information of the original PD pulse regarding its shape and amplitude. Denoising through wavelet thresholding degrades the signal features [Chang, Bin et al. 2000] for example magnitude and phase distortion. An empirical scaling factor of 1.1 is used to normalized the amplitude of the denoised pulses based on the simulations carried out for various SNR. Reconstructed signals are shown in Figure 7-10. Time domain signatures of pulses 1, 2 and 3 are shown in Figure 7-11.

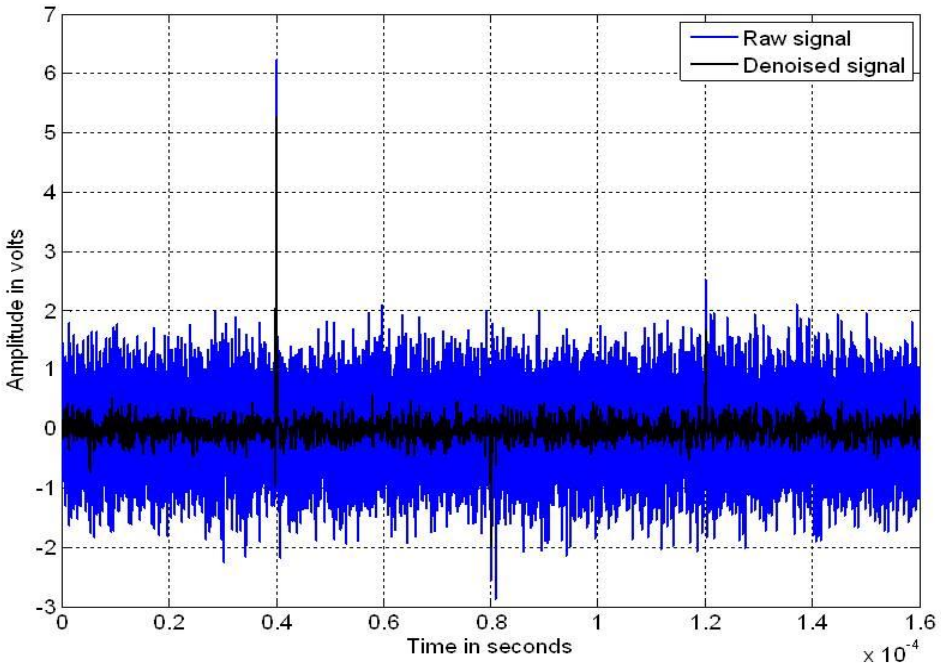


Figure 7-10 Denoised signal using kurtosis threshold *

* *Raw signal mean signal with added noise*

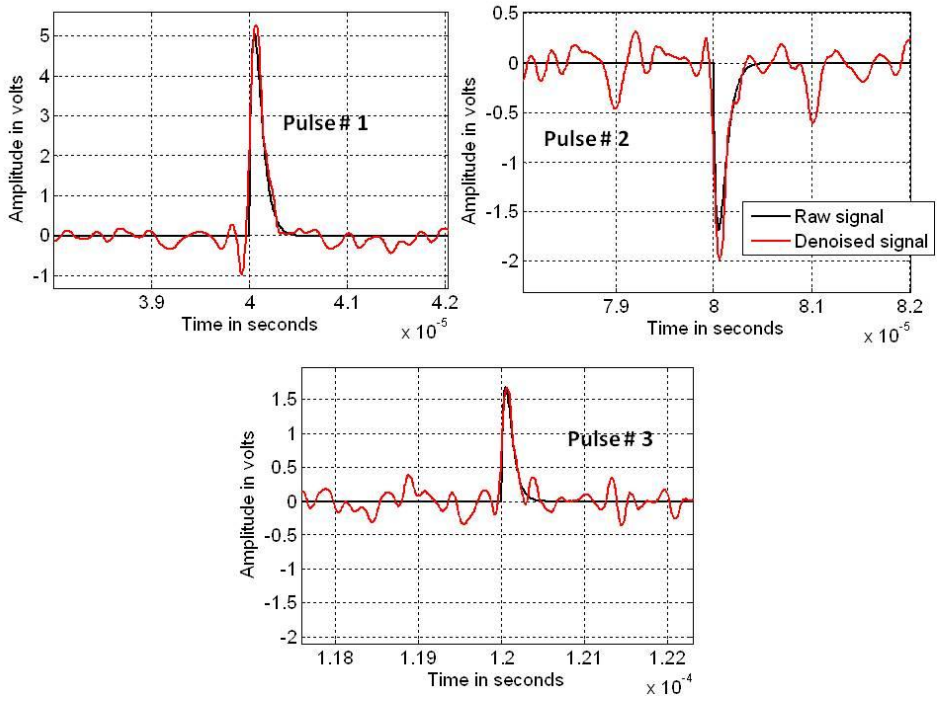


Figure 7-11 Denoised signal using kurtosis threshold (Zoomed)*

* *Raw signal mean noise free signal*

### 7.2.1.2 Experiment# 2 Synthetic data using damped oscillatory pulse

A damped oscillatory pulse having rise time of 100 ns and pulse width of 300 ns with added wide band noise is shown in Figure 7-12.

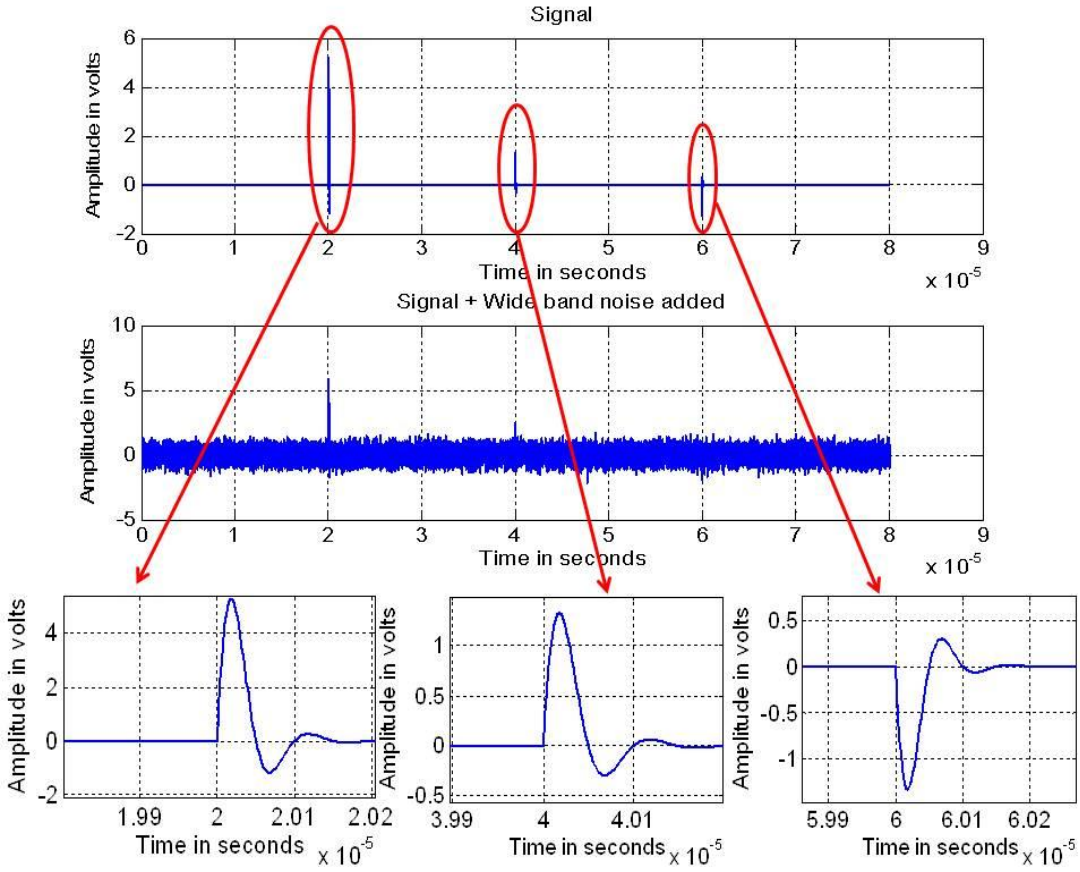


Figure 7-12 Damped oscillatory PD pulse with additive noise (SNR: -13 db)

Approximation and detail coefficients from first level to third level of decomposition are shown in Figure 7-13 and Figure 7-14 respectively. The rest of the coefficients are included in the Appendix E-2. Damped oscillatory signal signatures appear in the approximation coefficients, while most of the detail coefficients carry the noise components. Higher order coefficients show a flat trend which is used as the stopping criterion.

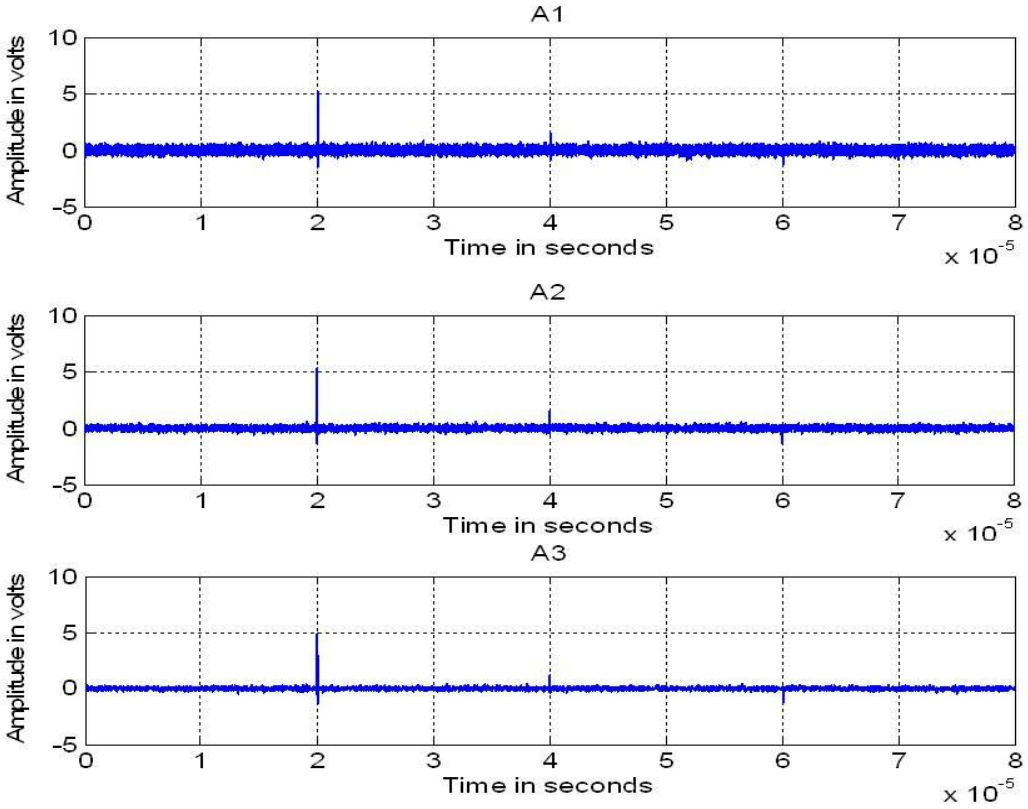


Figure 7-13 Approximation coefficients (leve1 # 1 – level # 3)

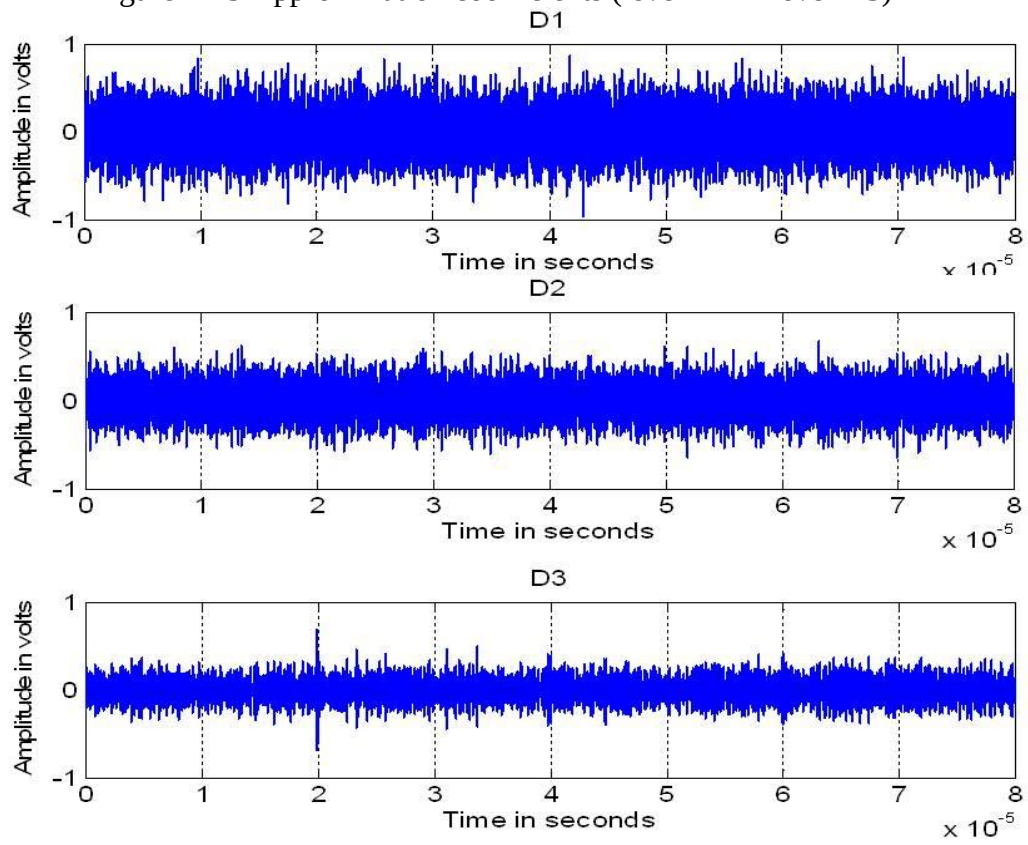


Figure 7-14 Detailed coefficients (leve1 # 1 – level # 3)

Kurtosis values of the approximation coefficients are shown in Figure 7-15. Approximation coefficient at level 4 shows a peak value which can be used as the threshold for denoising. Detail coefficients are discarded.

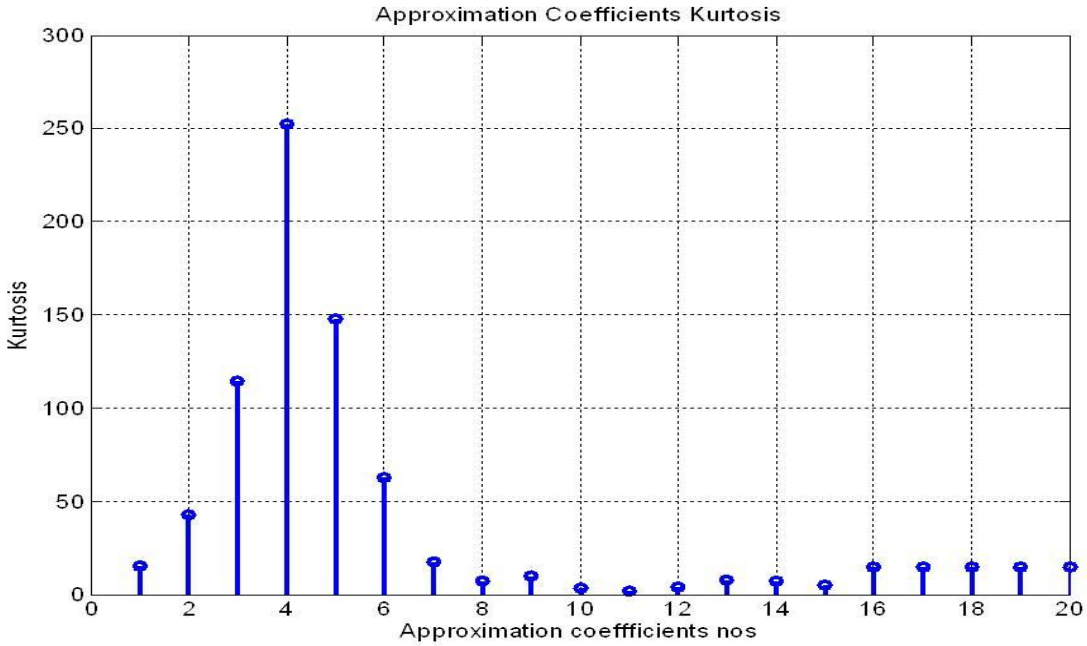


Figure 7-15 Kurtosis values of approximation coefficients (A1-A20)

Reconstructed signals are as shown in Figure 7-16. Time domain signatures of pulses 1, 2 and 3 are shown in Figure 7-17. Generally good signal preservation capability of this approach is evident from Figure 7-11 and Figure 7-17. Efficiency of this approach based on PD source location and PD quantification are discussed in the following sections.

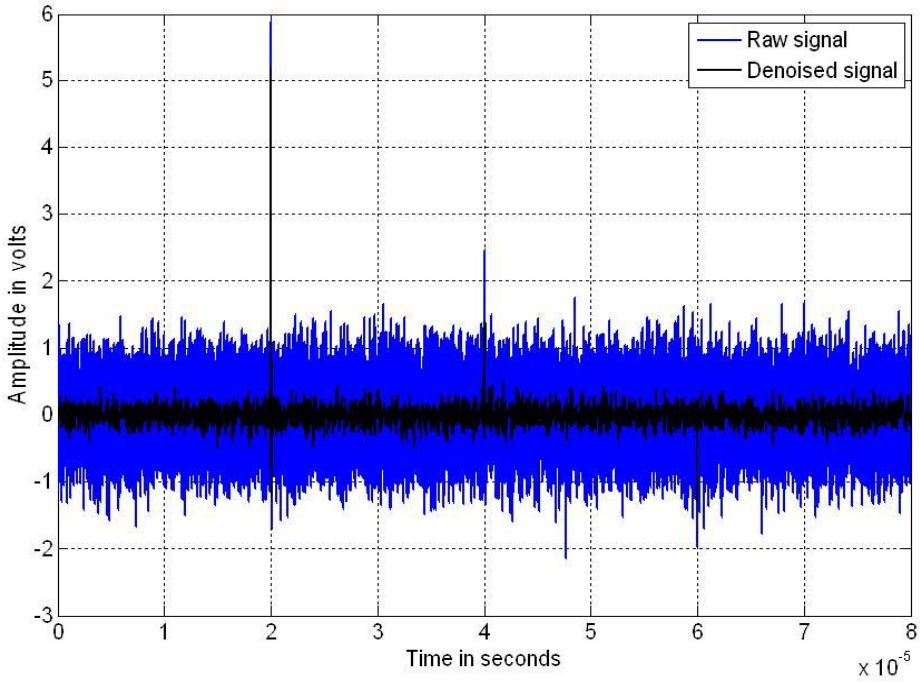


Figure 7-16 Denoised signal using kurtosis threshold (Zoomed) *

* *Raw signal mean signal with added noise*

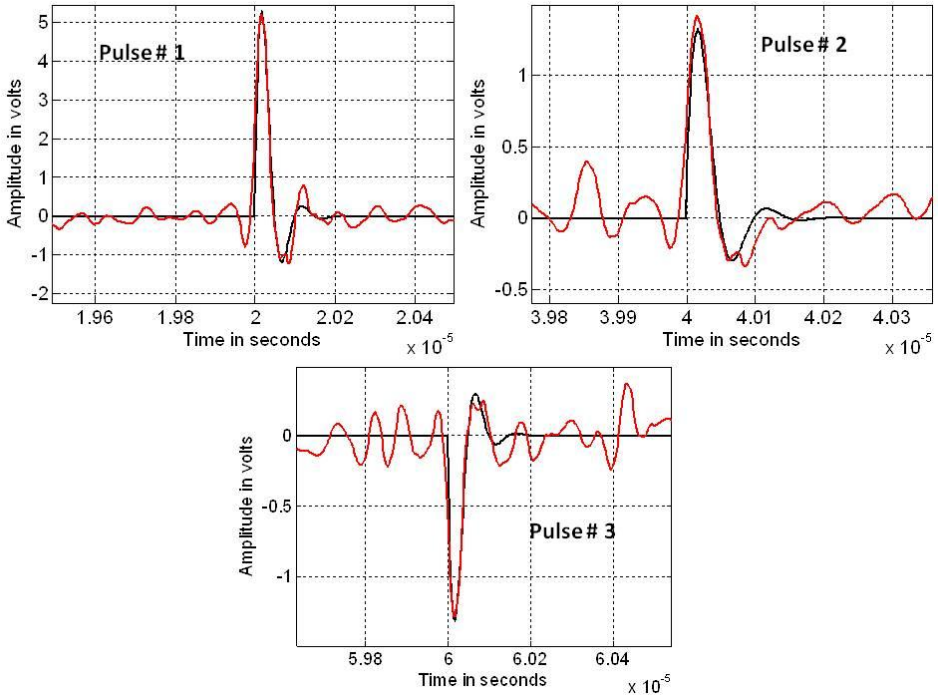


Figure 7-17. Denoised signal using kurtosis threshold (Zoomed) *

* *Raw signal means noise free signal*

#### 7.2.1.3 Comparison of KBT with existing thresholding methods

Performance of the KBT algorithm using SGWT is compared with existing thresholding methods,namely universal threshold, SURE, Minimax with same wavelet base, and ‘db5’ for various SNR. ‘db5’ is the optimum wavelet for denoising PD signals from cables[Xiaodi, Chengke et al. 2007].

Comparison of the KBT with exisiting thresholding methods is evaluated on the basis of edge error, maximum amplitude error and MSE. The SNR of pulse # 1 to pulse # 3 are in decreasing order. It has been observed that SURE, HeurSURE and Minimax thresholding are not effective when the raw data has double exponential waveform signatures. Hence in the case of the double exponential pulse, comparison is made between universal threshold and KBT. Results of the analysis are shown in (Figure 7-18 to Figure 7-23). Time domain waveforms are included in Appendix E-3 for brevity. Drift in the orgin of the pulse discussed in Figure 7-4, which is termed as edge error,is shown in the following figures (Figure 7-18 to Figure 7-23).

In this comparison, SNR is defined with respect to pulse # 1. Pulse # 2 and pulse # 3 represents the reflected pulses in the real case. SNR for pulse # 2 and pulse # 3 are much lower. Based on Figure 7-18 and Figure 7-19, case (i) universal thresholding is slightly better compare to KBT. Performance of other thresholding methods (heursure and minimax) are poor. Edge error in KBT is nearly consistent across the SNR band in both case ( i) and case (ii).

Based on (Figure 7-20 to Figure 7-23), pulse #2 and pulse # 3 which are of low SNR, performance of KBT is better in compare to the rest of the thresholding methods. Edge error margin is slightly higher in case (i) compared to universal and rigsure, which is possibly due to the filter kernel, thresholding and sub sampling process used in denoising. Overall performance of the KBT method, especially for lower SNR, is better compared to the other thresholding methods which is evident from the comparison.

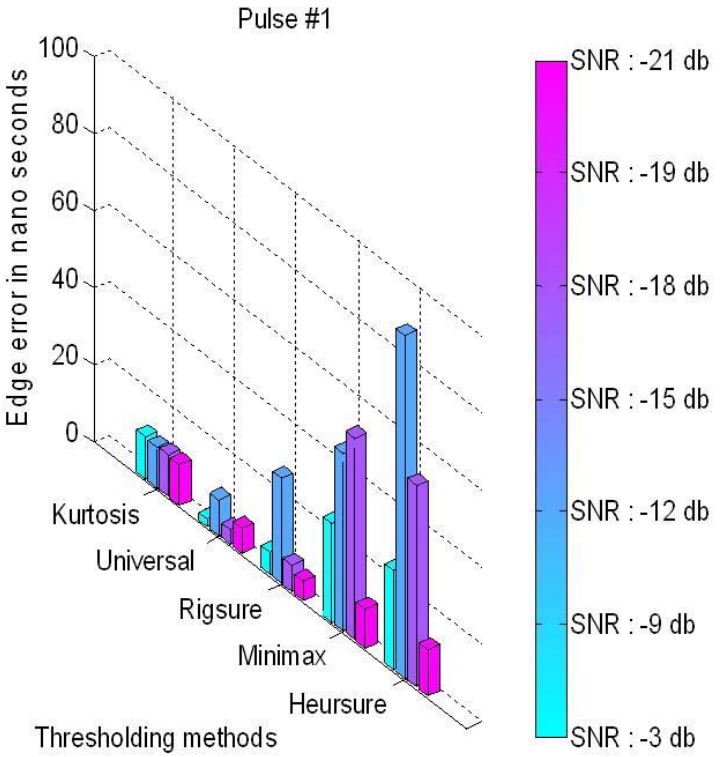


Figure 7-18 Case (i) Edge error for pulse # 1 (Damped oscillatory)

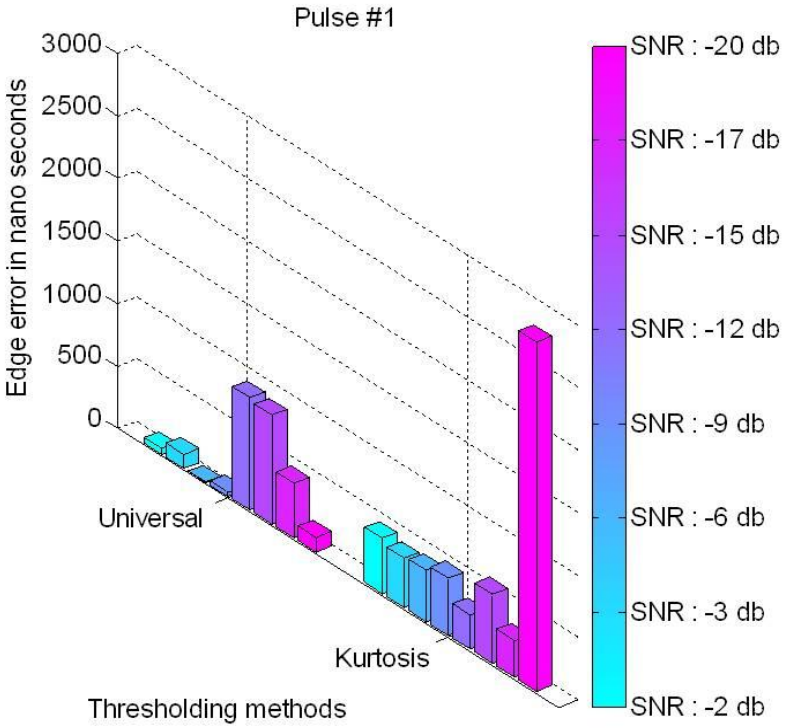


Figure 7-19 Case (ii) Edge error for pulse # 1 (Double exponential)

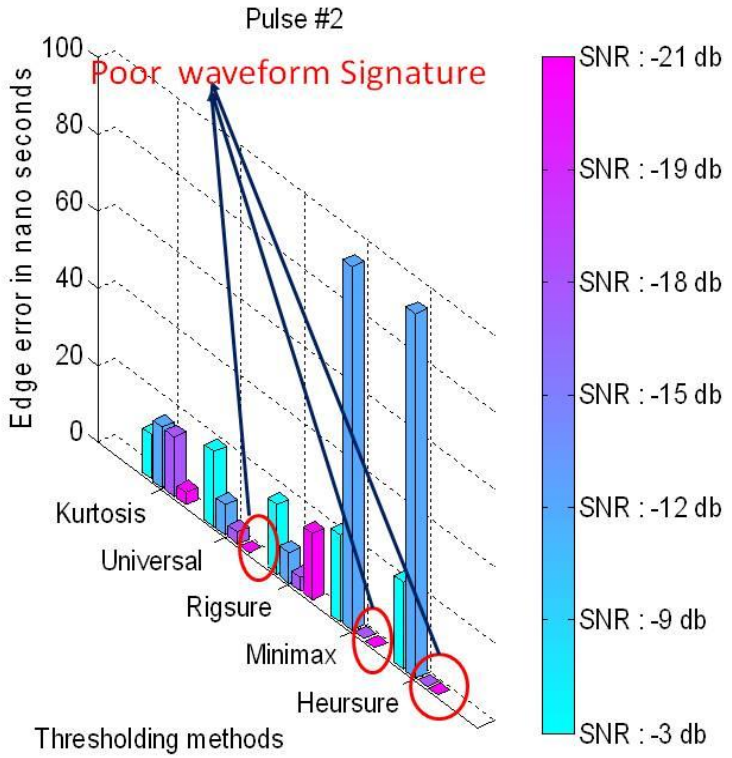


Figure 7-20 Case (i) Edge error for pulse # 2 (Damped oscillatory)

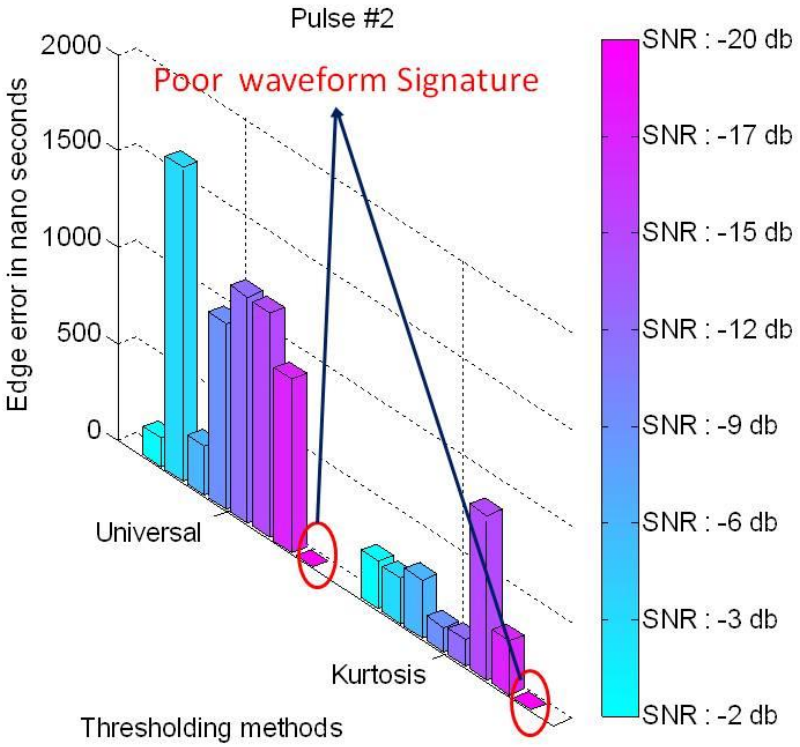


Figure 7-21 Case (ii) Edge error for pulse # 2 (Double exponential)

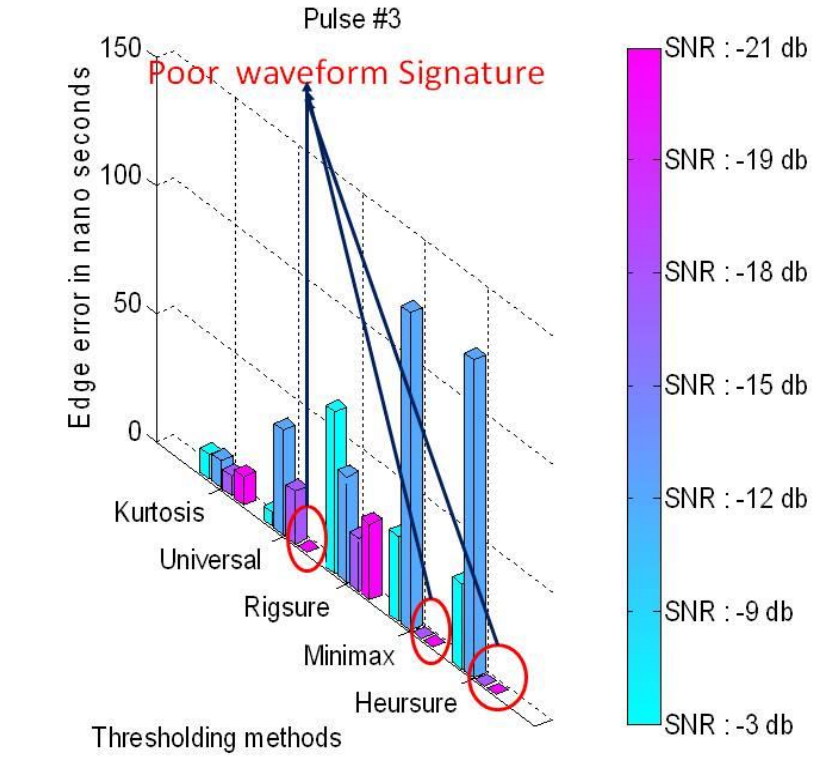


Figure 7-22 Case (i) Edge error for pulse # 3 (Damped oscillatory)

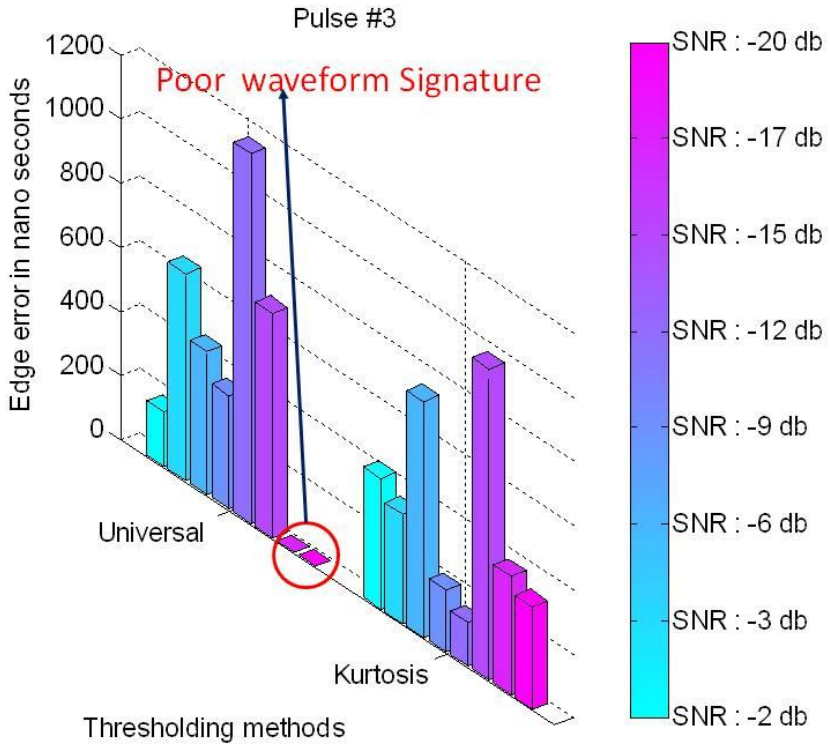


Figure 7-23 Case (ii) Edge error for pulse # 3 (Double exponential)

Peak amplitude error introduced by denoising algorithms affects PD quantification, which has an impact on prognostics methods. Peak amplitude error is given by

$$\text{Peak amplitude error} = \left[ \frac{A_i - A_d}{A_i} \right] \qquad 7\text{-}1$$

*Where, Ai* : *Peakamplitude of incident pulse*

$A_d$ : *Peak amplitude of denoised pulse*

Based on Figure 7-24, peak error in the KBT method is lower compare to other thresholding methods. In Figure 7-25, universal thresholding performs better than KBT. In the case of pulse # 2 and pulse # 3 as per figures (Figure 7-26 to Figure 7-29), KBT performance is better than other thresholding methods. MSE comparisons are also included in Appendix E-4.

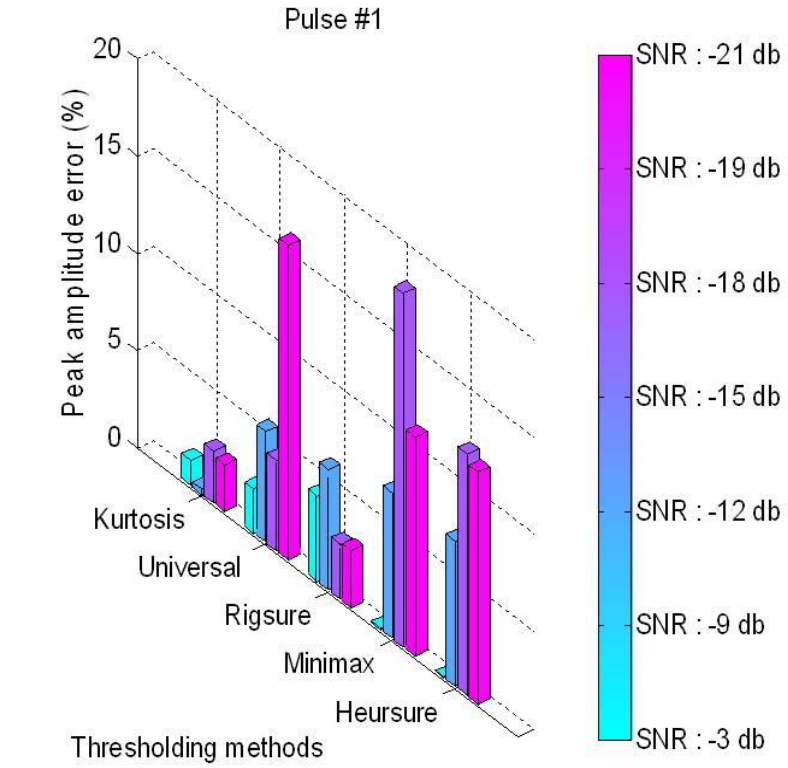


Figure 7-24 Case (i) Peak amplitude error for pulse # 1 (Damped oscillatory)

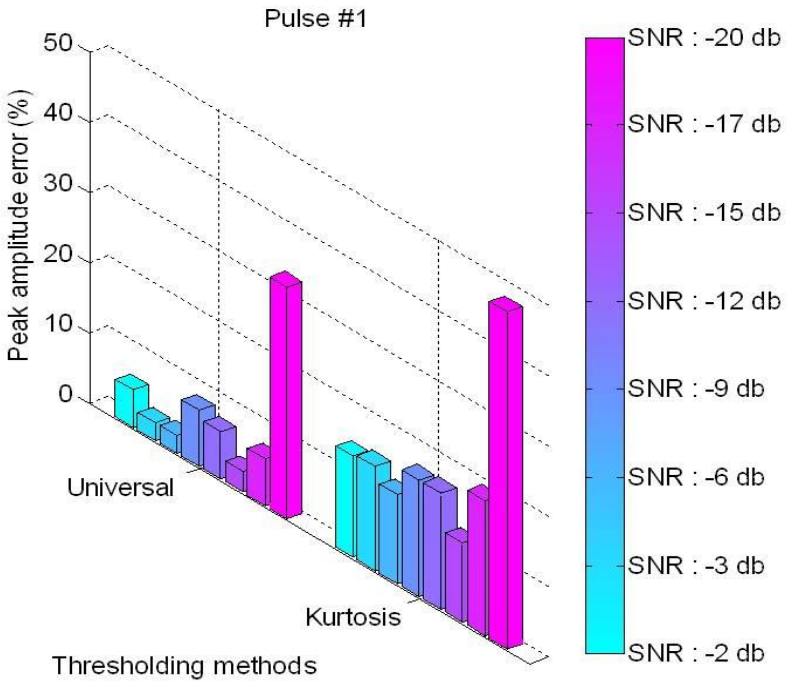


Figure 7-25 Case (ii) Peak amplitude error for pulse # 1 (Double exponential)

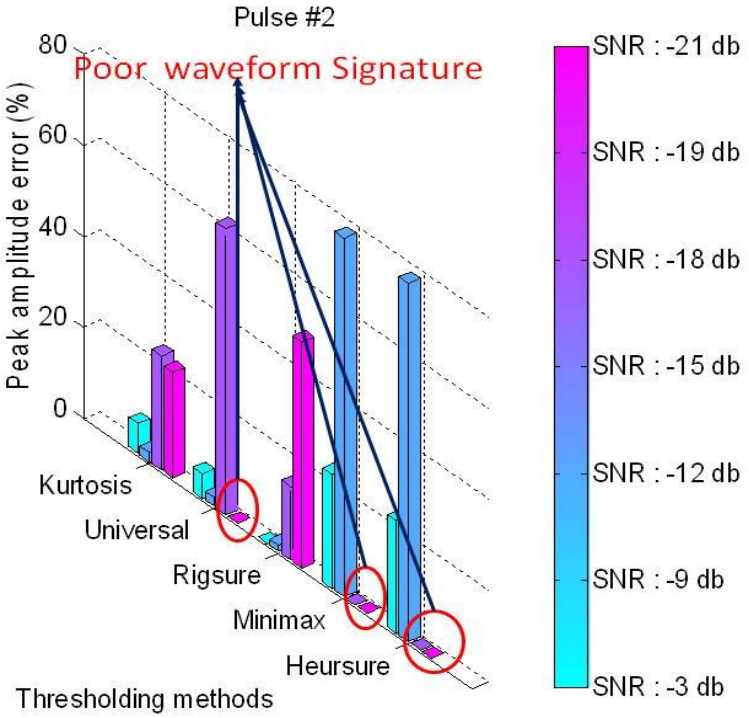


Figure 7-26 Case (i) Peak amplitude error for pulse # 2 (Damped oscillatory)

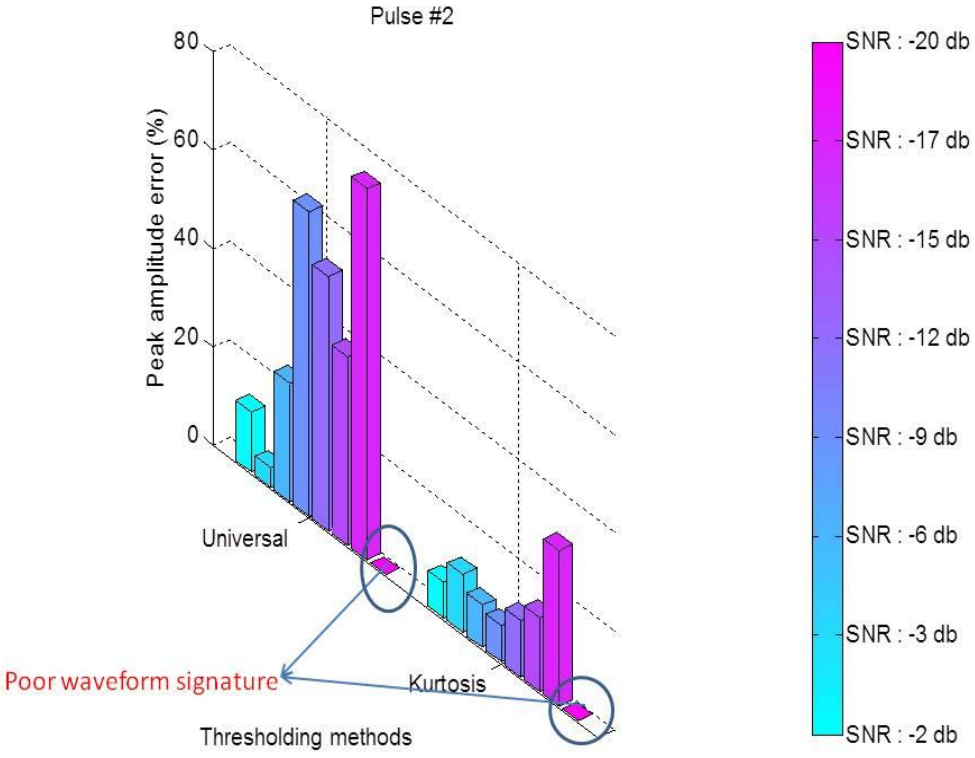


Figure 7-27 Case (ii) Peak amplitude error for pulse # 2 (Double exponential)

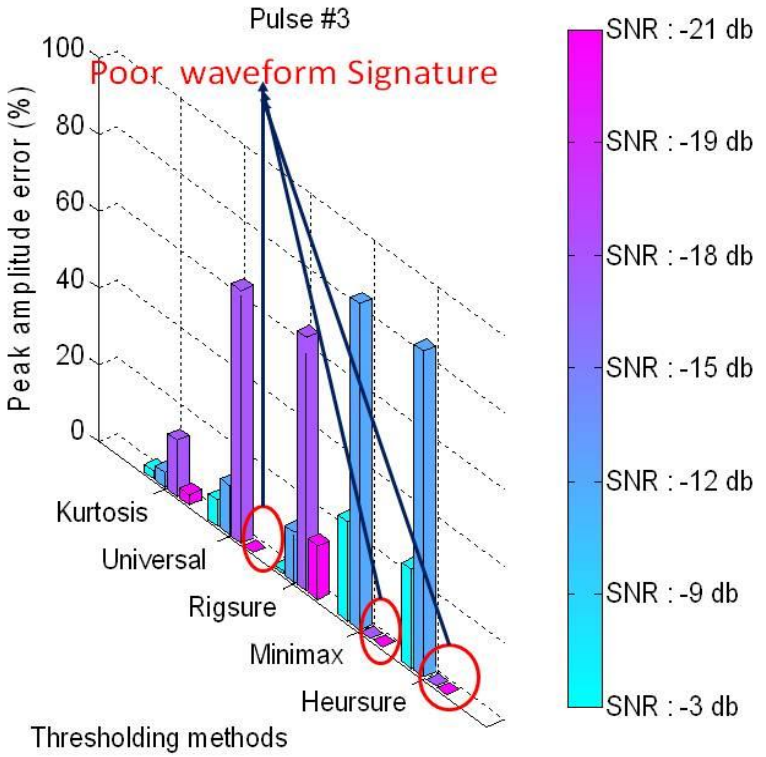


Figure 7-28 Case (i) Peak amplitude error for pulse # 3 (Damped oscillatory)

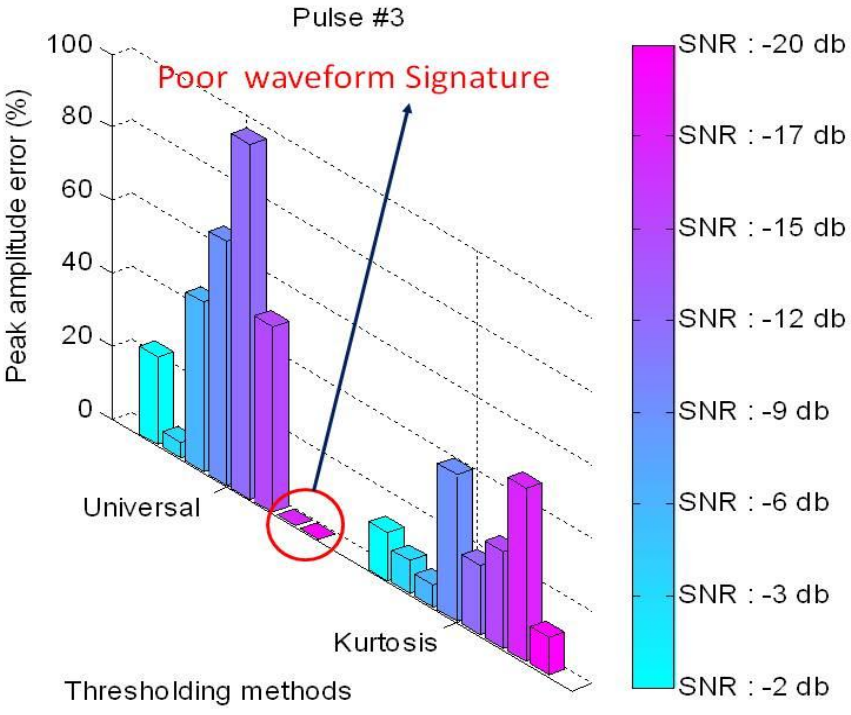


Figure 7-29 Case (ii) Peak amplitude error for pulse # 3 (Double exponential)

Based on the comparisons described above, for lower SNR, universal thresholding based on DWT performs better compare to KBT. This performance depends on the decomposition level selected based on human intervention in DWT based denoising, while in KBT automated stopping criterion is applied, which does not require any human intervention. Hence performance of KBT and universal threshold methods are balanced in higher SNR. For lower SNR, KBT performance is better compare to the other thresholding methods. DWT produces a smoother appearance. This smoother appearance depends on the level of decomposition used which may sometimes leads to loss of PD signature as evident in Figure 7-30. Overall performance of kurtosis based thresholding is better compared to rest of the thresholding methods.

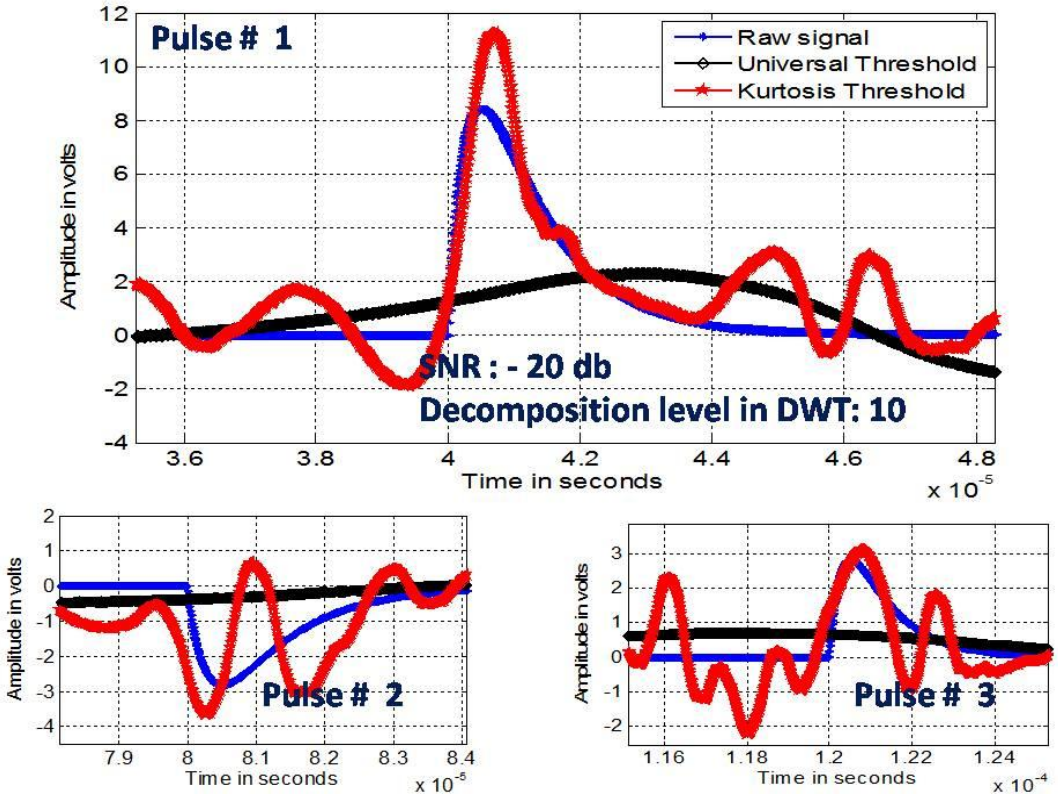


Figure 7-30 Denoising performance in time domain *

* *Raw signal mean noise free signal*

### 7.2.1.4 Testing the algorithm using on-site data

Denosing using KBT based on SGWT is applied to on-site data acquired from an 11kV PILC cable in a 33/11 kV substation. In this comparison using on-site data, only KBT and universal threshold are considered. Performance of other thresholding methods "SURE" and "*MINIMAX*" are poor. Figure 7-31 shows denosing results from KBT and universal with level 5 decomposition. Similar performance is seen in both cases.

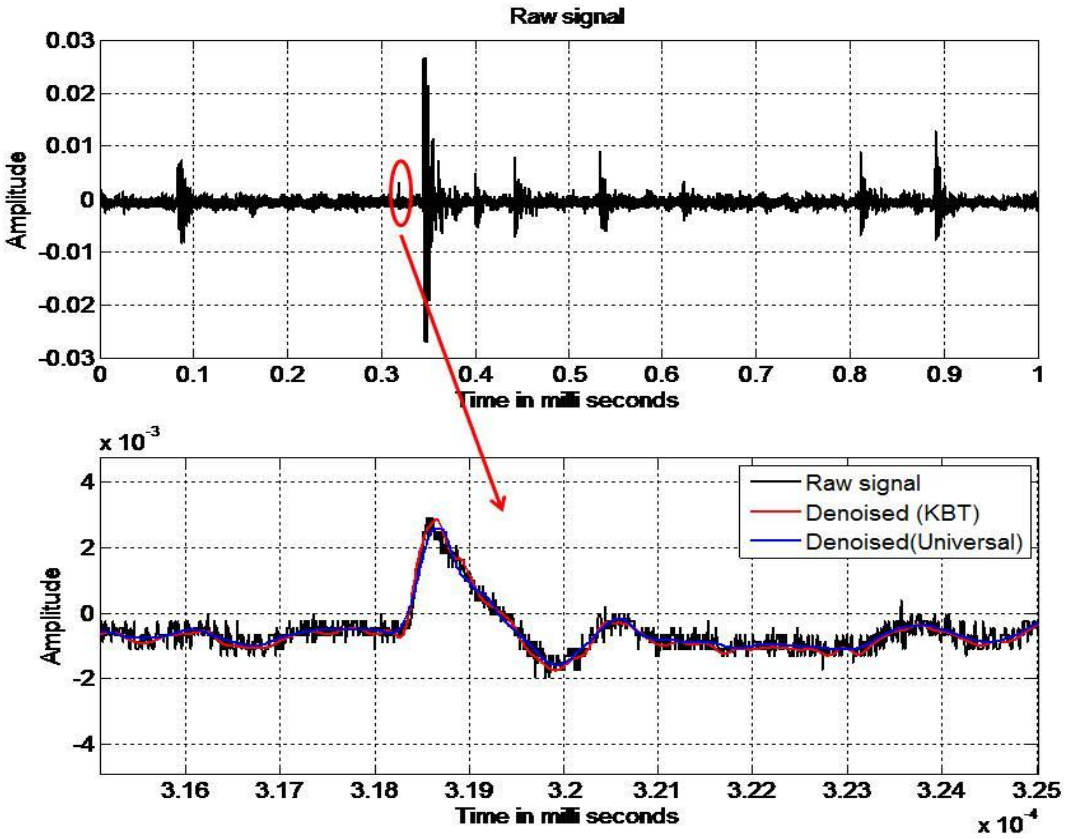


Figure 7-31 Denosing comparison (DWT level 5)

Figure 7-32 shows KBT compared with universal threshold using level 8. In this case universal thresolding produces poor signature which is due to over smoothing of the signal. Figure 7-33 shows the data acquired from an 11kV PILC cable using PFCT. Performance of KBT based denoising is better at extracting a wavelet signature over universal threshold. More time domain comparison results are included in the Appendix E-5.

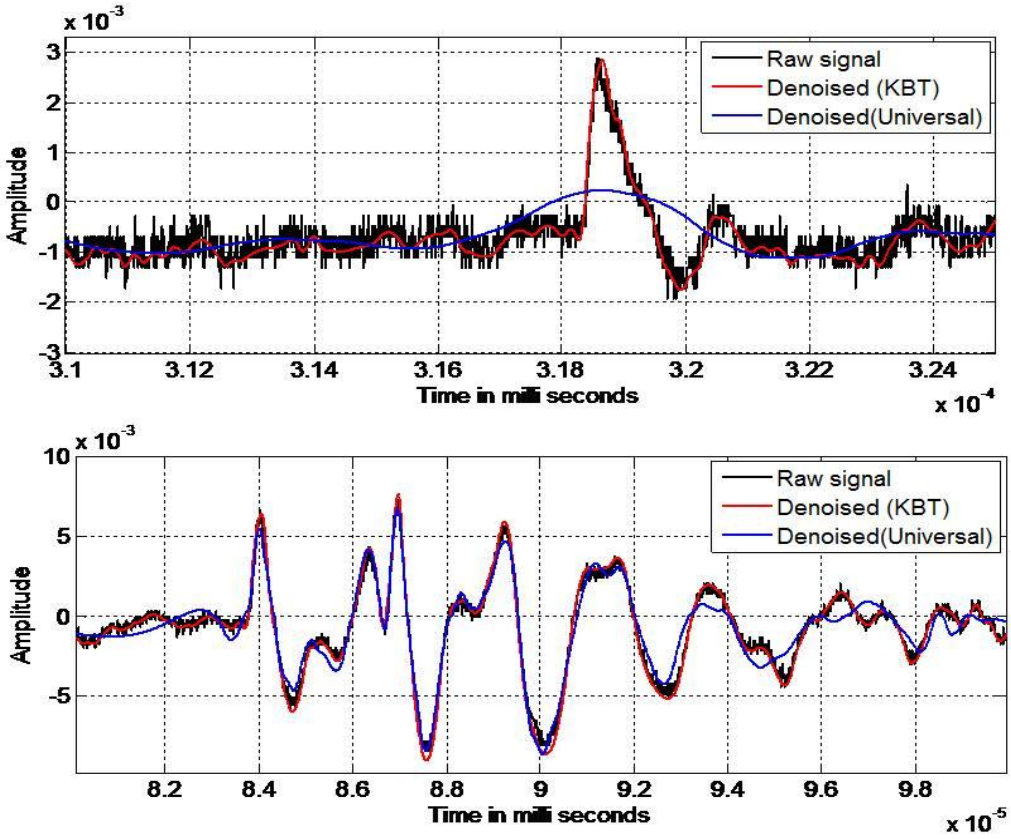


Figure 7-32 Denoising comparison (DWT level 8)

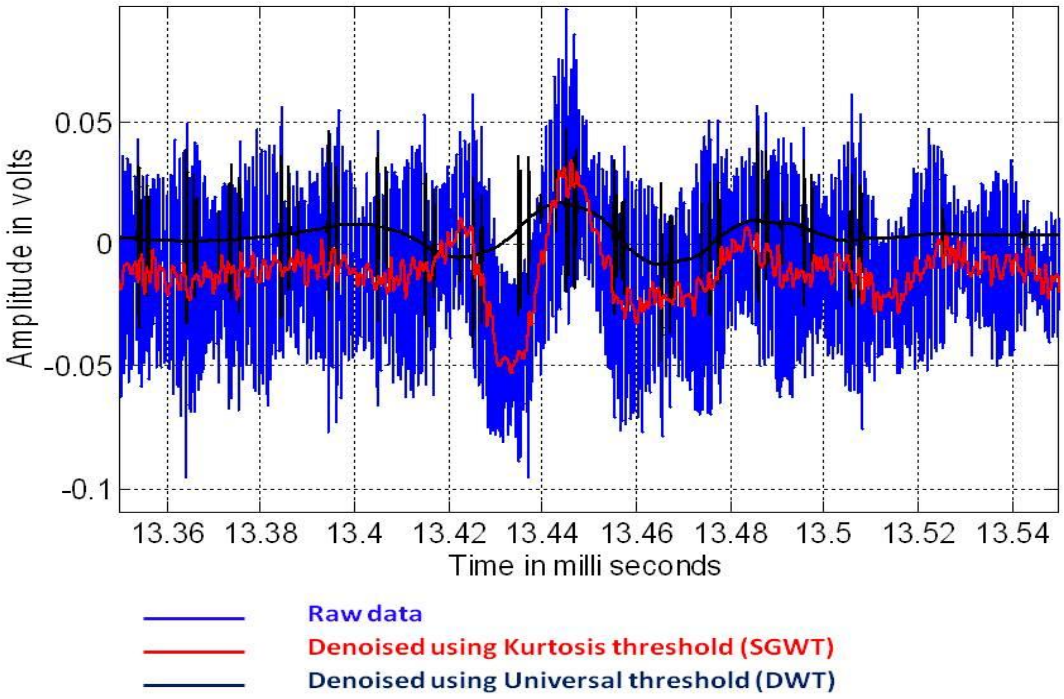


Figure 7-33 Denosing comparison (DWT level 8)

## 7.3 Kurtosis Based Thresholding using EMD

EMD is a signal processing method used to extract IMFs. These IMFs are derived from the signal itself, unlike approximation/detail coefficients from prerequisites like wavelete basis function used in wavelet based denoising. EMD is mostly used in processing of speech signals. Not much research is found for EMD based denoising of PD signals. In this section KBT is applied to IMFs from EMD for both synthetic and on-site data.

### 7.3.1 Synthetic data

Synthetic data includes an oscillatory PD pulse added with wide band noise as shown in Figure 7-34. IMFs derived from EMD are shown in Figure 7-35. Noise power decreases as the level of IMF increases and a higher value of kurtosis is seen for IMF3 as shown in Figure 7-36. This is set as the threshold followed by reconstruction. Time domain comparison of the KBT using EMD with SGWT is shown in Figure 7-37. There is much reduction in amplitude for the denoised signal. Signature preservation capability of EMD is poor compare to SGWT.

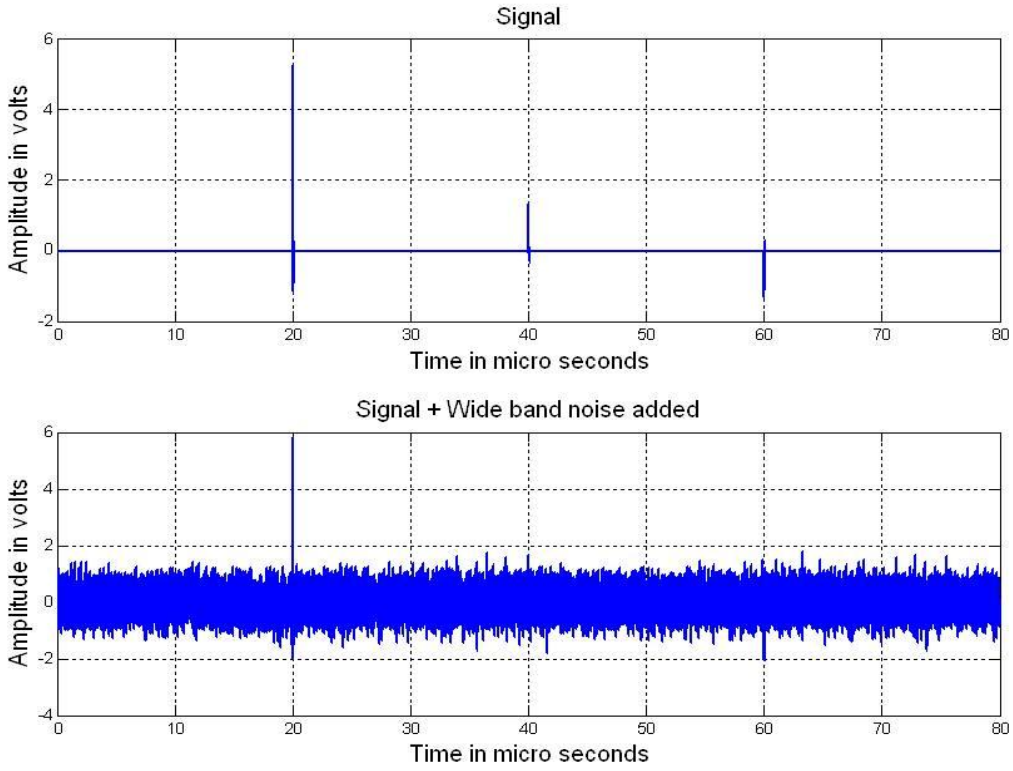


Figure 7-34 Synthetic data (oscillatory PD pulse + Wide band noise)

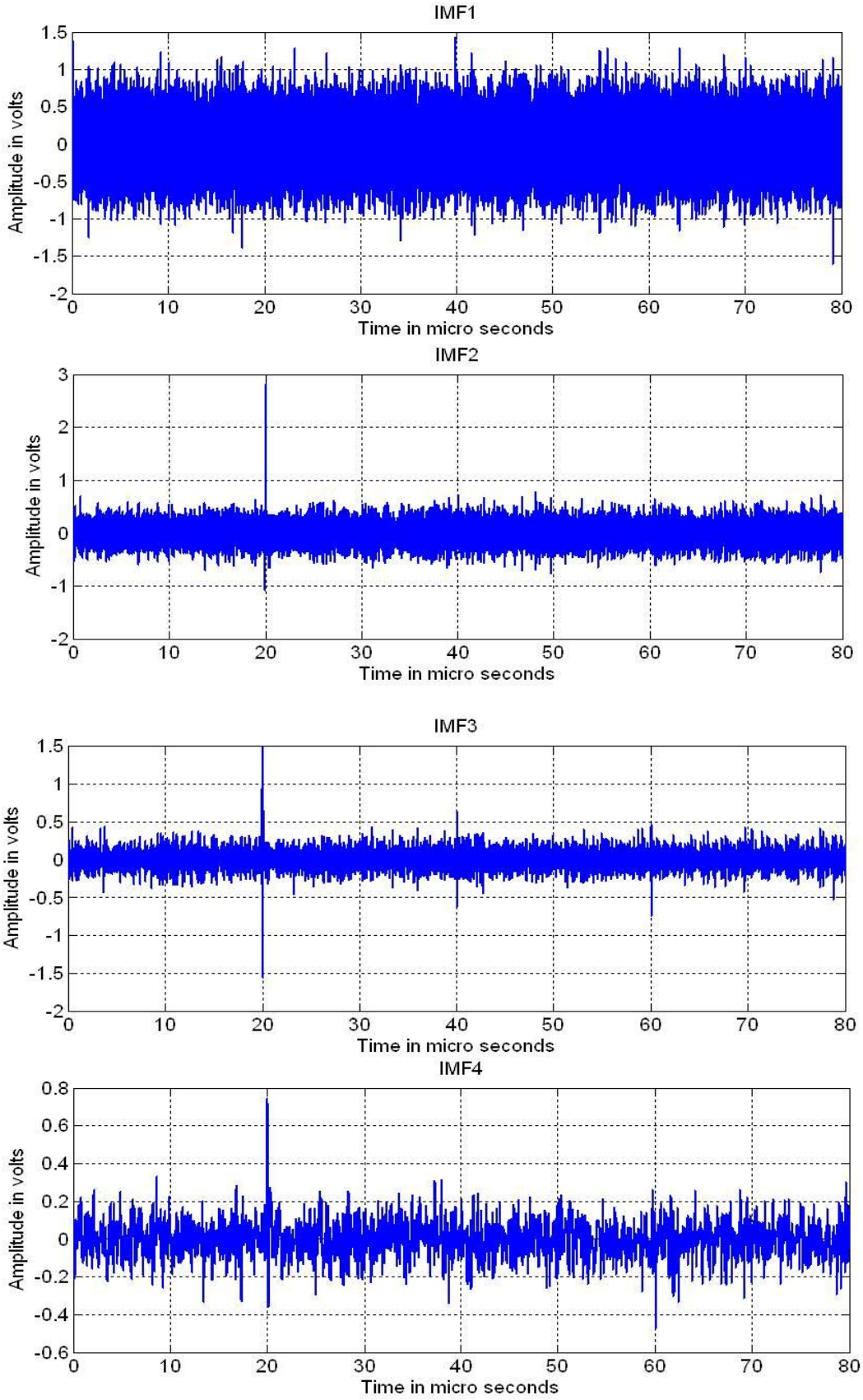


Figure 7-35 IMFs from EMD

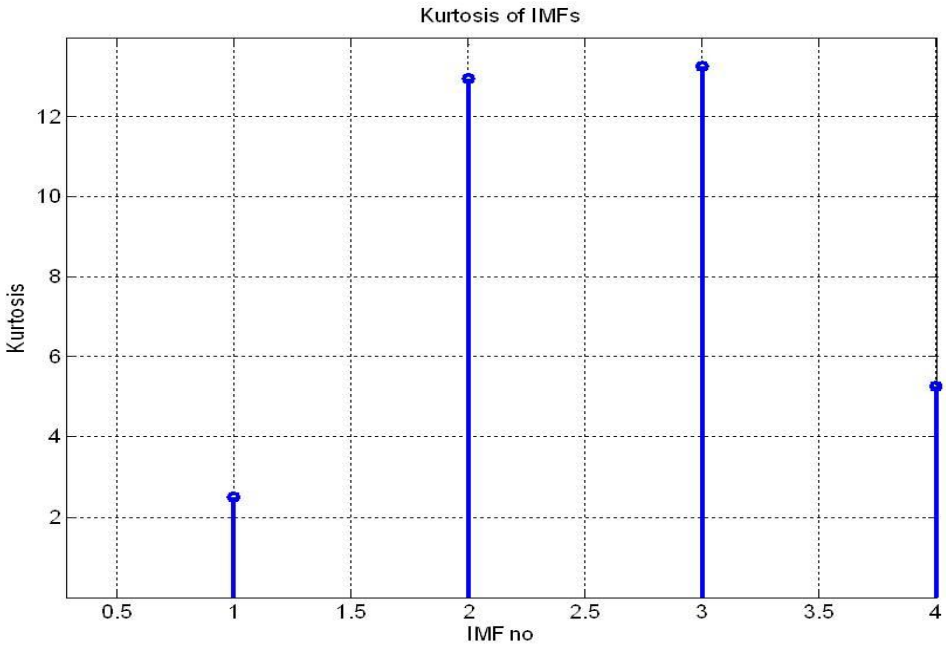


Figure 7-36 Kurtosis of IMFs

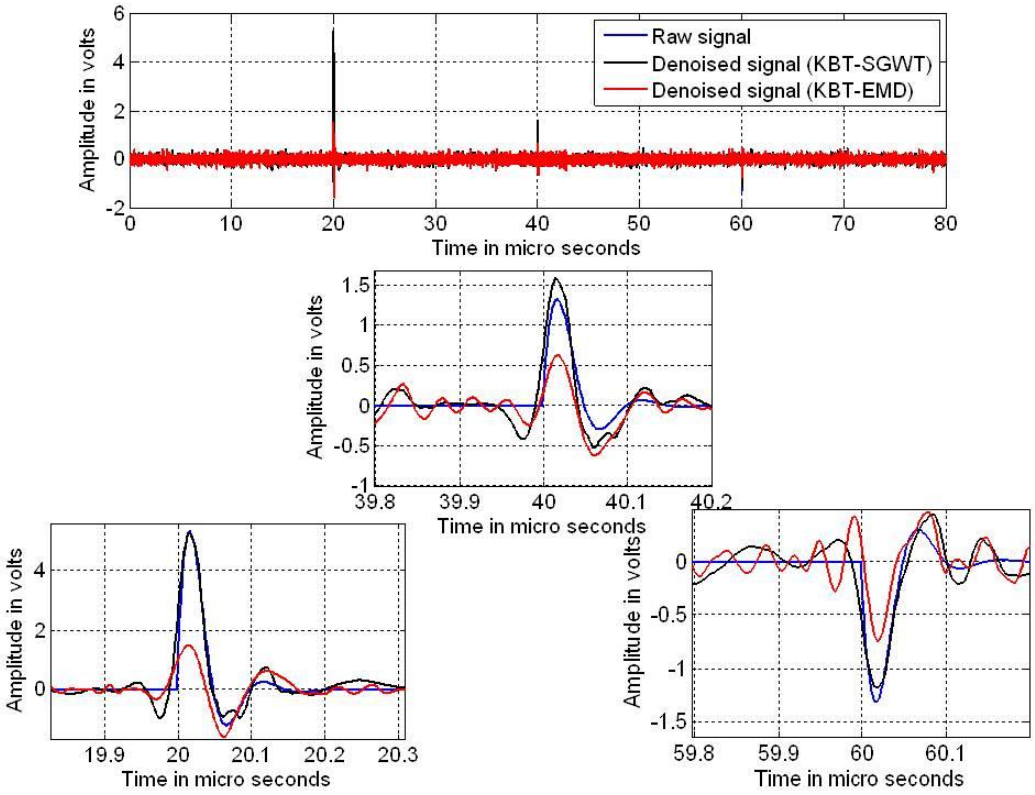


Figure 7-37 Denoising comparison of KBT, EMD vs SGWT *

* *Raw signal mean noise free signal*

### 7.3.2 On-site data

KBT based on EMD is applied to on-site data from an 11 kV PILC cable as shown in Figure 7-38. IMFS are shown in the Appendix E-6. A reconstructed signal after applying KBT is included in figures (Figure 7-38-Figure 7-40). Based on figures (Figure 7-38-Figure 7-40), Signature preservation is not consistent in EMD. Also in Figure 7-39, EMD using KBT fails to recover the pulse from the signal while KBT using SGWT performs better. Based on the literature, simulation using synthetic data and denoising using on-site data, performance of EMD in denoising of PD pulses is poor compare to wavelet based denoising. Also the Decomposition process in EMD is complex which makes this approach slower which eventually requires higher hardware resources to process such high sampled data like PD.

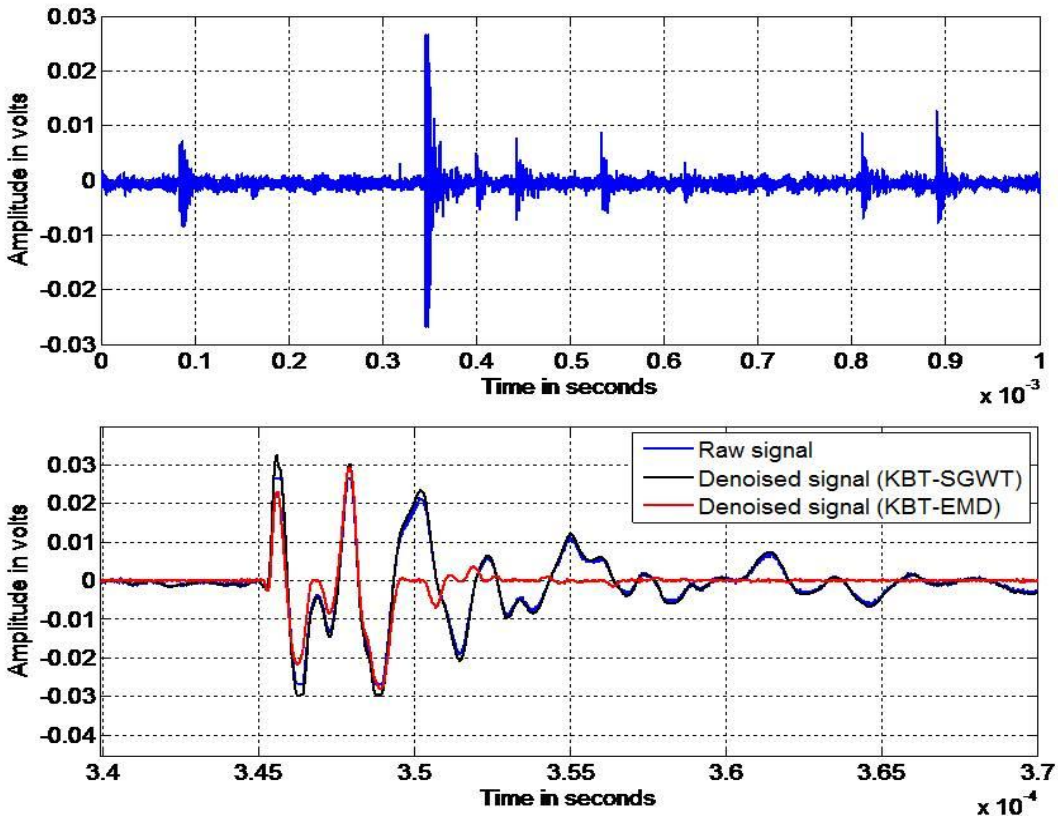


Figure 7-38 KBT based denoising comparison for on-site data

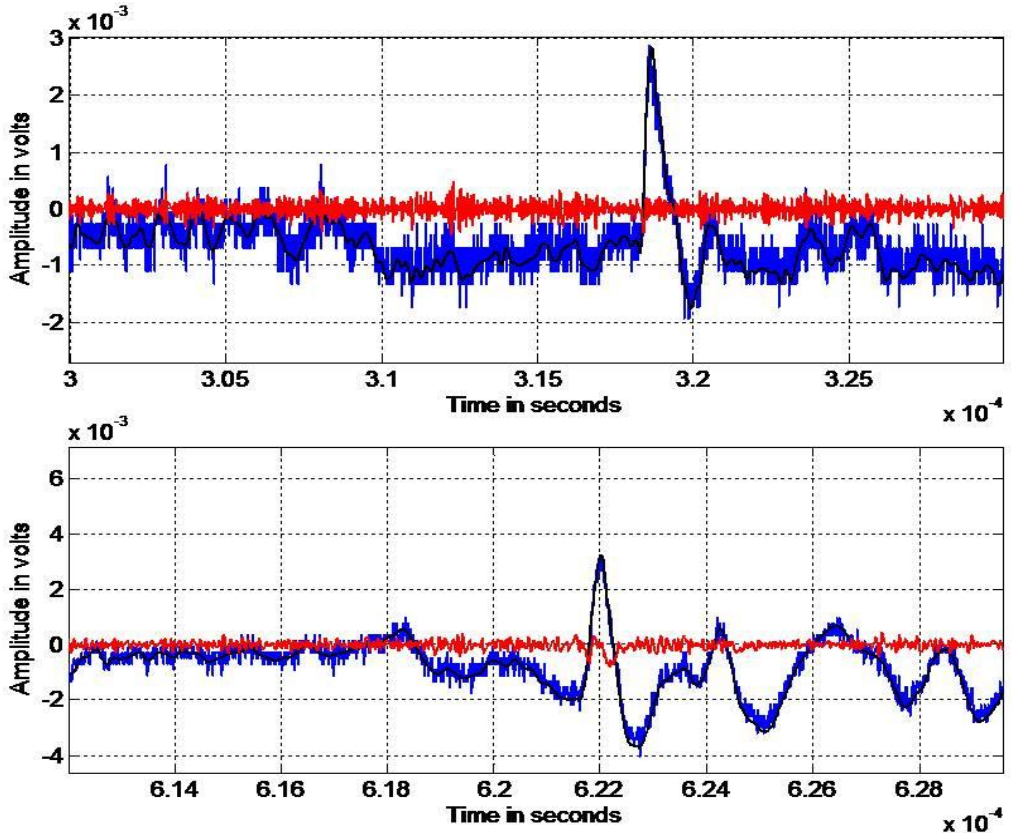


Figure 7-39 KBT based denoising comparison for on-site data

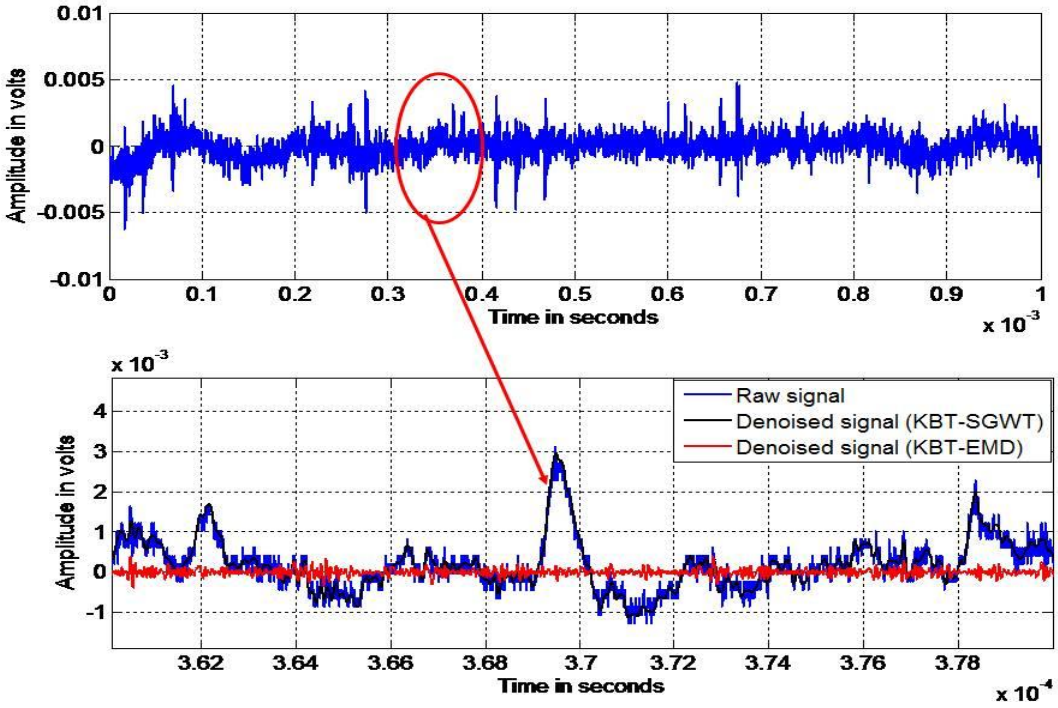


Figure 7-40 KBT based denoising comparison for on-site data

## 7.4 Conclusion

On-line PD signals are more prone to noise and it becomes more challenging to extract PD information from the raw data. Extracting PD information from the raw data is a two fold process namely denoising and data interpretation. The main objective of denoising is extracting the relevant information from the raw data by discarding the noise contained in the data. Wavelet based denoising of PD signals using DWT involves signal decomposition, thresoholding and reconstruction. The number of decomposition levels in DWT based denoising is selected by visual examination of the SNR of the decomposition coefficients. This makes this method less automatic. In this chapter fully automatic denoising of PD signals using SGWT based on KBT with stopping criterion was proposed.

Fast rising pulses like PD's exhibit a higher kurtosis value are used to extract pulses which have a transient signature. With the use of trend analysis, stopping criterion is achieved. In this way this method becomes fully automatic. Performance of the KBT based denoising method was evaluated on the basis of PD source location error and PD magnitude error. These error criterion plays an important role in determining the accuracy of locating PD source and prognostics tools for cable insulation life prediction.

Based on the tests using synthetic data and onsite data, signals having higher SNR, the performance of universal thresholding based on DWT was better compare to KBT. However such performance in DWT depends on the decomposition level selected based on the visual appearance using human intervention. While in KBT with automated stopping criterion, decomposition does not require any human intervention. Hence, performance of KBT and universal threshold methods were balanced for signals which are of higher SNR. For signals with lower SNR, KBT performance is better compared to the other thresholding methods. However, denoising by DWT produces smoother appearance over KBT. This smoother appearance depends on the level of decomposition used which may sometimes lead to loss of PD signature. Such loss of waveform signature in DWT was evident from the on-site data.

# Chapter 8 :
# Interpretation of PD Signals From On-site Data

## 8.1 Introduction

This chapter deals with analysis of data acquired from the hardware developed (described in Chapter 5) in this research project. Data acquired are denoised by applying a KBT using SGWT. To ascertain the PD activity from the denoised data, it needs to be analysed using the characteristics of PD pulses in cables. In this analysis, the data acquired from the 11 kV PILC cable in 33/11 kV substation and 11 kV distribution substation is included. Data interpretation discussed in this chapter has two purposes, namely comparative analysis of data from the earth strap using HFCT and cable core using PFCT to validate the approach of using PFCT (described in Chapter 5 :) as PD detection sensor in cables and identification of PD from the acquired data.

## 8.2 33/11 kV Cable Network Configuration

In this project one of the objectives was to investigate the possibility of using PFCT in detecting PD signals from cables. Though FRA of PFCT shows increased gain at higher frequencies, it is important to verify this approach using on-site measurements. Hence PD monitoring equipment (described in Chapter 5) was installed across solkar CT's at 33/11 kV substation in Glasgow. The Utility company has no record of PD history in the cable network, which made it difficult for this research project for the comparison of results. A network diagram of the 33/11 kV substation is included in the Appendix C-5. In this substation, there are few 11 kV feeders, but only two of them which includes substation end A and substation end B are shown. Both end A and end B of the substation was linked using an 11 kV, 3 core PILC cable of length 300 meters. This Feeder is dedicated for the University of Strathclyde purpose. In the substation end A, data is acquired from all the three cores and earth strap of the cable, while in the substation end B, data is acquired only from the earth strap, since PFCTs are not accessible at substation end B.

## 8.3 Signal Interpretation Algorithm

The signal interpretation algorithm is developed using Matlab to extract PD signals from the cable based on the properties of the PD pulse from the literature. A detailed flowchart of the proposed pulse interpretation algorithm is shown in Figure 8-1. This algorithm involves splitting the raw data into several segments of length, for example $\pi$ (20 ms) each. Then KBT based on SGWT (described in Chapter 7) is applied to extract the fast varying pulses from the raw data. Then each pulse is examined for features such as rise time, pulse width, pulse polarity, PRPD and load current correlation. Based on these features, noise and PD are segregated and updated in the data base with a waveform signature. Once the PD pulses associated with cable are extracted, the TDR method is applied to locate PD using the single ended or double ended method,depending on the hardware used to acquire the data.

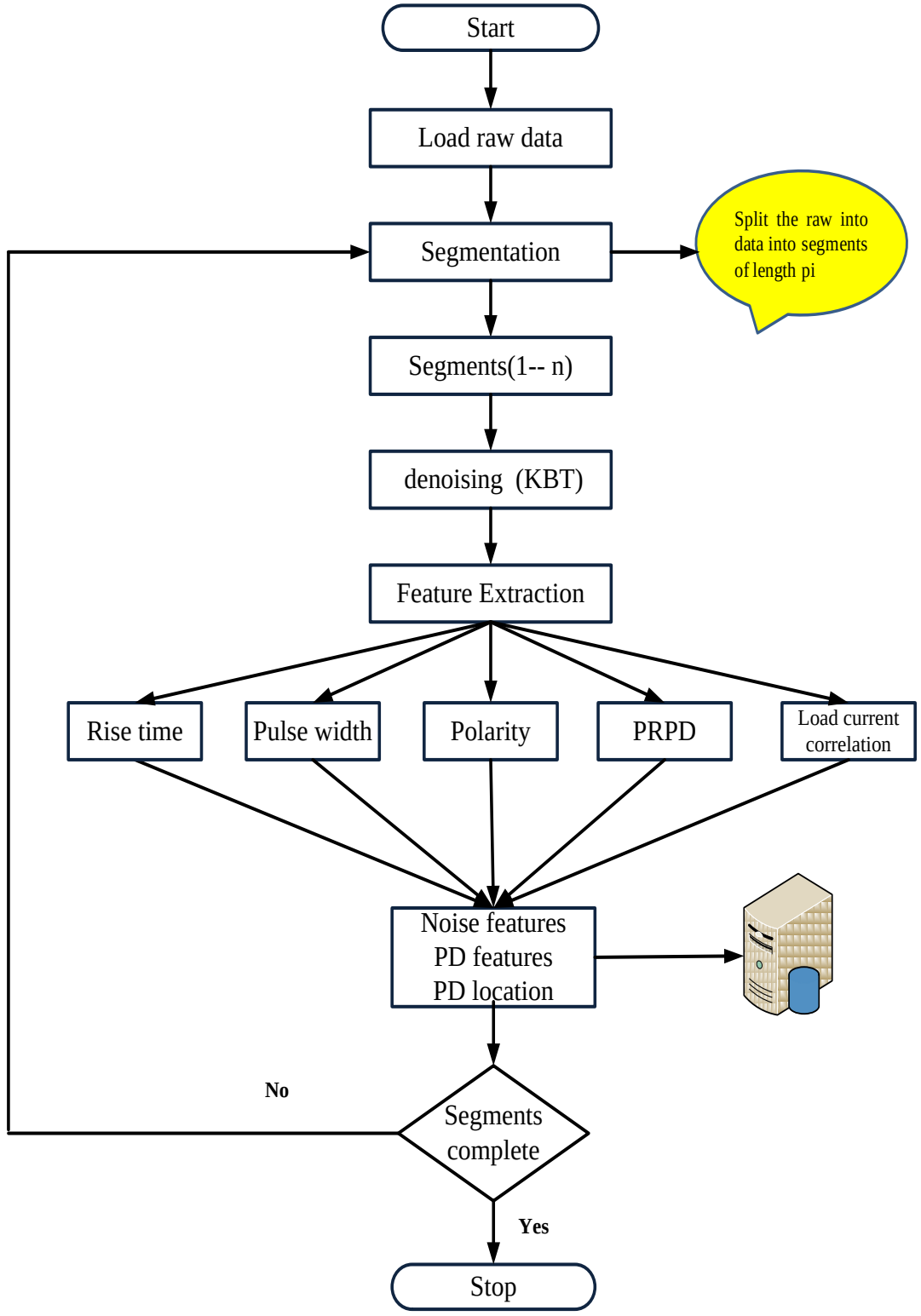


Figure 8-1 PD signal interpretation algorithm

## 8.4 Results from 33/11 kV substation

The remote PD monitoring system (discussed in Chapter 5) was installed in a 33/11 kV substation (decribed in the Appendix C-5). RPDMS acquires the data from all the three cores and earth strap of the PILC cable using PFCT and HFCT. The data acquisition interval used in RPDMS is 60 minutes with sampling rate of 50 Msps. The PD data frame has a time span of four power frequency cycles (80 ms) (described in 5.6.3.1).

### 8.4.1 Variation of load during the week

Variation of load current per hour expressed as maximum value in the respective cable network from April 2010 to June 2010 for certain days are shown in Figure 8-2 and Figure 8-3 respectively. In Figure 8-2, load current stays at minimum during 00:00:00 hrs to 08:00:00 hrs and then follows an increasing trend from 09:00:00 hrs to 11:00:00 hrs. Then the load variation stays at constant from 12:00:00 hrs to 04:00:00 hrs followed by a decreasing trend. This load cycle clearly reflects the power consumption during the University office hours. In Figure 8-3, different load current pattern showing constant load current of 100A approximately is maintained throughout the 24 hour period. The reason for such a load current pattern is not known.

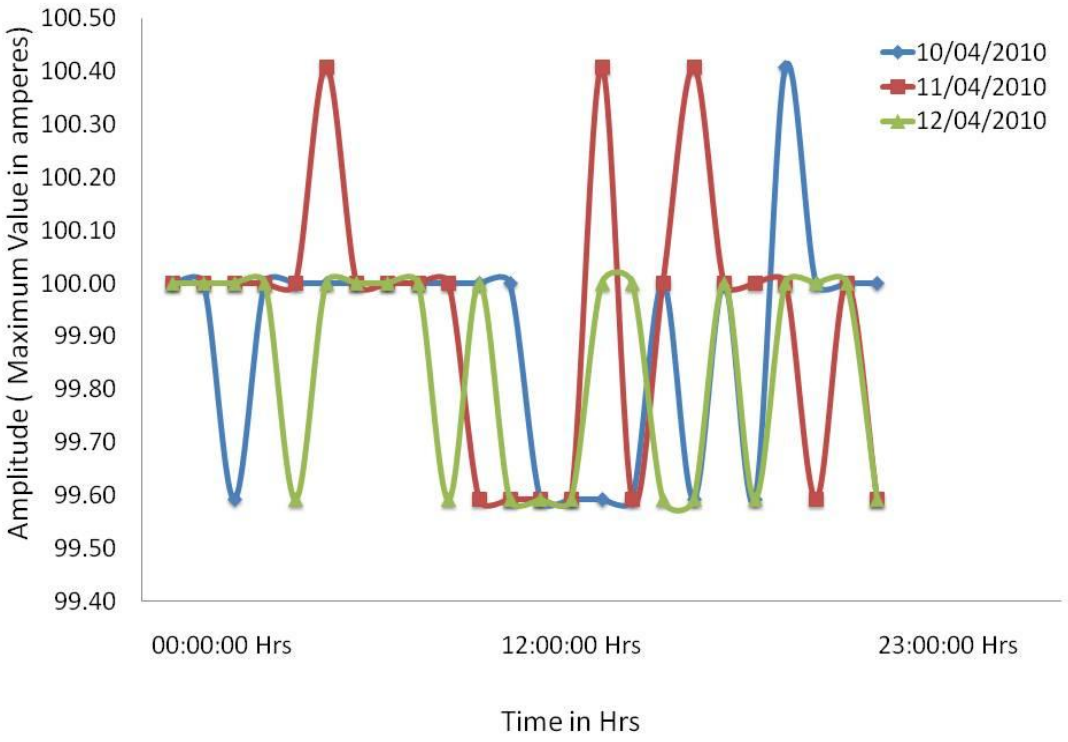


Figure 8-2 Load variation during April 2010

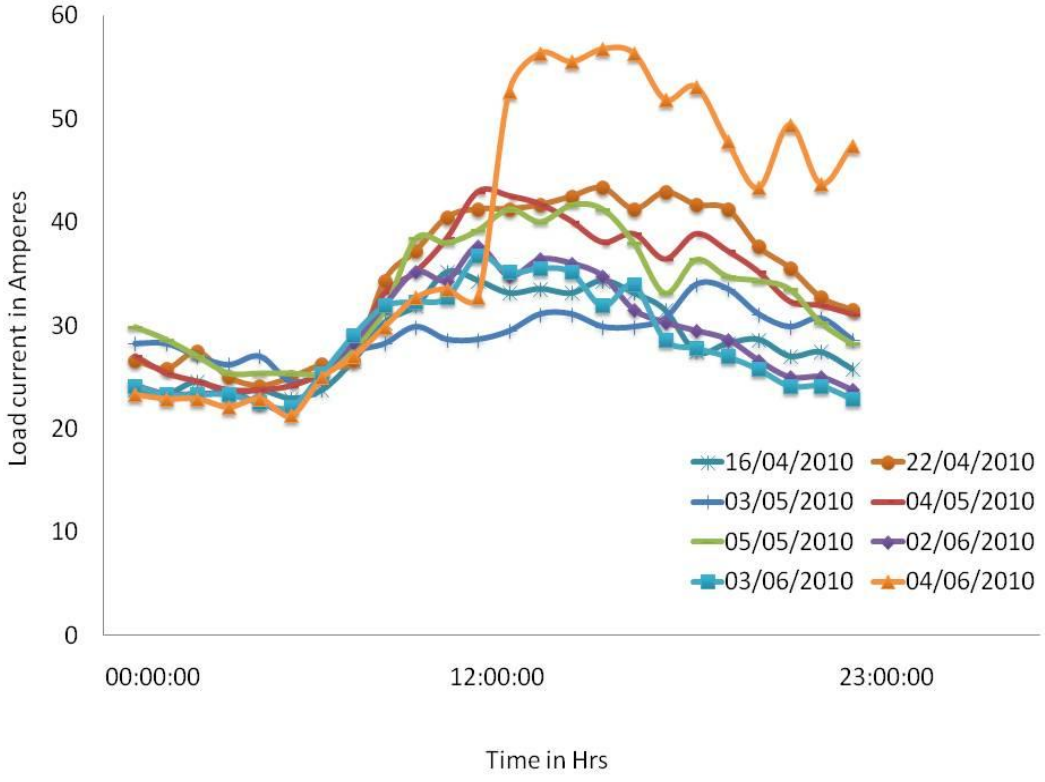


Figure 8-3 Load variation during April - June 2010

### 8.4.2 Signal power variation over time with respect to load

SNR is commonly used to describe the power level of any signal with respect to background noise level. In the unprocessed raw data, since the PD signal is not separated from the noise signal, total energy content includes noise and PD. The aim of this study is to compare this measurement data trend with the prviously published work by Glasgow Caledonian University [Song 2009].

$$\text{signal power} = \frac{\sum_{n=1}^{N} x[n]^2}{N} \qquad 8\text{-}1$$

Where, x[n] : discrete time sequence.

N : total number of samples

Normalised load current is given by the following formulae

$$\text{Normalized current} = \frac{I_{pc} - I_{p\min}}{I_{p\max} - I_{p\min}} \qquad 8\text{-}2$$

Where, $I_{pc}$ : load current at prsesent

$I_{p\min}$ : lowest load current for duration defined

$I_{p\max}$ : Highest load current for duration defined

In general normalized information is used to simplify the comparison of variation in range of values between the data sets. Hourly based normalized signal power trends from Y phase, B phase and Earth strap with respect to the cable circuit loading are shown in figures Figure 8-4 to Figure 8-7 during August and September for certain days in 2010. Based on the figures (Figure 8-4 to Figure 8-5), signal power gets lower when the circuit loading is high. However, data shown in figures Figure 8-6 and Figure 8-7 does not exhibit such a relation. Signal power variations during April 2010 are included in the Appendix F-1. During April 2010, signal power trends with respect to the load current exhibits different patterns as compared to September 2010. Similar signal power trends can be seen in [Song 2009].

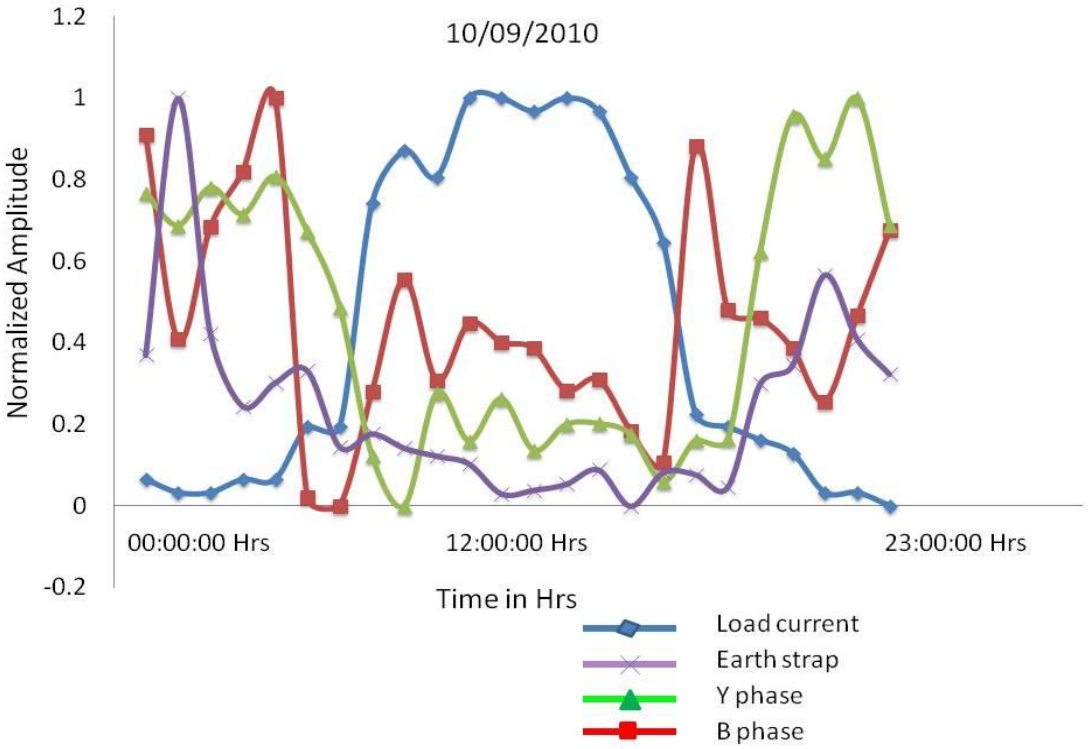


Figure 8-4 Signal power trend with respect to load

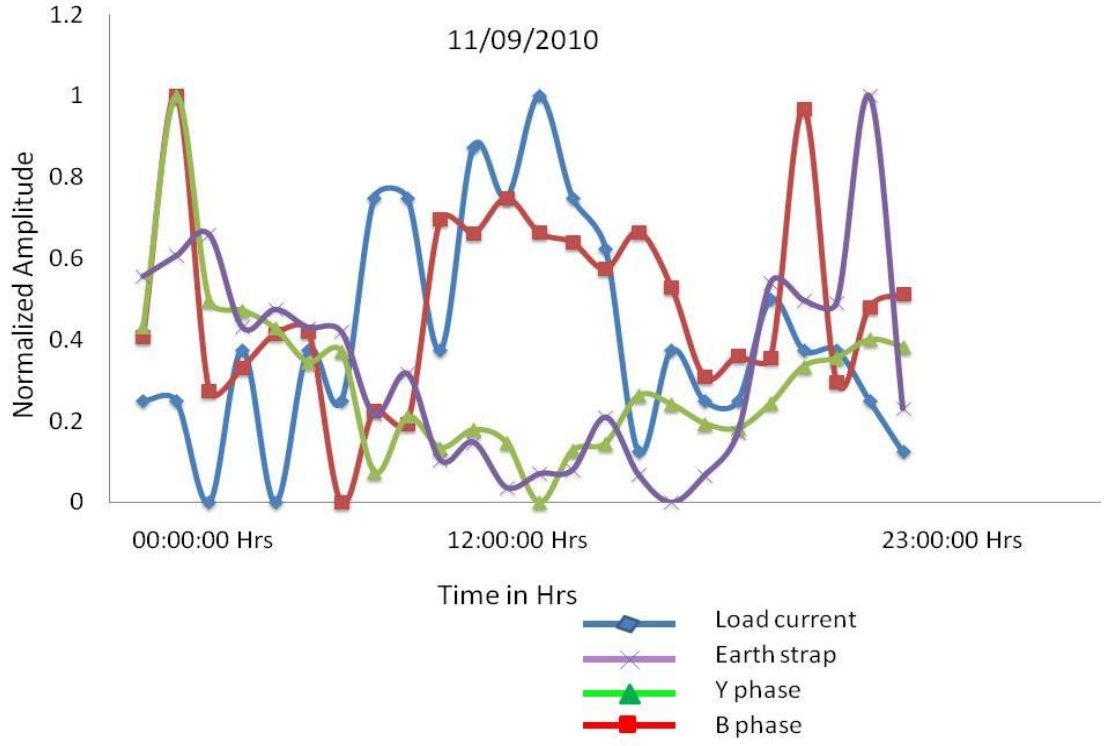


Figure 8-5 Signal power trend with respect to load

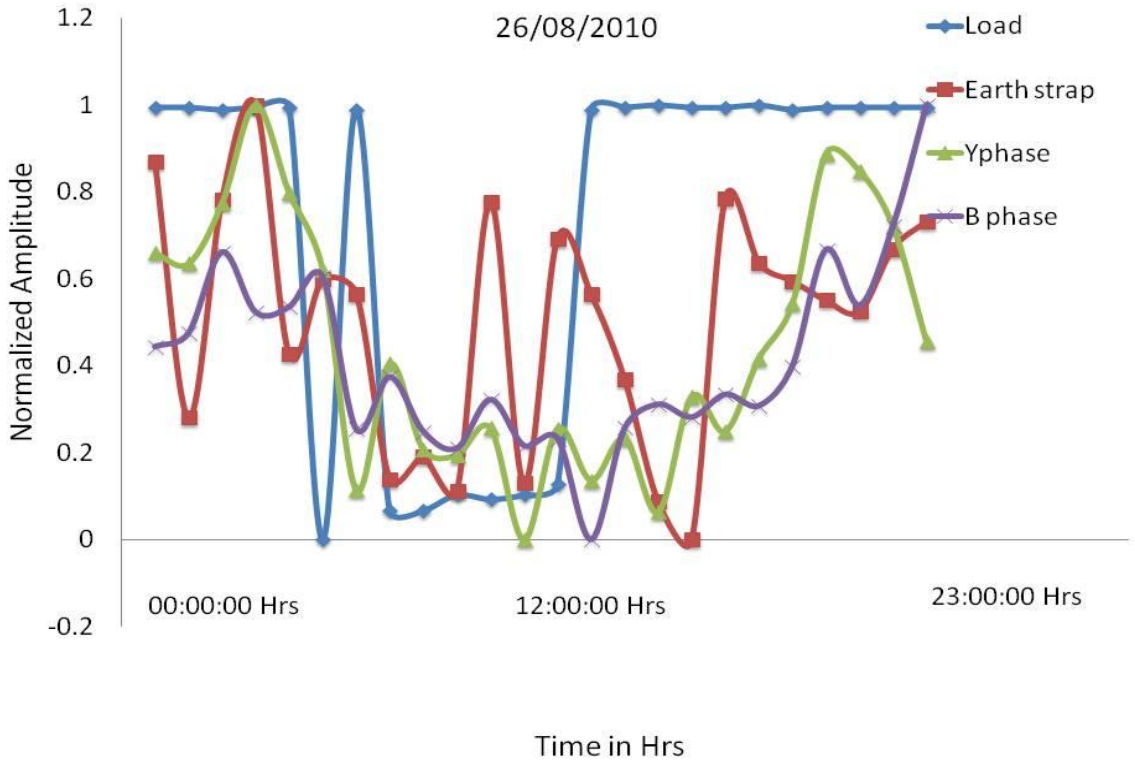


Figure 8-6 Signal power trend with respect to load

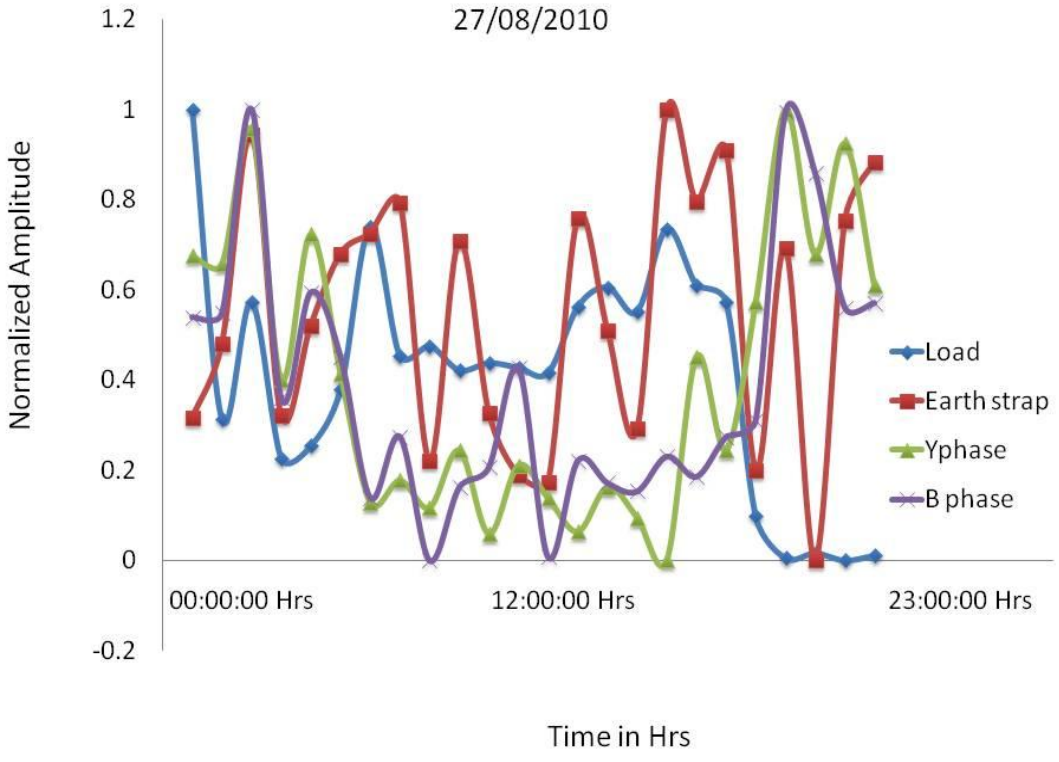


Figure 8-7 Signal power trend with respect to load

### 8.4.3 Data Denoising and Analysis

FFT is used to extract the frequency information contained in the raw data acquired using HFCT and PFCT from the cable earth strap and cable core (described in 5.6.3.1). The frequency spectrum of the raw data is shown in Figure 8-8. It is observed from Figure 8-8 that frequency components ranging from 1MHz to 1.21 MHz were found in the frequency spectrum of raw data from the earth strap, R phase and Y phase. Time domain signatures of these RF noise and associated frequency components are depicted in Figure 8-9 to Figure 8-11.

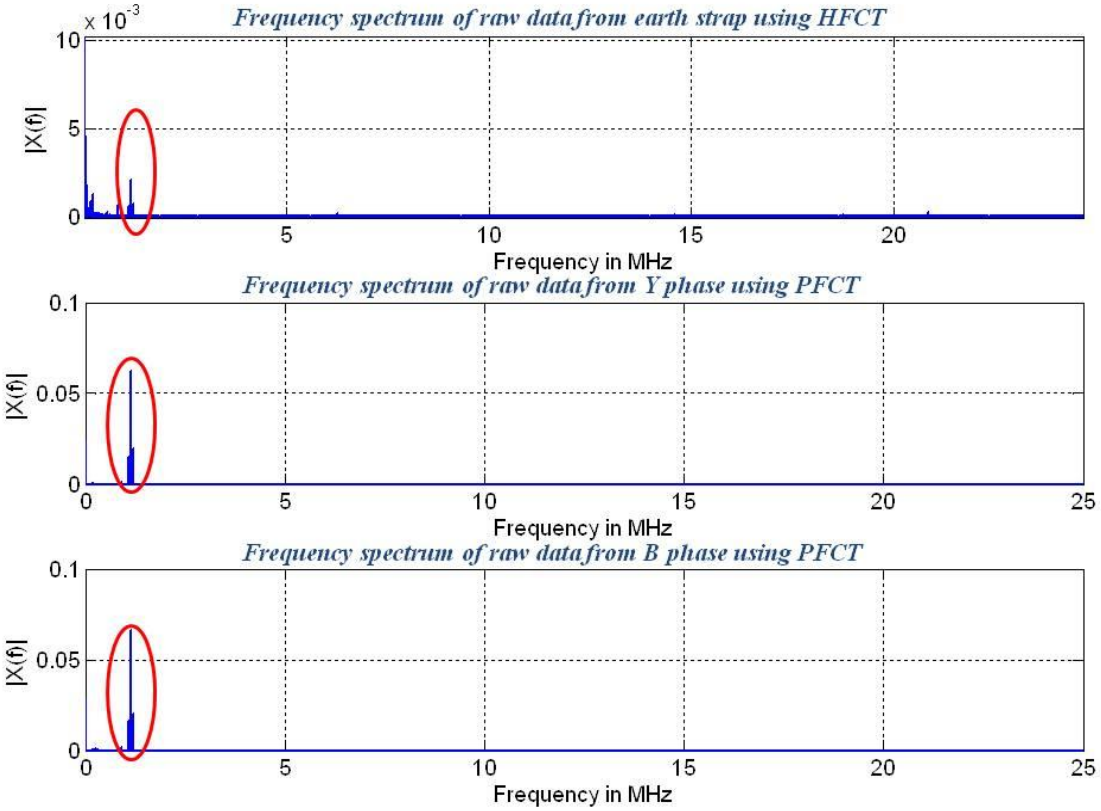


Figure 8-8 Frequency spectrum of the raw data

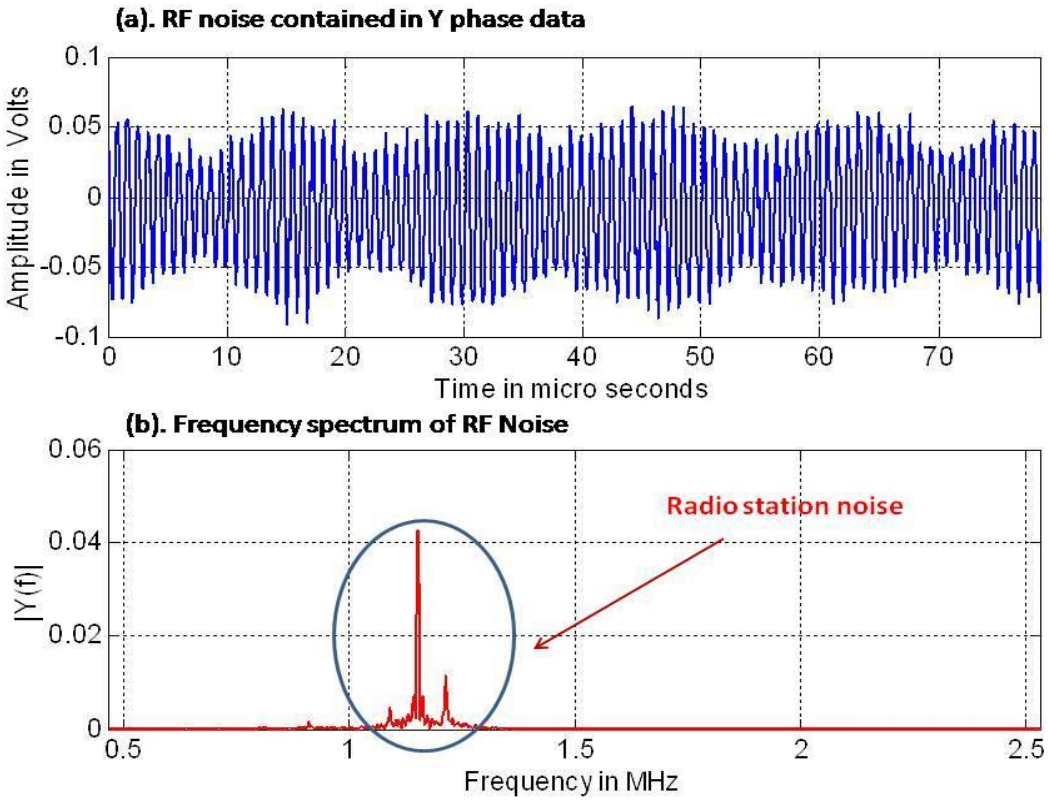


Figure 8-9 RF noise from Y phase and frequency spectrum

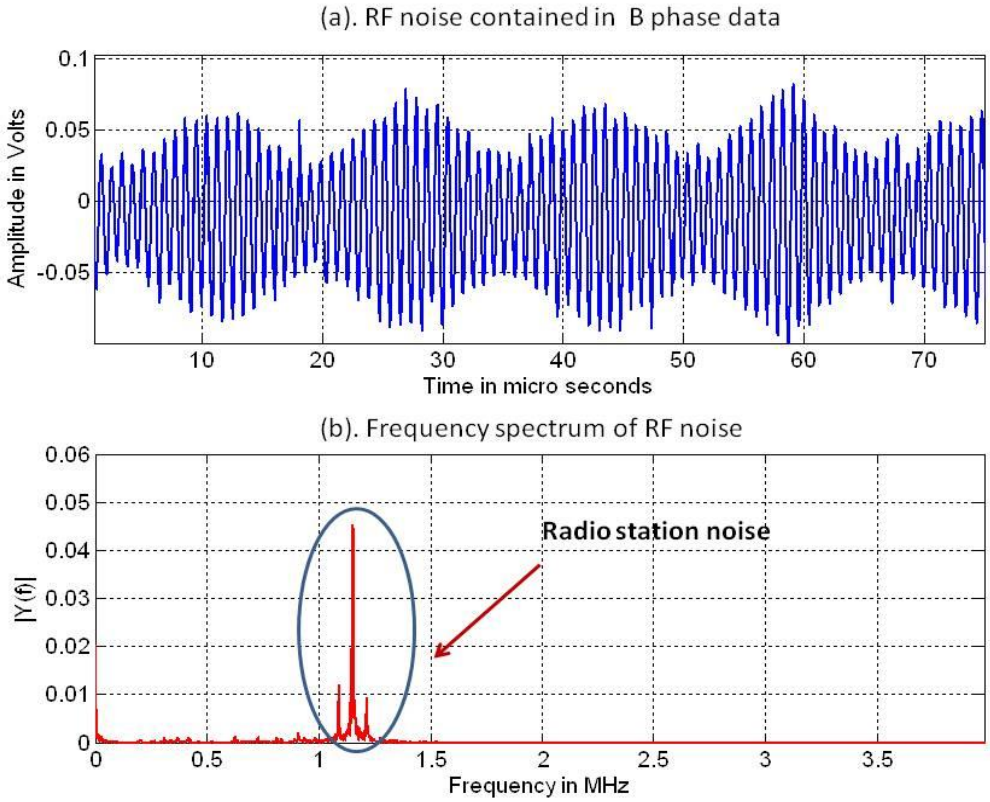


Figure 8-10 RF noise from Y phase and frequency spectrum

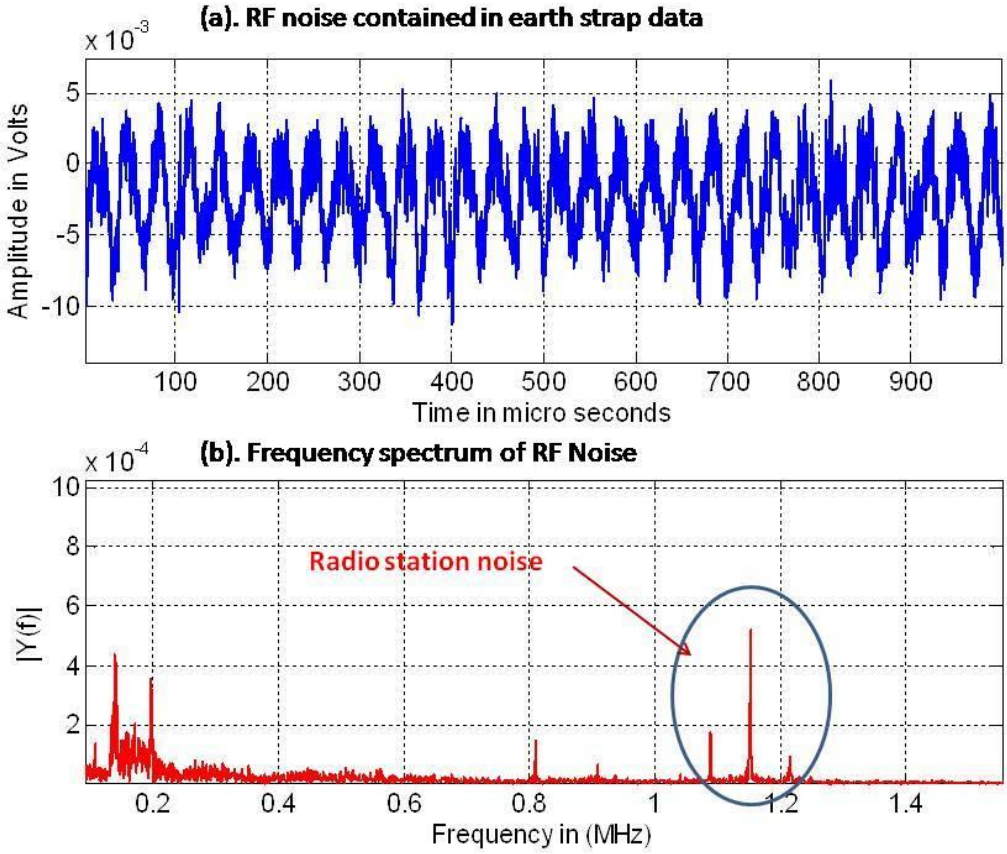


Figure 8-11 RF noise from earth strap and frequency spectrum

Figure 8-9 to Figure 8-11 indicate that these signals result from amplitude modulated (AM) radio transmission stations [Finder 2012]. Frequency components contained in the raw data are included in the Appendix F-2. These frequency components show varying signal power in the cable earth screen and cable core. Such varying signal power in the earth strap and cable core shows that these signals are resulted through conduction in the cable, not through radiated emission. In addition, there are more frequency components detected in HFCT. This is due to the fact that the cable earth strap is exposed and subsequently acts as an antenna becoming more susceptible to EMI, while the phase conductor of the cable to which the PFCT is attached is inside switch gear panel [Gavazza and Wiggins 1996]. The frequency band of a cable's PD normally falls in the range of 200kHz (if the PD site is 'far away' down the cable) up to or around 4MHz (if the cable PD site is 'nearby' i.e. a few meters to a few 10's of meters away) [Ltd 2009; Zhou, Song et al. 2009]. FRA results show a

nearly flat response in the PD frequency band (described in section 5.4). Based on FRA and the frequency power spectrum extracted from on-site measurements, PFCTS can be considered for detecting PD signals from cables.

### 8.4.4 Typical Fast Rising Pulses

Denoising is a process, which attempts to extract the required information from the corrupted data. Typical denoised signals for a window length of 20ms from the cable core and earth strap are as shown in Figure 8-12. The denoising method discussed in section 7.2 extracts fast rising pulses, which appear as bursts from the raw data. These pulses could be PD or transient disturbance. After analysing a few hundred datasets from the cable network, fast rising pulses which exhibit similar characteristics are isolated.

Observation of a dataset of 200 signals from each of the R phase, Y phase, B phase and earthstrap were used to extract wavelet signatures. Each signal is of 80ms length. The aim of the signature extraction process is to get the correlation in the time domain signature extracted from the cable core and earth strap which eventually increases the confidence level of using PFCT as a PD detection sensor. Typical fast rising waveform signatures from cable core and earth strap and associated frequency spectrum are shown in Figure 8-13 to Figure 8-20.

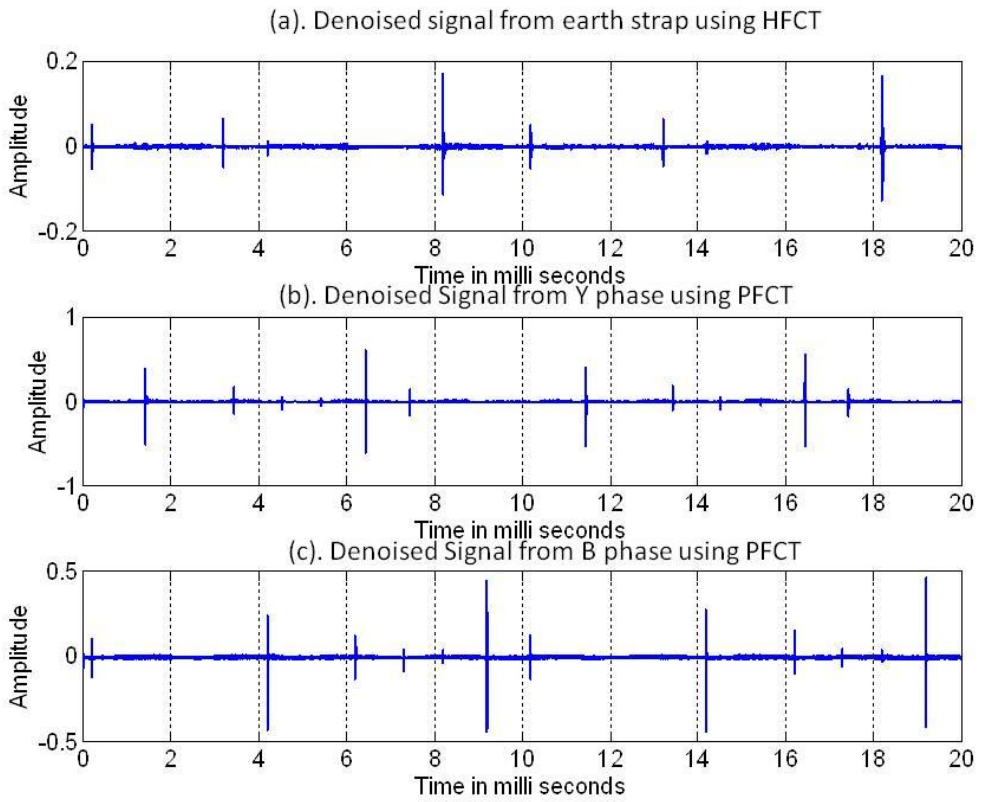


Figure 8-12 Denoised signal from cable core and earth strap

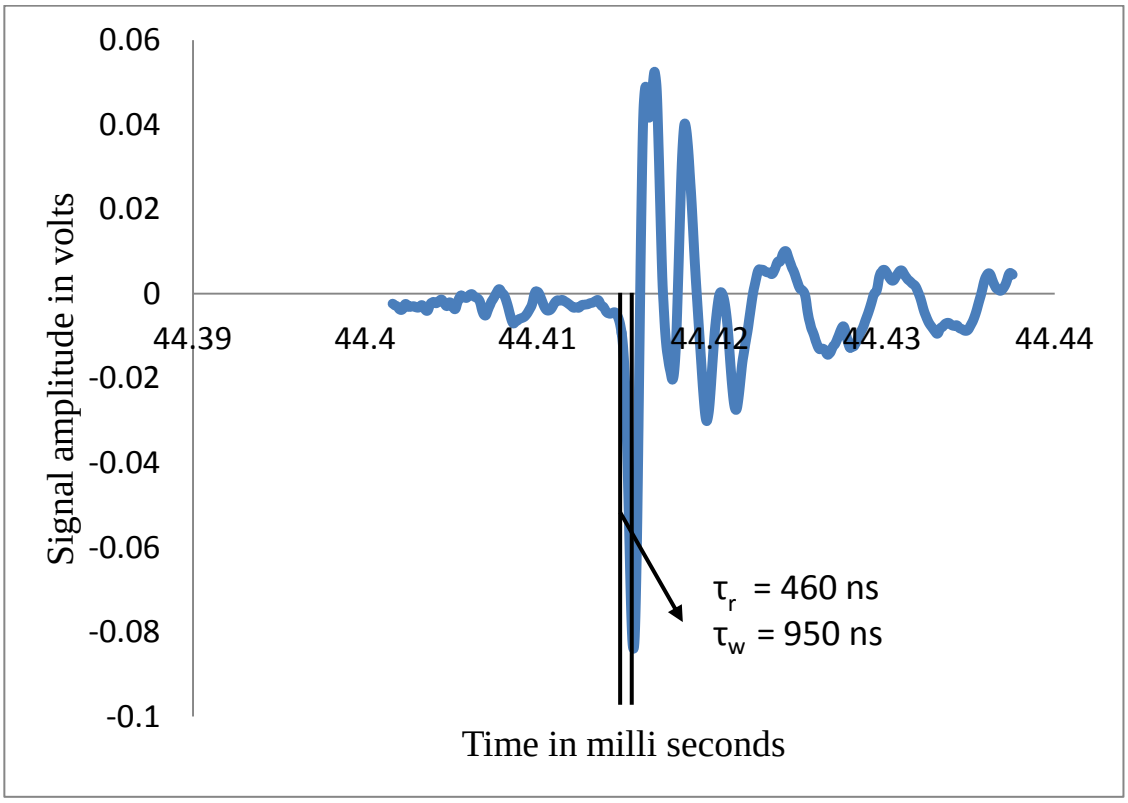


Figure 8-13 Fast rising pulse from earth strap

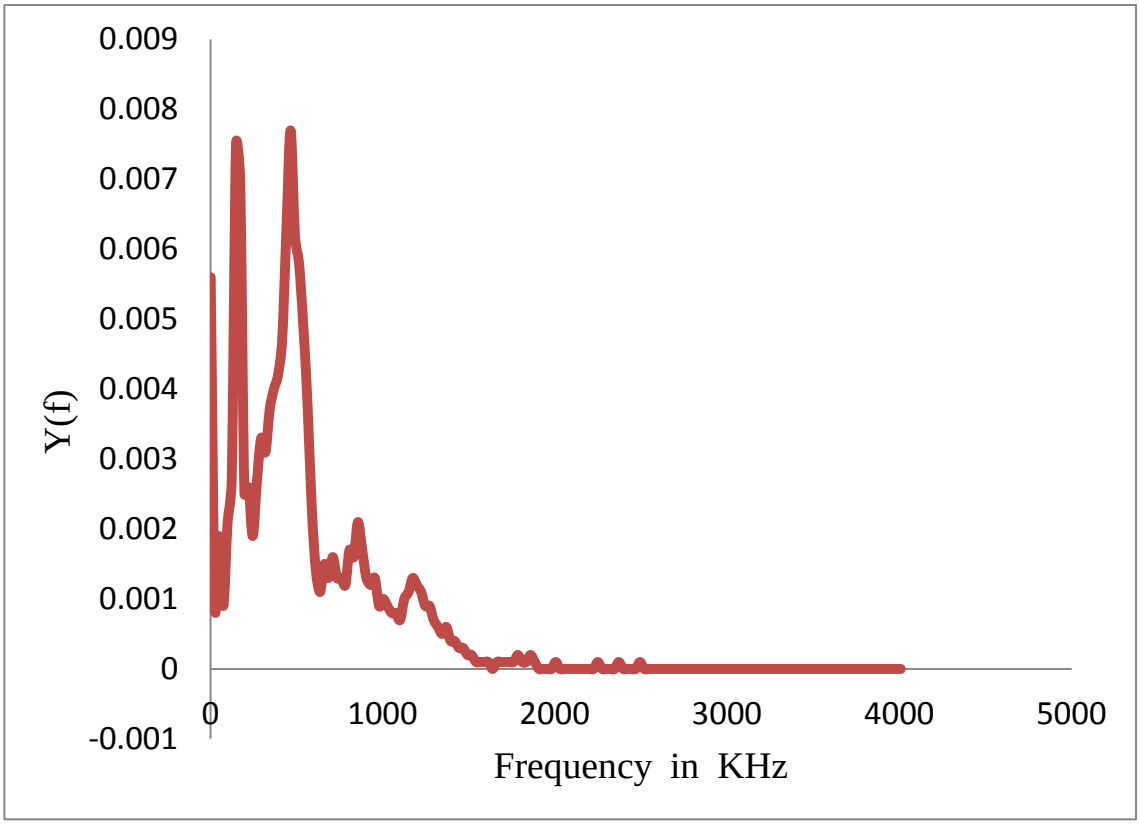


Figure 8-14 Frequency spectrum (earth strap)

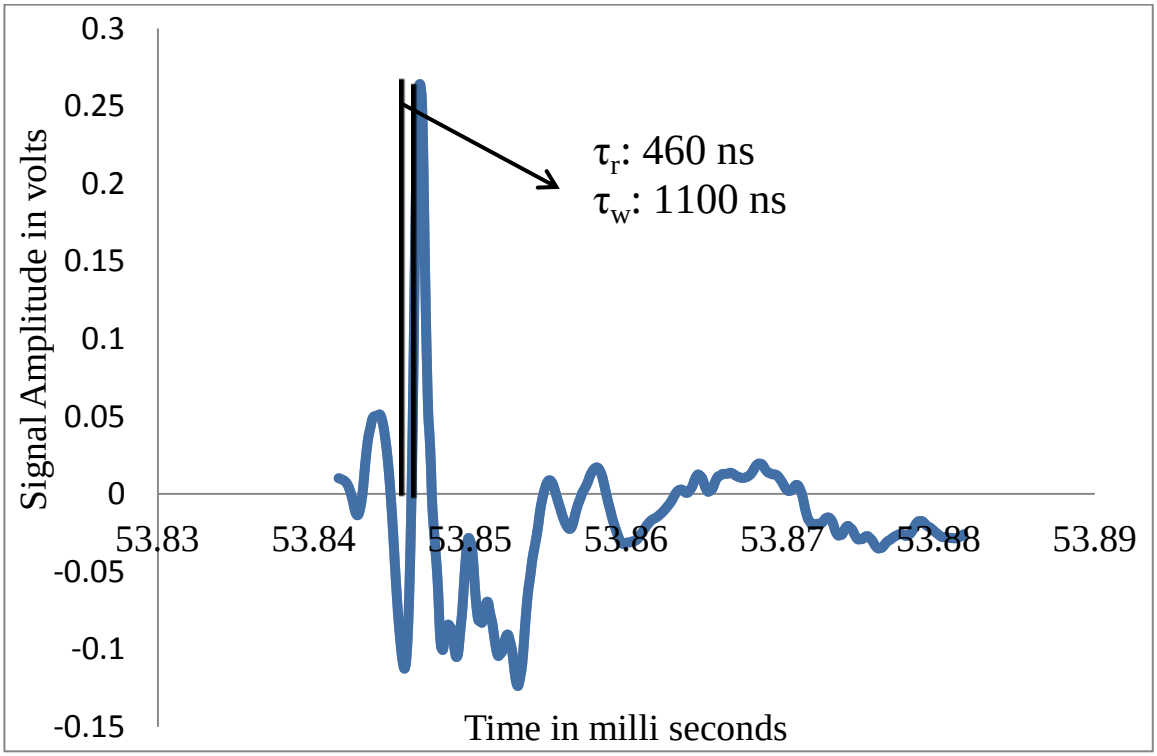


Figure 8-15 Fast rising pulse from Y phase

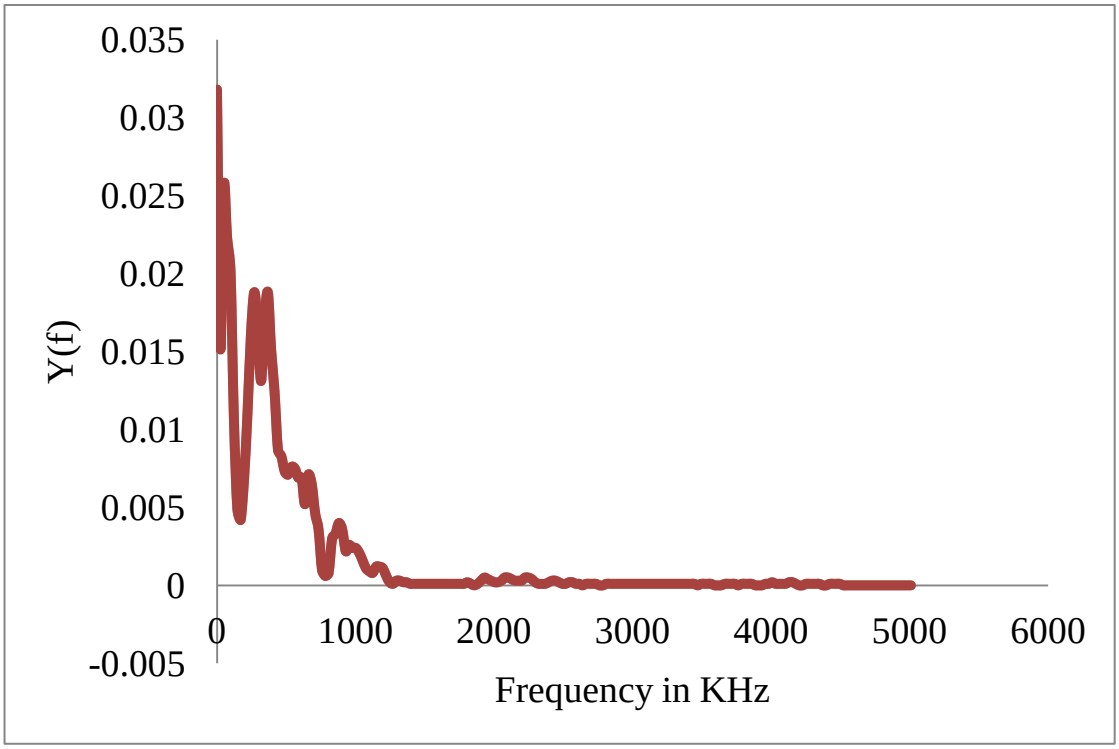


Figure 8-16 Frequency spectrum (Y phase)

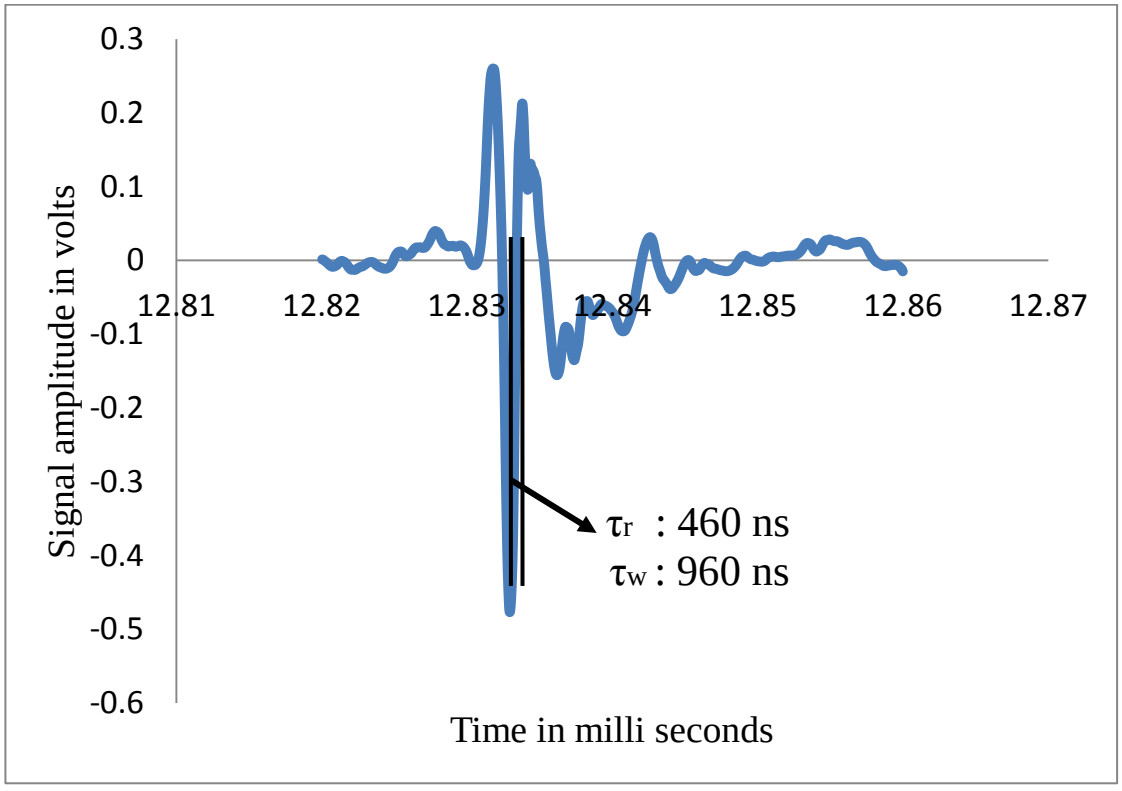


Figure 8-17 Fast rising pulse from B phase

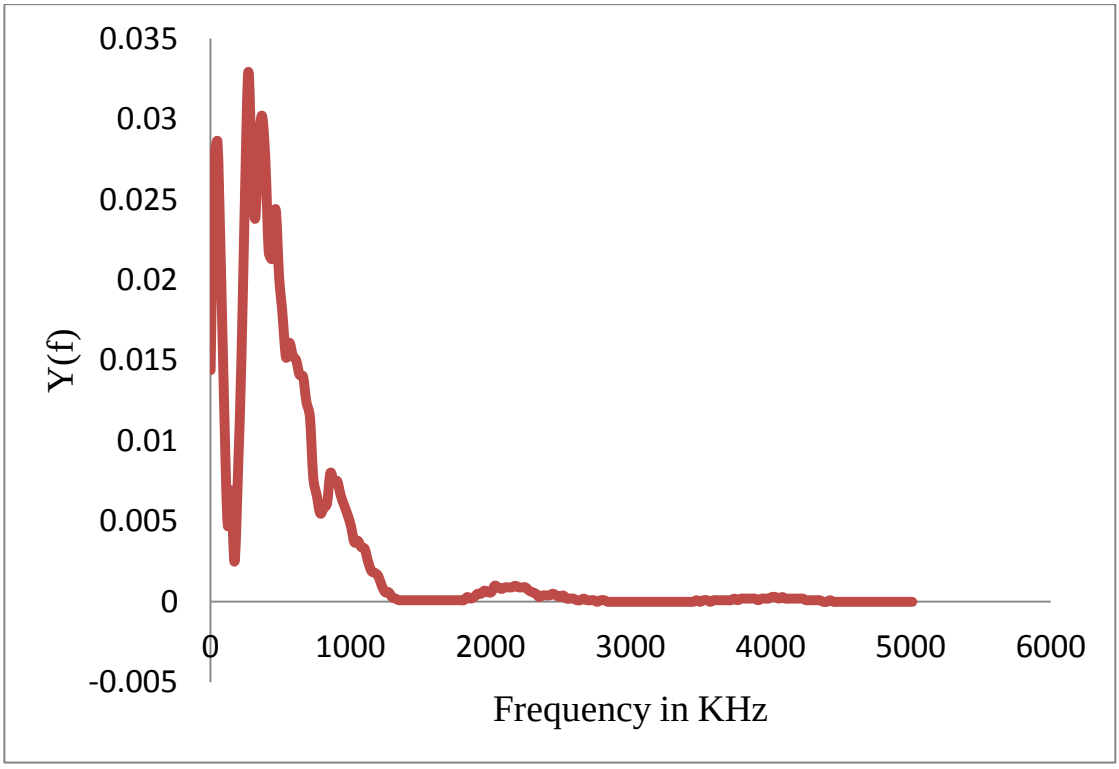


Figure 8-18 Frequency spectrum(B phase)

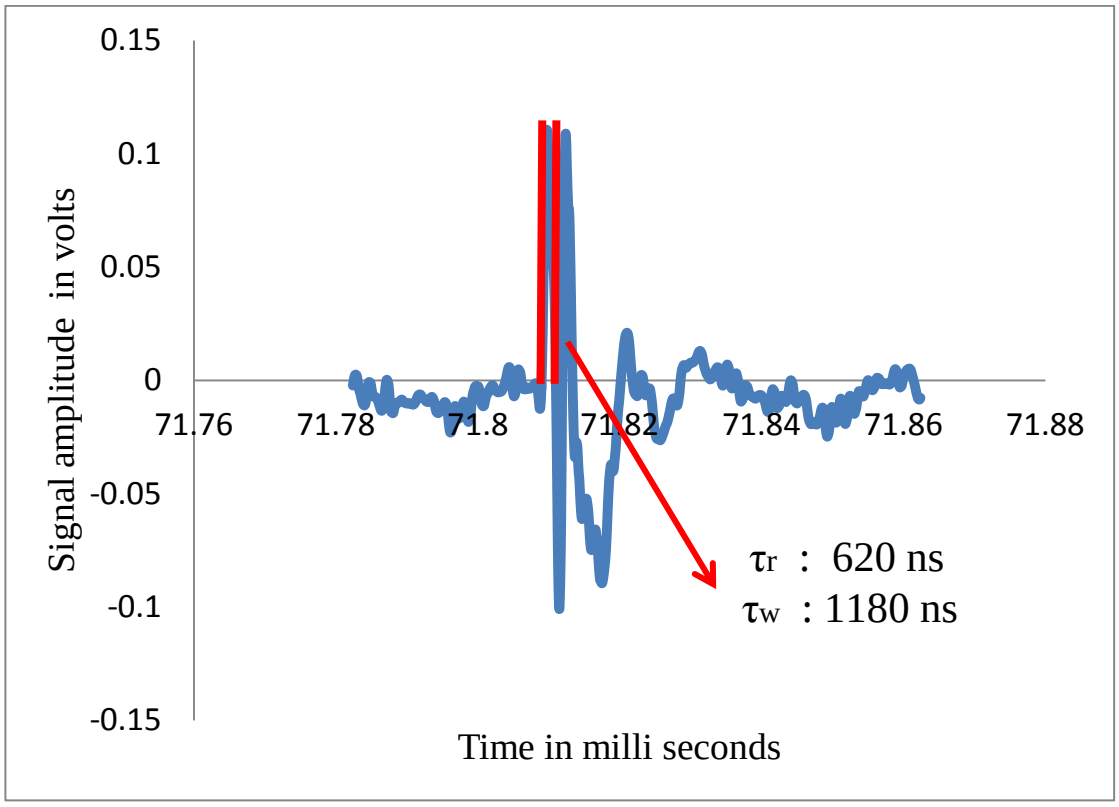


Figure 8-19 Fast rising pulse from R phase

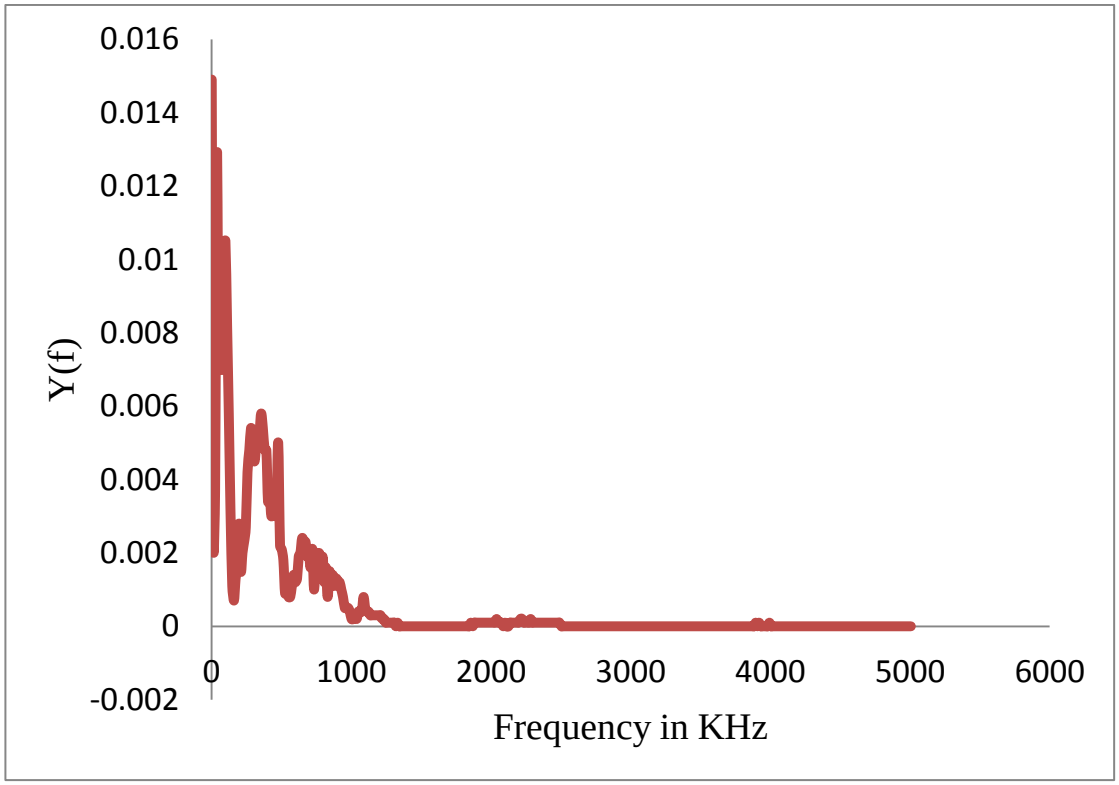


Figure 8-20 Frequency spectrum(R phase)

Based on Figure 8-13, pulses from the earth strap have an initial negative excursion followed a low frequency oscillation of smaller magnitude. In the case of the B phase, based on Figure 8-17, prior to the negative excursion there is positive portion of sufficiently larger amplitude. Such a positive portion is also seen in the Y phase (referring to Figure 8-16) with relatively lower amplitude. Rise time of the pulses from the R phase shown in

Figure 8-19 are slightly higher than the rest of the pulses. All of these pulses from the earth strap and cable core exhibit similar frequency spectrum based on Figure 8-14, Figure 8-16 and Figure 8-18. Based on the fact that the frequency spectrum signal power is mostly concentrated near to 500 KHz, a normalized time domain signature of a typical pulse is chosen from 50 numbers of pulses having a rise time in the order of 500ns within the frequency spectrum are shown in Figure 8-21.

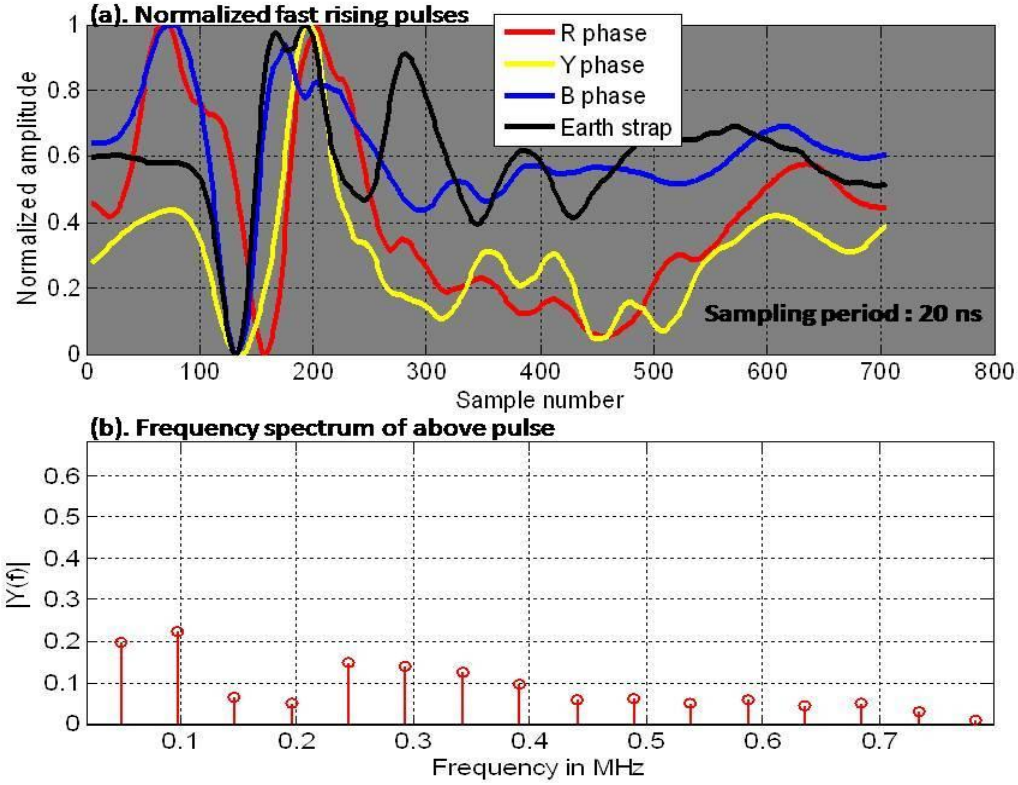


Figure 8-21 Normalized fast rising pulses and associated frequency spectrum

### 8.4.4.1 Statistical properties of fast rising pulses

The presence of PD in the insulation material has been known as a useful indicator of deteriorated insulation. PD exhibits different patterns which depend upon gas species, gas pressure, void conditions, dielectric etc. Interpretation of PD pattern can reveal the type of discharge and therefore, it has been used as a condition monitoring tool to assess the integrity of insulation [Yazici 2003]. Such variations cannot be realised from visual examinations. In addition to the time domain parameters, statistical parameters such as mean, standard deviation, skewnes and kurtosis can also be used to classify the various type of PD sources [Ariastina, Khawaja et al. 2003]. These statistical parameters along with the time domain parameter can be used as a template for classifying different types of PD signals. In this thesis since the PD measurement is done at one cable network, statistical parameters are used to find the similarities between pulses extracted (described in section 8.4.4) from all the three phases and the earth strap. Statistical parameters used for the feature extraction are given by

$$\eta = \frac{1}{N}\sum_{n=0}^{N-1} x[n] \qquad 8\text{-}3$$

$$\sigma = \sqrt{\frac{1}{N}\sum_{n=0}^{N-1}\left(x[n]-\eta\right)^2} \qquad 8\text{-}4$$

$$\gamma = \frac{1}{N\sigma^3}\sum_{n=0}^{N-1}\left(x[n]-\eta\right)^3 \qquad 8\text{-}5$$

$$k = \frac{1}{N\sigma^4}\sum_{n=0}^{N-1}\left(x[n]-\eta\right)^4 \qquad 8\text{-}6$$

$where, \eta$ : Mean

$\sigma$ : Standard deviation

$\gamma$ : Skewness

$k$ : Kurtosis

$n = 0,1,2---N-1$

Figure 8-22 and Figure 8-23 shows mean and standard deviation of 50 numbers of pulses respectively extracted from the R phase, Y phase, B phase and earth strap. As illustrated in Figure 8-22 and Figure 8-23, a high degree of correlation among the pulses is seen. Pulses from the cable exhibit negative skewness based on Figure 8-24. Also kurtosis shown in Figure 8-25 exhibits similar trend for the pulses from the earth strap and Y phase.

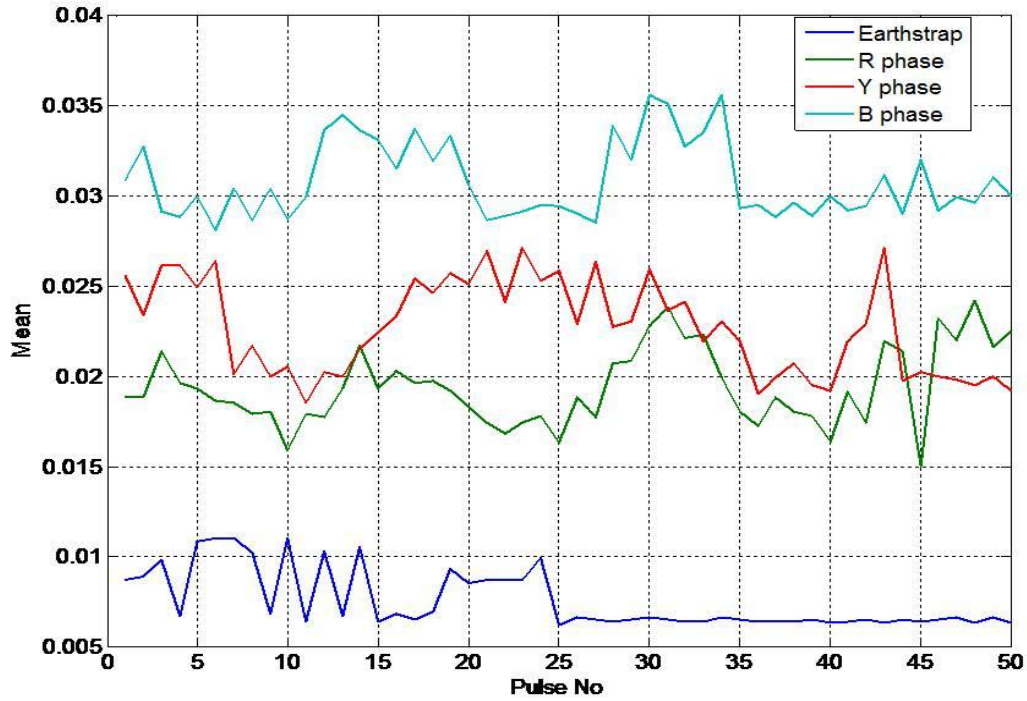


Figure 8-22 Statistical parameters - Mean

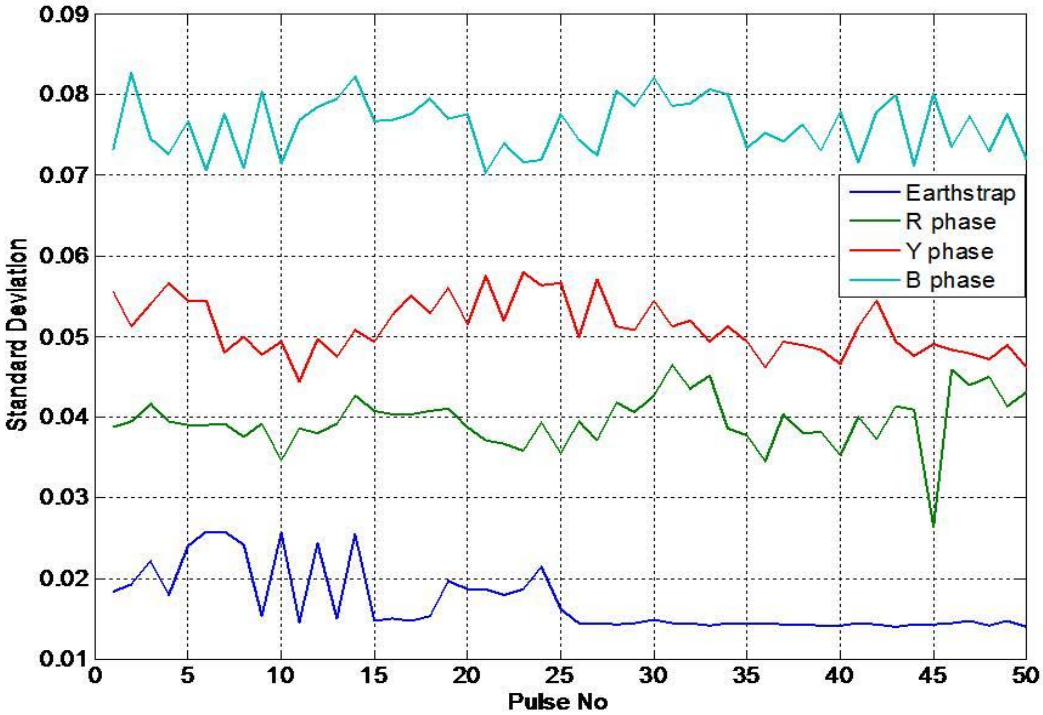


Figure 8-23 Statistical parameters - standard deviation

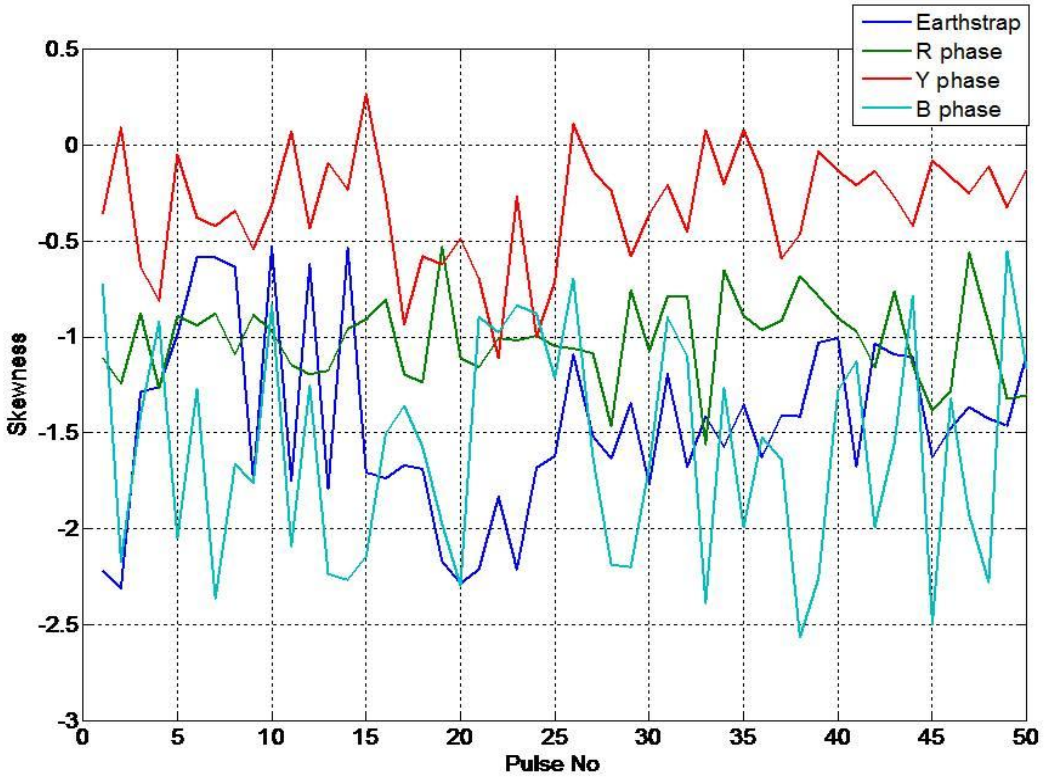


Figure 8-24 Statistical parameters- Skeweness

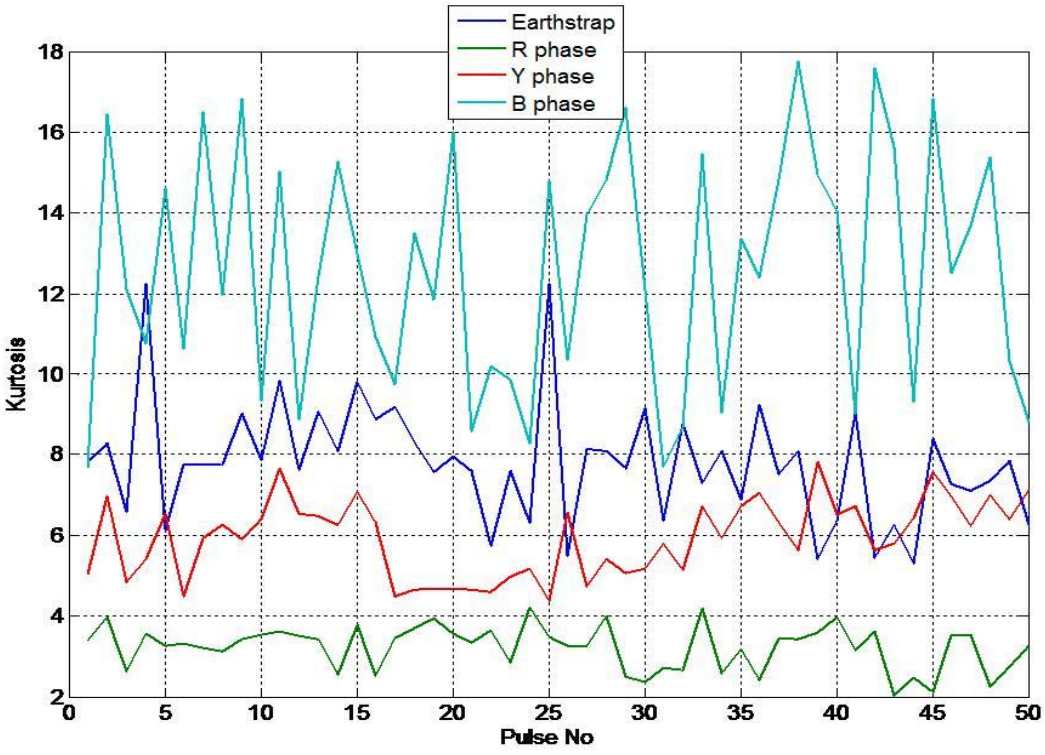


Figure 8-25 Statistical parameters - Kurtosis

### 8.4.5 Typical Switching Noise

Apart from the fast rising pulses extracted (described in section 8.4.4) from all the three phases and earth strap, typical noise interference pulses which exhibit similar characteristics are shown in Figure 8-26 and the associated frequency spectrum is shown in Figure 8-27. These noise signals have a similar time domain signature, frequency spectrum and repetition rate.

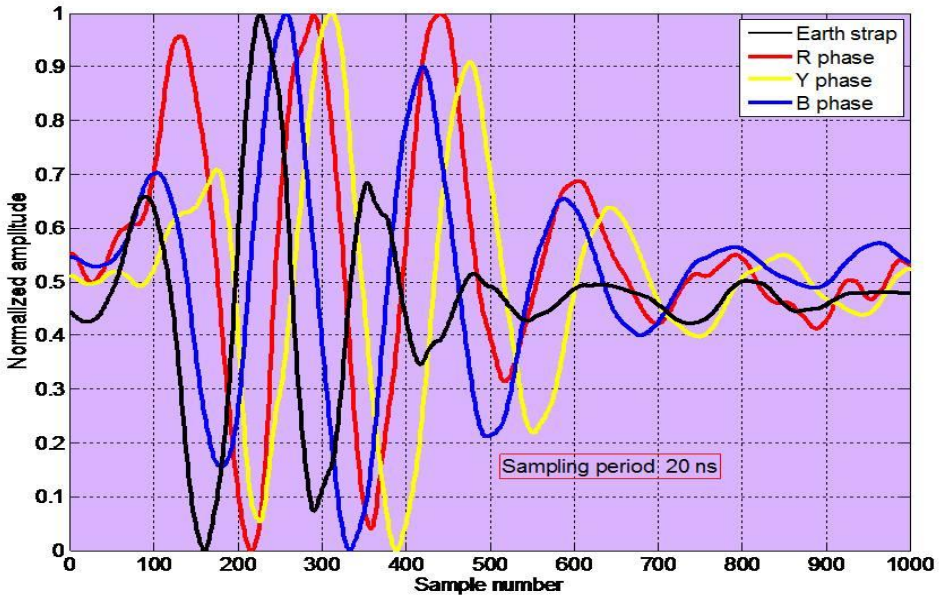


.

Figure 8-26 Typical noise signals from R, Y, B and earth strap

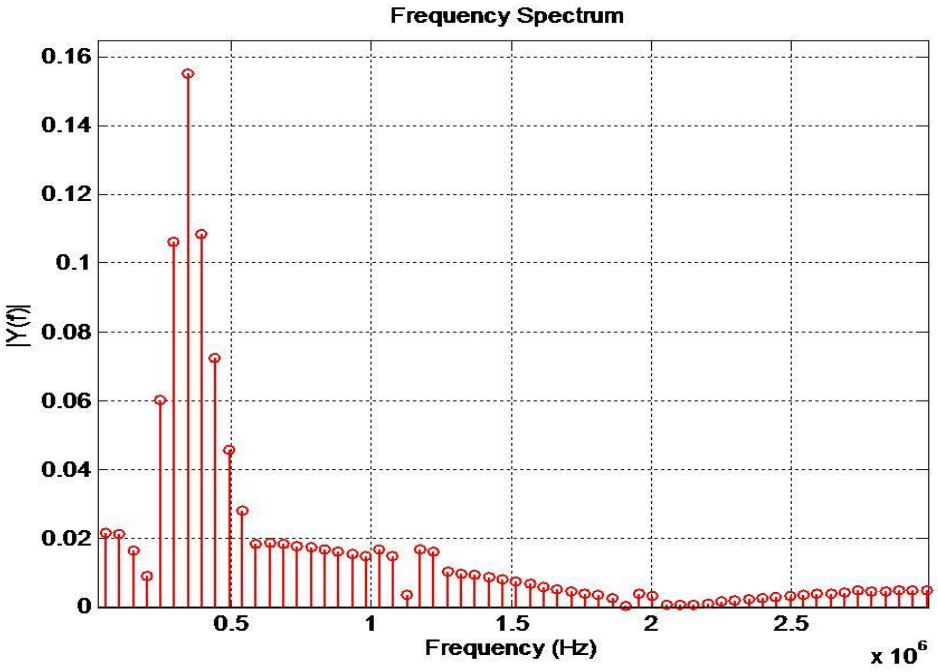


Figure 8-27 Frequency spectrum

### 8.4.6 Phase Resolved PD pattern

Position of PD pulses with respect to the phase of applied power frequency AC voltage in 20 ms window has been widely applied for both in the laboratory measurement of PD, as well as in industrial high voltage systems such as cables, transformers and rotating machines for PD characterisation. This method of PD charcterization is termed as PRPD. PD will occur with a specific polarity and phase position. Furthermore, depending on the location of the PD with respect to the electrodes, PRPD will change [Stone 2010]. In case of single core cables, electrical field inside cable geometry is linearly polarized at every point. In this scenario of linear field, PD will be concentrated between the zero crossing and maximum of the applied voltage. Hence well defined PRPD pattern exists for single core cables [Gross and Fruth 1998].

Typically MV cable consists of three cores with a common earth screen. During the normal operation, MV cable can be viewed as four conductor transmission lines with a three phase revolving electrical field. The rotating field has implications on the PD distribution with respect to the phase-angle. Hence, PD patterns for single core cable cannot be applied to characterise the PD activity in multicore cables like three core cables. In a three core cable, magnitude of the induced PD currents in the conductors will depend on the position of the defect within a cable cross section and the phase-angle of the energizing voltage. Geometry of three core cable is optimized for field control in such a way that narrow spacing is allowed among conductors and between conductor and earth screen. This makes the field distribution linear in most of the regions while in some critical regions the field is determined by the three phases of the applied voltage. However in case of cable joints which are more prone PD region, field optimization is difficult to maintain as in cable manufacturing. In such case, field is mostly elliptical as shown in Figure 8-28. In a three-phase four-conductor cable, charge displacement due to PD will not occur in all conductors to the same extent. This means that if PD detection is performed only in the earth screen, a PD may remain undetected, depending on the position of the discharge site within the dielectrics and its direction [van der Wielen, Steennis et al. 2003]. In addition to that a multi conductor transmission line exhibits various signal propagation modes. Magnitude of the induced currents in the phase conductors will therefore alter during signal propagation along the cable.

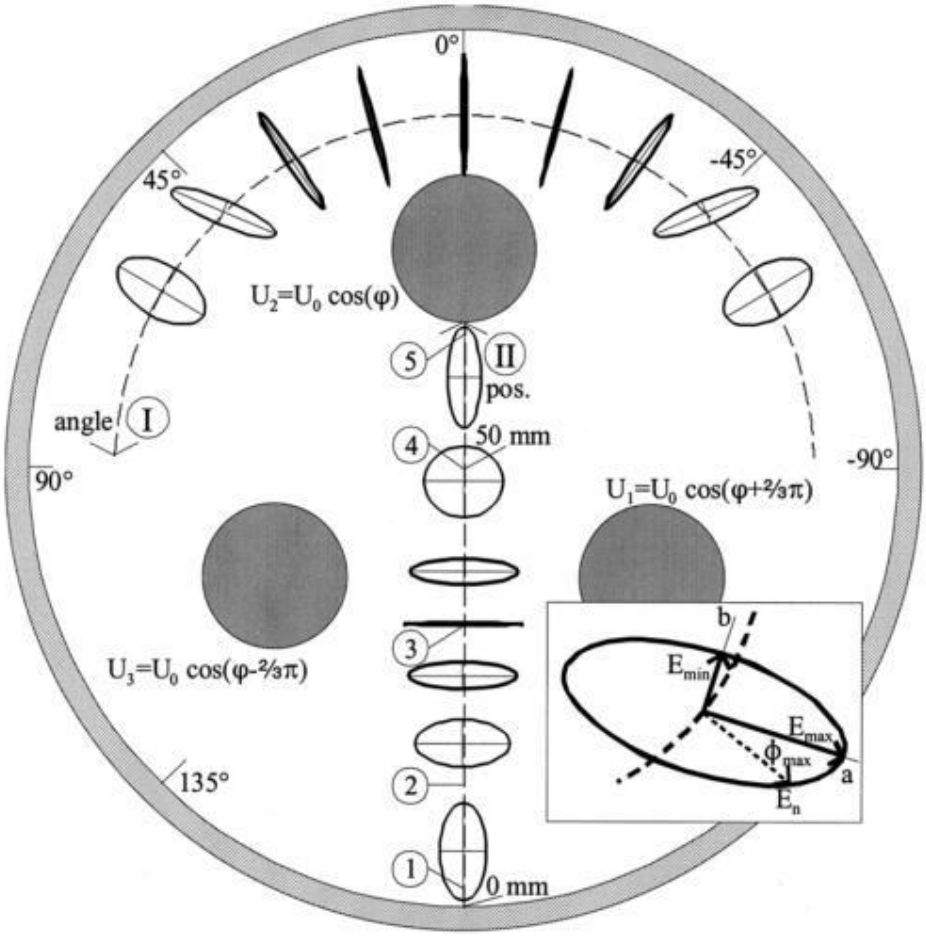


Figure 8-28 E field distribution in a three phase cable joint
[van der Wielen, Steennis et al. 2003]

Data acquired using RPDMS has a power frequency reference from the load current which was mainly aimed to get the interdependency of PD intensity with respect to loading on the cable network. In order to get PRPD, the power frequency reference must be taken from the output of the VT, which is an invasive method and is not possible. Some oscilloscopes have line triggering functionality which uses ac mains as a trigger source. RPDMS(described in Chapter 5) is triggered externally using the load current and hence load current is used as a power frequency reference. In general, load current and system voltage should have phase shift which depends on the connected load in the respective cable. PRPD pattern using load current as a reference does not give accurate results since PD inception with respect to the phase of the applied voltage cannot be obtained. Nevertheless by using the load current as a reference, some sort of phase correlation can be done among the multiple phases. PRPD distribution using

power frequency load current as the reference source is shown in Figure 8-29 and Figure 8-30.

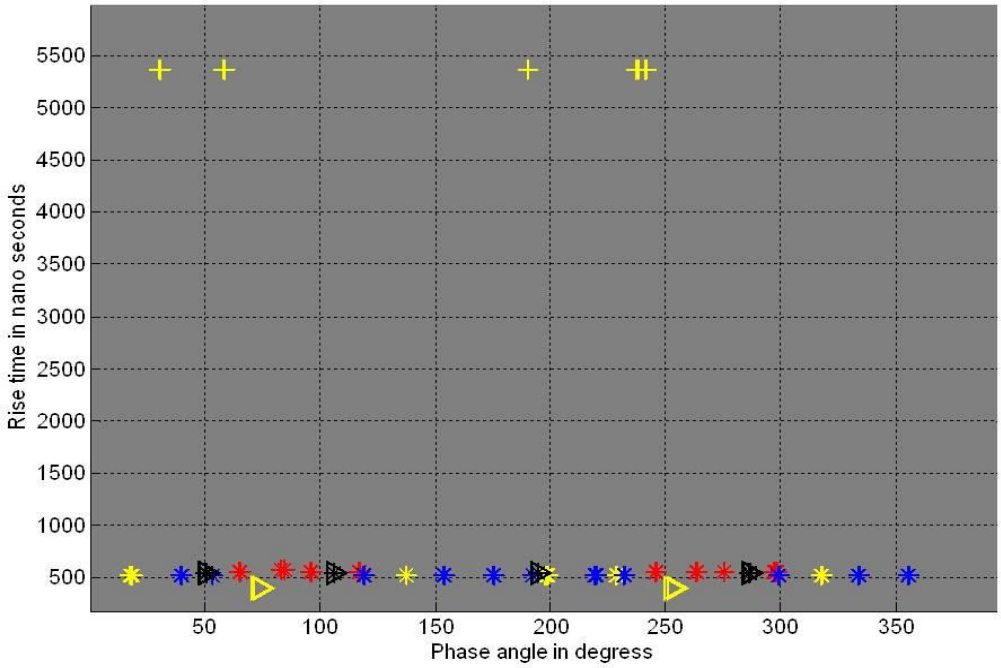


Figure 8-29 PRPD pattern (φ vs rise time)

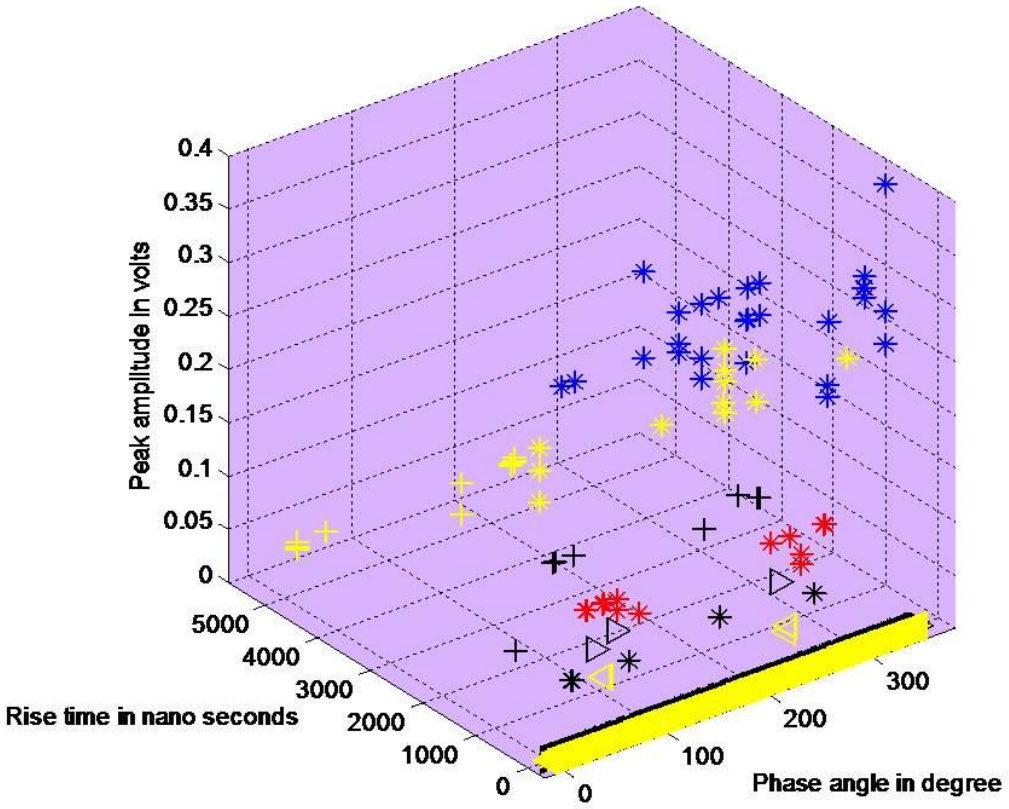


Figure 8-30 PRPD pattern (φ vs rise time and peak amplitude)

From Figure 8-29 and Figure 8-30 pulses having a rise time in the order of 500ns from all the three phases and earth strap are scattered throughout the $360^0$ phase window. This gives the impression that there is the possibility of multiple discharge sources in the cable with different inception voltages. Fast rising pulses resulted from all the three phases and earth strap have similar timing signatures and frequency spectrum. Also based on the polarity reversal character of PD, there is no polarity change between positive and negative halfcycles of the power frequency reference. PD's exhibit different waveform signatures from cable, switchgear, transformers e.t.c. PD pulses from switchgear are typically of high frequency (4MHz to 100MHz) and oscillatory in shape due to the multiple reflections within the switchgear panel. PD pulses from cables have a different wavelet signature in both time and and frequency (100kHz – 4MHz) and are monopolar (Appendix H) [Ltd 2009]. Pulses shown in the Figure 8-21 have multiple oscillations and are not monopolar. Based on timing signatures and risetime, pulses extracted from the substation end A data are more likely to originate away from the cable under test.

## 8.5 Results from 11kV secondary substation end B

In the 11 kV distribution substaion end B, (decribed in the Appendix C-5) PFCT access was not possible. So the only option was to use the HFCT from the earth strap. Hence RPDMS (described in Chapter 5) acquires the data from the earth strap of the three core PILC cable for every 60 minutes. The data acquisition interval used in RPDMS is 60 minutes, with a sampling rate of 50 Msps. The PD data frame has a time span four power frequency cycles (80ms). A typical dataset acquired and the corresponding frequency spectrum are shown in Figure 8-31. The main purpose of this analysis is to compare the data between between both ends of the cable. Since both datasets are taken at different times, which means they are not synchronized, propagation delay between both ends of the cable cannot be obtained from this data.

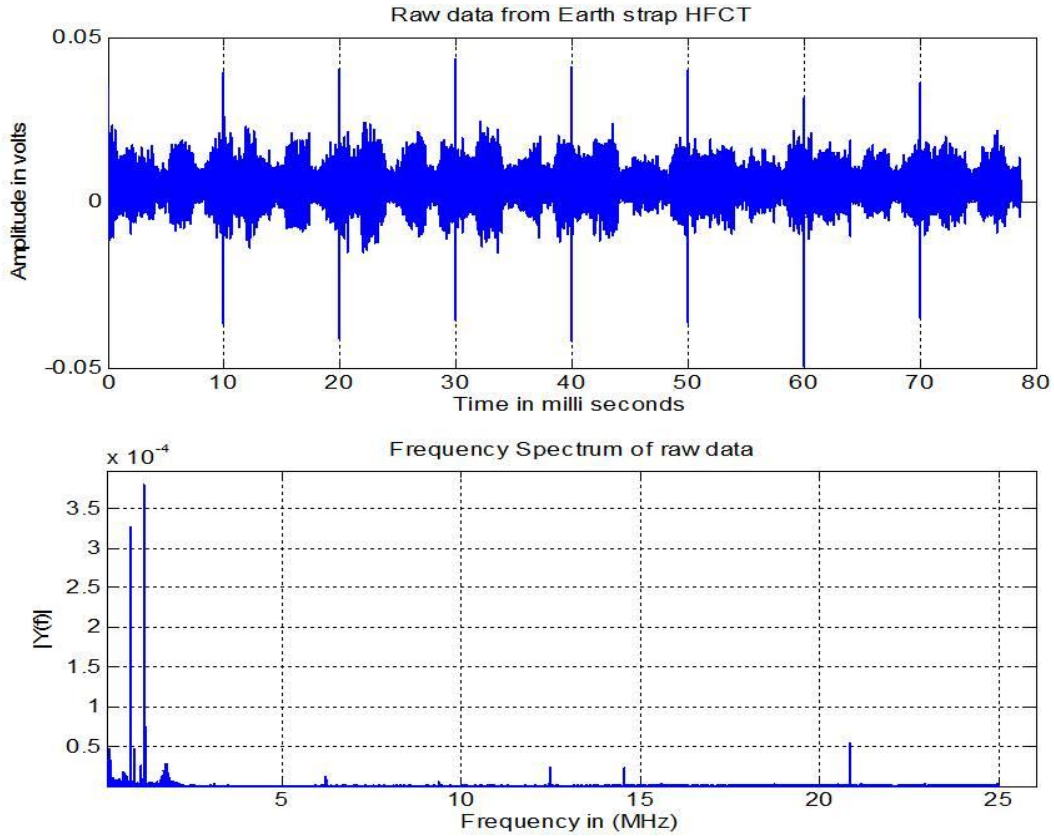


Figure 8-31 Acquired data from three core PILC cable – substation end B

## 8.5.1 Signal Power Variation Over Time

In this substation load current measurement was not possible since PFCT at this end was not accessible. Hence signal power variation with respect to load current in the cable was not possible. Hourly based normalized signal power from the earth strap during the third week of November 2011 is shown in Figure 8-32. Based on Figure 8-32, signal power reaches a maximum during 09:00:00 hrs to 20:00:00 hrs. Signal power during the fourth week of November 2011 are included in the Appendix F-3. Both of these data sets shows higher degree of similarity in signal power variation over the specified interval. However signal power trend dated 22 nd November 2011 in Figure 8-32 exhbits different pattern and the reason was not obvious.

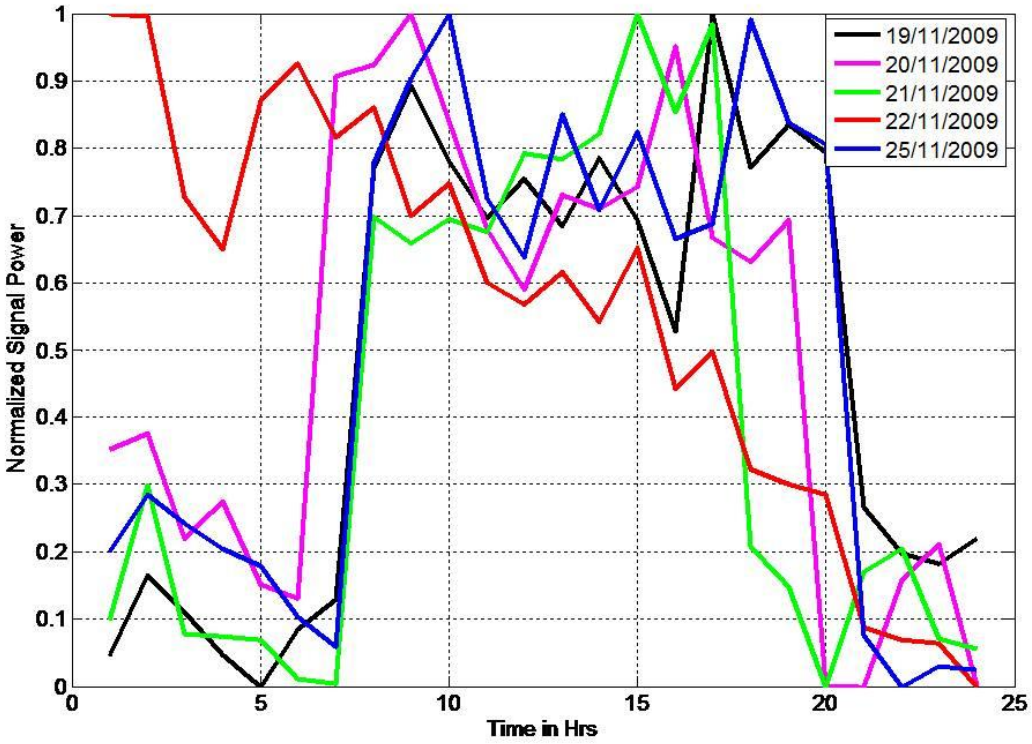


Figure 8-32 Signal power trend for 24 hours in substation end B

### 8.5.2 Fast rising pulses from substation end B

A typical fast rising pulse from both substation end A and substation end B is shown in Figure 8-33. The frequency spectrum of the pulse is shown in Figure 8-34. Both pulses exhibit a similar waveform signature which has negative excursion followed by an oscillation. The pulse from substation end A has a higher negative peak compared to substation end B pulse. In substation end B, pulse oscillations after the negative pulse are much slower than that of the substation end A . Based on the frequency spectrum depicted in Figure 8-34 , higher order frequency components are attenuated.

Statistical parameters (mean, standard deviation, skewness and kurtosis) of 50 numbers of pulses form substation end B are calculated and are compared with substation end A data from the earth strap. Results are included in Figure 8-35 to Figure 8-38. Based on Figure 8-37 skewness of both data are in agreement.

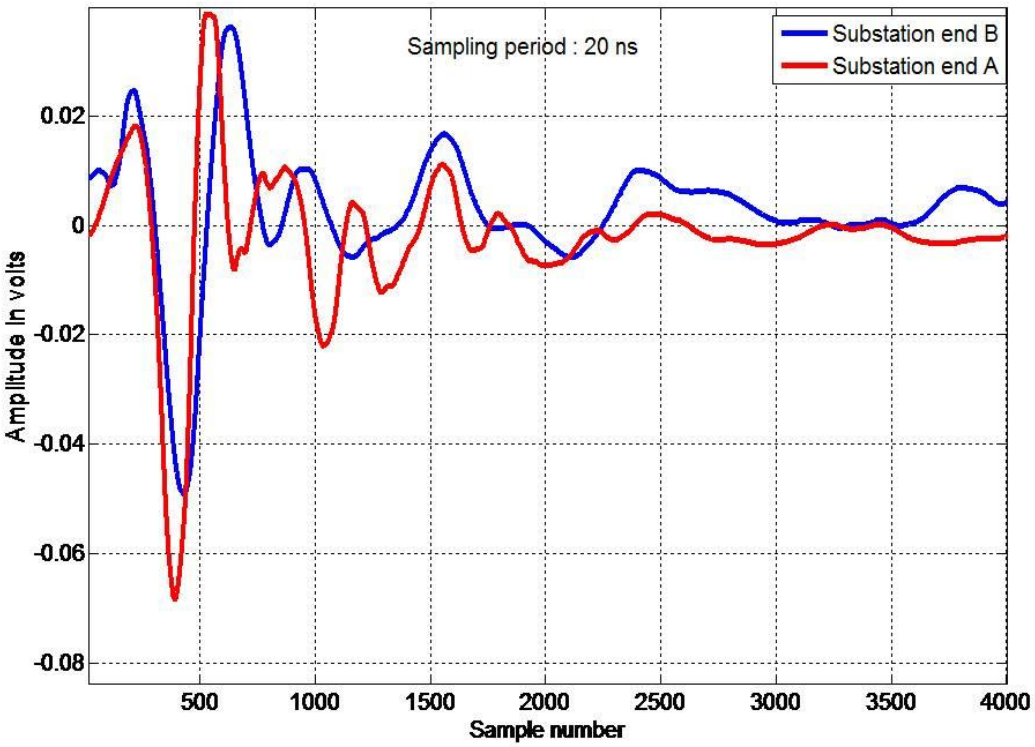


Figure 8-33 Typical pulses from substation end A and substation end B

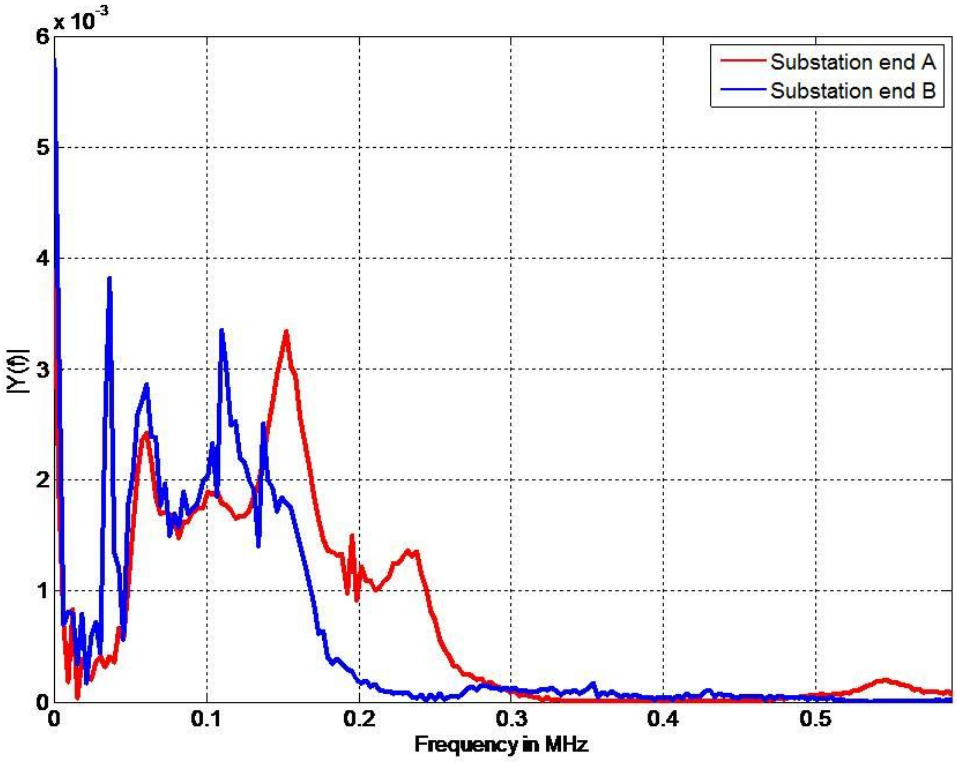


Figure 8-34 Frequency spectrum of the pulse, substation end A and substation end B

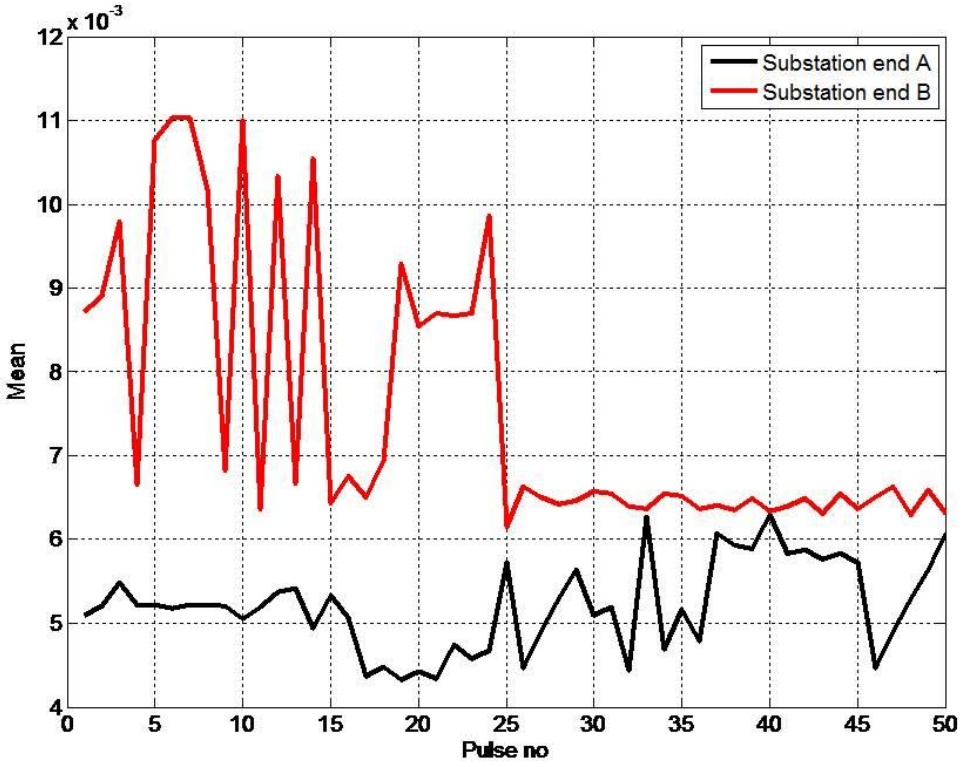


Figure 8-35 Statistical parameters – Mean

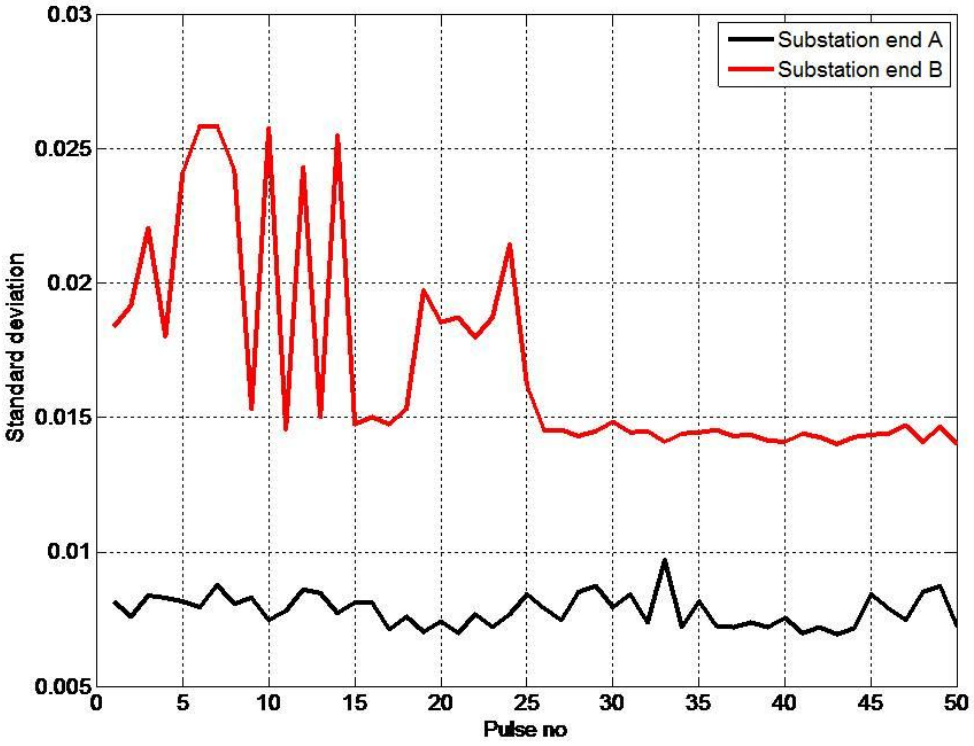


Figure 8-36 Statistical parameters - Standard deviation

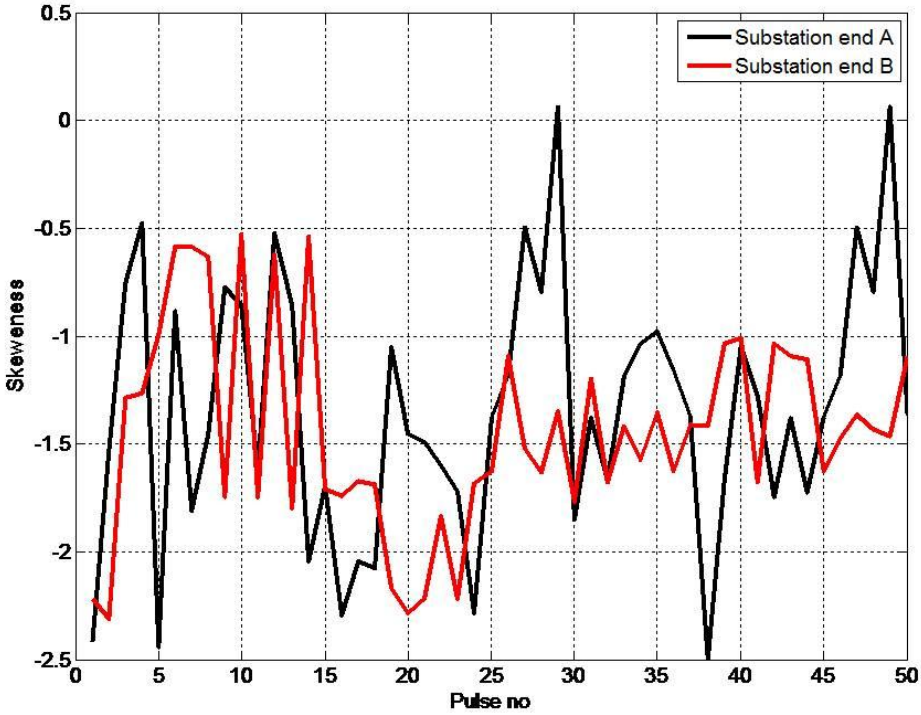


Figure 8-37 Statistical parameters -Skewness

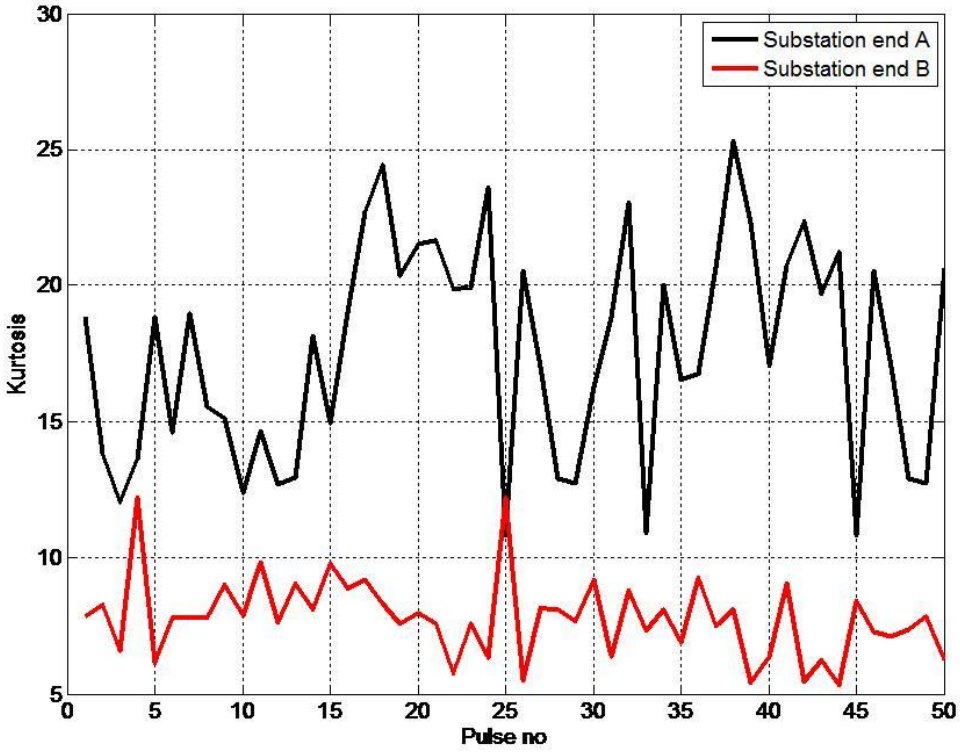


Figure 8-38 Statistical parameters - Kurtosis

## 8.6 Conclusion

Extracting PD information from the raw data is a two fold process namely denoising and data interpretation. In this chapter data acquired from the substation end A and substation end B using the developed PD montiring sytsem were analysed using the PD data interpreation alogorithm developed in Matlab. This method of PD interpreation split the raw data into segments of length $\pi$ followed by analysing the necessary parameters required to ascertain the PD signature. Parameters included in the PD signal interpretation are rise time, pulse width, PD pulse polarity, PRPD and load current correlation.

Based on the data acquired from the cable, signal power with respect to load current exhibits different patterns over time. Data from both substation end are enriched in AM radio transmission stations having frequency range 1MHz to 1.21 MHz. Similar frequency components were present in the data acquired from PFCT and HFCT. Also same repetition rate was seen from both data sets acquired from HFCT and PFCT. Furhermore, a high degree of correlation in time and frequency domain is seen for the typical fast rising pulses and switching noise extrcated from both of these sensors. Based on FRA and frequency power spectrum of on-site measurements, there is good potential for using PFCTs for detecting fast rising signals like PD from cables.

PRPD patterns are widely used for the charcaterisation of PD pulses using phase of the system voltage. However in RPDMS, load current was used as referrence which is mainly used to study the interdependancy of PD actvity with cable loading. Based on PRPD using load current as referrence, fast rising pulses from all the three phases and earth strap are scattered throughout the 360 degree phase window. There are three possibilites for such a distributed PRPD pattern such as multiple discharge sources in the cable with different inception voltages, there exists heterogenity of phase shift between system voltage and load current and finally the uneven distribution of charges during PD in case of three core cables. In addition to that, timing signature of extrcated pulse exhbits higher oscillations which are not monopolar. Based on the timing signatures, polarity dependence of phase angle and historical record of PD activity by the utility, pulses extracted from the substation end A and substation end B data are more likely originated away from the cable under test.

# Chapter 9 :
# Summary,Conclusions and Future Recommendations

This chapter summarises the research project presented in this thesis, identifies conclusions that may be drawn and indicates the direction of potential future Investigations.

## 9.1 Summary and conclusions

- This research project was focussed on the problems associated with online PD detection for medium voltage underground cables. The original contributions to the research community are: possibility of considering pre-installed PFCT for PD detection, improve the exisiting remote controlled on-line PD detction system, non invasive method of discarding a PD pulse from neighbouring cables, a novel double ended PD detection system with GPS synchronization, signal processing tools to enhance rapidly varying PD signals from the raw data and data interpretation algorithm for conforming the PD activity from the data acquired.

- Insulation degradation in cables or any high voltage equipment is caused by PD's. Such discharges do not completely bridges the electrodes in between the insulation. PD's can be triggered from normal working conditions in high voltage equipment which is due to the ageing of the insulator, stresses (electrical/thermal) in the insulation, improper insulation due to poor workmanship, and contaminants in the insulator such as metal particles and voids. PD's in cables can be detected using non-electrical and electrical methods. Electrical methods of PD detection using inductive couplers as a non-invasive technique are widely used since non-electrical detection of PD activity cannot able to locate the origin of the PD source. Though PD detection in cables using inductive couplers is easy to impelement, older switchgear with

completely bonded design, crosslinking of switchgear earth and substation earth often limits this technique to detect PD's from cables.

- Analysis and detection of PDs in cables is often hampered by noise in the signal which the process of extracting PD from the raw data a more difficult task.Various signal processing tools are used to denoise raw data acquired from cables. Due to stochastic nature of PD actvity and hardware requirements , design of digital signal processor for denoising PD signals from cables require experience in on -site PD signals. Matched filters apply cross correlating method between information to be extracted and filter kernel. Various sources of interference namely propagation characteristics of cable, PDs from neighbouring cable, transient noise sources which exhibits similar PD signatures makes difficult to select filter kernel. Filter coefficients defined in adaptive filter are updated with priory information. Though this method of denoising is applied to PD diagnostics, computational complexity and hardware resources requirement makes this method less suitable for on-line PD diagnostics. Data driven technique termed as EMD is basically an adapative technique which finds limited applications in denoising PD signals due to computational complexity.

  Denoising of PD signals using SGWT is relatively faster then classically DWT and also customization of filter cofficients in SGWT enhances the PD signals which provides better PD signature extraction. Wavelet Wavelet based techniques need an optimum wavelet base which maximizes the coefficient values within the time-scale (frequency) domain. Also the optimum level of decomposition is often selected manually which makes this approach semi-automatic.

  In this thesis a denoising algorithm using SGWT based on kurtosis based thresholding with stopping criterion was proposed. Performance of this algorithm was verified using synthetic and on-site data. For signals with low SNR, a KBT based denoising algorithm performs better compared to the existing thresholding methods. However, denoising by DWT produces a smoother appearance over KBT which is determined by the level of decomposition in DWT. This may lead to loss of PD signature and loss of edges in DWT based

denoising. This will have implications on PD quantification and PD source location.

- Older switchgear with completely bonded design, crosslinking of switchgear earth and substation earth often limits on-line PD detection in cables. In this thesis PD detection using pre-installed PFCT in cable networks for measurement/protection purposes was investigated by conducting FRA and on-site measurements. Results of the FRA shows increased gain from 1MHz onwards. This approach was validated by comparing the data acquired from the cable network at a 33/11 kV substation using both PFCT and HFCT. One of the problems that arose during the on site trial was the logistics and conforming to the regulations or protocols of the utility company. The process of acquiring online field data was tedious and many negotiations were performed before the final agreement was reached. Moreover on-line PD detection using PFCT is not starightforward since it is asscociated with protection issues. Hence RPDMS was developed. One of the other requirement in designing RPDMS was for continuous monitoring of PD without frequent site access. This is achieved using remote control and remote database storage. Other advantages of this system includes protection circuitry in the RPDMS maintains a constant burden across the PFCT and a health check algorithm isolates the systems in the event of faults. The flexible data transfer algorithm implemented in the RPDMS can transfer a large volume of data even with slow speed internet connection, and database storage of raw data makes easier handling and organisation of the data. Data acquired using RPDMS were denoised using a KBT based denoising algorithm using SGWT. Denoised data was analysed using a data interpretation algorithm formulated based on the properties of PD. This algorithm extracts the necessary parameters such as rise time, pulse width, PD pulse polarity, PRPD and load current correlation to ascertain the PD signature. Based on the analysis of several datasets acquired using HFCT and PFCT, both of these sensors detect similar time domain signatures having a rise time in the order of 500ns. In addition, datasets from both of these sensors follows a similar frequency spectrum. Similar switching noise signatures in both time and frequency domain were seen from the data acquired using both of these sensors. Hence based on

the laboratory results and on-site measurements, PFCT can be considered for detecting PD's in cables. This method of using a preinstalled PFCT (originally installed for protection or instrumentation purposes) to detect PD is not only a cost effective solution but also offers a non invasive method of detecting PD in cable cores irrespective of switchgear design.

- PRPD patterns are widely used for the characterisation of PD pulses using the phase of the system voltage. However in RPDMS, load current was used as the reference study the interdependancy of PD actvity with cable loading. Due to the limitation in hardware, voltage reference was not available. Based on the PRPD using load current as reference, fast rising pulses from all the three phases and earth strap are scattered throughout the 360 degree phase window. This could be due to multiple discharge sources in the cable with different inception voltages, or the existance of heterogeneous phase shift between system voltage and load current,or finally the uneven distribution of charges during PD in case of three core cables. In addition to that, timing signatures of fast rising pulses extracted exhibit higher oscillations which are almost multipolar. Based on the timing signatures, polarity dependence of phase angle and the historical record of PD activity by the utility company, pulses extracted from the substation end A and substation end B were more likely originated away from the cable under test.

- Success rate of PD daignostics depends upon the accuracy in PD source location which would reduce CI cost, CML cost and regulatory penalties. Single ended and double-ended methods based on TDR are widely used to locate PD sources. Accuracy of PD source location using the single ended method is determined by the signal power of the reflected pulse, which depends upon the impedance mismatch between the cable and termination, attenuation and dispersion in the cable and the dynamic range of the data acquisition system. In double-ended PD location method, incident PD pulses from measurement units at both ends of the cable are measured. Hence, uncertainties introduced by propagation channel effects, cable network structure and cable length is reduced. However, double ended PD detection methods are less common due to their complexity in system design, time synchronization and the communication link required between

measurement systems. Both of these methods suffer in distinguishing PD pulses from the neighbouring cable sections. Various invasive methods to discard PD pulses from the neighbouring cable were reviewed. A non invasive method of using a dual measurement unit was proposed with supporting simulation results. This method can distinguish PD from the neighbouring cable. However this method needs mutliple data acqusition systems with higher sampling rates which will eventually increase the cost of PD diagnostics. The cost of the system is negligible compared to CI and CML costs.

- Double ended PD source location with feasible and accurate time synchronization is the most suitable technique for on-line PD source location. A novel double ended PD detection system using the TBTL method based on GPS was proposed. This system acquires the data from both ends of the cable for a specific 1PPS from a GPS receiver using TBTL. Furthermore tracking of invalid data caused by flywheel 1PPS due to temporary loss of satellite signal can reduce PD source location accuracies which cannot be achieved using a conventional method of PD source location using flywheel 1PPS. With the use of communication between two PDDN's, invalid data acquiring is eliminated. Based on the measurements from laboratory and on-site, the proposed system with TBTL shows good PD source location accuracy compared to the conventional double ended PD source location methods. This system can be used to locate PD's with an error margin of less than ± 10 meters from the discharge source which would reduce the CI and CML costs. Further advantages of this system include low cost and portability compared with existing approaches to PD source location.

## 9.2 Recommendations For Future Work

During the course of this research, several aspects of research that may prompt future investigations have been discovered. Some of these aspects are the subsequent effects of the contributions made in this thesis.

- PFCTs are capable of detecting fast varying signals and have been verified using the laboratory and on-site results. However magnitude response of FRA from 1 MHz onwards does not exhibit flat trend rather a gradual increasing trend. This would have implication in quantifying discharge magnitude which eventually affects prognostics. Presence of inductive component in the CT burden affects the frequency response of PFCT. Hence in case of using PFCT as a PD sensor in cables, it is recommended to quantify the burden so that PFCTs can be characterized. Hence, it is necessary to calibrate the PFCTs before on-site PD measurement.

- Commercial data acquisition cards used in RPDMS has two analogue channels with a sampling frequency of 50 Msps which can get the synchronized PD data from two phases of the three core cable. Due to the absence of voltage reference measurement, PRPD patterns cannot be developed which is the most valuable tool for analyzing the PD signals from the raw data. Hence it is found that there is a necessity to upgrade the data acquisition card with three channels with an option to trigger using the system voltage. Furthermore, more on-site trials need to be attempted for testing the robustness of this approach.

- In RPDMS, data acquisition acquires the raw data for four power frequency cycles which occupies hard drive space of the order of 60 Mbytes. Though the flexible data transfer algorithm is successful in transferring such large volume of data via mobile broadband, this will increase the broadband cost and consumption hard drive space. Hence on-site signal processing needs to be implemented in RPDMS

- A double ended PD monitoring system with TBTL was successfully implemented on-site and the system shows higher PD source location accuracy. However due to time and hardware limitations, few functionalities like self-test logic, auto gain controllers and ADC protection are not implemented. This will affect the robustness of the system. Also laptops used in this system for control, reduce the portability. Hence it would be necessary to follow the design discussed in section 6.4.

- ADC used in the double ended PD monitoring system has a single channel. This needs to be upgraded with five analogue channels so that PD's from all the three cores, system voltage and load current can be monitored. Also the software developed for control of the hardware is based on a windows platform. It has been found that there is a necessity to consider for platform independency so that smart phones or tablet PCs can also be used for controlling the hardware. Due to the restrictions from the network owner, the double ended PD monitoring system was tested at one end of the cable. It is important to consider more site trials using both ends of the cable network.

- Denoising based on KBT using SGWT has been applied successfully to synthetic and raw data using a db5 wavelet base. Though this algorithm has been able to maintain time domain signatures, it is necessary to simulate this method for various wavelet basis functions. From this, there would be a potential to choose an optimum wavelet base which gives the highest degree of correlation with wavelet signatures to be extracted from the raw data. Also the algorithm needs to be tested with data from various cable networks.

# References

1996]. "IEEE Guide for the Application of Current Transformers Used for Protective Relaying Purposes." *IEEE Std C37.110-1996*: *i-59*.

[60270, B. E. 2001]. "High-voltage test techniques - Partial discharge measurements " *BS EN 60270:2001 IEC 60270:2000*

[Abbruzzese, G. 1989]. "Metallurgical conditions for development of adequate magnetic properties in grain oriented silicon iron." *Magnetics, IEEE Transactions on 25(5)*: *3955-3957*.

[Afonso, V. X. and W. J. Tompkins 1995]. "Detecting ventricular fibrillation." *Engineering in Medicine and Biology Magazine, IEEE 14(2)*: *152-159*.

[Alkan, R. M., H. Karaman, et al. 2005]. GPS, GALILEO and GLONASS satellite navigation systems & GPS modernization. *Recent Advances in Space Technologies, 2005. RAST 2005. Proceedings of 2nd International Conference on*.

[Anestis Antoniadis, J. B. 2001]. "Wavelet Estimators in Nonparametric Regression: A Comparative Simulation Study." *Journal of Statistical Software Vol. 6, Issue 6, Jun 2001*.

[Ariastina, W. G., R. H. Khawaja, et al. 2003]. The statistical properties of PD distribution in oil-impregnated insulation at elevated temperature. *Proceedings of the 7th International Conference on Properties and Applications of Dielectric Materials, 2003.*

[Bai, Y. 2005]. The Windows Serial Port Programming Handbook. *London, Auerbach publications*.

[Baker, P. C., M. D. Judd, et al. 2010]. "A frequency-based RF partial discharge detector for low-power wireless sensing." *Dielectrics and Electrical Insulation, IEEE Transactions on 17(1)*: *133-140*.

[Balch, M. 2003]. Complete Digital Design. *New York, McGraw Hill*.

[Battacharya, R. 2011]. Electrical Thermal And Thermo Mechanical Design Of Mv Cables. *Jicable'11 - 8th International Conference on Power Insulated Cables June 23, 2011, Versailles, France, JICABLE*.

[Bellanger, M. G. 2001]. Adaptive Digital Filters, *Marcel Dekker, Inc*.

[Berns, H. C. and R. J. Wilkes 2000]. "GPS time synchronization system for K2K." *Nuclear Science, IEEE Transactions on 47(2)*: *340-343*.

[Bewley, L. V. 1931]. "Traveling Waves on Transmission Systems." *Transactions of the American Institute of Electrical Engineers 50(2)*: *532-550*.

[Bodega, R. M., P. H. F.Lazzaroni, M.Wester, F. J. 2004]. "PD recurrence in cavities at different energizing methods." *IEEE Transactions on Instrumentation and Measurement 53(2)*: *251-258*.

[Bogg, S. A. 1990]. "Partial dischare - part 2 detection sensitivity." *IEEE Electrical Insulation Magazine 6(5)*.

[Boggs, S. A. 1990] "Partial discharge - Part 3 cavity induced PD in solid dielectrics ".

[Boggs, S. A., Stone, G. C. 1982]. "Fundamental Limitations in the Measurement of Corona and Partial Discharge." *IEEE Transactions on Electrical Insulation EI-17(2)*: *143-150*.

[Bojan Angelov , B. R. 2010]. "The Progression of WiMAX Toward a Peer-to-Peer Paradigm Shift " *CiteseerX*.

[C. Valens 1999]. "The Fast Lifting Wavelet Transform." *Citeseerx*.

[Cadence 2011] "CLOCK DOMAIN CROSSING."

[Carl Eastham , C. S., Fa-Chung Chen 2011]. Detection and Location of PD In MV Cables In Electrically Noisy Industrial Environments. *CIRED , 21st International Conference on Electricity Distribution, Frankfurt*

[Carpenter, K. H. 1991]. "A differential equation approach to minor loops in the Jiles-Atherton hysteresis model." *IEEE Transactions on Magnetics 27(6)*: *4404-4406*.

[Catterson, V. M. M., S.Judd, M. D.Zaher, A. S. 2008]. "Managing Remote Online Partial Discharge Data." *IEEE Transactions on Power Delivery 23(4)*: *1754-1762*.

[Cavallini, A., G. C. Montanari, et al. 2007]. "A novel method to locate PD in polymeric cable systems based on amplitude-frequency (AF) map." *Dielectrics and Electrical Insulation, IEEE Transactions on 14(3)*: *726-734*.

[Chang, S. G., Y. Bin, et al. 2000]. "Spatially adaptive wavelet thresholding with context modeling for image denoising." *IEEE Transactions on Image Processing 9(9)*: *1522-1531*.

[Claypoole, R. L., Jr., R. G. Baraniuk, et al. 1998]. Adaptive wavelet transforms via lifting. *Proceedings of the 1998 IEEE International Conference on Acoustics, Speech and Signal Processing, 1998.* .

[Cliff Walton, S. C., Mathew Michel and Carl Eastham 2009]. Avoidance of MV switchgear failure case studies of on-line condition monitoring. *CIRED ,20 th International conference on electricity distribution, Paper no : 0422*.

[Company, H.-P. 1997] "Traveling Wave Fault Location in Power Transmission Systems."

[Cooray, V. 2000]. "Charge and voltage characteristics of corona discharges in a coaxial geometry." *IEEE Transactions on Dielectrics and Electrical Insulation 7(6)*: *734-743*.

[Copeland, M. S., G. 1966]. "Minor loop loss predictions in devices using permanent magnet materials." *IEEE Transactions on Magnetics 2(3)*: *420-423*.

[Crichton, G. C., P. W. Karlsson, et al. 1989]. "Partial discharges in ellipsoidal and spheroidal voids." *IEEE Transactions on Electrical Insulation 24(2)*: *335-342*.

[Daubechies, I. 1990]. "The wavelet transform, time-frequency localization and signal analysis." *IEEE Transactions on Information Theory 36(5)*: *961-1005*.

[David L. Donoho , I. M. J., Gerard Kerkyacharian , Dominique Picard 1995]. "Wavelet Shrinkage: Asymptopia?" *CiteseerX*.

[Delechelle, E., J. Lemoine, et al. 2005]. "Empirical mode decomposition: an analytical approach for sifting process." *IEEE Signal Processing Letters 12(11)*: *764-767*.

[Doberstein, D. 2011]. Fundamentals of GPS Receivers a Hardware Approach. *California, United States, DKD Instruments & Independent Publisher Services*.

[Dobrogowski, A. and M. Kasznia 2002]. "Maximum time interval error assessment based on the sequential reducing data volume." *IEEE Transactions on Ultrasonics, Ferroelectrics and Frequency Control 49(7)*: *987-994*.

[Dong-Jun, W., C. Il-Yop, et al. 2002]. Development of power quality monitoring system with central processing scheme. *IEEE Power Engineering Society Summer Meeting, 2002*.

[Donoho, D. L. 1995]. "De-noising by soft-thresholding." *IEEE Transactions on Information Theory 41(3)*: *613-627*.

[E. Kuffel, W. S. Z., J. Kuffel 2006]. High Voltage Engineering Fundamentals. *Oxford, Butterworth-Heinemann*.

[Ercegovac, A. F. T. M. D. 1997]. "Synchronous Up/Down Binary Counter for LUT FPGAs with Counting Frequency independent of counter size." *IEEE Transactions on VLSI systems*.

[Ericsson 2009]. Universal Cable Handbook. *Sweden, Ericsson Cables & Interconnect*.

[F P Mohamed, W. H. S., K.Y. Liu, S.S.Strachan, Neil. Donald, Jamie McWilliams 2011]. Investigation of power frequency current transformer as partial discharge sensor in medium voltage cables. *8 th international conferrence on insulated power cables, Versailles, France*.

[F.Ramsey, N. 1983]. "History of atomic clocks." *Journal of research of the national buraeu of standards 8(5)*: *301-320*.

[F.W.Peek 1920]. Dielectric phenomena in high voltage engineering, *McGraw-hill book company 1920 p.48*.

[Farrow, C. 2008] "Absolute Timing Integrity Monitoring Using a Multiple Reference Mash-Up."

[Fastrax 2011] "Fastrax IT520 datasheet."

[Federic Leuser, V. L., Matthieu surdon 2011]. Economical design of cable conductors *Jicable'11 - 8th International Conference on Power Insulated Cables June 23, 2011, Versailles, France, JICABLE*.

[Ferrara, E. and B. Widrow 1981]. "The time-sequenced adaptive filter." *IEEE Transactions on circuits and systems 28(6)*: *519-523*.

[Ferrari, P., A. Flammini, et al. 2008]. Non invasive time synchronization for ZigBee Wireless Sensor Networks. *IEEE International Symposium on Precision Clock Synchronization for Measurement, Control and Communication, 2008. ISPCS 2008.*

[Institution. 2012]). "Frequency finder UK." *from http://frequencyfinder.org.uk/tc/glasgow.html*.

[Foley, J. B. and F. M. Boland 1987]. "Comparison between steepest descent and LMS algorithms in adaptive filters." *IEE Proceedings of Communications, Radar and Signal Processing 134(3)*: *283-289*.

[Foo, D. 2003]. Online Partial Discharge Detection and ,Signal Analysis for High Voltage Cables. PhD, *University of Strathclyde, Andersonian Library Thesis reference*.

[Francois Gahungu, P. S., Pierre Mirebeu 2011]. Performance test on large conductor connectors. *Jicable'11 - 8th International Conference on Power Insulated Cables June 23, 2011, Versailles, France, JICABLE*.

[Ftdi 2010] "FTDI , UM 232R data sheet."

[Gary stevens, B. p., Janet Thomas,Mike Fairhurst,Ankit Gorwadia
2011]. Whole life costs and environmental assessment of high voltage power cable systems. *Jicable'11 - 8th International Conference on Power Insulated Cables June 23, 2011, Versailles, France, JICABLE*.

[Gavazza, R. J. and C. M. Wiggins 1996]. "Reduction of interference on substation low voltage wiring." *Power Delivery, IEEE Transactions on 11(3)*: *1317-1329*.

[Geraldo De Almedia, L. C. Z., Carla Dasmackeno peixoto,Athyede macedo 2011]. Backfill replacement save underground transmission lines cost and postpone investments. *JICABLE '11, 8 th international conferrence on insulated power cables., Versailles, France, JICABLE*.

[Ginosar, R. 2011]. "Metastability and Synchronizers: A Tutorial." *IEEE Design & Test of Computers 28(5)*: *23-35*.

[Giscard F. C. Veloso, L. E. B. d. S., Ismael Noronha, Germano Labert Torres 2009]. "Detecting Partial Discharges Using Empirical Mode Decomposition."

[GJ Catlin, H. D. S. 2010]. Practical Application of Tan Delta Diagnostic Testing In Cables. *Conference on Power Cables CABLE TECH 2010*.

[Gottin, B., C. Ioana, et al. 2009]. "Detection and localization of transient sources: comparative study of complex-lag distribution concept versus wavelets and spectrogram-based methods." *EURASIP J. Adv. Signal Process 2009(doi:10.1155/2009/864185)*: *4-4*.

[Gracias, D. J. 1994]. Historical review of UK MV (11-33 kV) cable designs. *IEE Colloquium on Design of Medium Voltage Polymeric Cables*.

[Gross, D. W. and B. A. Fruth 1998]. Characteristics of phase resolved partial discharge pattern in spherical voids. *Annual Report. Conference on Electrical Insulation and Dielectric Phenomena, 1998.* .

[Grundgeiger, D. 2002]. Programming Visual Basic .NET, *O'Reilly*.

[Gu, J. 2009]. Wavelet Threshold De-noising of Power Quality Signals. *Fifth International Conference on Natural Computation, 2009. ICNC '09.*

[guide, I. 2005]. "IEEE Guide for Field Testing of Shielded Power Cable Systems Using Very Low Frequency (VLF)." *IEEE Std 400.2-2004*: *0_1-22*.

[Gulski, E., J. J. Smit, et al. 1998]. PD measurements on-site using oscillating wave test system. *IEEE International Symposium on Electrical Insulation, 1998*.

[Gulski, E., J. J. Smit, et al. 2005]. "PD knowledge rules for insulation condition assessment of distribution power cables." *IEEE Transactions on Dielectrics and Electrical Insulation 12(2)*: *223-239*.

[Guven, S. 2012]. PD pattern classification system in GIS using adaptive neuro fuzzy inferrence system. Msc, *National Taiwan University of Science and Technology , Thesis referrence*.

[Hao, L., P. L. Lewin, et al. 2011]. "Discrimination of multiple PD sources using wavelet decomposition and principal component analysis." *Dielectrics and Electrical Insulation, IEEE Transactions on 18(5)*: *1702-1711*.

[Hao, Z., T. R. Blackburn, et al. 2007]. "A novel wavelet transform technique for on-line partial discharge measurements. 1. WT de-noising algorithm." *IEEE Transactions on Dielectrics and Electrical Insulation 14(1)*: *3-14*.

[He, Q., Y. Liu, et al. 2011]. "Machine fault signature analysis by midpoint-based empirical mode decomposition." *IET Measurement Science and Technology 22(1)*: *015702*.

[Helwig, A., G. Offermans, et al. 2006]. LORADD UTC timing trials & developments. *LA – 35 th Convention and Technical Symposium, Groton, CT, Groton, CT*.

[Hemmati, E. and S. M. Shahrtash 2012]. Evaluation of unshielded Rogowski coil for measuring partial discharge signals. *Environment and Electrical Engineering (EEEIC), 2012 11th International Conference on*.

[Hewlett-Packard 1996] "Eye Diagrams and Sampling Oscilloscopes." *Hewlett-Packard Journal*.

[HVPD 2009] "HVPD Technical Guide for PD Levels in MV and HV Cables and Joints."

[Ivy Shim, J. J. S., W.H.siew 2000]. Signal Processing Techniques for Partial Discharge Detection and Mapping in High Voltage Phd *University of Strathclyde,Andersonian Library Thesis referrence (T10243)*.

[Jaideva C. Goswami, A., K. Chan 2010]. Fundamentals of Wavelets Theory, Algorithms, and Applications. *New Jersey, John Wiley & Sons, Inc*.

[Jiles, D. 1998]. Introduction to magnetism and magnetic materials second edition, *Chapman and Hall London 1998*.

[Jiles, D. C. 1994]. "Frequency dependence of hysteresis curves in conducting magnetic materials." *Journal of applied physics 76(10)*: *5849-5855*.

[Jiles, D. C., J. B. Thoelke, et al. 1992]. "Numerical determination of hysteresis parameters for the modeling of magnetic properties using the theory of ferromagnetic hysteresis." *IEEE Transactions on Magnetics 28(1)*: *27-35*.

[Jones, W. D. 2011]. "The ultimate in precision--the cesium clock--has been miniaturized." *IEEE spectrum, March 2011*.

[Judd, M. D., Y. Li, et al. 2005]. "Partial discharge monitoring for power transformer using UHF sensors. Part 2: field experience." *Electrical Insulation Magazine, IEEE 21(3)*: *5-13*.

[Kaplan, E. D. and C. J. Hegarty 2006]. Understanding GPS Principles and Applications. *Boston, Artech house, Boston*.

[Karmakar, S., N. K. Roy, et al. 2009]. Partial discharge measurement of transformer with ICT facilities. *International Conference on Power Systems, 2009. ICPS '09.* .

[Kemp, I. J. 1995]. "Partial discharge plant-monitoring technology: present and future developments." *IEE Proceedings Science, Measurement and Technology 142(1)*: *4-10*.

[Kwak, H., B. Lee, et al. 1999]. "Effects of multithreading on cache performance." *IEEE Transactions onComputers 48(2)*: *176-184*.

[Kwang Hoi Ku, K. C. C., Seyung bum kwon ,Jae soon lee, 2011]. Developments of new recyclable material for power cable. *Jicable'11 - 8th International Conference on Power Insulated Cables June 23, 2011, Versailles, France, JICABLE*.

[Lee Renforth, R. M., Malcolm Seltzer-Grant 2009]. Deployment of Distributed On-Line Partial Discharge Monitoring Devices on Medium Voltage Electricity Networks. *20 th International Conference on Electricity Distribution, Prague,*.

[Lelekakis, N., D. Martin, et al. 2011]. "Comparison of dissolved gas-in-oil analysis methods using a dissolved gas-in-oil standard." *IEEE Electrical Insulation Magazine 27(5)*: *29-35*.

[Lemke, E., T. Strehl, et al. 1999]. New developments in the field of PD detection and location in power cables under on-site condition. *Eleventh International Symposium on High Voltage Engineering, 1999 (Conf. Publ. No. 467)*.

[Liu, K. Y. 2009]. Design and Implementation of Automatic Wireless High-speed Data Acquisition System for EMI Measurements in Power Substations PhD, *University of Strathclyde, Andersonian Library Theses Moratorium (T12402 )*.

[Liu, K. Y., W. H. Siew, et al. 2010]. Wireless distributed EMI measurement system. *Asia-Pacific Symposium on Electromagnetic Compatibility (APEMC), 2010*

[Liu Ying, L. M., Cao Xialolong,Xu Yang, Xian 2011]. Evalauation of magnetic induction on pipe-lines by ac power cable circuits. *Jicable'11 - 8th International Conference on Power Insulated Cables June 23, 2011, Versailles, France, JICABLE*.

[Lowe, R. D. 1968]. "Portable, Rugged Cable Fault Locator For VHF Communications and CATV " *HEWLETT-PACKARD JOURNAL June volume 20 -Number 10 Copr 1949-1998 Hewlett-Packard Co*.

[Ltd, H. V. P. D. 2009] "Application Notes for On-Line Partial Discharge (PD) Testing of Medium Voltage (MV) Switchgear With the HVPD Longshot TM PD 'Spot' Tester."

[Lundback, J., S. Nordebo, et al. 2008]. "A Digital Directional Coupler With Applications to Partial Discharge Measurements." *IEEE Transactions on Instrumentation and Measurement 57(11)*: *2561-2567*.

[M. Muhr, R. S. 2009]. "Experience with optical partial discharge detection." *Materials Science-Poland Vol. 27, No. 4/2*: *1139-1146*.

[M.C.E . Rosas orea M Hernandezdias Universidad de las Américas, P. 2005]. A Comparative Simulation Study of Wavelet Based Denoising Algorithms. *Proceedings of the 15th International Conference on Electronics, Communications and Computers (CONIELECOMP 2005)*

[M.E. Ardeleanu , A. M., Gh. Opran, Al. Manta, D. Popa 2008]. On Damped A.C. Voltage Use for On-Site Measurement of Partial Discharges in HV Equipment Insulation *2 nd International Conference on Modern Power Systems Mps 2008, , CLUJ -NAPOCA, ROMANIA*

[Ma, X., C. Zhou, et al. 2002]. "Automated wavelet selection and thresholding for PD detection." *IEEE Electrical Insulation Magazine 18(2)*: *37-45*.

[Makky, A. R. A. M., H. Abo-Zied, et al. 2008]. Design of the instrument current transformer for high frequency high power applications. *12th International Middle-East Power System Conference, 2008. MEPCON 2008*.

[Mallat, S. G. 1989]. "A theory for multiresolution signal decomposition: the wavelet representation." *IEEE Transactions on Pattern Analysis and Machine Intelligence 11(7)*: *674-693*.

[Mazen Abdel-Salam, H. A., Ahdab El-Morshedy, Roshdy Radwan 2012]. High voltage engineering Theory and Practice. *New York, CRC Press, 31 Aug 2000 - Technology & Engineering*.

[McAllister, I. W. 1997]. "Partial discharges in spheroidal voids. Void orientation." *IEEE Transactions on Dielectrics and Electrical Insulation 4(4)*: *456-461*.

[Mehta, K. P. a. N. 2003]. Programmable Logic Design, Quck start handbook, *Xilinx*.

[Mellon, U. o. C. 2010]. "Department of Statistics Lecture notes." *Chapter 8, Minimax theory*.

[Michel, M. 2007] "EDF energy Identifies high-risk cable sections."

[Micron 2011] "Async/Page/Burst CellularRAMTM 1.5MT45W8MW16BGX."

[Mohamed, F. P., W. H. Siew, et al. 2009]. High frequency modeling of protection / measurement current transformers for partial discharge detection. *Proceedings of the 44th International Universities Power Engineering Conference (UPEC), 2009*

[Mohamed, F. P., W. H. Siew, et al. 2011]. Improved Algorithm for on-line Partial Discharge Location in Cables. *CIRED, 21st International Conference on Electricity Distribution, Frankfurt, Germany*.

[Mohamed, F. P., W. H. Siew, et al. 2012]. Synchronised power quality monitoring system using global positioning system (GPS). *Asia-Pacific Symposium on Electromagnetic Compatibility (APEMC), 2012*

[Moore, D. A. a. H. 2004]. Electric Power Transformer Engineering Second Edition, *CRC Press LLC*.

[Moore, G. F. 2006]. Electric Cables Handbook *Oxford, United Kingdom, Blackwell Science*

[Moore, P. J., I. E. Portugues, et al. 2006]. "Partial discharge investigation of a power transformer using wireless wideband radio-frequency measurements." *IEEE Transactions on Power Delivery 21(1)*: *528-530*.

[Musa, B. U., S. Wah Hoon, et al. 2010]. "Computation of Transient Electromagnetic Fields Due to Switching in High-Voltage Substations." *IEEE Transactions on Power Delivery 25(2)*: *1154-1161*.

[Naus, H. W. L. 2002]. "Ferromagnetic hysteresis and the effective field." *IEEE Transactions on Magnetics 38(5)*: *3417-3419*.

[Niang, O., Dele, et al. 2010]. "A Spectral Approach for Sifting Process in Empirical Mode Decomposition." *IEEE Transactions on Signal Processing 58(11)*: *5612-5623*.

[Norden E. Huang1, Z. S., Steven R. Long3, Manli C. W u4, Hsing H. Shih5, Quanan Zheng6, Nai-Chyuan Yen7, Chi Chao Tung8 and Henry H. Liu9 1998]. "The empirical mode decomposition and the Hilbert spectrum for nonlinear and non-stationary time series analysis." *Royal society NASA Proc. R. Soc. Lond.A (1998) 454*: *903-995*.

[Okubo, H., N. Hayakawa, et al. 2002]. "The relationship between partial discharge current pulse waveforms and physical mechanisms." *IEEE Electrical Insulation Magazine 18(3)*: *38-45*.

[Pesquet, J. C., H. Krim, et al. 1996]. "Time-invariant orthonormal wavelet representations." *IEEE Transactions on Signal Processing 44(8)*: *1964-1970*.

[Ponniran, A. K., M. S. 2008]. Study on the performance of underground XLPE cables in service based on tan delta and capacitance measurements. *IEEE 2nd International on Power and Energy Conference, 2008. PECon 2008*.

[Qu, T., S. Wang, et al. 2002]. Adaptive denoising based on wavelet thresholding method. *6th International Conference on Signal Processing, 2002*

[Quan, P., Z. Lei, et al. 1999]. "Two denoising methods by wavelet transform." *IEEE Transactions on Signal Processing 47(12)*: *3401-3406*.

[R.T. Rato, M. D. O., A.G. Batista 2008]. "On the HHT, its problems, and some solutions." *Elsevier,Mechanical Systems and Signal Processing 2(6)*: *1374–1394*.

[Rabbany, A. E. 2002]. Introduction to GPS: The Global Positioning System. *Noorwood MA, Artech House*.

[Rad, M. 2003]. Two-Dimensional Adaptive Perfect Reconstruction Filter Banks Using Lifting Scheme. Msc, *University of Zagreb Faculty of Electrical Engineering and Computing, Thesis Referrence*.

[Ramachandran, S. a. 2000]. Insight into wavelets from theory and practice, *Prentice hal of India , EEE*.

[Redfern, M. A., S. C. Terry, et al. 2004]. The application of distribution system current transformers for high frequency transient based protection. *Eighth IEE International Conference on Developments in Power System Protection, 2004*.

[Reynolds, D., A. Brown, et al. 1999]. Miniaturized GPS Antenna Array Technology And Predicted Anti-Jam Performance. *Proceedings of the 12th International Technical Meeting of the Satellite Division of The Institute of Navigation (ION GPS 1999)*.

[Riley, W. J. 2008]. Handbook of Frequency Stability Analysis. *Beaufort, SC 29907, NIST SpecialPublication 1065*.

[Robertson, D. C., O. I. Camps, et al. 1996]. "Wavelets and electromagnetic power system transients." *IEEE Transactions on Power Delivery 11(2)*: *1050-1058*.

[Robertson, S. D. T. and S. Z. G. Zaky 1969]. "Analysis of the Hysteresis Machine - Part I." *IEEE Transactions on Power Apparatus and Systems PAS-88(4)*: *474-483*.

[Rosa M de castro M fernandez , H. N. D. R. 2002]. An overview of wavelet transforms application in power systems. *14 th Power System Computation Conferrence, Sevilla*.

[S. Sumathi, S. E. 2007]. Fundamentals of Relational Database Management Systems *Springer*.

[Satish, L. and B. Nazneen 2003]. "Wavelet-based denoising of partial discharge signals buried in excessive noise and interference." *IEEE Transactions on Dielectrics and Electrical Insulation 10(2)*: *354-367*.

[Schwarz, R. and M. Muhr 2007]. Modern technologies in optical partial discharge detection. *Annual Report - Conference on Electrical Insulation and Dielectric Phenomena, 2007. CEIDP 2007*.

[Schwarz, R., M. Muhr, et al. 2005]. Partial discharge detection in oil with optical methods. *IEEE International Conference on Dielectric Liquids, 2005. ICDL 2005. 2005*.

[Seifzadeh, S., M. Rostami, et al. 2011]. Parameter selection for smoothing splines using Stein's Unbiased Risk Estimator. *International Joint Conference on Neural Networks (IJCNN), The 2011*

[Seralathan, K. E. and G. Nandini 2006]. Stochastic Modeling of Electric Tree Progression due to Partial Discharge Activity. *Properties and applications of Dielectric Materials, 2006. 8th International Conference on*.

[Shim, I., J. J. Soraghan, et al. 2001]. "Detection of PD utilizing digital signal processing methods. Part 3: Open-loop noise reduction." *IEEE Electrical Insulation Magazine 17(1)*: *6-13*.

[Shim, I., J. J. Soraghan, et al. 1999]. Partial discharge location on high voltage cables. *Eleventh International Symposium on High Voltage Engineering, 1999. (Conf. Publ. No. 467)*.

[Shu, E. W. and S. Boggs 2008]. "Feature article - Dispersion and PD detection in shielded power cable." *IEEE Electrical Insulation Magazine 24(1)*: *25-29*.

[Siemens. 2009]. "Protective and Measuring Transformers,Medium Voltage Equipment Selection and Ordering Data." *HG 24 · 2009*

[Soloviev, A. and F. van Graas 2008]. Utilizing multipath reflections in deeply integrated GPS/INS architecture for navigation in urban environments. *IEEE/ION Position, Location and Navigation Symposium, 2008*.

[Song, H., L. Gao, et al. 2007]. Development of Digital Measuring Instrument for Dielectric Loss Tangent. *8th International Conference on Electronic Measurement and Instruments, 2007. ICEMI '07.*

[Song, X. 2009]. The Automation and Optimisation of Wavelet Transform Techniques for PD Denoising and Pulse Shape Classification in Power Plant PhD, *Glasgow Caledonian University , Thesis referrence*.

[Steennis, E. F., R. Ross, et al. 2001]. Partial Discharge Diagnostics Of Long And Branched Medium-Voltage Cables. *Proceedings of the 2001 IEEE 7th International Conference on Solid Dielectrics. ICSD '01*. .

[Stone, G. C. 2010]. Relevance of phase resolved PD analysis to insulation diagnosis in industrial equipment. *10th IEEE International Conference on Solid Dielectrics (ICSD), 2010*

[Sweldens, W. 1996]. "The Lifting Scheme: A Construction Of Second Generation Wavelets." *SIAM Journal on Mathematical Analysis*: *1-42*.

[T.Exon, D. A. W. a. J. L. 1993]. "Rogowski coil." *engineering science and education*

[Institution. 2013]). "U1065A Acqiris 10-bit High-Speed cPCI Digitizers."_ *Retrieved 04/02/2013, 2013, from http://www.home.agilent.com/en/pd-1184897-pn-U1065A/acqiris-10-bit-high-speed-cpci-digitizers?&cc=GB&lc=eng*.

[Institution. 2013], 01/02/2013). "MSO/DPO5000 Mixed Signal Oscilloscope." *Retrieved 04/02/2013, 2013, from http://www.tek.com/oscilloscope/mso5000-dpo5000*.

[Ulaby, F. T. 2006]. Fundamentals of applied electromagnetics. *USA, Pearson international edition*.

[van der Wielen, P. C. J. M., E. F. Steennis, et al. 2003]. "Fundamental aspects of excitation and propagation of on-line partial discharge signals in three-phase medium voltage cable systems." *IEEE Transactions on Dielectrics and Electrical Insulation 10(4)*: *678-688*.

[van der Wielen, P. C. J. M., P. A. F. Wouters, et al. 2002]. Signal interpretation of partial discharges in three-phase medium voltage cable systems measured on-line. *Conference Record of the 2002 IEEE International Symposium on Electrical Insulation*.

[Vaseghi, S. S. 2000]. Advanced digital signal processing and noise reduction. *New York, John Wiley & sons*.

[Veen, J., P. C. J. M. van der Wielen, et al. 2002]. Propagation characteristics of three-phase belted paper cable for on-line PD detection. *Conference Record of the 2002 IEEE International Symposium on Electrical Insulation*.

[Veen, J. and P. C. J. M. van der Wiellen 2003]. "The application of matched filters to PD detection and localization." *IEEE Electrical Insulation Magazine 19(5)*: *20-26*.

[Veloso, G. F. C., L. E. B. da Silva, et al. 2009]. Detection of partial discharge in power transformers using Rogowski coil and multiresolution analysis. *Brazilian Power Electronics Conference, 2009. COBEP '09.* .

[Vierra, R. 2005]. Professional SQL server 2005 programming, *Wiley Publishing, Inc*.

[Wagenaars, P., P. A. A. F. Wouters, et al. 2011]. "Adaptive templates for matched filter bank for continuous online partial discharge monitoring." *IEEE Transactions on Dielectrics and Electrical Insulation 18(5)*: *1693-1701*.

[Wang, H. T. M. 1989]. "Subcompact hydrogen maser atomic clocks." *IEEE Proceedings of 77(7)*: *982-992*.

[Wasim Ahma, H. H. g., and Ahmet M. Kondoz 2010]. Discrete Wavelet Transform Based Shift-Invariant Analysis Scheme For Transient Sound Signals. *Proceedings of the 13th International Conference on Digital Audio Effects (DAFx-10), Graz, Austria , September 6-10, 2010*.

[Widrow, B., J. R. Glover, Jr., et al. 1975]. "Adaptive noise cancelling: Principles and applications." *Proceedings of the IEEE 63(12)*: *1692-1716*.

[wielen, P. C. J. M. V. 2005]. On-Line Detection and Location of Partial Discharges In Medium Voltage Cables. PhD, *University of Eindhoven, Thesis referrence*.

[Wielen, P. C. J. M. V. D., J. Veen, et al. 2005]. On-Line Partial Discharge Detection Of MV Cables With Defect Localisation (Pdol) Based On Two Time Synchronised Sensors. *18 th International Conference on Electricity Distribution CIRED 2005, Turin*.

[Xiaodi, S., Z. Chengke, et al. 2007]. "Second generation wavelet transform for data denoising in PD measurement." *IEEE Transactions on Dielectrics and Electrical Insulation 14(6)*: *1531-1537*.

[Xiaoguang, Q. and S. Boggs 2006]. "Thermal and mechanical properties of EPR and XLPE cable compounds." *IEEE Electrical Insulation Magazine 22(3)*: *19-24*.

[Xilinx 2008] "SPARTAN 3 series FPGA data sheet."

[Xn, Y., M. Yn, et al. 2000]. Comparison between optical and electrical methods for partial discharge measurement. *Proceedings of the 6th International Conference on Properties and Applications of Dielectric Materials, 2000.*

[Yazici, B. 2003]. Statistical pattern analysis of partial discharge measurements for quality assessment of insulation systems in high voltage electrical machinery. *4th IEEE International Symposium on Diagnostics for Electric Machines, Power Electronics and Drives, 2003. SDEMPED 2003.* .

[Yonghua, Z., W. Changshun, et al. 2006]. Discussion on Resistivity Testing Method of Semi-conducting screen in Power Cables. *8th International Conference on Properties and applications of Dielectric Materials, 2006*.

[Zhang, Y., W. Yu, et al. 2002]. Partial discharge denoising via lifting scheme. *International Conference on Power System Technology, 2002. Proceedings. PowerCon 2002.* .

[Zhifang, D., P. K. Willett, et al. 1997]. "Performance limits of PD location based on time-domain reflectometry." *IEEE Transactions on Dielectrics and Electrical Insulation 4(2)*: *182-188*.

[Zhou, C., X. Song, et al. 2009]. "On-line partial discharge monitoring in medium voltage underground cables." *Science, Measurement & Technology, IET 3(5)*: *354-363*.

[Zhou, X., C. Zhou, et al. 2005]. "An improved methodology for application of wavelet transform to partial discharge measurement denoising." *IEEE Transactions on Dielectrics and Electrical Insulation 12(3)*: *586-594*.

[Zhu, D., A. J. McGrail, et al. 1994]. Partial discharge detection in cable termination using acoustic emission techniques and adaptive signal processing. *Conference Record of the IEEE International Symposium on Electrical Insulation, 1994.*, .

This page is left intentionally blank.

# Appendix : A

## A.1 Multiple PD sources from the Cable

In Figure A-1, PD monitoring equipment at cable end A and at cable end B, PD source at 500 meters from cable end A , 700 meters from cable end A and 1000 meters from cable end A. TDR plot is shown in Figure A-2.

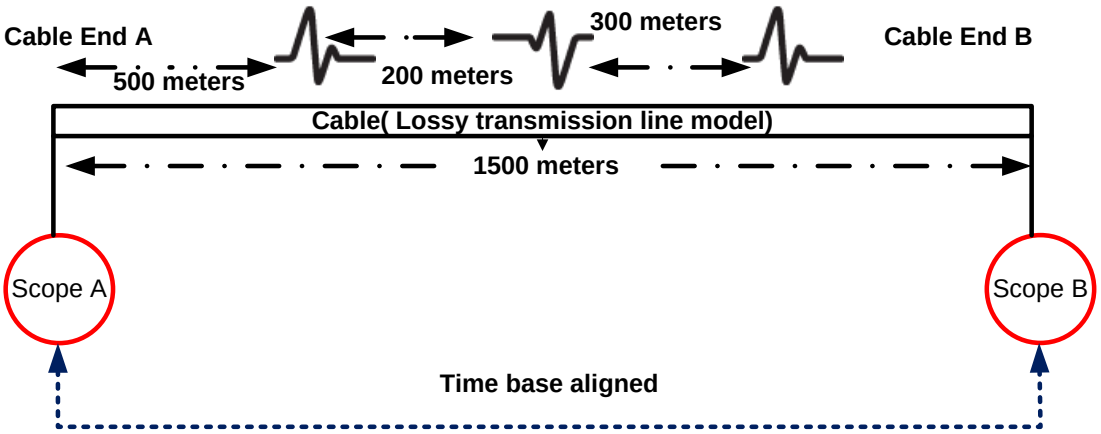


Figure A-1 Cable network, multiple PD pulses, double ended method

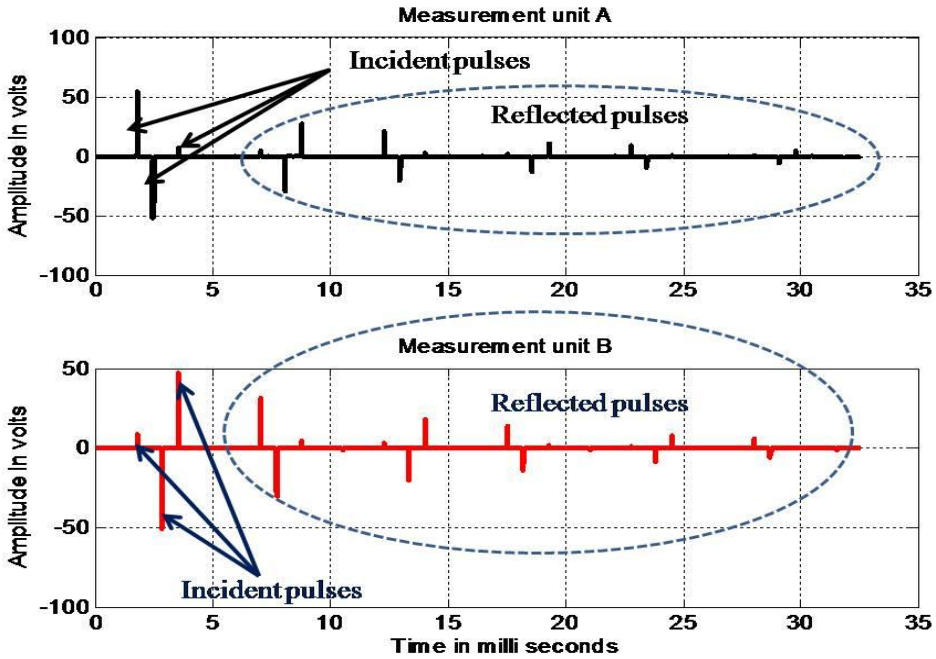


Figure A-2 TDR plot, double ended method

PD source #1

$\Delta t = \left(1.75\times10^{-3}\right) - \left(3.5\right)$ seconds

$= 1.75\times10^{-3}$ seconds

$$PD_l = \frac{1500 - \left(1.75\times10^{-3} \times 2.8571\times10^{5}\right)}{2}$$

$= 500.00375$ meters

$\approx 500$ meters from Cable end A

$\approx \left(1500-500\right)$ meters from Cable end B

PD source # 2

$\Delta t = \left(2.8\times10^{-3}\right) - \left(2.45\times10^{-3}\right)$ seconds

$= 0.35\times10^{-3}$ seconds

$$PD_l = \frac{1500 - \left(0.35\times10^{-3} \times 2.8571\times10^{5}\right)}{2}$$

$= 700.00075$ meters

$\approx$ 700 meters from Cable end A

$\approx \left(1500 - 700\right)$ meters from Cable end B

PD source # 3

$\Delta t = \left(1.75\times10^{-3}\right) \sim \left(3.5\times10^{-3}\right)$ seconds

$= 1.75\times10^{-3}$ seconds

$$PD_l = \frac{1500 - \left(1.75\times10^{-3} \times 2.8571\times10^{5}\right)}{2}$$

$= 500.00375$ meters

$\approx$ 500 meters from Cable end B

$= \left(1500 - 500\right)$ meters from Cable end A

# Appendix : B

## B.1 Downsampling Operation

Let x[n] be a finite sequence where n € Z. Down sampling of x[n] is denoted as $x_d[n]$ which is given by

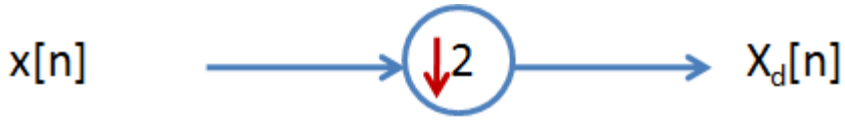


Down sampling by 2 is expressed as

$$x_d[n] = \{x[2n] \text{ , for all values of } n\}$$

$$Z[x_d[n]] = \sum_{n=-\infty}^{n=\infty} (x_d[n])(z^{-n})$$

$$= \sum_{n=-\infty}^{n=\infty} (x_d[2n])(z^{-n})$$

substitute $2n = k$ ie $n = \frac{k}{2}$ which gives

$$= \sum_{k=\ldots-2,0,2,\ldots} x[k]\left[z^{1/2}\right]^{-k}$$

$$= \sum_{k=-\infty}^{k=\infty} \frac{1}{2}\left\{x[k]\left[z^{1/2}\right]^{-k} + x[k]\left[-z^{-1/2}\right]^{-k}\right\}$$

$$X_d(z) = \frac{1}{2}\left\{X\ (z^{1/2}) + X\ (-z^{1/2})\right\}$$

## B.2 Upsampling operaion

Let x[n] be a finite sequence where n € Z, Up sampling of x[n] is denoted as $x_u[n]$ which is given by


Upsampling by 2 is expressed as

$$x_u[n] = \begin{cases} 0, & \text{if n is odd} \\ x\left[\frac{n}{2}\right], & \text{if n is even} \end{cases}$$

$$Z[x_u[n]] = \sum_{n=-\infty}^{n=-\infty} (x_u[n])(z^{-n})$$

$$= \sum_{n=\ldots-2,0,2} \left(x\left[\frac{n}{2}\right]\right)(z^{-n})$$

Let $\frac{n}{2} = m$

$$= \sum_{m=\ldots-1,0,1,\ldots} (x[m])(z^{-2m})$$

$$= \sum_{m=\ldots-1,0,1,\ldots} (x[m])(z^{2})^{-m}$$

$$X_u(z) = X(z^2)$$

# Appendix : C

## C.1 Current Transformer

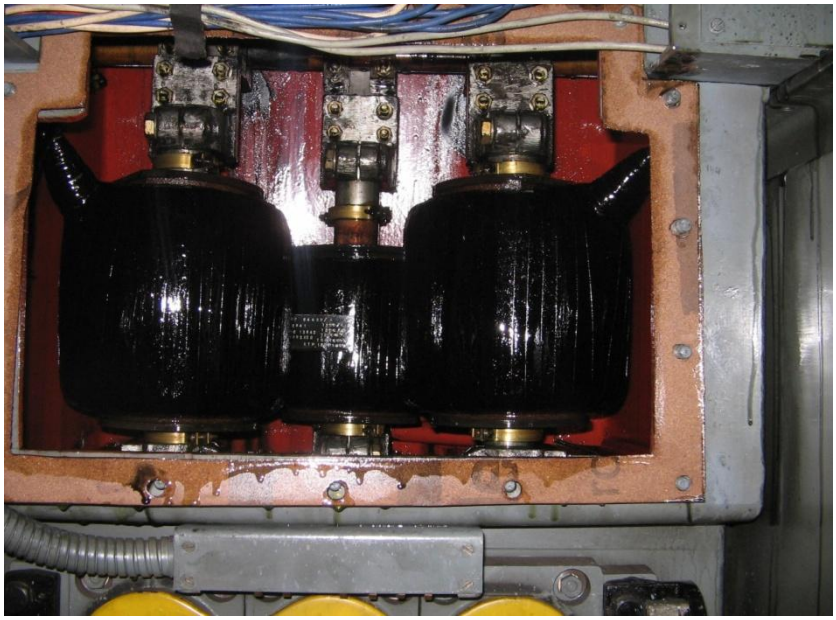

Figure C-1 Wound type CT in switchgear panel [Courtesy: SP energy networks]

## C.2 Solution of Jiles-Artherton Equation

$$\mu_0 \int M_{an}(dH_e) = \mu_0 \int M(dH_e) + \mu_0 \int \frac{n\varepsilon_\pi}{2M_s}\left[\frac{dM}{dH}\right](dH) + \frac{\mu_0 d^2}{2\rho\beta}\left(\frac{dM}{dt}\right)^2 dt \quad \text{C-1}$$

$$\left(\frac{dM}{dt}\right)^2 dt = \left(\frac{dM}{dt}\right)\left(\frac{dM}{dHe}\right)dHe \quad \text{C-2}$$

Classical hysteresis equation gives

$$\mu_0 \int M_{an}(dH) = \mu_0 \int M(dH) + \mu_0 \int \frac{n\varepsilon_\pi}{2M_s}\left[\frac{dM}{dH}\right](dH) \quad \text{C-3}$$

Also

$$M = M_{irr} + M_{rev} \quad \text{C-4}$$

From the energy balance equation

$$M_{an} = M_{irr} + M_{rev} + k\delta(1-c)\left(\frac{dM_{irr}}{dH_e}\right) \quad \text{C-5}$$

$$\mu_0 \int M_{an}(dH_e) = \mu_0 \int M(dH_e) + k\delta(1-c) \int \left[\frac{dM_{irr}}{dH_e}\right](dH_e) + \frac{\mu_0 d^2}{2\rho\beta}\left(\frac{dM}{dt}\right)\int\left(\frac{dM}{dH_e}\right)dH_e \quad \text{C-6}$$

$$M_{an} = M + k\delta(1-c)\left(\frac{dM_{irr}}{dH_e}\right) + \frac{\mu_0 d^2}{2\rho\beta}\left(\frac{dM}{dt}\right)\left(\frac{dM}{dH_e}\right) \quad \text{C-7}$$

$$M_{an} = M + k\delta(1-c)\left(\frac{dM_{irr}}{dH_e}\right) + k'\left(\frac{dM}{dH_e}\right) \quad \text{C-8}$$

where

$$k' = \frac{\mu_0 d^2}{2\rho\beta}\left(\frac{dM}{dt}\right) \quad \text{C-9}$$

$$\left(\frac{dM}{dHe}\right) = \left(\frac{Man - M - k\delta(1-c)\frac{dMirr}{dHe}}{k'}\right) \quad \text{C-10}$$

$$\left(\frac{dM}{dH}\right) = \left(\frac{Man - M - k\delta(1-c)\frac{dMirr}{dHe}}{k' - \alpha\left(Man - M - k\delta(1-c)\frac{dMirr}{dHe}\right)}\right) \quad \text{C-11}$$

Numerical solution of the above equation can be obtained by decoupling of M into $M_{irr}$ and $M_{rev.}$ Irreversible and reversible component of magnetization are

$$Man = Mrev + Mirr + k\delta(1-c)\frac{dMirr}{dHe} + \frac{\mu_0 d^2}{2\rho\beta}\left(\frac{dM}{dt}\right)\left(\frac{dM}{dH_e}\right) \quad \text{C-12}$$

substituting $M_{rev}$= 0 and C=0

$$Man = Mirr + k\delta \frac{dMirr}{dHe} + \frac{\mu_0 d^2}{2\rho\beta}\left(\frac{dM}{dt}\right)\left(\frac{dM}{dH_e}\right)$$

C-13

$$Mirr = Man - k\delta \frac{dMirr}{dHe} - \frac{\mu_0 d^2}{2\rho\beta}\left(\frac{dM}{dt}\right)\left(\frac{dM}{dH_e}\right)$$

$$Mirr = Man - \frac{dMirr}{dHe}\left(k\delta + \frac{\mu_0 d^2}{2\rho\beta}\left(\frac{dM}{dt}\right)\right)$$

C-14

$$Mirr = Man - k'\left(\frac{dMirr}{dHe}\right)$$

C-15

$$\left(\frac{dMirr}{dHe}\right) = \left(\frac{M_{an} - M_{irr}}{k'}\right)$$

C-16

Where, $k' = k\delta + \frac{\mu_0 d^2}{2\rho\beta}\left(\frac{dM}{dt}\right)$

C-17

Simplifying

$$\left(\frac{dM}{dH}\right) = \left(\frac{dMirr}{dH}\right) + c\left(\frac{dMan}{dH}\right) - c\left(\frac{dMirr}{dH}\right)$$

$$\left(\frac{dMan}{dH}\right) = \left(\frac{dMan}{dHe}\right)\left(\frac{dHe}{dH}\right)$$

$$\left(\frac{dMan}{dH}\right)=\left(\frac{dMan}{dHe}\right)\left(1+\alpha\frac{dM}{dH}\right)$$

$$\left(\frac{dMirr}{dH}\right)=\left(\frac{dMirr}{dHe}\right)\left(\frac{dHe}{dH}\right)$$

$$\left(\frac{dM_{irr}}{dH}\right)=\left(\frac{dM_{irr}}{dHe}\right)\left(1+\alpha\frac{dM}{dH}\right)$$

After substitution

$$\left(\frac{dM}{dH}\right)=\left\{\frac{(1-c)\left(\frac{dMirr}{dHe}\right)+c\left(\frac{dMan}{dHe}\right)}{1-\alpha(1-c)\left(\frac{dMirr}{dHe}\right)-\alpha c\left(\frac{dMan}{dHe}\right)}\right\}$$

C-18

Where

$$\left(\frac{dMan}{dHe}\right)=\frac{Ms}{a}\left\{1-\coth^2\left(\frac{He}{a}\right)+\left(\frac{a}{He}\right)^2\right\}$$

C-19

Where , $\left(\frac{dMirr}{dHe}\right)=\left(\frac{M_{an}-M_{irr}}{k'}\right)$

$$Coth(He/a)=\left\{\frac{1}{He/a}+\frac{He/a}{3}-\left(\frac{(He/a)^3}{45}\right)+2\left(\frac{(He/a)^5}{945}\right)\right\}$$

$$Man(t)=Ms\left(\frac{He}{3a}\right)$$

$$\left(\frac{dMan}{dHe}\right)=\left(\frac{Ms}{3a}\right)$$

# C.3 RPDMS Hardware Photographs

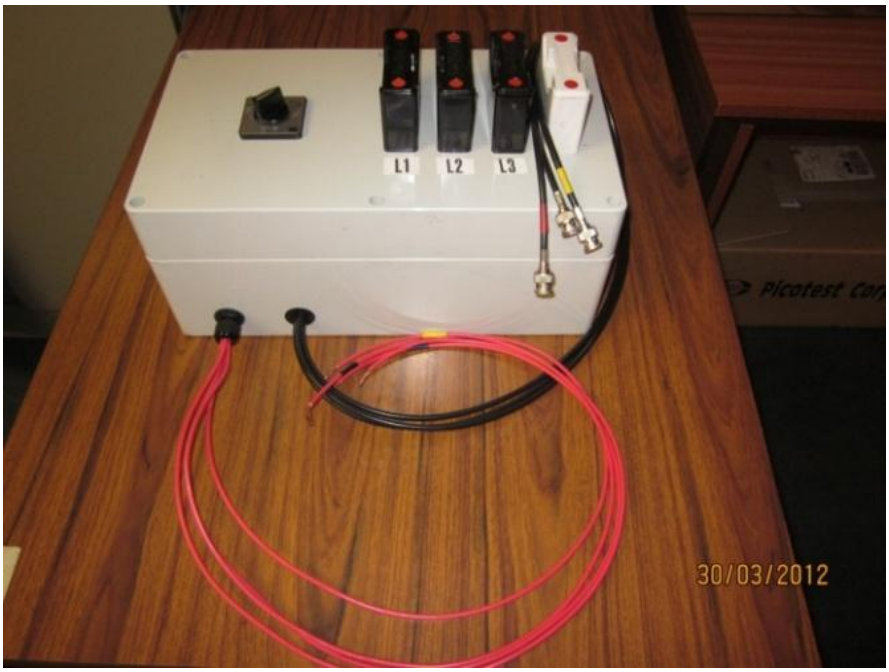


Figure C-2 Three pole switch

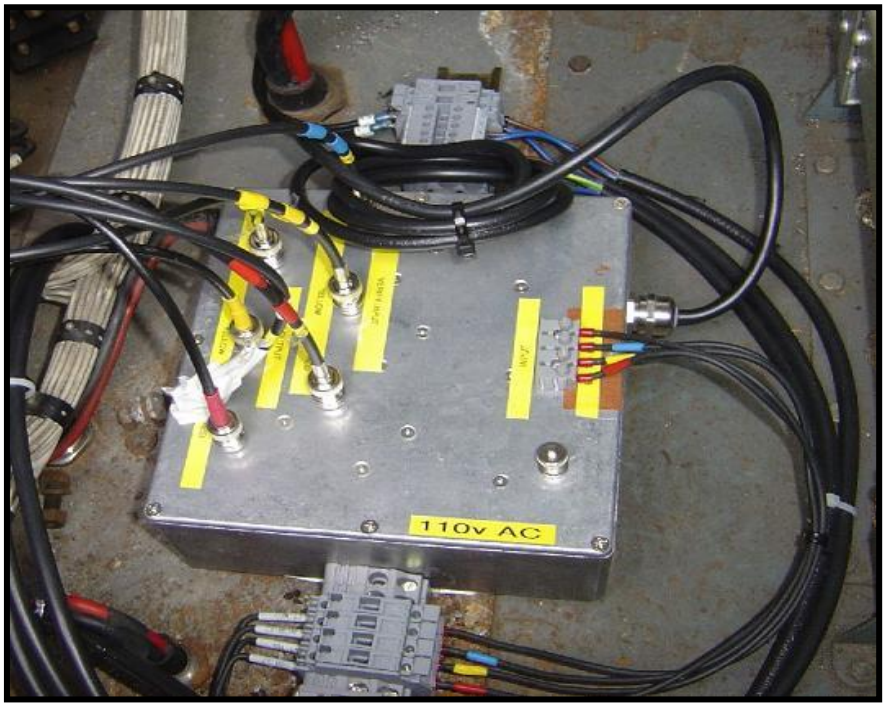


Figure C-3 Photograph of source follower[Foo 2003]

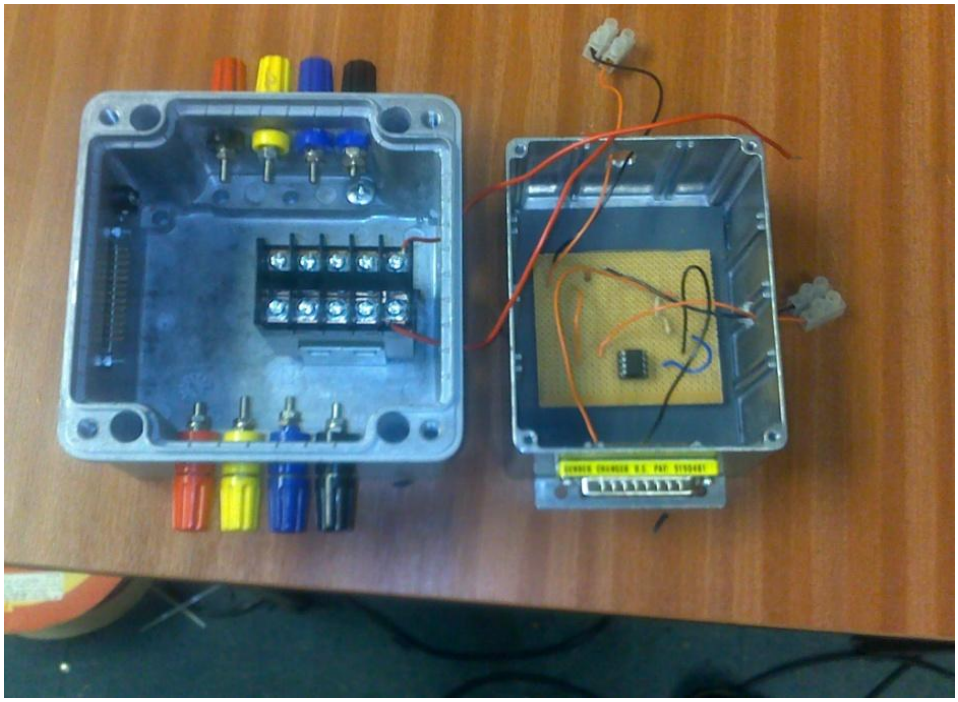

Figure C-4 Photograph of PC controlled isolator[Foo 2003]


Figure C-5 Photograph of signal conditioning unit[Foo 2003]


Figure C-6 Digitizer # 1 [Foo 2003]

Figure C-7 HFCT [courtesy www.ipec.co.uk]


Figure C-8 Clamp on current probe (MN60 Chauvin Arnoux)


Figure C-9 Digitizer # 2 (NI-USB6008)

# C.4 Graphical User Interface

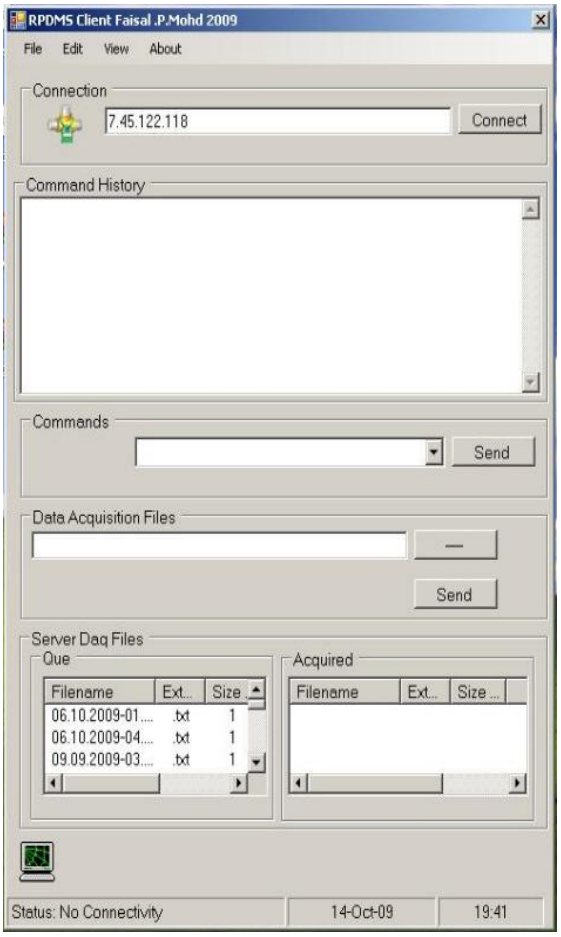


Figure C-10 Advanced user interface

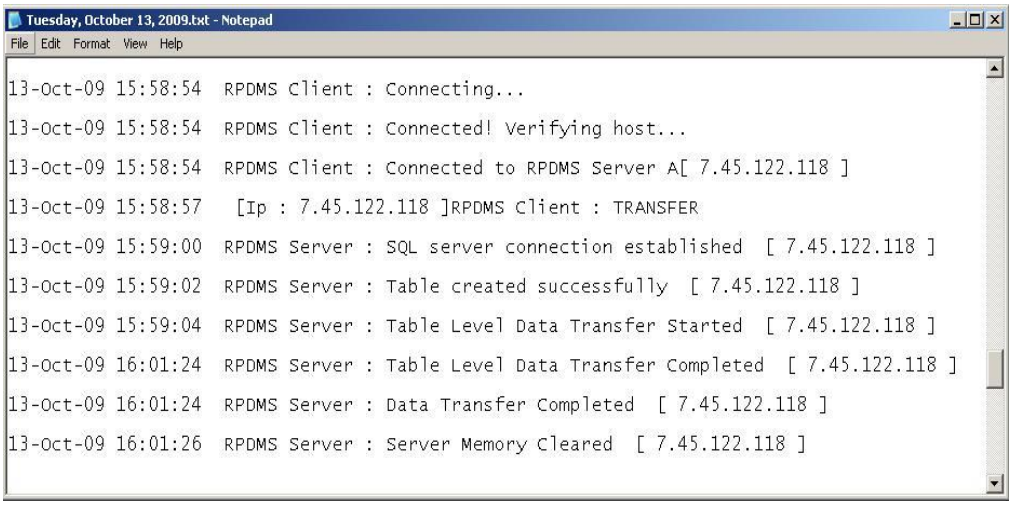


Figure C-11 RPDMS client logs

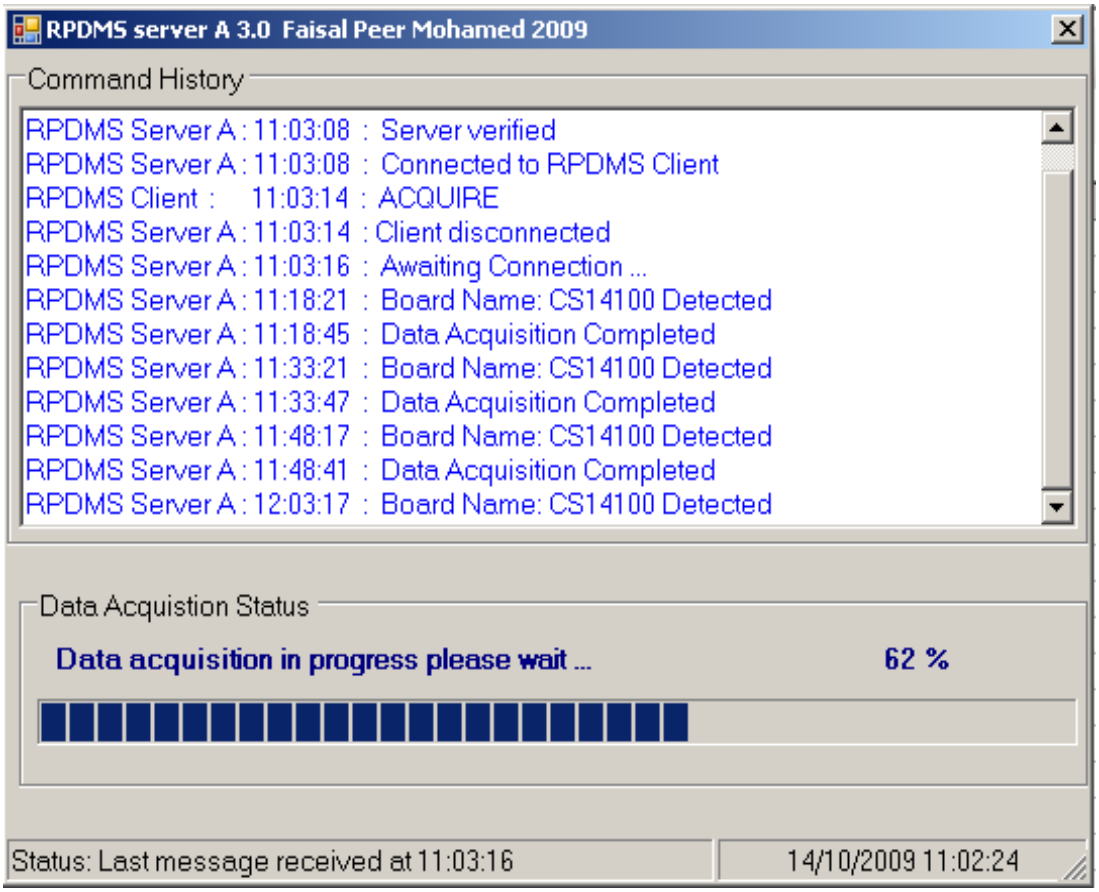


Figure C-12 Remote system interface

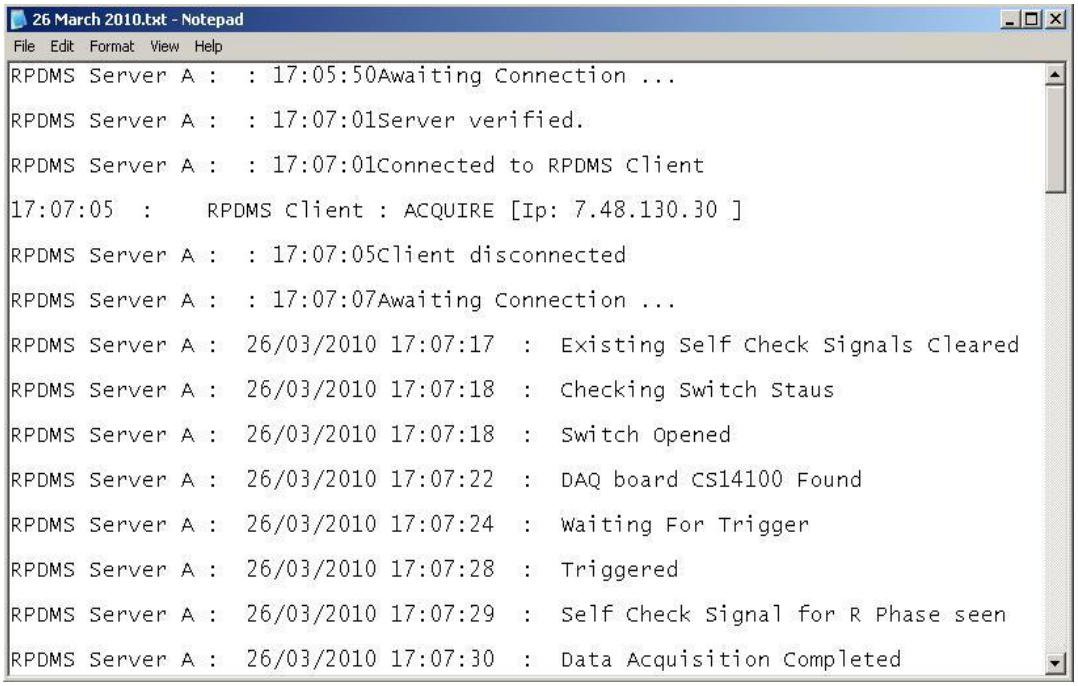


Figure C-13 RPDMS server logs

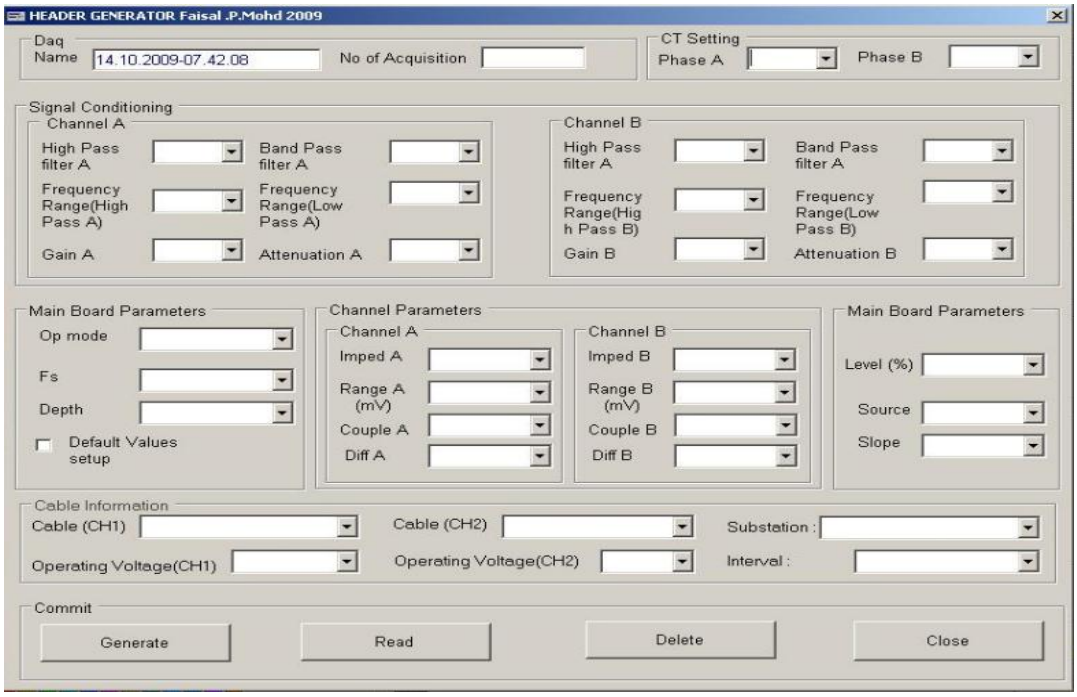


Figure C-14 Daq file generation wizard

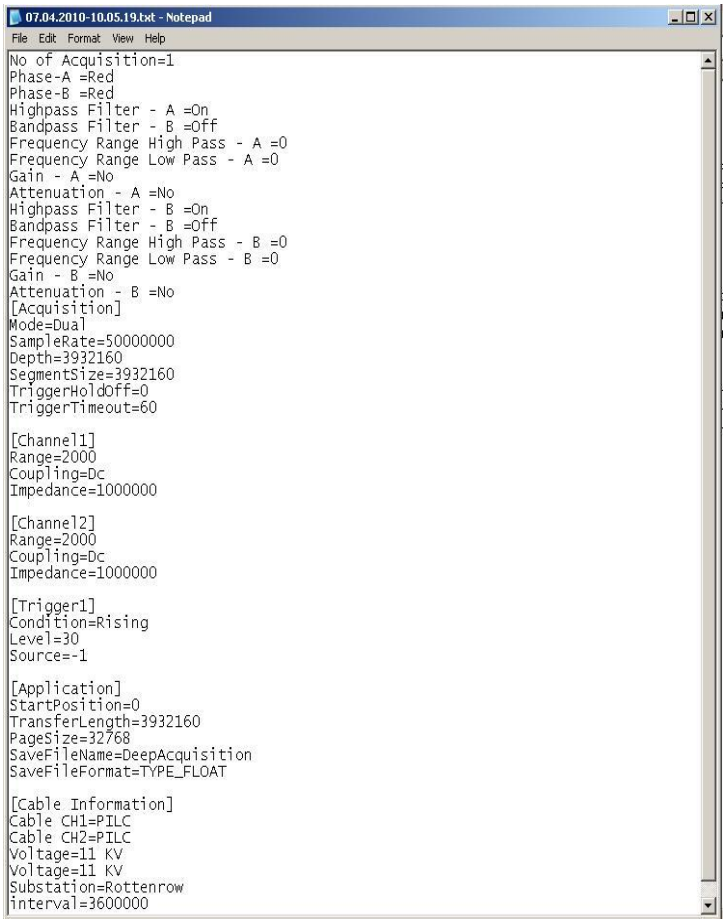


Figure C-15 Sample DAQ file

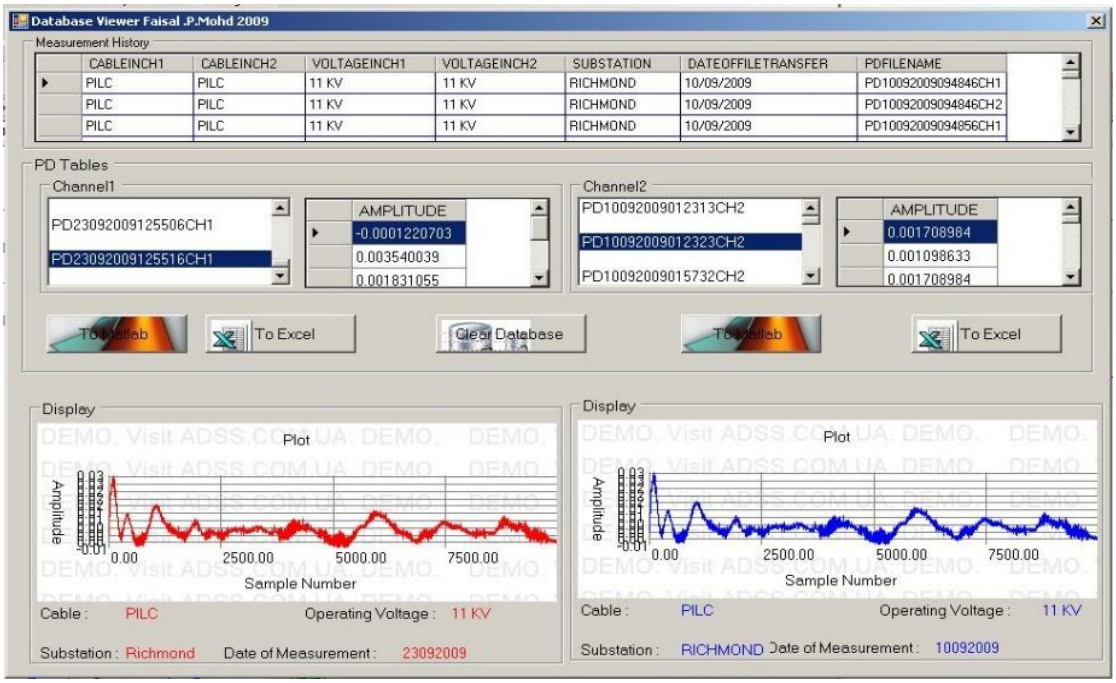


Figure C-16 PD database viewer

# C.5 33/11kV Cable Network Configuration, Glasgow

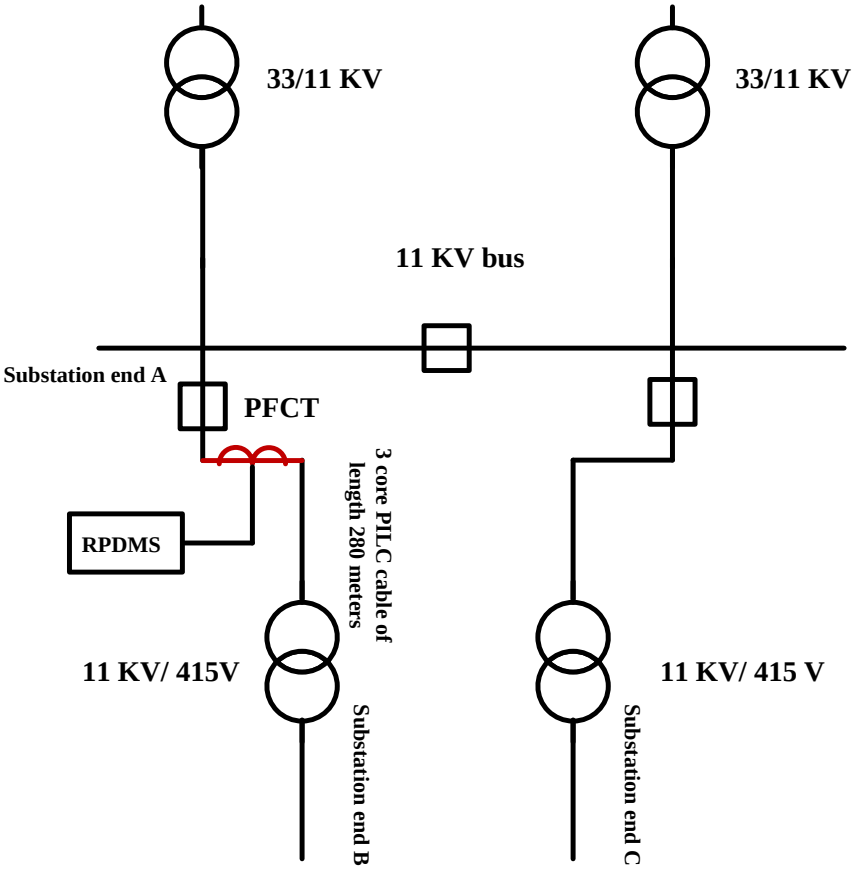


Figure C-17 Cable network configuration, 33/11 kV substation, Glasgow

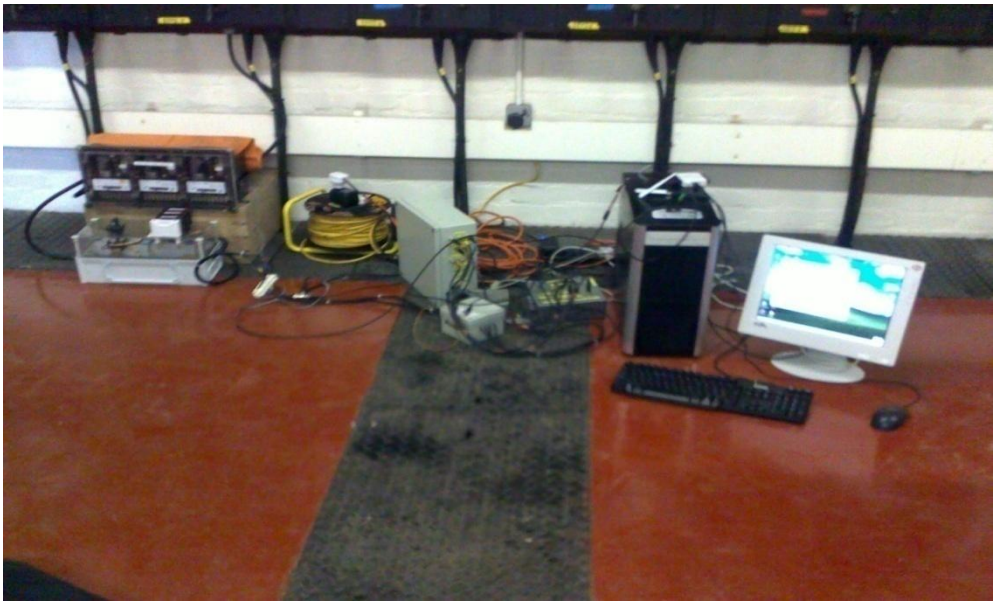

Figure C-18 RPDMS at 33/11 kV substation, Glasgow

# Appendix : D

## D.1 PDDN, PCB

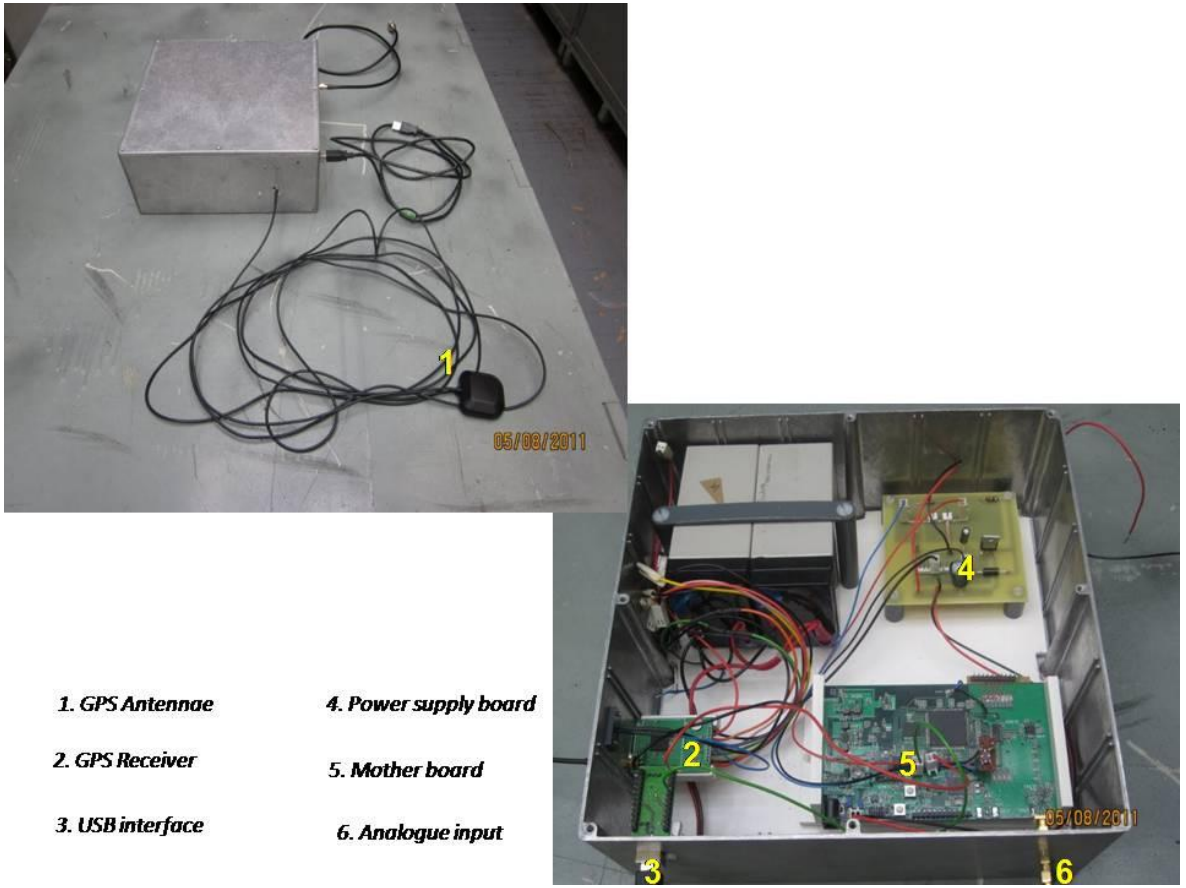


Figure D-1 PDDN, PCB

# D.2 GPS Reciever Specification


Figure D-2 IT 520 Fastrax GPS receiver[Fastrax 2011]

| Sl # | Electrical spec | Value |
|---|---|---|
| 1 | Time to First Fix, Cold acquisition. | 35 seconds |
| 2 | Time to First Fix, Hot acquisition | 1 seconds |
| 3 | 1 PPS accuracy | jitter  50 ns (RMS) |
| 4 | Supply voltage, | 3.3 V |
| 5 | Serial port protocol | NMEA-0183 |
| 6 | Serial data format (UART) | 8 bits, no parity, 1 stop bit |
| 7 | Serial data speed (UART) | 9600 baud (configurable) |
| 8 | Power consumption | 75mW |

Table D-1 GPS receiver electrical specification

# D.3 USB-UART Bridge

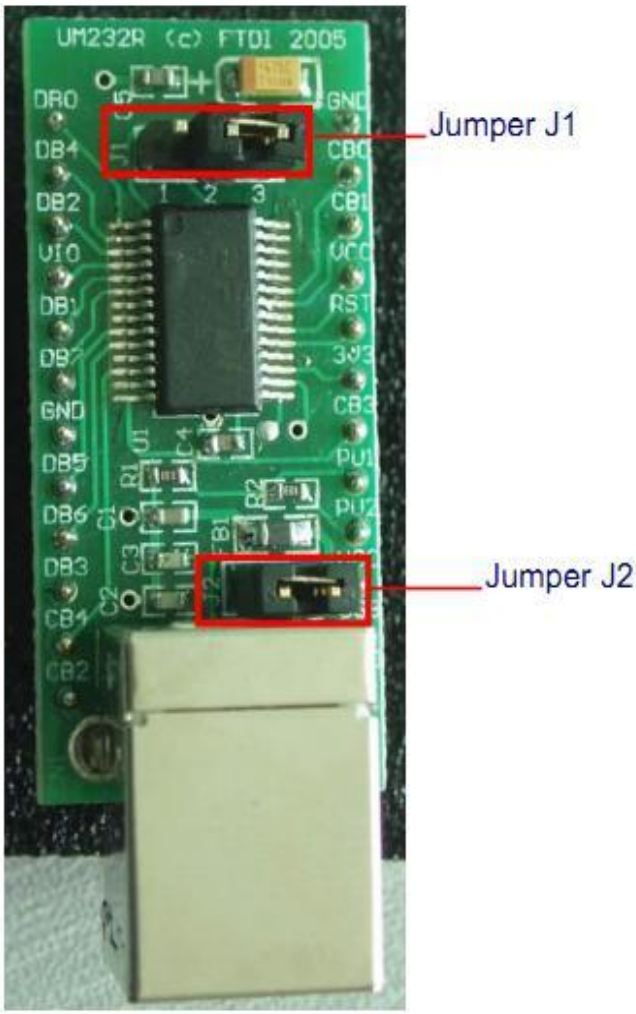


Figure D-3 UM232R USB-UART bridge[www.ftdi.com]

| Sl # | Description | Value |
|---|---|---|
| 1. | I/O standard | CMOS |
| 2 | Data transfer rate | 300 baud to 3 Mega Baud |
| 3 | PC interface | USB 2.0 full speed |
| 4 | Power supply | 3.3 V |
| 5. | Flow control | Hardware based |

Table D-2 Electrical specifications of UM-232R

# D.4 Attenuator Design Formulae

## D.4.1 π attenuator

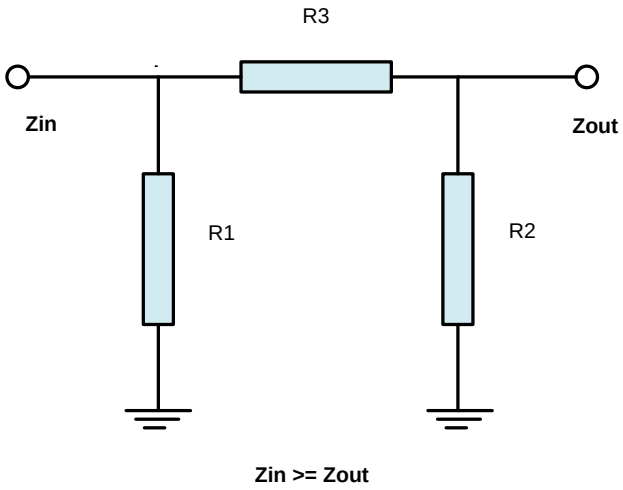


Figure D-4 π type attenuator

$$R_3 = \left(\frac{1}{2}\right)\left(10^{\frac{L}{10}} - 1\right)\sqrt{\frac{Z_{in} * Z_{out}}{10^{\frac{L}{10}}}}$$

D-1

$$R_2 = \frac{1}{\frac{10^{\frac{L}{10}} + 1}{Z_{out}\left(10^{\frac{L}{10}} - 1\right)} - \frac{1}{R_3}}$$

D-2

$$R_1 = \frac{1}{\frac{10^{\frac{L}{10}} + 1}{Z_{in}\left(10^{\frac{L}{10}} - 1\right)} - \frac{1}{R_3}}$$

D-3

Where,

L : desired attenuation in db

Zin : input impedance

Zout : Ouput impedance

## D.4.2 T type attenuator

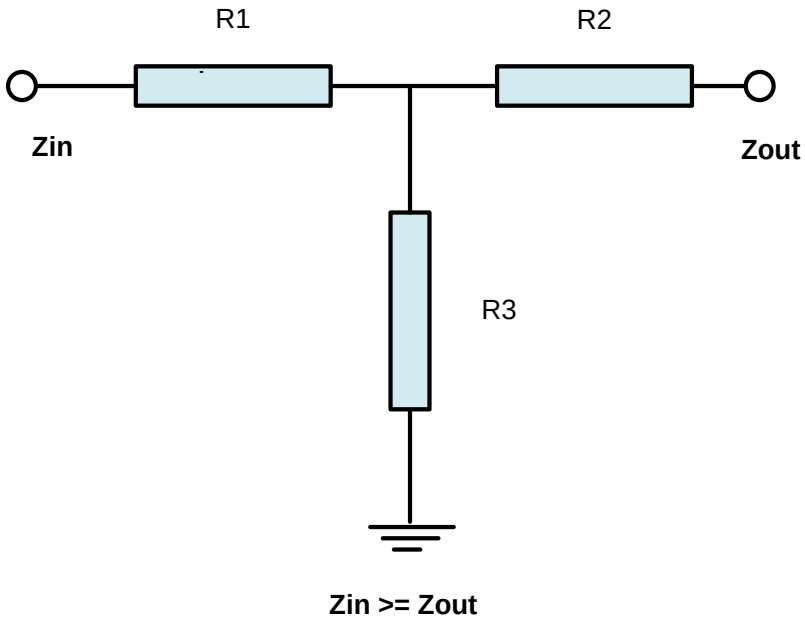


Figure D-5 T type attenuator

$$R_3 = \frac{2 * \sqrt{\left( Z_{in} * Z_{out} * 10^{\frac{L}{10}} \right)}}{10^{\frac{L}{10}} - 1}$$

D-4

$$R_1 = \frac{10^{\frac{L}{10}} + 1}{\left( 10^{\frac{L}{10}} - 1 \right)} Z_{in} - R_3$$

D-5

$$R_2 = \frac{10^{\frac{L}{10}} + 1}{\left(10^{\frac{L}{10}} - 1\right)} Z_{out} - R_3$$

D-6

Where,

L : desired attenuation in db

Zin : input impedance

Zout : Ouput impedance

## D.4.3 Bridged T type Attenuator

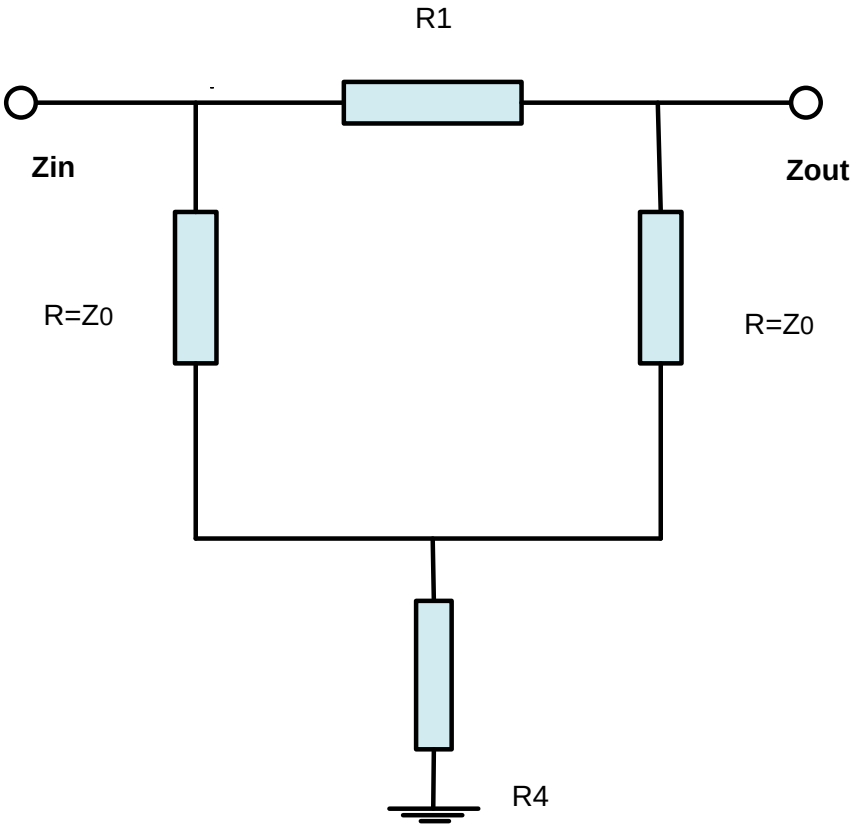


Figure D-6 Bridge type attenuator

$$R_1 = Z_0\left(10^{\frac{L}{20}} - 1\right)$$

D-7

$$R_4 = \frac{Z_0}{\left(10^{\frac{L}{20}} - 1\right)}$$

D-8

Where,

L : desired attenuation in db

Zin : input impedance

Zout : Ouput impedance

# D.5 PDDN drift Measurements

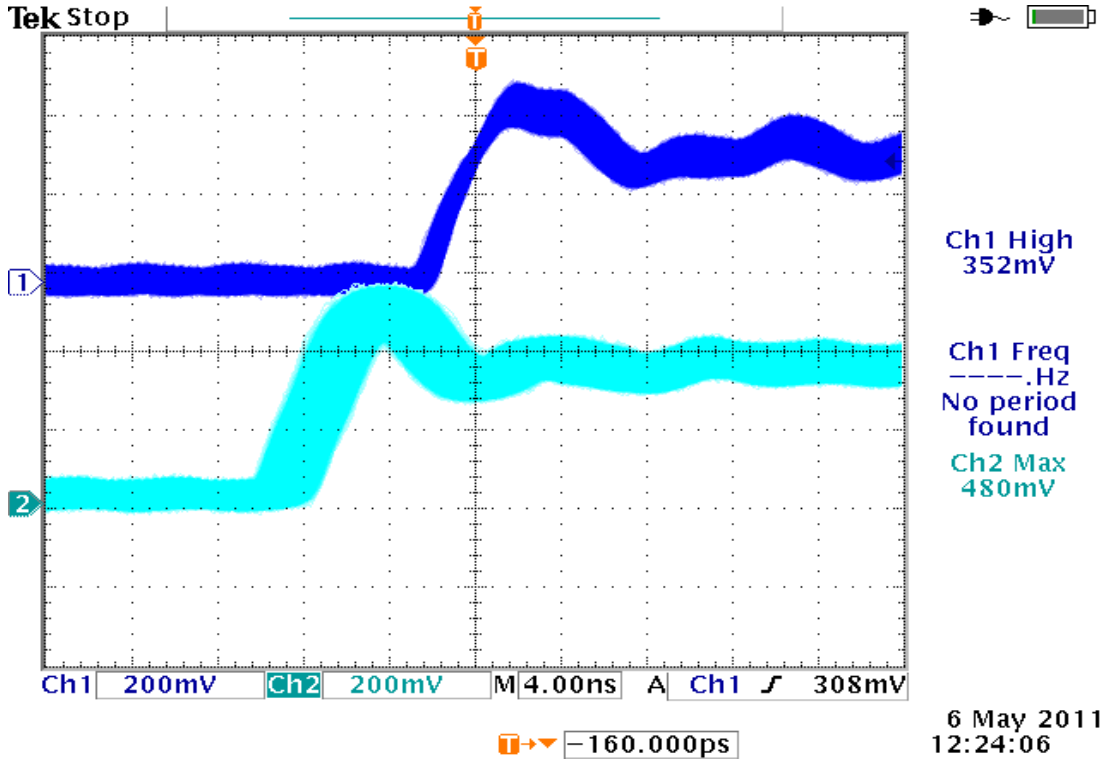


Figure D-7 16 th bit of the test counter

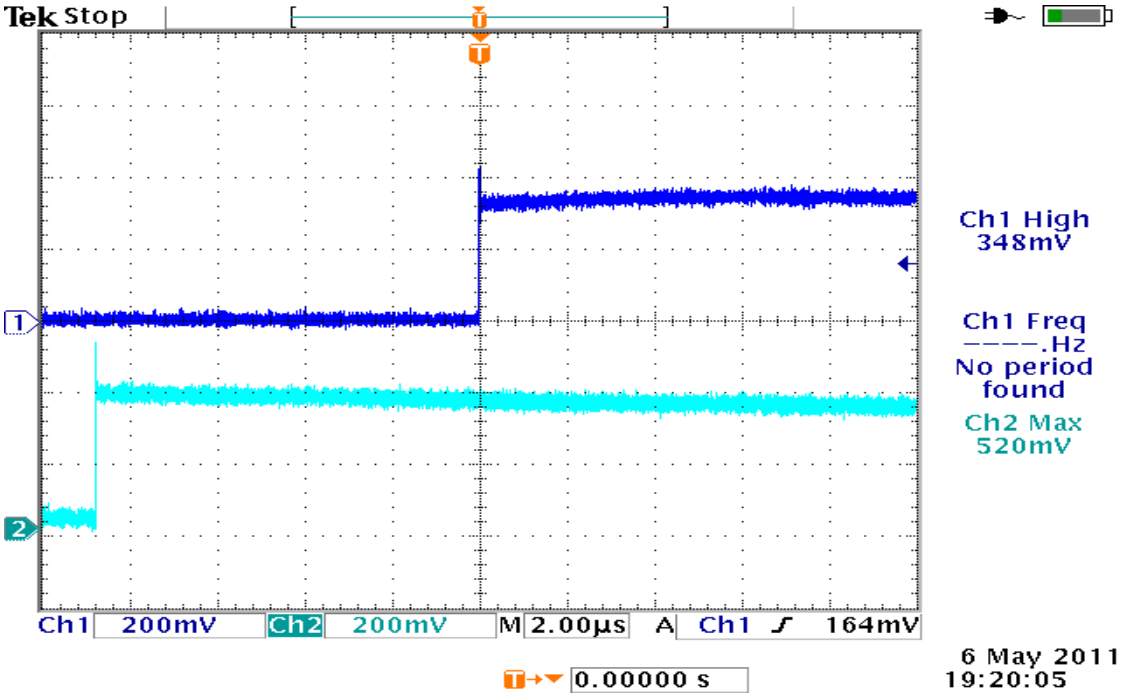


Figure D-8 38 th bit of the test counter

# D.6 PDDN data Acquisition Test

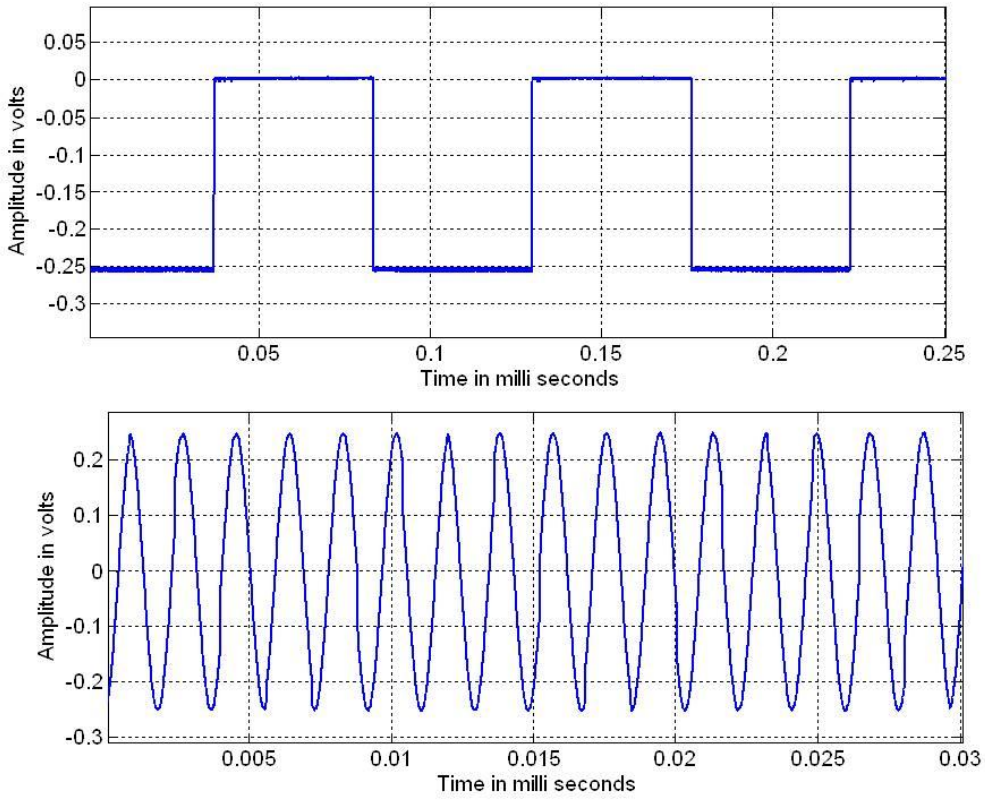


Figure D-9 Data acquisition test # 2

# D.7 Handshaking Signals

| Sl # | Control signal | Meaning |
|---|---|---|
| 1. | SW | Waiting for Start Signal |
| 2. | SR | Start command received from PC |
| 3. | PR | PPS detected from GPS |
| 4 | NR | NMEA messages were transferred to PC |
| 5. | NM | NMEA configuration in GPS successful |
| 6 | NO | GPS acknowledgement failure |
| 7. | TO | GPS timeout received |
| 8 | PS | PPS configuration successful |
| 9. | TC | Timestamp information from GPS has sent to PC |
| 10. | DR | Time delay received from PC |
| 11. | TS | Hardware triggered |
| 12. | GS | Informs PC that data transfer completed |
| 13. | CS | GPS cold start successful |
| 14. | TF | Trigger time data transfer complete |

Table D-3 Handshaking signals

# D.8 Software Screenshots of PDDN

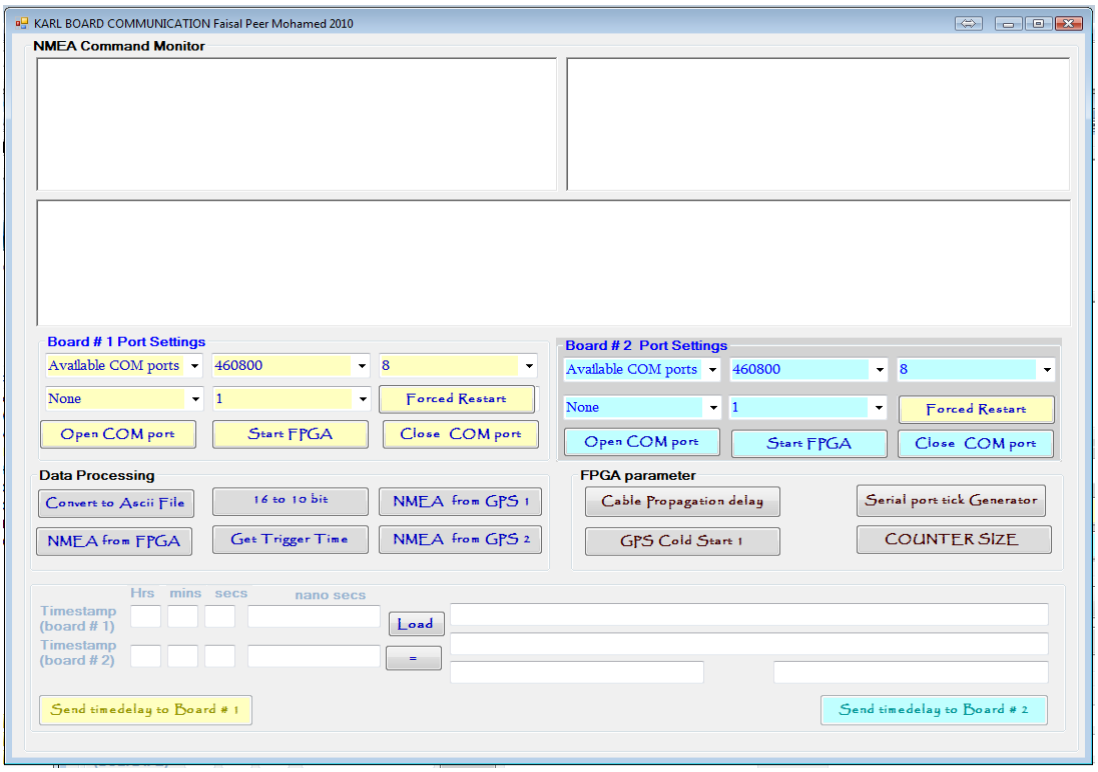


Figure D-10 Test GUI for PDDN

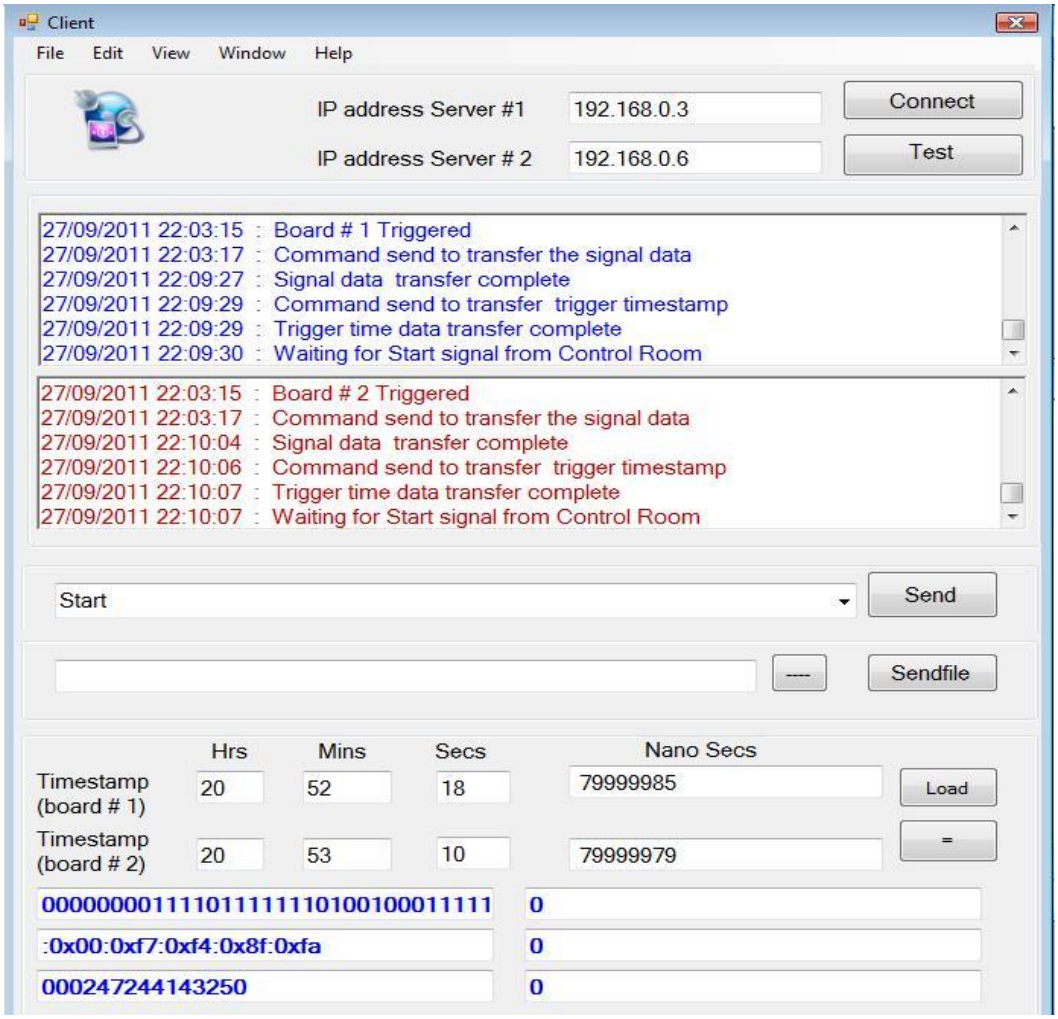


Figure D-11 Client GUI for PDDN

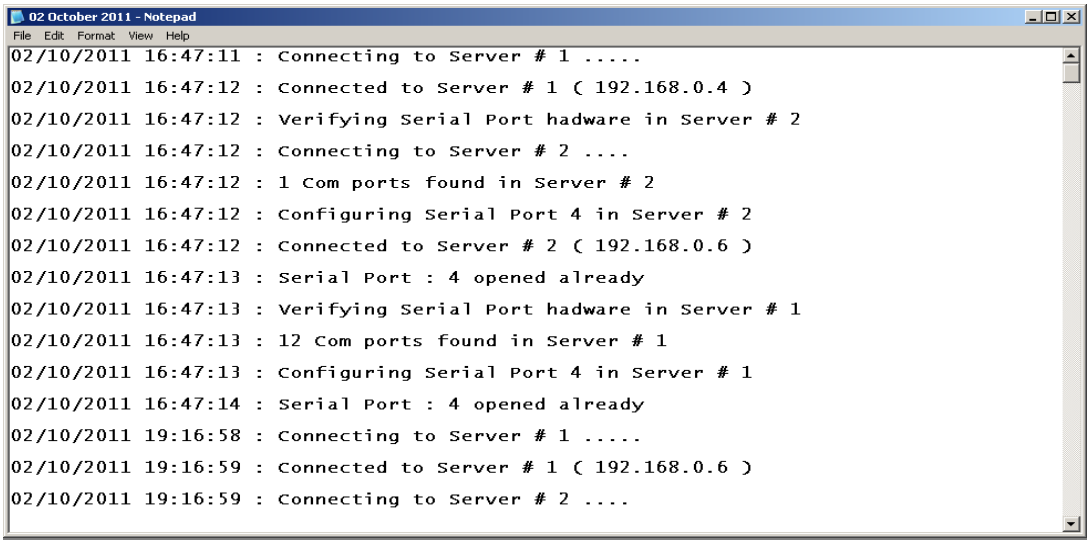


Figure D-12 PDDN Client logs

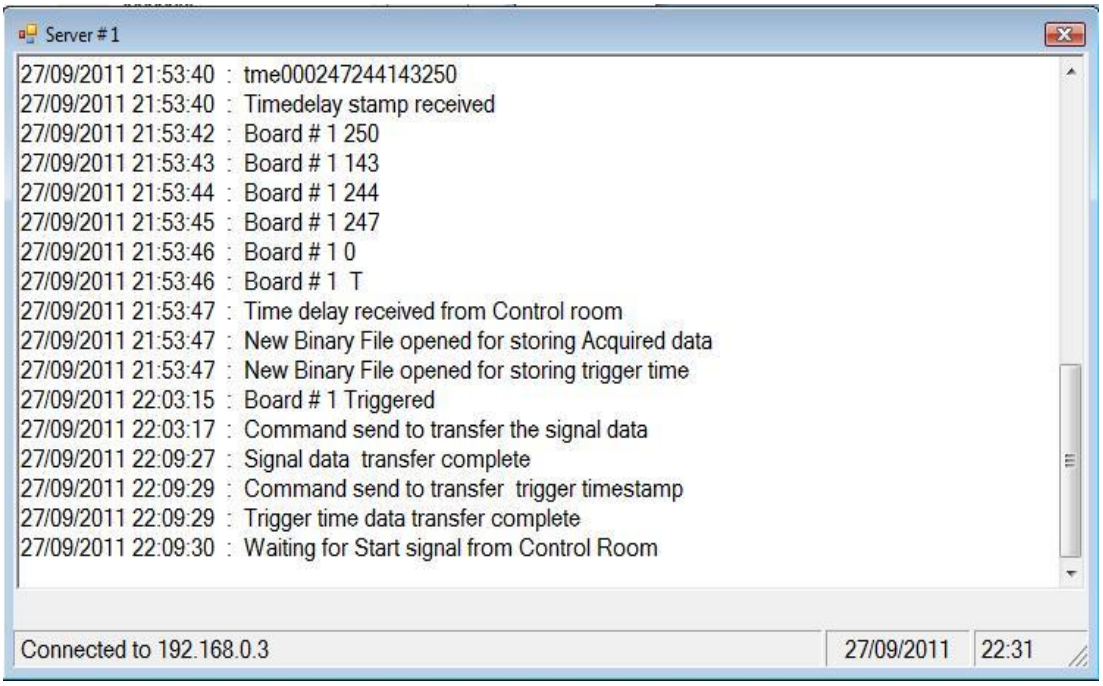


Figure D-13 Server GUI for PDDN

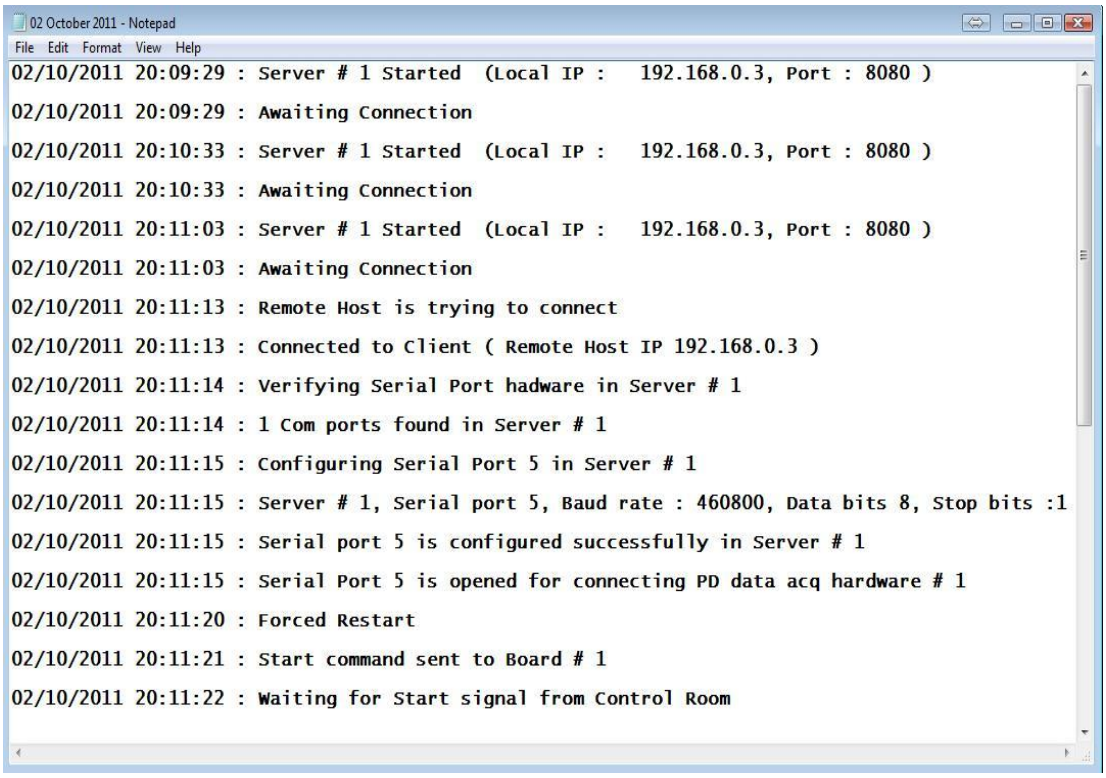


Figure D-14 Server logs


Figure D-15 PDDN on-site trial @ 33/11 KV Substation, Edinburgh

# Appendix : E

## E.1 Wavelet Coefficients # 1

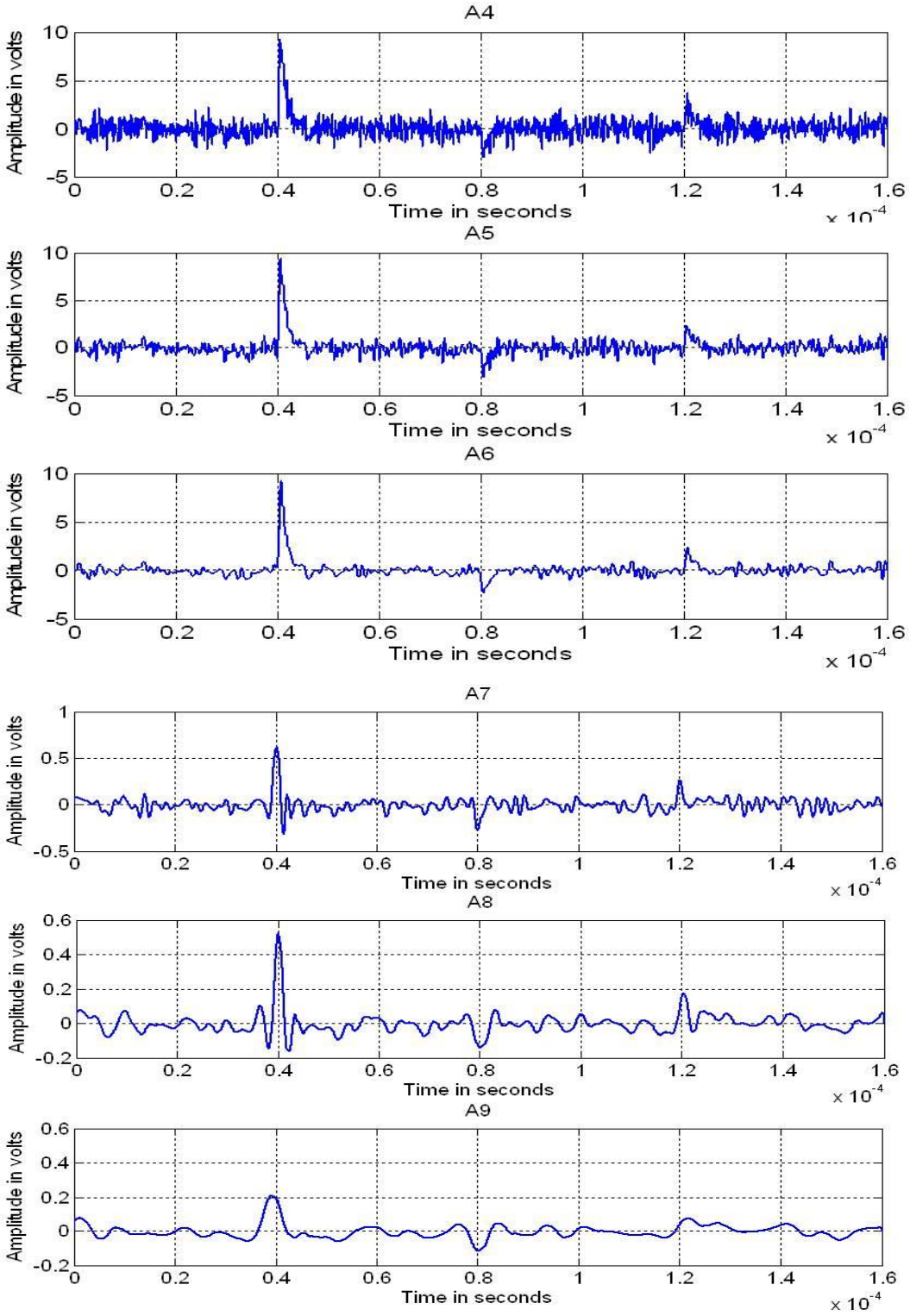


Figure E-1 Approximation coefficients ($A_4$-$A_9$)

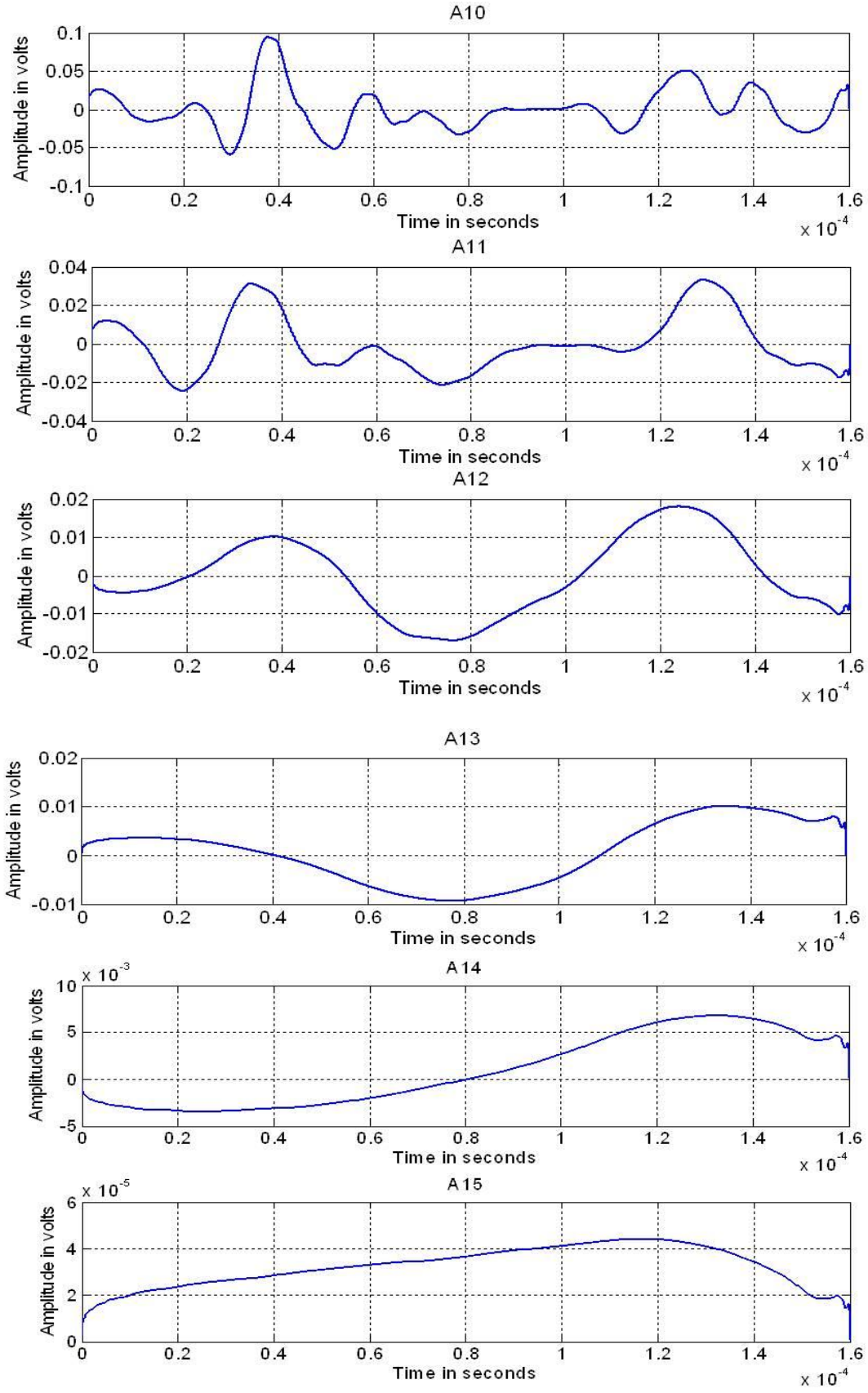


Figure E-2 Approximation coefficients ($A_{10}$-$A_{15}$)

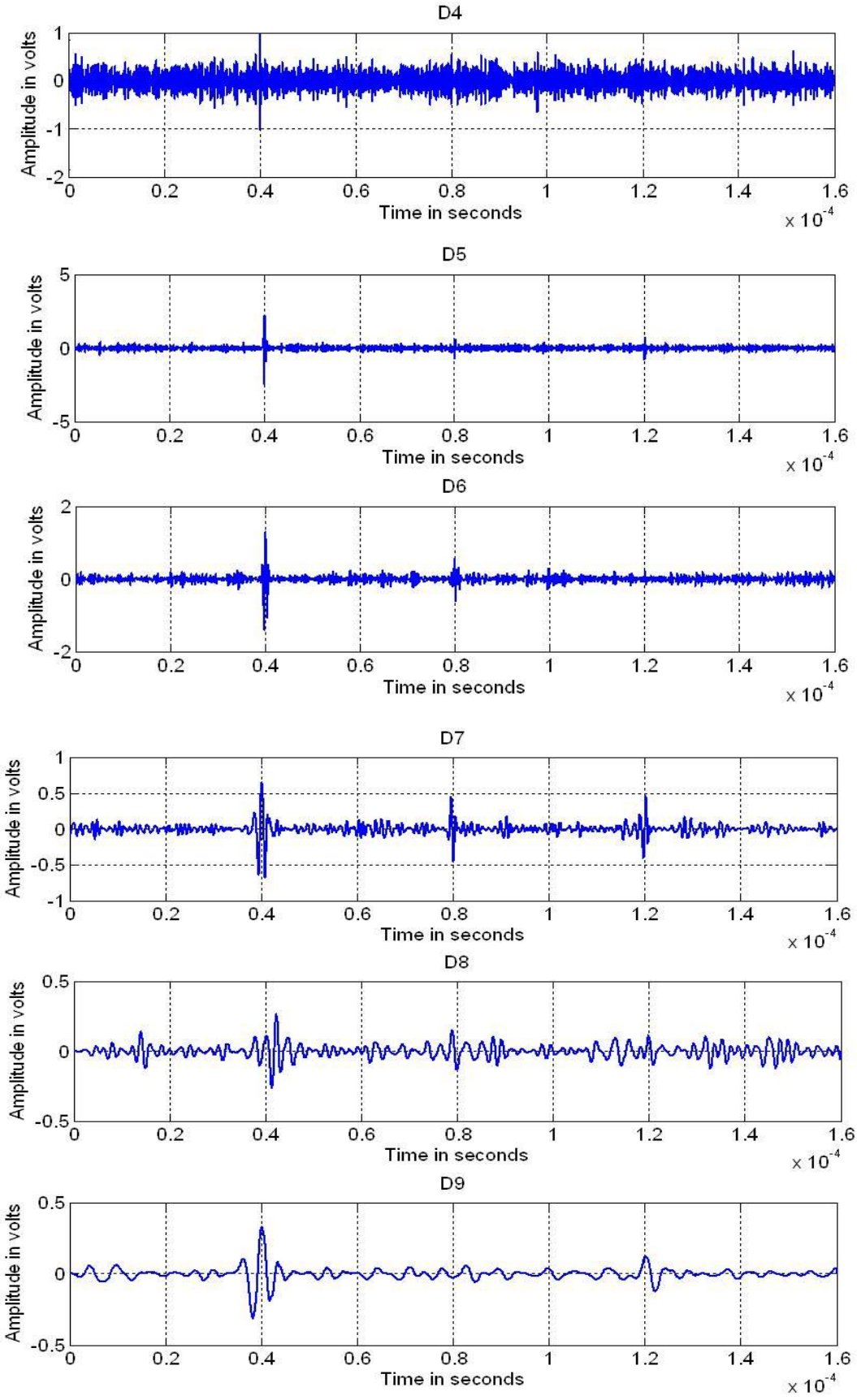


Figure E-3 Detail coefficients ($D_4$-$D_9$)

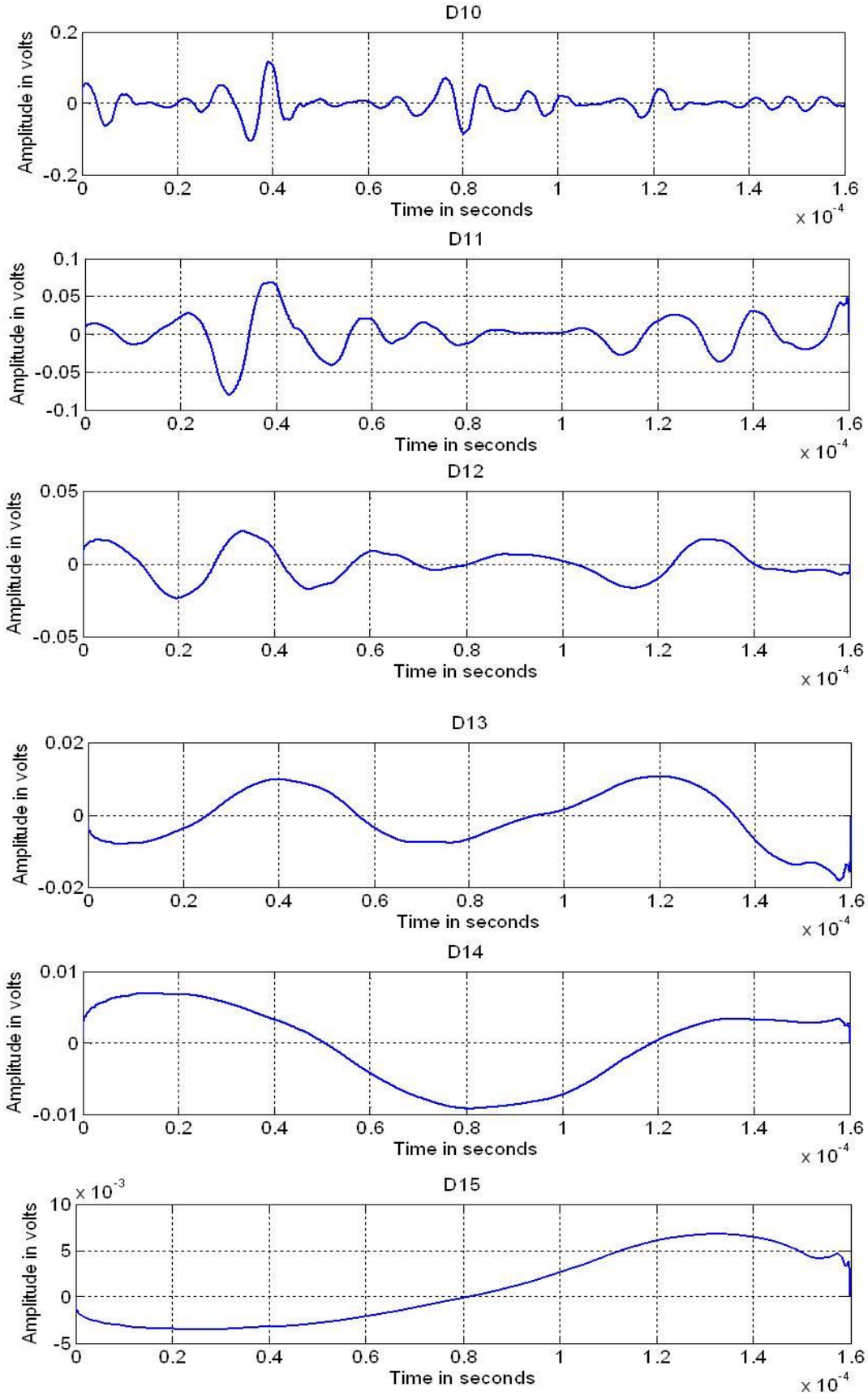


Figure E-4 Detail coefficients for double exponential pulse ($D_{10}$-$D_{15}$)

# E.2 Wavelet Coefficients # 2

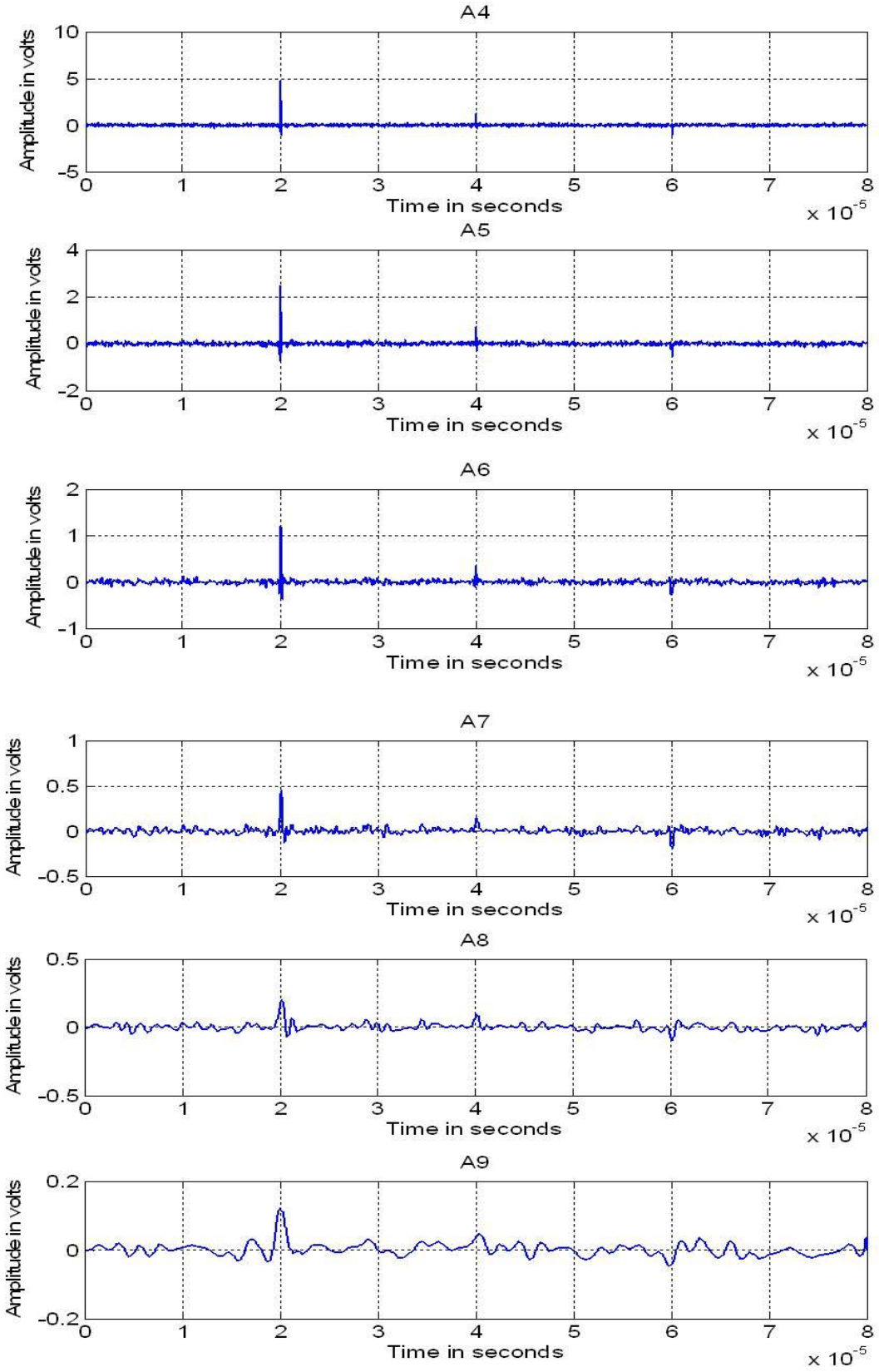


Figure E-5 Approximation coefficients for damped oscillatory pulse ($A_4$-$A_9$)

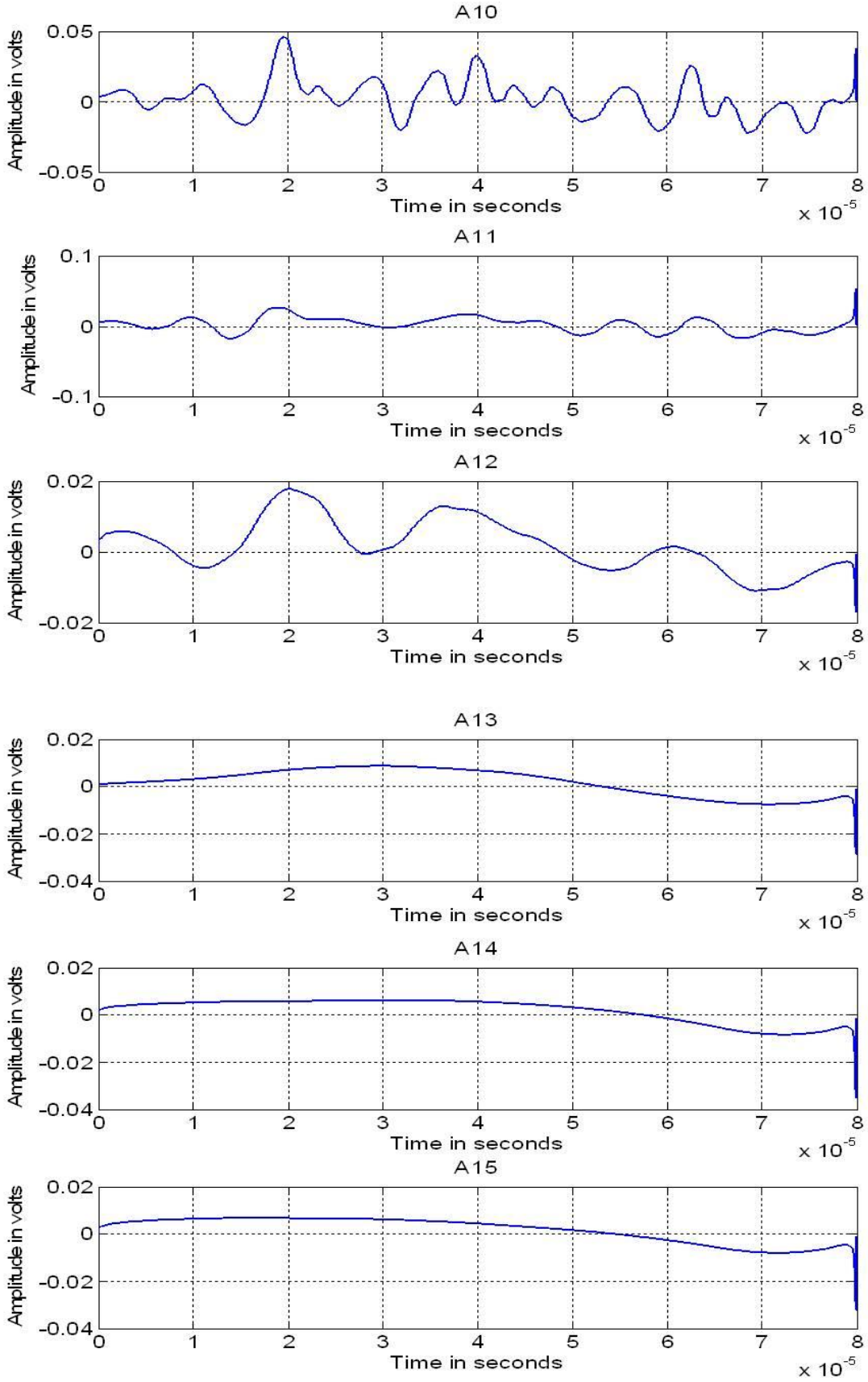


Figure E-6 Approximation coefficients for damped oscillatory pulse ($A_{10}$-$A_{15}$)

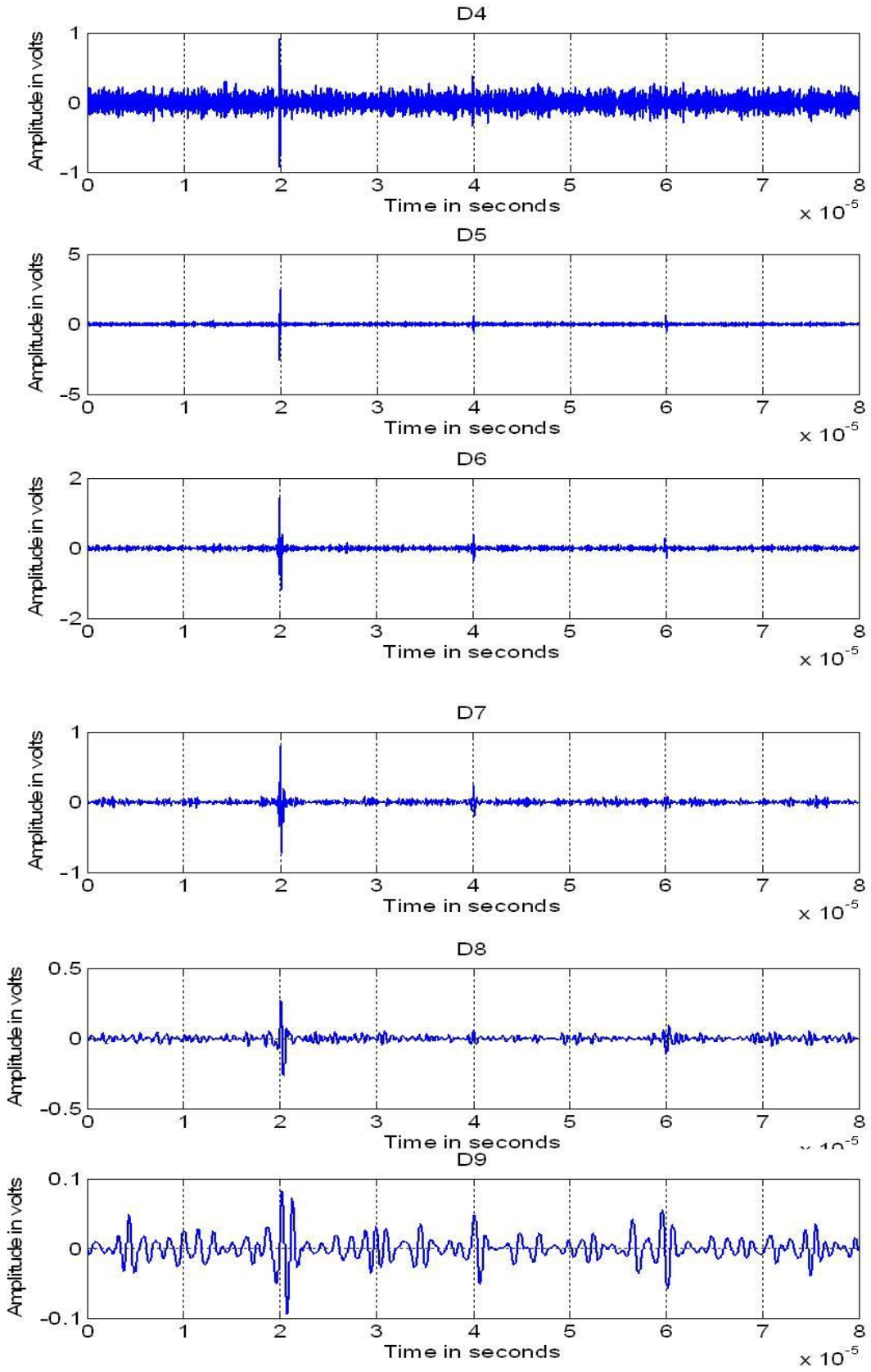


Figure E-7 Detail coefficients for damped oscillatory pulse ($D_1$-$D_9$)

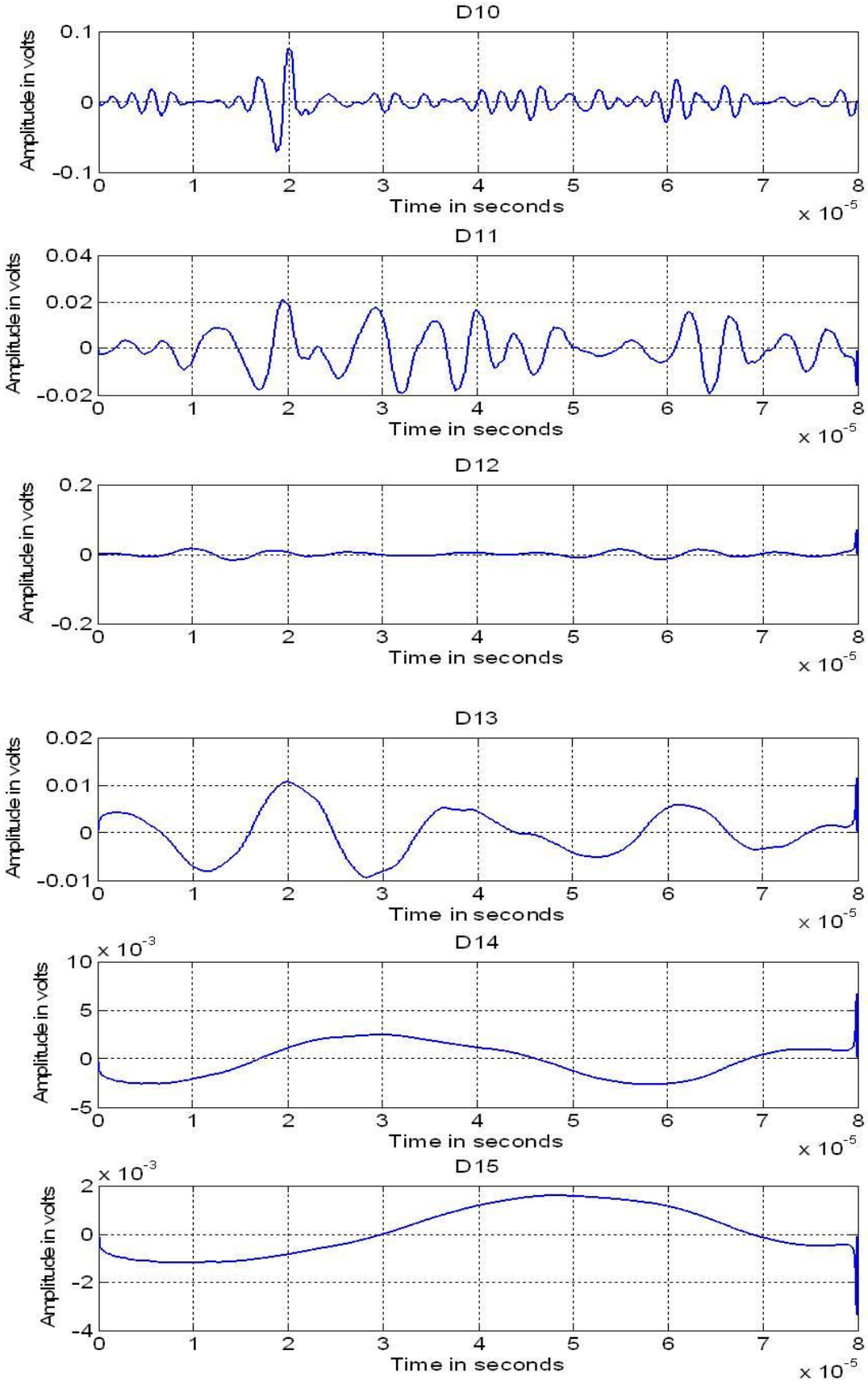


Figure E-8 Detail coefficients for damped oscillatory pulse ($D_{10}$-$D_{15}$)

# E.3 Comparison in Time domain

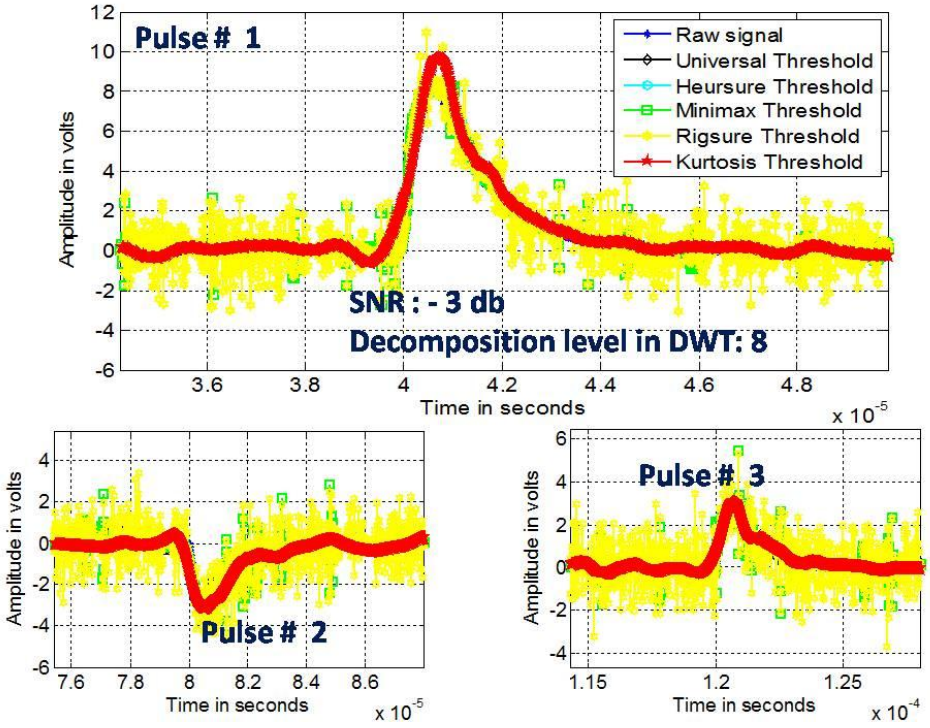


Figure E-9 Time domain comparison (SNR: - 3 db)

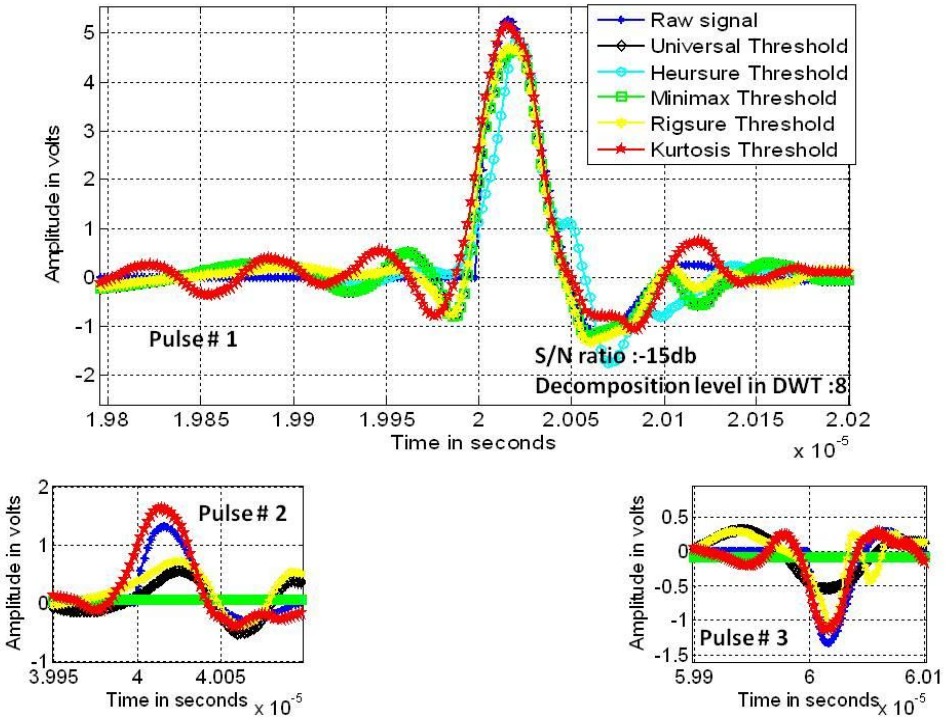


Figure E-10 Time domain comparison (SNR: - 15 db) *

* *Raw signal means Noise free signal*

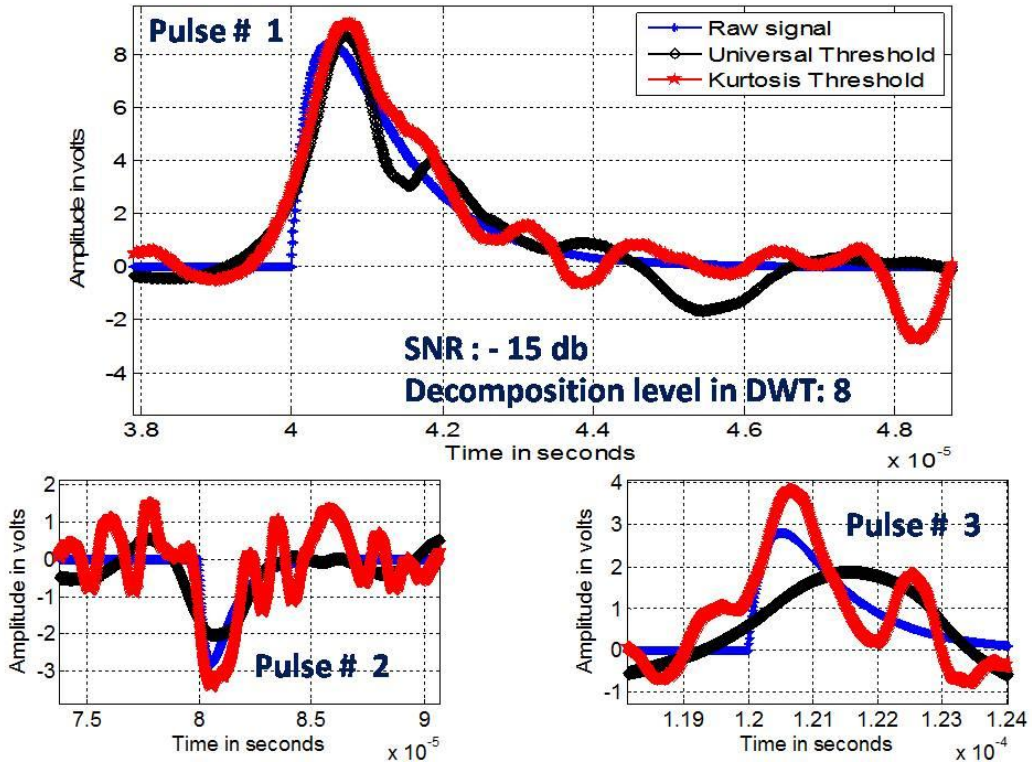


Figure E-11 Time domain comparison (SNR: - 15 db)

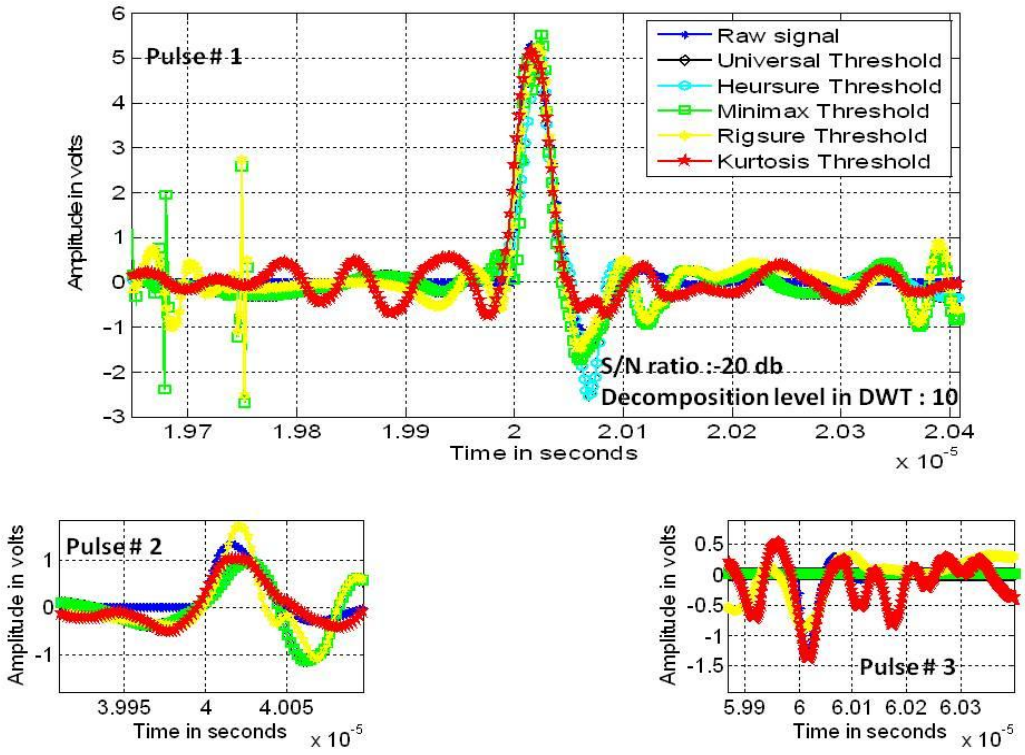


Figure E-12 Time domain comparison (SNR : - 20 db)*

* *Raw signal means Noise free signal*

# E.4 Mean Square Error (MSE) Comparison

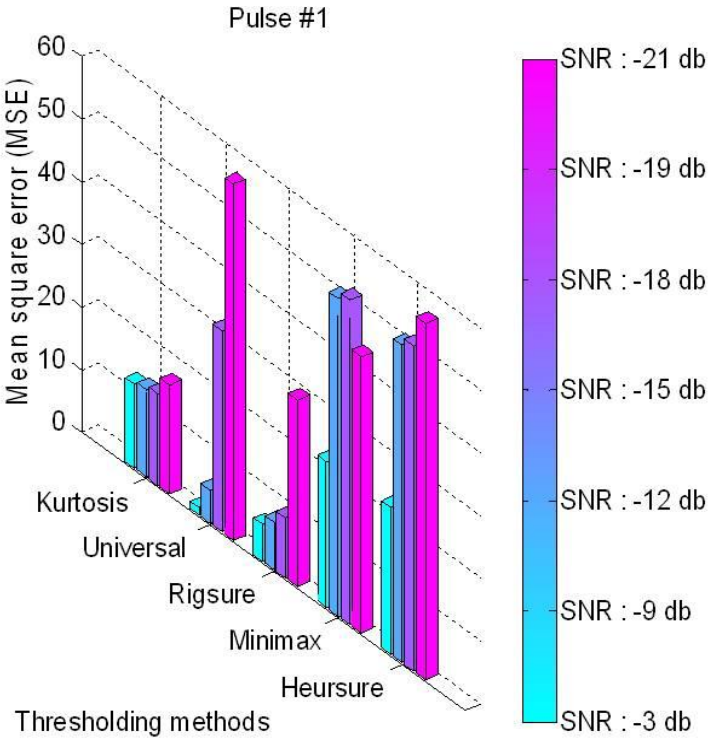


Figure E-13 MSE for pulse # 1 (Damped oscillatory)

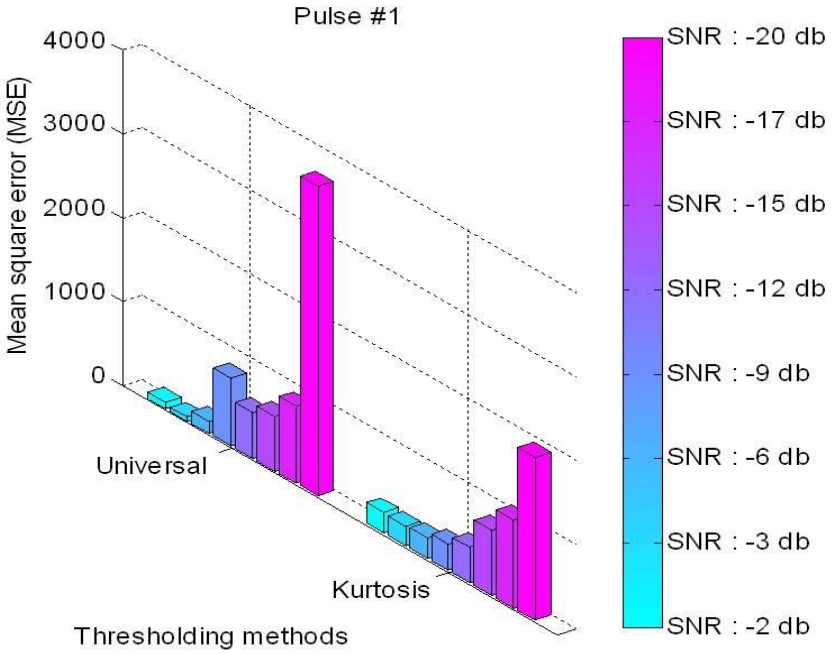


Figure E-14 MSE for pulse # 1 (Double exponential)

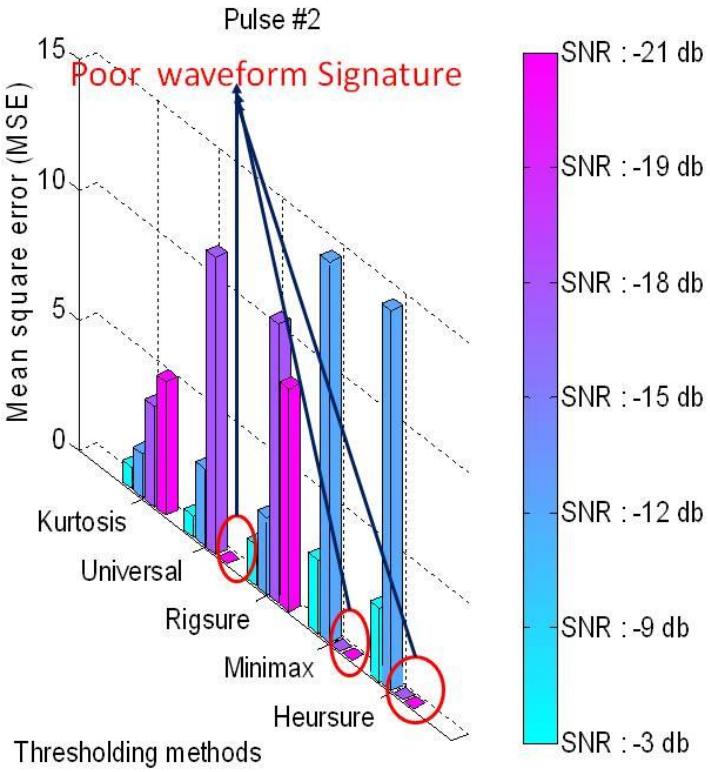


Figure E-15 MSE for pulse # 2 (Damped oscillatory)

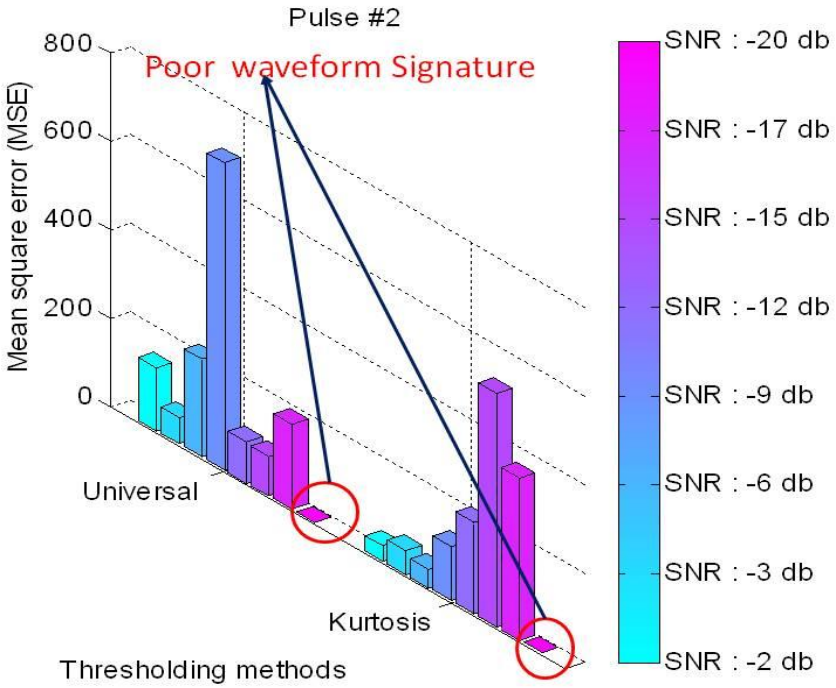


Figure E-16 MSE for pulse # 2 (Double exponential)

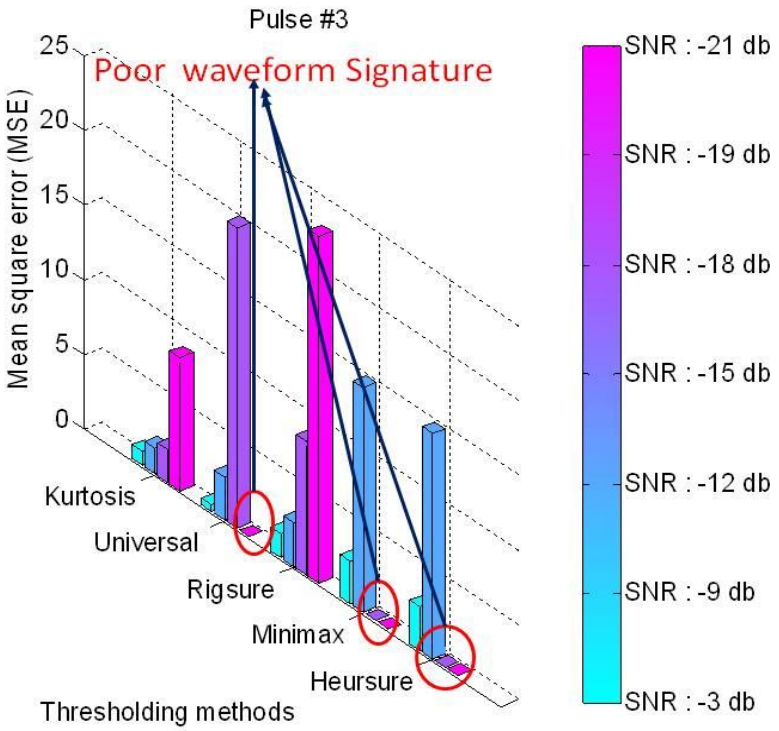


Figure E-17 MSE for pulse # 3 (Damped oscillatory)

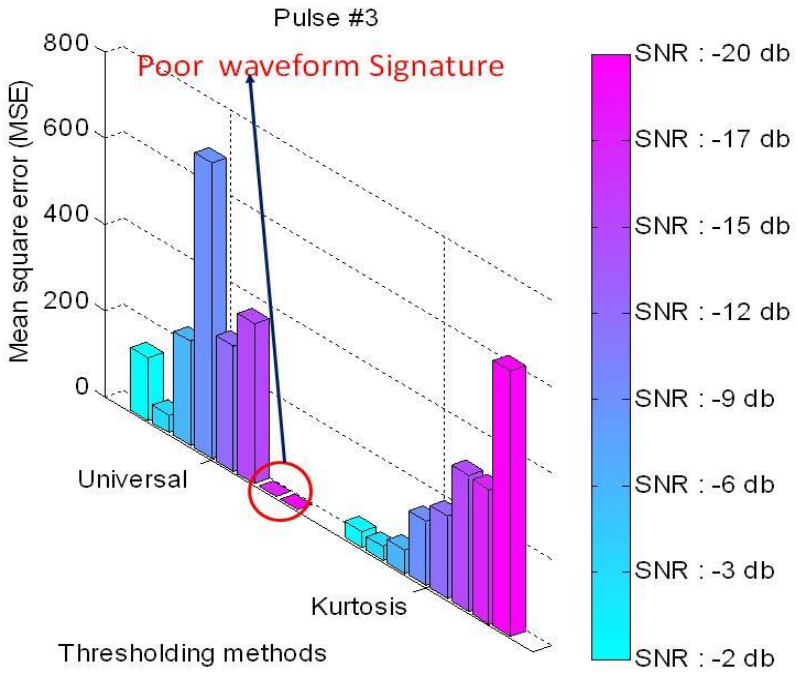


Figure E-18 MSE for pulse # 3 (Double exponential)

# E.5 Denoising Comparison using on-site Data

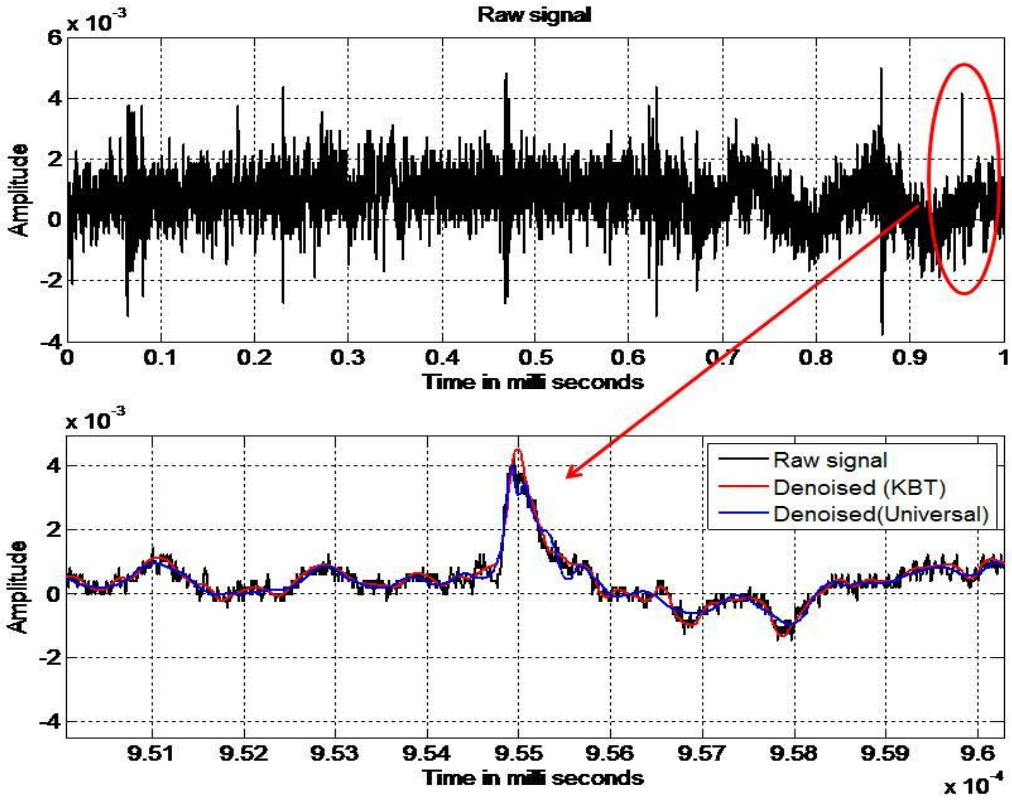


Figure E-19 Denoising comparison (DWT level # 5)

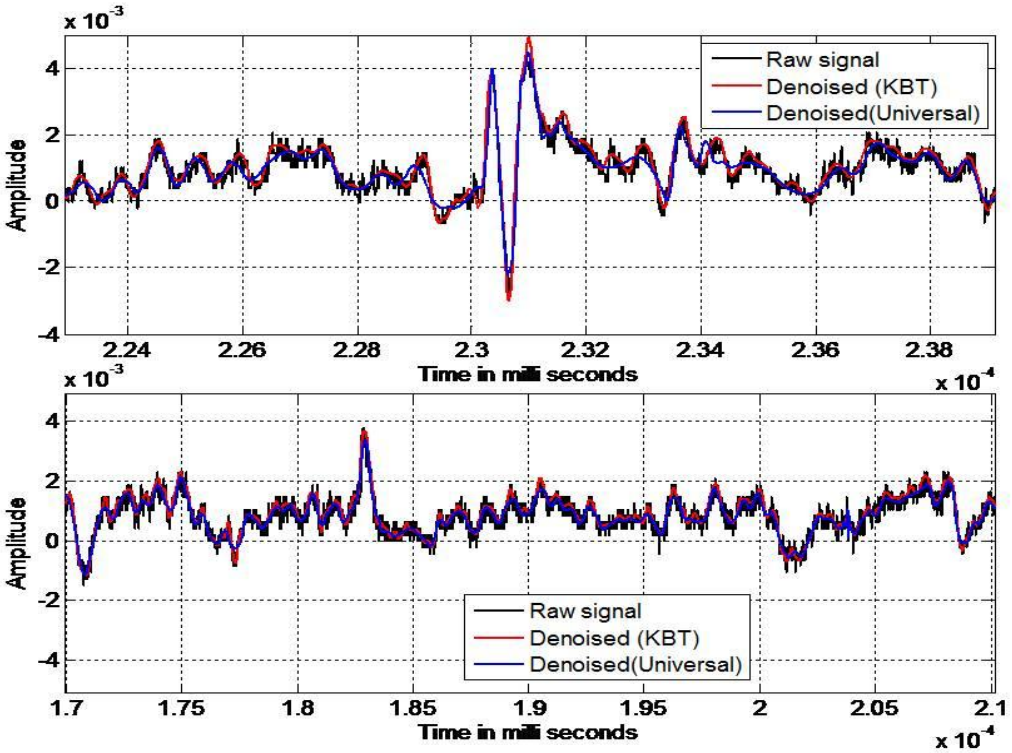


Figure E-20 Denoising comparison (DWT level # 5)

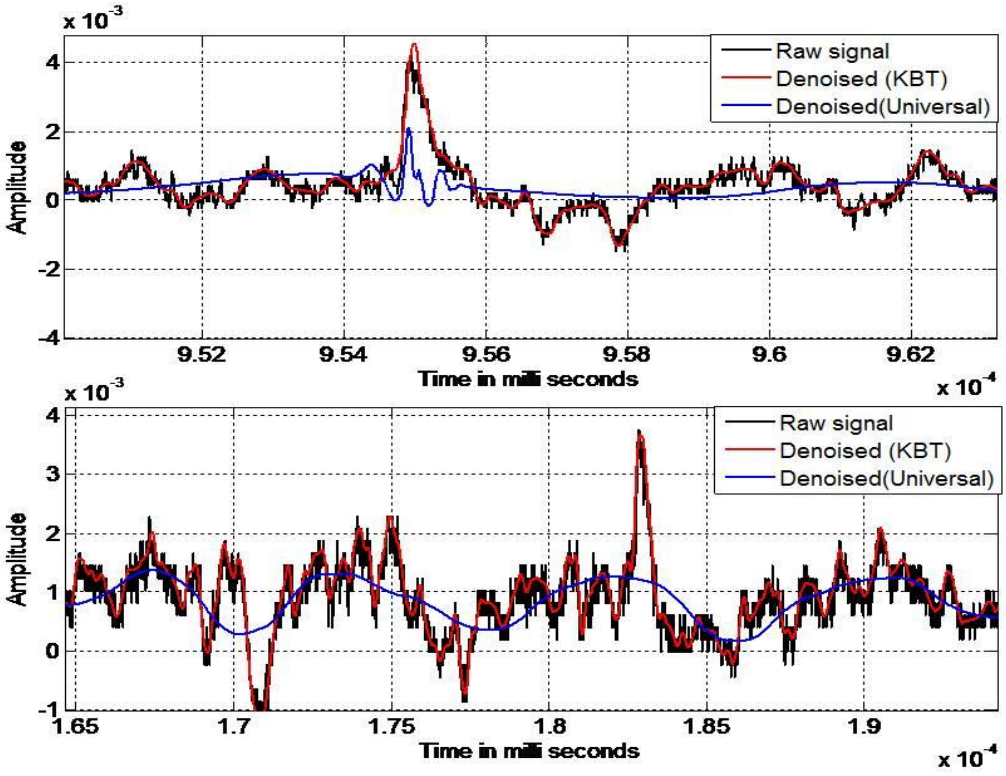


Figure E-21 Denoising comparison (DWT level # 8)

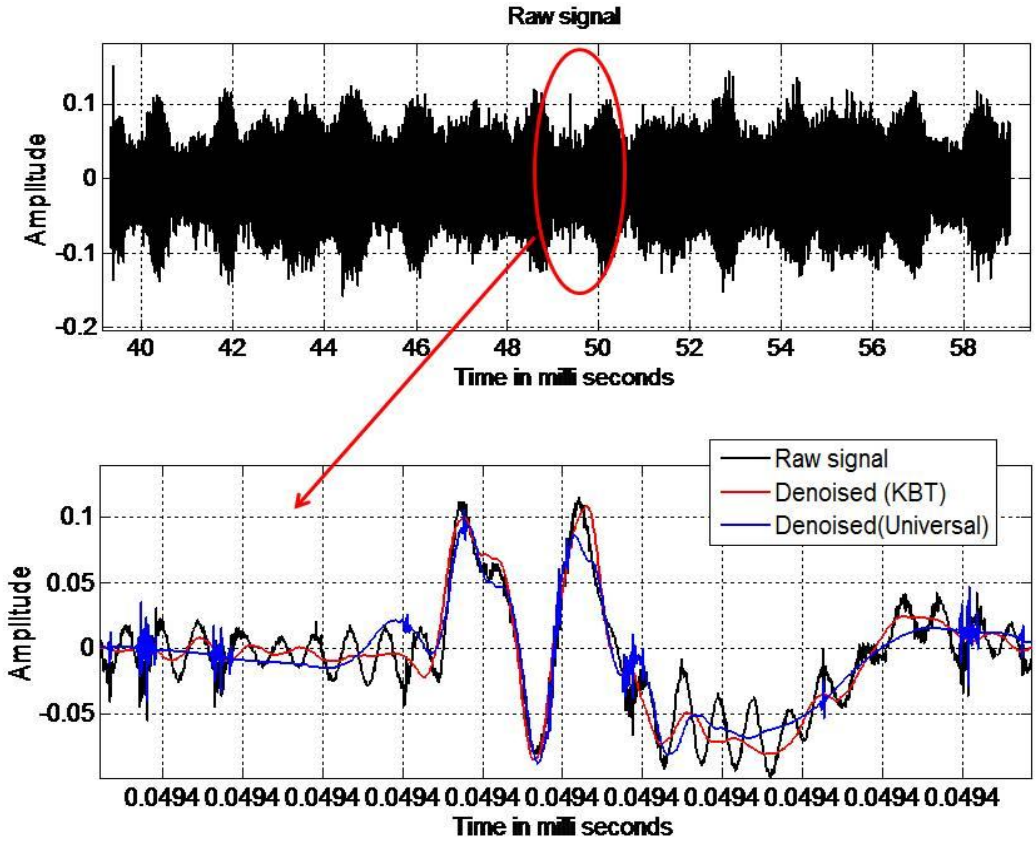


Figure E-22 Denoising comparison (DWT level 5)

# E.6 Intrinsic Mode Functions from on-site Data

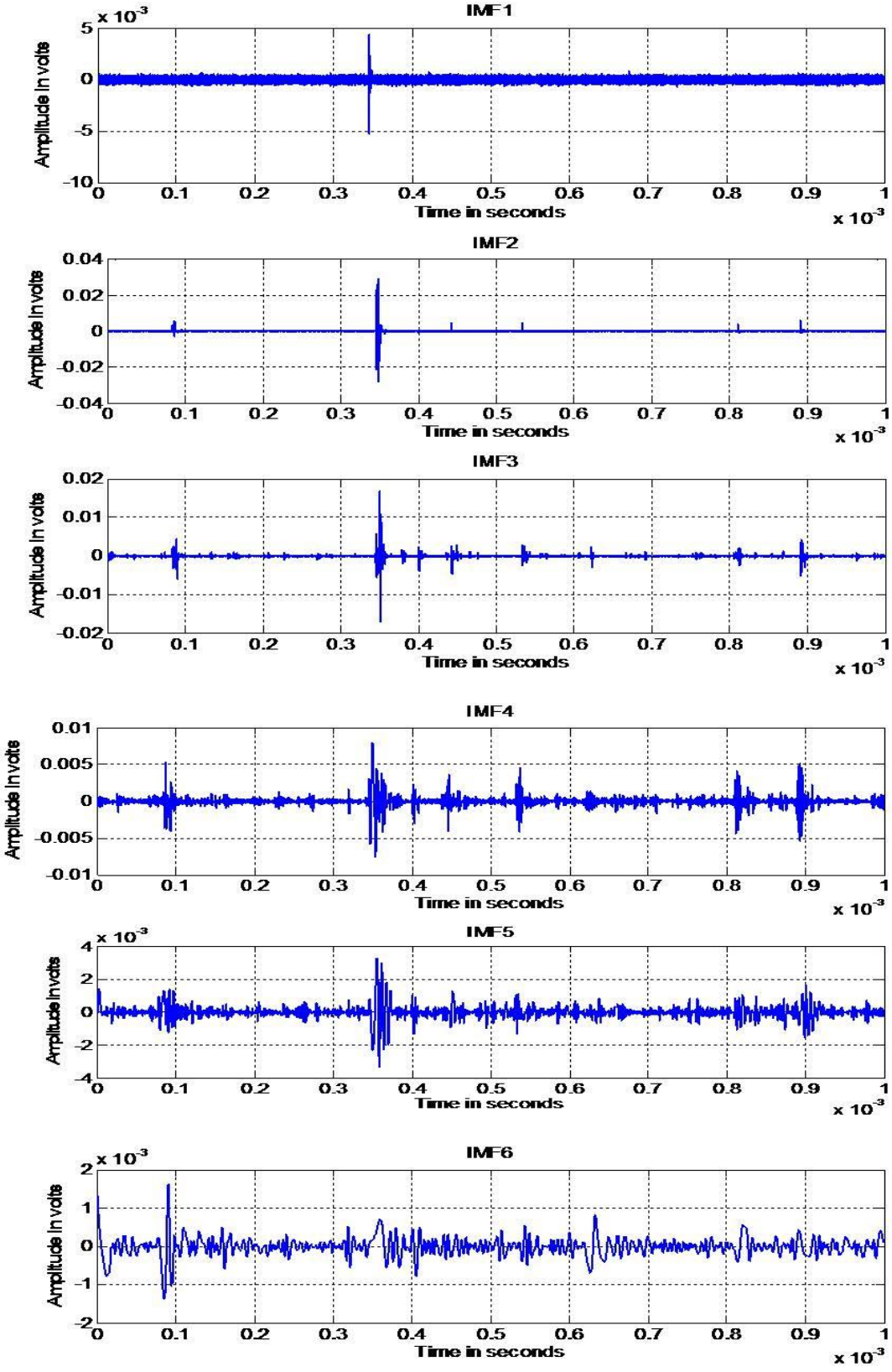


Figure E-23 Intrinsic mode functions ($IMF_1$- $IMF_6$) from on-site data

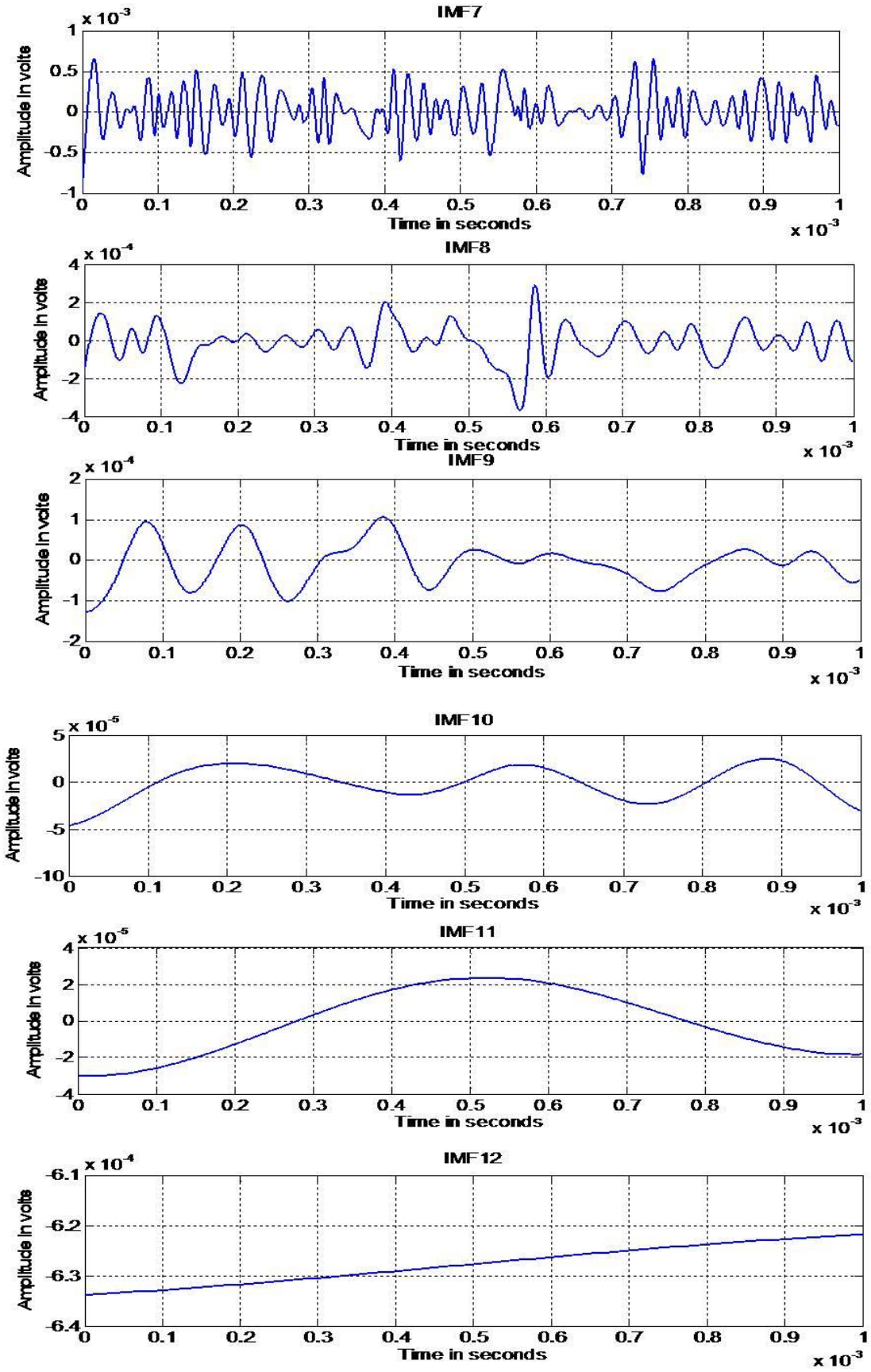


Figure E-24 Intrinsic mode functions ($IMF_7$- $IMF_{12}$) from on-site data

# Appendix : F

## F.1 Signal Power Trend – Substation end A

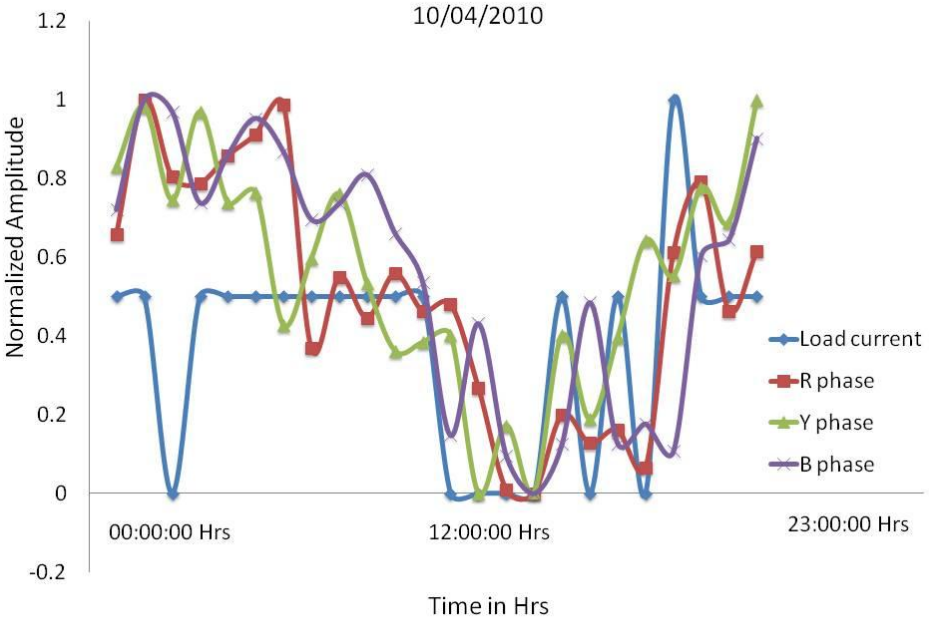


Figure F-1 Signal power trend with respect to load

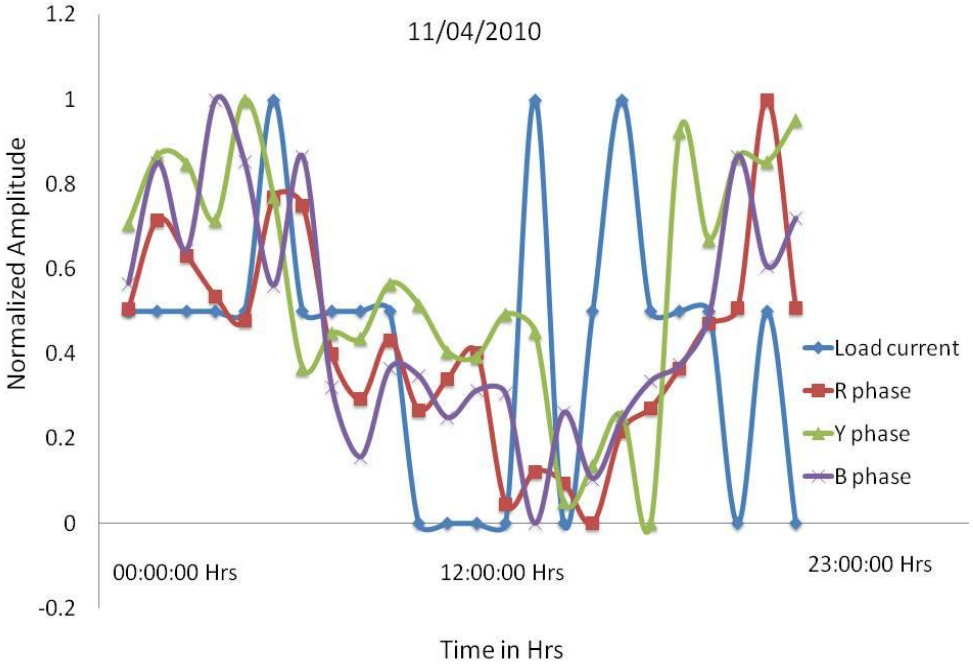


Figure F-2 Signal power trend with respect to load

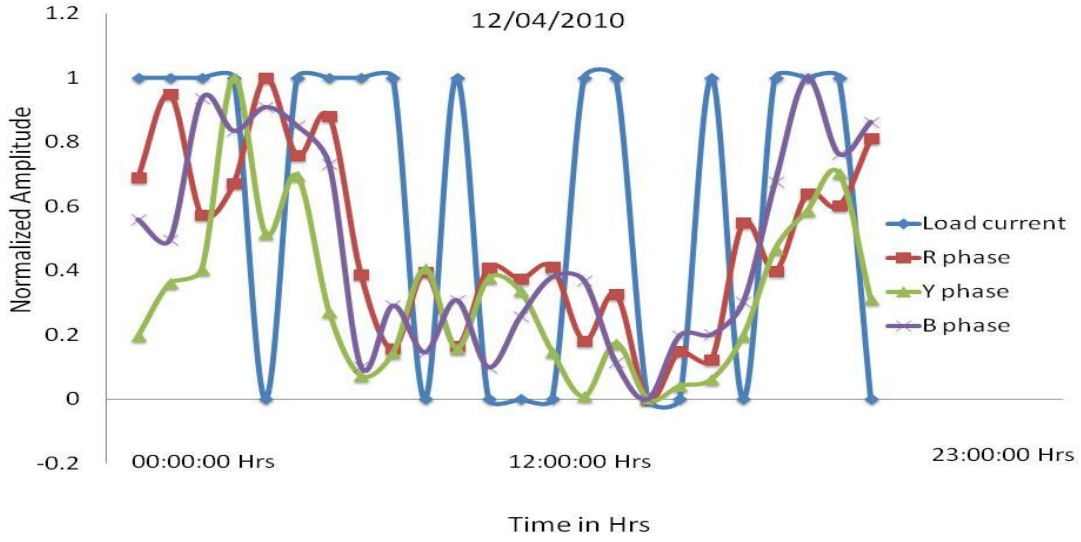


Figure F-3 Signal power trend with respect to load

## F.2 Frequency Components

| Sl # | Earth strap (kHz) | Yphase (kHz) | B phase (kHz) |
|---|---|---|---|
| 1 | 61 | 268 | 256 |
| 2 | 67 | 280 | 286 |
| 3 | 115 | 286 | 1000 |
| 4 | 150 | 568 | 1120 |
| 5 | 158 | 1000 | 1140 |
| 6 | 161 | 1120 | 1200 |
| 7 | 274 | 1150 | 1250 |
| 8 | 329 | 1150 | - |
| 9 | 1100 | 1200 | - |
| 10 | 1150 | - | - |
| 11 | 1220 | - | - |
| 12 | 1526 | - | - |

Table F-1 RF components, UK

# F.3 Signal Power – Substation end B

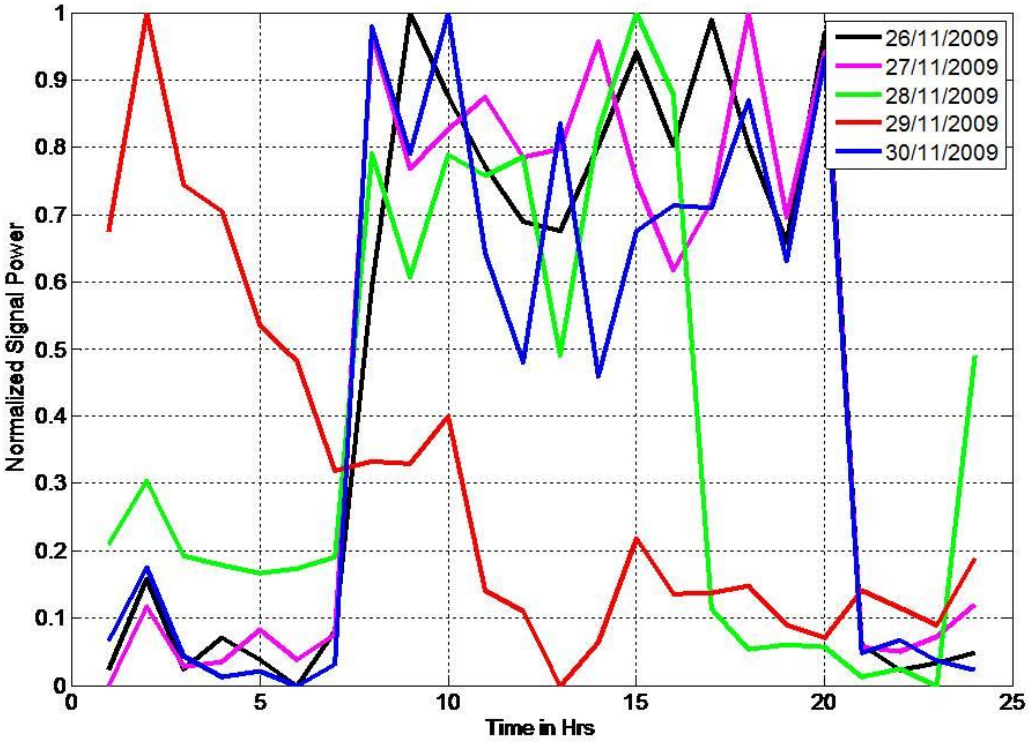


Figure F-4 Signal power trend with respect to load

# Appendix : G

## G.1 Conference Publications

1. F P Mohamed, W.H.Siew, J.J.Soraghan, S.S.Strachan. "Generic data acquisition system with high-speed sampling and synchronized triggering for measurements in any electromagnetic environment." *Fifth UHV net Colloquium, University of Strathclyde, Glasgow, United Kingdom, January 2012*

2. F P Mohamed, W.H.Siew, J.J.Soraghan. "High Speed Data Acquisition System For High Frequency Signals In Harsh Environments". *Advances in Wireless Sensor Networks for Hostile Environments, Derby, May 3 rd 2012, Sensors & Instrumentation Group, United Kingdom.*

3. F P Mohamed, W.H.Siew, "High Speed Wireless Monitoring System", *AFRC Metrology Workshop Day, Glasgow, United Kingdom 28th March 2012.*

4. F P Mohamed, W.H.Siew, K.Y. Liu, S.S.Strachan, N.M. Donald, Jamie McWilliams. "Synchronised Powe Quality Monitoring System using Global Positioning System". *Asia Pacific Symposium on Electromagnetic Compatibility 2012 , Singapore*

5. F P Mohamed, W.H.Siew, J.J.Soraghan, S.S.Strachan, N.M.Donald, J.McWilliams. "Error Sources in Partial Discharge Location in Cables using Time Domain Reflectometry". *Fourth UHV net Colloquium, University of Leicester , United Kingdom, January 2012*

6. F P Mohamed, W.H.Siew, J.J.Soraghan, S.S.Strachan, N.M.Donald, J.McWilliams. "Problems Associated With On-Line Partial Discharge Detection And Location In High Voltage Cables And Solutions". *Jicable'11 - 8th International Conference on Power Insulated Cables, Versailles, France June 23, 2011.*

7. F P Mohamed, W.H.Siew, J.J.Soraghan, S.S.Strachan, N.M.Donald, J.McWilliams. "Investigation of Power Frequency Current Transformer as Partial Discharge Sensors in Medium Voltage Cables." *Jicable'11 - 8th*

*International Conference on Power Insulated Cables , Versailles, France June 22, 2011*

*8.* F P Mohamed, W.H.Siew, J.J.Soraghan, S.S.Strachan, N.M.Donald, J.McWilliams. " Improved Algorithm For On-Line Partial Discharge Location In Cables" *21st International Conference and Exhibition on Electricity Distribution, Frankfurt, CIRED , Germany, 6-9 June, 2011.*

*9.* F P Mohamed, W.H.Siew, J.J.Soraghan, S.S.Strachan, N.M.Donald, J.McWilliams "Study of Signal Processing Techniques Used For Denoising Partial Discharge Signals In Cables."*Fourth UHV net Colloquium, University of Southampton, United Kingdom, January 2011.*

10. F.P.Mohamed, W.H.Siew, J. J. Soraghan. "Remote Partial Discharge Monitoring System For Medium Voltage Cables Using Power Frequency Current Transformers". *Third UHV net Colloquium, University of Manchester, United Kingdom, January 2010.*

11. F.P.Mohamed, W.H.Siew, J. J. Soraghan. "High Frequency Modelling of Protection/Measurement Current Transformers For Partial Discharge Detection". *44th International Universities Power Engineering Conference UPEC, University of Strathclyde, United Kingdom, September 2009*

*12.* F P. Mohamed, W. H. Siew, J. J. Soraghan. "On-Line Partial Discharge Detection In Medium Voltage Cables Using Protection/Instrument Current Transformers". *Second UHV net Colloquium, Glasgow Caledonian University, United Kingdom, 21 January 2009*

*13.* F. P Mohamed, W. H. Siew, Q.M Li. "*Online Partial Discharge Detection In HV Cables Using Conventional Current Transformers*." *2008 International Conference on Condition Monitoring and Diagnosis, Beijing, China, 21-24 April 2008.*

## G.2 Journal Publications

1. The Use of Power Frequency Current Transformers as Partial Discharge Sensor for Underground Cables. *Submitted to IEEE Transactions on Dielectric and Electrical Insulation dated 28/08/2012. Comments received on 17/01/2013. Under review.*

2. PD Location in Power Cables using a Double Ended Method based on Time Triggering with Global Positioning System. *Submitted to IEEE Transactions on Dielectric and Electrical Insulation dated 17/09/2012 . Comments received on 29/10/2012. Under review.*

3. Remote Monitoring of Partial Discharges in Insulated Power Cables. *Submitted to IET Science Measurement & Technology dated 19/11/2012. Under review.*

4. Denosing of partial discharge signals using kurtosis based thresholding with second generation wavelet transforms. *Under preparation for submitting to IEEE Transactions on Dielectric and Electrical Insulation.*

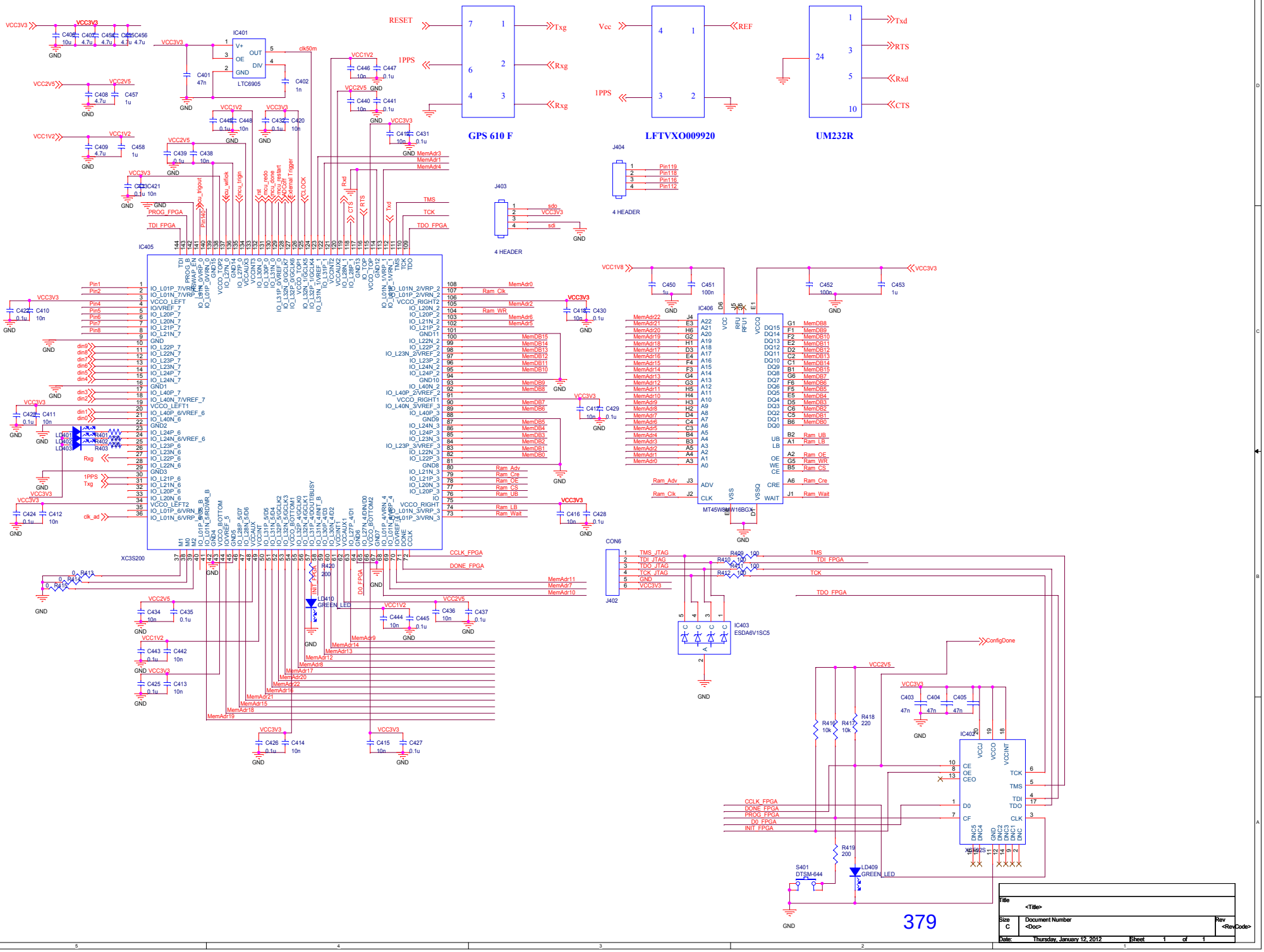
GPS 610 F
LFTVXO009920
UM232R
4 HEADER
IC405
XC3S200
IC406
MT45W8MW16BGX
IC401
LTC6905
IC403
ESDA6V1SC5
IC402
XC9572S
J402
J403
J404
LD409
GREEN_LED
LD410
GREEN_LED
S401
DTSM-644
ConfigDone
379

# Power supply



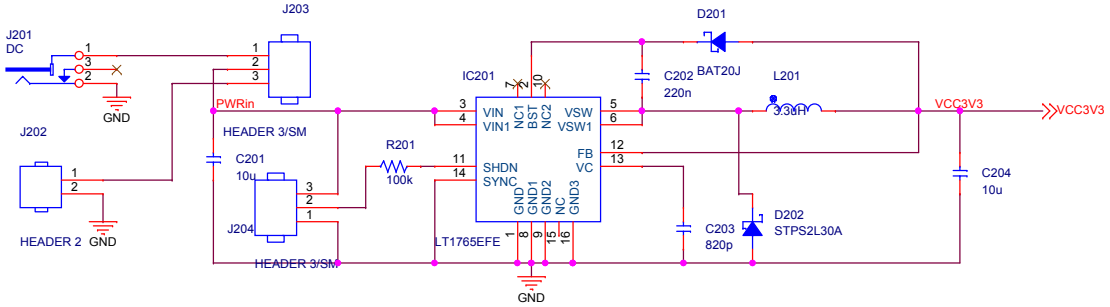


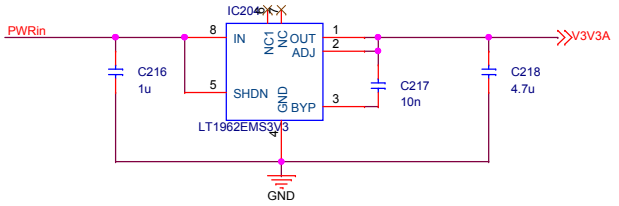


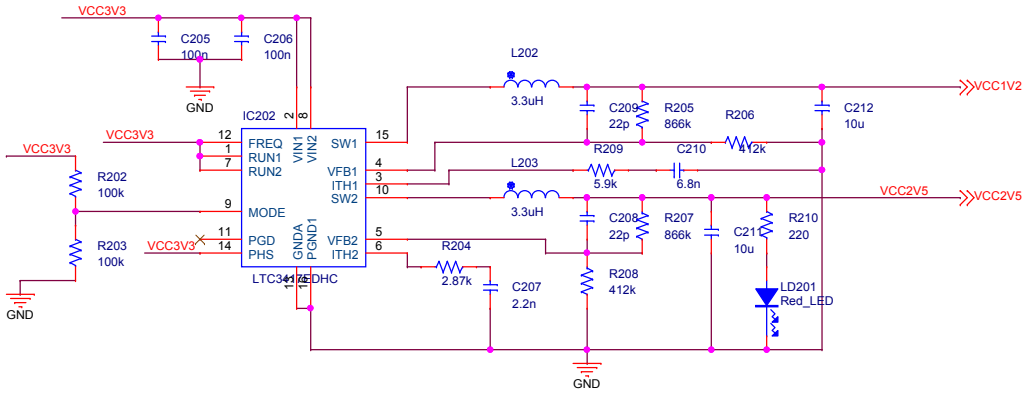


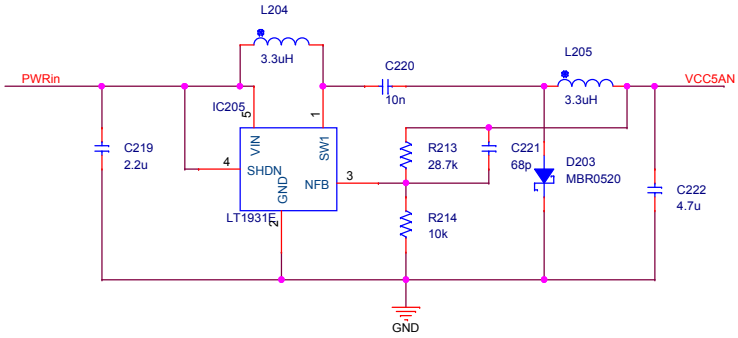


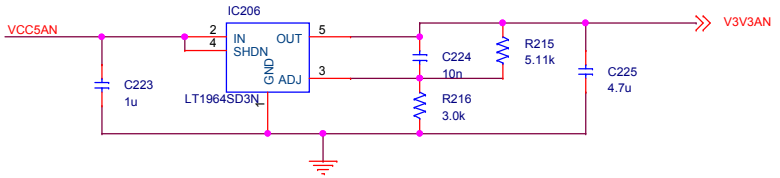


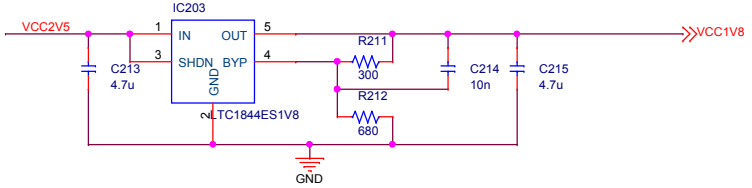


380

| | | |
|---|---|---|
| Title | <Title> | |
| Size B | Document Number <Doc> | Rev <RevCode> |
| Date: Wednesday, January 11, 2012 | Sheet 1 of 8 | |

# Analoge Front-end

H.3

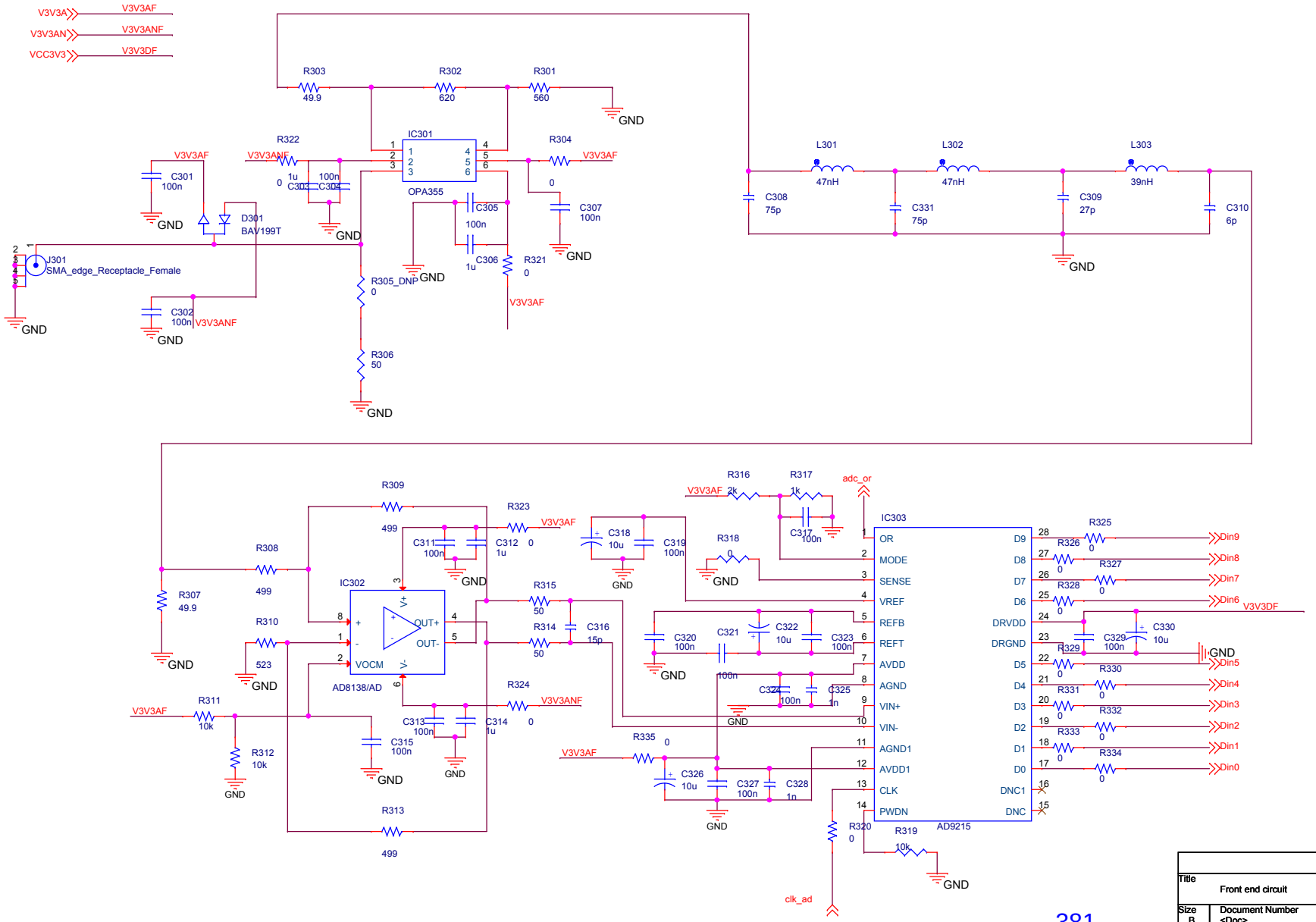


381

| | | |
|---|---|---|
| Title: Front end circuit | | |
| Size: B | Document Number: <Doc> | Rev: <RevCod |
| Date: Wednesday, January 11, 2012 | Sheet 3 of 8 | |

# Zigbee circuit



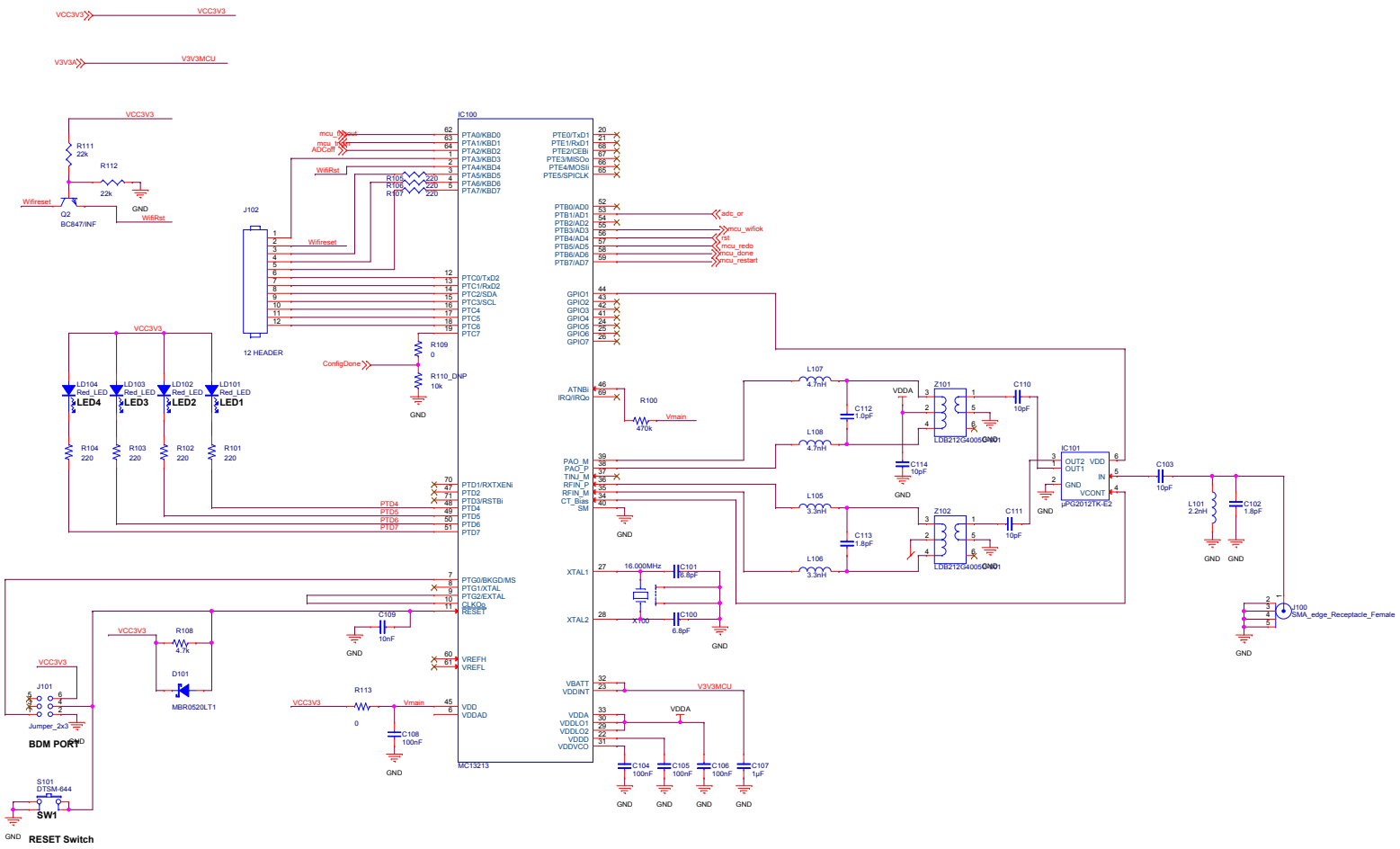




| | | | |
|---|---|---|---|
| Title | <Title> | | |
| Size A2 | Document Number <Doc> | | Rev <RevCode> |
| Date: Wednesday, January 11, 2012 | Sheet 1 of 8 | | |

# Signal Conditioning Circuit

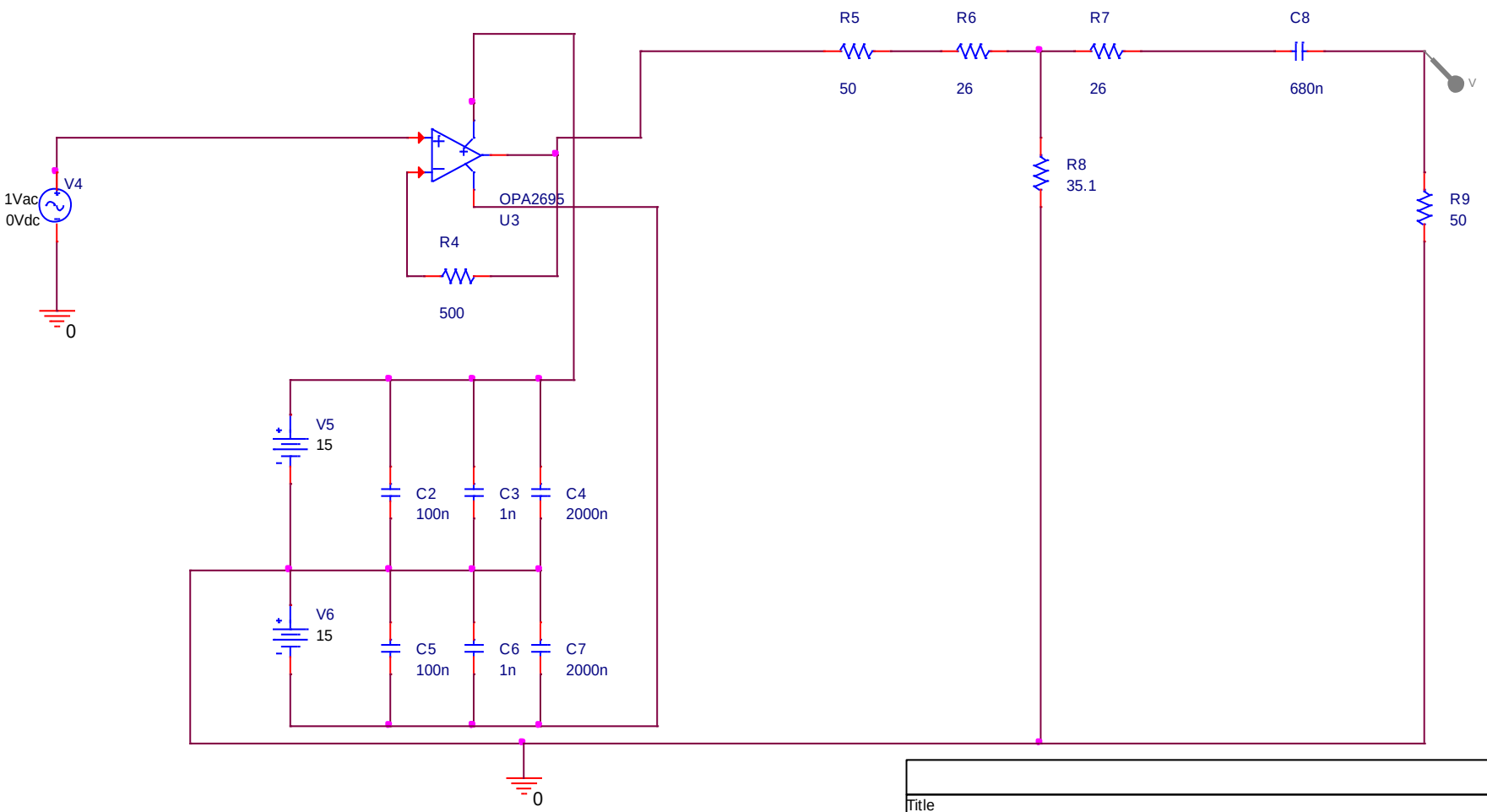

# GPS receiver

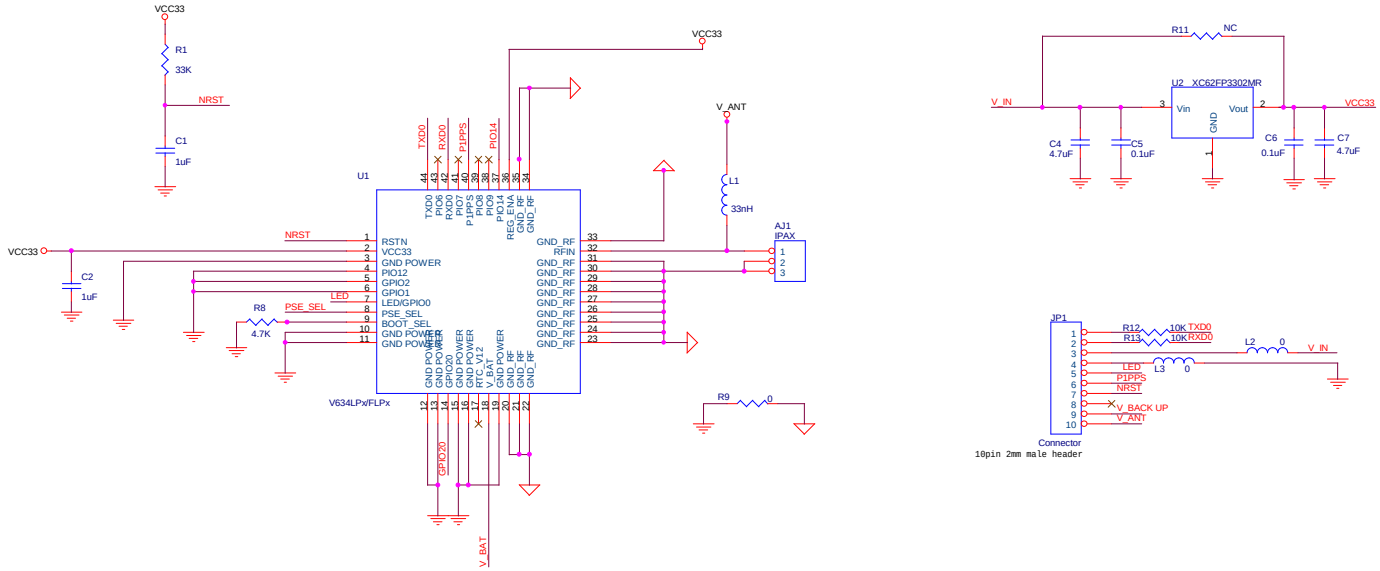








**BAUD_SEL[1:0]:**
**0 0:9600**
**0 1:4800**
**1 0:38400**
**1 1:115200**

**PSE_SEL:**
**0: 4PSE**
**1: 2PSE**

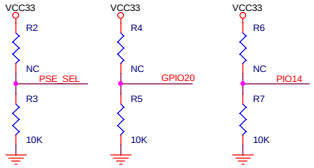


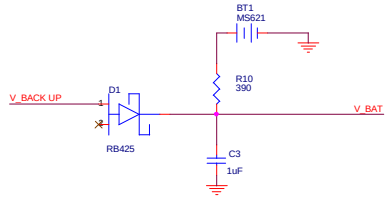


384

| | | |
|---|---|---|
| Title | GM634 | |
| Size C | Document Number Venus 634LP/LPx/FLPx | Rev 0.1 |
| Date: Wednesday, April 08, 2009 | Sheet 1 of 1 | |

# HVPD Technical Guide for PD Levels in MV and HV Cables and Joints

## May 2009

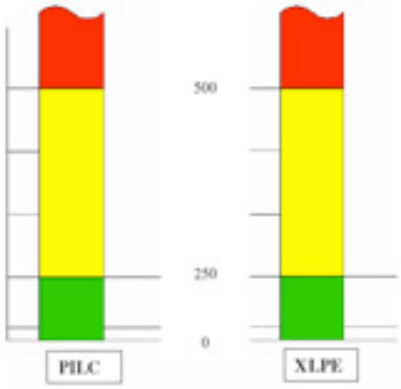


**High Voltage Partial Discharge Ltd**
**Manchester, UK**

Tel: +44 (0) 161 877 6142
Fax:+44 (0) 161 877 6139
e-mail: info@hvpd.co.uk
Web: www.hvpd.co.uk

## PD Testing of MV and HV Cables – *Guideline* PD Levels for Diagnostics

Through work carried out by the HVPD Directors over the past 10 years with utility and industrial MV and hv power plant owners in the UK, Europe and the Rest of the World a large database of results has been generated. From this database it has been possible to produce Cable and Switchgear Insulation Condition 'Knowledge Rules' which allow the plant owner to assess the condition of their MV Cables and Cable Accessories through the on-line PD Test results. These Knowledge Rules can be used in conjunction with the HVPD range of On-line PD test and monitoring equipment and the HVPD 4 Phase Asset Management Solution for the insulation condition assessment of both paper and polymeric-insulated MV cables and solid and air-insulated MV switchgear.

In order to place PD Test results obtained from PD testing of MV cables and cables accessories into some context tables 1 and 2 below provide *Guideline**, PD threshold levels for medium voltage cable networks.

** N.B. It should be noted that these PD levels are based on HVPD's own experience of PD testing (mainly in the UK) and are not definitive figures. The levels given are meant as a guideline only and could be considered in some cases to be conservative whilst in others not conservative enough. They do nevertheless provide a basis for developing a 'League Table' of in-service MV plant and cables based on their insulation condition from which to make Asset Management Decisions.*

*It is recommended that the user/customer develop their own 'at risk' MV Cable and Switchgear PD levels as part of HVPD's Diagnostic Consultancy and Training course on PD Diagnostics. In this way the PD levels for different levels of concern or action can be developed in line with the general condition of the plant owner's equipment and their maintenance schedules and budgets.*

| Insulation Condition Assessment | Colour Code | PD in XLPE | PD in PILC |
|---|---|---|---|
| Discharge within acceptable limits | | 0pC – 250pC | 0pC – 2500pC |
| Some Concern Monitoring recommended | | 250pC – 350pC | 2500pC – 5000pC |
| Some Concern, regular monitoring recommended | | 350pC- 500pC | 5000pC – 7000pC |
| Major Concern, Locate PD and then repair or replace | | > 500pC | >7000pC |

**Table 1: Medium Voltage (6.6 - 45kV) Cables - Guideline PD Levels**

| PILC Cable Accessories | XLPE Cable Accessories |
|---|---|
| 0-4000 pC | 0 – 500 pC |
| 4000 pC – 6000 pC | 500 pC – 1000 pC |
| 6000 pC – 10000 pC | 1000 pC – 2500 pC |
| >10000 pC | >2500 pC |

**Table 2: PD Level Guidelines for MV (6.6 - 45kV) Cable Accessories**

**PD Tolerance Levels for HV XLPE Cables and Cable Accessories (66kV+)**

Through work carried out by HVPD over the past 10 years with Electricity Utility Customers in the UK, Europe and the Rest of the World a large database of results has been generated. From this database it has been possible to *produce Cable Insulation Condition 'Knowledge Rules'* which allow the plant owner to assess the condition of their high voltage cables and accessories through the on-line PD Test results. The Maintenance/Asset Management activity required vs. Level of PD Activity Guidelines from this work are given below in Tables 3 and 4.

The PD Guideline Levels given below in Tables 3 and 4 can be used in conjunction with the *HVPD-Longshot™* PD Spot Tester to provide Guidelines for the On-line condition assessment of polymeric-insulated (XLPE) cables of operating voltages from 66kV up to 400kV.

The On-Line Partial Discharge (PD) testing of high voltage (66kV to 400kV) cables, cable accessories and cable sealing ends is a relatively new application and has been developed by HVPD through the application of our synchronous, 4-Channel HVPD-Longshot™ PD Test Technology over the past 6 years. Whilst the techniques employed are similar to those developed for medium voltage cables and their accessories there are a number of important differences between the testing of HV/EHV cables and their lower voltage, MV counterparts. These differences and the test methods employed are explained in the HVPD document: *"HVPD – Technical Document for HV & EHV Cable Sealing End On-line PD Testing - May 2009"*

| XLPE HV Cables | | |
|---|---|---|
| **PD Level** | **Assessment** | **Colour Code** |
| 0 – 50 pC | Discharge within tolerable limits | |
| 50 – 200 pC | Some concern, monitoring recommended | |
| 200 – 400 pC | Higher concern, regular monitoring recommended | |
| > 400 pC | Major concern, repair or replace | |

**Table 3: High Voltage (66kV - 400kV) Cables - Guideline PD Levels**

| XLPE HV Cable Accessories | | |
|---|---|---|
| **PD Level** | **Assessment** | **Colour Code** |
| 0 – 250 pC | Discharge within tolerable limits | |
| 250 – 1,000 pC | Some concern, regular monitoring recommended | |
| > 1,000 pC | Major concern, repair or replace | |

**Table 4: PD Level Guidelines for HV (66kV - 400kV) Cable Accessories**

**High Voltage Partial Discharge Ltd**
Empress Business Centre
380 Chester Road
Manchester M16 9EA, UK
Tel: +44 161 877 6142
e-mail: info@hvpd.co.uk

# Application Notes for *On-Line* Partial Discharge (PD) Testing of Medium Voltage (MV) Switchgear With the HVPD Longshot™ PD 'Spot' Tester


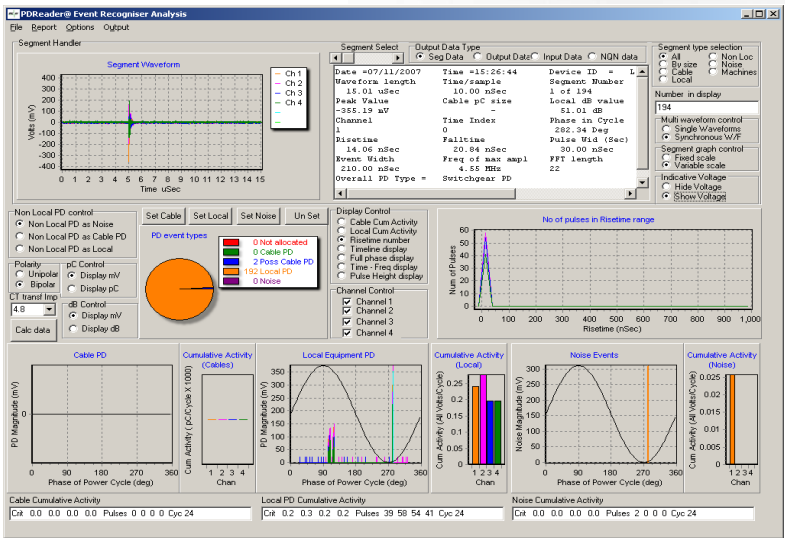


**Issue 4 – May 2009**
**Prepared by:**

**High Voltage Partial Discharge Ltd**

info@hvpd.co.uk

# Partial Discharge (PD) Detection within Medium Voltage Switchgear

## Introduction to these Application Notes

These application notes describe the application of the *Longshot™ On-line Partial Discharge (PD) Test Technology* for the *On-line* PD Testing and Screening of *Medium Voltage (MV) Switchgear (voltage range of 3.3kV to 36kV).* The test system, PD sensors and the test techniques described are suitable for testing both the older type of in-service, Solid Insulated Switchgear (SIS) and the newer type of 'dry' Air-Insulated Switchgear (AIS). It should be noted at this point that the LongshotTM system and the 3x PD sensors described herein is not suitable for the On-line PD testing of the internal insulation of fully enclosed Gas Insulated HV Switchgear (GIS). HV GIS requires internal capacitive PD couplers to measure internal PD.

## Background to the Longshot™ Test Technology

The Longshot™ system has been developed for the On-Line PD testing, monitoring and screening of a wide range of medium voltage (MV) and high voltage (HV) plant. More recently, the system has also been adapted for use in the more conventional Off-Line PD Testing of MV plant in conjunction with adjustable HV power supplies and blocking capacitors. The technologies and techniques described herein have been developed through direct industrial application over a 10-year period, initially in the UK, and more recently (over the past 5 years) in an increasing number of countries around the World. This development has been made in conjunction with HV plant end users (utilities and private plant owners), test service providers and MV/HV plant manufacturers to produce a highly effective, flexible but focused PD testing solution.

The new technology has been built around the development of the versatile PDGold© software which is used in conjunction with high-speed, digital storage oscilloscope (DSO) technology to produce the robust and portable LongshotTM PD 'Spot' Tester for the On-line (and also Off-Line), diagnostic PD testing of HV plant insulation. The applications to which the technology has been applied include:

- **MV Switchgear PD testing and location**
- MV Cable PD testing, monitoring and mapping (PD site location)
- MV and HV VT & CT PD testing
- MV Rotating Machine PD testing
- HV Cable and Cable Sealing End PD testing and cable mapping (PD site location)

These Application Notes refer specifically to the *On-Line* PD testing of MV Switchgear. For further information on the *Off-Line* PD testing of MV Switchgear and other types of MV and HV plant listed above the reader should contact HVPD at info@hvpd.co.uk.

## A Summary Introduction to Partial Discharge Detection in MV Switchgear

### Background

The On-Line Partial Discharge testing of Medium Voltage Switchgear originated in the UK in the early 1980's through the use of Transient Earth Voltage (TEV) / External Capacitive Coupler sensors which are attached to the outer casing of the switchgear at strategic positions. These sensors pick-up the high frequency (radio-frequency) pulses (in the frequency range of 4MHz to 100MHz) which emanate from discharges occurring within the insulation of the metal clad switchgear. This is illustrated in Figure 1 below:

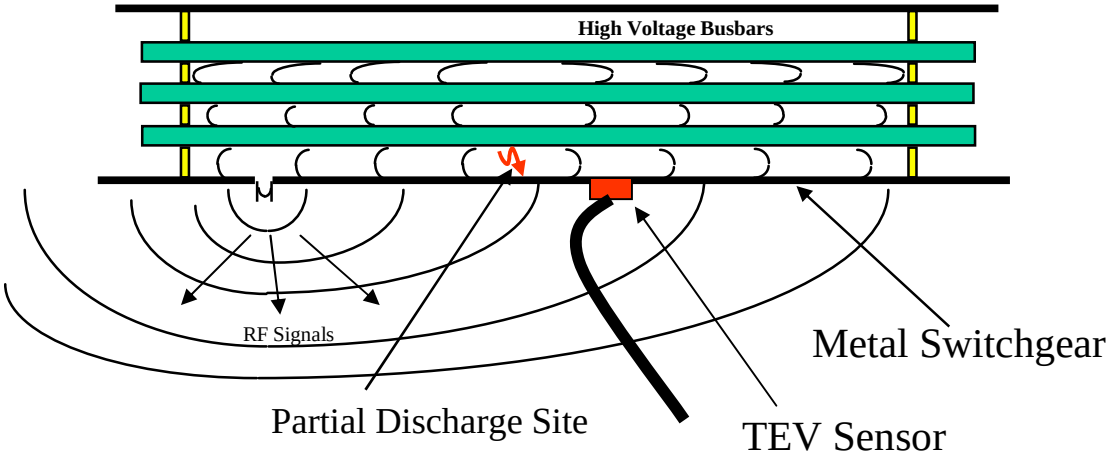


**Figure 1: TEV Signals emanating from within Metal clad Switchgear**

Through work carried out by the UK Electricity Association in conjunction with UK Electricity Distribution Customers a large database of results has been generated which *compares* off-line PD testing of MV Switchgear (measurements in pico Coulombs, pC's) with those made on-line using the TEV Sensor (measurements in decibels, dB). From these results it has been possible to produce Plant Condition 'Knowledge Rules' which allow the plant owner to assess the condition of their MV Switchgear through the on-line PD Test results. PD Level Guidelines vs. Action from this work are provided in Appendix 1. These guideline PD Level Figures are given in dB (as is the convention) for both Solid Insulated and Air Insulated Switchgear.

The Knowledge Rules given in Appendix 1 can be used in conjunction with the Longshot™ PD Spot Tester to provide quick and simple on-line PD Spot Testing and condition assessment of both solid-insulated and air-insulated MV switchgear of operating voltage up to 36kV. However, a word of warning should be made here as this method cannot be directly calibrated, as there is no *prima facie* way of measuring the relationship between the discharge size in pC, and the received electromagnetic signal in Volts. However, a rough guide often is very useful and around 100pC translates to 0dB. This technique is best used for comparative measurements between the same types of switchgear where it provides an excellent comparative tool, and a reasonable absolute tool. It should be noted however that for an accurate, absolute measurement of the PD activity in pico Coulombs an Off-Line test with a pC Calibrator must be used.

## Technical Rationale

At the site of the discharging cavity in the switchgear insulation, the characteristics of PD pulses are as determined by electron travel times across the void space, These result in *very fast* pulses with the following characteristics:-

- small pulse widths, typically 1 nsec – 20 nsec wide (high speed detection circuits are required to measure these characteristics)
- pulse risetimes in the region of 100 psec to 5 nsec
- magnitudes vary from 100 μVolts - 1 V.

With such a large bandwidth of electromagnetic signals, some methods take advantage of the high bandwidth. Bear in mind that the measurements made on these pulses depend greatly on the suitability of the detection circuits used. IEC 270 gives methods for constructing the classical circuits for the detection of these types of signal, but no standards exist to show the interpretation of the measurements, or even the expected values if the detection circuits use on-line components. At the original frequency of the PD pulse, the resulting electromagnetic disturbance is partly describable in 'lumped' components, but is fast enough to show the characteristics of guided waves and transmission lines. With PD events in switchgear, one must deal with pulses which have wavelengths which are similar in size to the physical size of the switchgear. This means that the PD events will travel more like microwaves than lumped circuit electrical signals. This is the basis of the so called *Transient Earth Voltage (TEV)* method, which detects the electromagnetic waves from the PD sites using a probe sat on the outside of the metalclad switchgear. This is a very useful way of measuring PD data on-line.

The values in dB are traditionally (from the original UK Electricity Council Research Centre work in the 1970's) defined as:

$$\text{Measurement (in dB)} = 20\,\text{Log}\left(\frac{\text{Peak PD value in mV}}{1\,\text{mV}}\right)$$

Hence the 0 dB level represents 1 mV into 50 Ohms peak signal, translating to around 100pC. This is now used as a guide for making on-line PD measurements in many electricity utilities around the world. As a rough guide, the tables given in Appendix 1 give some advice on measured levels and their significance. Be aware of all the pitfalls in the measurements, and treat the guides as an indicator rather than an accurate scientific measurement. Nevertheless, the big advantage of this technique is the speed at which in-service MV switchgear can be 'screened' for PD activity prior to carrying out more detailed testing such as Off-Line PD Testing.

In order to make an accurate, laboratory-style measurement of the PD activity in the switchgear an Off-Line PD test with a portable HV power supply, a blocking capacitor and a pC Calibrator must be made. The application of the HVPD Longshot© Test System to Off-line PD Testing of MV Switchgear is not covered in this document. For further information on this application the reader should contact HVPD at info@hvpd.co.uk.

## On-Line PD Testing – Sensor Configuration and Test Set-up

HVPD Ltd recommends the use of 2x PD Sensors for the On-line PD Testing of MV Switchgear and their corresponding cable feeders. These are the TEV sensor, as described previously, and the split-core, High Frequency Current Transformer (HFCT) sensor, as described below.

## TEV – Transient Earth Voltage Sensor

The most effective sensor to use to measure 'local' PD in the switchgear/cable termination is the TEV (Transient Earth Voltage) sensor which is an externally mounted *capacitive coupler* device. The sensor acts as a capacitive coupler to detect PD pulses flowing out of the switchgear panel onto its earthed metal surfaces. The TEV sensors are magnetically latched onto the outside of the switchgear panel. The bandwidth of the TEV sensor is >100MHz and is designed to pick-up PD pulses in the frequency range of 4 to 100MHz.


**Figure 2: Transient Earth Voltage (TEV) Sensor**

## HFCT – High Frequency Current Transformer

Alongside the TEV sensor, the user should also use a calibrated, split-core HFCT sensor which is connected on the earth strap of the cable at the switchgear (a schematic of this connection is shown in Figure 3 below). The HFCT uses *inductive coupling* to detect PD pulses flowing to earth, converting the high frequency (HF) current pulses from the discharges into HF voltage pulses. The split-core HFCT is clipped around the cable earth strap at the bottom of the switchgear. The HFCT sensor (bandwidth 100KHz - 50MHz) is capable of picking-up both 'local' discharge from the switchgear (as per the TEV sensor) and also lower frequency PD pulses coming from down the cable (to enable differentiation between these cable pulses and the switchgear pulses).

**Figure 3: Split-Core High Frequency Current Transformer (HFCT) Sensor**

The ideal On-line PD Test Set-up for MV switchgear is shown below in the schematic in Figure 4. This shows the TEV sensor attached to the outside of the cable box of the switchgear and the HFCT sensor connected around the earth strap of the cable. It can also be noted that the schematic shows an *insulated gland* between the cable and the switchgear, this is a pre-requisite for picking up PD pulses from the switchgear and the cable with the HFCT sensor. For switchgear/cable installations without an insulated gland (such as a lead plumbed termination) then only the TEV sensor can be used. In this case it is recommended that 2x TEV sensors are used with one placed on the cable box (as shown below) and the second placed higher up the switchgear panel.

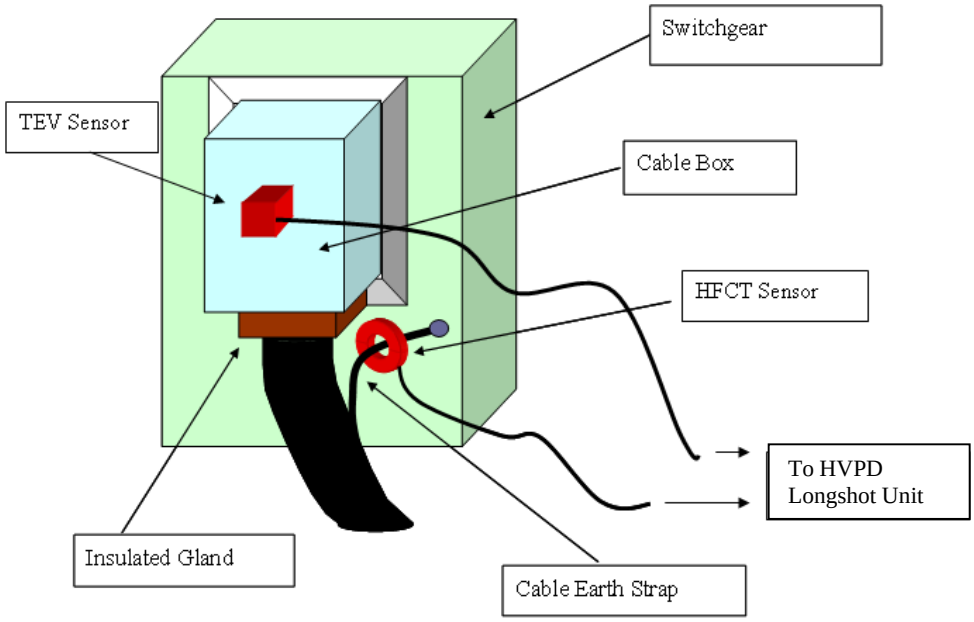


**Figure 4: On-Line PD Test Set-Up for MV Switchgear with 2x PD Sensors**

Figure 5 below shows the above test set-up in the substation with a TEV sensor attached to cable box of an 11kV solid-insulated switchgear panel and an HFCT sensor connected around the earth bar connection of the switchgear/cable to measure both 'local' switchgear PD and also cable PD from along the cable.

**Figure 5: Photo of TEV Sensor Attachment to Cable Box & HFCT connection to Cable Earth Bar**

## PD PULSE RECOGNITION

Partial discharges (PD) in voids and cavities in insulation systems produce very fast pulses with widths of a few tens or hundreds of picoseconds at the source of the discharge being typical. Switchgear PD pulses are characterized by very fast risetimes (in the range of a few hundred picoseconds) and a pulse widths of a few tens of nanoseconds. A typical Switchgear PD pulse is shown below in Figure 6. Switchgear PD pulses are typically of high frequency (4MHz to 100MHz) and oscillatory in shape due to the original PD pulse producing multiple reflections within the switchgear panel.

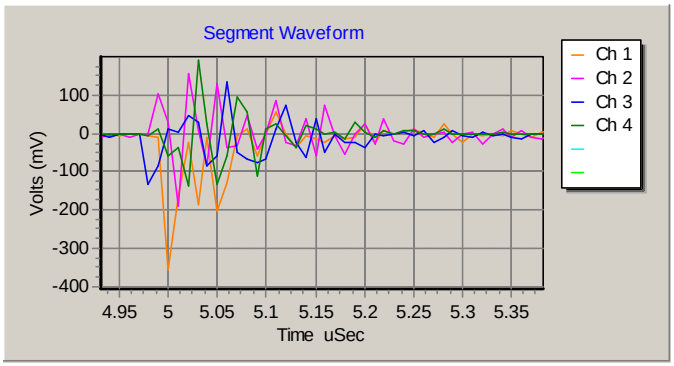


**Figure 6: Switchgear PD pulse in 11kV metal clad AIS**

Cable PD pulses are somewhat different to the Switchgear PD pulses in both shape and frequency content (cable PD frequency range; 100kHz – 4MHz). In the case of cables, the cavity responsible for the PD discharges into a real impedance (the 'surge impedance' of the cable) which is purely resistive at the point of launch. The resulting PD pulse initiated at the pd source is virtually monopolar with a fast pulse risetime and very short pulse width. This pulse travels outward from the originating site, and arrives at the detection point (at the switchgear termination) both wider and smaller due to attenuation and dispersion on its travel down the cable. A typical cable PD pulse which has travelled some way down a 33kV PILC cable is shown below in Figure 7.

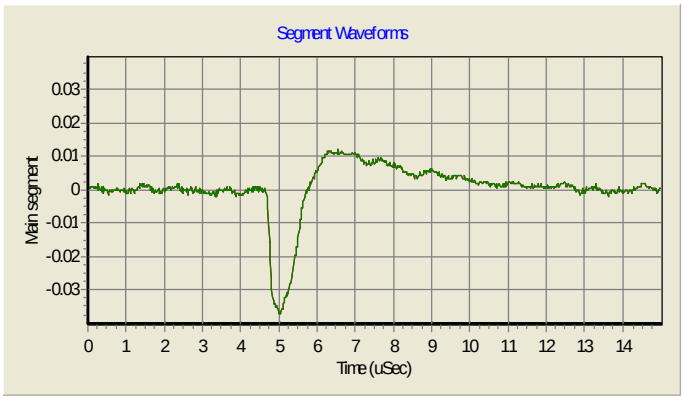


**Figure 7: Example of Typical Monopolar Cable PD Pulse on 33kV PILC Cable**

When measuring cable PD pulses it should be noted that two PD pulses will travel down the cable to the termination, with one on the conductor and one on the earth screen. These pulses have an equal and opposite polarity and so it does not matter whether the HFCTs are placed on the earth strap, or around the conductor (insulated core).The important criterion is that *only one of* either the earth or conductor PD currents is intercepted (if they are both intercepted then they effectively 'cancel each other out'). The HFCT connection options available are illustrated below in Figure 8.

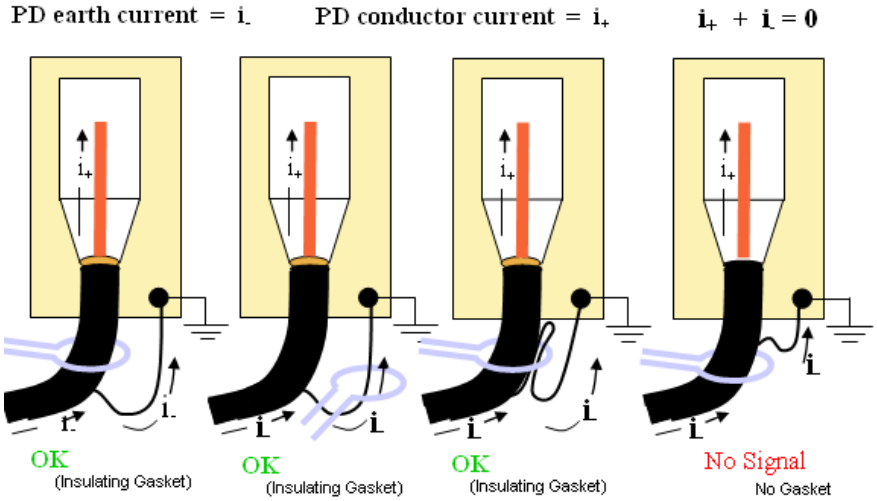


**Figure 8: HFCT sensor connection options for PD pulse detection in power cables**

**Electrical 'Noise' Pulses** are the other type of signals which are picked up during On-Line PD Testing and these must be differentiated from the real PD signals (in the switchgear or cable). Noise pulses are typically of three forms, switching noise/generator exciter pulses (typically in the frequency range of 30-100kHz), RF noise from AM radio broadcasts (in frequency range 500kHz to 1.2MHz) or from signalling schemes (Power Line Carrier - PLC signals) used for signal communications along the overhead lines between substations. The PDGold© software identifies these noise pulses via frequency analysis in the case of switching noise (this being of too low frequency for PD) and through waveshape analysis in the case of RF and PLC Noise (the sinusoidal nature of these signals is rejected by the software as being from a PD source). Two examples of a switching noise and RF noise are shown below in Figure 9 (these would be automatically characterised as noise by the PDGold© software).

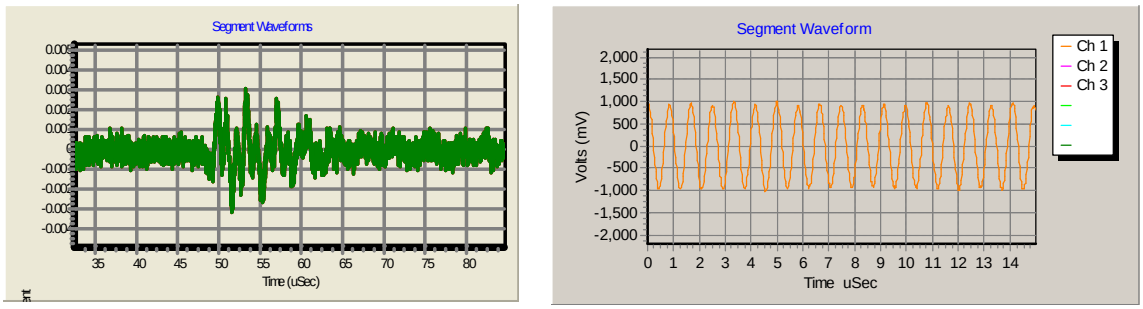


**Figure 9: Examples of Typical Noise Pulses**
(Left: Switching noise at 40KHz, right: RF noise at 600KHz)

By automatically identifying the various wave shapes shown above in Figures 7 to 9 the PDGold© software provides an instant diagnostic as to the presence and magnitude of any PD activity present whilst automatically removing the noise pulses. Unlike other commercially-available systems, the LongshotTM will collect and analyze the noise pulses and display them to the user so that they can be viewed manually if required. It should be noted that other systems use hardware filters to block-out bands of frequencies to try to reduce noise, which whilst they can work also block-out real PD pulses). The PDGold© software has been designed to be easy and quick to use with automatic diagnosis of the signals, thus allowing large numbers of HV plant items to be scanned for PD.

## PDGold© Event Recognizer Page

As explained above, Switchgear or 'Local Equipment' PD (such as in the cable termination) has a very different waveshape and frequency content than the PD's coming from along the cable. Figure 10 overleaf shows Screenshot's from the PDGold© software which compare an example of *Switchgear/Local Equipment PD* activity (top screenshot) with that from *Cable PD* activity (bottom screenshot). The top screenshot shows Switchgear/Local Equipment PDs of up to 10mV (20dB) in the bottom middle graph with a few noise pulses (bottom right graph). The 'Segment Waveform' box in the top left-hand corner of the screen shows the 'Waveform' of one of the Switchgear/Local Equipment PD pulses measured in this test. This pulse has been identified by the

software as a 'Local' PD due to it having the right waveshape (high frequency and 'ringing'/oscillating pulse shape) with a risetime, fall-time and pulse width in the correct range and the much higher frequency (22.5MHz) than would be seen for a cable PD (these are typically in the range of 200kHz to 3MHz).

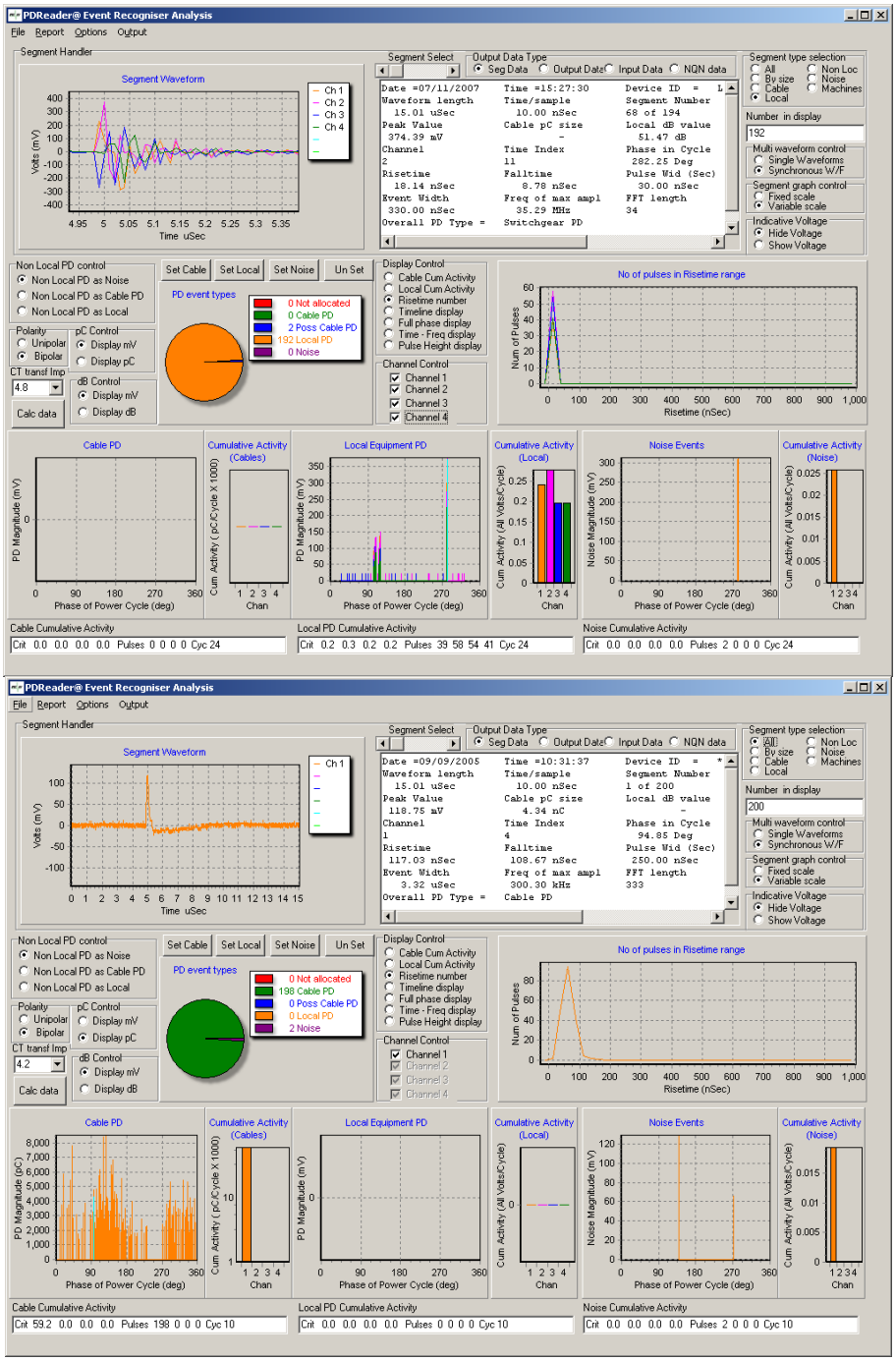


**Figure 10: Screenshots from PDGold© Software Event Recogniser Page**
Top: Switchgear/Local Equipment PD
Bottom: Cable PD (and Noise)

The bottom screenshot in Figure 10 of the PDGold© Event Recogniser pages shows a combination of Cable PDs (of up to 8,500pC - bottom left graph) and noise pulses of up to 17mV (bottom right graph). The 'Segment Waveform' box in the top left-hand corner of the screen shows the 'Waveform' of one of the cable PD pulses measured in this test. This pulse has been identified by the software as a cable PD due to it having the right waveshape (similar to a 'sharks fin') with a risetime, fall-time and pulse width in the correct range and the correct frequency (0.625MHz/625kHz) for a cable PD.

As mentioned earlier, Switchgear PD pulses are typically oscillatory in waveshape and normally have frequencies in the range of 4MHz and higher (up to 100MHz if the source of the discharge is very close by to the sensor\). This is an important point to note as it is known that whilst discharges measured at their source produce very high frequency signals (up to 100MHz) the high frequency content of these signals is stripped out as the pulse travels outwards from its source. This results in a lowering of the main frequency of the pulse as it travels through the insulation and air around the site.

## On-Line PD *Location* in Switchgear with Time-Of-Flight Measurements

The source of partial discharge activity can be located along a row of switchgear panels and also within a switchgear panel itself by using the HVPD Longshot© Unit with two or more TEV sensors and then applying Time of Flight (TOF) analysis. By placing TEV sensors at different points on the switchgear panel (with matching signal cables of the same length) it is possible to measure the time of arrival of the PD pulses on each of the sensors to provide a good estimation of the origin of the PD within the switchgear (the sensor where the pulse arrives first is nearest to the source of discharge).

This measurement is carried out in the ScopeControl© Software on the LongshotTM system which allows the user to measure and record signals and differentiates time-of-flight signals down to less than 500 pico-Seconds. In air the TEV signals will travel typically at a speed of 300mm (30cm) per 1ns and thus the resolution of the system is typically around 15cm (assuming that matched length signal cables are used).

An example of this PD location method is given overleaf for a test where 2x TEV sensors were placed at different points on an air-insulated switchgear panel to locate the PD source. Through a series of tests where the 2x TEV sensors were placed at various positions on the switchgear panel it was possible to locate the position of the discharge activity in the switchgear panel. Figure 11 shows the test set-up for the final test in this series where one TEV sensor was placed on the top of the panel and the other on the front of the panel above the cable box.

The ScopeControl© measurement screen in Figure 12 shows the first signal (green) coming from is the TEV sensor positioned on the top of panel whilst the second signal (red) is from a TEV sensor positioned on the front of the panel. The first signal is around 3ns in advance of the second signal which equates to a physical distance of around 90cm (the propagation speed of TEV signals in air is around 30cm per nanosecond).This confirms that the source of the discharge is in the top section of the switchgear panel.


**Figure 11: Placement of 2xTEV Sensors on Switchgear Panel for TOF Measurements**

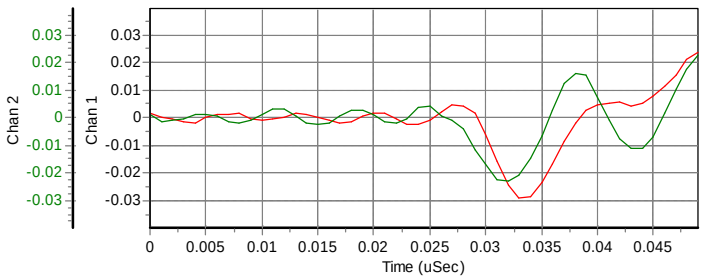


**Figure 12: Time Of Flight Measurement for PD Site Location Using 2x TEV sensors (green signal – top, red signal –front)**

### Example of PD measurements on 22kV Air Insulated Switchgear with TEV Probes

This example describes the results from application of the HVPD Longshot© PD Spot Tester to test 22kV air-insulated switchgear. The testing was carried out over a 10-minute period with the TEV probe initially placed near the top of the switchgear housing over the first 5 minutes, a gap of around 1 minute when the probe was repositioned, and then 4 minutes of the TEV probe placed on the switchgear cable box. The results of this test are shown in Figure 13 with traces for the Peak PD Signal (red), 1% Level (yellow) and Number of Counts (above an automatic threshold) in grey. It can be noted here that the Peak TEV signals (in dB) are higher (at around 30dB) when the sensor is placed near the top of the panel than on the cable box (20dB) which suggest that the discharge source is at the top of the housing.

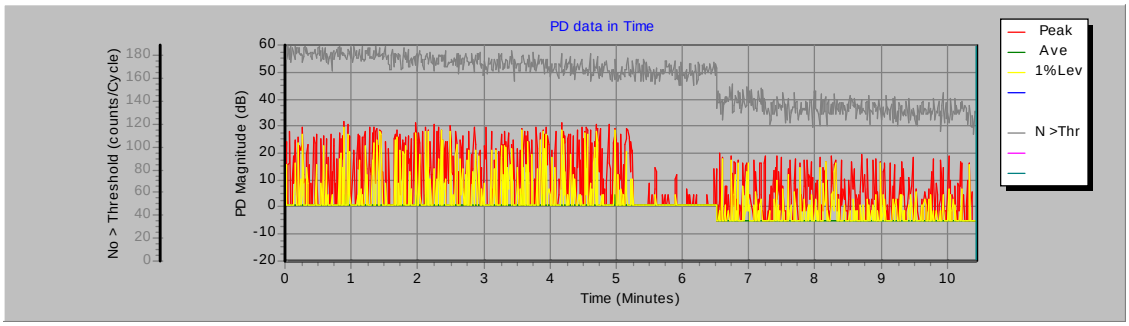


**Figure 13: PD Results vs. Time from Testing of 22kV Air Insulated Switchgear**

It can be noted from the above plot that the PD activity near to the bushings has a level of around 30dB which is a cause for concern for 22kV air-insulated switchgear and this should be investigated further (refer to Appendix 1 for Guideline PD Levels).

For comparison purposes, an example of the results from testing the same type of 22kV Air-Insulated Switchgear with no discharge is given below in Figure 14.

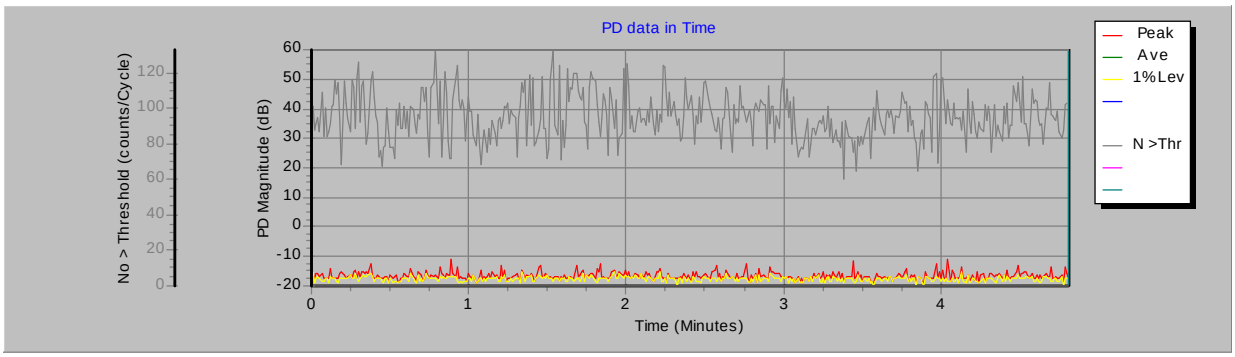


**Figure 14: Test Results for 22kV Air Insulated Switchgear - No Discharge**

### PD measurements on MV Switchgear combining HFCT and TEV Probes

As mentioned earlier in this document, it is recommended that for On-line PD Testing of MV switchgear a combination of the HFCT and TEV sensors are used in order to provide the highest level of confidence in picking up PD activity. For the HFCT to pick-up PD activity in the Switchgear Panel (and also the corresponding cable feeder) it should be placed around *either* the cable core, above the earth strap, with the HFCT picking up the discharge pulses from within the conductor, or alternatively, around the cable earth strap with the HFCT picking up the discharge pulse travelling to earth.

TEV sensors are normally magnetically latched to the outside of the cable earth box and/or higher up the switchgear panel. Depending on the source of the discharge in the switchgear panel the TEV signals will be higher in magnitude on the sensor which is nearer to source (this is illustrated above in Figure 13).

## Airborne Acoustic Emission (Ultrasonic) Probes

The third and final PD Sensor used by HVPD for testing MV Switchgear is the Airborne Acoustic Emission Probe. This is used for detecting PD's into air from corona and surface tracking insulated switchgear and is the most sensitive way of measuring PD activity in this type of switchgear with measurements down to a few pC's possible. This sensor is particularly useful in detecting surface discharge on cable terminations, sealing ends and within air-insulated switchgear (line-of-sight to discharge site required). It has also been found to be very useful to record the electromagnetic signals (from a TEV or HFCT sensor) synchronously with the acoustic ones useful when Time-of-Flight (TOF) measurements are carried out to locate the source of airborne discharges. This adds a further confirmation of the origin of the PD signals when used in conjunction with TEV/HFCT sensors. The HVPD Airborne Acoustic Probe is shown below in Figure 15.

**Figure 15: HVPD Airborne Acoustic (Ultrasonic) PD Sensor**

For this sensor to work it should be noted that there must be a **clear air path** from the sensor to the discharge site. This means that fully enclosed switchgear with no grills, vents air gaps etc, will not be suitable for measurements using ultrasonic probes.

If the ultrasonic probe is used in conjunction with a TEV or HFCT, when looking across the power cycle on the PD spot tester, bear in mind that the ultrasonic signals take time to arrive at the detectors compared with the electromagnetic signals. Delays of a few milliseconds (ms) are common. The Electromagnetic signals travel at a speed of around 150m/μsec (around 50% the speed of light) whilst sound travels much slower, at around 330m/Sec in air, so a distance of 1m would produce a delay of 3mSec between the very fast electromagnetic signal and the much slower acoustic signal. This is best described as the time difference between the thunder (ultrasonic signal) and the lightning (electromagnetic signals) as is illustrated in Figure 16 overleaf. Also the acoustic signal may be more spread out than the e/m signal. Both of these should be borne in mind when using the ultrasonic probes.

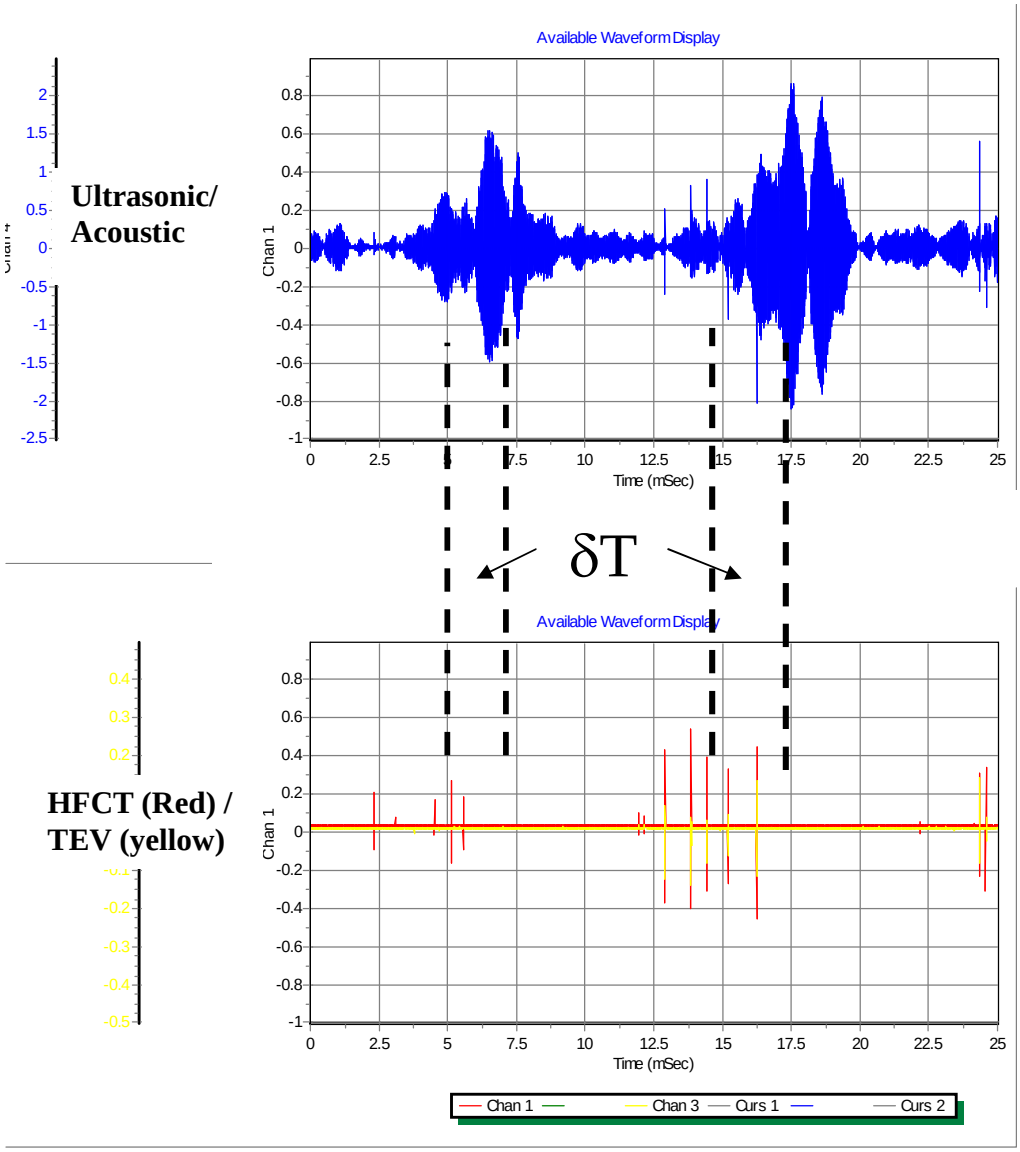


**Figure 16: Time difference between HFCT/TEV electromagnetic signals ('the lightning') and Ultrasonic signals ('the thunder')**

Internal discharges in insulation do produce ultrasound signals, but these will generally not be picked up when using an ultrasonic probe. This is due to the attenuation of the signal in the insulation, and poor coupling of the air/solid interfaces which means that acoustic signals which originate inside the insulation, are generally not accessible via ultrasonic methods. Hence the Airborne Acoustic probes are best reserved for air discharges in air insulated switchgear, for which they work remarkably well.

Using the Longshot™ spot tester method for ultrasonic measurements is a much more reliable method than listening to the output of an ultrasonic detector. This is especially true when the used in conjunction with the TEV or HFCT sensors. The ultrasonic detectors are more sensitive than TEV signals for air discharges (sensitivity

down to around 2pC). Hence it is possible for lower magnitude PD events, to detect the acoustic PD signals, and see no detectable TEV signals. In general, the PD levels in switchgear must be above 100pC before reliable TEV signals can be measured. The ultrasonic probe however, can easily make measurements at levels well below this, down to around 2pC. This sensitivity is based on the proviso that there exists the continuous air path between the acoustic detector and the originating PD site.

The HVPD Ultrasonic sensor relies on a line-of sight detection (+/- 30$^{o}$) has been designed to supplement the TEV and HFCT sensors and is highly suitable for detecting discharge into the air or along polymeric surfaces (tracking) such as that shown below in Figure 17.

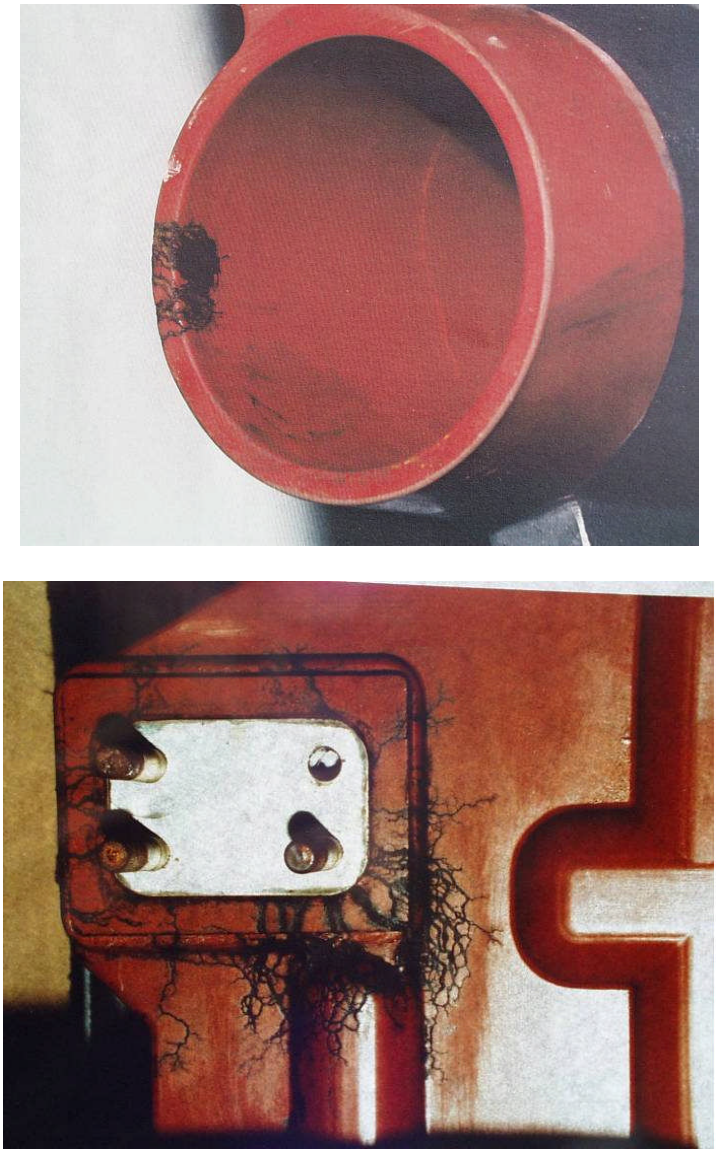

**Figure 17: Examples of Tracking on Air-Insulated Switchgear**
Top – Start of Tracking on the Spouts of Air-Insulated Switchgear
Bottom – Advanced Tracking Damage on Epoxy Resin bus bar

## Conclusions

HVPD recommends that for the maximum sensitivity and to detect the widest range of PD types that *all three of the non-intrusive PD sensors* are used to carry out On-Line PD Testing of MV Switchgear. It is through the *combination of the TEV, HFCT and Airborne Acoustic probes* that this maximum PD test sensitivity can be achieved in the field.

Improved sensitivities for PD measurements on switchgear can be made using a combination of the TEV, HFCT and Airborne Acoustic Probes. Results of in-field testing show, in general, an improvement of about 5 or 6 times in the sensitivity of PD measurements (for internal discharge) can be achieved using an HFCT connected around the cable conductor compared with a TEV type aerial probe. A similar improvement in sensitivity is seen with the HVPD Airborne Acoustic Sensor compared to the TEV when detecting surface and air discharge.

These results have significant implications for on-line testing for switchgear, where much better sensitivity can be used to monitor switchgear using HFCT's and Acoustic Probes. These results do not discount the use of TEV sensors for a number of reasons, as follows:

- Locations of PD to a particular Switchgear Panel within the substation can be made using Time-Of-Flight (TOF) analysis of TEV signals as discussed herein.

- There is a large, historical database in the UK for TEV testing of MV switchgear (level of activity given in dB). Results from switchgear testing with TEV probes can therefore be compared back to this reference data (refer to Appendix 1 for details).

- The combination of the three sensors allows for 'type of discharge' diagnosis to be made, providing the opportunity to assess the seriousness of the PD activity in more detail.

To summarise, for testing switchgear with an identified PD problem, measurements using a combination of sensors (TEV's, HFCT's and Acoustic Probes) give a much better monitoring outlook than only using conventional TEV probes alone.

# Appendix 1: Guide to TEV levels for Switchgear

## Background

The measurement of PD magnitudes and rates can be enormously variable when measurements on power systems are made. The nature of the system makes a large difference in the interpretation of the results. What is very bad in one type of equipment may just be acceptable in another. Hence the interpretation of PD activity must take into account all the factors which can influence the outcome. The largest influence comes with the detailed location of the PD activity. Hence for example, if the PD originates between two metal structures one of which is not grounded, then this may be benign for the life of the equipment. However, if the PD originates in a cavity in a high stress part of the insulation, then this is very serious, and has to be treated to avoid failure. Hence it is mostly *the position of the PD site* which determines the 'badness' of the measured PD activity. A list of the factors which influence the weighting of the PD measurements are given below for guidance purposes.

The PD level guide is really for medium voltage systems (typically 11kV and 33kV) as the plant at higher voltages should run discharge free. The advice that power systems should be operated discharge free is a very good one although in practice this is not normally practicable due to limited maintenance and operational budgets. In addition it is known that some insulation types in HV plant are more resilient to PD activity than others (see Insulation Materials) below. For example the mica-based insulation in Medium Voltage Motors is known to be able to withstand PD activity of tens and sometimes hundreds of thousands of pico-Coulombs (10,000 to 100,000pC) one of the most resilient. With HV plant with a high resilience to

Most polymer based insulation now has standards which set by IEC guidelines (at least in the factory/type test) to have a PD level of better than 10pC. It is difficult to see that properly installed plant which is discharging less than this level is going to fail by insulation failure. All other failure modes can be sorted with maintenance programs and hence the aim should be to run any new system discharge-free (this can be tested at commissioning stage to provide a 'base-line, at-installation' PD level).

**Operating Voltage**

As the voltage increases, the same size PD becomes more serious. This is partly because the stresses tend to increase in larger voltage plant, partly because there are simply more volts available and partly due to the geometry. Probably a rough rule would be to weight the voltage level linearly. Hence a discharge of 50pC in a 33kV system would be three times more damaging than the same size discharge in an 11kV system. Again these depend on geometry; the type of PD event, location etc, but the rough scaling is there. Notice that at transmission voltages, PD events are significant at a small level, and tend to be more difficult to measure. Measurements at medium voltage (e.g. 11kV) are probably the easiest to make as the signal to noise ratio tends to be smaller.

**Type of discharge**
These can be cavities bounded by dielectric, or bounded by metal, surface discharges, PD in layered media, corona in air etc. Internal PD events in dielectric cavities tend to be the most damaging. The daughter products from the PD events remain within the cavity. (These can be acids, corrosive chemicals, or simply active elements from the gases in the discharge). No ventilation is possible, and cavities like this almost always end up in failure. The time scale is the only variable. The important part here is the damage the PD events do to the surrounding insulation.

**Insulation materials**
The materials of the insulation are critical. Hence old switchgear with porcelain and metal parts, were virtually indestructible unless nests of mice shorted out the porcelain insulators. In this case, PD activity had almost no effect. With polymers, paper, oil, bitumen etc, this is no longer true, and the rate of deterioration will depend on the nature of the degradation of the insulation material. The route of deterioration will also depend on the material. For example, in air insulated switchgear, surface discharges will damage the hydrophobicity of the materials, with the result that the surfaces will wet out distorting the fields, and causing a tracking/erosion failure.

**Thermo-mechanical variations**
The effect of load (i.e. temperature) is vital in the development of discharges. The variation will temperature can come simply because the insulation is hotter. Polymers (both thermoset and thermoplastic) will become softer and less resistant to PD as they heat up. Whereas mass impregnated non draining (MIND) impregnated paper cables tend to improve with temperature, as the wax based oils flows more easily into any cavities. Temperature variations can produce a large change in the mechanical movements of the equipment as the components expand. Movement at terminations and joints are a good example of this. These movements can make a large change in the PD activity, depending on which parts of the high voltage region they move or distort.

**Mechanical movement**
Clearly the movement of parts in the high voltage system can cause PD to appear, increase or decrease. Tap changer selectors, switchgear circuit breaker trolleys, earthing arms, knife blade switches etc, can all cause changes in the equipment which can affect the PD activity. With cables, external damage is probably the most common cause of failures of all.

**Environmental conditions**
Other than temperature, there are some environmental conditions, which can affect the performance of high voltage plant. For air insulated switchgear, the effect of temperature and humidity is a vital component of damage due to PD activity. Water condensation is the vital part of the induction of PD on surfaces in air insulated switchgear. In fact water condensation should be avoided for all high voltage plant. Only outdoor insulators are designed for operation in wet condition, and only in a fully ventilated state. All other plant should be operated dry.

## 11-33 kV Switchgear systems

In these cases, the levels are in dB. In these cases 1mV into 50Ohms is the level for 0dB. The following are measurements which are above the noise, and clearly PD activity. They are for switchgear and apply to solid insulation discharges.

### Switchgear (solid insulation)

This category also applies to bitumen filled cable terminations.

| | | |
|---|---|---|
| **Below 0dB (or discharge free)** | No insulation difficulties. Can be left out of any monitoring programme. Re-test as legally required. | |
| **0dB to 15dB** | Some discharge but probably not implying short term failure. This should be re-tested in 6 or 12 months to watch for any change | |
| **15dB to 25dB** | System is quite active, but still not likely to fail in the very short term. This needs to be monitored, or re-tested soon. Prudent system operators may choose to do something now | |
| **25dB to 35dB** | These are bad discharges, and some monitoring should be installed immediately. Recommend that plans be put in place to locate and sort out the origin of the PD activity | |
| **Above 35dB** | These are serious, and the substation should be restricted. The switchgear should be tested offline and the origin of the PD located and repaired. | |

### Switchgear (Air insulated)

This category also applies to dry cable terminations which are discharging in air either on the surface or between cores.

| | | |
|---|---|---|
| **Below 0dB (or discharge free)** | No insulation difficulties. Can be left out of any monitoring programme. Re-test as legally required. | |
| **0dB to 10dB** | This level of PD in or on the air insulating surfaces is potentially quite serious. These are not failure levels, but should be monitored as the discharges vary with the atmospheric conditions, and spot testing may miss the majority of the activity. Use ultrasonic air probe to confirm diagnosis of surface discharges. | |
| **10dB to 15dB** | If this is combined with audible discharges, then this is much more serious. Monitoring or even restricted access is desirable here. Plans should be put in place to find out the cause of the PD and correct it. | |
| **15dB – 30dB** | These are bad discharges, and some monitoring should be installed. Recommend that plans be put in place to locate and sort out the origin of the PD activity | |
| **Above 30dB** | These are serious, and the substation should be restricted & the switchgear tested offline and the origin of the PD located and repaired. | |